

FABAD JOURNAL of PHARMACEUTICAL SCIENCES

ISSN 1300-4182
e-ISSN: 2651-4648
www.fabad.org.tr

Volume: 49 • Issue: 1 • March 2024

An Official Journal of The Society of Pharmaceutical Sciences of Ankara (FABAD)



Publisher

Sevgi AKAYDIN (Gazi University, Department of Biochemistry, Ankara, Turkey)

Editor in Chief

Nesrin Gökhan KELEKÇİ (Hacettepe University, Department of Pharmaceutical Chemistry, Ankara, Turkey)

Co-Editors

Selen ALP (Ankara University, Department of Pharmaceutical Chemistry, Ankara, Turkey)
Fatma Sezer ŞENOL DENİZ (Gazi University, Department of Pharmacognosy, Ankara, Turkey)
Sibel İLBASMIŞ TAMER (Gazi University, Department of Pharmaceutical Technology, Ankara, Turkey)

Technical Editors

Gökçen TELLİ (Hacettepe University, Department of Pharmacology, Ankara, Turkey)
Vahap Murat KUTLUAY (Hacettepe University, Department of Pharmacognosy, Ankara, Turkey)

Biostatistics Editor

Hatice Yağmur ZENGİN Hacettepe University, Faculty of Medicine, Department of Biostatistics, Ankara, Turkey

Editorial Board

Almira RAMANAVIČIENĖ Vilnius University, Nanotechnology and Material Sciences Center, Vilnius, Latvia
Alper GÖKBULUT Ankara University, Department of Pharmacognosy, Ankara, Turkey
Ashok K. SHAKYA Al Ahliyya Amman University, Department of Pharmaceutical Chemistry, Amman, Jordan
Aygin EKİNÇIOĞLU Hacettepe University, Department of Clinical Pharmacy, Ankara, Turkey
Ayşe KURUÜZÜM UZ Hacettepe University, Department of Pharmacognosy, Ankara, Turkey
Bharat JHNAWAR Lovely Professional University, Pharmaceutical Sciences, Punjab, India
Bülent KIRAN Ege University, Department of Pharmacy Management, Izmir, Turkey
Ceyda Tuba ŞENGEL TÜRK Ankara University, Department of Pharmaceutical Technology, Ankara, Turkey
Chia-Yi TSENG Chung Yuan Christian University, Biomedical Engineering, Taoyuan, Taiwan
Didem DELİORMAN ORHAN Gazi University, Department of Pharmacognosy, Ankara, Turkey
Emel Öykü ÇETİN UYANIKGİL Ege University, Department of Pharmaceutical Technology, Izmir, Turkey
Filiz BAKAR ATEŞ Ankara University, Department of Biochemistry, Ankara, Turkey
Gerardo EPIFANIO G. D'Annunzio* University, Department of Pharmaceutical Chemistry, Chieti-Pescara, Italy
Gerard LIZARD University of Burgundy, French Institute for Medical and Health Research, Dijon, France
Gökçe CİHAN ÜSTÜNDAG Istanbul University, Department of Pharmaceutical Chemistry, Ankara, Turkey
Gökçen EREN Gazi University, Department of Pharmaceutical Chemistry, Ankara, Turkey
Hande GÜRER ORHAN Ege University, Department of Pharmaceutical Toxicology, Izmir, Turkey
Hasan Abougazar YUSUFOĞLU King Saud University, Department of Pharmacognosy, Riyadh, Saudi Arabia
Hasan KIRMIZIBEKMEZ Yeditepe University, Department of Pharmacognosy, Istanbul, Turkey
İkhlas KHAN University of Mississippi, National Center for Natural Product Research, USA.
İşıl ÖZAKCA GÜNDÜZ Ankara University, Department of Pharmacology, Ankara, Turkey
İnci Selin DOĞAN Karadeniz Technical University, Department of Pharmaceutical Chemistry, Trabzon, Turkey
Leyla YURTTAŞ Anadolu University, Department of Pharmaceutical Chemistry, Eskisehir, Turkey
Melike H. ÖZKAN Hacettepe University, Department of Pharmacology, Ankara, Turkey
Meltem ÜNLÜSOY Ankara University, Department of Pharmaceutical Chemistry, Ankara, Turkey
Merve BACANLI University of Health Sciences, Department of Pharmaceutical Toxicology, Ankara, Turkey
Merve BECİT Afyonkarahisar University of Health Sciences, Department of Pharmaceutical Toxicology, Afyonkarahisar, Turkey
Mesut SANCAR Marmara University, Department of Clinical Pharmacy, Istanbul, Turkey
Ming-Wei CHAO Chung Yuan Christian University, Department of Bioscience Technology, Taoyuan, Taiwan
Muhammed ÖLÇER Afyonkarahisar University of Health Sciences, Department of Pharmaceutical Technology, Afyonkarahisar, Turkey
Natalizia MICELI University of Messina, Department of Chemistry and Biology, Messina, Italy
Özlem Nazan ERDOĞAN Istanbul University, Department of Pharmacy Management, Ankara, Turkey
Sevda ŞENEL Hacettepe University, Department of Pharmaceutical Technology, Ankara, Turkey
Sevta AYDIN DİLSİZ Hacettepe University, Department of Pharmaceutical Toxicology, Ankara, Turkey
Suryakanta SWAIN The Assam Kaziranga University, Department of Pharmaceutical Sciences, Assam, India
Şükrü BEYDEMİR Anadolu University, Department of Pharmaceutical Microbiology, Ankara, Turkey
Tuba İNCEÇAYIR Gazi University, Department of Pharmaceutical Technology, Ankara, Turkey
Tuğba TÜYLÜ KÜÇÜKKİLİNÇ Hacettepe University, Department of Biochemistry, Ankara, Turkey
Tuğçe YEŞİL Marmara University, Department of Pharmaceutical Toxicology, Istanbul, Turkey
Uğur TAMER Gazi University, Department of Analytical Chemistry, Eskisehir, Turkey
Vu Dang HOANG Hanoi University of Pharmacy, Department of Analytical Chemistry and Toxicology, Hanoi, Vietnam
Wolfgang SCHUHLY University of Graz Institute of Pharmaceutical Sciences, Department of Pharmacognosy, Graz, Austria

The FABAD Journal of Pharmaceutical Sciences is published three times a year by the
Society of Pharmaceutical Sciences of Ankara (FABAD)

All expressions of opinion and statements of supposed facts appearing in articles and / or advertisements carried in this journal are published on the responsibility of the author and / or advertiser, and are not to be regarded those of the Society of Pharmaceutical Sciences of Ankara. The manuscript submitted to the Journal has the requirement of not being published previously and has not been submitted elsewhere. Manuscript should be prepared in accordance with the requirements specified as in the back cover. The submission of the manuscript to the Journal is not a condition for acceptance; articles are accepted or rejected on merit alone. This Journal is published electronically and it is an open-access journal without publication fee. All rights reserved. Neither this work nor any part may be reproduced or transmitted in any form or by any means, electronic or mechanical, microfilming and recording, or by any information storage and retrieval systems without written permission from FABAD Journal of Pharmaceutical Sciences.

The FABAD Journal of Pharmaceutical Sciences is indexed in Chemical Abstracts,
Analytical Abstracts, International Pharmaceutical Abstracts, Excerpta Medica (EMBASE), Scopus and TR Index

CONTENTS

Research Articles

- 1 In Silico Target Prediction of 6-Gingerol and Similar Compounds as Potential Anticancer Agents
Nour Osama AL-MASSRI*, **Enise Ece GURDAL **°**, **Gulcin TUGCU ***°**
- 19 Mineral contents, Antioxidant and Antimicrobial Activities of Algerian *Terfezia claveryi* extracts
Hadjira GUENANE*, **Boulanouar BAKCHICHE**°**, **Ramazan ERENLER*****, **Ilyas YILDIZ******, **Asmaa S. MOHAMED*******, **Maha A.M. El-SHAZLY*******
- 37 Dipyridamole Cocrystal Tablets with Enhanced Solubility and Dissolution at Intestinal pH
Monika NIJHAWAN*° **Sadhna DHYAGALA**** , **Gunnam SAILAJA*****, **Rajeswari ALETI******, **Trapti SAXENA*******
- 51 Formulation and Evaluation of Mixed Micelles Containing Quercetin for Inhibiting Intestinal Metabolism of Atorvastatin
Narahari N. PALEI*°, **Jayaraman RAJANGAM****, **Ramu SAMINENI*****, **Arghya K DHAR******, **Anna BALAJI*******
- 65 Development and Evaluation of Pullulan-Based Mouth Dissolving Film of Furosemide
Aafreen SAHA*, **Umesh Kumar ATNERIYA**°**, **Umashankar JOSHI*****, **Dharmendra SOLANKI******
- 81 Investigation of the Effects of Oleuropein on Mouse Detrusor Muscle Contractility
Elif Nur BARUT*°, **Ahmet Can OZTURK****, **Seckin ENGIN*****, **Gulin RENDA******
- 91 Immunosuppressive and Ameliorative Effects of Dietary Combined Herbs Extract of *Curcuma zedoaria* (Christm.) Roscoe and *Phyllanthus niruri* L. in DMBA-induced Breast Cancer Mouse Model
Wira Eka PUTRA*, **Anoraga Mona Larasati Sekar MENTARI****, **Devita RATNASARI*****, **Dhaniar CHAIRUNNIZA******, **Arief HIDAYATULLAH*******, **Muhaimin RIFA'I*****°**
- 111 Metronidazole Loaded Novel Microemulsion Formulation for Topical Delivery and Characterization With Validated New UPLC Method
Tilbe ÇEVİKELİ*°, **Umay Merve GÜVEN****, **Ahmet Alper ÖZTÜRK*****
- 129 *In vitro* Evaluation of the Effects of *Inula viscosa's* Different Extracts on Wound Healing and Oxidative Stress in Mouse L929 Fibroblast Cell Line
Ahmet HARMANKAYA*°, **İrfan ÇINAR****, **Muhammed YAYLA*****, **Sezen HARMANKAYA******, **Murat BEYTUR*******, **Cem ÖZİÇ*******

- 143 Design, Development, and Characterization of Lyophilized Posaconazole-Loaded Mixed Micelles for Improved Fungal Treatment and Stability
Adesh KURANE*, **Rutuja CHOUGALE****, **Vibhuti THAKUR*****, **Kiran PATIL****°**, **Shalaka PATKI*******, **John Disouza*******, **Ashok HAJARE*******
- 163 Bilayer Nanofiber Scaffold Incorporated with Mupirocin and Thyme Essential Oil for Synergistic Activity Against Bacterial Wound Infections
Kisan JADHAV*°, **Shivani GHARAT ****, **Shradha B. ADHALRAO*****
- 181 Protective Role of Pistacia palaestina Boiss. Fruit and Leaf Extracts in Isoproterenol-Induced Cardiac Ischemia
Mehmet Sina İÇEN*, **Hande YÜCE****, **Neşe BAŞAK TÜRKMEN*****, **Aslı TAŞLIDERE******, **Dilan AŞKIN ÖZEK*****°**, **Songül ÜNÜVAR*******
- 197 Comparative Study of The Anti-Inflammatory Pathway Enzyme Activities of Selected Plant Extracts from Lamiaceae Family
Kubra SENER *, **Murat EKİCİ****, **Ekrem Murat GONULALAN*****, **Ebru BODUR****°**
- 211 Financial Development of the Turkish Pharmaceutical Sector During and After the Pandemic: Sector Panel Data Analysis for the Period 2018-2022
Mustafa ÖZYEŞİL*°, **Havane TEMBELO****
- 227 The Inhibitory Effect of Trimethylamine (TMA), an Intestinal Bacterial Metabolite, on Endothelial Vasorelaxation in Rat Mesenteric Artery
Melike Hacer ÖZKAN*°
- 233 Effect of n-Hexane Extract from Tanacetum argenteum (Lam.) Willd. subsp. argenteum on the Secretion of Proinflammatory Cytokines in THP-1 Cell Line
Ege ARZUK*°, **Fuat KARAKUŞ****, **Gökay ALBAYRAK*****, **Ali ERGÜÇ******, **İclal TAN*******, **Ecrin ATIŞ *******

Review Article

- 245 Endocrine Disrupting Effects of Flame Retardants on Thyroid System
İrem İYİGÜNDOĞDU*, **İsmet ÇOK**°**

In Silico Target Prediction of 6-Gingerol and Similar Compounds as Potential Anticancer Agents

Nour Osama AL-MASSRI*, Enise Ece GURDAL **, Gulcin TUGCU ***

In Silico Target Prediction of 6-Gingerol and Similar Compounds as Potential Anticancer Agents

SUMMARY

Ginger (*Zingiber officinale* Roscoe) has been widely recognized for its culinary and medicinal applications; however, its potential anticancer activity remains understudied. This research aimed to identify novel lead compounds exhibiting high bioavailability and low toxicity, akin to 6-gingerol, through an in silico screening approach using ChemMine Tools depending on the PubChem fingerprints. The screened compounds were further analyzed using target fishing servers to identify putative kinase targets. Molecular docking studies were conducted on selected kinases including BRAF, JAK1/2, ERK1(MAPK3), and p38 γ . Computational analysis was performed to evaluate the pharmacokinetics, drug-likeness, and toxicity profiles of the compounds, shedding light on their safety and bioavailability. Notably, the following compounds exhibited promising anticancer potential: 6-gingerol, vanilyl glycol, vanillylmandelic acid, L-(+)-vanilmandelic acid, dehydrozingerone, 2-methoxyestrone, methylvanillate, dihydroconiferyl aldehyde, pratensein, acetovanillone, acetosyringone, licochalcone B, isoferulic acid, curcumin PE, and coniferaldehyde. These findings suggest that these compounds warrant further investigation as potential candidates for anticancer therapies and should be considered for future lead optimization studies.

Key Words: 6-gingerol, anticancer, chemical similarity, computational toxicity, molecular docking, pharmacokinetics, target fishing

Potansiyel Antikanser Ajanlar Olarak 6-Gingerol ve Benzer Bileşiklerin In Silico Hedef Tabmini

ÖZ

Zencefil (*Zingiber officinale* Roscoe), mutfak ve tıbbi uygulamalarıyla yaygın olarak tanınmaktadır; ancak potansiyel antikanser aktivitesi yeterince araştırılmamıştır. Bu araştırma, PubChem parmak izlerine bağlı olarak ChemMine araçlarını kullanan bir in silico tarama yaklaşımı aracılığıyla 6-gingerol'e benzer şekilde yüksek biyoyararlanım ve düşük toksisite sergileyen yeni öncü bileşikler tanımlamayı amaçlamıştır. Taranan bileşikler, varsayılan kinaz hedeflerini belirlemek için hedef balıkçılık sunucuları kullanılarak daha fazla analiz edildi. BRAF, JAK1/2, ERK1(MAPK3) ve p38 γ dahil olmak üzere seçilen kinazlar üzerinde moleküler yerleştirme çalışmaları yapılmıştır. Bileşiklerin farmakokinetiğini, ilaca benzerliğini ve toksisite profillerini değerlendirmek, güvenliklerine ve biyoyararlanımlarına ışık tutmak için hesaplamalı analizler yapılmıştır. Özellikle, aşağıdaki bileşikler umut verici antikanser potansiyeli sergilemiştir: 6-gingerol, vanilglükol, vanilmandelik asit, L-(+)-vanilmandelik asit, dehidrozingeron, 2-metoksiestron, metilvanillat, dihidrokoniiferil aldehit, pratensein, asetovanillon, asetosiringon, likokalkon B, izoferulik asit, kurkumin PE ve koniferaldehit. Bu bulgular, bu bileşiklerin anti-kanser tedaviler için potansiyel adaylar olarak daha fazla araştırılması gerektiğini ve gelecekteki öncü optimizasyon çalışmaları için dikkate alınması gerektiğini göstermektedir.

Anahtar Kelimeler: 6-gingerol, antikanser, kimyasal benzerlik, hesaplamalı toksisite, moleküler yerleştirme, farmakokinetik, hedef tabmini

Received: 15.08.2023

Revised: 05.10.2023

Accepted: 06.10.2023

* ORCID: 0009-0004-8699-3003, Department of Pharmaceutical Chemistry, Faculty of Pharmacy, Yeditepe University, 34755 Istanbul, Turkey

** ORCID: 0000-0003-1064-8639, Department of Organic Chemistry, Institute of Chemistry, Martin-Luther-Universität Halle-Wittenberg, 06120 Halle, Germany

*** ORCID: 0000-0002-9750-6563, Department of Pharmaceutical Toxicology, Faculty of Pharmacy, Yeditepe University, 34755 Istanbul, Turkey

INTRODUCTION

Cancer, a leading cause of death worldwide, poses significant challenges to effective treatment. Chemotherapy remains a widely utilized therapeutic approach for all stages of cancer (Rayan et al., 2017). However, it is associated with high doses, severe side effects due to toxicity, activation of pro-survival pathways with prolonged exposure, and the emergence of treatment resistance (Rastogi et al., 2015; Rayan et al., 2017). To overcome these drawbacks, researchers have turned their attention to natural resources. Various alkaloids, flavonoids, terpenoids, polysaccharides, saponins, and other natural substances are known to have anticancer activities by modulating immune function, inducing autophagy, or inhibiting cell proliferation (Rayan et al., 2017). Ginger (*Zingiber officinale Roscoe*), a member of the Zingiberaceae family and genus *Zingiber*, has a long history of use as a culinary spice and herbal medicine. Rich in bioactive compounds, ginger contains phenolic compounds such as gingerols, shogaols, and paradols, with 6-gingerol, 8-gingerol, 10-gingerol, and terpene compounds being the major polyphenols found in fresh ginger. Recent studies have revealed a range of biological effects exhibited by these bioactive compounds, including antioxidant, anti-inflammatory, antimicrobial, and intriguingly, anticancer properties. Numerous studies have demonstrated the anticancer effects of 6-gingerol in various human cancers, including leukemia, breast, colon, pancreatic, prostate, and liver (Wang et al., 2014; Zhang et al., 2017; Mao et al., 2019). In particular, the hydroxyl group-containing aliphatic chain moiety in 6-gingerol (1-[4'-hydroxy-3'-methoxyphenyl]-5-hydroxy-3-decanone) (Figure 1) has been linked to its biological activities (Wang et al., 2014).

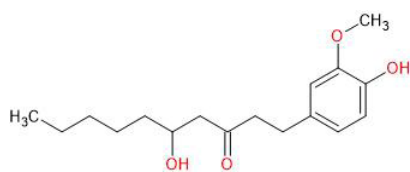


Figure 1. Structure of 6-gingerol

Kinases are cellular intermediaries that facilitate the phosphorylation process by transferring the gamma-phosphate group from an ATP molecule to the serine (Ser), threonine (Thr), or tyrosine (Tyr) residues in target molecules. They play a pivotal role in regulating cellular signaling pathways by controlling a wide range of cellular functions such as transcription, metabolism, nervous system activity, immune response, cell division, and migration (Modi et al., 2019; Schwarz et al., 2019; Wang et al., 2021). Dysregulation and mutations of protein kinases have been associated with a range of human diseases including cancer, diabetes, autoimmune disorders, cardiovascular diseases, inflammatory conditions, and neurological disorders. As a result, protein kinases have emerged as key therapeutic targets, particularly in cancer treatment (Roskoski, 2016).

In silico target fishing is widely used in drug discovery to discover the most probable biological targets of a given molecule (Galati et al., 2021). This approach allows us to anticipate the biological activity of a given molecule in question or its mechanism of action. Additionally, target fishing can be useful for predicting side effects, revealing multiple effects of a drug, and uncovering new applications for existing drugs (Cereto-Massagué et al., 2015). A commonly used similarity approach is the target fishing strategy, which suggests that molecules with similar structural patterns may exhibit comparable bioactivities and, thus, interact with similar targets (Galati et al., 2021).

In light of existing research, this study aims to identify novel lead compounds that are similar to 6-gingerol and exhibit potent anticancer activity, while also demonstrating high bioavailability and a low toxicity profile. For this purpose, an *in silico* screening was performed using ChemMine Tools based on PubChem fingerprints, to search for compounds with structural similarity to 6-gingerol. To investigate the anticancer potential of 6-gingerol and the identified similar compounds, they were screened using *in silico* target fishing servers, focusing on their putative

kinase targets. Selected kinase targets were then used in docking studies to assess potential interactions with the compound dataset. Furthermore, computational assessments were performed to determine the pharmacokinetics, drug-likeness, and toxicity profiles of these compounds, with the goal of highlighting the safety and bioavailability of both 6-gingerol and its structurally similar compounds. The results of this computational study include the discovery of putative kinase targets of 6-gingerol-like molecules and potential lead compounds for further development.

MATERIAL AND METHOD

Compounds Studied

The primary focus of this study was on 6-gingerol (1-[4'-hydroxy-3'-methoxyphenyl]-5-hydroxy-3-decanone), a known active anti-tumor compound. In addition to 6-gingerol, compounds with chemical structures similar to 6-gingerol were identified for further investigation. The selection of structurally similar compounds was based on a predetermined cut-off value. For the similarity search, Tanimoto score calculations were performed using PubChem fingerprints in ChemMine Tools (<https://chemminetools.ucr.edu/eisearch/query/>) (Backman et al., 2011).

In silico Target Fishing

The biological activities of 6-gingerol were predicted using the PASSOnline, Swiss Target Prediction, MolTarPred, and SEA web servers (Keiser et al., 2007; Filimonov et al., 2014; Peón et al., 2017; Daina et al., 2019). These servers utilize fingerprint similarity to known bioactive compounds to generate a list of potential biological targets for the molecules under investigation. The first tool used in this study was PASSOnline, which can be accessed at (<http://www.way2drug.com/PASSOnline/predict.php>). The SMILES format of 6-gingerol was submitted to the PASSOnline server, and the results were subsequently evaluated. This tool provides estimates with an average accuracy of 95% for approximately 4,000 different types of biological activity. Compound

activity prediction is based on structure-activity relationship analysis of a training set of over 300,000 compounds (Filimonov et al., 2014). The PASSOnline output provides a list of expected activity types, along with estimated probabilities expressed as probable activity (Pa) and probable inactivity (Pi). Pa and Pi values range from 0 to 1. When with Pa > Pi were considered potential for a given compound. When Pa is greater than 0.7, there is a greater likelihood that the compound has novel pharmacological activity while being structurally similar to an existing drug. Pa values between 0.5 and 0.7 indicated a lower probability of experimental pharmacological activity. When Pa is less than 0.5, the likelihood of finding the compound's activity experimentally is low, suggesting its potential as a parent compound to study biological activity (Filimonov et al., 2014).

The second server used in this study was Swiss Target Prediction (<http://www.swisstargetprediction.ch/>). This server, which has been operational since 2014, employs ligand-based target prediction to identify the most likely protein targets for a given bioactive small molecule. Predictions were performed by assessing the 2D and 3D similarity between the input query and compounds with known *in vitro* activity data in the ChEMBL library (ChEMBL 23 is the version used). The 2D similarity measure used the Tanimoto index on FP2 (2D) with a threshold of 0.65. For 3D similarity, multiple conformations of the molecule were generated, and Manhattan distances were calculated for each conformation. Target scores were calculated using logistic regression with the 2D and 3D similarity scores of the most similar ligands. The server provided a list of up to 100 potential protein targets for the 6-gingerol compound, with target scores ranging from 0 to 1. The same approach was applied to its structurally similar compounds (Daina et al., 2019).

The third method used in this screening was the MolTarPred web server (<http://moltarpred.marseille.inserm.fr/>). It was used to predict protein

targets utilizing ChEMBL22 data. When 6-gingerol was submitted, the server determined the Tanimoto similarity between the Morgan fingerprint of the query molecule and each of the 607,659 ChEMBL compounds that will be tested. The predicted targets were obtained from the top 10 most similar molecules to the query. To claim that a drug candidate is among the 607,659 ChEMBL and has single-protein targets annotated with activity equal to or less than 10 micromolar, the confidence score needed to be between 7.8 and 9. However, if the query contained more than one protein target with activity less than 7.8 micromolar, further prospective validation of these targets was required (Peón et al., 2017).

The Similarity Ensemble Approach (SEA) server was the fourth tool used to select the putative biological target for the query (<https://sea.bkslab.org/>). This server employs a 2D ligand-based similarity ensemble approach to predict the biological targets of a compound based on its resemblance to ligands found in a reference database, such as ChEMBL. The comparison of the input ligands (6-gingerol and related compounds) was performed against all ligands within the target sets, using the Tanimoto similarity of ECFP4 fingerprints. The Tanimoto similarities were summed, and z-scores were calculated for each ligand. This tool has been successfully applied to identify new targets for old drugs and natural products, and to predict side effects and potential anatomical therapeutic indications (ATCs) of approved drugs (Keiser et al., 2006; Wang et al., 2016; Irwin et al., 2018). In this study, the query (6-gingerol) and its similar molecules were screened using these *in silico* approaches, with the corresponding SMILES serving as the query input. The resulting list of predicted targets was downloaded and further analyzed manually, with a particular focus on kinase targets.

Molecular Docking

To prepare the compounds for molecular docking, ionization and protonation were performed based on physiological pH. The compounds were subjected to

conformational search in the Molecular Operating Environment (MOE) v2019.01 (MOE Release V2019.01; ULC) software from Chemical Computing Group ULC, Montreal, QC, Canada was employed for conformational search using the Stochastic Conformational Search module. The global minimum energy of each molecule was minimized using the MMFF94x force field. The structure of the proteins [V-Raf Murine Sarcoma Viral Oncogene Homolog B1 (BRAF) active and inactive conformation PDB ID: 3OG7, 6N0Q, Janus Tyrosine Kinase 1 (JAK1) active conformation PDB ID: 3EYG, Janus Tyrosine Kinase 2 (JAK2) active and inactive conformation PDB ID: 2B7A, 3UGC, Extracellular Signal-Regulated Kinase 1 (ERK1) PDB ID: 2ZOQ, human p38 mitogen-activated protein kinase p38 γ (MAPK) active and inactive conformation PDB ID:1CM8, PDB ID:6UNA] were downloaded from Protein Data Bank (<https://www.rcsb.org/>) (Berman et al., 2000). Unnecessary chains, ions, water molecules, and solvents were removed, and hydrogen atoms and partial charges were added to the protein structures. Missing loops and side chains were also fixed. Each conformation of the compounds was docked into the structures using MOE with London dG rescoring and triangle matcher placement settings (MOE Release V2019.01; ULC).

The Pharmacokinetic Properties and Drug-likeness

The *in silico* evaluation of pharmacokinetic properties and drug-likeness, including absorption, distribution, metabolism, and excretion (ADME) properties, was conducted for 6-gingerol and similar molecules. The SwissADME web server was used to assess these properties (<http://www.swissadme.ch/>) (Daina et al., 2017). Additionally, the excretion properties of the compounds were predicted by using the pkCSM web server (<https://biosig.lab.uq.edu.au/pkcsm/prediction>) (Pires et al., 2015). The user-friendly web interface allows the input of structures in SMILES format and after submission, the results

were presented in an output table. Drug-likeness is a crucial concept in the screening of drug candidates in the early stages of drug discovery, with a focus on achieving oral bioavailability. Lipinski's Rule of Five (Ro5) is a widely used criterion for evaluating the drug-like properties of molecules. According to this rule, a molecule may exhibit poor absorption or permeation if it violates more than two of the following criteria, it: molecular weight (MW) < 500, number of hydrogen bond donors (HBD) < 5 (counting the sum of all NH and OH groups), octanol/water partition coefficient $\log P < 5$, number of hydrogen bond acceptors (HBA) < 10 (counting all N and O atoms) (Bickerton et al., 2012; Leeson et al., 2015; Daina et al., 2017). In addition, there were two other descriptors were identified by Veber *et al.* (Veber et al., 2002): Number of Rotatable Bonds (NRB) <10 and Polar Surface Area (PSA) <140 Å². Furthermore, the ability of the investigated compounds to cross the blood-brain barrier (BBB) was also evaluated as a distribution parameter (Daina et al., 2017).

Cytochrome P450 (CYP450) enzymes, particularly the major isoforms CYP1A2, 2C9, 2C19, 2D6, and 3A4, play a significant role in the metabolic biotransformation and elimination of drugs. Inhibition of these isoenzymes can lead to toxic or adverse effects due to drug-drug interactions (Daina et al., 2017). Drug clearance is measured by the proportionality constant (CL_{tot}) and expressed as a log(mL/min/kg). It is related to bioavailability and is important in determining dosing rates to achieve steady-state concentrations. The Organic Cation Transporter 2 (OCT2) was also determined to determine whether the compounds were substrates for it or not. It plays an essential role in the clearance of drugs and endogenous substances, and was evaluated by using the pkCSM server (Pires et al., 2015).

Toxicity Assessment

Toxicity prediction is a critical aspect of the drug development process, as many drugs fail to reach the market due to ineffectiveness or adverse effects.

Computational approaches have been widely used to assess the potential cytotoxicity and adverse effects of chemical structures on both normal and tumor cells, as well as general organ toxicity. These approaches help to identify structures that can improve efficacy and therapeutic success (Capuzzi et al., 2016). In this study, the drug cytotoxicity on tumor and non-tumor cells was computationally screened using PASS CLC Pred (<http://www.way2drug.com/cell-line/index.php>) (Lagunin et al., 2018). Adverse effects commonly associated with anticancer drugs, such as hepatotoxicity and cardiotoxicity, were evaluated. Hepatotoxicity and hERG I-II inhibitory activities of the compounds were predicted by using pkCSM (<https://biosig.lab.uq.edu.au/pkcsm/prediction>) (Pires et al., 2015). Hepatotoxicity prediction was also performed using the ProTox-II program (https://tox-new.charite.de/protox_II/index.php?site=compound_input) (Banerjee et al., 2018).

Furthermore, the investigated compounds were evaluated for mutagenicity, carcinogenicity, cytotoxicity, and immunotoxicity. The ProTox-II program was used to predict their effects on stress response pathways, specifically mitochondrial membrane potential (MMP) and phosphoprotein tumor suppressor (p53) (Banerjee et al., 2018). The SMILES structures of the compounds were used to predict the aforementioned toxicity endpoints.

RESULTS AND DISCUSSION

Similarity Search

A similarity search was performed using the Chemmine server to identify chemical structures similar to the query compound, 6-gingerol. The similarity cut-off value was set at 0.80, resulting in 49 compounds, including 6-gingerol (Table S1). All of these similar compounds are originated from natural sources and exhibit diverse biological activities. Here are some examples of the activity of the investigated compounds.

Calycosin (N-G-12) is a bioactive phytoestrogenic isoflavone that is isolated from *Trifolium pratense*

(red clover), which is able to suppress carcinogenesis and progression by modulating estrogen receptor (ER) β expression. Furthermore, the antiproliferative effects of calycosin were found to be mediated through ER β -dependent regulation of the The phosphatidylinositol 3-kinase (PI3K)/protein kinase B (Akt) pathways in human osteosarcoma cell line (MG-63) (Tian et al., 2020). While Curcumin (N-G-5), Demethoxycurcumin (N-G-24), and Tetrahydrocurcumin (N-G-41) are bioactive non-flavonoid polyphenolic compounds extracted from the rhizome of the plant *Curcuma longa* and found in the spice turmeric. Many studies have been conducted to assess the effects of curcumin metabolites, analogs, or derivatives. Curcumin or its metabolite tetrahydrocurcumin has been shown to promote cell death in chemotherapy-resistant (Ara-C) human AML cells (HL-60) using two different methods. Indeed, curcumin mainly induced apoptotic cell death mainly via the regulation of poly(ADP-ribose) polymerase (PARP), caspase-9, and caspase-3, whereas tetrahydrocurcumin primarily promoted autophagy mainly via the regulation of LC3 and p62. Tetrahydrocurcumin has also been used in human NSCLC A549 cells. The therapy suppressed cell growth and induced autophagic flux by suppressing the PI3K/Akt/mammalian target of rapamycin (mTOR) pathway and increasing Beclin 1 gene expression (Benvenuto et al., 2020). Additionally, pratensein (N-G-39) is a member of the flavonoid family that is found in many plants such as *Trifolium pratense*. The anticancer activity of pratensein was recently demonstrated in breast cancer cells. The result of the study showed that pratensein can induce caspase-3 and Bcl-2-associated X protein (Bax) and increase the expression level of p53. It also inhibits B-cell lymphoma 2 (Bcl-2) activation in a time-dependent manner (Behbahani et al., 2020). In addition, vanillyl alcohol (N-G-18) is one of the phenolic compounds that can be found in a variety of plants that can be produced enzymatically from the reduction of vanillin. A previous study has shown the anti-angiogenic activity of vanillyl alcohol by using the chick chorioallantoic membrane (CAM)

assay. The results showed that vanillyl alcohol has a significant anti-angiogenic effect due to the decrease in membrane transport, possibly due to its methoxy group at the 3-position (Jung et al., 2008). Eugenol (N-G-3) is the active component of the essential oil isolated from clove (*Syzygium aromaticum*) and has antimutagenic, antigenotoxic, and anti-inflammatory properties. It also has cytotoxic activity and can induce cell death in various cancer cells (Carvalho et al., 2015). Methyleugenol (N-G-6), on the other hand, is a substituted allylbenzene that can be found in many foods and essential oils. It has been shown to induce cytotoxicity in rat and mouse hepatocytes and leukemia. Methyleugenol has also been reported to enhance the inhibition of cancer cell growth and induce apoptosis when it was combined with cisplatin (Carvalho et al., 2015; Yi et al., 2015).

Licochalcone B (Lico B) (N-G-38), which shares a similar structure to 6-gingerol, is a recently synthesized molecule belonging to the chalcone group extracted from licorice root, also known as *Glycyrrhiza* root. Chalcone groups serve as precursors to flavonoids. Numerous *in vitro* and *in vivo* studies have demonstrated the therapeutic effects of Lico B, particularly its anti-inflammatory, anticancer, antioxidant, and hepatoprotective properties. In a 2016 *in vitro* study, Lico B was found to significantly inhibit cell proliferation in oral squamous cell carcinoma (OSCC) cells, depending on the duration and concentration of treatment. Treatment with Lico B up-regulated pro-apoptotic proteins such as Bax and down-regulated anti-apoptotic proteins such as BH3 domain-only death agonist protein and B-cell lymphoma-extra large, while promoting myeloid leukemia cell differentiation protein Mcl-1 (Bax). Lico B induced apoptosis through the release of cytochrome C and loss of mitochondrial membrane potential. In addition, these studies provided evidence for the activation of multiple caspases and the cleavage of the PARP protein following Lico B therapy. Based on these findings, Lico B is considered a promising natural drug for the treatment of human oral cancer

through its induction of apoptosis (Maria Pia et al., 2019).

The Putative Anticancer Target of the Molecules

To identify the most promising target for 6-gingerol and its related compounds, a comprehensive screening process was conducted. First, the anticancer activities of 6-gingerol were evaluated using four different web servers. Subsequently, the potential targets of small molecules sharing a 6-gingerol scaffold were identified by screening the compounds through various web servers, namely PASS Online, Swiss Target Prediction, MolTarPred, and SEA. Each server employs different algorithms to predict potential targets. The results from each server are presented in Tables S3, S4, S5, and S6. Based on the methods used and the results of these computational analyses, the most notable anticancer activities were identified. The corresponding results are presented in Table S2. Given the data collected, our focus for the subsequent docking studies was primarily centered around tyrosine kinases, including B-RAF, JAK1/2, ERK1 (MAPK3), and p38 γ . These kinases have been strongly implicated in a variety of diseases, particularly cancer, which is the main focus of our study.

Evaluation of Docking on the Selected Targets with the Studied Molecules

To identify the most promising targets for 6-gingerol and related compounds, a comprehensive screening process was conducted. The anticancer activities of 6-gingerol were first evaluated using various web servers, and the potential targets of similar compounds were identified through screening using various algorithms. The focus was primarily on tyrosine kinases, including B-RAF, JAK1/2, ERK1, and p38 γ , which are strongly associated with cancer.

The majority of approved protein kinase inhibitors work by interacting with the ATP-binding pocket and acting as competitive enzyme antagonists. In particular, the interaction with the hinge region is critical for ATP binding and substrate

phosphorylation. Successful kinase inhibitors have been developed based on this strategy (Roskoski, 2016; Wang et al., 2021). Most BRAF inhibitors also interact with the ATP-binding and hinge regions, known as type I inhibition (Roskoski, 2016; Wang et al., 2017; Umar et al., 2020). Docking studies on the BRAF protein with the X-ray data of 3OG7 showed that the co-crystallized ligand (PLX4032) formed two hydrogen bonds with Cys532 and Gln530, in the hinge region. Vanlyglycol (N-G-42) and N-G-1 were identified as potential type I inhibitors of BRAF kinase by forming two hydrogen bonds with the specific hinge region residues with docking scores: -5.341 and -7.585, respectively (Figure 2).

Selective BRAF inhibitors that target the RAF-MEK-ERK pathway without inducing paradoxical activation are desired. Interaction with the DFG loop enhances inhibitor potency, known as type II inhibition (Ramurthy et al., 2020). Docking studies on inactive BRAF revealed that the conformation of the co-crystallized ligand [N-(4-methyl-3-(1-methyl-2-oxo-2,3-dihydro-1H-benzo[d]imidazol-5-yl)phenyl)-3-(trifluoromethyl)benzamide] formed hydrogen bonds with specific residues Phe595, Asp594, and α C-Glu501. L-(+)-vanilmandelic acid (N-G-44) showed potential as a selective type II inhibitor of BRAF with a docking score of - 5.5003 (Figure 2).

In general, most of the studied compounds studied with the active conformation of the BRAF protein by forming hydrogen bonds with hinge residues. The side chain hydroxyl group of certain compounds (N-G-12, 17, 26, 31, 38, 39, 40, 42, and 47) played an important role in interacting with the BRAF receptor (Figure S1).

Overall, the screening and docking studies identified potential targets and modes of inhibition for 6-gingerol and its related compounds, with a particular on kinase proteins.

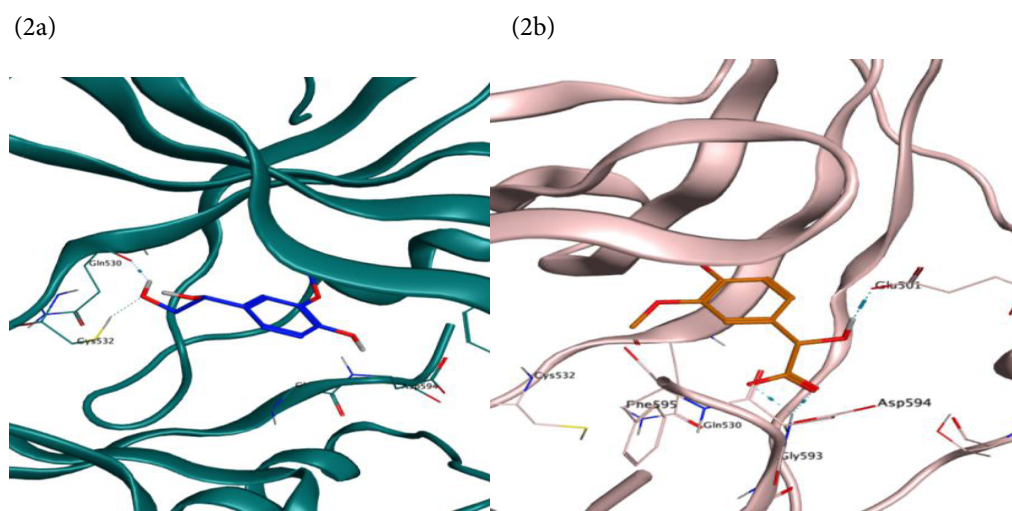


Figure 2. (a) Structure of BRAF^{V600E}; PDB ID: 3OG7 complex with: vanlyglycol (N-G-42) and (b) Structure of BRAF; PDB ID: 6N0Q complex with: L- (+)-vanilmandelic acid (N-G-44)

JAK proteins are non-receptor tyrosine kinases that play critical roles in cytokine and growth factor signaling pathways. Dysregulation of the JAK-STAT signaling cascade may contribute to various immunological disorders and malignancies (Alicea-Velázquez et al., 2011; Sanachai et al., 2020). JAK1, JAK2, and JAK3 are frequently found in cancer cells, with JAK1 and JAK2 being particularly abundant, making them promising targets for anticancer agents (Lucet et al., 2006; Hornakova et al., 2011; Andraos et al., 2012; Sanachai et al., 2020). Most JAK inhibitors act as type I inhibitors, enhancing phosphorylation in the JAK activation loop while inhibiting kinase activity and phosphorylation of STAT proteins (Andraos et al., 2012).

Binding to JAK1 in its active state involves interactions with Glu957 and Leu959 residues in the hinge region (Williams et al., 2009; Lin et al., 2018). Docking studies on JAK1 demonstrated that the co-crystallized ligand (CP-690-550) formed hydrogen bonds with Glu957 and Leu959. When 6-gingerol and its similar molecules were docked into the active conformation of JAK1, paradol (N-G-30) formed a

hydrogen bond with the carbonyl backbone of Leu959, indicating its potential as an inhibitor of JAK1 with a docking score of - 6.9492 (Figure 3).

Similarly, to achieve good binding to JAK2 in its active state, the inhibitor should interact with Glu930 and Leu932 residues in the hinge region. Docking studies on JAK2 revealed that the co-crystallized ligand (CMP6) formed hydrogen bonds with Glu930 and Leu932 (Lucet et al., 2006). In the case of dihydroconiferyl aldehyde (N-G-43), docking simulations showed that it formed two hydrogen bonds with the carbonyl backbone and the nitrogen backbone of Leu932, indicating its potential as a JAK2 inhibitor with a docking score of -5.478 (Figure 3).

Based on these findings, paradol (N-G-30) showed potential as a JAK1 inhibitor, while dihydroconiferyl aldehyde (N-G-43) showed potential as a JAK2 inhibitor. These results suggest that 6-gingerol and its related compounds have the potential to inhibit JAK proteins and may serve as promising agents in the development of anticancer treatments targeting the JAK-STAT signaling pathway.

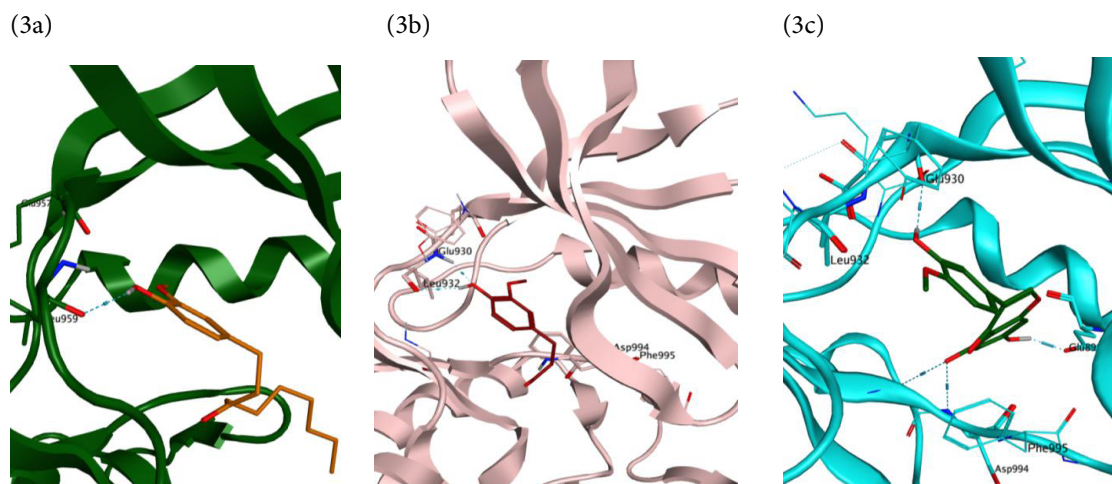


Figure 3. (a) Structure of JAK1: PDB ID-3EYG complex with paradol (N-G-30), (b) structure of JAK2: PDB ID-2B7A complex with dihydroconiferyl aldehyde (N-G-43), and (c) structure of JAK2: PDB ID: 3UGC complex with pratensein (N-G-39)

The development of a selective JAK2 inhibitor has been challenging due to the conserved ATP site of the JAK family. However, efforts are underway to discover selective JAK2 inhibitors to minimize undesired side effects (Lin et al., 2018). Inhibition of JAK2 activity can lead to several alterations in myeloid cell function. Binding to the inactive conformation of the JAK protein, known as DFG-out, reduces phosphorylation in the activation loop. Critical residues, including Leu932, α -C-Glu898, and Asp994, play a pivotal role in achieving selectivity towards JAK2. Docking studies on JAK2 using X-ray data revealed that the co-crystallized ligand (NVP-BBT494) formed hydrogen bonds with Leu932, Asp994, and α -C-Glu898 (Andraos et al., 2012; Lin et al., 2018). Pratensein (N-G-39) formed hydrogen bonds with Glu898, Glu930, and Asp994, indicating its potential as a selective JAK2 inhibitor with a docking score of -6.5816 (Figure 3).

For both JAK1 and JAK2, most of the compounds interacted with the active conformation of the proteins. The phenol group of the compounds formed hydrogen bonds with hinge region residues, predominantly Leu959 for JAK1 and Glu930 and Leu932 for JAK2.

The phenolic hydroxyls of the compounds played an important role in the interaction with the receptors (Figure S2 and S3).

Mitogen-activated protein kinases (MAP kinases), such as ERK1 and ERK2, regulate cell proliferation, differentiation, and various physiological responses. Dysregulation of ERK signaling has been implicated in several cancers (Halder et al., 2019; Pegram et al., 2019). Most inhibitors targeting ERK1/2 exhibit a type I binding mode. Co-crystal structures of ERK1/2 5-iodotubericidin (5ID) have revealed a type I binding mode with hydrogen bonds formed with hinge residues (Met125 and Asp123) and Lys131 (Chaikwad et al., 2014). Docking studies on ERK1 showed that isoferulic acid (N-G-47) formed hydrogen bonds with Met125 and Lys131, indicating its potential as an ERK1 inhibitor with a docking score of -5.413 (Figure 4). The phenol group of 6-gingerol also formed a hydrogen bond with Met125. Several other compounds exhibited hydrogen bonding interactions with Met125 and Lys131 through their phenol and carbonyl groups or phenolic hydroxyl group and carboxylate group (Figure S4).

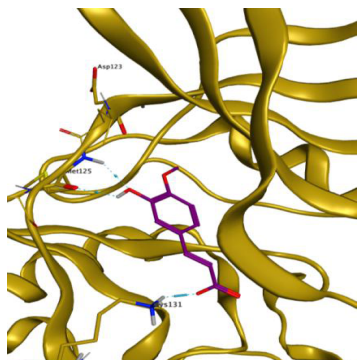


Figure 4. Structure of ERK1: PDB ID: 2ZOQ complex with isoferulic acid (N-G-47)

The p38 mitogen-activated protein kinase (MAPK) family consists of four isoforms: p38 α , p38 β , p38 γ , and p38 δ . These isoforms are activated by dual phosphorylation of tyrosine and threonine residues in a Thr-X-Tyr motif. The p38 MAPK pathway is involved in the regulation of the inflammatory response and may contribute to tumorigenesis. Elevated levels of p38 γ have been observed in cutaneous T-cell lymphoma (CTCL) and various malignancies, making it a potential therapeutic target (Sahu et al., 2019; Zhang et al., 2021).

Docking studies were performed on both

the active and inactive conformations of p38 γ to understand how the compounds under study interact with the protein. X-ray data from 1CM8, using the non-hydrolyzable ATP-like inhibitor AMP-PNP, revealed two hydrogen bonds with the hinge residues (Met112 and Pro110) (Bellon et al., 1999). However, the compounds in this study did not interact with the hinge region. Instead, they showed interactions with residues located outside of the ATP pocket (Figure 5).

No co-crystallized ligands were available for the inactive conformation of p38, represented by the X-ray data of 6UNA. The binding pocket was identified based on the active conformation of p38, particularly involving α C-Glu74 and Asp171 of the DFG region (Bellon et al., 1999; Aoto et al., 2019). Docking studies on 6UNA showed that most of the compounds interacted with the hinge region or with Asp171 of the DFG region. For example, Curcumin PE (N-G-40) formed hydrogen bonds with the backbone of Met112, Phe111, Asp115, and α C-Glu74, indicating its potential as an inhibitor with a docking score of -5.979 (Figure 5). More information about the docking scores of the 6-gingerol-like series and the co-crystallized ligands is presented in (Table S7).

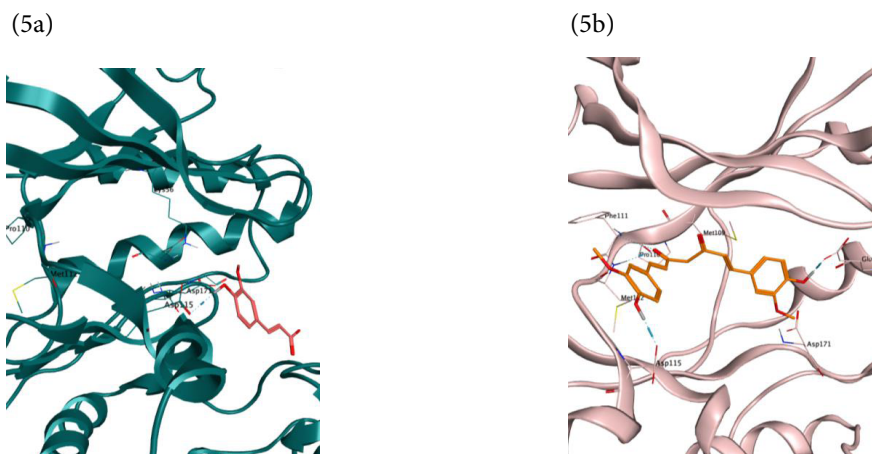


Figure 5. (a) Structure of p38 γ : PDB ID: 1CM8 complex with Ferulic acid (N-G-2) and (b) structure of p38 γ : PDB ID: 6UNA complex with curcumin PE (N-G-40)

Prediction of Drug-likeness and Pharmacokinetics Properties of the Molecules

To assess the drug-likeness and pharmacokinetic properties of the molecules, an analysis was conducted to ensure their potential as drugs. For this purpose, the SwissADME online tool, designed for easy submission and analysis of the results, was used to predict the drug-likeness and ADME properties. The results of drug-likeness and ADME properties are presented in Tables S8, S9, and S10, respectively. The evaluation showed that 6-gingerol and the similar molecules investigated in this study met Lipinski's and Veber's rules of five. This suggests that these molecules possess favorable oral bioavailability based on their physicochemical properties. These parameters are associated with desirable aqueous solubility and intestinal permeability, which are crucial initial factors in determining oral bioavailability. Furthermore, the bioavailability score (BA) was assessed, revealing that most of the molecules studied obtained a value of 0.55. This score indicates compliance with the Rule of Five and predicts a 55% bioavailability in rats, indicating a higher probability compared to the 10% threshold (Martin, 2005; Daina et al., 2017). Notably, N-G (2, 22, 46, 47, and 48) showed a BA value of 0.85. The synthetic accessibility was also evaluated using a scale ranging from 1 (easy to synthesize) to 10 (very difficult and complex to synthesize) (Daina et al., 2017). The synthetic accessibility of all the studied molecules falls within the range of 1-4, indicating that they are relatively easy to synthesize (Table S8).

The ADME properties of 6-gingerol and similar compounds are summarized in Tables S8 and S9. These compounds exhibit high gastrointestinal (GI) absorption, consistent with the Rule of Five (Ro5). P-glycoprotein (P-gp), a transmembrane efflux pump involved in drug transport, regulates the uptake and efflux of various drugs and toxins (Finch et al., 2014; Leeson et al., 2015). Our results showed that the molecules N-G-(16, 27, and 31) are the only substrates for P-gp among the molecules

studied, while the others are not substrates for P-gp. Furthermore, the blood-brain barrier (BBB) controls cerebral homeostasis and provides the central nervous system (CNS) with a unique protection against the toxicity of many xenobiotics and pathogens (Weiss et al., 2009). Analysis of the molecules in this study indicates that the N-G (5, 9, 12, 14, 17, 22, 24, 28, 31, 38- 42, 44, and 46) lack the ability to cross the BBB, while the remaining compounds studied possess BBB permeability.

The results presented in Tables S8 and S9 are consistent with the BOILED-Egg (Brain Or Intestinal EstimateD permeation predictive model) shown in Figure 6. The BOILED-Egg model predicts the behavior of small molecules based on their polarity and lipophilicity, using an egg visualization. Molecules located in the yolk of the egg are expected to pass through the BBB, while those in the white are expected to be absorbed by the human gastrointestinal tract (HIA) (Daina et al., 2016). Blue-white circles indicate molecules predicted to be effluxed from the CNS by P-glycoprotein (PGP+), while red-white circles represent molecules not expected to be effluxed by P-glycoprotein (PGP-). As depicted in Figure 6, most of the compounds, except those mentioned above, are located within the yolk of the egg, suggesting their permeability across the BBB. However, 6-gingerol and its similar compounds are predicted to be absorbed from the gastrointestinal tract.

Furthermore, our results indicate that most of the compounds do not inhibit CYP2C19, except for N-G-15, which exhibits inhibitory effects on CYP2C19. Among the compounds studied, N-G-(5, 12, 17, 24, 27, 32, 38- 41) specifically affects CYP3A4, while the remaining molecules do not inhibit this isoform. Only N-G-(1, 12, 15, 16, 17, 27, 30, 31, 32, 39, and 41) exhibit inhibition against CYP2D6, while the other compounds do not affect this isoform. Regarding CYP2C9, compounds N-G-(5, 24, 32, 38- 40) show inhibitory activity, while the remaining compounds do not impact this isoform. Moreover, the compounds

N-G-(1, 3, 6, 7, 11- 13, 15, 19, 23, 24, 29, 30, 33, 37-39, and 45) inhibit the CYP1A2 isoform, while the other compounds do not exhibit any effect on this isoform. Overall, the compounds N-G-(5, 12, 17, 24, 27, 32, 38- 40, and 41) show inhibitory activity against multiple CYP isoforms.

Regarding excretion, clearance was determined by calculating the sum of hepatic and renal clearance, which represents the rate at which a drug is eliminated from the body. A low total clearance value indicates a longer persistence of the drug in the body. In our study, most of the compounds exhibited low clearance rates. However, the compounds N-G-(1, 2, 4, 8- 10, 15, 16, 20, 30, 34, 35, 38, 46, 47, and 49) exhibited high clearance values (Table S10). The organic cation transporter 2 (OCT2), which is responsible for renal uptake, plays a critical role in the clearance of drugs and endogenous substances. When substances are OCT2 substrates, there is a possibility of adverse reactions when co-administered with OCT2 inhibitors (Pires et al., 2015). It is noteworthy that none of the compounds studied in this research were identified as OCT2 substrates. Therefore, it is unlikely that these compounds would interact or cause adverse effects when used with OCT2 inhibitors.

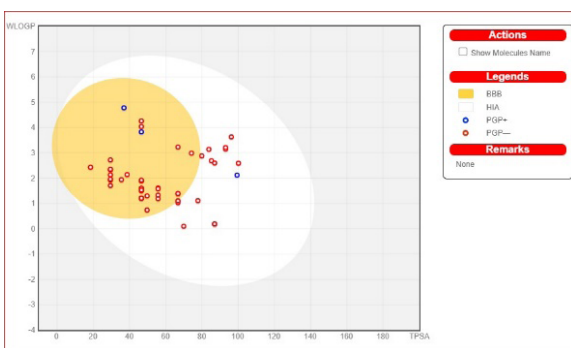


Figure 6. BOILED-Egg representation of the studied molecules

Prediction of the Toxicity Profiles of the Molecules

The toxicity profiles of the compounds were predicted using various computational tools, and the results are summarized in (Table S11, S12, and S13).

Cytotoxicity predictions (Way2Drug) on tumor and non-tumor cell lines revealed that 21 compounds showed activity against various tumor cell lines from 8 different tissues. Among them, coniferaldehyde exhibited the highest predicted activity against 6 cell lines. Vanylglycol demonstrated the highest predicted activity (0.747) against PC-3 cells. However, the majority of the compounds did not exhibit significant effects on non-tumor cells when their probability was above 0.50, and only 6 compounds showed negative effects on non-tumor cells. This lack of activity was consistent with the predictions from ProTox-II (Table S12), which indicated that most of the compounds were expected to be safe with low probabilities of toxicity.

Hepatotoxicity predictions made by ProTox-II suggested that most of the compounds were unlikely to cause liver toxicity (Table S12). The compounds predicted to have positive effects had low probabilities, ranging from 50% to 52%. Furthermore, the toxicity effects of hepatotoxicity, hERG I inhibitor, and hERG II inhibitor were assessed using pkCSM (Table S13). Most of the compounds showed no significant effects on hepatotoxicity, hERG I inhibitor, and hERG II inhibitor.

Regarding the predictions of mutagenicity, carcinogenicity, cytotoxicity, and immunotoxicity by ProTox-II, not all compounds were expected to show mutagenic or cytotoxic effects. Only two compounds had low probabilities of a positive mutagenicity result, ranging from 53% to 67%. Immunotoxicity predictions revealed that 17 compounds, including the query compound, had a high probability of affecting the immune system (79% to 98%). For carcinogenicity, methyleugenol exhibited the highest potential to induce tumors, with a probability of 76%. Most of the compounds showed no toxicity to MMP and p53. However, seven compounds were predicted to have positive effects on MMP with probabilities ranging from 78% to 100%, and two compounds were predicted to have positive effects on p53 with

probabilities from 80% to 100%. Notably, curcumin showed a toxic effect on MMP and p53 with a high probability of 100%.

CONCLUSION

In this study, we used virtual screening to identify potential leads and molecular targets for natural chemical compounds, with a particular focus on 6-gingerol and its similar compounds. Through target prediction servers, we discovered anticancer targets, with a particular focus on kinase proteins due to their role in cellular signaling pathways (Roskoski, 2016; Wang et al., 2021).

Our findings showed that the compounds interacted with various kinases, including B-RAF, JAK1/2, ERK1, and p38 γ . These interactions were determined by through molecular docking studies using MOE. The majority of the compounds acted as type I inhibitors, forming hydrogen bonds with specific residues in the hinge region of the active conformation of the target proteins.

The drug-like characteristics and ADMET properties of the compounds were also evaluated. They complied with Lipinski's and Veber's rule of five, indicating good oral bioavailability and absorption. However, some compounds inhibited multiple CYP isoforms, while most showed low clearance. None of the studied molecules were substrates for OTC2.

Toxicity assessments were conducted using computational approaches. Most compounds did not show cytotoxicity to normal cells, but several demonstrated toxicity to cancer cells. Coniferaldehyde, Vanlyglycol, and L-(+)-vanilmandelic acid exhibited the highest potency on various cell lines. Each compound showed potent inhibitory activity against specific kinases. With respect to organ toxicity, the compounds did not show hepatotoxicity or hERG inhibitory effects on the liver and heart. None of the compounds exhibited mutagenicity or carcinogenicity, except for two with a low probability

of positive mutagenicity. A few compounds had a high probability of affecting the immune system. Additionally, the majority of compounds were predicted to be inactive with respect to the MMP and p53 stress response pathways, indicating safe use for non-cancerous cells.

In conclusion, our computational approach identified the potential anticancer targets for 6-gingerol and its similar molecules including vanlyglycol, vanillylmandelic acid, L-(+)-vanilmandelic acid, dehydrozingerone, 2-methoxyestrone, methylvanillate, dihydroconiferyl aldehyde, pratensein, acetovanillone, acetosyringone, licochalcone B, isoferulic acid, curcumin PE, and coniferaldehyde that could inhibit (B-RAF, JAK1/2, and ERK1 (MAPK3)) proteins primarily in their active state while they could modulate p38 γ primarily in its inactive state. In addition, our computational analysis showed that the majority of the compounds have good drug-likeness and ADMET profiles without toxicity. In the future, *in vitro* enzymatic assays are planned to validate the computational results and optimize the lead compounds.

CONFLICT OF INTEREST

The authors declare that there is no conflict of interest.

AUTHOR CONTRIBUTIONS STATEMENT

Author contribution: . Enise Ece Gurdal and Gulcin Tugcu contributed equally. Enise Ece Gurdal and Gulcin Tugcu designed the experiments. Nour Osama Al-Massri, Enise Ece Gurdal and Gulcin Tugcu performed computational studies. All authors contributed to the data analyses and writing of the manuscript. All authors read and approved the final version of the manuscript.

REFERENCES

Alicea-Velázquez, N.L., & Boggon, T.J. (2011). The Use of Structural Biology in Janus Kinase Targeted Drug Discovery. *Current Drug Targets*, 12(4), 546-555. doi: 10.2174/138945011794751528

- Andraos, R., Qian, Z., Bonenfant, D., Rubert, J., Vangrevelinghe, E., Scheufler, C., Marque, F., Régnier, C. H., De Pover, A., Ryckelynck, H., Bhagwat, N., Koppikar, P., Goel, A., Wyder, L., Tavares, G., Baffert, F., Pissot-Soldermann, C., Manley, P. W., Gaul, C., Voshol, H., & Radimerski, T. (2012). Modulation of Activation-Loop Phosphorylation by JAK Inhibitors Is Binding Mode Dependent. *Cancer Discovery*, 2(6), 512-523. doi: 10.1158/2159-8290.CD-11-0324
- Aoto, P.C., Stanfield, R.L., Wilson, I.A., Dyson, H.J., & Wright, P.E. (2019). A Dynamic Switch in Inactive p38 γ Leads to an Excited State on the Pathway to an Active Kinase. *Biochemistry*, 58 (51), 5160-5172. doi: 10.1021/acs.biochem.9b00932.
- Backman, T.W., Cao, Y., & Girke, T. (2011). ChemMine tools: an online service for analyzing and clustering small molecules. *Nucleic Acids Research*, 39 (Web Server issue), W486- W491. doi: 10.1093/nar/gkr320
- Banerjee, P., Eckert, A.O., Schrey, A.K., & Preissner, R. (2018). ProTox-II: a webserver for the prediction of toxicity of chemicals. *Nucleic Acids Research*, 46 (W1), W257- W263. doi: 10.1093/nar/gky318
- Behbahani, M., & Moghaddam, M. (2020). Study of Anticancer Activity of Pratensein and Pratensein Glycoside Isolated from *Cuscuta kotchiana*. *Journal of Molecular Biology Research*, 10(1), 73. doi: 10.5539/jmbr.v10n1p73
- Bellon, S., Fitzgibbon, M.J., Fox, T., Hsiao, H.M., & Wilson, K.P. (1999). The structure of phosphorylated P38 γ is monomeric and reveals a conserved activation-loop conformation, Structure. *Structure*, 7(9), 1057- 1065. doi: 10.1016/s0969 2126(99)80173-7.
- Benvenuto, M., Albonici, L., Focaccetti, C., Ciuffa, S., Fazi, S., Cifaldi, L., Miele, M.T., De Maio, F., Tresoldi, I., Manzari, V., Modesti, A., Masuelli, L., & Bei, R. (2020). Polyphenol-Mediated Autophagy in Cancer: Evidence of In Vitro and In Vivo Studies. *International Journal of Molecular Sciences*, 21(18), 6635. doi: 10.3390/ijms21186635
- Berman, H.M., Westbrook, J., Feng, Z., Gilliland, G., Bhat, T.N., Weissig, H., Shindyalov, I.N., & Bourne, P.E. (2000). The Protein Data Bank. *Nucleic Acids Research*, 28(1), 235-242. doi: 10.1093/nar/28.1.235
- Bickerton, G.R., Paolini, G.V., Besnard, J., Muresan, S., & Hopkins, A.L. (2012). Quantifying the chemical beauty of drugs. *Nature Chemistry*, 4(2), 90- 98. doi: 10.1038/nchem.1243
- Capuzzi, S., Politi, R., Isayev, O., Farag, S., & Tropsha, A. (2016). QSAR Modeling of Tox21 Challenge Stress Response and Nuclear Receptor Signaling Toxicity Assays. *Frontiers in Environmental Science*, 4(3). doi: 10.3389/fenvs.2016.00003
- Carvalho, A.A., Andrade, L.N., de Sousa, É.B., & de Sousa, D.P. (2015). Antitumor Phenylpropanoids Found in Essential Oils. *Biomed Research International*, 2015, 392674. doi: 10.1155/2015/392674.
- Cereto-Massagué, A., Ojeda, M.J., Valls, C., Mulero, M., Pujadas, G., & Garcia-Vallve, S. (2015). Tools for in silico target fishing. *Methods*, 71, 98- 103. doi: 10.1016/j.ymeth.2014.09.006
- Chaikuad, A., Tacconi, E.M.C., Zimmer, J., Liang, Y., Gray, N.S., Tarsounas, M., & Knapp, S. (2014). A unique inhibitor binding site in ERK1/2 is associated with slow binding kinetics. *Nature Chemical Biology*, 10, 853- 860. doi: 10.1038/nchembio.1629
- Daina, A., Michielin, O., & Zoete, V. (2017). SwissADME: a free web tool to evaluate pharmacokinetics, drug-likeness and medicinal chemistry friendliness of small molecules. *Scientific Reports*, 7, 42717. doi: 10.1038/srep42717
- Daina, A., Michielin, O., & Zoete, V. (2019). SwissTargetPrediction: updated data and new features for efficient prediction of protein targets of small molecules. *Nucleic Acids Research*, 47(W1), W357- W364. doi: 10.1093/nar/gkz382

- Daina, A., & Zoete, V. (2016). A BOILED-Egg To Predict Gastrointestinal Absorption and Brain Penetration of Small Molecules. *ChemMedChem*, 11(11), 1117- 1121. doi: 10.1002/cmdc.201600182
- Filimonov, D.A., Lagunin, A.A., Glorizova, T.A., Rudik, A.V., Druzhilovskii, D.S., Pogodin, P.V., & Poroikov, V.V. (2014). Prediction of the Biological Activity Spectra of Organic Compounds Using the Pass Online Web Resource. *Chemistry of Heterocyclic Compounds*, 50(3), 444- 457. doi: 10.1007/s10593-014-1496-1
- Finch, A., & Pillans, P. (2014). P-glycoprotein and its role in drug-drug interactions. *Australian Prescriber*, 37(4), 137- 139. doi: 10.18773/austprescr.2014.050
- Galati, S., Di Stefano, M., Martinelli, E., Poli, G., & Tuccinardi, T. (2021). Recent advances in in silico target fishing. *Molecules*, 26 (17), 5124. doi: 10.3390/molecules26175124
- Halder, A.K., Giri, A.K., & Cordeiro, M.N.D.S. (2019). Multi-Target Chemometric Modelling, Fragment Analysis and Virtual Screening with ERK Inhibitors as Potential Anticancer Agents. *Molecules*, 24, 3909. doi: 10.3390/molecules24213909
- Hornakova, T., Springuel, L., Devreux, J., Dusa, A., Constantinescu, S.N., Knoops, L., & Renaud, J.C. (2011). Oncogenic JAK1 and JAK2-activating mutations resistant to ATP-competitive inhibitors. *Haematologica*, 96(6), 845- 853. doi: 10.3324/haematol.2010.036350
- Irwin, J., Gaskins, G., Sterling, T., Mysinger, M., & Keiser, M. (2018). Predicted Biological Activity of Purchasable Chemical Space. *Journal of Chemical Information and Modeling*, 58, 148-164. doi: 10.1021/acs.jcim.7b00316
- Jung, H., Song, Y., Lim, C., & Park, E. (2008). Anti-angiogenic, anti-inflammatory and anti-nociceptive activities of vanillyl alcohol. *Archives of Pharmacal Research*, 31(10), 1275-1279. doi: 10.1007/s12272-001-2106-1
- Keiser, M.J., Roth, B. L., Armbruster, B. N., Ernsberger, P., Irwin, J.J., & Shoichet, B.K. (2007). Relating protein pharmacology by ligand Chemistry. *Nature Biotechnology*, 25(2), 197- 206. doi: 10.1038/nbt1284
- Lagunin, A.A., Dubovskaja, V.I., Rudik, A.V., Pogodin, P.V., Druzhilovskiy, D.S., Glorizova, T.A., Filimonov, D.A., Sastry, G.N., & Poroikov, V.V. (2018). CLC-Pred: a freely available web-service for in silico prediction of human cell line cytotoxicity for drug-like compounds. *PLOS One*, 13(1). doi: 10.1371/journal.pone.0191838
- Leeson, P.D., & Young, R.J. (2015). Molecular Property Design: Does Everyone Get It?. *ACS Medicinal Chemistry Letters*, 6(7), 722-725. doi: 10.1021/acsmmedchemlett.5b00157
- Lin, T.E., HuangFu, W.C., Chao, M.W., Sung, T.Y., Chang, C.D., Chen, Y.Y., Hsieh, J.H., Tu, H.J., Huang, H.L., Pan, S.L., & Hsu, K.C. (2018). A Novel Selective JAK2 Inhibitor Identified Using Pharmacological Interactions. *Frontiers in Pharmacology*, 9(1379). doi: 10.3389/fphar.2018.01379
- Lucet, I.S., Fantino, E., Styles, M., Bamert, R., Patel, O., Broughton, S.E., Walter, M., Burns, C.J., Treutlein, H., Wilks, A.F., & Rossjohn, J. (2006). The structural basis of Janus kinase 2 inhibition by a potent and specific pan-Janus kinase inhibitor. *Blood*, 107, 176- 183. doi: 10.1182/blood-2005-06-2413

- Mao, Q.Q., Xu, X.Y., Cao, S.Y., Gan, R.Y., Corke, H., Beta, T., & Li, H.B. (2019). Bioactive compounds and bioactivities of ginger (*zingiber officinale roscoe*). *Foods*, 8, 1-21. doi: 10.3390/foods8060185
- Maria Pia, G.D., Sara, F., Mario, F., & Lorenza, S. (2019). Biological Effects of Licochalcones. *Mini Reviews in Medicinal Chemistry*, 19(8), 647- 656. doi: 10.2174/1389557518666180601095420
- Martin, Y.C. (2005). A bioavailability score. *Journal of Medicinal Chemistry*, 48(9), 3164- 3170. doi: 10.1021/jm0492002
- Modi, V., & Dunbrack, R.L. (2019). Defining a new nomenclature for the structures of active and inactive kinases. *Proceedings of the National Academy of Sciences*, 116, 6818-6827. doi: 10.1073/pnas.1814279116
- MOE. Molecular Operating Environment, Release v2019.01; Chemical Computing Group ULC, 1010 Sherbooke St. West, Suite #910, Montreal, QC, Canada, H3A 2R7, 2021
- Pegram, L.M., Liddle, J.C., Xiao, Y., Hoh, M., Rudolph, J., Iverson, D.B., Vigers, G.P., Smith, D., Zhang, H., Wang, W., Moffat, J.G., & Ahn, N.G. (2019). Activation loop dynamics are controlled by conformation-selective inhibitors of ERK2. *Proceedings of the National Academy of Sciences*, 116, 15463- 15468. doi: 10.1073/pnas.1906824116
- Peón, A., Naulaerts, S., & Ballester, P. J. (2017). Predicting the Reliability of Drug-target Interaction Predictions with Maximum Coverage of Target Space. *Scientific Reports*, 7, 3820. doi: 10.1038/s41598-017-04264-w
- Pires, D.E., Blundell, T.L., & Ascher, D.B. (2015). pkCSM: predicting small-molecule pharmacokinetic and toxicity properties using graph-based signatures. *Journal of Medicinal Chemistry*, 58(9), 4066-4072. doi: 10.1021/acs.jmedchem.5b00104
- Ramurthy, S., Taft, B.R., Aversa, R.J., Barsanti, P.A., Burger, M.T., Lou, Y., Nishiguchi, G.A., Rico, A., Setti, L., Smith, A., Subramanian, S., Tamez, V., Tanner, H., Wan, L., Hu, C., Appleton, B.A., Mamo, M., Tandeske, L., Tellew, J.E., Huang, S., Yue, Q., Chaudhary, A., Tian, H., Iyer, R., Hassan, A.Q., Griner, L.A.M., La Bonte, L.R., Cooke, V.G., Abbema, A.V., Merritt, H., Gampa, K., Feng, F., Yuan, J., Mishina, Y., Wang, Y., Haling, J.R., Vaziri, S., Hekmat-Nejad, M., Polyakov, V., Zang, R., Sethuraman, V., Amiri, P., Singh, M., Sellers, W.R., Lees, E., Shao, W., Dillon, M.P., & Stuart, D.D. (2020). Design and Discovery of N-(3-(2-(2-Hydroxyethoxy)-6-morpholinopyridin-4-yl)-4-methylphenyl)-2(trifluoromethyl)isonicotinamide, a Selective, Efficacious, and Well-Tolerated RAF Inhibitor Targeting RAS Mutant Cancers: The Path to the Clinic. *Journal of Medicinal Chemistry*, 63, 2013- 2027. doi: 10.1021/acs.jmedchem.9b00161
- Rastogi, N., Duggal, S., Singh, S.K., Porwal, K., Srivastava, V.K., Maurya, R., Bhatt, M.L.B., & Mishra, D.P. (2015). Proteasome inhibition mediates p53 reactivation and anticancer activity of 6-Gingerol in cervical cancer cells. *Oncotarget*, 6, 43310-43325. doi: 10.18632/oncotarget.6383
- Rayan, A., Raiyn, J., & Falah, M. (2017). Nature is the best source of anticancer drugs: Indexing natural products for their anticancer bioactivity. *PLoS One*, 12, 1- 12. doi: 10.1371/journal.pone.0187925
- Roskoski, R. (2016). Classification of small molecule protein kinase inhibitors based upon the structures of their drug-enzyme complexes. *Pharmacology Research*, 103, 26- 48. doi: 10.1016/j.phrs.2015.10.021

- Sahu, V., Nigam, L., Agnihotri, V., Gupta, A., Shekhar, S., Subbarao, N., Bhaskar, S., & Dey, S. (2019). Diagnostic Significance of p38 Isoforms (p38 α , p38 β , p38 γ , p38 δ) in Head and Neck Squamous Cell Carcinoma: Comparative Serum Level Evaluation and Design of Novel Peptide Inhibitor Targeting the Same. *Cancer Research and Treatment*, 51(1), 313- 325. doi: 10.4143/crt.2018.105
- Sanachai, K., Mahalapbutr, P., Choowongkamon, K., Poo-arporn, R., Wolschann, P., & Rungrotmongkol, T. (2020). Insights into the Binding Recognition and Susceptibility of Tofacitinib toward Janus Kinases. *American Chemical Society Omega*, 5, 369-377. doi: 10.1021/acsomega.9b02800
- Schwarz, D., Merget, B., Deane, C., & Fulle, S. (2019). Modeling conformational flexibility of kinases in inactive states. *Proteins: Structure, Function and Bioinformatics*, 87, 943-951. doi: 10.1002/prot.25756
- Tian, W., Wang, Z.W., Yuan, B.M., & Bao, Y.G. (2020). Calycosin induces apoptosis in osteosarcoma cell line via ER β mediated PI3K/Akt signaling pathways. *Molecular Medicine Reports*, 21(6), 2349- 2356. doi: 10.3892/mmr.2020.11039
- Umar, A.B., Uzairu, A., Shallangwa, G.A., & Uba, S. (2020). Docking-based strategy to design novel flavone-based arylamides as potent V600E-BRAF inhibitors with prediction of their drug-likeness and ADMET properties. *Bulletin of the National Research Center*, 44, 179. doi: 10.1186/s42269-020-00432-7
- Veber, D.F., Johnson, S.R., Cheng, H.Y., Smith, B.R., Ward, K.W., & Kopple, K.D. (2002). Molecular properties that influence the oral bioavailability of drug candidates. *Journal of Medicinal Chemistry*, 45(12), 2615- 2623. doi: 10.1021/jm020017n
- Wang, B., Wu, H., Hu, C., Wang, H., Liu, J., Wang, W., & Liu, Q. (2021). An overview of kinase downregulators and recent advances in discovery approaches. *Signal Transduction and Targeted Therapy*, 6, 1-19. doi: 10.1038/s41392-021-00826-7
- Wang, G.M., Wang, X., Zhu, J.M., Guo, B.B., Yang, Z., Xu, Z.J., Li, B., Wang, H.Y., Meng, L.H., Zhu, W.L., & Ding, J. (2017). Docking-based structural splicing and reassembly strategy to develop novel deazapurine derivatives as potent B-Raf^{V600E} inhibitors. *Acta Pharmacologica Sinica*, 38(7), 1059- 1068. doi: 10.1038/aps.2016.173
- Wang, S., Zhang, C., Yang, G., & Yang, Y. (2014). Biological properties of 6-Gingerol: A brief review. *Natural Product Communications*, 9(7), 1027-1030. doi: 10.1177/1934578x1400900736
- Wang, Z., Liang, L., Yin, Z., & Lin, J. (2016). Improving chemical similarity ensemble approach in target Prediction. *Journal of Cheminformatics*, 8(1). doi: 10.1186/s13321-016-0130-x
- Weiss, N., Miller, F., Cazaubon, S., & Couraud, P.O. (2009). The blood brain barrier in brain homeostasis and neurological diseases. *Biochimica et biophysica acta*, 1788(4), 842- 857. doi: 10.1016/j.bbamem.2008.10.022
- Williams, N.K., Bamert, R.S., Patel, O., Wang, C., Walden, P.M., Wilks, A.F., Fantino, E., Rossjohn, J., & Lucet, I.S. (2009). Dissecting Specificity in the Janus Kinases: The Structures of JAK-Specific Inhibitors Complexed to the JAK1 and JAK2 Protein Tyrosine Kinase Domains. *Journal of Molecular Biology*, 387, 219- 232. doi: 10.1016/j.jmb.2009.01.041

- Yi, J. L., Shi, S., Shen, Y. L., Wang, L., Chen, H. Y., Zhu, J., & Ding, Y. (2015). Myricetin and methyl eugenol combination enhances the anticancer activity, cell cycle arrest and apoptosis induction of cis-platin against HeLa cervical cancer cell lines. *International Journal of Clinical and Experimental Pathology*, 8(2), 1116– 1127.
- Zhang, F., Zhang, J.G., Qu, J., Zhang, Q., Prasad, C., & Wei, Z.J. (2017). Assessment of anti-cancerous potential of 6-gingerol (Tongling White Ginger) and its synergy with drugs on human cervical adenocarcinoma cells. *Food and Chemical Toxicology*, 109, 910- 922. doi: 10.1016/j.fct.2017.02.038
- Zhang, X.H., Chen, C.H., Li, H., Hsiang, J., Wu, X., Hu, W., Horne, D., Nam, S., Shively, J., & Rosen, S.T. (2021). Targeting the non-ATP-binding pocket of the MAP kinase p38 γ mediates a novel mechanism of cytotoxicity in cutaneous T-cell lymphoma (CTCL). *FEBS Letters*, 595(20), 2570-2592. doi: 10.1002/1873-3468.1418

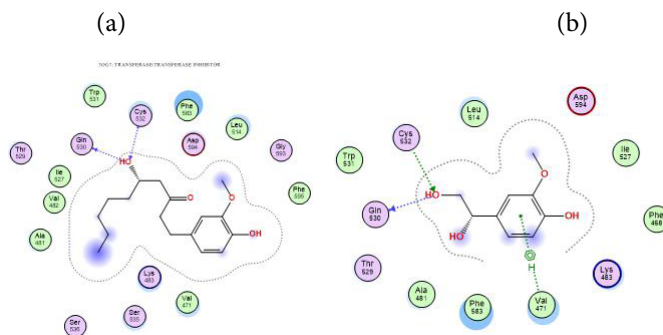


Figure S1. Predicted interaction of (a) N-G-1 and (b) N-G-42 with BRAF: PDB:ID: 3OG7.

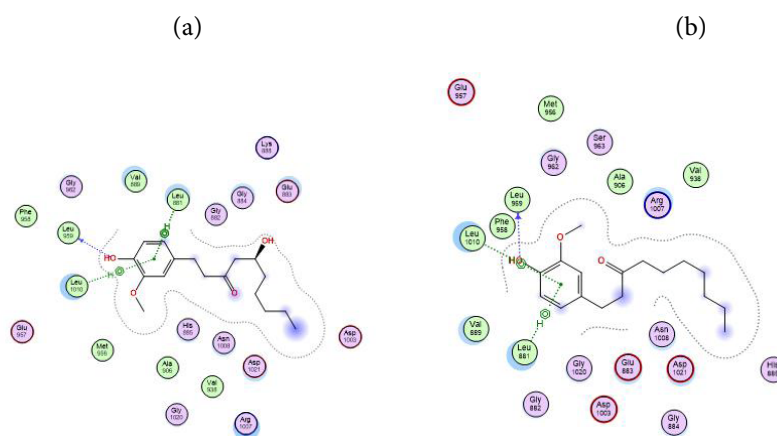


Figure S2. Predicted interaction of (a) N-G-1 and (b) N-G-30 with JAK 1: PDB:ID: 3EYG.

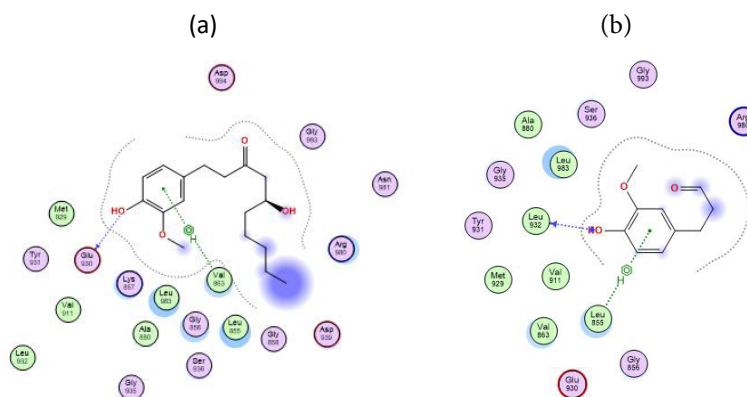


Figure S3. Predicted interaction of (a) N-G-1 and (b) N-G-43 with JAK 2: PDB:ID: 2B7A.

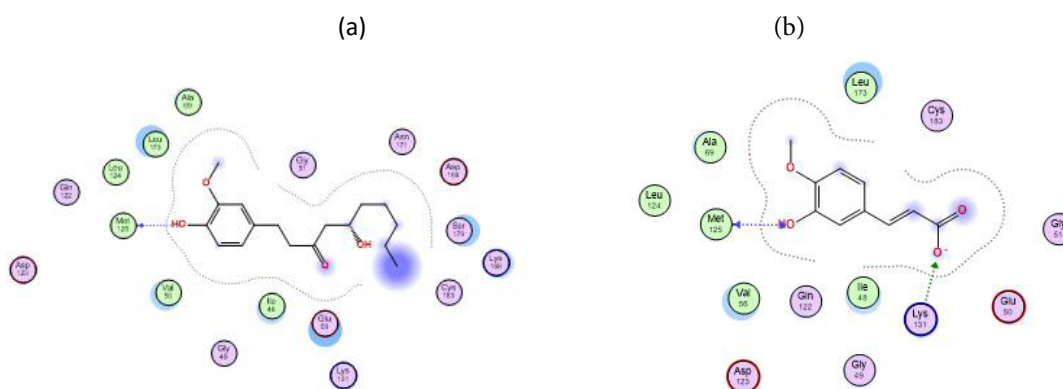
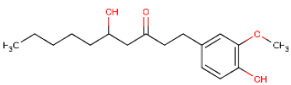
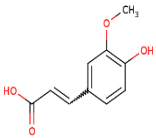
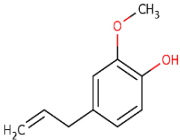
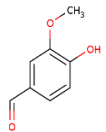
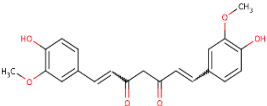
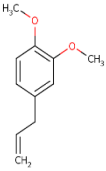
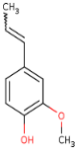
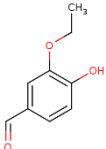
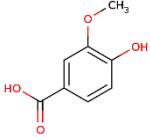
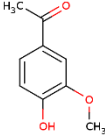
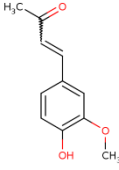
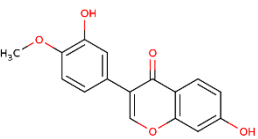
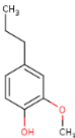
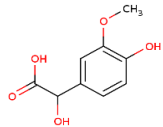
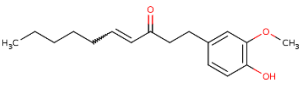
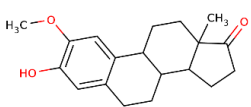
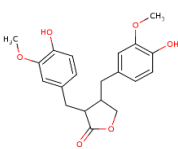
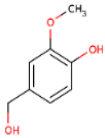
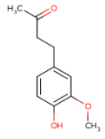
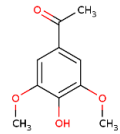
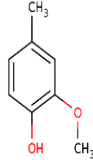
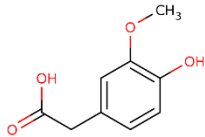
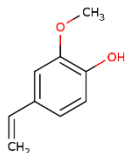
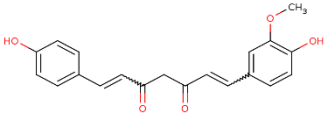
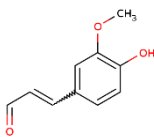
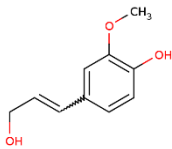
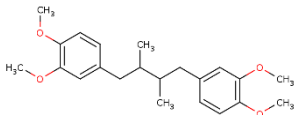
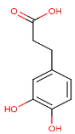
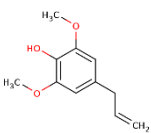


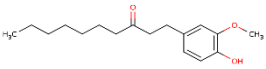
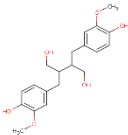
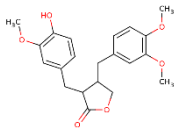
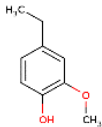
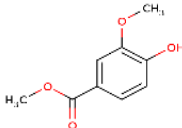
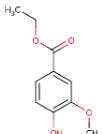
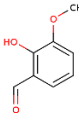
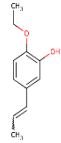
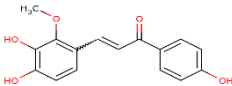
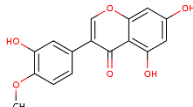
Figure S4. Predicted interaction of (a) N-G-1 and (b) N-G-47 with Erk 1 : PDB:ID: 2ZOQ.

Table S1. ID and structure information of 6-gingerol and structurally similar compounds

Compound code	Compound name	CAS no	Structure
N-G-1	6-Gingerol	23513-14-6	
N-G-2	Ferulic acid	537-98-4	
N-G-3	Eugenol	97-53-0	
N-G-4	Vanillin	121-33-5	
N-G-5	Curcumin	458-37-7	
N-G-6	Methyl eugenol	93-15-2	
N-G-7	(E)Isoeugenol	97-54-1	
N-G-8	Ethyl vanillin	121-32-4	
N-G-9	Vanillic acid	121-34-6	

Compound code	Compound name	CAS no	Structure
N-G-10	Acetovanillone	498-02-2	
N-G-11	Dehydrozingerone	1080-12-2	
N-G-12	Calycosin	20575-57-9	
N-G-13	2-methoxy-4-propylphenol (Dihydroeugenol)	2785-87-7	
N-G-14	Vanillylmandelic acid	55-10-7	
N-G-15	Shogaol	555-66-8	
N-G-16	2-methoxyestrone	362-08-3	
N-G-17	Matairesinol	580-72-3	
N-G-18	Vanillyl alcohol	498-00-0	
N-G-19	Zingerone	122-48-5	

Compound code	Compound name	CAS no	Structure
N-G-20	Acetosyringone	2478-38-8	
N-G-21	2-methoxy-4-methylphenol (Cresol)	93-51-6	
N-G-22	Homovanillic acid	306-08-1	
N-G-23	2-methoxy-4-vinylphenol	7786-61-0	
N-G-24		22608-11-3	
N-G-25	Coniferaldehyde	20649-42-7	
N-G-26	Coniferyl alcohol	32811-40-8	
N-G-27	Terameprocol	24150-24-1	
N-G-28	Dihydrocaffeic acid	1078-61-1	
N-G-29	4-allyl-2,6-dimethoxyphenol ((Methoxyeugenol))	6627-88-9	

Compound code	Compound name	CAS no	Structure
N-G-30	Paradol	27113-22-0	
N-G-31	Secoisolariciresinol	29388-59-8	
N-G-32	Arctigenin	7770-78-7	
N-G-33	4-ethyl-2-methoxyphenol	2785-89-9	
N-G-34	Methyl vanillate	3943-74-6	
N-G-35	Ethyl vanillate	617-05-0	
N-G-36	2-hydroxy-3-methoxybenzaldehyde	148-53-8	
N-G-37	Vanitrope	63477-41-8	
N-G-38	Licochalcone B	58749-23-8	
N-G-39	Pratensein	2284-31-3	

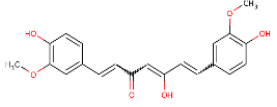
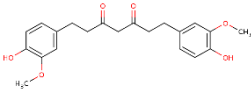
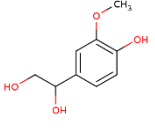
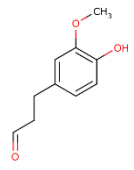
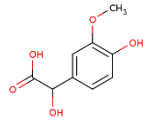
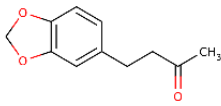
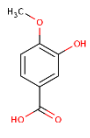
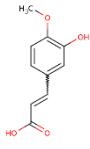
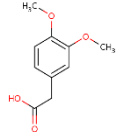
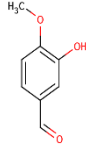
Compound code	Compound name	CAS no	Structure
N-G-40	Curcumin PE	NG	
N-G-41		36062-04-1	
N-G-42	Vanylglycol	534-82-7	
N-G-43	3-(4-Hydroxy-3-methoxyphenyl) propanal [dihydroconiferyl aldehyde]	80638-48-8	
N-G-44	L-(+)-vanilmandelic acid	13244-77-4	
N-G-45	Piperonyl acetone	55418-52-5	
N-G-46	3-hydroxy-4-methoxybenzoic acid (Isovanillic acid)	645-08-9	
N-G-47	Isoferulic acid	25522-33-2	
N-G-48	Homoveratric acid	93-40-3	
N-G-49	(3-hydroxy-4	621-59-0	

Table S2. Common anti-cancer targets for 6-gingerol and similar compounds via four different web servers

PASSonline	SwissTargetPrediction	MolTarPred	SEA
MAP Kinase Stimulant	MAP Kinase ERK1		
Apoptosis Agonist	MAP2K1		
Caspase3 Stimulant	mTOR		
Caspase8 Stimulant	STAT3		
	SYK		
JAK2 expression Inhibitor	JAK2		
	(PIK3CB) \ (PIK3CA)		
BRAF expression Inhibitor	BRAF		
AR expression Inhibitor	Androgen Receptor (AR)		
TP53 expression enhancer	p53-binding protein Mdm-2 (MDM2)		
Transcription Factor NFκB Inhibitor			NF-kappa B essential modulator
			Nuclear factor NF-kappa B p105 subunit (NF-κB1)
Beta Tubulin Antagonist	Tubulin beta-1 chain (TUBB1)		Beta-tubulin
Histone acetyltransferase Inhibitor			Histone acetyltransferase p300 (EP300)
Toll-like receptor Antagonist			Toll-like receptor 1
Beta-adrenergic receptor kinase Inhibitor			Beta-1 adrenergic receptor (ADRB1)
5-lipoxygenase Inhibitor	Arachidonate 5-lipoxygenase (ALOX5)	Arachidonate 5-lipoxygenase	Arachidonate 5-lipoxygenase (ALOX5)
	Arachidonate 15-lipoxygenase (ALOX15)		Arachidonate 15-lipoxygenase (ALOX15)

Table S3. Results of PASSonline server

Compounds	Glucanate 2-dehydrogenase (acceptor) inhibitor	TP53 expression enhancer	Preneoplastic conditions treatment	GST A substrate	GST M substrate	Lipid peroxidase inhibitor	JAK2 expression inhibitor	NOS2 expression inhibitor	TNF expression inhibitor
N-G-1	0.765	0.600	0.772	0.717	0.687	0.670	0.679	0.632	0.633
N-G-2	0.833	0.788	0.903	0.768	0.673	0.618	0.915	0.560	0.819
N-G-3	0.797	0.724	0.803	0.633	0.543	0.501	0.873	0.618	0.525
N-G-4	0.737	0.608	0.777	0.532	0.572	0.711	0.886	0.465	0.546
N-G-5	0.833	0.671	0.676	0.778	0.777	0.598	0.369	0.649	0.764
N-G-6	0.825	0.649	0.748	0.632	0.437	0.383	0.819	0.545	0.437
N-G-7	0.772	0.766	0.879	0.719	0.730	0.613	0.942	0.724	0.852
N-G-8	0.496	0.549	0.637	0.622	0.439	0.729	0.710	0.378	0.433
N-G-9	0.794	0.713	0.905	0.537	0.535	0.564	0.871	0.485	0.670
N-G-10	0.780	0.681	0.798	0.584	0.542	0.467	0.883	0.531	0.691
N-G-11	0.927	0.745	0.905	0.861	0.888	0.582	0.953	0.801	0.847
N-G-12	0.759	0.797	0.571	0.314	0.541	0.734	0.837	0.567	0.453
N-G-13	0.747	0.686	0.861	0.638	0.630	0.535	0.876	0.527	0.638
N-G-14	0.823	0.652	0.794	0.560	0.472	0.426	0.821	0.418	0.758
N-G-15	0.759	0.757	0.873	0.730	0.707	0.603	0.828	0.544	0.754
N-G-16	0.698	0.755	0.351		0.246	0.501	0.964	0.505	0.568
N-G-17	0.646	0.536	0.683	0.304	0.395	0.371	0.709	0.426	0.483
N-G-18	0.747	0.720	0.796	0.523	0.549	0.587	0.876	0.591	0.618
N-G-19	0.921	0.744	0.841	0.655	0.641	0.602	0.870	0.600	0.715
N-G-20	0.768	0.680	0.740	0.594	0.468	0.463	0.845	0.474	0.618
N-G-21	0.772	0.739	0.814	0.544	0.585	0.614	0.924	0.606	0.723
N-G-22	0.831	0.775	0.878	0.668	0.560	0.517	0.836	0.512	0.647
N-G-23	0.916	0.723	0.824	0.700	0.609	0.462	0.922	0.597	0.613
N-G-24	0.822	0.693	0.950	0.751	0.802	0.627	0.978	0.674	0.901
N-G-25	0.706	0.830	0.834	0.830	0.864	0.438	0.925	0.540	0.634
N-G-26	0.715	0.735	0.867	0.711	0.661	0.560	0.919	0.595	0.804
N-G-27	0.755	0.584	0.593	0.480	0.431	0.339	0.798	0.389	0.549
N-G-28	0.801	0.699	0.816	0.771	0.574	0.507	0.747	0.405	0.580
N-G-29	0.788	0.723	0.746	0.642	0.468	0.496	0.832	0.559	0.451
N-G-30	0.797	0.760	0.892	0.646	0.625	0.726	0.811	0.577	0.678
N-G-31	0.658	0.633	0.859	0.468	0.459	0.420	0.801	0.458	0.589
N-G-32	0.646	0.536	0.683	0.304	0.395	0.371	0.709	0.426	0.483
N-G-33	0.765	0.725	0.848	0.598	0.622	0.497	0.888	0.548	0.620
N-G-34	0.757	0.652	0.872	0.531	0.548	0.584	0.871	0.501	0.628
N-G-35	0.727	0.652	0.825	0.469	0.416	0.631	0.784	0.453	0.605
N-G-36	0.770	0.541	0.706	0.568	0.498	0.580	0.848	0.387	0.447
N-G-37	0.525	0.711	0.786	0.767	0.614	0.616	0.868	0.620	0.749
N-G-38	0.706	0.657	0.754	0.584	0.569	0.697	0.882	0.640	0.563
N-G-39	0.727	0.857	0.507	0.244	0.464	0.797	0.792	0.612	0.492
N-G-40	0.825	0.686	0.883	0.721	0.720	0.403	0.941	0.589	0.788
N-G-41	0.822	0.744	0.874	0.555	0.573	0.405	0.913	0.599	0.639
N-G-42	0.688	0.647	0.727	0.469	0.460	0.543	0.827	0.459	0.736
N-G-43	0.672	0.716	0.783	0.670	0.670	0.375	0.839	0.444	0.478
N-G-44	0.823	0.652	0.794	0.560	0.472	0.426	0.821	0.418	0.758
N-G-45	0.902	0.572	0.479	0.569	0.324	0.468	0.546	0.330	0.587
N-G-46	0.794	0.713	0.905	0.537	0.535	0.564	0.871	0.485	0.670
N-G-47	0.833	0.788	0.903	0.768	0.673	0.618	0.915	0.560	0.819
N-G-48	0.864	0.738	0.851	0.694	0.482	0.422	0.784	0.457	0.581
N-G-49	0.737	0.608	0.777	0.532	0.572	0.711	0.886	0.465	0.546

Table S3. Results of PASSonline server (continued)

Compounds	Free radical scavenger	Prostaglandin-A1 DELTA-isomerase inhibitor	Antimutagenic	Caspase 3 stimulant	GST P substrate	GST P1-I substrate	Nitric oxide antagonist	Apoptosis agonist
N-G-1	0.617	0.602	0.597	0.575	0.546	0.511	0.494	0.518
N-G-2	0.731	0.431	0.900	0.749	0.541	0.521	0.324	0.702
N-G-3	0.563	0.309	0.878	0.873	0.491	0.467	0.335	0.743
N-G-4	0.546	0.387	0.618	0.754	0.379	0.350	0.247	0.705
N-G-5	0.766	0.294	0.814	0.747	0.184	0.188	0.346	0.803
N-G-6	0.536	0.362	0.807	0.840	0.465	0.438	0.297	0.726
N-G-7	0.717	0.365	0.805	0.778	0.538	0.517	0.329	0.733
N-G-8	0.481	0.380	0.469	0.651	0.356	0.305	0.189	0.588
N-G-9	0.643	0.731		0.640	0.358	0.330	0.258	0.512
N-G-10	0.560	0.446	0.609	0.658	0.384	0.356	0.284	0.547
N-G-11	0.704	0.322	0.848	0.819	0.654	0.640	0.280	0.760
N-G-12	0.506	0.221	0.864	0.603	0.220	0.216	0.454	0.779
N-G-13	0.528	0.477	0.783	0.734	0.393	0.364	0.249	0.482
N-G-14	0.482		0.575	0.439	0.386	0.351	0.220	0.405
N-G-15	0.743	0.344	0.851	0.551	0.676	0.663	0.475	0.711
N-G-16	0.440		0.335	0.737			0.253	0.484
N-G-17	0.330	0.249	0.372	0.582	0.202	0.192	0.207	0.422
N-G-18	0.579	0.394	0.816	0.787	0.364	0.325	0.270	0.562
N-G-19	0.551	0.376	0.796	0.659	0.364	0.336	0.315	0.488
N-G-20	0.547	0.439	0.573	0.534	0.323	0.299	0.282	0.578
N-G-21	0.546	0.447	0.730	0.756	0.375	0.346	0.271	0.600
N-G-22	0.612	0.530	0.748	0.634	0.393	0.364	0.266	0.471
N-G-23	0.540	0.342	0.791	0.768	0.784	0.772	0.362	0.663
N-G-24	0.785	0.269	0.834	0.719	0.813	0.803	0.356	0.861
N-G-25	0.487	0.276	0.752	0.945	0.765	0.754	0.277	0.871
N-G-26	0.565	0.281	0.796	0.784	0.529	0.491	0.305	0.590
N-G-27	0.340	0.454	0.356	0.529	0.200	0.199	0.138	0.326
N-G-28	0.516	0.758	0.818	0.401	0.413	0.384	0.249	0.363
N-G-29	0.652	0.304	0.868	0.816	0.459	0.432	0.336	0.794
N-G-30	0.631	0.438	0.789	0.544	0.420	0.392	0.350	0.538
N-G-31	0.439	0.303	0.523	0.543	0.315	0.269	0.194	0.436
N-G-32	0.330	0.249	0.372	0.582	0.202	0.192	0.207	0.422
N-G-33	0.529	0.456	0.769	0.761	0.366	0.338	0.284	0.516
N-G-34	0.575	0.542	0.700	0.728	0.356	0.329	0.263	0.521
N-G-35	0.539	0.462	0.628	0.657	0.318	0.271	0.243	0.440
N-G-36	0.503	0.387	0.435	0.647	0.285	0.267	0.175	0.889
N-G-37	0.643	0.336	0.715	0.698	0.520	0.480	0.275	0.648
N-G-38	0.737	0.276	0.650	0.805	0.389	0.361	0.640	0.829
N-G-39	0.593		0.896	0.660	0.178	0.181	0.590	0.844
N-G-40	0.562	0.269	0.736	0.626	0.632	0.618	0.253	0.799
N-G-41	0.710	0.353	0.718	0.539	0.675	0.662	0.406	0.625
N-G-42	0.518	0.315	0.486	0.483	0.361	0.304	0.216	0.513
N-G-43	0.390	0.324	0.650	0.700	0.530	0.509	0.220	0.435
N-G-44	0.482	0.475	0.575	0.439	0.386	0.351	0.220	0.405
N-G-45	0.408	0.401	0.245	0.646			0.243	0.371
N-G-46	0.643	0.731	0.834	0.640	0.358	0.330	0.258	0.512
N-G-47	0.731	0.431	0.900	0.749	0.541	0.521	0.324	0.702
N-G-48	0.520	0.638	0.630	0.570	0.350	0.323	0.223	0.394
N-G-49	0.546	0.387	0.618	0.754	0.379	0.350	0.247	0.705

Table S3. Results of PASSonline server (continued)

Compounds	Platelet derived growth factor receptor kinase inhibitor	Histone acetyltransferase inhibitor	MAP kinase stimulant	Prostaglandin-E2 9-reductase inhibitor	Caspase 8 stimulant	Histidine kinase inhibitor	Anticarcinogenic	Myc inhibitor
N-G-1	0.509	0.470	0.482	0.461	0.433	0.390	0.364	0.350
N-G-2		0.555	0.709	0.464	0.551	0.400	0.616	0.357
N-G-3		0.457	0.735	0.298	0.598	0.331	0.459	0.476
N-G-4		0.284	0.744	0.240	0.525	0.473	0.388	0.307
N-G-5		0.305	0.737	0.235	0.487	0.317	0.611	0.313
N-G-6		0.350	0.663	0.285	0.566		0.362	0.492
N-G-7		0.524	0.806	0.324	0.545	0.344	0.408	0.350
N-G-8		0.432	0.597	0.195	0.449	0.443	0.353	0.278
N-G-9		0.619	0.717	0.702	0.573	0.405	0.413	0.358
N-G-10		0.470	0.764	0.510	0.519	0.467	0.341	0.343
N-G-11	0.400	0.584	0.756	0.241	0.491	0.315	0.609	0.319
N-G-12		0.170	0.794	0.167	0.536	0.937	0.703	0.327
N-G-13	0.346	0.561	0.781	0.435	0.566	0.435	0.367	0.390
N-G-14		0.333	0.608	0.389	0.505	0.433	0.370	0.464
N-G-15	0.559	0.614	0.564	0.454	0.536	0.389	0.475	0.386
N-G-16		0.547	0.875	0.521	0.521	0.259	0.496	0.444
N-G-17		0.210	0.578	0.487	0.487	0.251	0.566	0.337
N-G-18		0.357	0.720	0.342	0.649	0.372	0.469	0.392
N-G-19	0.854	0.399	0.728	0.257	0.478	0.360	0.419	0.346
N-G-20		0.390	0.691	0.513	0.474	0.473	0.341	0.350
N-G-21	0.379	0.397	0.838	0.438	0.606	0.407	0.402	0.398
N-G-22		0.414	0.733	0.705	0.608	0.706	0.453	0.389
N-G-23		0.502	0.810	0.324	0.610	0.342	0.402	0.370
N-G-24		0.703	0.760	0.248	0.461	0.388	0.649	0.299
N-G-25		0.362	0.735	0.196	0.498	0.385	0.498	0.286
N-G-26		0.565	0.711	0.332	0.550	0.298	0.595	0.369
N-G-27		0.227	0.721	0.439	0.470		0.270	0.431
N-G-28		0.501	0.652	0.705	0.482	0.553	0.412	0.367
N-G-29		0.378	0.660	0.301	0.553	0.326	0.459	0.488
N-G-30	0.630	0.471	0.647	0.350	0.507	0.438	0.415	0.359
N-G-31		0.344	0.691	0.379	0.506	0.307	0.477	0.407
N-G-32		0.210	0.578		0.487	0.251	0.566	0.337
N-G-33	0.286	0.377	0.826	0.401	0.644	0.410	0.394	0.471
N-G-34		0.567	0.717	0.453	0.608	0.376	0.364	0.392
N-G-35	0.268	0.684	0.630	0.386	0.511	0.323	0.341	0.339
N-G-36		0.218	0.660	0.271	0.461	0.493	0.353	0.391
N-G-37		0.624	0.673	0.237	0.461	0.326	0.367	0.302
N-G-38		0.511	0.644	0.315	0.351	0.457	0.382	0.219
N-G-39			0.744		0.570	0.954	0.781	0.329
N-G-40		0.503	0.682	0.187	0.432	0.289	0.455	0.284
N-G-41	0.680	0.475	0.733	0.241	0.472	0.359	0.495	0.330
N-G-42		0.344	0.610	0.268	0.504	0.331	0.421	0.475
N-G-43	0.251	0.277	0.707	0.208	0.484	0.430	0.341	0.316
N-G-44		0.333	0.608	0.389	0.505	0.433	0.370	0.464
N-G-45	0.850	0.159	0.658		0.481	0.235	0.251	
N-G-46		0.619	0.717	0.702	0.573	0.405	0.413	0.358
N-G-47		0.555	0.709	0.464	0.551	0.400	0.616	0.357
N-G-48		0.348	0.675	0.735	0.579	0.675	0.381	0.396
N-G-49		0.284	0.744	0.240	0.525	0.473	0.388	0.307

Table S3. Results of PASSonline server (continued)

Compounds	AR expression inhibitor	Transcription factor NF kappa B inhibitor	BRAF expression inhibitor	Endothelial growth factor antagonist	G-protein-coupled receptor kinase inhibitor	Beta-adrenergic receptor kinase inhibitor	Pin1 inhibitor	DNA polymerase I inhibitor
N-G-1	0.339	0.264	0.273	0.297	0.332	0.332	0.340	0.277
N-G-2	0.627	0.407	0.395	0.386	0.641	0.641	0.562	0.253
N-G-3	0.608	0.488	0.126	0.376	0.807	0.807	0.607	0.249
N-G-4	0.582	0.378	0.176	0.377	0.753	0.753	0.617	0.258
N-G-5	0.527	0.399	0.219	0.375	0.427	0.427	0.567	0.237
N-G-6	0.529	0.405	0.162	0.388	0.811	0.811	0.585	
N-G-7	0.702	0.520	0.296	0.414	0.539	0.539	0.612	0.252
N-G-8	0.465	0.451	0.185	0.290	0.882	0.882	0.479	0.237
N-G-9	0.594	0.296	0.172	0.393	0.698	0.698	0.606	0.289
N-G-10	0.666	0.290	0.188	0.424	0.388	0.388	0.631	0.292
N-G-11	0.697	0.422	0.230	0.479	0.407	0.407	0.556	0.229
N-G-12	0.871	0.332		0.264			0.680	0.245
N-G-13	0.559	0.246	0.230	0.490	0.447	0.447	0.674	0.302
N-G-14	0.560	0.133	0.183	0.370	0.562	0.562	0.507	0.303
N-G-15	0.570	0.452	0.217	0.382	0.406	0.406	0.428	0.271
N-G-16	0.846	0.255		0.216	0.256	0.256	0.398	0.315
N-G-17	0.393	0.155		0.383	0.290	0.290	0.467	0.240
N-G-18	0.529	0.288	0.148	0.416	0.617	0.617	0.654	0.354
N-G-19	0.551	0.272	0.145	0.747	0.309	0.309	0.620	0.260
N-G-20	0.664	0.278	0.243	0.487	0.392	0.392	0.620	0.268
N-G-21	0.634	0.356	0.270	0.685	0.541	0.541	0.660	0.318
N-G-22	0.544	0.207	0.206	0.447	0.515	0.515	0.668	0.288
N-G-23	0.639	0.375	0.152	0.349	0.551	0.551	0.630	0.235
N-G-24	0.810	0.560	0.193	0.343	0.425	0.425	0.534	
N-G-25	0.675	0.289	0.447	0.302	0.419	0.419	0.542	
N-G-26	0.598	0.458	0.181	0.370	0.675	0.675	0.589	0.276
N-G-27	0.526	0.189	0.172	0.411	0.323	0.323	0.631	
N-G-28	0.494	0.133	0.413	0.361	0.749	0.749	0.611	0.269
N-G-29	0.605	0.474	0.163	0.432	0.810	0.810	0.596	
N-G-30	0.504	0.267	0.193	0.433	0.319	0.319	0.522	0.292
N-G-31	0.492	0.177		0.356	0.401	0.401	0.630	0.294
N-G-32	0.393	0.155		0.383	0.290	0.290	0.467	0.240
N-G-33	0.619	0.281	0.196	0.481	0.417	0.417	0.715	0.291
N-G-34	0.561	0.350	0.141	0.418	0.628	0.628	0.606	0.316
N-G-35	0.496	0.547	0.115	0.355	0.655	0.655	0.580	0.266
N-G-36	0.566	0.253	0.176	0.413	0.755	0.755	0.657	0.233
N-G-37	0.612	0.559	0.260	0.311	0.788	0.788	0.492	0.230
N-G-38	0.648	0.497	0.170	0.259	0.359	0.359	0.542	
N-G-39	0.905	0.471		0.308			0.616	0.275
N-G-40	0.642	0.295	0.160	0.318	0.337	0.337	0.478	
N-G-41	0.596	0.406	0.122	0.552	0.305	0.305	0.638	0.260
N-G-42	0.524	0.141	0.107	0.354	0.598	0.598	0.534	0.323
N-G-43	0.575	0.188	0.227	0.359	0.316	0.316	0.605	0.247
N-G-44	0.560	0.133	0.183	0.370	0.562	0.562	0.507	0.303
N-G-45	0.242	0.130	0.187	0.422			0.487	
N-G-46	0.594	0.296	0.172	0.393	0.698	0.698	0.606	0.289
N-G-47	0.627	0.407	0.395	0.386	0.641	0.641	0.562	0.253
N-G-48	0.473	0.167	0.303	0.459	0.582	0.582	0.664	0.247
N-G-49	0.582	0.378	0.176	0.377	0.753	0.753	0.617	0.258

Table S3. Results of PASSonline server (continued)

Compounds	Leukopoiesis inhibitor	Toll-Like receptor antagonist	Transcription factor inhibitor	Tumour necrosis factor alpha release inhibitor	Glutamate decarboxylase inhibitor	Antineoplastic (breast cancer)	Transcription factor NF kappa A inhibitor	Antineoplastic (cervical cancer)
N-G-1	0.288	0.166	0.243	0.200	0.162	0.210	0.228	0.151
N-G-2	0.431		0.329		0.263	0.467	0.338	0.308
N-G-3	0.434		0.410	0.171	0.202	0.419	0.351	0.276
N-G-4	0.443		0.379		0.191	0.466	0.329	0.139
N-G-5	0.335		0.334		0.175	0.528	0.325	0.323
N-G-6	0.476		0.377	0.270	0.151	0.402	0.316	0.315
N-G-7	0.427		0.494	0.160	0.148	0.463	0.377	0.318
N-G-8	0.312		0.425		0.146	0.365	0.341	
N-G-9	0.570		0.304		0.513	0.298	0.371	0.155
N-G-10	0.582		0.415	0.176	0.225	0.413	0.382	0.264
N-G-11	0.348		0.339		0.153	0.552	0.342	0.512
N-G-12	0.300		0.361		0.097	0.565	0.294	0.355
N-G-13	0.499		0.254	0.158	0.183	0.252	0.366	0.181
N-G-14	0.443				0.360		0.292	
N-G-15	0.254		0.334		0.134	0.256	0.268	0.148
N-G-16	0.317		0.229			0.563	0.353	0.163
N-G-17	0.777					0.231	0.278	0.115
N-G-18	0.477		0.296		0.172	0.384	0.357	0.271
N-G-19	0.414		0.253	0.124	0.189	0.242	0.316	0.400
N-G-20	0.605		0.389	0.138	0.229	0.401	0.357	0.280
N-G-21	0.571		0.406	0.163	0.185	0.399	0.387	0.267
N-G-22	0.558		0.190		0.478	0.181	0.333	0.113
N-G-23	0.395		0.340	0.174	0.191	0.411	0.341	0.320
N-G-24	0.304		0.504		0.184	0.547	0.310	0.309
N-G-25	0.321		0.239		0.203	0.279	0.316	0.331
N-G-26	0.364		0.379		0.128	0.357	0.400	0.280
N-G-27	0.488	0.137	0.257	0.215	0.105	0.282	0.368	0.190
N-G-28	0.514	0.124	0.166		0.603		0.363	
N-G-29	0.465		0.384	0.136	0.206	0.410	0.327	0.292
N-G-30	0.305	0.121	0.255	0.137	0.194	0.227	0.288	0.254
N-G-31	0.381	0.122	0.181	0.131	0.126	0.179	0.398	0.103
N-G-32	0.777					0.231	0.278	0.115
N-G-33	0.588		0.305	0.171	0.192	0.302	0.371	0.229
N-G-34	0.647		0.382	0.145	0.248	0.349	0.404	0.259
N-G-35	0.652	0.145	0.519	0.140	0.177	0.309	0.357	0.164
N-G-36	0.510		0.295		0.173	0.437	0.298	0.177
N-G-37	0.307		0.535	0.159	0.120	0.391	0.379	0.179
N-G-38	0.283		0.449		0.183	0.597	0.320	0.537
N-G-39	0.252		0.468	0.131	0.092	0.602	0.267	0.376
N-G-40	0.293		0.245		0.146	0.727	0.307	0.406
N-G-41	0.423		0.375	0.134	0.202	0.250	0.305	0.156
N-G-42	0.374				0.195	0.174	0.348	
N-G-43	0.379				0.250		0.291	0.140
N-G-44	0.443				0.360		0.292	
N-G-45			0.210		0.172		0.231	0.345
N-G-46	0.570		0.304		0.513	0.298	0.371	0.155
N-G-47	0.431		0.329		0.263	0.467	0.338	0.308
N-G-48	0.597	0.119		0.137	0.358		0.307	0.107
N-G-49	0.443		0.379		0.191	0.466	0.329	0.139

Table S3. Results of PASSonline server (continued)

Compounds	Antineoplastic (endocrine cancer)	Phosphomevalonate kinase inhibitor	Tubulin antagonist	Nucleotidase inhibitor	Glutaminase inhibitor	Antineoplastic (thyroid cancer)	Antineoplastic (bone cancer)	Antineoplastic (non-Hodgkin's lymphoma)
N-G-1	0.171	0.115	0.121	0.126	0.180	0.161	0.205	0.295
N-G-2		0.482	0.283	0.137	0.335	0.163	0.219	0.424
N-G-3	0.172	0.170	0.344		0.214	0.189	0.206	
N-G-4		0.619	0.480		0.287		0.272	
N-G-5		0.267	0.238		0.274	0.160	0.211	0.387
N-G-6	0.174	0.115	0.315		0.201	0.188		
N-G-7		0.297	0.514		0.259	0.165	0.230	0.420
N-G-8		0.523	0.248		0.392	0.150	0.261	
N-G-9		0.320	0.254	0.194	0.594	0.168	0.235	0.388
N-G-10	0.187	0.171	0.347		0.316	0.176	0.222	0.432
N-G-11		0.264	0.272		0.313	0.163	0.208	0.426
N-G-12		0.129	0.327		0.178		0.274	
N-G-13	0.167	0.184	0.248		0.293	0.151	0.242	0.382
N-G-14		0.203	0.169	0.153	0.346	0.176	0.211	0.348
N-G-15		0.135	0.154		0.176		0.206	0.352
N-G-16			0.371			0.228	0.214	
N-G-17	0.187	0.112	0.172		0.162	0.173		0.336
N-G-18		0.205	0.271	0.120	0.322	0.160	0.251	0.467
N-G-19		0.164	0.203		0.351		0.209	0.356
N-G-20	0.205	0.138	0.383		0.309	0.172	0.192	0.444
N-G-21		0.197	0.447		0.352	0.178	0.246	0.415
N-G-22		0.233	0.231	0.150	0.390	0.150	0.225	0.362
N-G-23	0.189	0.233	0.521		0.254	0.208	0.232	0.316
N-G-24		0.286	0.234		0.253	0.153	0.209	0.375
N-G-25	0.175	0.292	0.288		0.202	0.179	0.253	0.320
N-G-26		0.313	0.384		0.305	0.159	0.227	0.442
N-G-27	0.155	0.093	0.176		0.227		0.258	0.315
N-G-28		0.344		0.226	0.618		0.206	0.400
N-G-29	0.186	0.140	0.377		0.208	0.187		
N-G-30		0.138	0.151		0.279	0.171	0.227	0.327
N-G-31		0.171	0.167		0.284		0.246	0.378
N-G-32	0.187	0.112	0.172		0.162	0.173		0.336
N-G-33	0.176	0.181	0.327		0.305	0.157	0.244	0.431
N-G-34		0.233	0.365	0.131	0.423	0.195	0.219	0.366
N-G-35	0.165	0.203	0.234	0.111	0.507	0.191	0.219	0.401
N-G-36		0.411	0.502		0.305		0.257	
N-G-37		0.260	0.326		0.351	0.165	0.216	0.391
N-G-38	0.166	0.229	0.353		0.202	0.184		0.319
N-G-39		0.114	0.386		0.171		0.272	
N-G-40		0.257	0.186		0.236			0.320
N-G-41		0.171	0.179		0.297	0.171	0.206	0.288
N-G-42		0.176	0.183		0.316	0.173	0.220	0.376
N-G-43	0.167	0.186	0.187		0.233	0.161	0.253	
N-G-44		0.203	0.169	0.153	0.346	0.176	0.211	0.348
N-G-45			0.179		0.282			0.339
N-G-46		0.320	0.254	0.194	0.594	0.168	0.235	0.388
N-G-47		0.482	0.283	0.137	0.335	0.163	0.219	0.424
N-G-48		0.201	0.184	0.163	0.410		0.212	0.297
N-G-49		0.619	0.480		0.287		0.272	

Table S3. Results of PASSonline server (continued)

Compound	Prostaglandin F2 alpha antagonists	Anticancer (liver cancer)	Aspartate kinase inhibitor	Anticancer	Dual specificity protein phosphatase VHR inhibitor	Glutamate dehydrogenase (NADP+) inhibitor	Prostaglandin EP2 antagonists	Adenylate kinase inhibitor	Glutamate-tRNA ligase inhibitor	Glutamate synthase (ferredoxin) inhibitor	Beta tubulin antagonists	5-Lipoxygenase inhibitor
NG-1	0.063	0.175	0.115	0.241	0.062	0.081	0.043	0.127	0.198	0.129	0.050	0.064
NG-2	0.051	0.241	0.121	0.601		0.133	0.055	0.148	0.291	0.172	0.163	0.172
NG-3		0.239		0.461	0.057		0.029	0.135	0.203		0.237	0.154
NG-4		0.190	0.115	0.636	0.050	0.160		0.136	0.254	0.149	0.462	0.094
NG-5	0.045	0.194		0.672		0.065			0.217	0.143	0.168	0.156
NG-6		0.245		0.417			0.037	0.144	0.221		0.195	0.113
NG-7	0.046	0.205	0.097	0.679				0.121	0.225	0.136	0.387	0.210
NG-8			0.148	0.448		0.192		0.148	0.239	0.145	0.227	0.089
NG-9		0.250	0.193	0.326	0.079	0.207		0.258	0.457	0.274	0.150	0.105
NG-10		0.234	0.117	0.404	0.075			0.132	0.264	0.161	0.169	0.166
NG-11	0.043	0.216		0.773		0.078		0.146	0.199	0.138	0.189	0.135
NG-12				0.708							0.145	0.156
NG-13	0.042	0.208	0.126	0.222	0.071	0.072		0.129	0.255	0.152	0.173	0.131
NG-14	0.042		0.134			0.090		0.149	0.324	0.180	0.058	0.068
NG-15	0.015	0.230		0.338	0.066	0.062	0.019	0.152			0.085	0.141
NG-16				0.731							0.251	
NG-17		0.183		0.574	0.056						0.074	0.086
NG-18	0.258	0.121	0.500	0.662		0.082		0.157	0.292	0.163	0.168	0.122
NG-19	0.190	0.100	0.283	0.055	0.055	0.090		0.143	0.226	0.155	0.095	0.089
NG-20	0.213	0.134	0.513	0.079	0.076	0.076		0.151	0.284	0.174	0.180	0.165
NG-21	0.244	0.117	0.478	0.065	0.065	0.070		0.145	0.179	0.179	0.321	0.138
NG-22	0.043	0.217	0.145		0.054	0.118		0.225	0.337	0.197	0.104	0.121
NG-23		0.220		0.617	0.057			0.143	0.231	0.135	0.442	0.150
NG-24	0.045	0.193		0.678					0.202	0.133	0.169	0.152
NG-25	0.042	0.202	0.113	0.551		0.060		0.150	0.191		0.218	0.140
NG-26	0.046	0.232	0.107	0.674		0.069		0.118	0.204	0.151	0.312	0.158
NG-27		0.160	0.118						0.313	0.156	0.063	0.102
NG-28	0.058	0.165	0.214		0.050	0.262	0.070	0.252	0.501	0.280		0.118
NG-29		0.220		0.564	0.059		0.031	0.155	0.219	0.127	0.265	0.153
NG-30	0.042	0.219	0.110	0.268	0.076	0.109		0.127		0.157	0.060	0.095
NG-31		0.230	0.114	0.247					0.235	0.139	0.071	0.072
NG-32		0.183		0.574	0.056						0.074	0.086
NG-33		0.259	0.116	0.329	0.063	0.064		0.130	0.262	0.157	0.219	0.115
NG-34		0.242	0.148	0.378	0.116	0.099		0.239	0.335	0.194	0.208	0.116
NG-35		0.196	0.185	0.270	0.088	0.091		0.214	0.277	0.186	0.139	0.120
NG-36		0.187	0.115	0.693	0.052	0.166		0.141	0.259	0.151	0.498	0.104
NG-37	0.046		0.117	0.545		0.066		0.129	0.217	0.131	0.226	0.190
NG-38	0.043			0.786			0.030		0.191		0.251	0.378
NG-39		0.161		0.775							0.203	0.193
NG-40	0.042			0.888						0.125	0.107	0.102
NG-41				0.260	0.053	0.064		0.118	0.233	0.153	0.096	0.090
NG-42		0.170	0.118	0.287		0.065		0.119	0.229	0.158	0.071	0.086
NG-43		0.174	0.153	0.250	0.059			0.146	0.217	0.124	0.125	0.077
NG-44	0.042		0.134			0.090		0.149	0.324	0.180	0.058	0.068
NG-45				0.226		0.088		0.144	0.245	0.132	0.049	
NG-46		0.250	0.193	0.326	0.079	0.200		0.258	0.457	0.274	0.150	0.105
NG-47	0.051	0.241	0.121	0.601		0.133	0.055	0.148	0.251	0.172	0.163	0.172
NG-48	0.042	0.218	0.164			0.143	0.019	0.261	0.387	0.212	0.059	0.091
NG-49		0.190	0.115	0.636	0.050	0.160		0.136	0.254	0.149	0.462	0.094

Table S4. SwissTarget prediction results

Target	N-G-1	N-G-2	N-G-3	N-G-4	N-G-5	N-G-6	N-G-7	N-G-8	N-G-9	N-G-10	N-G-11	N-G-12	N-G-13	N-G-14	N-G-15	N-G-16	N-G-17	N-G-18	N-G-19	N-G-20	N-G-21	N-G-22	N-G-23	N-G-24	N-G-25
ESR1	+																								
ALOX5	+	+																							
ALOX15	+	+	+																						
LYPLA1	+																								
LYPLA2	+																								
PDE4B	+																								
PPARG	+																								
MAP2K1	+																								
NR3C1	+																								
CHEK1	+		+		+		+																		
WEE1	+																								
PTGES	+			+	+																				
KIF11	+																								
PIK3CB	+																								
PIK3CG	+			+																					
PIK3CA	+			+		+																			
CDK2	+			+																					
MTOR	+																								
KDR	+		+			+	+																		
ERN1	+																								
RET	+																								
ITK	+																								
PDK1	+				+																				
PARP1	+	+	+	+		+	+																		
PIK3C2B	+																								
STAT3	+	+			+		+																		
PIM2	+																								
PIM3	+			+																					
IGF1R	+																								
PIK3CD	+			+																					
SYK	+																								
MAPK3	+																								
LIMK1	+																								
LRRK2	+			+		+		+		+															
AR	+		+	+		+	+																		
CDK2 CCNA1 CCNA2	+				+		+	+		+	+														
JAK3	+					+	+			+	+														
JAK1	+		+		+	+	+			+	+														
JAK2	+		+		+	+	+			+	+														
TYK2	+		+		+	+	+			+	+														
CDK5R1 CDK5	+				+			+		+	+														
CCNE1 CDK2	+																								
CDK7 CCNH	+																								
CDK9 CCNT1	+																								
PRKDC	+			+																					
PDPK1	+							+																	
FLT1	+																								
ROCK2	+																								
ROCK1	+																								
TUBB1	+	+	+	+				+		+	+														
BRAF	+		+	+		+	+	+		+	+														
TNK2	+																								
EPHB4	+																								
HSP90AA1	+																								
GAK	+																								
MDM2	+																								
CCND1 CDK4	+																								
CDK1 CCNB1	+																								
CCNE2 CDK2 CCNE1	+																								
GSK3B	+	+			+					+	+														
GSK3A	+										+														

Table S4. SwissTarget prediction results (continued)

Target	N-G-26	N-G-27	N-G-28	N-G-29	N-G-30	N-G-31	N-G-32	N-G-33	N-G-34	N-G-35	N-G-36	N-G-37	N-G-38	N-G-39	N-G-40	N-G-41	N-G-42	N-G-43	N-G-44	N-G-45	N-G-46	N-G-47	N-G-48	N-G-49
ESR1		*	*		*	*	*					*	*	*	*			*			*			*
ALOX5		*	*		*	*	*					*	*	*	*	*			*	*	*		*	*
ALOX15		*	*	*	*	*	*	*	*	*		*	*	*	*	*			*	*	*		*	*
LYPLA1					*	*	*									*							*	*
LYPLA2			*		*	*	*								*									
PDE4B					*	*	*																	
PPARG					*	*	*							*								*		
MAP3K1		*	*		*	*	*								*							*		
NR3C1		*	*		*	*	*	*							*					*	*		*	*
CHEK1					*	*	*	*	*	*		*	*	*	*	*			*	*	*		*	*
WEE1					*	*	*	*	*	*		*	*	*	*	*			*	*	*		*	*
PTGES					*	*	*	*	*	*		*	*	*	*	*			*	*	*		*	*
KIF11					*	*	*	*	*	*		*	*	*	*	*			*	*	*		*	*
PIK3CB		*			*	*	*	*	*	*		*	*	*	*	*			*	*	*		*	*
PIK3CG		*			*	*	*	*	*	*		*	*	*	*	*			*	*	*		*	*
PIK3CA		*			*	*	*	*	*	*		*	*	*	*	*			*	*	*		*	*
CDK2			*	*	*	*	*	*	*	*		*	*	*	*	*			*	*	*		*	*
MTOR					*	*	*	*	*	*		*	*	*	*	*			*	*	*		*	*
KDR		*	*	*	*	*	*	*	*	*		*	*	*	*	*			*	*	*		*	*
ERN1			*	*	*	*	*	*	*	*		*	*	*	*	*			*	*	*		*	*
RET					*	*	*	*	*	*		*	*	*	*	*			*	*	*		*	*
ITK					*	*	*	*	*	*		*	*	*	*	*			*	*	*		*	*
PDK1					*	*	*	*	*	*		*	*	*	*	*			*	*	*		*	*
PARP1			*	*	*	*	*	*	*	*		*	*	*	*	*			*	*	*		*	*
PIK3C2B					*	*	*	*	*	*		*	*	*	*	*			*	*	*		*	*
STAT3					*	*	*	*	*	*		*	*	*	*	*			*	*	*		*	*
PIM2					*	*	*	*	*	*		*	*	*	*	*			*	*	*		*	*
PIM3					*	*	*	*	*	*		*	*	*	*	*			*	*	*		*	*
IGF1R		*	*	*	*	*	*	*	*	*		*	*	*	*	*			*	*	*		*	*
PIK3CD		*	*	*	*	*	*	*	*	*		*	*	*	*	*			*	*	*		*	*
SYK					*	*	*	*	*	*		*	*	*	*	*			*	*	*		*	*
MAPK3					*	*	*	*	*	*		*	*	*	*	*			*	*	*		*	*
LIMK1					*	*	*	*	*	*		*	*	*	*	*			*	*	*		*	*
LRRK2					*	*	*	*	*	*		*	*	*	*	*			*	*	*		*	*
AR			*	*	*	*	*	*	*	*		*	*	*	*	*			*	*	*		*	*
CDK2 CCNA1 CCNA2				*	*	*	*	*	*	*		*	*	*	*	*			*	*	*		*	*
JAK3					*	*	*	*	*	*		*	*	*	*	*			*	*	*		*	*
JAK1					*	*	*	*	*	*		*	*	*	*	*			*	*	*		*	*
JAK2					*	*	*	*	*	*		*	*	*	*	*			*	*	*		*	*
TYK2					*	*	*	*	*	*		*	*	*	*	*			*	*	*		*	*
CDK5R1 CDK5				*	*	*	*	*	*	*		*	*	*	*	*			*	*	*		*	*
CCNE1 CDK2				*	*	*	*	*	*	*		*	*	*	*	*			*	*	*		*	*
CDK7 CCNH				*	*	*	*	*	*	*		*	*	*	*	*			*	*	*		*	*
CDK9 CCNT1			*	*	*	*	*	*	*	*		*	*	*	*	*			*	*	*		*	*
PRKDC		*			*	*	*	*	*	*		*	*	*	*	*			*	*	*		*	*
PDPK1		*	*		*	*	*	*	*	*		*	*	*	*	*			*	*	*		*	*
FLT1				*	*	*	*	*	*	*		*	*	*	*	*			*	*	*		*	*
ROCK2				*	*	*	*	*	*	*		*	*	*	*	*			*	*	*		*	*
ROCK1				*	*	*	*	*	*	*		*	*	*	*	*			*	*	*		*	*
TUBB1		*	*	*	*	*	*	*	*	*		*	*	*	*	*			*	*	*		*	*
BRAF				*	*	*	*	*	*	*		*	*	*	*	*			*	*	*		*	*
TNK2				*	*	*	*	*	*	*		*	*	*	*	*			*	*	*		*	*
EPHB4				*	*	*	*	*	*	*		*	*	*	*	*			*	*	*		*	*
HSP90AA1				*	*	*	*	*	*	*		*	*	*	*	*			*	*	*		*	*
GAK				*	*	*	*	*	*	*		*	*	*	*	*			*	*	*		*	*
MDM2				*	*	*	*	*	*	*		*	*	*	*	*			*	*	*		*	*
CCND1 CDK4			*	*	*	*	*	*	*	*		*	*	*	*	*			*	*	*		*	*
CDK1 CCNB1			*	*	*	*	*	*	*	*		*	*	*	*	*			*	*	*		*	*
CCNE2 CDK2 CCNE1			*	*	*	*	*	*	*	*		*	*	*	*	*			*	*	*		*	*
GSK3B			*	*	*	*	*	*	*	*		*	*	*	*	*			*	*	*		*	*
GSK3A			*	*	*	*	*	*	*	*		*	*	*	*	*			*	*	*		*	*

Table S5. MolTarPred (Compounds 1-25)

Compounds	Targets	
	Vanilloid receptor (Homo sapiens)	Arachidonate 5-lipoxygenase (Homo sapiens)
N-G-1	+	+
N-G-2		
N-G-3		+
N-G-4		+
N-G-5		+
N-G-6		
N-G-7		+
N-G-8		
N-G-9		
N-G-10		+
N-G-11		+
N-G-12		
N-G-13		+
N-G-14		
N-G-15	+	+
N-G-16		
N-G-17		
N-G-18		+
N-G-19	+	+
N-G-20		+
N-G-21		
N-G-22		+
N-G-23		+
N-G-24		+
N-G-25		+
N-G-26		+
N-G-27		
N-G-28		
N-G-29		+
N-G-30	+	+
N-G-31		
N-G-32		
N-G-33		+
N-G-34		
N-G-35		
N-G-36		
N-G-37		
N-G-38		+
N-G-39		
N-G-40		+
N-G-41	+	+
N-G-42		
N-G-43	+	+
N-G-44		
N-G-45	+	
N-G-46		
N-G-47		+
N-G-48		
N-G-49		

Table S6. SEA online

Compounds	Targets																								
	APP	NDUFAB1	Adrb1	ADRB1	EP300	GPR174	LPAR1	IKBKG	NFE2L2	NFKB1	Ptger2	beta-tubulin	CXCL12	MAPT	TLR1	Tlr1	Tlr2	YWHAG	NDUFAB1	Erpp2	FOS	ALOX15	ALOX5	Alox5	Trpv2
N-G-1	*	*	*	*	*	*	*	*	*	*	*	*	*	*	*	*	*	*	*	*	*	*	*	*	*
N-G-2	*	*	*	*	*	*	*	*	*	*	*	*	*	*	*	*	*	*	*	*	*	*	*	*	*
N-G-3	*	*	*	*	*	*	*	*	*	*	*	*	*	*	*	*	*	*	*	*	*	*	*	*	*
N-G-4	*	*	*	*	*	*	*	*	*	*	*	*	*	*	*	*	*	*	*	*	*	*	*	*	*
N-G-5	*	*	*	*	*	*	*	*	*	*	*	*	*	*	*	*	*	*	*	*	*	*	*	*	*
N-G-6	*	*	*	*	*	*	*	*	*	*	*	*	*	*	*	*	*	*	*	*	*	*	*	*	*
N-G-7	*	*	*	*	*	*	*	*	*	*	*	*	*	*	*	*	*	*	*	*	*	*	*	*	*
N-G-8	*	*	*	*	*	*	*	*	*	*	*	*	*	*	*	*	*	*	*	*	*	*	*	*	*
N-G-9	*	*	*	*	*	*	*	*	*	*	*	*	*	*	*	*	*	*	*	*	*	*	*	*	*
N-G-10	*	*	*	*	*	*	*	*	*	*	*	*	*	*	*	*	*	*	*	*	*	*	*	*	*
N-G-11	*	*	*	*	*	*	*	*	*	*	*	*	*	*	*	*	*	*	*	*	*	*	*	*	*
N-G-12	*	*	*	*	*	*	*	*	*	*	*	*	*	*	*	*	*	*	*	*	*	*	*	*	*
N-G-13	*	*	*	*	*	*	*	*	*	*	*	*	*	*	*	*	*	*	*	*	*	*	*	*	*
N-G-14	*	*	*	*	*	*	*	*	*	*	*	*	*	*	*	*	*	*	*	*	*	*	*	*	*
N-G-15	*	*	*	*	*	*	*	*	*	*	*	*	*	*	*	*	*	*	*	*	*	*	*	*	*
N-G-16	*	*	*	*	*	*	*	*	*	*	*	*	*	*	*	*	*	*	*	*	*	*	*	*	*
N-G-17	*	*	*	*	*	*	*	*	*	*	*	*	*	*	*	*	*	*	*	*	*	*	*	*	*
N-G-18	*	*	*	*	*	*	*	*	*	*	*	*	*	*	*	*	*	*	*	*	*	*	*	*	*
N-G-19	*	*	*	*	*	*	*	*	*	*	*	*	*	*	*	*	*	*	*	*	*	*	*	*	*
N-G-20	*	*	*	*	*	*	*	*	*	*	*	*	*	*	*	*	*	*	*	*	*	*	*	*	*
N-G-21	*	*	*	*	*	*	*	*	*	*	*	*	*	*	*	*	*	*	*	*	*	*	*	*	*
N-G-22	*	*	*	*	*	*	*	*	*	*	*	*	*	*	*	*	*	*	*	*	*	*	*	*	*
N-G-23	*	*	*	*	*	*	*	*	*	*	*	*	*	*	*	*	*	*	*	*	*	*	*	*	*
N-G-24	*	*	*	*	*	*	*	*	*	*	*	*	*	*	*	*	*	*	*	*	*	*	*	*	*
N-G-25	*	*	*	*	*	*	*	*	*	*	*	*	*	*	*	*	*	*	*	*	*	*	*	*	*
N-G-26	*	*	*	*	*	*	*	*	*	*	*	*	*	*	*	*	*	*	*	*	*	*	*	*	*
N-G-27	*	*	*	*	*	*	*	*	*	*	*	*	*	*	*	*	*	*	*	*	*	*	*	*	*
N-G-28	*	*	*	*	*	*	*	*	*	*	*	*	*	*	*	*	*	*	*	*	*	*	*	*	*
N-G-29	*	*	*	*	*	*	*	*	*	*	*	*	*	*	*	*	*	*	*	*	*	*	*	*	*
N-G-30	*	*	*	*	*	*	*	*	*	*	*	*	*	*	*	*	*	*	*	*	*	*	*	*	*
N-G-31	*	*	*	*	*	*	*	*	*	*	*	*	*	*	*	*	*	*	*	*	*	*	*	*	*
N-G-32	*	*	*	*	*	*	*	*	*	*	*	*	*	*	*	*	*	*	*	*	*	*	*	*	*
N-G-33	*	*	*	*	*	*	*	*	*	*	*	*	*	*	*	*	*	*	*	*	*	*	*	*	*
N-G-34	*	*	*	*	*	*	*	*	*	*	*	*	*	*	*	*	*	*	*	*	*	*	*	*	*
N-G-35	*	*	*	*	*	*	*	*	*	*	*	*	*	*	*	*	*	*	*	*	*	*	*	*	*
N-G-36	*	*	*	*	*	*	*	*	*	*	*	*	*	*	*	*	*	*	*	*	*	*	*	*	*
N-G-37	*	*	*	*	*	*	*	*	*	*	*	*	*	*	*	*	*	*	*	*	*	*	*	*	*
N-G-38	*	*	*	*	*	*	*	*	*	*	*	*	*	*	*	*	*	*	*	*	*	*	*	*	*
N-G-39	*	*	*	*	*	*	*	*	*	*	*	*	*	*	*	*	*	*	*	*	*	*	*	*	*
N-G-40	*	*	*	*	*	*	*	*	*	*	*	*	*	*	*	*	*	*	*	*	*	*	*	*	*
N-G-41	*	*	*	*	*	*	*	*	*	*	*	*	*	*	*	*	*	*	*	*	*	*	*	*	*
N-G-42	*	*	*	*	*	*	*	*	*	*	*	*	*	*	*	*	*	*	*	*	*	*	*	*	*
N-G-43	*	*	*	*	*	*	*	*	*	*	*	*	*	*	*	*	*	*	*	*	*	*	*	*	*
N-G-44	*	*	*	*	*	*	*	*	*	*	*	*	*	*	*	*	*	*	*	*	*	*	*	*	*
N-G-45	*	*	*	*	*	*	*	*	*	*	*	*	*	*	*	*	*	*	*	*	*	*	*	*	*
N-G-46	*	*	*	*	*	*	*	*	*	*	*	*	*	*	*	*	*	*	*	*	*	*	*	*	*
N-G-47	*	*	*	*	*	*	*	*	*	*	*	*	*	*	*	*	*	*	*	*	*	*	*	*	*
N-G-48	*	*	*	*	*	*	*	*	*	*	*	*	*	*	*	*	*	*	*	*	*	*	*	*	*
N-G-49	*	*	*	*	*	*	*	*	*	*	*	*	*	*	*	*	*	*	*	*	*	*	*	*	*

Table S8. Predicted drug-likeness based on the RO5 including bioavailability (BA) and synthetic accessibility (SA) of the molecules

Compound code	Mol.wt	HBA	HBD	TPSA	iLOGP	NRB	BA Score	SA
N-G-1	294.39	4	2	66.76	3.48	10	0.55	2.81
N-G-2	194.18	4	2	66.76	1.62	3	0.85	1.93
N-G-3	164.2	2	1	29.46	2.37	3	0.55	1.58
N-G-4	152.15	3	1	46.53	1.57	2	0.55	1.15
N-G-5	368.38	6	2	93.06	3.27	8	0.55	2.97
N-G-6	178.23	2	0	18.46	2.65	4	0.55	1.71
N-G-7	164.2	2	1	29.46	2.38	2	0.55	1.81
N-G-8	166.17	3	1	46.53	1.82	3	0.55	1.37
N-G-9	168.15	4	2	66.76	1.4	2	0.55	1.42
N-G-10	166.17	3	1	46.53	1.77	2	0.55	1.36
N-G-11	192.21	3	1	46.53	2.11	3	0.55	2.13
N-G-12	284.26	5	2	79.9	2.4	2	0.55	2.95
N-G-13	166.22	2	1	29.46	2.46	3	0.55	1.4
N-G-14	198.17	5	3	86.99	1.21	3	0.55	2.2
N-G-15	276.37	3	1	46.53	3.28	9	0.55	2.51
N-G-16	300.39	3	1	46.53	2.92	1	0.55	3.52
N-G-17	358.39	6	2	85.22	2.47	6	0.55	3.3
N-G-18	154.16	3	2	49.69	1.79	2	0.55	1.26
N-G-19	194.23	3	1	46.53	2.09	4	0.55	1.52
N-G-20	196.2	4	1	55.76	1.98	3	0.55	1.65
N-G-21	138.16	2	1	29.46	1.94	1	0.55	1
N-G-22	182.17	4	2	66.76	1.18	3	0.85	1.49
N-G-23	150.17	2	1	29.46	2.14	2	0.55	1.45
N-G-24	338.35	5	2	83.83	2.78	7	0.55	2.82
N-G-25	178.18	3	1	46.53	1.75	3	0.55	1.88
N-G-26	180.2	3	2	49.69	2.16	3	0.55	1.86
N-G-27	358.47	4	0	36.92	4.31	9	0.55	3.32
N-G-28	182.17	4	3	77.76	0.86	3	0.55	1.2
N-G-29	194.23	3	1	38.69	2.46	4	0.55	1.87
N-G-30	278.39	3	1	46.53	3.65	10	0.55	2.28
N-G-31	362.42	6	4	99.38	2.98	9	0.55	3.21
N-G-32	372.41	6	1	74.22	2.8	7	0.55	3.43
N-G-33	152.19	2	1	29.46	2.21	2	0.55	1.18
N-G-34	182.17	4	1	55.76	2.13	3	0.55	1.67
N-G-35	196.2	4	1	55.76	1.98	4	0.55	1.85
N-G-36	152.15	3	1	46.53	1.6	2	0.55	1.16
N-G-37	178.23	2	1	29.46	2.63	3	0.55	1.89
N-G-38	286.28	5	3	86.99	1.7	4	0.55	2.8
N-G-39	300.26	6	3	100.13	2.38	2	0.55	3.02
N-G-40	368.38	6	3	96.22	3.21	7	0.55	3.42
N-G-41	372.41	6	2	93.06	3.21	10	0.55	2.45

Compound code	Mol.wt	HBA	HBD	TPSA	iLOGP	NRB	BA Score	SA
N-G-42	184.19	4	3	69.92	1.61	3	0.55	2.11
N-G-43	180.2	3	1	46.53	1.77	4	0.55	1.4
N-G-44	198.17	5	3	86.99	1.21	3	0.56	2.2
N-G-45	192.21	3	0	35.53	2.21	3	0.55	2.03
N-G-46	168.15	4	2	66.76	0.89	2	0.85	1.24
N-G-47	194.18	4	2	66.76	1.79	3	0.85	1.9
N-G-48	196.2	4	1	55.76	1.67	4	0.85	1.62
N-G-49	152.15	3	1	46.53	1.44	2	0.55	1.05

Table S9. Predicted ADME properties of molecules under study

Compound code	GI absorption	BBB permeant	Pgp substrate	CYP1A2 inhibitor	CYP2C19 inhibitor	CYP2C9 inhibitor	CYP2D6 inhibitor	CYP3A4 inhibitor
N-G-1	High	+	-	+	-	-	+	-
N-G-2	High	+	-	-	-	-	-	-
N-G-3	High	+	-	+	-	-	-	-
N-G-4	High	+	-	-	-	-	-	-
N-G-5	High	-	-	-	-	+	-	+
N-G-6	High	+	-	+	-	-	-	-
N-G-7	High	+	-	+	-	-	-	-
N-G-8	High	+	-	-	-	-	-	-
N-G-9	High	-	-	-	-	-	-	-
N-G-10	High	+	-	-	-	-	-	-
N-G-11	High	+	-	+	-	-	-	-
N-G-12	High	-	-	+	-	-	+	+
N-G-13	High	+	-	+	-	-	-	-
N-G-14	High	-	-	-	-	-	-	-
N-G-15	High	+	-	+	+	-	+	-
N-G-16	High	+	+	-	-	-	+	-
N-G-17	High	-	-	-	-	-	+	+
N-G-18	High	+	-	-	-	-	-	-
N-G-19	High	+	-	+	-	-	-	-
N-G-20	High	+	-	-	-	-	-	-
N-G-21	High	+	-	-	-	-	-	-
N-G-22	High	-	-	-	-	-	-	-
N-G-23	High	+	-	+	-	-	-	-
N-G-24	High	-	-	+	-	+	-	+
N-G-25	High	+	-	-	-	-	-	-
N-G-26	High	+	-	-	-	-	-	-
N-G-27	High	+	+	-	-	-	+	+
N-G-28	High	-	-	-	-	-	-	-
N-G-29	High	+	-	+	-	-	-	-
N-G-30	High	+	-	+	-	-	+	-
N-G-31	High	-	+	-	-	-	+	-
N-G-32	High	+	-	-	-	+	+	+
N-G-33	High	+	-	+	-	-	-	-
N-G-34	High	+	-	-	-	-	-	-
N-G-35	High	+	-	-	-	-	-	-
N-G-36	High	+	-	-	-	-	-	-
N-G-37	High	+	-	+	-	-	-	-
N-G-38	High	-	-	+	-	+	-	+
N-G-39	High	-	-	+	-	+	+	+
N-G-40	High	-	-	-	-	+	-	+
N-G-41	High	-	-	-	-	-	+	+
N-G-42	High	-	-	-	-	-	-	-
N-G-43	High	+	-	-	-	-	-	-
N-G-44	High	-	-	-	-	-	-	-
N-G-45	High	+	-	+	-	-	-	-
N-G-46	High	-	-	-	-	-	-	-
N-G-47	High	+	-	-	-	-	-	-
N-G-48	High	+	-	-	-	-	-	-
N-G-49	High	+	-	-	-	-	-	-

Table S10. The excretion properties of the studied compounds

Compound code	Total Clearance Log (ml/min/kg)	Renal OCT2 substrate
N-G-1	1.339	No
N-G-2	0.623	No
N-G-3	0.282	No
N-G-4	0.601	No
N-G-5	-0.002	No
N-G-6	0.338	No
N-G-7	0.221	No
N-G-8	0.642	No
N-G-9	0.628	No
N-G-10	0.62	No
N-G-11	0.16	No
N-G-12	0.18	No
N-G-13	0.244	No
N-G-14	0.446	No
N-G-15	1.44	No
N-G-16	0.719	No
N-G-17	0.147	No
N-G-18	0.215	No
N-G-19	0.307	No
N-G-20	0.641	No
N-G-21	0.202	No
N-G-22	0.246	No
N-G-23	0.233	No
N-G-24	0.026	No
N-G-25	0.183	No
N-G-26	0.233	No
N-G-27	0.197	No
N-G-28	0.245	No
N-G-29	0.293	No
N-G-30	1.411	No
N-G-31	0.248	No
N-G-32	0.214	No
N-G-33	0.232	No
N-G-34	0.687	No
N-G-35	0.769	No
N-G-36	0.159	No

Compound code	Total Clearance Log (ml/min/kg)	Renal OCT2 substrate
N-G-37	0.268	No
N-G-38	0.555	No
N-G-39	0.165	No
N-G-40	0.089	No
N-G-41	0.230	No
N-G-42	0.206	No
N-G-43	0.325	No
N-G-44	0.446	No
N-G-45	0.158	No
N-G-46	0.626	No
N-G-47	0.621	No
N-G-48	0.304	No
N-G-49	0.599	No

Table S11. Results of the cytotoxicity predictions by Way2Drug server on the tumor and non-tumor cell lines

	Cell-line	NCI-H322M	NCI-H226	PC-6	HOP-18	NCI-H187	DMS-114	Malme-3M	M14	SK-MEL-	M19-MEL
	Full name	Non-small cell	Non-small cell	Small cell lung	Non-small cell	Small cell lung ca	Lung carcin	Melanoma	Melanoma	Melanoma	Melanoma
Compound code	Tissue	Lung	Lung	Lung	Lung	Lung	Lung	Skin	Skin	Skin	Skin
	N-G-1	-									
	N-G-2	-									
	N-G-3	-									
	N-G-4	-				0.537					
	N-G-5	-									
	N-G-6	-									
	N-G-7	-									
	N-G-8	-									
	N-G-9	-									
	N-G-10	-									
	N-G-11	-									
	N-G-12	-									
	N-G-13	-									
	N-G-14	-					0.539				
	N-G-15	-									
	N-G-16	-									
	N-G-17	-									
	N-G-18	-									
	N-G-19	-									
	N-G-20	-									
	N-G-21	-			0.587						0.514
	N-G-22	-									
	N-G-23	-									
	N-G-24	-									
	N-G-25	0.7	0.64					0.646	0.564	0.514	
	N-G-26	-									
	N-G-27	-									
	N-G-28	-									
	N-G-29	-									
	N-G-30	-									
	N-G-31	-									
	N-G-32	-									
	N-G-33	-		0.628							
	N-G-34	-		0.534							
	N-G-35	-									
	N-G-36	-				0.741					
	N-G-37	-									
	N-G-38	-									
	N-G-39	-									
	N-G-40	-									
	N-G-41	-									
	N-G-42	-					0.512				
	N-G-43	-									
	N-G-44	-					0.539				
	N-G-45	-									
	N-G-46	-									
	N-G-47	-									
	N-G-48	-									
	N-G-49	-									

Table S11. Results of the cytotoxicity predictions by Way2Drug server on the tumor and non-tumor cell lines (Continued)

Cell-line	RPMI-8226	K562	Hs 683	SF-539	MDA-MB	MCF7	OVCAR-1	IGROV-1	PC-3	DU-145	SN12C	SNB-75	cytotoxicity on non-tumor cell line when pa>0.5
Full name	Multiple myeloma	Erythroleu	Oligodend	Glioblasto	Breast adenocarcin	Breast	Ovarian a	Ovarian a	Prostate c	Prostate c	Renal car	Glioblasto	
Tissue	Haematopoietic and lymph	Haematop	Brain	Brain	Breast	Breast	Ovarium	Ovarium	Prostate	Prostate	Kidney	Nervous s	
N-G-1													no
N-G-2		0.542						0.529					no
N-G-3													no
N-G-4													no
N-G-5													no
N-G-6													no
N-G-7													no
N-G-8													no
N-G-9													no
N-G-10		0.53											no
N-G-11		0.586											no
N-G-12													no
N-G-13													no
N-G-14													no
N-G-15					0.601								no
N-G-16				0.528	0.53						0.524		yes (on endothelium)
N-G-17													yes (on lung)
N-G-18			0.612										no
N-G-19													no
N-G-20		0.517								0.503			no
N-G-21			0.591										no
N-G-22													yes (on lung)
N-G-23													no
N-G-24													no
N-G-25	0.578												no
N-G-26													no
N-G-27													no
N-G-28													no
N-G-29													no
N-G-30													no
N-G-31													no
N-G-32													yes (on lung)
N-G-33													no
N-G-34													no
N-G-35													no
N-G-36			0.512										no
N-G-37													no
N-G-38		0.646											no
N-G-39													no
N-G-40									0.733				no
N-G-41													no
N-G-42							0.53		0.747				no
N-G-43					0.551								no
N-G-44													no
N-G-45			0.598									0.535	yes (on lung)
N-G-46													no
N-G-47		0.542						0.529					no
N-G-48													yes (on lung)
N-G-49													no

Table S12. Results of the toxicity prediction by ProTox-II server

Compound code	Organ Toxicity	Toxicity end points				Tox21 Stress response pathways	
	Hepatotoxicity	Carcinogenicity	Immunotoxicity	Mutagenicity	Cytotoxicity	(MMP)	p53
N-G-1	inactive(0.83)	inactive(0.76)	active(0.95)	inactive(0.65)	inactive(0.88)	inactive(0.59)	inactive(0.69)
N-G-2	inactive(0.51)	inactive(0.61)	active(0.91)	inactive(0.96)	inactive(0.88)	inactive(0.92)	inactive(0.93)
N-G-3	inactive(0.67)	inactive(0.73)	inactive(0.83)	inactive(0.97)	inactive(0.90)	inactive(0.98)	inactive(0.99)
N-G-4	inactive(0.52)	inactive(0.60)	inactive(0.55)	inactive(0.98)	inactive(0.94)	inactive(0.99)	inactive(1.0)
N-G-5	inactive(0.61)	inactive(0.84)	active(0.92)	inactive(0.88)	inactive(0.88)	active(1.0)	active(1.0)
N-G-6	inactive(0.65)	active(0.76)	inactive(0.92)	inactive(0.86)	inactive(0.89)	inactive(0.99)	inactive(0.99)
N-G-7	inactive(0.67)	active(0.55)	active(0.85)	inactive(0.97)	inactive(0.85)	inactive(0.97)	inactive(0.99)
N-G-8	inactive(0.69)	inactive(0.70)	inactive(0.68)	inactive(0.92)	inactive(0.90)	inactive(0.97)	inactive(0.99)
N-G-9	inactive(0.55)	inactive(0.64)	inactive(0.97)	inactive(0.96)	inactive(0.93)	inactive(0.93)	inactive(0.98)
N-G-10	inactive(0.52)	inactive(0.57)	inactive(0.78)	inactive(0.99)	inactive(0.94)	inactive(0.97)	inactive(0.99)
N-G-11	active(0.51)	inactive(0.59)	active(0.87)	inactive(0.87)	inactive(0.91)	inactive(0.96)	inactive(0.98)
N-G-12	inactive(0.72)	inactive(0.59)	active(0.92)	inactive(0.71)	inactive(0.89)	active(0.89)	inactive(0.88)
N-G-13	inactive(0.65)	inactive(0.54)	inactive(0.72)	inactive(0.83)	inactive(0.87)	inactive(0.91)	inactive(0.98)
N-G-14	inactive(0.6)	inactive(0.52)	inactive(0.95)	inactive(0.95)	inactive(0.92)	inactive(0.95)	inactive(0.99)
N-G-15	inactive(0.72)	inactive(0.74)	active(0.86)	active(0.67)	inactive(0.75)	inactive(0.68)	inactive(0.92)
N-G-16	inactive(0.73)	inactive(0.68)	active(0.98)	inactive(0.86)	inactive(0.83)	inactive(0.53)	inactive(0.76)
N-G-17	inactive(0.78)	inactive(0.61)	active(0.98)	inactive(0.72)	inactive(0.92)	active(0.63)	inactive(0.70)
N-G-18	inactive(0.87)	inactive(0.64)	inactive(0.78)	inactive(0.88)	inactive(0.93)	inactive(0.93)	inactive(0.98)
N-G-19	inactive(0.51)	inactive(0.73)	inactive(0.90)	inactive(0.89)	inactive(0.89)	inactive(0.93)	inactive(0.98)
N-G-20	inactive(0.55)	inactive(0.61)	inactive(0.78)	inactive(0.95)	inactive(0.94)	inactive(0.81)	inactive(0.99)
N-G-21	inactive(0.71)	active(0.61)	inactive(0.95)	inactive(0.98)	inactive(0.86)	inactive(0.99)	inactive(1.0)
N-G-22	inactive(0.61)	inactive(0.79)	inactive(0.94)	inactive(0.92)	inactive(0.91)	inactive(0.95)	inactive(0.98)
N-G-23	inactive(0.66)	inactive(0.61)	active(0.59)	inactive(0.97)	inactive(0.88)	inactive(0.98)	inactive(0.99)
N-G-24	inactive(0.61)	inactive(0.82)	active(0.94)	inactive(0.79)	inactive(0.85)	active(0.94)	active(0.80)
N-G-25	active(0.50)	inactive(0.63)	active(0.79)	inactive(0.85)	inactive(0.90)	inactive(0.97)	inactive(0.98)
N-G-26	inactive(0.82)	inactive(0.68)	active(0.76)	inactive(0.81)	inactive(0.93)	inactive(0.92)	inactive(0.96)
N-G-27	inactive(0.63)	inactive(0.57)	inactive(0.80)	inactive(0.75)	inactive(0.93)	active(0.52)	inactive(0.89)
N-G-28	inactive(0.67)	inactive(0.64)	inactive(0.99)	inactive(0.79)	inactive(0.86)	inactive(0.88)	inactive(0.95)
N-G-29	inactive(0.64)	inactive(0.63)	inactive(0.73)	inactive(0.72)	inactive(0.93)	inactive(0.97)	inactive(0.96)
N-G-30	inactive(0.71)	inactive(0.75)	active(0.62)	active(0.53)	inactive(0.80)	inactive(0.69)	inactive(0.93)
N-G-31	inactive(0.87)	inactive(0.70)	inactive(0.71)	inactive(0.80)	inactive(0.94)	inactive(0.58)	inactive(0.80)
N-G-32	inactive(0.74)	inactive(0.60)	active(0.98)	inactive(0.72)	inactive(0.94)	active(0.55)	inactive(0.84)
N-G-33	inactive(0.71)	active(0.53)	inactive(0.82)	inactive(0.93)	inactive(0.88)	inactive(0.98)	inactive(0.99)
N-G-34	active(0.52)	inactive(0.70)	inactive(0.92)	inactive(0.95)	inactive(0.96)	inactive(0.96)	inactive(0.99)
N-G-35	inactive(0.70)	inactive(0.74)	inactive(0.94)	inactive(0.87)	inactive(0.94)	inactive(0.91)	inactive(0.98)
N-G-36	inactive(0.55)	inactive(0.62)	inactive(0.68)	inactive(0.96)	inactive(0.93)	inactive(0.98)	inactive(1.0)
N-G-37	inactive(0.76)	inactive(0.62)	active(0.87)	inactive(0.78)	inactive(0.88)	inactive(0.92)	inactive(0.99)
N-G-38	inactive(0.62)	inactive(0.57)	active(0.97)	inactive(0.61)	inactive(0.86)	active(0.85)	inactive(0.53)
N-G-39	inactive(0.72)	inactive(0.68)	active(0.66)	inactive(0.94)	inactive(0.95)	active(0.92)	inactive(0.86)
N-G-40	inactive(0.58)	inactive(0.69)	active(0.93)	inactive(0.69)	inactive(0.97)	active(0.94)	active(0.56)
N-G-41	inactive(0.70)	inactive(0.71)	inactive(0.91)	inactive(0.75)	inactive(0.85)	active(0.78)	inactive(0.59)
N-G-42	inactive(0.94)	inactive(0.79)	active(0.52)	inactive(0.83)	inactive(0.92)	inactive(0.94)	inactive(0.97)
N-G-43	inactive(0.55)	inactive(0.72)	inactive(0.69)	inactive(0.87)	inactive(0.91)	inactive(0.92)	inactive(0.98)
N-G-44	inactive(0.6)	inactive(0.52)	inactive(0.95)	inactive(0.95)	inactive(0.92)	inactive(0.95)	inactive(0.99)
N-G-45	inactive(0.68)	active(0.64)	inactive(0.91)	inactive(0.79)	inactive(0.88)	inactive(0.96)	inactive(0.98)
N-G-46	inactive(0.55)	inactive(0.64)	inactive(0.96)	inactive(0.96)	inactive(0.93)	inactive(0.93)	inactive(0.98)
N-G-47	inactive(0.51)	inactive(0.61)	active(0.95)	inactive(0.96)	inactive(0.88)	inactive(0.92)	inactive(0.93)
N-G-48	active(0.50)	inactive(0.80)	inactive(0.97)	inactive(0.93)	inactive(0.92)	inactive(0.95)	inactive(0.97)
N-G-49	inactive(0.52)	inactive(0.60)	active(0.63)	inactive(0.98)	inactive(0.94)	inactive(0.99)	inactive(1.0)

Table S13. Results of the toxicity prediction by using pkCSM server

Compound code	Hepatotoxicity	hERG I inhibitor	hERG II inhibitor
N-G-1	no	no	no
N-G-2	no	no	no
N-G-3	no	no	no
N-G-4	no	no	no
N-G-5	no	no	no
N-G-6	no	no	no
N-G-7	yes	no	no
N-G-8	no	no	no
N-G-9	no	no	yes
N-G-10	no	no	no
N-G-11	no	no	no
N-G-12	no	no	no
N-G-13	yes	no	no
N-G-14	no	no	no
N-G-15	no	no	yes
N-G-16	no	no	no
N-G-17	no	no	yes
N-G-18	no	no	no
N-G-19	yes	no	no
N-G-20	no	no	no
N-G-21	no	no	no
N-G-22	no	no	no
N-G-23	no	no	no
N-G-24	no	no	yes
N-G-25	no	no	no
N-G-26	no	no	no
N-G-27	no	no	yes
N-G-28	yes	no	no
N-G-29	no	no	no
N-G-30	no	no	yes
N-G-31	no	no	yes
N-G-32	no	no	no
N-G-33	yes	no	no
N-G-34	no	no	no
N-G-35	no	no	no
N-G-36	no	no	no
N-G-37	no	no	no
N-G-38	no	no	no
N-G-39	no	no	no
N-G-40	no	no	no
N-G-41	no	no	yes
N-G-42	no	no	no
N-G-43	yes	no	no
N-G-44	no	no	no
N-G-45	yes	no	no
N-G-46	no	no	no
N-G-47	no	no	no
N-G-48	no	no	no
N-G-49	no	no	no

Mineral contents, Antioxidant and Antimicrobial Activities of Algerian *Terfezia claveryi* extracts

Hadjira GUENANE*, Boulanouar BAKCHICHE**, Ramazan ERENLER***, Ilyas YILDIZ****, Asmaa S. MOHAMED****, Maha A.M. El-SHAZLY*****

Mineral contents, Antioxidant and Antimicrobial activities of Algerian *Terfezia claveryi* extracts

SUMMARY

Terfezia species are known for their high nutritional value and diverse biological activities due to their unique chemical composition. The current study aims to evaluate the different extracts of *Terfezia claveryi* Chatin for their in vitro antioxidant, antibacterial, total phenolic content, total flavonoid content and mineral content. The antioxidant activity was evaluated via 1,1-diphenyl-2-picrylhydrazyl (DPPH), ABTS and phosphomolybdenum assays. While the in vitro antibacterial activity was evaluated via disc diffusion method against *Staphylococcus aureus* a Gram-positive bacteria as well as *Escherichia coli* and *Pseudomonas aeruginosa* as Gram-negative bacteria. The total phenolic content (TPC) and total flavonoid content (TFC) were evaluated via Folin-Ciocalteu's and $AlCl_3$ assays, respectively. The mineral content was evaluated via using atomic absorption spectrophotometer. In the antioxidant assays, the aqueous extract showed the most potent activity IC_{50}^{DPPH} equal to 0.09mg/mL, IC_{50}^{ABTS} equal to 0.24mg/mL and total antioxidant capacity equal to 0.10. Among all the tested extracts, the aqueous extract showed the highest TPC (176.67 mg GAE / g DW) and the highest TFC (14.53 mg ER / g DW). Obviously, the antioxidant activities are exist in a positive correlation with the TPC and TFC. On the other side, the tested extracts exhibited strong to moderate antibacterial activity against tested pathogenic microbial strains. The methanolic and aqueous extracts showed the most potent antibacterial activity against *Pseudomonas aeruginosa* with inhibition zones 21.91 and 15.79 mm, respectively. The extracts contain macroelements like Na (3293.01 mg·kg⁻¹dw) and K (21092.19 mg·kg⁻¹dw). Additionally, they contain micro-elements like Fe (16.45 mg·kg⁻¹dw), Cu (22.80 mg·kg⁻¹dw) and Ni (27.88 mg·kg⁻¹dw). LC/ESI-MS-MS was used to determine the chemical profile of the extract obtained from *Terfezia claveryi*. A total of seven phenolic compounds were selected. Rutin and hesperidin were primary compounds in the extract with 38.0089 and 22.4629 mg/g. In conclusion, *T. claveryi* extracts are considered promising sources of naturally occurring antioxidant and antimicrobial agents as well as their high nutritional values

Key Words: *Terfezia claveryi*, Antioxidant, Antimicrobial, Mineral content, TPC, TFC

Cezayir *Terfezia claveryi* Ekstrelerinin Mineral İçerikleri, Antioksidan ve Antimikrobiyal Aktiviteleri

ÖZ

Terfezia türleri, benzersiz kimyasal bileşimleri nedeniyle yüksek besin değeri ve çeşitli biyolojik aktiviteleriyle bilinmektedir. Bu çalışmada, *Terfezia claveryi* Chatin'in farklı ekstrelerinin in vitro antioksidan, antibakteriyel, toplam fenolik içerik, toplam flavonoid içeriği ve mineral içeriği açısından değerlendirilmesini amaçlamaktadır. Antioksidan aktivite 1,1-difenil-2-pikrilhidrazil (DPPH), ABTS ve fosfomolibden analizleri yoluyla değerlendirildi. İn vitro antibakteriyel aktivite, Gram-pozitif bakterilerden *Staphylococcus aureus*'ün yanı sıra Gram-negatif bakterilerden *Escherichia coli* ve *Pseudomonas aeruginosa*'ya karşı disk difüzyon yöntemiyle değerlendirildi. Toplam fenolik içerik (TPC) ve toplam flavonoid içeriği (TFC), sırasıyla Folin-Ciocalteu ve $AlCl_3$ analizleri ile değerlendirildi. Mineral içeriği atomik absorpsiyon spektrofotometresi kullanılarak değerlendirildi. Antioksidan analizlerinde sulu ekstre, DPPH radikaline karşı 0,09 mg/mL'ye eşit IC_{50} , ABTS radikaline karşı 0,24 mg/mL'ye eşit IC_{50} ve 0,10'a eşit toplam antioksidan kapasiteyi gösterdi. Test edilen tüm ekstreler arasında sulu ekstre en yüksek TPC'yi (176,67 mg GAE/g DW) ve en yüksek TFC'yi (14,53 mg ER/g DW) gösterdi. Antioksidan aktiviteler TPC ve TFC ile pozitif bir korelasyon içinde bulundu. Öte yandan, test edilen ekstreler, test edilen patojenik mikrobiyal türlere karşı güçlü ila orta dereceli antibakteriyel aktivite sergiledi. Metanolik ve sulu ekstreler, sırasıyla 21.91 ve 15.79 mm'lik inhibisyon bölgeleriyle *Pseudomonas aeruginosa*'ya karşı en güçlü antibakteriyel aktiviteyi gösterdi. Ekstraktlar Na (3293.01 mg·kg⁻¹dw) ve K (21092.19 mg·kg⁻¹dw) gibi makro elementler içermiştir. Ek olarak Fe (16,45 mg·kg⁻¹dw), Cu (22,80 mg·kg⁻¹dw) ve Ni (27,88 mg·kg⁻¹dw) gibi mikro elementler içerirler. *Terfezia claveryi* den elde edilen ekstraktın kimyasal profilini belirlemek için LC/ESI-MS-MS kullanıldı. Toplamda yedi fenolik bileşik belirlendi. Rutin ve hesperidin, 38.0089 ve 22.4629 mg/g ile ekstrakttaki ana bileşikti. Sonuç olarak, *T. claveryi* ekstraktlarının yüksek besin değerlerinin yanı sıra doğal olarak oluşan antioksidan ve antimikrobiyal ajanlar açısından da umut verici kaynaklar olduğu düşünülmektedir.

Anahtar Kelimeler: *Terfezia claveryi*, Antioksidan, Antimikrobiyal, Mineral içeriği, TPC, TFC

Received: 14.07.2023

Revised: 11.10.2023

Accepted: 16.10.2023

* ORCID: 0000-0002-3598-5343, Laboratory of Biological and Agricultural Sciences (LBAS), Amar Telidji University, Laghouat 03000, Algeria

** ORCID: 0000-0002-3124-5153, Laboratory of Biological and Agricultural Sciences (LBAS), Amar Telidji University, Laghouat 03000, Algeria

*** ORCID: 0000-0002-0505-3190, Department of Chemistry, Faculty of Arts and Sciences, Tokat, Gaziosmanpaşa University, 60240 Tokat, Turkey

**** ORCID: 0000-0003-1254-1069, Department of Chemistry, Faculty of Arts and Sciences, Tokat, Gaziosmanpaşa University, 60240 Tokat, Turkey

***** ORCID: 0000-0001-9397-0556, Medicinal Chemistry Department, Theodor Bilharz Research Institute, Kornaish El-Nile, Warrak El-Hadar, Imbaba (P.O. 30), Giza 12411, Egypt

***** ORCID: 0000-0002-8229-449x, Medicinal Chemistry Department, Theodor Bilharz Research Institute, Kornaish El-Nile, Warrak El-Hadar, Imbaba (P.O. 30), Giza 12411, Egypt

© Corresponding Author; Boulanouar BAKCHICHE

E-mail: b.bakchiche@lagh-univ.dz

INTRODUCTION

Desert truffles are edible fungi with important gastronomic, nutritional and medicinal properties, locally named « terfess ». They are mostly endemic to semi-arid and arid areas of Arabian Peninsula, the North-Africa and Mediterranean Region (Kagan-Zur and Roth Bejerano, 2008). Desert truffles grow in arid desert climate characterized by very hot summers with high humidity and relatively cooler winters (Mandeel and Al-Laith, 2007). They are socio-economically important fungi and are widely consumed in North Africa (Morocco, Algeria, Tunisia and Egypt) and in the Middle East (Saudi Arabia, Kuwait, Iraq, Iran, Lebanon, Syria and Jordan), the productive area of desert truffles are characterized by its aridity and high average temperatures. At Northern Sahara of Algeria, three species of desert truffles have been identified: *Tirmania nivea* (Desf.) (Trappe 1971), *Terfezia arenaria* (Moris, 1829) Trappe 1971 and *Terfezia claveryi* Chatin 1892 (Bradai et al., 2014).

The main nutritional constituents of truffle are carbohydrates, followed by proteins (Dahham et al., 2018, Khalifa et al., 2019; Lee et al., 2020). Most of their carbohydrates are considered dietary fibers such as chitin, -glucans and other polysaccharides, and they also include mannitol and trehalose (Tejedor-Calvo et al., 2020) as well as smaller sugars such as D-glucose, D-mannose or D-galactose (Tejedor-Calvo et al., 2020). Although truffles show low fat levels, their lipid content is important since they are involved in flavor and aroma properties. To maintain their hyphal membranes it is necessary to obtain unsaponifiable molecules such as ergosterol (ergosta-5,7,22-trienol), ergosta7,22-dienol, stigmasterol or ergosta-5,8-dieno-3-ol (Harki et al., 1996; Tang et al., 2012). Brassicasterol (ergosta-5,22-dienol) is also frequently detected in truffles; however, it is mainly reported in plants and algae species but is also found in species belonging to the subphylum Taphrinomycotina, a dimorphic plant parasite (Weete et al., 2012). Recently, truffles have shown interesting bioactive compounds, and their potential

bioactivities are now being studied, e.g., antitumoral, antioxidant, immunomodulatory and hypoglycemic properties (Tejedor-Calvo et al., 2020; Bhotmange et al., 2019; Mudliyar et al., 2019; Farzaneh et al., 2018; Zhao et al., 2014). Therefore, the aim of this study is to evaluate the antioxidant, antibacterial activities and mineral analysis of different extracts of *T. claveryi*. Also, the phytochemical investigation was performed using LC-MS/MS.

MATERIALS AND METHODS

Sample extraction

T. claveryi truffles were collected from the Algerian northern Sahara region, cleaned, peeled, and sliced. The samples were dried in an oven at (35-40 °C) and ground mechanically. Approximately 10 g of the sample was extracted separately with 100 mL of different solvents (water, ethyl acetate, ethanol, methanol, acetone and chloroform) using the maceration method. The extracts were filtered and concentrated using a rotary evaporator (Buchi, USA) at 40 °C. Extracts were stored at -20 °C for further analysis.

Total phenolic content (TPC)

The concentration of total phenolic compounds was measured according to Bakchiche et al., 2022 with some modifications. A 0.1 mL sample of extract was mixed with 0.2 mL of Folin-Ciocalteu's phenol reagent and 2 mL of water. The mixture was shaken and allowed to stand for 3 min, before addition of 1 mL of Na₂CO₃ (20 %). After the addition, the solution was incubated in the dark at room temperature for 30 min. Finally, the absorbance of the solution was measured at 765 nm and compared to a gallic acid calibration curve.

Total flavonoid content (TFC)

Total flavonoids were assessed using the method reported by Sun et al. with some modifications. A 1 mL sample of extract was mixed with 1 mL of 2% methanolic AlCl₃. The solution was incubated at room temperature for 10 min. Finally, the absorbance of the solution was measured at 430 nm.

Assay of DPPH scavenging activity

The DPPH radical scavenging activity was determined by a spectrophotometric method based on the reduction of methanol solution of 1,1-diphenyl-2-picrylhydrazyl (DPPH). 200 μ L of each extract at different solvents was added to 1.8 mL methanolic solution of DPPH (0.2 mM). The mixture was allowed to react at room temperature in the dark for 30 min. After 30 min, the absorbance (A) was measured at 517 nm. The experiment was repeated for three times for each test sample (Apriliyanti et al., 2020). IC₅₀ values denote the concentration of sample which is required to scavenge 50% of DPPH free radicals. DPPH free radical-scavenging activity was calculated according to the following equation: DPPH radical-scavenging activity (%) = $(\text{Abs}_{\text{control}} - \text{Abs}_{\text{sample}}) / (\text{Abs}_{\text{control}}) \times 100$. Where Abs_{control} is the absorbance of DPPH radical + methanol; Abs sample is the absorbance of DPPH radical + sample extract / standard.

ABTS cation radical scavenging assay

ABTS radical scavenging activity was determined according to the method by Bakchiche et al., 2022 The ABTS⁺ solution was prepared and stored in the dark at room temperature for 16 h. Then, 1 mL of the solution was diluted with 40 mL deionized water to yield working ABTS⁺ solution with an absorbance equal to 0.70 ± 0.02 at 734 nm. To 1.485 mL ABTS⁺ working solution, 15 μ L test samples were added. After 10 min, the absorbance of the plate was read at 734 nm.

ABTS free radical-scavenging activity was calculated according to the following equation: ABTS radical-scavenging activity (%) = $(\text{Abs control} - \text{Abs sample}) / (\text{Abs control}) \times 100$. Where Abs control is the absorbance of ABTS radical + methanol; Abs sample is the absorbance of ABTS radical + sample extract / standard. The lower value of IC₅₀ has the most critical antioxidant activity.

The extract concentration providing 50% radical scavenging activity (IC₅₀) was calculated from the graph of ABTS⁺ scavenging effect percentage against extract concentration. Trolox was used an antioxidant standard for comparison of the activity.

Evaluation of total antioxidant activity by phosphomolybdenum method

The total antioxidant capacity of the extracts was evaluated according to the method described by Saravanakumar et al. (2021). An aliquot of 0.3 mL of samples solution was combined with 3 mL of reagent solution (0.6 M sulfuric acid, 28 mM sodium phosphate, and 4 mM ammonium molybdate). In case of blank, 0.5 mL of 45% ethanol was used in place of sample. The tubes were incubated in a boiling water bath at 95 °C for 90 min. After the samples were cooled to room temperature, the absorbance of the aqueous solution of each sample was measured at 695 nm against blank in UV-2450 spectrophotometer (Shimadzu, Japan). The total antioxidant activity was expressed as the absorbance of the sample at 695 nm. The higher absorbance value indicated higher antioxidant activity.

Antimicrobial assay

Microbial strains

All the microorganisms were obtained from the laboratoire de Microbiologie, Department of Biology, University AMAR TELIDHI-LAGHOUAT. One Gram-positive bacteria (*Staphylococcus aureus* ATCC 25923) and two Gram-negative bacteria (*Escherichia coli* ATCC 25922, *Pseudomonas aeruginosa* ATCC 27853) were chosen as test bacteria.

Inoculum preparation

The bacterial strains were grown overnight at 37 °C in Nutrient Agar. Inoculum for the assays was prepared by inoculating three to five colonies from the agar plate culture into 10 mL of nutrient broth and then incubated at 37 °C for 24h. After growing, the microbial suspension was standardized with sterile saline to turbidity equivalent to 0.5 Mc Farland scale (108 CFU/mL for bacteria and 106 CFU/mL for *C. albicans*).

Antimicrobial activity

The antimicrobial tests were carried out by the disc diffusion method (Alpay et al., 2019) using 100

μL of suspension containing 106 per/mL of bacteria, inoculated into Mueller Hinton Agar (Difco). The discs (6 mm) were then impregnated with 100 μL of extract and then placed on the inoculated agar. Petridishes were prepared at 4 °C for 2 h, standard discs of Gentamycin (10 $\mu\text{g}/\text{disc}$), Tetracycline (10 $\mu\text{g}/\text{disc}$) and Ampicillin (10 $\mu\text{g}/\text{disc}$) were used as positive controls for bacteria whereas DMSO discs were used as a negative control. Then, the inoculated plates were incubated at 37 ± 0.1 °C for 24 h for bacterial strains. At the end of the incubation period, the inhibition zones were measured.

Mineral analysis

Each truffle sample was air-dried at room temperature and drying was finished at 105 °C overnight, crushed with a mortar and pestle. About 1 g of truffle dry matter was weighed in a crucible and was ashed at 550 °C. The ash was then dissolved in 5 mL of HCl (20%) and the solution was transferred to a 50 mL volumetric flask, the final volume was achieved with deionized water and then all was filtered. Analysis of the trace metals was carried out using an atomic absorption spectrophotometer (Vahdani et al., 2017).

Phytochemical investigation

LC-MS/MS

A stock solution of standard compounds were prepared by dissolving them in methanol (1.0 mg/ml) and then diluted to 0.8 $\mu\text{g}/\text{ml}$. after serial dilution of standard mixture, titration levels were separated. The solutions of *Terezia clavary* were prepared as 2.0 mg/ml. finally; they were filtered (0.45 μm) and pipette to vials for LC-MS/MS analysis (Atalar et al., 2021, Erenler et al., 2023). The standard compounds are Shikimic acid (1), Gallic acid (2), Protocatechuic acid (3), Epigallocatechin(4), Catechin(5), Chlorogenic acid(6), Hydroxybenzaldehyde (7), Vanillic acid (8), Caffeic acid (9), Syringic acid (10), Caffein (11), Vanillin (12), o-coumaric acid (13), Salicylic acid (14), Taxifolin (15), Resveratrol (16), Polydatine (17), *trans*-ferulic acid (18), Sinapic acid (19), Scutellarin (20), p-coumaric acid (21), Coumarin

(22), Protocatehuic ethyl ester (23), Hesperidin (24), Isoquercitrin (25), Rutin (26), Quercetin-3-xyloside (27), Kaempferol-3-glucoside (28), Fisetin (29), Baicalin (30), Chrysin (31), Daidzein (32), *trans*-cinnamic acid (33), Quercetin (34), Naringenin (35), Silibinin (36), Hesperetin (37), Morin (38), Kaempferol (39), Baicalein (40), Luteolin (41), Biochanin A (42), Capcaicin (43), Dihydrocapcaicin (44), and Diosgenin (45).

LC-MS/MS conditions

Quantitative analysis of natural compounds in methanol extract was performed using the spectrophotometer (An Agilent Technologies 1260 Infinity II, jonted 6460 Triple Quad mass spectrophotometre (Spectrometer). A Poroshell 120 EC-C18 (100 mm x 4.6 mm I.D., 2.7 μm) column was used 0.1% formic acid and 5.0 mM ammonium formate in water A, 0.1% formic acid, and 5.0 mM ammonium formate in methanol B mobile phase were used. The flow rate was modified to 0.4 mL/min. The gradient program fixed as 15% for 1-12 min, 50% for 12-30 min, 90% for 30-32 min, and 10% for 32-35 min was applied in the mobile phase B. The injection volume was 4.0 μL and the column temperature was 40 °C. The mass ratio in compound to ion (m/z) was determined by negative and positive ionization modes using an electrospray ionization (ESI) source. The capillary voltage was set at 4000 V, nebulizing gas (N) flow was 11 L/min, the nebulizer pressure was 15 psi, and the gas temperature was 300 °C. Each compound's precursor and product ions, collision energies, and cleavage voltage were detected for quantitative analysis as a multiplex reaction control.

Statistical analysis

Data were analyzed with a statistical software program (SPSS 21). Comparisons between multiple numeric data sets were performed using one-way ANOVA followed by Tukey multiple-range test. Results are expressed as mean \pm SEM., and statistical significance was accepted at $P < 0.05$.

RESULTS AND DISCUSSION

Extraction yields (%)

Herein, the collected *T. claveryi* materials were extracted separately with different solvents in descending polarity. The extraction yield (%) was recorded in which the aqueous extract showed the

highest yield (40 %), followed by the methanolic extract (19.0 %). The extraction yields of the rest the extracts are in the order: of ethanolic (11.4%), ethyl acetate (10.1 %), acetone (9.4%), and chloroform extract (4.5 %) (Table 1). The high yields of the *T. claveryi* may be due to their high amounts of phenolic components, soluble sugars, and sugar alcohols.

Table 1. Extraction yields (%) of *T. claveryi* extracts

<i>T. claveryi</i> extracts	Yields (%)
Aqueous	40 %
Methanolic	19 %
Ethanolic	11.4 %
Acetone	9.4 %
Ethyl acetate	10.1 %
Chloroform	4.5 %

Total phenolic and flavonoid contents (TPCs & TFCs)

Polyphenols have a unique chemical structure that combines aromatic properties and a high density of hydroxyl groups, which gives them strong activity as free radical scavenging agents. Accordingly, there is a positive correlation between the presence of polyphenols in the tested extracts and their

antioxidant activities (Ghareeb et al., 2018 a; Hamed et al., 2020). The total phenolic and flavonoid contents of the investigated extract are present in Table 2, the TPCs were ranged from 176.67 to 19.92 mg GAE / g DW and the TFCs were ranged from 14.53 to 1.71 mg ER / g DW. The standard curve is shown in Figure 1.

Table 2. Total phenolic and flavonoids contents in *T. claveryi* extracts

<i>T. claveryi</i> extracts	Total phenolic content (mg GAE / g DW)	Total flavonoids content (mg RE / g DW)
Aqueous	176.67 ± 6,48 ^a	14.53 ± 0,53 ^a
Methanolic	58.89 ± 3,00 ^c	4.89 ± 0,25 ^c
Ethanolic	19.92 ± 1,47 ^d	1.71 ± 0,12 ^d
Acetone	117.05 ± 11,16 ^b	9.65 ± 0,91 ^b
Ethyl acetate	97.86 ± 6,55 ^b	8.08 ± 0,54 ^b
Chloroform	---	---

Each value in the table is represented as mean ± SE (n = 3). GAE, gallic acid equivalents; RE, rutin equivalents; dw, dry weight. Means followed by the same letter are not different according to ANOVA (analysis of variance) (p < 0.05). The results are sorted in decreasing order: a > b > c > d.

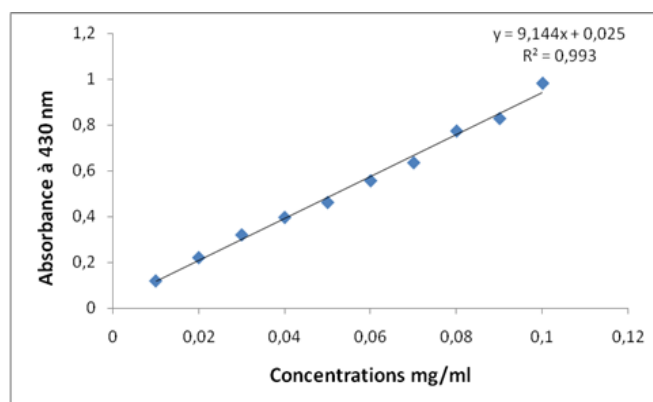


Figure 1. Rutin calibration curve.

In vitro antioxidant activities

Free radicals are highly energetic active molecules that cause many health problems when they penetrate the human cells, it is also considered the main cause of cardiovascular and cancer diseases (Ghareeb et al., 2018 a,b; Khalaf et al., 2021). Natural products have a great role in mitigating the side effects of free radicals and as a safe source of natural antioxidants (Ghareeb et al., 2018 c; Nasr et al., 2018; Sobeh et al., 2018). The antioxidant activities are mainly due to the presence of bioactive ingredients like polyphenolics and others (Bakchiche et al., 2019, 2022; Khalaf et al., 2019; Abdelfattah et al., 2022).

The results presented in Table 3 reveal that the different extracts of *T. claveryi* showed antioxidant activity against DPPH free radical expressed in IC_{50} (mg/ mL) in the order: Aqueous (0.09), methanolic (0.87), ethyl acetate (1.53), ethanolic (2.86), acetone (3.09), and chloroform (6.53) compared to vitamin C (0.001). Also, the extracts exhibited antioxidant effects against ABTS radical with IC_{50} values ranged from 0.24 to 4.24 compared to Trolox (0.033). While in the phosphomolybdate assay the values were ranged from 0.10 to 0.001.

Reviewing the literature revealed that the methanol extract of Turkish *T. claveryi* showed total phenolic content value of 0.0084 mgGAE/mg extract (Taşkın et al., 2018). While, the aqueous methanolic extract of Algerian *T. claveryi* showed total phenolic content value of 15.4 ± 0.11 mg GAE/g) and total flavonoid content value of 12.03 ± 0.27 mg CE/g (Wahiba et al., 2016). On the other side, several previous studies demonstrated the ability of *Terfezia* extracts to scavenge free radicals and as a vital source of antioxidants (Dundar et al., 2012; Taşkın et al., 2018; Wu et al., 2022). The Aqueous extract exhibited an antioxidant effect using DPPH and ABTS assays with an IC_{50} value of 0.09 and 0.24 mg/ml, respectively. Neggaz et al. (2015) reported that the methanolic extract of Algerian *T. claveryi* showed strong free radical scavenging activity against DPPH radical with IC_{50} value of 8.56 mg/mL. Moreover, the methanolic extract of *T. claveryi* from Algeria exhibited antiradical activity with IC_{50} value of 1.02 mg/mL (Wahiba et al., 2016).

Table 3. Antioxidant activity of the phenolic extracts for *T. claveryi* extracts, expressed in IC₅₀ (mg/mL) for DPPH and ABTS assay, VCEAC (vitamin C equivalents mmol of vitamin C/ g dry weight) for Phosphomolybdate assay

<i>T. claveryi</i> extracts	IC ₅₀ /DPPH (mg/mL)	IC ₅₀ /ABTS (mg/mL)	Phosphomolybdate assay
Aqueous	0.09±0.01 ^a	0.24±0.05 ^a	0.10±0.02 ^a
Methanolic	0.87±0.17 ^{a,b}	0.33±0.09 ^a	0.01±0.001 ^b
Ethanollic	2.86±0.07 ^c	4.24±0.21 ^d	0.03± 0.006 ^b
Acetone	3.09±1.01 ^c	2.01±0.09 ^c	0.005± 0.0005 ^c
Ethyl acetate	1.53±0.07 ^b	1.30±0.28 ^b	0.007± 0.001 ^c
Chloroform	6.53±0.23 ^d	-----	0.001±0.002 ^c
Vitamin C	0.001±5.98E ^{-05a}	-----	-----
Trolox	-----	0.003±0.0002 ^a	-----

Values are presented as mean ± standard error of three replicates. Values followed by the same letter within a column are not statistically different according to Tukey’s multiple range test.

In vitro antimicrobial activity

The rapid spread of infectious microbial diseases as a result of bad habits and also as a result of the fierce resistance of some microbial strains to current antibiotics encouraged scientists to search for alternative natural sources to obtain promising and safe antibiotics (Ghareeb et al., 2015; Mohammed et al., 2019; Abdel-Motleb et al., 2022; El-Shazly et al., 2022). Natural extracts have a long history in eliminating infectious diseases, especially their activities against pathogenic microbial strains (El-Neekety et al., 2016; Ghareeb et al., 2016a,b; Hathout et al., 2016; Saad et al., 2017; Abdel-Aziz et al., 2018; Elkhouly et al., 2021a,b).

Our current findings showed that the different extracts of *T. claveryi* showed variable antimicrobial activities against *Pseudomonas aeruginosa*, *Escherichia coli* and *Staphylococcus aureus* with inhibition zones ranged from 5.80 to 21.91 mm, from 4.43 to 13.53 mm and from 4.53 to 6.67 mm, respectively. The methanolic extract exhibited the most potent antimicrobial activity against *Pseudomonas aeruginosa* with inhibition zone value of 21.91 mm followed by the aqueous extract with inhibition zone value of 15.79 mm. Also, the methanol and aqueous extracts showed the strongest effects against *Escherichia coli*

with inhibition zones value of 13.53 and 12.68 mm, respectively. All extracts showed a moderate effect against *Staphylococcus aureus* (Table 4).

Among the tree different types of antibiotics used in the study, Gentamycin has wide range of impact on all the three species of human pathogenic bacteria. The maximum zone of inhibition was observed against *Pseudomonas aeruginosa*. The maximum zone of inhibition was obtained using Gentamycin (25.12 mm) against *Pseudomonas aeruginosa*, (16.35 mm) against *Escherichia coli* and (11.85 mm) against *Staphylococcus aureus* whereas the minimum zone of inhibition was exhibited in Ampicillin (8.25 mm) against *Staphylococcus aureus* (Table 4). Altogether, the antibiotics Gentamycin, Tetracycline and Ampicillin have higher antimicrobial activity on the selected test organisms.

Previous reports revealed that different *Terfezia* species showed strong antimicrobial activities against various pathogenic microbial strains due to the presence of several bioactive compounds (İnci and Kirbağ, 2018; Neggaz et al., 2019; Ghareeb et al., 2020). Dib-Bellahouel and Fortas (2019) reported that the extract of the culture filtrate of *T. claveryi* inhibits the growth of *Gliocladium roseum*, *Candida albicans* and *Staphylococcus aureus* with inhibition

zone values of 11, 23 and 10.8 mm, respectively. The acid-soluble protein extract of *T. claveryi* exhibited an antimicrobial effect against gram-positive and gram-negative phytopathogenic bacteria including *Pseudomonas corrugate* (CFBP 5454), *Pseudomonas mediterranea* (CFBP 5447T), *Pectobacterium carotovorum* (CFBP 2046T), *Pectobacterium syringae* (PVCT 28.3.1), *Clavibacterium higanensis* (PVCT 156.1.1) and *Xanthomona vesicatoria* (CFBP 2537T) with inhibition zone values of 0.38, 0.40, 0.33, 0.52, 1.26 and 1.88 cm, respectively (Gargano et al., 2017). Moreover, the aqueous extract of *T. claveryi* showed antibacterial activity against three strains of *P. aeruginosa* including *P. aeruginosa* ATCC14028, *P. aeruginosa* ATCC 27853 and *P. aeruginosa* ATCC 9027 with inhibition zone values of 21.0, 28.0 and 19.0 mm, respectively (Saddiq et al., 2016). Alhussaini et

al (2016) reported that the methanol extract of Saudi *T. claveryi* showed antibacterial activity against some bacterial strains including *Staphylococcus aureus*, *Bacillus subtilis*, *Escherichia coli* and *Pseudomonas aeruginosa* with inhibition zone values of 5.0, 4.0, 5.0 and 4.0 mm, respectively. Additionally, the aqueous extract of *T. claveryi* showed antibacterial effect against *Staphylococcus aureus* (ATCC 6538), *Staphylococcus epidermidis* (ATCC 12228), *Streptococcus faecalis*, *Escherichia coli* (ATCC 29425), *Pseudomonas aeruginosa* (ATCC 9027), *Proteus vulgaris* (ATCC 8427) and *Klebsiella pneumonia* (ATCC 13883) with inhibition zone values of 19.0, 18.0, 17.0, 15.33, 20.33, 15.33 and 14.66 mm, respectively (Aldebasi et al., 2013). In addition, it is noted for its antimicrobial and antioxidant activities, *T. claveryi* is strongly affected by the nature of the solvents used.

Table 4. Diameter of zone of inhibition of *T. claveryi* extracts

<i>T. claveryi</i> extracts	Gram (-)		Gram (+)
	<i>Pseudomonas aeruginosa</i> ATCC 23853	<i>Escherichia coli</i> ATCC 23822	<i>Staphylococcus aureus</i> ATCC 23823
Zone of inhibition (mm)			
Aqueous	15.79	12.68	5.67
Methanolic	21.91	13.53	4.53
Acetone	7.67	5.43	4.88
Ethyl acetate	10.96	7.45	6.67
Chloroform	5.80	4.43	4.65
Ampicillin	23.85	15.36	8.25
Gentamycin	25.12	16.35	11.85
Tetracycline	24.54	14.21	10.51

Mineral content

Different *Terfezia* species contain important nutritional components for the growth of the human body, especially the mineral elements (Dundar et al., 2012; Wahiba et al., 2016; Khlaif et al., 2021). Herein,

the truffle extracts showed a varied mineral content including macroelements like Na (3293.01mg·kg⁻¹dw) and K (21092.19mg·kg⁻¹dw). Also, there are microelements like Fe (16.45 mg·kg⁻¹dw), Cu (22.80 mg·kg⁻¹dw), and Ni (27.88 mg·kg⁻¹dw). While, other elements like Pb, Cd, and Co are absent (Table 5).

Table 5. Mineral content of truffle extracts

	Truffle extracts
	Macroelements (mg·kg⁻¹dw)
Na	3293.01±95.04 ^b
K	21092.19±96.67 ^a
	Micro-elements (mg·kg⁻¹dw)
Fe	16.45± 0.008 ^c
Cu	22.80± 0.27 ^c
Ni	27.88±0,40 ^c
Pb	ND
Cd	ND
Co	ND

Values are presented as mean ± SE (n = 3). Different letters above the average bars denote significant differences at p < 0.05 - Tukey's test.

Phytochemical investigation using LC-MS/MS

LC-MS/MS analysis was performed on the methanol extract of *T. claveryi* in order to determine the chemical components compared to 46 standards (Table 6). The analysis showed the presence of six compounds viz., caffeine, scutellarin, hesperidin, isoquercitrin, rutin, quercetin-3-xyloside, and morin. These compounds were identified in the extract at contents equal to 0.9229, 0.0322, 22.4629, 1.2009, 38.0089, 2.5611, and 0.0358 mg/g, respectively. Rutin and hesperidin were dominant in the extract (Figures 2, 3 and Table 7). Our current findings are in agreement to some extent with the previous reports. Al-Atassi et al. (2022) stated that LC-MS/MS analysis of 70% ethanolic extract of *T. claveryi* led to identification of 14 compounds belonging to phenolic acids and flavonoids including

p-hydroxy benzoic acid, syringic acid, *trans*-cinnamic acid, p-coumaric acid, gallic acid, homogentisic acid, protocatechuic acid, vanillin, ferulic acid, rutin, vanillic acid, apigenin, catechin, and hesperidin. In the same context, UPLC-ESI-MS analysis of the *T. claveryi* aqueous extract led to identification of some phenolic, organic and fatty acids including succinic acid, coumaric acid, vanillic acid, scopoletin, palmitic acid, *trans*-vaccenic acid, and stearic acid as well as protocatechuic aldehyde (Abu-Odeh et al., 2022). Additionally, Vahdani et al (2017) reported that HPLC investigation of *T. claveryi* led to detection of several phenolic compounds including gallic acid, catechin, chlorogenic acid, rutin, p-coumaric acid, hesperidin, and eugenol.

Table 6. Phenolic content of *T. claveryi* extract using LC/ESI-MS-MS

Peak No.	Compound name	RT (min)	Content (mg/g)
1	Shikimic acid	1.406	ND
2	Gallic acid	3.292	ND
3	Protocatechuic acid	5.537	ND
4	Epigallocatechin	6.878	ND
5	Catechin	6.880	ND
6	Chlorogenic acid	7.498	ND
7	Hydroxybenzaldehyde	7.791	ND
8	Vanillic acid	7.860	ND
9	Caffeic Acid	7.875	ND
10	Syringic acid	8.383	ND
11	Caffein	8.404	0.9229
12	Vanillin	8.631	ND
13	o-coumaric acid	9.628	ND
14	Salicylic Acid	9.316	ND
15	Taxifolin	9.921	ND
16	Resveratrol	9.545	ND
17	Polydatine	9.975	ND
18	Trans-ferulic acid	10.323	ND
19	Sinapic acid	10.424	ND
20	Scutellarin	11.289	0.0322
21	p-coumaric acid	11.427	ND
22	Coumarin	11.525	ND
23	Protocatehuic ethyl ester	11.496	ND
24	Hesperidin	12.094	22.4629
25	Isoquercitrin	12.110	1.2009
26	Rutin	12.078	38.0089
27	Quercetin-3-Xyloside	12.676	2.5611
28	Kaempferol-3-glucoside	13.443	ND
29	Fisetin	13.461	ND
30	Baicalin	13.637	ND
31	Chrysin	14.204	ND
32	Daidzein	14.263	ND
33	Trans-cinnamic acid	14.281	ND
34	Quercetin	15.074	ND
35	Naringenin	15.184	ND
36	Silibinin	15.211	ND
37	Hesperetin	15.983	ND
38	Morin	15.845	0.0358
39	Kaempferol	16.599	ND
40	Baicalein	17.135	ND
41	Luteolin	18.002	ND
42	Biochanin A	17.926	ND
43	Capcaicin	18.245	ND
44	Dihydrocapcaicin	18.817	ND
45	Diosgenin	23.601	ND

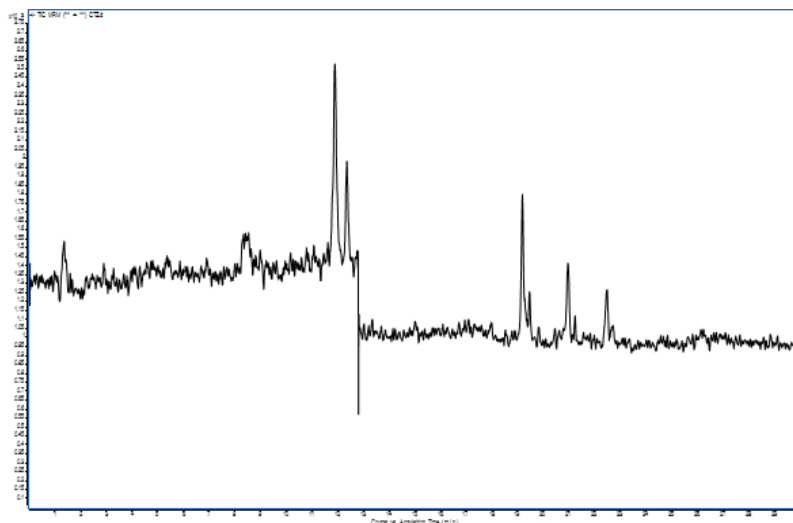


Figure 2. LC-MS chromatogram of *T. claveryi* extract

Table 7. Detected compounds in the methanol extract using LC-MS/MS

Peak No.	Name	RT (min)	Content (mg/g)	Classification	Reported bioactivity	References
1	Caffein	8.404	0.9229	Alkaloids	Anti-inflammatory, antiapptotic and antioxidant	Saud and Salamatullah, 2021
2	Scutellarin	11.289	0.0322	Flavonoids	Antioxidant, antimicrobial, anti-rheumatoid, and anti-coagulation	Vesaghhamedani et al., 2023
3	Hesperidin	12.094	22.4629	Flavonoids	Antiradical, antioxidant, and anti-cancer	Öngün et al., 2021
4	Isoquercitrin	12.110	1.2009	Flavonoids	Antioxidant	Razavia et al., 2009
5	Rutin	12.078	38.0089	Flavonoids	Antioxidant	-
6	Quercetin-3-xyloside	12.676	2.5611	Flavonoids	Antioxidant	-
7	Morin	15.845	0.0358	Flavonoids	Antioxidant Anti-lipid peroxidation, antifungal, anticancer, and treatment diabetes mellitus	Hussain et al., 2014; Yang and Lee, 2012; Nazir et al., 2021

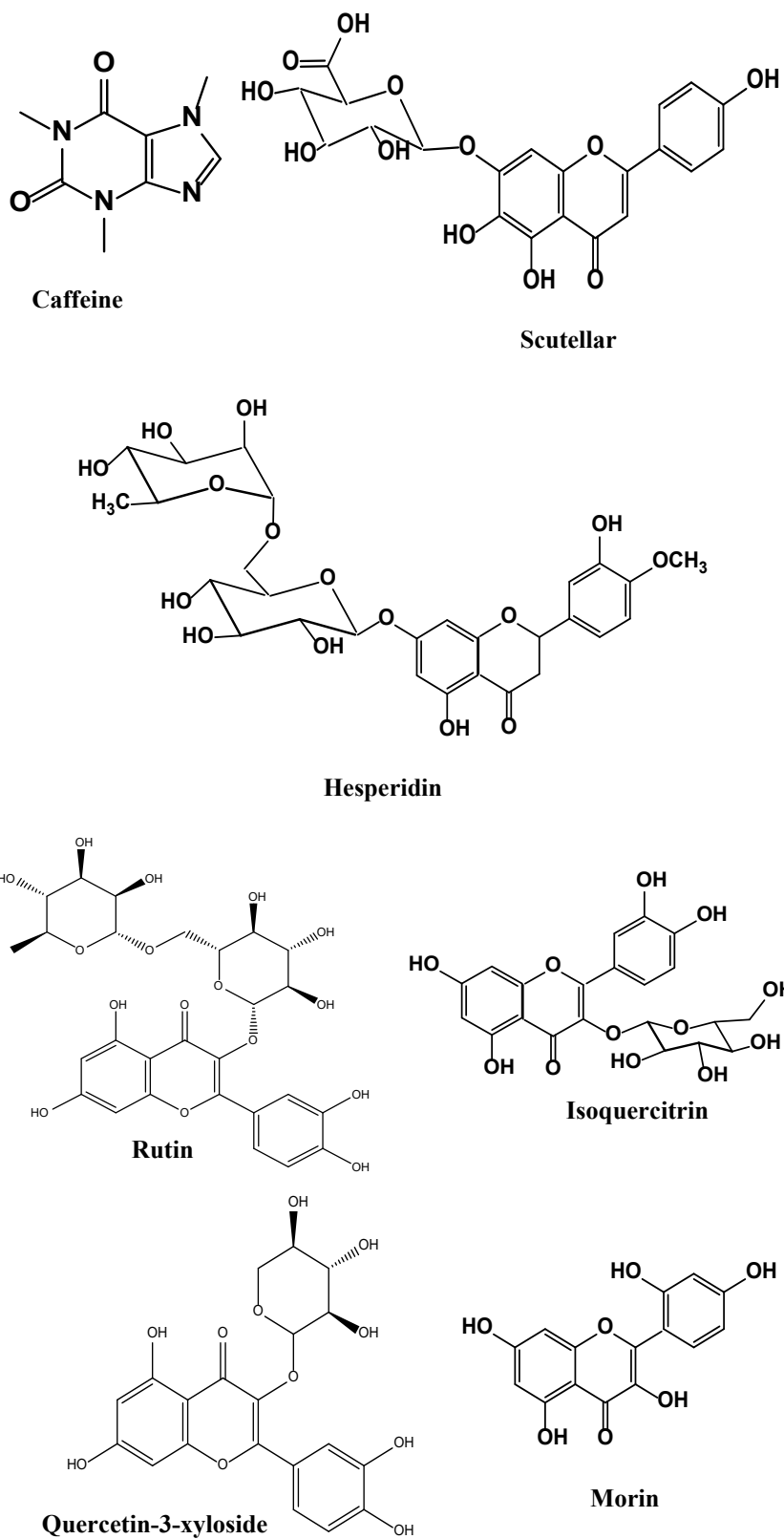


Figure 3. Chemical structures of the identified compounds using LC-MS/MS

CONCLUSION

In this work, we discovered the antioxidant and antimicrobial potential of different solvent extracts of *T. claveryi*. Also, the study aimed to the determination of their mineral content, accompanied by the identification of the chemical components of the methanol extract using LC-MS/MS technique, which led to the identification of some phenolic compounds which are known for its multiple biological activities. To sum up, *T. claveryi* extracts are considered as promising sources of natural antioxidant and antimicrobial agents. Additionally, its high nutritional content also makes it a promising source for nutritional supplements.

ACKNOWLEDGMENT

The authors are grateful to the DGRSDT and the Ministry of Higher Education and Scientific Research of Algeria the PRFU Project (A16N01UN030120230001), and the team of Medicinal Chemistry Department, Theodor Bilharz Research Institute, Egypt.

CONFLICT OF INTEREST

The author declare that there is no conflict of interest.

AUTHOR CONTRIBUTION

Hadjira GUENANE: Plants collection, perform extraction, antioxidant activity evaluation, and writing-original draft preparation. Boulanouar BAKCHICHE: writing-original draft preparation and supervision. Ramazan ERENLER and Ilyas YILDIZ: Perform LC-ESI-MS/MS analysis. Asmaa S. MOHAMED and Maha A.M. El-SHAZLY: Formal analysis, investigation, data curation, visualization, writing-original draft preparation, review and editing,

REFERENCES

- Abdel-Aziz MS, Ghareeb MA, Saad AM, Refahy LA, Hamed AA. (2018). Chromatographic isolation and structural elucidation of secondary metabolites from the soil-inhabiting fungus *Aspergillus fumigatus* 3T-EGY. *Acta Chromatographica*, 30(4): 243-249.
- Abdelfattah MAO, Dmirieh M, Ben Bakrim W, Mouhtady O, Ghareeb MA, Wink M, Sobeh M. (2022). Antioxidant and anti-aging effects of *Warburgia salutaris* bark aqueous extract: Evidences from *in silico*, *in vitro* and *in vivo* studies. *Journal of Ethnopharmacology*; 292: 115187.
- Abu-Odeh A, Shehadeh M, Suaifan GARY, Karameh N, Abdel Rahman D, Kandil Y. (2022) . *In vitro* and *in vivo* antidiabetic activity, phenolic content and microscopical characterization of *Terfezia claveryi*. *Molecules*.; 27: 4843.
- Al-Atassi AZ, Al-Khatib RA, Othman MA. (2022) . Comparison of phenolic contents and antioxidant activities for black and white desert truffles spread in Syria, *Iraqi Journal of Pharmaceutical Sciences* , 31(2): 184-192.
- Aldebasi YH, Aly SM, Qureshi MA, Khadri H. (2013). Novel antibacterial activity of *Terfizia claveryi* aqueous extract against clinical isolates of corneal ulcer. *African Journal of Biotechnology*. 12: 6340-6346.
- Alpay M, Dulger G, Sahin IE, Dulger B. (2019). Evaluating antimicrobial and antioxidant capacity of endemic *Phlomis russeliana* from Turkey and its antiproliferative effect on human Caco-2 cell lines. *Anais da Academia Brasileira de Ciências*.; 91(3): e 20180404.
- Apriliyanti MW, Ardiyansyah M, Febrianti W, Arum P, Jayus, Sjaifullah A. Effect of time and temperature on vitamin c contents and antioxidant activity in the hot water extraction of melinjo peels. *IOP Conf. Series: Earth and Environmental Science*. 2022; 980; 012045.

- Atalar MN, Aras A, Türkan F, Barlak N, Yildiko Ü, Karatas OF Alma MH.(2021). The effects of *Daucus carota* extract against PC3, PNT1a prostate cells, acetylcholinesterase, glutathion S-transferase, and α -glycoside; an *in vitro-in silico* study. *Journal of Food Biochemistry* , 45(12): e13975.
- Bakchiche B, Gherib A, Bronze MR, Ghareeb MA.(2019). Identification, quantification, and antioxidant activity of hydroalcoholic extract of *Artemisia campestris* from Algeria. *Turkish Journal of Pharmaceutical Sciences* ; 16(2): 234-239.
- Bakchiche B, Gören AC, Aydoğmuş Z, Mataraci-Kara E, Ghareeb MA. (2022) . *Artemisia campestris* and *Artemisia herba-alba*: LC-HRESI-MS profile alongside their antioxidant and antimicrobial evaluation. *Acta Pharmaceutica Scientia*; 60(2): 131-152.
- Bhotmange DU, Wallenius JH, Singhal RS, Shamekh SS. (2017). Enzymatic extraction and characterization of polysaccharide from *Tuber aestivum*. *Bioactive Carbohydrates and Dietary Fibre* ; 10: 1-9.
- Bradai L, Bissati S, Chenchouni H. Desert trues of the North Algerian Sahara: Diversity and bioecology. *Emir J Food Agric*. 2014; 26: 429-435
- Dahham SS, Al-Rawi SS, Ibrahim AH, Abdul Majid AS, Abdul Majid AMS. (2018). Antioxidant, anticancer, apoptosis properties and chemical composition of black truffle *Terfezia clavaryi*. *Saudi Journal of Biological Sciences*.; 25(8): 1524-1534.
- Dib-Bellahouel S., Fortas Z. (2019). Antimicrobial activities of desert Truffle extracts and their chemical identification. *Journal of Pharmacy and Pharmacology* ; 7: 593-597.
- Dundar A, Yesil OF, Acay H, Okumus V, Ozdemir S, Yildiz A. (2012). Antioxidant properties, chemical composition and nutritional value of *Terfezia boudieri* (Chatin) from Turkey. *Food Science and Technology International* ; 18(4): 317-328
- Elkhoully HI, Hamed AA, El Hosainy AM, Ghareeb MA, Nagwa M. Sidkey. (2021). Bioactive secondary metabolite from endophytic *Aspergillus Tubenginses*ASH4 isolated from *Hyoscyamus muticus*: Antimicrobial, antibiofilm, antioxidant and anticancer activity. *Pharmacognosy Journal* ; 13(2): 434-442.
- Elkhoully HI, Sidkey NM, Ghareeb MA, El Hosainy AM, Hamed AA. (2021). Bioactive Secondary Metabolites from Endophytic *Aspergillus terreus* AH1 Isolated from *Ipomoea carnea* Growing in Egypt. *Egyptian Journal of Chemistry* ; 64(12): 7511-7520.
- El-Neekety AA, Abdel-Aziz MS, Hathout AS, Hamed AA, Sabry BA, Ghareeb MA, Aly SE, Abdel-Wahhab MA.(2016) . Molecular identification of newly isolated non-toxicogenic fungal strains having antiaflatoxicogenic, antimicrobial and antioxidant activities. *Der Pharma Chemica* ; 8: 121-134.
- El-Shazly MAM, Hamed AA, Kabary HA, Ghareeb MA. (2022). LC-MS/MS profiling, antibiofilm, antimicrobial and bacterial growth kinetic studies of *Pluchea dioscoridis* extracts. *Acta Chromatographica* ; 34(3): 338-350.
- Erenler R, Yaman C, Demirtas I, Alma MH. (2023) Phytochemical investigation of *Hypericum heterophyllum* flowers: LC-ESI-MS/MS analysis, total phenolic and total flavonoid contents, antioxidant activity. *Journal of Natural Products*, 13: e12012321672.

- Farzaneh P, Khanahamadi M, Ehsani MR, Sharifan A. (2018). Bioactive properties of *Agaricus bisporus* and *Terfezia claveryi* proteins hydrolyzed by gastrointestinal proteases. *LWT - Food Science and Technology* ; 91: 322-329.
- Fouad MS, Ghareeb MA, Hamed AA, Aidy EA, Tabudravu J, Sayed AM, Tammam MA, Mwaheb MA. (2024). Exploring the antioxidant, anticancer and antimicrobial potential of *Amaranthus viridis* L. collected from Fayoum depression: Phytochemical, and biological aspects. *South African Journal of Botany*. 166: 297-310.
- Gargano ML, Bella P, Panno S, Arizza V, Inguglia L, Catara V, Venturella G, Davino S. (2017). Antimicrobial activity of the extracts of *Terfezia claveryi* and *Tirmania pinoyi* against gram-positive and gram-negative bacteria causal agent of diseases in tomato. *Chemical Engineering Transactions* ; 58: 73-78.
- Ghareeb MA, Ahmed WS, Refahy LA, Abdou AM, Hamed MM, Abdel-Aziz MS. (2016). Isolation and characterization of the bioactive phenolic compounds from *Morus alba* L. growing in Egypt. *Pharmacologyonline* ; 3: 157-167.
- Ghareeb MA, Khalaf OM, Abdel-Aziz MS, Saad AM, Madkour HMF, El-Ziaty AK, Refahy LA. (2020). Chemical profiles and bio-activities of different extracts of *Terfezia* species and their other associated fungi. *Current Bioactive Compounds* ; 16(3): 308-319.
- Ghareeb MA, Mohamed T, Saad AM, Refahy LA, Sobeh M, Wink M. (2018). HPLC-DAD-ESI-MS/MS analysis of fruits from *Firmiana simplex* (L.) and evaluation of their antioxidant and antigenotoxic properties. *Journal of Pharmacy and Pharmacology* ; 70: 133-142.
- Ghareeb MA, Refahy LA, Saad AM, Osman NS, Abdel-Aziz MS, El-Shazly MA, Mohamed AS. (2015). *In vitro* antimicrobial activity of five Egyptian plant species. *Journal of Applied Pharmaceutical Science*; 5: 045-049.
- Ghareeb MA, Saad AM, Abdel-Aleem AH, Abdel-Aziz MS, Hamed MM, Hadad AH. (2016). Antioxidant, antimicrobial, cytotoxic activities and biosynthesis of silver & gold nanoparticles using *Syzygium jambos* leaves growing in Egypt. *Der Pharma Chemica* ; 8: 277-286.
- Ghareeb MA, Saad AM, Ahmed WS, Refahy LA, Nasr SM. (2018). HPLC-DAD-ESI-MS/MS characterization of bioactive secondary metabolites from *Strelitzia nicolai* leaf extracts and their antioxidant and anticancer activities *in vitro*. *Pharmacognosy Research* ; 10(4): 368-378.
- Ghareeb MA, Sobeh M, Rezaq S, El-Shazly AM, Mahmoud MF, Wink M. (2018). HPLC-ESI-MS/MS profiling of polyphenolics of a leaf extract from *Alpinia zerumbet* (Zingiberaceae) and its anti-inflammatory, anti-nociceptive, and antipyretic activities *in vivo*. *Molecules* ; 23: 3238.
- Hamed AA, Soldatou S, Qader MM, Arjunan S, Miranda KJ, Casolari F, Pavesi C, Diyaolu OA, Thissera B, Eshelli M, Belbahri L, Luptakova L, Ibrahim NA, Abdel-Aziz MS, Eid BM, Ghareeb MA, Rateb ME, Ebel R. (2020). Screening fungal endophytes derived from under-explored Egyptian marine habitats for antimicrobial and antioxidant properties in fractionalised textiles. *Microorganisms* ; 8: 1617.

- Harki E, Klaebe A, Talou T, Dargent R. (1996). Identification and quantification of *Tuber melanosporum* Vitt. sterols. *Steroids* ; 61:609-612.
- Hathout AS, EL-Neekety AA, Abdel Aziz MS, Sabry BA, Hamed AA, Ghareeb MA, Aly SE. (2016). Novel Egyptian bacterial exhibiting antimicrobial and antiaflatoxic activity. *Journal of Applied Pharmaceutical Science* ; 6: 001-010.
- Hussain J, Ali L, Khan AL, Rehman NUr, Jabeen F, Kim J and Al-Harrasi A. (2014). Isolation and Bioactivities of the Flavonoids Morin and Morin-3-O- β -D-glucopyranoside from *Acridocarpus orientalis*—A Wild Arabian Medicinal Plant. *Molecules*, 19, 17763-17772.
- İnci Ş, Kirbağ S. Nutritional content, antioxidant and antimicrobial activity of *Terfezia clavaryi* Chatin. *Journal of Forestry Faculty*. 2018; 19(2): 138-143.
- Kagan-Zur V, Roth-Bejerano N. (2008) . Desert trues. *Fungi* ; 1: 32-37.
- Khalaf OM, Abdel-Aziz MS, El-Hagrassi AM, Osman AF, Ghareeb MA. (2021). Biochemical aspect, antimicrobial and antioxidant activities of *Melaleuca* and *Syzygium* species (Myrtaceae) grown in Egypt. *Journal of Physics: Conference Series* ; 1879: 022062.
- Khalaf OM, Ghareeb MA, Saad AM, Madkour HMF, El-Ziaty AK, Abdel-Aziz MS. (2019). Phenolic constituents, antimicrobial, antioxidant and anticancer activities of ethyl acetate and *n*-butanol extracts of *Senna italica*. *Acta Chromatographica* ; 31(2): 138-145.
- Khalifa SAM, Farag MA, Yosri N, Sabir JSM, Saeed A, Al-Mousawi SM, Taha W, Musharraf SG, Patel S, El-Seedi HR. Truffles: From Islamic culture to chemistry, pharmacology, and food trends in recent times. *Trends Food Sci. Technol.* 2019; 91:193-218.
- Khlaif DK, Kadum H, Abod NS. (2021) . Nutritional and chemical compositions of the desert Truffle (*Terfezia clavaryi*) in Samawa city of Iraq. *IOP Conf. Series: Earth and Environmental Science* ; 923: 012050.
- Kuhkheil A, Badi HN, Mehrafarin A, Abdossi V. (2020). Phytochemical and morpho-physiological variations in sea buckthorn (*Hippophae rhamnoides* L.) populations of Taleghan region in Iran . *Journal of Medicinal Plants* ; 19(76): 21-35.
- Lee H, Lee H, Nam K, Zahra Z, Zahra Z, Farooqi MQU. (2020). Potentials of truffles in nutritional and medicinal applications: A review. *Fungal Biology and Biotechnology* ; 7(9): 1-17.
- Li Y, Chen J, Cao L, Li L, Wang F, Liao Z, Chen J, Wu S, Zhang L.(2018). Characterization of a novel polysaccharide isolated from *Phyllanthus emblica* L. and analysis of its antioxidant activities. *Journal of Food Science and Technology* ; 55(7): 2758-2764.
- Mahmoud HNS, Elshazly MAM, Saad AM, Refahy LA, Ghareeb MA, Rizk SA. (2023). UPLC-QTOF/MS-assisted chemical profiling of *Daucus carota* leaf extract and evaluation of its antioxidant, antimicrobial and antibiofilm activities: Evidence from in vitro and in silico studies. *Egyptian Journal of Chemistry*. 66(SI 13): 2175-2190.
- Mandael QA, Al-Laith AA. (2007). Ethnomycological aspects of the desert true among native Bahraini and non Bahraini peoples of the Kingdom of Bahrain. *Journal of Ethnopharmacology* ; 110: 118-129.
- Mudliyar DS, Wallenius JH, Bedade DK, Singhal RS, Madi N, Shamekh SS.(2019) . Ultrasound assisted extraction of the polysaccharide from *Tuber aestivum* and its *in vitro* anti-hyperglycemic activity. *Bioactive Carbohydrates and Dietary Fibre* ; 20: 100198.

- Nasr SM, Ghareeb MA, Mohamed MA, Elwan NM, Abdel-Aziz AA, Abdel-Aziz MS. (2018) . HPLC-fingerprint analyses, *in vitro* cytotoxicity, antimicrobial and antioxidant activities of the extracts of two *Cestrum* species growing in Egypt. *Pharmacognosy Research* ; 10(2): 173-180.
- Nazir N, Zahoor M, Nisar M, Khan I, Ullah R and Alotaibi A. (2021). Antioxidants Isolated from *Elaeagnus umbellata* (Thunb.) Protect against Bacterial Infections and Diabetes in Streptozotocin-Induced Diabetic Rat Mode. *Molecules* : 26: 4464.
- Neggaz S, Fortas Z, Chenni M, El Abed D, Ramli B, Kambouche N.(2015). *In vitro* evaluation of antioxidant, antibacterial and antifungal activities of *Terfezia claveryi* Chatin. *Phytothérapie*; 16(1): 1-7.
- Neggaz S, Fortas Z, Zitouni FE. (2019). Antimicrobial activity of medicinal mushroom: Algerian desert Truffle. *International Journal of Advances in Science Engineering and Technology* ; 7(1): 33-34.
- Razavia SM, Zahria S, Zarrini G, Nazemiyeh H & Mohammadia S. (2009). Biological Activity of Quercetin-3-O-Glucoside, a Known Plant Flavonoid. *Russian Journal of Bioorganic Chemistry* : 35(3): 376–378.
- Saad AM, Mohammed MMD, Ghareeb MA, Ahmed WS, Farid MA. (2017). Chemical composition and antimicrobial activity of the essential oil of the leaves of *Cupressus macrocarpa* Hartweg. ex Gordon. *Journal of Applied Pharmaceutical Science* ; 7: 207-212.
- Saddiq AA, Yousef JM, Mohamed AM. (2016). The potential antibacterial role of *Terfezia claveryi* extract against immune-inflammatory disorder and oxidative damage induced by *Pseudomonas aeruginosa* in rat corneas. *Romanian Biotechnological Letters* ; 21(4):11781- 11801.
- Saravanakumar K, Sarikurkcu C, Sahinler SS, Sarikurkcu RB, Wang M. (2021). Phytochemical composition, antioxidant, and enzyme inhibition activities of methanolic extracts of two endemic *Onosma* species. *Plants* ; 10(7): 1373.
- Saud S, Salamatullah AM.(2021). Relationship between the Chemical Composition and the Biological Functions of Coffee. *Molecules* : 26: 7634.
- Sedighi Hamedani S, Kiapey SS M, Shabgah AG, Amiresmaili, Jahanara A, Oveisee M, Shekarchi A, Gheibihayat SM, Farhad J, Navashenaq JG. (2023). From traditional medicine to modern oncology: Scutellarin, a promising natural compound in cancer treatment. *Progress in Biophysics & Molecular Biology*: 180–181: 19-27.
- Sobeh M, Mahmoud MF, Hasan RA, Abdelfattah MAO, Sabry OM, Ghareeb MA, El-Shazly AM, Wink M. (2018). Tannin-rich extracts from *Lannea stuhlmannii* and *Lannea humilis* (Anacardiaceae) exhibit hepatoprotective activities *in vivo* via enhancement of the anti-apoptotic protein Bcl-2. *Scientific Reports* ; 8: 9343.
- Soltane R, Alasiri A, Taha MN, Abd El-Aleam RH, Alghamdi KS, Ghareeb MA, Keshke DEG, Cardoso SM, Sayed AM. (2023). Norlobaridone inhibits quorum sensing-dependent biofilm formation and some virulence factors in *Pseudomonas aeruginosa* by disrupting its transcriptional activator protein LasR dimerization. *Biomolecules*. 13: 1573.
- Sun S, He J, Liu M, Yin G, Zhang X. (2019). A great concern regarding the authenticity identification and quality control of Chinese propolis and Brazilian green propolis. *Journal of Food and Nutrition Research* ; 7(10): 725-735.

- Tang Y, Li H-M, Tang Y-J. (2012). Comparison of sterol composition between Tuber fermentation mycelia and natural fruiting bodies. *Food Chemistry* ; 132: 1207-1213.
- Taşkın T, Devecioğlu TY, Şenkardeş İ.(2018). Antioxidant, anti-urease activities and genotoxic effects of *Terfezia claveryi* methanol extracts on human Lymphocytes. *Clinical and Experimental Health Sciences* : 190-195.
- Tejedor-Calvo E, Amara K, Reis FS, Barros L, Martins A, Calhella RC, Venturini M, Blanco D, Redondo D, Marco P. (2020). Chemical composition and evaluation of antioxidant, antimicrobial and antiproliferative activities of Tuber and *Terfezia* truffles. *Food Research International* ; 140: 110071.
- Tejedor-Calvo E, Morales D, Marco P, Sánchez S, Garcia-Barreda S, Smiderle FR, Iacomini M, Villalva M, Santoyo S, Soler-Rivas C. (2020). Screening of bioactive compounds in truffles and evaluation of pressurized liquid extractions (PLE) to obtain fractions with biological activities. *Food Research International* ; 132: 109054.
- Vahdani M, Rastegar S, Rahimzadeh M, Ahmadi M, Karmostaji A.(2017) . Physicochemical characteristics, phenolic profile, mineral and carbohydrate contents of two truffle species. *Journal of Agricultural Science and Technology* ; 19: 1091-1101.
- Wahiba B, Wafaà T, Asmaà K, Bouziane A, Mohammed B. Nutritional and antioxidant profile of red truffles (*Terfezia claveryi*) and white truffle (*Tirmania nivea*) from southwestern of Algeria. *Der Pharmacia Lettre*. 2016; 8(17):134-141.
- Weete JD, Abril M, Blackwell M. Phylogenetic distribution of fungal sterols. *PLoS ONE* ; 5: e10899.
- Wu Z, Jayachandran M, Cheang WS, Xu B. Black Truffle extract exerts antidiabetic effects through inhibition of inflammation and lipid metabolism regulation. *Oxidative Medicine and Cellular Longevity*. 2022, Article ID 6099872: 1-10.
- Yang J & Hoi-Seon Lee. (2012). Evaluation of Antioxidant and Antibacterial Activities of Morin Isolated from *Mulberry Fruits* (*Morus alba* L.). *Journal of the Korean Society for Applied Biological Chemistry* ; 55: 485–489.
- Zhao W, Wang XH, Li HM, Wang SH, Chen T, Yuan ZP, Tang YJ. (2014). Isolation and characterization of polysaccharides with the antitumor activity from Tuber fruiting bodies and fermentation system. *Applied Microbiology and Biotechnology* ; 98: 1991-2002.

Dipyridamole Cocrystal Tablets with Enhanced Solubility and Dissolution at Intestinal pH

Monika NIJHAWAN[°], Sadhna DHYAGALA^{**}, Gunnam SAILAJA^{***},
Rajeswari ALETI^{****}, Trapti SAXENA^{*****}

Dipyridamole Cocrystal Tablets with Enhanced Solubility and Dissolution at Intestinal pH

SUMMARY

Aim of the study was to prepare dipyridamole (DPM) cocrystals to alter its physicochemical properties as it is poorly soluble in water, 6.8 pH buffer and belongs to BCS class II. Cocrystals were prepared using neat grinding method. Initial screening of cocrystals was done with melting point determination indicating formation of nine cocrystals. Based upon interference studies nine cocrystals were finalized for solubility and dissolution studies. DPM-citric acid, DPM-hippuric acid, DPM-tartaric acid and DPM-oxalic acid cocrystals showed the significant enhancement in solubility and dissolution in 6.8 pH buffer. Further confirmation was done by Differential Scanning Calorimetry (DSC) and Powder X-ray diffraction (PXRD) studies. DPM-hippuric acid cocrystals have shown promising results for formation of cocrystals and considered for tablet formulation. DPM-hippuric acid cocrystal tablets were prepared by using various levels of carboxymethyl cellulose and microcrystalline cellulose. These tablets showed acceptable physical characteristics with subsequent rapid dissolution.

Key Words: Dipyridamole (DPM), Cocrystals, Neat grinding, DSC, Solubility, Dissolution.

Bağırsak pH'sında Geliştirilmiş Çözünürlük ve Çözünme Özelliğine Sahip Dipyridamol Kokristal Tabletler

ÖZ

Çalışmanın amacı, suda ve 6,8 pH tamponunda az çözünen ve BCS sınıf II'ye ait olan dipiridamol'un (DPM) fizikokimyasal özelliklerini değiştirmek üzere ko-kristallerinin hazırlanmasıdır. Ko-kristaller düzenli öğütme metodu kullanılarak hazırlanmıştır. Ko-kristallerin ilk taraması, dokuz ko-kristalin oluşumunu gösteren erime noktası tayini ile gerçekleştirilmiştir. Girişim çalışmalarına dayanarak, çözünürlük ve çözünme çalışmaları için dokuz ko-kristal seçilmiştir. DPM-sitrik asit, DPM-hippurik asit, DPM-tartarik asit ve DPM-oksalik asit ko-kristalleri, 6,8 pH tamponunda çözünürlük ve çözünmede anlamlı bir artış göstermiştir. İleri doğrulama, Diferansiyel Taramalı Kalorimetre (DSC) ve Toz X-Ray Difraksiyonu (PXRD) çalışmaları yapılmıştır. DPM-hippurik asit ko-kristalleri, ko-kristallerin oluşumu için umut verici sonuçlar vermiş ve tablet formülasyonu için düşünülmüştür. DPM-hippurik asit ko-kristal tabletleri, çeşitli seviyelerde karboksimetil selüloz ve mikrokristalin selüloz kullanılarak hazırlanmıştır. Bu tabletler, daha sonra hızlı çözünme ile kabul edilebilir fiziksel özellikler göstermiştir.

Anahtar Kelimeler: Dipiridamol (DPM), Ko-kristaller, Düzenli öğütme, DSC, Çözünürlük, Çözünme Hızı.

Received: 22.06.2023

Revised: 19.10.2023

Accepted: 19.10.2023

[°] ORCID: 0000-0002-3564-0257, GokarajuRangaraju College of pharmacy, Department of Pharmaceutics, Associate Professor, Osmania University, Hyderabad, Telangana, India

^{**} ORCID: 0000-0003-1834-7750, GokarajuRangaraju College of pharmacy, Department of Pharmaceutics, Osmania University, Hyderabad, Telangana, India.

^{***} ORCID: 0009-0007-2550-4001, GokarajuRangaraju College of pharmacy, Department of Pharmaceutics, Associate Professor, Osmania University, Hyderabad, Telangana, India.

^{****} ORCID: 0009-0001-8894-9063, GokarajuRangaraju College of pharmacy, Department of Pharmaceutics, Assistant Professor Osmania University, Hyderabad, Telangana, India.

^{*****} ORCID: 0009-0001-8894-9063, G Pulla Reddy College of Pharmacy, Department of Pharmaceutics, Associate Professor, Hyderabad, Telangana, India.

INTRODUCTION

Cocrystals are multicomponent system consisting of API and GRAS listed cofomers that are held together by nonionic interaction such as hydrogen bonding or Vanderwall forces (Qiao et al., 2011; Thimmasetty et al., 2021). The cofomer selected can be a drug, excipient or nutraceuticals having functional groups like amine, alcohol, amide, and carboxylic acid that form hydrogen bonding with the API (Stahl et al., 2002; Gadade et al., 2016; Thipparaboina et al., 2016). Crystal engineering approach can alter physicochemical behavior such as solubility, dissolution, and stability of an API for improvement in bioavailability of poorly soluble drug (Blagden et al., 2007; Izutsu et al., 2016). In the market, cocrystals of caffeine-citric acid/citrate, valproic acid/Na-valproate, and escitalopram-oxalic acid/oxalate are available though many more under investigation (Kumar et al., 2014).

Dipyridamole (DPM) is BCS class II drug having pH dependent solubility and is primarily absorbed in the stomach. DPM has low oral bioavailability (37-66%) because of its insolubility at alkaline pH (Paul et al., 2018). Solid dispersion, self emulsifying drug delivery system, micronization, cyclodextrin complexation are reported techniques in the literature to alter the dissolution behavior of DPM (Guo et al., 2011; Savjani et al., 2012). Cocrystals are suitable alternative approach to improve physicochemical properties of DPM to overcome the problem of poor bioavailability (Yadav et al., 2009; Gawade et al., 2021). Since there is only one literature support for the formation of co-crystals of DPM with tartaric acid, there is a scope for obtaining the DPM cocrystals with acidic cofomers to enhance its solubility and absorption (Kojo et al., 2017). An attempt was made to formulate DPM cocrystal tablets to enhance solubility and dissolution rate.

MATERIALS AND METHODS

Materials

DPM was procured as a gift sample from Aurobindo Laboratories, Hyderabad. All other chemicals and excipients used in this research were obtained from S D Fine-Chem Limited, Mumbai.

Methods

Preparation of DPM-cocrystals

Neat grinding method was opted for DPM cocrystal preparation. DPM and cofomers were grinded in (1:1 molar ratio) in mortar and pestle for 30 minutes at room temperature. Products were stored in desiccators for further use (Thimmasetty et al., 2021). List of cofomers used in this study was represented in **Table 1**.

Characterization of DPM cocrystals

Melting point

Initial screening of cocrystals was done based on melting point. Fifteen cofomers were selected given in **Table 1**. Melting point of DPM and cocrystals was determined by open capillary tube method using melting point apparatus (Biotech, India) (Schultheiss et al., 2009). The procedure was repeated in triplicate (n=3).

Saturation solubility studies of DPM-cocrystals

Solubility of DPM and its cocrystals was carried out in 0.1N hydrochloric acid, 6.8 phosphate buffer and distilled water. The DPM and cocrystals were added in excess quantity separately in volumetric flasks containing different media to form supersaturated solutions and rotated in orbital shaker (Kemi industries, Kerala) at room temperature (25°C), with a 50 rpm, for 24 h. After attainment of equilibrium, samples were withdrawn, filtered using 0.45µm whattmann filter paper, diluted and analyzed by UV spectrophotometer. Procedure was repeated in triplicate (Dai et al., 2018; Nijhawan et al., 2014).

Dissolution studies of DPM-cocrystals

DPM dissolution studies were carried out at acidic (0.1N HCl) and alkaline basic pH (6.8) for 1 hr using USP dissolution test apparatus II (Electrolab, Dissolution tester, TDT-08L) by paddle method in 900 mL of pH 1.2 and 6.8 phosphate buffer at 50 rpm maintained at 37±0.5°C. DPM and its cocrystals containing the drug equivalent to 25 mg were filled in hard gelatin capsule. 5 ml of sample was withdrawn at 10 minutes interval for a period of 1 hr and analyzed spectrophotometrically (Panzade et al., 2017).

Differential Scanning Calorimetry (DSC) of DPM-cocrystals

A differential calorimetry scanning (DSC7020 thermal analysis system HITACHI) was used for thermal analysis of DPM and DPM cocrystal samples. Powder samples of approximately 2.0 mg were placed in aluminum open crucibles and heated at a rate of 10°C/min up to 400°C (Cheney et al., 2011;

Saganowska et al., 2018).

Powder X-ray diffraction (PXRD) of DPM-cocrystals

The cocrystals of dipyrindamole and pure drug were characterized at 25 °C using XPERT-PRO diffractometer with Cu-Kα (λ = 1.54060 Å) at 45 kV and 40 mA (Bevill et al., 2014; Nijhawan et al., 2022).

Preparation of DPM-hippuric acid cocrystal tablets

Based on dissolution results, DPM-hippuric acid cocrystals were selected for tablet compression as per formulae given in Table 1. DPM-hippuric acid cocrystals were geometrically mixed for 15 min with other additives (CMC, MCC, mannitol, magnesium stearate) and compressed by Rimek 12 station rotary mini tablet compression machine at sufficient compression force to obtain hardness in the range of 3-4 kg/cm² using 4 mm round punch with flat surface.

Table 1: Formulation of DPM-hippuric acid cocrystal tablets.

S.No	Drug and other excipients (mg)	Formulations (200 mg)			
		DPMF1	DPMF2	DPMF3	DPMF4
1	DPM-hippuric acid cocrystals	26	26	26	26
2	Carboxy methyl cellulose (CMC)	8	4	4	8
3	Microcrystalline cellulose (MCC)	60	64	60	64
4	Mannitol	102	102	106	98
5	Magnesium stearate	4	4	4	4

Characterization of DPM-hippuric acid tablets

For evaluation of DPM-hippuric acid tablets post compression parameters such as hardness, thickness, friability, weight variation, disintegration studies, drug content, and dissolution studies were carried out. The thickness of tablets was determined by using Vernier calipers. Friability was determined using tablet friability tester (FT 1020, LABINDIA), the device that subjects the tablet to the combined effect of abrasion and shock in a plastic chamber revolving and dropping the tablet at a height of 6 inches in each revolution. The tablets were subjected to 100 revolutions and

dedusted by muslin cloth and reweighed. The percent loss in weight (F) was calculated as shown by Eq. 1. For Uniformity of weight, twenty tablets from each batch were randomly selected, weighed together and individually to check the average weight. Percent weight variation calculated (Eq. 2) (Indian Pharmacopoeia, 2018).

$$F = \frac{\text{initial weight} - \text{final weight}}{\text{initial weight}} \times 100 \quad (1)$$

$$\% \text{weight variation} = \frac{\text{individual weight} - \text{final weight}}{\text{individual weight}} \times 100 \quad (2)$$

In vitro disintegration test of tablets was performed in tablet disintegration test apparatus (DT

1000, LABINDIA) containing six cylindrical tubes with #10 (aperture size 2 ± 0.2 mm) sieve. Randomly chosen six tablets were added to tubes containing pH 6.8 phosphate buffer as the medium maintained at $37\pm 2^\circ\text{C}$ and disintegration time was recorded.

RESULTS AND DISCUSSION

Melting point determination

Melting point of the prepared cocrystals was determined up to four weeks. All the observed values are compared with reported values (Marydele et al., 2006; Raymond CR et al., 2009; Cheney et al., 2010). From Table 2 it can be observed that nine cocrystals are formed based on the principle of lowering of melting point.

DPM-citric acid cocrystals showed melting point

of $80-110^\circ\text{C}$ which is neither nearer to DPM (165°C) nor to the coformer (citric acid- 153°C), similar is the case of DPM-hippuric acid, DPM-tartaric acid, DPM-malonic acid, DPM-succinic acid, DPM-fumaric acid, DPM-adipic acid, DPM-oxalic acid, and DPM-cinnamic acid cocrystals. These observations indicated that the cocrystals might have formed with the respective coformer. Cocrystals with salicylic acid, benzoic acid aspirin, maleic acid, glutamic acid and glutaric acid showed melting within the 7 days of preparation of cocrystals hence rejected for further evaluation. DPM-citric acid, DPM-hippuric acid, DPM-tartaric acid, DPM-malonic acid, DPM-succinic acid, DPM-fumaric acid, DPM-adipic acid, DPM-benzoic acid, DPM-cinnamic acid cocrystal preparations were selected for further analysis.

Table 2: Melting point values of DPM, cofomers and cocrystals

S. No.	Name	MP ($^\circ\text{C}$) (Reported Values)	MP ($^\circ\text{C}$) (Obs. values)	Inference
	DPM	164-167 (drug)	165	-
1	DPM - citric acid anhydrous	153 (coformer)	80-110	Cocrystals might have formed
2	DPM - hippuric acid	187-188 (coformer)	110-130	Cocrystals might have formed
3	DPM - tartaric acid	168-170 (coformer)	110-120	Cocrystals might have formed
4	DPM - malonic acid	135-137 (coformer)	150-160	Cocrystals might have formed
5	DPM - Succinic acid	184-190 (coformer)	110-120	Cocrystals might have formed
6	DPM - fumaric acid	287 (coformer)	120-140	Cocrystals might have formed
7	DPM - adipic acid	152.1 (coformer)	110-120	Cocrystals might have formed
8	DPM - oxalic acid	101-102 (coformer)	90-100	Cocrystals might have formed
9	DPM - cinnamic acid	133 (coformer)	80-90	Cocrystals might have formed
10	DPM - salicylic acid	158.6 (coformer)	converted into liquid within 7days of preparation	Cocrystals might not have formed
11	DPM - benzoic acid	122 (coformer)	converted into liquid within 7days	Cocrystals might not have formed
12	DPM - Aspirin	136 (coformer)	converted into liquid within 7days	Cocrystals might not have formed
13	DPM - maleic acid	135 (coformer)	converted into liquid within 7days of preparation	Cocrystals might not have formed
14	DPM - glutamic acid	213-224 (coformer)	converted into liquid within 7days	Cocrystals might not have formed
15	DPM - glutaric acid	115 (coformer)	converted into liquid after 7days	Cocrystals might not have formed

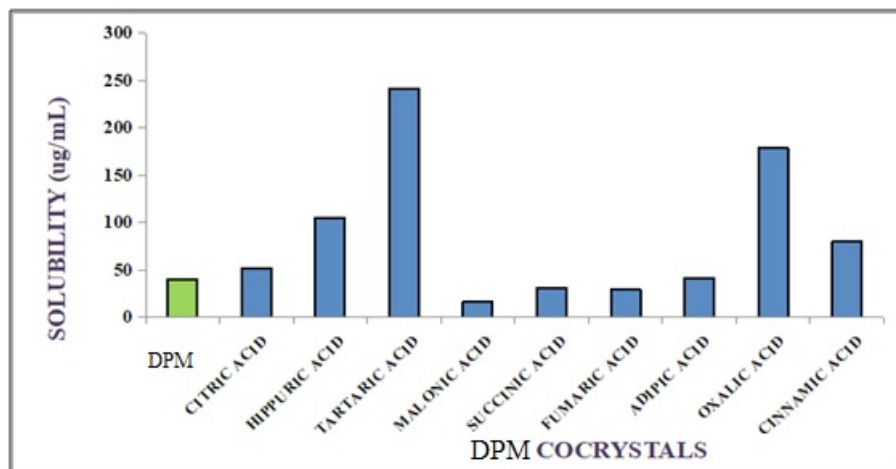


Figure 1: Solubility profile of DPM co-crystals in pH 1.2 at 25 °C

Physicochemical Properties of DPM-co-crystals

Saturation solubility studies of DPM-co-crystals

The data of solubility studies was recorded and the solubility profile of DPM-co-crystals is graphically represented in Figure 1-3.

Among nine cocrystals, six: DPM-citric acid,

DPM-hippuric acid, DPM-tartaric acid, DPM-adipic acid, DPM-oxalic acid and DPM-cinnamic acid showed higher solubility in the 1.2 pH buffer than DPM (40.18 mg/mL). The order of the solubility of the cocrystals in 1.2 pH buffer was found to be tartaric acid > oxalic acid > hippuric acid > cinnamic acid > citric acid > adipic acid > DPM.

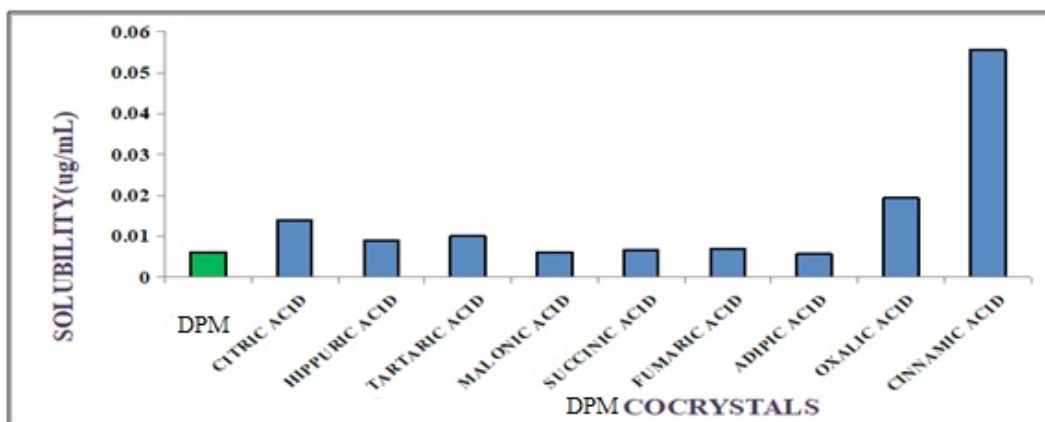


Figure 2: Solubility profile of DPM co-crystals in pH 6.8 phosphate buffer at 25 °C

Among nine cocrystals, DPM-citric acid, DPM-hippuric acid, DPM-tartaric acid, DPM-succinic acid, DPM-fumaric acid, DPM-oxalic acid and DPM-cinnamic acid showed higher solubility in 6.8 pH buffer than DPM (0.0062 mg/mL). The order of

the solubility of the co-crystals in 6.8 pH buffer was found to be cinnamic acid > oxalic acid > citric acid > tartaric acid > hippuric acid > fumaric acid > succinic acid > DPM.

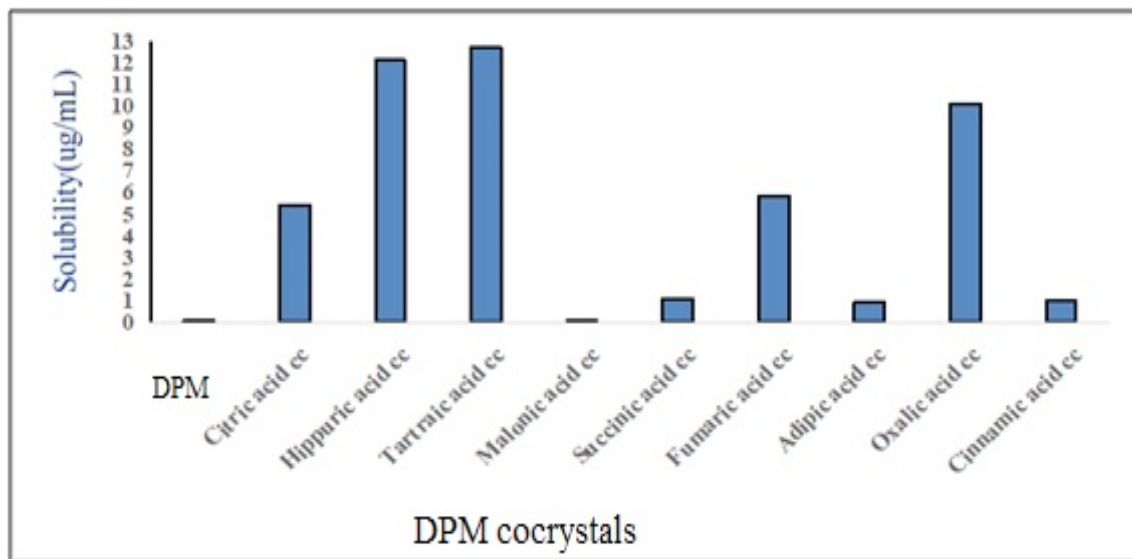


Figure 3: Solubility profile of DPM co-crystals in distilled water at 25 °C

Among nine co-crystals, all nine: DPM-citric acid, DPM-hippuric acid, DPM-tartaric acid, DPM-malonic acid, DPM-succinic acid, DPM-fumaric acid, DPM-adipic acid, DPM-oxalic acid and DPM-cinnamic acid showed higher solubility in distilled water than DPM (0.01096 mg/mL). The order of the solubility of the co-crystals in distilled water was found to be tartaric acid > hippuric acid > oxalic acid > fumaric acid > citric acid > succinic acid > cinnamic acid > adipic acid > malonic acid > DPM.

Based upon the melting points and solubility studies, six co-crystals, DPM-citric acid co-crystals, DPM-hippuric acid co-crystals, DPM-tartaric acid co-crystals, DPM-succinic acid co-crystals, DPM-oxalic acid co-crystals and DPM-cinnamic acid co-crystals were selected for the further studies.

Dissolution studies of DPM co-crystals

The dissolution-time profile of DPM-co-crystals in pH 6.8 and 1.2 buffers was recorded in Figure 4 and 5.

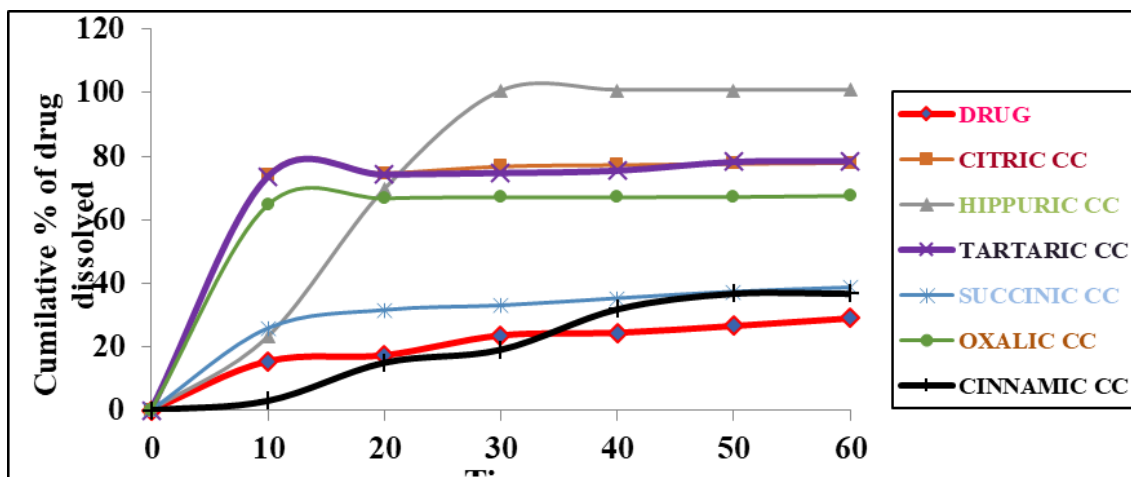


Figure 4: Dissolution profiles of DPM and its co-crystals in 6.8 phosphate buffer

The dissolution-time profiles of DPM and cocrystals in pH 6.8 buffer showed the following order: hippuric acid > tartaric acid > citric acid > oxalic acid > succinic acid > cinnamic acid > DPM. 100% drug release was observed for DPM-hippuric

acid cocrystals within 60 min while, the DPM showed only 28.98% in 60 min. The rate and extent of dissolution was found to be maximum for DPM-hippuric acid cocrystals.

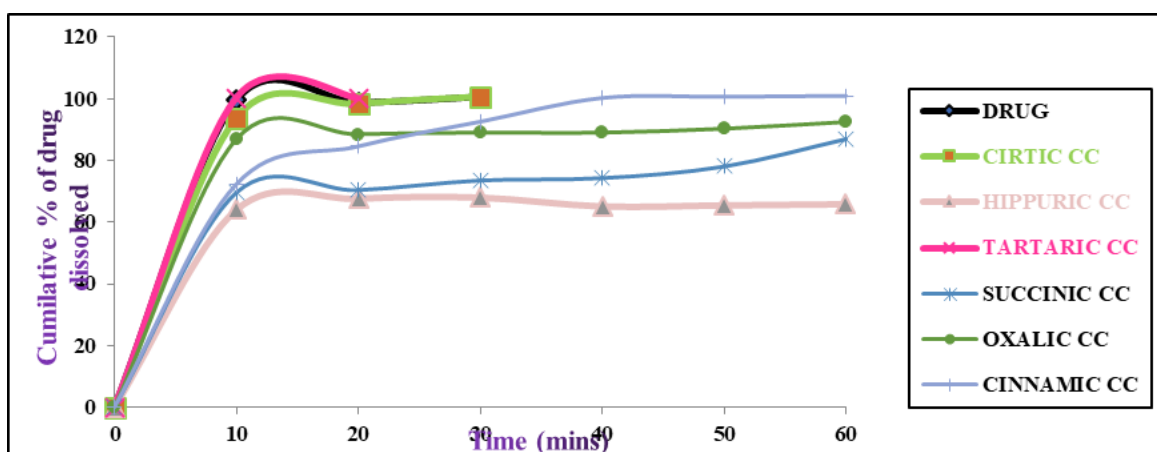


Figure 5: Dissolution profiles of DPM and its cocrystals in 0.1N HCl

In pH 1.2 buffer dissolution rate of DPM was 100% within 30 min, citric acid and tartaric acid cocrystals also showed 100% dissolution profile whereas, DPM-hippuric acid cocrystals, DPM-succinic acid cocrystals, DPM-oxalic acid cocrystals and DPM-cinnamic acid cocrystals showed 68.14%, 73.67%, 88.9% and 92.51% of dissolution rates respectively within 30 min.

The cocrystals showed marked increase in the dissolution in the 6.8 pH buffer as compared to 1.2 pH buffers. Based upon the dissolution studies in 6.8 pH buffer DPM-citric acid cocrystals, DPM-hippuric acid cocrystals, DPM-tartaric acid cocrystals and DPM-oxalic acid cocrystals were selected for further characterization by DSC.

DSC of DPM-Cocrystals

The DSC thermogram of DPM was recorded and the melting point was observed to be 166.27 °C indicating the purity of DPM. Thermograms of drug cocrystals were shown in Figure 6. In DPM-

citric acid, DPM-hippuric acid, DPM-tartaric acid and DPM-oxalic acid preparations endothermic peaks were observed at 127°C, 122°C, (118°C,134°C) and 90°C respectively. Literature value for melting of citric acid, hippuric acid, tartaric acid and oxalic acid are reported as 153°C, 188°C, 169°C and 101°C respectively (Marydele et al., 2006; Raymond CR et al., 2009; Cheney et al., 2010). The endothermic peak of co-crystal was found to be different than drug and co-crystal former, thus confirming the formation of new phase. In DPM-citric acid, DPM-hippuric acid, DPM-tartaric acid and DPM-oxalic acid preparations endothermic peaks were observed, which were neither near to the melting point of drug nor the cofomer. This inferred absence of physical mixture and the formation of cocrystals. Single sharp endothermic peak was observed incase of DPM-hippuric acid cocrystal which was neither near to the DPM nor to the hippuric acid. Hence DPM-hippuric cocrystals were further selected for PXRD studies and preparation of tablet dosage formulation.

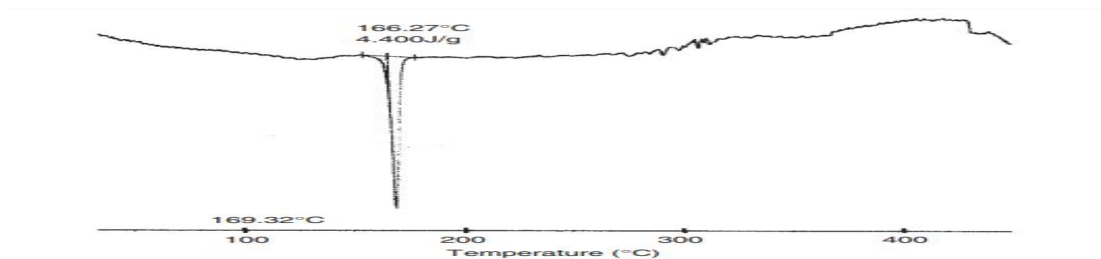
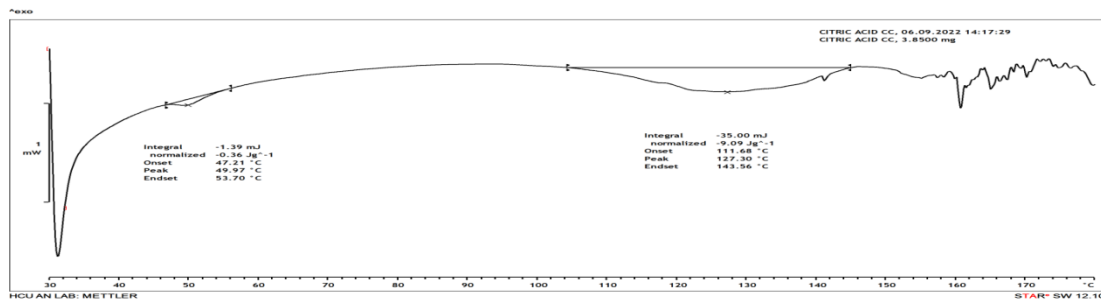
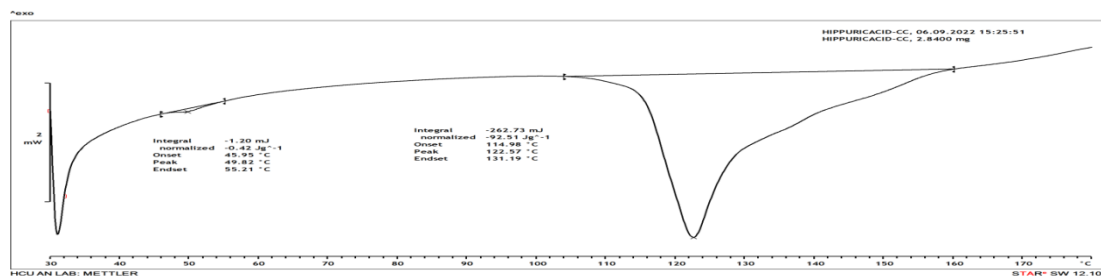


Figure 2. Differential scanning calorimetry thermogram of dipyrnidamole.

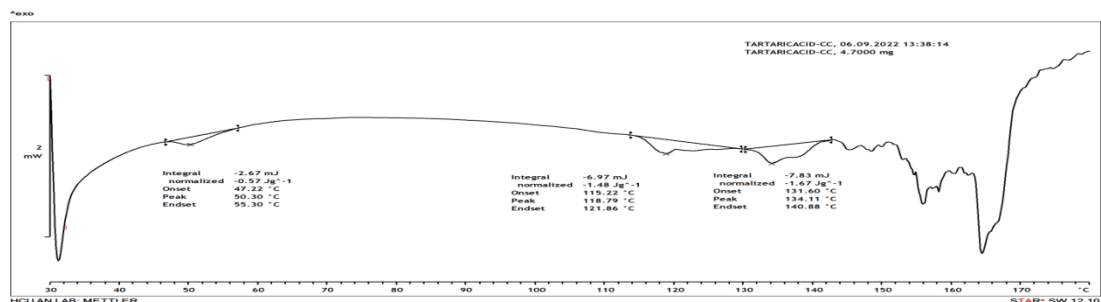
A



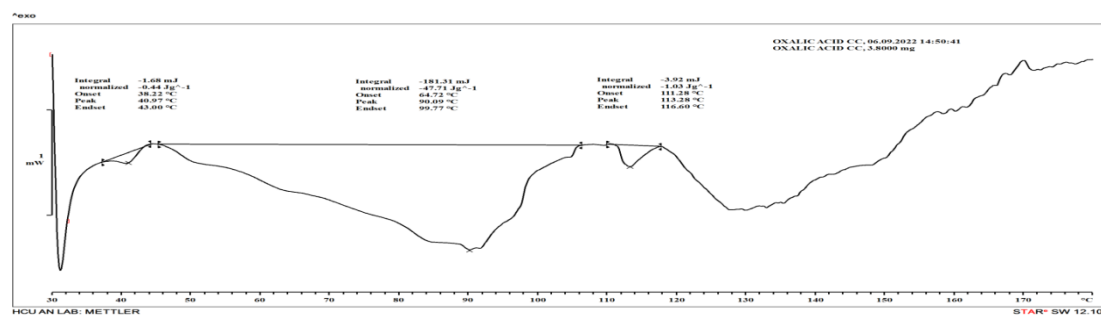
B



C



D



E

Figure 6: DSC thermogram of (A) DPM, (B) DPM-citric acid, (C) DPM-hippuric acid, (D) DPM-tartaric acid, and (E) DPM-oxalic acid cocrystals.

Powder X-Ray Diffraction of DPM-Cocrystals

PXRD provides a distinctive fingerprint diffraction pattern characteristic of a particular crystal structure. The 2θ value for 100% intensity of DPM was found at 20.4 and intense peaks of crystallinity were observed,

indicating its crystalline nature. Overlay of PXRD of DPM, cocrystals and cofomers were shown in Figure 7. The 2θ value for 100 % intensity of hippuric acid was observed at 18.4.

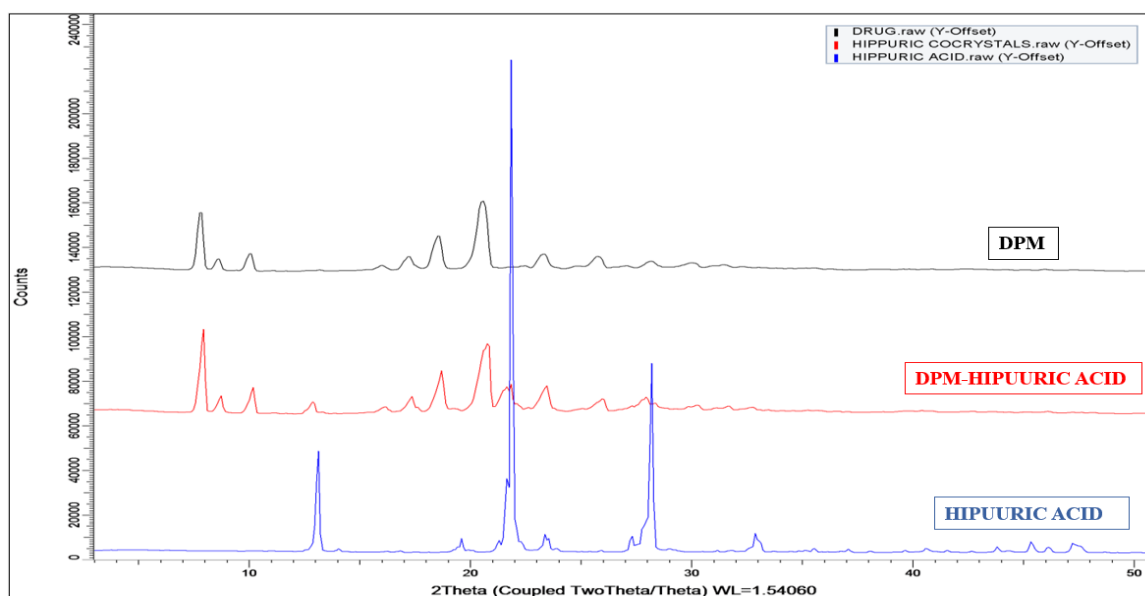


Figure 7. Overlay PXRD pattern of DPM-hippuric acid co-crystal with its individual components.

PXRD pattern of above prepared DPM cocrystals showed the presence of new peaks, alteration in peak intensities that infers different crystal habits and arrangement of molecules indicating generation of distinct crystalline forms.

DPM-hippuric acid cocrystals tablets were formulated with various levels of MCC (super disintegrating agent) and carboxy methyl cellulose as a binder.

Characterization of DPM-Hippuric Acid Tablets

Disintegration time, hardness, thickness, friability, drug content & % weight variation for DPMF₁, DPMF₂, DPMF₃ and DPMF₄ formulations were reported in Table 3. All parameters were found to be satisfactory. Hardness of tablets was found to be in

the range of 3-4 kg/cm² that confirms the resistance of tablets to shipping or breakage under conditions of storage and transportation. Friability results indicated good mechanical strength of tablets as the percentage of friability is less than 1% confirming to the compendial limits. Percentage deviation of weight was less than $\pm 7.5\%$, complying with Pharmacopeial specifications confirming uniformity of weight. Drug content was found to be within the specified limits of 90 to 110% of the stated amount. Disintegration time of all the prepared tablets was within the range of 54-61 seconds that comply with the disintegration time for uncoated tablets as per IP (<15 minutes) (Indian Pharmacopoeia, 2018)

Table 3. Characterization of DPM-hippuric acid tablet formulations

	DPMF ₁	DPMF ₂	DPMF ₃	DPMF ₄
Disintegration time(sec)*	54±0.81	60±0.81	56±0.47	55±0.81
Hardness(kg/cm ²)*	4±0.81	3±0.4	3±0.47	4±0.8
Thickness(cm*10 ⁻² m)*	0.36	0.36	0.36	0.36
Friability(%)	0.847±0.002	0.826±0.003	0.833±0.001	0.819±0.002
Drug content(AM±SD)*	96±0.53	95±0.81	95±0.81	95.33±0.54
% Weight variation	0	1	0.5	1

*Mean of three determinations (n=3)

Dissolution studies of DPM-hippuric acid cocrystal tablets

Dissolution studies of DPM-hippuric acid cocrystal tablets were performed in pH 6.8 buffer and

reported in (Figure 8).

The order of dissolution profiles of DPM-hippuric acid formulations (DPMF₁, DPMF₂, DPMF₃, DPMF₄) in pH 6.8 phosphate buffer resulted as F1>F2>F3>F4.

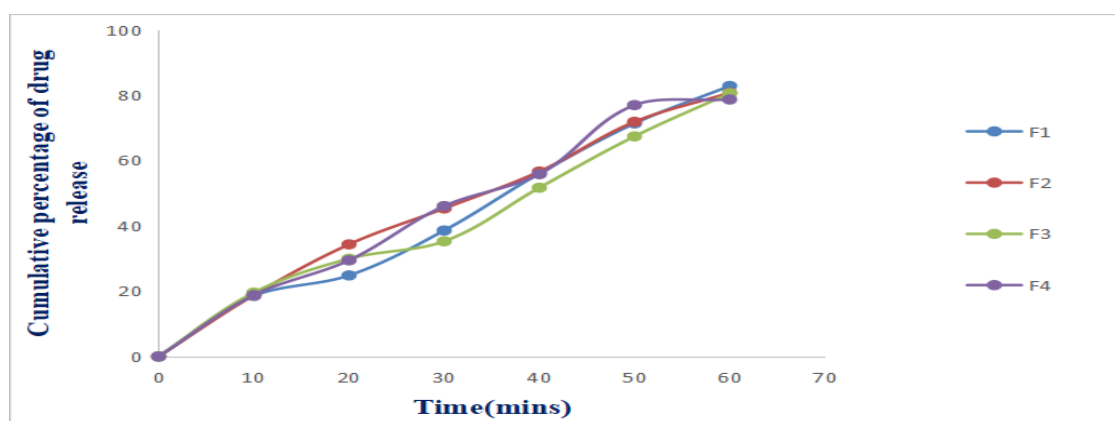


Figure 8. Dissolution profiles of DPM-hippuric acid formulations in pH 6.8 phosphate buffer.

Optimization of formulation of DPM-hippuric acid tablets

Factorial design analysis of DPM release at 60 min

The 60 min cumulative % DPM release data was analysed and recorded in the Table 4 and 5. The

coefficients were recorded in the standard format and equation (3) was obtained. From the software analysis, the following polynomial equation was obtained at 10mins.

$$Y = 82.78 - 4.43X_1 - 4.5X_2 + 1.94X_1X_2 \dots\dots\dots (3)$$

Table 4: DPM release data at 60 min

S. No.	Treatments	Cumulative DPM Release (%)
1	1	82.78
2	CMC, X ₁	80.7
3	MCC, X ₂	80.58
4	Interaction term, X ₁ X ₂	78.65

Table 5. 2² Factorial analysis of DPM at 60 min.

S. No.	Combination	Coefficient	significance	SS ratio
1	b0	82.7875	---	----
2	b1	-4.4375	---	44.9957%
3	b2	-4.5075	----	46.4265%
4	b12	1.9375	-----	8.5778%

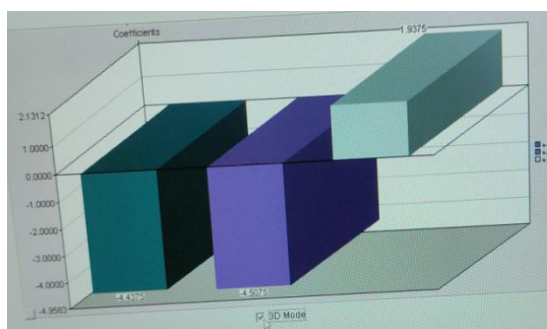


Figure 9: Graph identifying the influence of factors on DPM release at 60mins.

The MCC, (X_2) was highest (SS ratio = 46.426 %). The coefficient has negative sign, i.e., the higher the amount of X_2 , less will be the DPM release. The CMC, (X_1) is the second main factor (SS ratio = 44.99 %). The coefficient has negative sign, i.e., the higher the amount of X_1 , less will be the DPM release. The interaction term, (X_1X_2) was negligible (SS ratio = 8.577 %). The coefficient has a positive sign, i.e., the higher the amount of X_1X_2 , greater will be the DPM release.

Further, analysis is attempted by observing the simulation and search method. The main factors,

say X_1 and X_2 , are larger (nearly 50%) compared to the effects of their interactions (X_1X_2) and hence, the curvature effect was insignificant. The steepest ascent method was used for the simulation and optimization of the conditions or theoretical formulation.

Method of calculation – Simulation: Steepest ascent method was systematic simulation that is made with MCC jump by 2 mg, The CMC and other concentrations are automatically fixed. Then, responses are calculated using equations. The data are given in Table 6.

Table 6: Random simulation for steepest ascent method for 60 min release analysis

S.No	CMC	MCC	Estimated response
1	4	60	82.78
2	8	64	

The decision is taken regarding the ingredient concentrations. The concentrations finalized are: CMC (8 mg) and MCC (60 mg) for the desired cumulative % drug release of 82.78.

CONCLUSIONS

The melting point of DPM-cocrystals indicated a decrease in the melting point as compared to DPM (166.27 °C), suggesting the possibility of cocrystals

formation. Melting point data suggested formation of eleven cocrystals. Solubility studies were conducted for the 9 cocrystals. Among those, 6 cocrystals: DPM-citric acid, DPM-hippuric acid, DPM-tartaric acid, DPM-succinic acid, DPM-oxalic acid and DPM-cinnamic acid cocrystals showed increased solubility in pH 1.2, 6.8 buffers and distilled water. Dissolution studies of 6 cocrystals resulted in improved dissolution

rate in pH 6.8 buffer compared to the DPM. The 100% drug release was observed for DPM-hippuric acid cocrystals within 60 min while the DPM showed only 28.98% in 60 min. DPM-citric acid, DPM-hippuric acid, DPM-tartaric acid and DPM-oxalic acid preparation showed endothermic peaks, which were neither near to the melting point of DPM nor the coformer that inferred absence of physical mixture and the formation of cocrystals. PXRD pattern of cocrystals showed distinct diffraction pattern. DPM-hippuric acid tablets were prepared and among four formulations (F₁, F₂, F₃, F₄), F₁ formulation resulted as the optimised formula with the highest dissolution rate with accordance to the theoretical response. As anticipated in the objectives of the present work, the attempts were met. DPM-cocrystals with improved physicochemical properties were obtained.

ACKNOWLEDGEMENT

Authors are thankful to Hyderabad Central University for providing DSC and PXRD facility.

CONFLICT OF INTEREST

The authors declare that there is no conflict of interest

AUTHOR CONTRIBUTION STATEMENT

Author contributions: Concept -Monika Nijhawan; Design - Monika Nijhawan, Gunnam Sailaja; Supervision- Monika Nijhawan ; Data Collection and/or Processing -Sadhna Dhyagala; Analysis and/or Interpretation – Monika Nijhawan; Literature Search Rajeswari Aleti; Critical Reviews -Monika Nijhawan, Trapti Saxena, Gunnam Sailaja

REFERENCES

- Bevill, M. J., Vlahova, P. I., & Smit, J. P. (2014). Polymorphic cocrystals of nutraceutical compound p-coumaric acid with nicotinamide: Characterization, relative solid-state stability, and conversion to alternate stoichiometries. *Crystal growth & design*, 14(3), 1438-1448.
- Blagden, N., de Matas, M., Gavan, P. T., & York, P. (2007). Crystal engineering of active pharmaceutical ingredients to improve solubility and dissolution rates. *Advanced drug delivery reviews*, 59(7), 617-630.
- Cheney, M. L., Weyna, D. R., Shan, N., Hanna, M., Wojtas, L., & Zaworotko, M. J. (2010). Supramolecular architectures of meloxicam carboxylic acid cocrystals, a crystal engineering case study. *Crystal growth & design*, 10(10), 4401-4413.
- Cheney, M. L., Weyna, D. R., Shan, N., Hanna, M., Wojtas, L., & Zaworotko, M. J. (2011). Coformer selection in pharmaceutical cocrystal development: a case study of a meloxicam aspirin cocrystal that exhibits enhanced solubility and pharmacokinetics. *Journal of pharmaceutical sciences*, 100(6), 2172-2181.
- Dai, X. L., Chen, J. M., & Lu, T. B. (2018). Pharmaceutical cocrystallization: an effective approach to modulate the physicochemical properties of solid-state drugs. *CrystEngComm*, 20(36), 5292-5316.
- Gadade, D. D., & Pekamwar, S. S. (2016). Pharmaceutical cocrystals: Regulatory and strategic aspects, design and development. *Advanced pharmaceutical bulletin*, 6(4), 479.
- Gawade, A., Kuchekar, A., Boldhane, S., & Baheti, A. (2021). Improvement of physicochemical and solubility of dipyridamole by cocrystallization technology. *Journal of Drug Delivery and Therapeutics*, 11(1-s), 43-48.
- Guo, F., Zhong, H., He, J., Xie, B., Liu, F., Xu, H., Liu, M., & Xu, C. (2011). Self-microemulsifying drug delivery system for improved oral bioavailability of dipyridamole: preparation and evaluation. *Archives of pharmacal research*, 34(7), 1113-1123. <https://doi.org/10.1007/s12272-011-0709-8>

- Indian Pharmacopoeia, Govt of India, Ministry of Health and Family Welfare, The Indian Pharmacopoeia Commission, Ghaziabad, India, 2018; 8thEdition, 2.5.5:309,308
- Izutsu, K. I., Koide, T., Takata, N., Ikeda, Y., Ono, M., Inoue, M., Fukami, T., &Yonemochi, E. (2016). Characterization and Quality Control of Pharmaceutical Cocrystals. *Chemical & pharmaceutical bulletin*, 64(10), 1421–1430.
- Kojo, Y., Matsunaga, S., Suzuki, H., Taniguchi, C., Kawabata, Y., Wada, K., Yamauchi, Y., Seto, Y., Sato, H., &Onoue, S. (2017). Improved Dissolution of Dipyridamole with the Combination of pH-Modifier and Solid Dispersion Technology. *Chemical & pharmaceutical bulletin*, 65(5), 426–431. <https://doi.org/10.1248/cpb.c16-00714>
- Kumar, S. S., Thakuria, R., &Nangia, A. (2014). Pharmaceutical cocrystals and a nitrate salt of voriconazole. *CrystEngComm*, 16(22), 4722-4731.
- Marydele J. The Merck Index: An Encyclopedia of Chemicals, Drugs and Biologicals. 2006; 14th Ed. New Jersey, Merck and Co. Inc: pp 30, 384, 389, 1191
- Nijhawan, M., Godugu, M., Saxena, T., Farheen, T., & Dwivedi, K. (2022). Pharmaceutical co-crystals of posaconazole for improvement of physicochemical properties. *Brazilian Journal of Pharmaceutical Sciences*, 58.
- Nijhawan, M., Santhosh, A., Babu, P. S., & Subrahmanyam, C. V. S. (2014). Solid state manipulation of lornoxicam for cocrystals–physicochemical characterization. *Drug development and industrial pharmacy*, 40(9), 1163-1172.
- Panzade, P., Shendarkar, G., Shaikh, S., & Balmukund Rathi, P. (2017). Pharmaceutical Cocrystal of Piroxicam: Design, Formulation and Evaluation. *Advanced pharmaceutical bulletin*, 7(3), 399–408. <https://doi.org/10.15171/apb.2017.048>
- Pol, S., Nawale, R., Puranik, P., Chalak, H., & Pol, H. (2018). Scientific cofomer screening, preparation and evaluation of Dabigatran Etxilate Mesylate Cocrystal. *Asian Journal of Pharmacy and Pharmacology*, 4(6), 810-820.
- Qiao, N., Li, M., Schlindwein, W., Malek, N., Davies, A., &Trappitt, G. (2011). Pharmaceutical cocrystals: an overview. *International journal of pharmaceuticals*, 419(1-2), 1-11.
- Raymond CR, Sheskey, PJ, Quinn ME. Editors, Handbook of Pharmaceutical Excipients. 6th Edition. London: Pharmaceutical Press; 2009. P. 185,770.
- Saganowska, P., &Wesolowski, M. (2018). DSC as a screening tool for rapid co-crystal detection in binary mixtures of benzodiazepines with co-formers. *Journal of Thermal Analysis and Calorimetry*, 133, 785-795.
- Savjani, K. T., Gajjar, A. K., &Savjani, J. K. (2012). Drug solubility: importance and enhancement techniques. *ISRN pharmaceuticals*, 2012, 195727. <https://doi.org/10.5402/2012/195727>
- Schultheiss, N., &Newman, A. (2009). Pharmaceutical cocrystals and their physicochemical properties. *Crystal growth and design*, 9(6), 2950-2967.
- Stahl, P. H., &Wermuth, C. G. (2002). Handbook of pharmaceutical salts: properties, selection and use. *Chem. Int*, 24, 21.

- Thimmasetty, J., Ghosh, T., Nayak, N. S., & Raheem, A. (2021). Oral bioavailability enhancement of paliperidone by the use of cocrystalization and precipitation inhibition. *Journal of Pharmaceutical Innovation*, 16, 160-169.
- Thipparaboina, R., Kumar, D., Chavan, R. B., & Shastri, N. R. (2016). Multidrug co-crystals: towards the development of effective therapeutic hybrids. *Drug Discovery Today*, 21(3), 481-490.
- Yadav, A. V., Shete, A. S., Dabke, A. P., Kulkarni, P. V., & Sakhare, S. S. (2009). Co-crystals: a novel approach to modify physicochemical properties of active pharmaceutical ingredients. *Indian journal of pharmaceutical sciences*, 71(4), 359.

Formulation and Evaluation of Mixed Micelles Containing Quercetin for Inhibiting Intestinal Metabolism of Atorvastatin

Narahari N. PALEI*, Jayaraman RAJANGAM**, Ramu SAMINENI***, Arghya K DHAR****, Anna BALAJI*****

Formulation and Evaluation of Mixed Micelles Containing Quercetin for Inhibiting Intestinal Metabolism of Atorvastatin

Atorvastatinin Bağırsak Metabolizmasını İnhibe Etmek İçin Kersetin İçeren Karışık Misellerin Formülasyonu ve Değerlendirilmesi

SUMMARY

Atorvastatin is a poorly bioavailable drug due to fast-pass metabolism. The objective of the study was to prepare quercetin-containing mixed micelles to inhibit intestinal metabolism of Atorvastatin. Mixed micelles of Atorvastatin were prepared using the film hydration method, and optimization of the formulations were based on different ratios of poloxamer 188 and sodium deoxycholate (SDC). The drug permeation and permeability coefficients of mixed micelles were calculated from an ex vivo study using goat intestines. To the optimized formulation (F7), quercetin was added to improve the permeability of Atorvastatin. The vesicle size, % entrapment efficiency, and % in vitro drug release of optimized formulation (F7) were found to be 273.11 nm, 91.34%, and 72.14%, respectively. The ex vivo results of Atorvastatin with quercetin (25 mg) showed two times more permeation (flux = 2.69 µg/cm²h), and Atorvastatin mixed micelles with quercetin (25 mg) showed three times (flux = 4.33 µg/cm²h) compared to Atorvastatin without quercetin (flux = 1.34 µg/cm²h). The improvement of Atorvastatin permeation of mixed micelles may be due to the blockage of the p glycoprotein efflux pump in the presence of quercetin. The histopathology analysis revealed that the utilization of mixed micelles resulted in alterations to the tissue microenvironment, whereas no significant changes were observed in the control tissue. Based on the obtained results, we can conclude that the mixed micelles containing Atorvastatin enhanced the permeability effect in the presence of quercetin compared to the plain formulation without quercetin.

Key Words: Atorvastatin; mixed micelles; permeability; ex-vivo studies; histopathology

ÖZ

Atorvastatin, hızlı geçiş metabolizması nedeniyle biyoyararlanımı zayıf bir ilaçtır. Çalışmanın amacı, Atorvastatinin bağırsak metabolizmasını inhibe etmek için kersetin içeren karışık miseller hazırlamaktır. Atorvastatinin karışık miselleri, film hidrasyon yöntemi kullanılarak hazırlanmıştır ve formülasyonlar, farklı poloksamer 188 ve sodyum deoksikolat (SDC) oranlarına dayalı olarak optimize edilmiştir. Karışık misellerin ilaç geçirgenliği ve geçirgenlik katsayıları, keçi bağırsağı kullanılarak yapılan ex vivo çalışmadan hesaplanmıştır. Optimize edilmiş formülasyona (F7), Atorvastatinin geçirgenliğini iyileştirmek için kersetin eklenmiştir. Optimize edilmiş formülasyonun (F7) vezikül boyutu, % yakalama etkinliği ve in vitro ilaç salımı %'si sırasıyla 273.11 nm, % 91.34 ve % 72.14 bulunmuştur. Kersetin (25 mg) içeren Atorvastatin'in ex vivo sonuçları ve kersetin (25 mg) içeren Atorvastatin karışık miselleri, kersetin içermeyen Atorvastatin'e (akı = 1,34 µg/cm²h) kıyasla sırasıyla iki kat (akı = 2,69 µg/cm²h) ve üç kat (akı = 4,33 µg/cm²h) daha fazla permeabilite göstermiştir. Atorvastatin permeasyonunun karışık misel formundaki gelişimi, kersetin varlığında p glikoprotein akış pompasının bloke edilmesine bağlı olabilir. Histopatoloji çalışması, kontrol dokusu sırasında hiçbir önemli değişiklik meydana gelmemesine kıyasla, karışık miseller kullanıldığında formülasyonun dokunun mikro ortamını değiştirdiğini göstermiştir. Elde edilen sonuçlara dayanarak, Atorvastatin içeren karışık misellerin, kersetin içermeyen formülasyona kıyasla, kersetin varlığında permeabilite etkisini arttırdığı sonucuna varabiliriz.

Anahtar Kelimeler: Atorvastatin; karışık miseller; permeabilite; ex-vivo çalışmalar; histopatoloji

Received: 23.05.2023

Revised: 04.11.2023

Accepted: 06.11.2023

* ORCID: 0000-0002-2041-1849, Amity Institute of Pharmacy, Amity University Uttar Pradesh, Lucknow Campus, India

** ORCID: 0000-0002-6367-0365, Shri Venkateshwara College of Pharmacy, Ariyur, Pondicherry, India

*** ORCID: 0000-0002-8652-2883, Department of Pharmaceutics, School of Pharmaceutical Sciences, Sandip University, Mahiravani, Maharashtra, India

**** ORCID: 0000-0003-1081-9143, School of Pharmacy, The Neotia University, Sarisha, West Bengal, India

***** ORCID: 0000-0002-3233-9637, IIMT College of Pharmacy, Greater Noida, Uttar Pradesh, India

© Corresponding Author; Narahari N. PALEI

E-mail: narahari.palei@gmail.com

INTRODUCTION

Atorvastatin (ATV) is an 3-hydroxy-3-methylglutaryl coenzyme (HMG-Co) reductase inhibitor with 12% oral bioavailability because of its poor water solubility and high first-pass metabolism. Oral administration is the most extensively used method of drug delivery because it is convenient and affordable, especially for long-term treatment (Qu, 2018). When the polymer concentrations are higher than the critical micellar concentration (CMC) and mostly amphiphilic polymers self-assemble in water to form nanostructures with a hydrophobic core and a hydrophilic shell, they are called mixed micelles. A lipophilic core amplifies the solubility of lipophilic drugs and allows controlled drug release. In addition, the small particle size increases cellular absorption and the capacity to overcome epithelial barriers while extending the residence period in blood circulation, skipping liver, spleen, and glomerular clearance processes. The cumulative effects of all these factors enhance drug bioavailability (Lu, 2013; Pepic, 2013). Mixed micelles contain phospholipids that help enhance drug permeation through lymphatic vessels, which can directly carry the drug to the systemic circulation, resulting in improved bioavailability. As the central part of the cell membrane, phospholipids have many benefits as drug carriers. They are biocompatible, emulsifying, and surface-active wetting agents that improve drug permeability and retention (Abd-Elsalam, 2019). The development of a novel micellar carrier for improving intestinal permeability is influenced by the saturation of phospholipid levels (Kassem, 2017). Recent research has demonstrated that lipid-containing micelles may retain the fluidity of cell membranes and facilitate the absorption and utilization of poorly soluble drugs (Wang, 2014; Li, 2015). In addition, many researchers have studied the potential of cholate-mixed micelles for solubilizing poorly soluble drugs (Dongowski, 2005; Weng, 2021). Researchers are increasingly interested in the formulation of mixed micelles because of their enhanced drug solubility, high drug loading, good stability, and extended

systemic circulation. Mixed micelles have also shown better tissue targeting, suppressing the P-glycoprotein (Pgp) effect, hypersensitivity of multidrug-resistant cells, and subcellular drug distribution properties (Kulthe, 2011; Chiappetta, 2013; Bothiraja, 2013). Pgp, a 170-kDa membrane transporter and a member of the ATP-binding cassette, is an example of an efflux transporter that uses ATP as an energy source. Pgp, a transmembrane protein predominantly located in the intestinal epithelium, plays a crucial role in the efflux of drugs, hence diminishing their oral bioavailability. It is possible to control Pgp activity to enhance drug bioavailability (Genevieve, 2010). By blocking Pgp, several studies have been conducted to increase the penetration of first metabolite drugs such as resveratrol (Jadhav, 2016; Nguyen, 2021), berberine (Kwon, 2020), and silymarin (Piazzini, 2019). Mixed micelles have been used to enhance the bioavailability of various poorly bioavailable drugs by improving lymphatic circulation and inhibiting Pgp efflux and CYP3A4 enzyme metabolism. Quercetin, a type of flavonoid, has been identified as a potential bioenhancer capable of inhibiting Pgp efflux and CYP3A4 enzyme drug metabolism. This inhibition mechanism has the potential to enhance drug bioavailability (Kesarwani, 2013; Mu, 2019). Quercetin can be used as an enhancer for improving the drug permeability and bioavailability. Hence, we have included quercetin in the formulations of mixed micelles in order to reduce the amount of metabolism that occurs in the gut wall in order to improve the presentation of the drug in the systemic circulation and, as a result, the oral bioavailability. Therefore, this work aimed to develop quercetin containing ATV mixed micelles and assess its impact on gut wall permeability in formulations of mixed micelles.

MATERIALS AND METHODS

ATV and quercetin were procured from Yarrow chem India, Mumbai. Poloxamer 188, sodium deoxycholate (SDC), and lecithin were procured from Himedia, Mumbai. Hematoxylin and eosin were procured from Sigma, Bangalore. The dialysis bag

was procured from Himedia, Mumbai. HPLC-grade chemicals and reagents were utilized for this study.

Preparation of ATV suspension

ATV (20 mg) and different amounts of quercetin (12.5, 25, 37.5, and 50 mg) were added to 10 mL distilled water containing 1% of poloxamer188 and appropriately stirred using a mechanical stirrer at a speed of 700 RPM to obtain ATV suspension. The ATV suspension was stored at 2 to 8°C for 24 h.

Preparation of ATV mixed micelles formulation

ATV mixed micelles were developed using the film hydration method with slight modification (Sun, 2016). Different ratios of lecithin, and surfactants were prepared and dissolved in a round-bottomed

flask with 10 mL each of chloroform and methanol (2:1 V/V). The ATV was weighed and then added to the solvent. A smooth film was produced by evaporating the solvent in a rotavapor (RV 10, IKA) using a vacuum of 20 in Hg at 60°C and 100 rpm. The film was dried at room temperature. Mixed micelles were obtained by hydrating the dried film in 10 mL of phosphate buffer (PB) pH 6.8 for 3 h at 37 ± 2°C. The mixed micelle formulation was stored at 2 to 8°C for 24 h. The formulation of mixed micelles is depicted in Table 1. Quercetin (25 mg) was added to the organic phase along with lecithin and surfactants and the same procedure was followed to formulate the quercetin ATV mixed micelles.

Table1. Formulation of ATV mixed micelles

Ingredients	F1	F2	F3	F4	F5	F6	F7	F8
ATV(mg)	20	20	20	20	20	20	20	20
Lecithin(mg)	75	75	75	75	75	75	100	150
Polaxomer188(mg)	150	-	120	112.5	100	75	75	75
SDC(mg)	-	150	30	37.5	50	75	75	75

Evaluation of Mixed Micelle Formulations

Particle Size and Zeta Potential

The particle size of mixed micelles was determined using the dynamic light scattering technique (Horiba SZ 100, Japan). Appropriate dilution was made before measuring the particle size of mixed micelles and poured into a 10 mm diameter cell. The estimation was performed at 25°C at an angle of 90°. The same method was adopted for measuring the zeta potential.

Entrapment Efficiency (EE) and Drug Loading (DL)

Mixed micelles formulations (10 mL) were put into a stopper tube and centrifuged at 15,000 rpm for 60 min while keeping the temperature at 10°C. The sample was then filtered using filter paper to get a clear supernatant. The untrapped drug was determined from the apparent, fraction by applying a UV visible spectrophotometer set at 246 nm. The %EE and %DL were determined using the formula(Xie, 2017).

$$EE (\%) = [(Wt-Wu)/Wt] \times 100$$

Where Wt is the amount of total drug, and Wu is the amount of untrapped drug.

$$DL (\%) = [\text{Weight of entrapped ATV in micelles} / \text{Total weight of micelles}] \times 100$$

Cumulative Drug Release (CDR) study

The vesicle suspension was transferred into a dialysis bag using a pipette, and subsequently sealed. The dialysis bag was put into a beaker with 500 mL of PB pH 6.8. The beaker was placed on the magnetic stirrer, and the speed was maintained at 50 rpm. Throughout the entire experiment, the temperature was kept at 37 ± 0.5°C. At predetermined intervals, samples were withdrawn, and substituted the same quantity of PB pH 6.8 throughout the experiment. Samples were adequately diluted using PB pH 6.8, and the amount of drug was determined using a UV-visible spectrophotometer at 246nm.

Release Kinetics study

In vitro release kinetics of different mixed micelles formulations were determined and analyzed to find the drug release patterns. The *in vitro* release data were fitted to zero order (cumulative % release versus time), first order (log % drug remaining versus time), Higuchi order (cumulative % drug release versus square root of time), and Korsmeyer-Peppas model (log drug release versus log time). Values of r^2 and k were calculated from the linear curve obtained by regression analysis of the plots. In the Korsmeyer-Peppas model, n value was calculated (Kushwaha, 2013).

Fourier Transform Infrared (FT-IR) analysis

FT-IR spectrophotometer (Agilent) was used to record the FT-IR spectra of ATV, lecithin, SDC, mixed micelles, and ATV-mixed micelles between 600 cm^{-1} and 4000 cm^{-1} .

Transmission Electron Microscopy (TEM) study

The TEM instrument (Jeol, Japan) was utilized to conduct a morphological analysis of ATV mixed micelles. A single droplet consisting of mixed micelles was carefully deposited onto a carbon-coated copper grid, resulting in the formation of a thin film. The sample was examined and photographed using an electric voltage of 15 KeV.

Stability study

Freshly prepared ATV mixed micelles (F7) were put into glass vials and kept there for 0, 2, 4, and 8 weeks at 4 and 25°C . At predefined intervals, the particle size (nm), %EE, and %CDR were calculated (Tang, 2021).

Ex vivo studies using goat intestine

Ex vivo studies were conducted by selecting goat ileum (Jha, 2014). The 4 cm ileum was appropriately

washed and placed in a 100 mL container containing 50 mL PB, pH 6.8. Mixed micelles (2 mL) were kept in the ileum. The ileum was tied using thread at both sides and dipped in PB solution with proper aeration. 2 mL of the sample was extracted at specific intervals up to 6 h, and fresh PB pH 6.8 was replaced to maintain sink condition. The sample was quantified using a UV-visible spectrophotometer at 246 nm.

Histopathology study

After the test formulation was put on the goat ileum, it was cut in half and stained with hematoxylin and eosin so that changes in the histology could be seen. The results were compared to goat intestines that had not been treated.

Statistical analysis

All data are represented in Mean \pm standard deviation ($n = 3$). The t-test was used to assess the significance level of data, and $p < 0.05$ was considered significant.

RESULTS AND DISCUSSION

Characterizations of Mixed micelles

The vesicle sizes ranging from 321.66 nm to 587.22 nm and are depicted in Table 2. The various ratios of SDC and Poloxamer 188, such as 1:0, 1:1, 2:3, 1:4, 0:1 were used for formulating mixed micelles. From that, we found a 1:1 ratio (F6) of SDC and Poloxamer 188 having less particle size. Lecithin played a significant role in the reduction of particle size. With increasing the amount of lecithin, the particle size decreased to 273.11 nm (F7). This providing a proper place for ATV in mixed micelles, resulting in the size reduction. The surfactants also help to reduce the particle size of mixed micelles by lowering the interfacial tension. In the presence of quercetin in the mixed micelles, the particle size and PDI were not significantly different.

Table 2. Characterizations of ATV mixed micelles (Mean ± S.D., n = 3)

Formulation	Particle Size (nm)	PDI	ZP (mV)	EE (%)	DL (%)	CDR (%)
F1	560.23 ± 7.9	0.26 ± 0.03	- 28.9 ± 1.2	72.11 ± 3.8	6.40 ± 0.81	59.33 ± 4.2
F2	587.22 ± 10.3	0.29 ± 0.04	- 31.5 ± 2.4	72.44 ± 2.7	6.43 ± 0.92	57.28 ± 3.9
F3	412.22 ± 6.4	0.29 ± 0.02	- 34.7 ± 1.9	86.23 ± 3.4	7.64 ± 0.87	67.24 ± 3.7
F4	478.14 ± 7.9	0.31 ± 0.04	- 29.2 ± 1.7	70.13 ± 3.3	6.23 ± 0.65	57.19 ± 2.6
F5	501.23 ± 9.7	0.25 ± 0.06	- 30.3 ± 2.6	76.22 ± 2.8	6.77 ± 0.23	66.76 ± 4.4
F6	321.66 ± 6.4	0.24 ± 0.03	- 36.8 ± 3.7	91.34 ± 3.9	8.11 ± 0.37	72.14 ± 3.6
F7	273.11 ± 8.2	0.27 ± 0.03	-38.2 ± 2.9	93.17 ± 2.1	8.28 ± 0.54	76.45 ± 2.9
F8	282.56 ± 9.1	0.24 ± 0.06	-36.5 ± 1.8	91.45 ± 1.7	8.12 ± 0.34	73.28 ± 3.7

The poly dispersive index (PDI) of prepared ATV mixed micelles was found in the range of 0.24 to 0.31. A PDI value of 0.3 or lower is deemed appropriate within the context of drug delivery systems that utilize lipid-based formulations. This value signifies the presence of a uniformly dispersed population of phospholipid vesicles (Putri, 2017; Danaei, 2018). The zeta potential influenced the stability of a colloidal dispersion system. The lower the zeta potential is likely to aggregate the particles due to insufficient electric repulsion or steric barriers between each other (Helmy, 2013). According to various reported zeta potential values, formulations with zeta potentials greater than +30 or -30 mV are highly stable (Palei, 2013). The zeta potential of the F7 formulation was found to be -36 mV. Based on the zeta potential, it might be considered as the optimum for stabilizing the mixed micelles formulation. The particle size and zeta potential of blank and ATV-loaded mixed micelles are depicted in Figure 1. The % entrapment efficiency was found in the range from

70.13% to 93.17%. The entrapment efficiency of drug-loaded mixed micelles was seen to vary when SDC and poloxamer 188 were combined in different ratios. However, when the ratio of SDC and poloxamer 188 was 1:1, the entrapment efficiency was significantly higher ($p < 0.05$) compared to the other ratios. When SDC and poloxamer 188 were used alone in mixed micelles, the entrapment efficiency decreased. This because of two things. First, increasing the amount of lecithin maintained hydrophobicity, stability, and permeability of mixed micelles, which may make it easier to trap the hydrophobic drug in micelles. Secondly, the proper ratio of SDC and poloxamer 188 may provide adequate space to entrap the drug into mixed micelles. The 1:1 ratio of SDC and poloxamer 188 showed maximum entrapment efficiency, which may be due to adequate solubilization of, ATV in mixed micelles (Choi, 2015). The characterizations of ATV mixed micelles are depicted in Table 2.

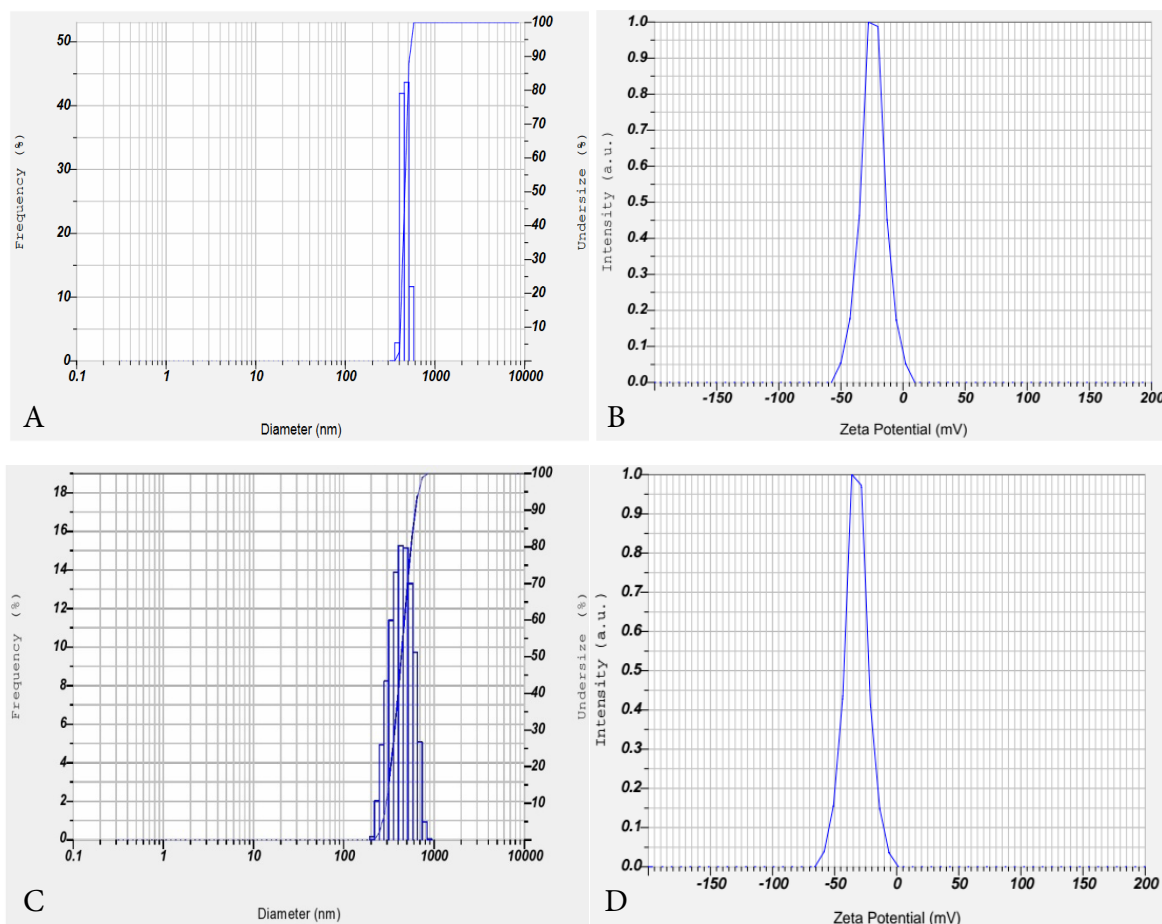


Figure 1. (A) Particle size of mixed micelles (Blank), (B) Zeta potential of mixed micelles (Blank), (C) Particle size of F7, and (D) Zeta potential of F7

***In vitro* drug release**

In vitro studies of mixed micelle formulations were performed using a dialysis method. The % drug release of different mixed micelle formulations was found in the range from 57.28 to 76.45 up to 12 h and is depicted in Figure 2. The drug release from the mixed micelle formulation containing a 1:1 ratio of SDC and Poloxamer 188 showed 72.14% release up to 12 h. The different ratios of SDC and poloxamer 188 influenced the release of ATV. The blend of surfactants may provide suitable space for ATV, resulting in better release. Lecithin concentration was raised, resulting in an increase in drug release to 76.45% (F7). Lecithin

may improve the solubility of ATV, making it easier for the dissolution fluid to transport the drug and thus enhance the drug release.

From release kinetics data, it was found that all mixed micelle formulations followed better in zero order kinetics and the Higuchi model compared to first-order kinetics (Table 3). The release pattern indicated that drug release from mixed micelles happened in a diffusion-like way. The *n* values of the Korsmeyer-Peppas model were found to be less than 0.79. Therefore, the drug release followed non-Fickian diffusion.

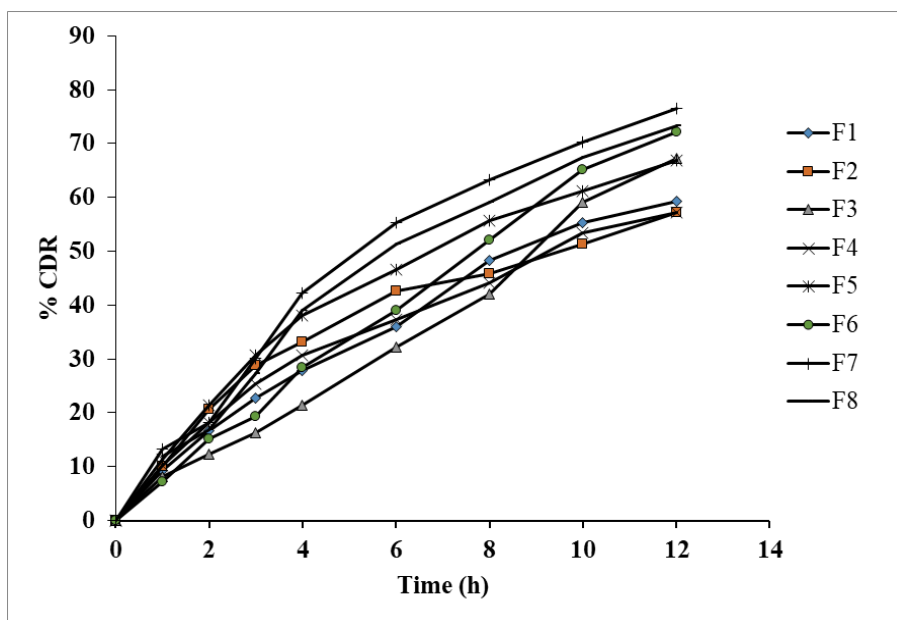


Figure 2. *In vitro* cumulative drug release of various ATV mixed micelles formulations (n=3)

Table 3. Release kinetics of ATV Mixed micelles

FC	Zero order		First order		Higuchi		Korsmeyer-Peppas		
	K_0	R^2	K_1	R^2	K_h	R^2	n	K_{kp}	R^2
F1	4.89	0.97	0.105	0.96	18.37	0.97	0.74	9.54	0.99
F2	4.47	0.98	0.098	0.97	17.83	0.98	0.67	7.58	0.99
F3	5.37	0.98	0.105	0.95	19.61	0.93	0.72	11.48	0.98
F4	4.43	0.95	0.098	0.94	17.33	0.98	0.78	7.24	0.99
F5	5.18	0.94	0.107	0.95	20.61	0.98	0.73	10.71	0.99
F6	6.13	0.99	0.099	0.96	22.36	0.93	0.72	12.58	0.98
F7	6.34	0.95	0.119	0.99	24.7	0.96	0.75	12.88	0.98
F8	5.72	0.96	0.110	0.99	23.12	0.97	0.77	11.48	0.97

FT-IR studies

The FT-IR spectrum of ATV showed a distinctive peak at 3065 cm^{-1} because of the presence of -NH stretching vibration and aromatic -CH stretching vibration. The peak was detected at 1641 cm^{-1} because of the C=O stretching in primary amide. A distinctive peak was detected at 1422 cm^{-1} and 1386 cm^{-1} , allocated to bending of the N-H group and stretching of -CO of the carboxylic group, respectively. The stretching vibration of the C-N group appeared at 1231 cm^{-1} . The spectrum of ATV mixed micelles exhibited characteristic peaks of ATV at 3062 cm^{-1} ,

1639 cm^{-1} , 1426 cm^{-1} , and 1388 cm^{-1} due to -NH stretching, -CO stretching, -NH bending, and -CO stretching in the carboxylic group, respectively (Figure 3). When the spectra of ATV and mixed micelles were compared, there was no discernible variation in the positions of the peaks for ATV, which indicated that the drug was compatible with the excipients used in the formulation. However, a concurrent decline in the intensity of the corresponding peaks allocated for ATV was seen in the spectrum of the formulation due to the inclusion of other excipients in the formulations (Kim, 2008).

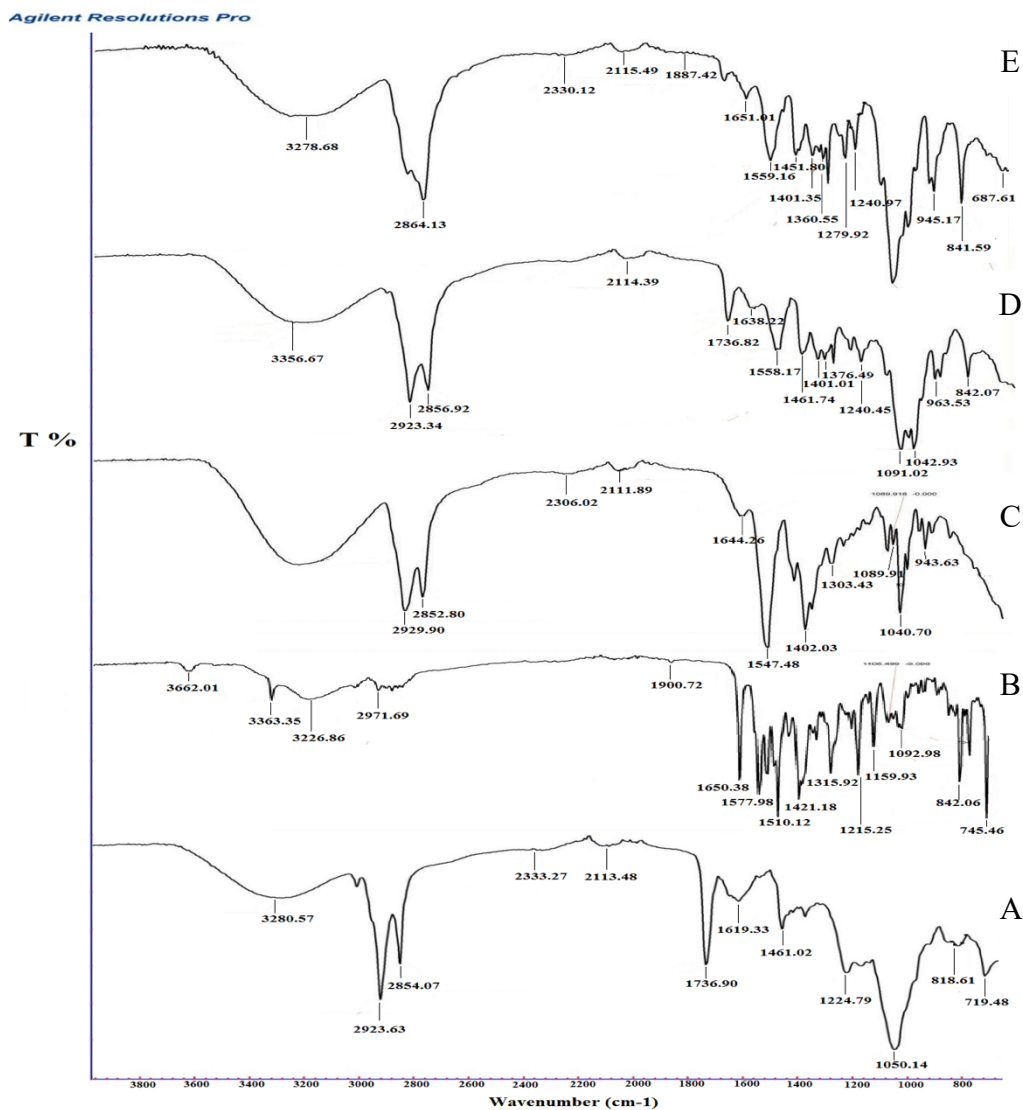


Figure 3. FTIR study of (A) ATV, (B) Lecithin, (C) SDC, (D) Mixed micelles, (E) ATV mixed micelles(F7)

TEM analysis

TEM analysis observed ATV-loaded mixed micelles (F7) and quercetin ATV loaded mixed micelles having a spherical shape. Still some irregular

fashion was observed because of the presence of surfactant network and water layer on the surface of mixed micelles represented in Figure 4. The TEM analysis results are quite acceptable compared to dynamic light scattering method.

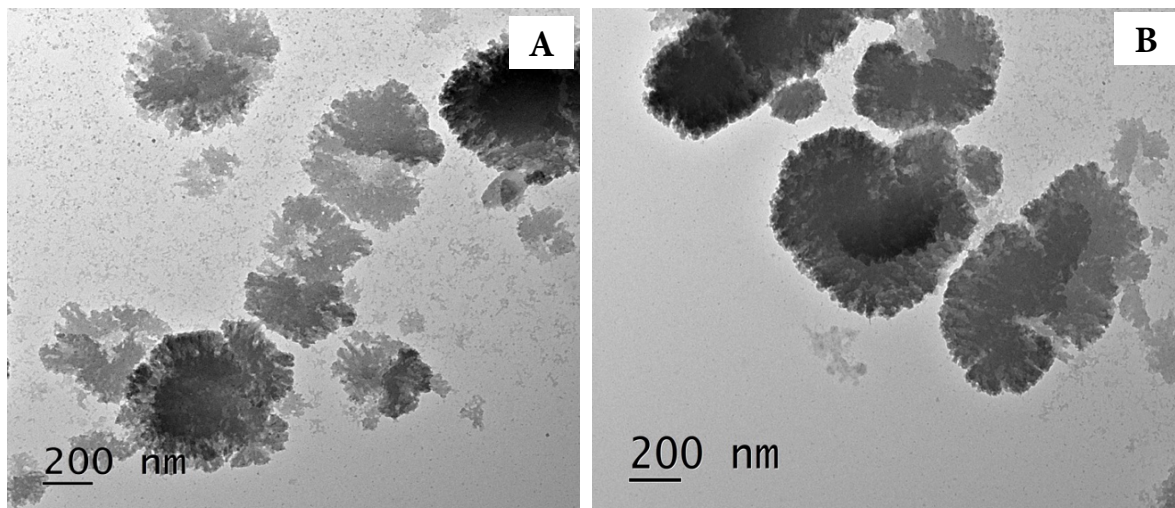


Figure 4. TEM analysis of (A) ATV loaded Mixed Micelles (F7); (B) Quercetin ATV loaded mixed micelles

Stability study

The size, % EE, and % CDR of freshly prepared ATV mixed micelles (F7) were determined at 4°C and 25°C for 8 weeks to evaluate the stability of the mixed micelles. The particle size, % EE, and % CDR of the mixed micelles did not significantly change at 4°C, as shown

in Table 4. The particle size of the composite micelles significantly increased. In contrast, the % EE and % CDR slightly decreased when the mixed micelles were maintained at 25°C, and no sedimentation was observed after eight weeks. As a result, the F7 formulation was stable at a temperature of 4°C compared to 25°C.

Table 4. Stability study of ATV loaded mixed micelles (F7) at different temperatures (Mean ± S.D., n=3)

Time (weeks)	4°C			25°C		
	Particle size (nm)	EE (%)	CDR (%)	Particle size (nm)	EE (%)	CDR (%)
0	273.11 ± 8.2	93.17 ± 2.1	76.45 ± 2.9	273.11 ± 8.2	93.17 ± 2.1	76.45 ± 2.9
2	277.11 ± 9.3	93.10 ± 3.6	76.12 ± 1.7	281.56 ± 7.1	92.86 ± 1.8	75.36 ± 2.1
4	286.11 ± 6.2	92.13 ± 2.9	75.65 ± 1.2	294.23 ± 9.3	91.36 ± 1.4	75.11 ± 1.7
8	294.23 ± 7.9	90.76 ± 2.3	75.19 ± 1.6	321.11 ± 6.8	89.31 ± 2.3	74.35 ± 1.6

Ex vivo permeation studies

The amount of drug permeated from ATV mixed micelles and ATV suspension was found to be 19.29 ± 1.8 µg/cm² and 8.31 ± 1.1 µg/cm², respectively. The ATV mixed micelle formulations showed higher intestinal permeation than the plain ATV suspension. Based on the results, the flux of ATV mixed micelles was found to be 3.15 ± 0.36 µg/cm²h, which was significantly more than the flux of ATV suspension (1.4 ± 0.22 µg/cm²h). The ability of mixed micelles to influence drug transport across the goat ileum has been explained by several different mechanisms,

including adsorption and fusion of the mixed micelles on the surface of the intestinal wall, which creates a high thermodynamic activity gradient of the drug at its interface and enhances penetration of lipophilic drugs. This result could be attributed to the superiority of the ATV mixed micelles over the ATV suspension because of their higher penetration capabilities. The nanosize of mixed micelles can improve cellular and paracellular transport, thereby increasing intestinal drug absorption and protecting intestinal drug metabolism. Because of their firm adherence to the intestinal membrane, mixed micelles may increase passive drug absorption (Alqahtani, 2017).

Table 5. *Ex vivo* permeation parameters of ATV suspension with quercetin (Mean ± S.D., n=3)

Formulations	Amt of drug permeated (µg/cm ²)	Flux (µg/cm ² h)	Permeability coefficient (cm/h × 10 ⁻³)	Enhancement ratio
ATV Suspension	8.31 ± 1.1	1.34 ± 0.30	0.33 ± 0.08	-
ATV+12.5 mg quercetin	11.04 ± 1.3	1.88 ± 0.46	0.47 ± 0.11	1.4 ± 0.002
ATV+ 25 mg quercetin	15.32 ± 0.9	2.69 ± 0.51	0.67 ± 0.12	2.01 ± 0.003
ATV+ 37.5 mg quercetin	15.8 ± 1.2	2.74 ± 0.47	0.69 ± 0.11	2.05 ± 0.002
ATV+ 50 mg quercetin	16.52 ± 1.1	2.57 ± 0.40	0.64 ± 0.10	1.92 ± 0.002

Proper intestinal absorption of different biopharmaceutical classification systems (BCS) II and III drugs was significantly impeded by Pgp. The BCS II classes of drugs have good permeability efficiency. Still, they cannot enter the systemic circulation because they are susceptible to the gut wall and first-pass metabolism. Mixed micelles strengthened

the attraction between the micelles and intestinal membrane, improved the water solubility of the lipophilic drug, and inhibited Pgp by d-α-tocopheryl polyethylene glycol succinate (TPGS), increasing drug permeability as well as oral bioavailability and therapeutic efficacy of DBAE-loaded mixed micelles (Collnot, 2007).

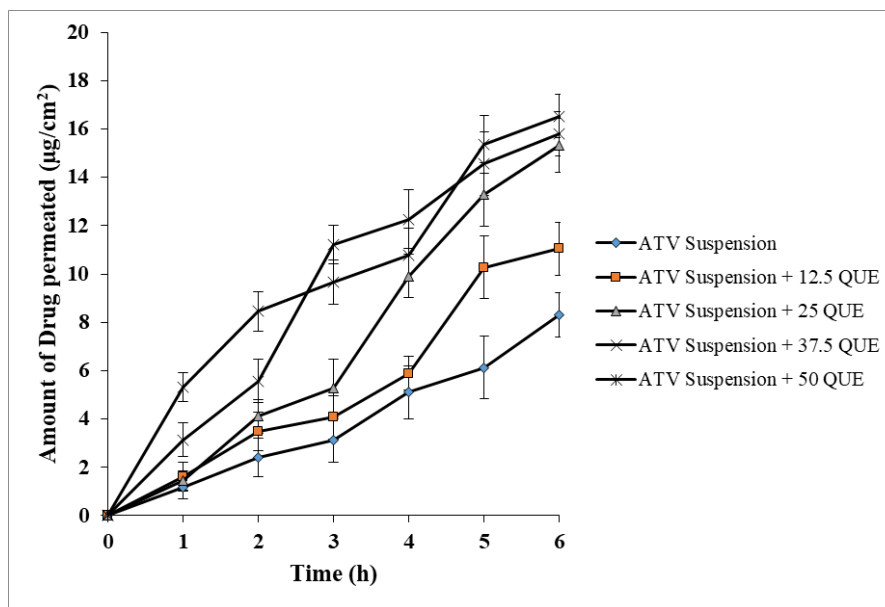


Figure 5. *Ex vivo* permeation parameters of ATV suspension with quercetin (n=3). (Abbreviation: ATV: atorvastatin, QUE: quercetin)

In this study, the utilization of quercetin as a Pgp inhibitor was explored within mixed micelle formulations, resulting in enhanced permeability across the gastrointestinal barrier. As different quercetin concentrations were introduced to free ATV suspension, it was found that the drug permeability significantly increased as compared to

ATV suspension without quercetin. While comparing the gut wall permeation of ATV using various concentrations of quercetin in the ATV suspension, it was found that the permeation of ATV was increased by increasing the concentration of quercetin in suspension up to 25 mg and further increasing the quercetin concentration, there were no significant

changes in gut wall permeation of ATV. ATV suspension containing 25 mg of quercetin, showed a significant ($p < 0.05$) increase in permeability almost two times compared to plain ATV suspension and

is depicted in Table 5 and Figure 5. Thus, 25 mg of quercetin was used in ATV-mixed micelles for the gut wall permeability study.

Table 6. *Ex vivo* permeation parameters of various formulations of ATV (Mean \pm S.D., n=3)

Formulations	Amt of drug permeated ($\mu\text{g}/\text{cm}^2$)	Flux ($\mu\text{g}/\text{cm}^2\text{h}$)	Permeability coefficient ($\text{cm}/\text{h} \times 10^{-3}$)	Enhancement ratio
ATV Suspension	8.31 \pm 1.1	1.4 \pm 0.22	0.35 \pm 0.05	-
ATV Mixed micelles(F7)	19.29 \pm 1.8	3.15 \pm 0.36	0.78 \pm 0.09	2.25 \pm 0.002
ATV Mixed micelles (F7)+ 25 mg quercetin	24.75 \pm 2.1	4.33 \pm 0.42	1.08 \pm 0.10	3.09 \pm 0.003

Therefore, ATV-mixed micelles containing 25 mg of quercetin were found three times more permeability compared to free ATV suspension and two times more permeability compared to ATV-mixed micelles. According to the findings, the enhancement ratio of quercetin containing ATV mixed micelles was found to be significantly more compared to ATV mixed micelles and ATV suspension. The permeability data

are depicted in Table 6 and Figure 6. Quercetin exhibits a regulatory effect on efflux transporters, potentially influencing the bioavailability of the administered drug. According to Hsiu et al., quercetin significantly impairs CYP3A4 and Pgp activity in the gut. Thus, the presence of quercetin in mixed micelles can improve the intestinal permeability of ATV (Hsiu, 2002; Mu, 2019).

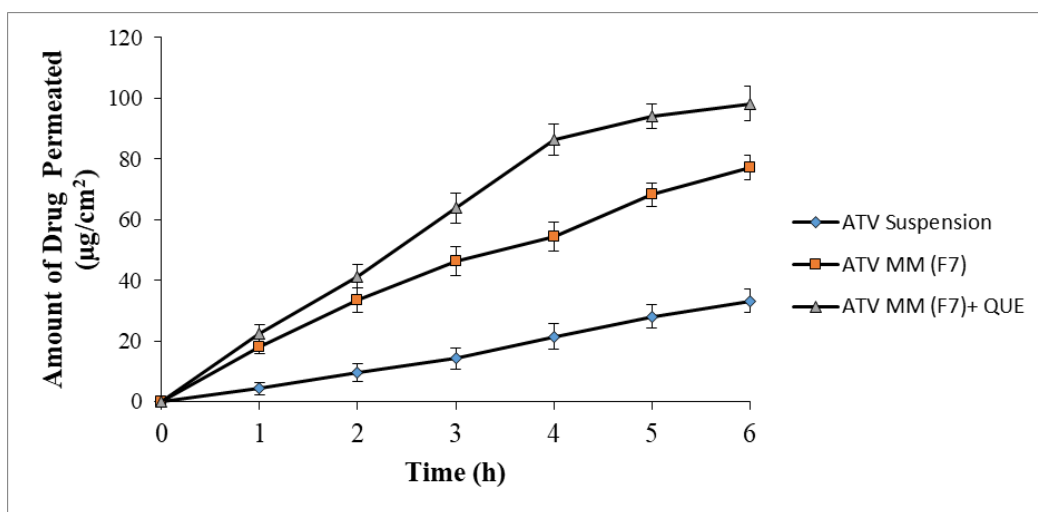


Figure 6. *Ex vivo* permeation study of various formulations of ATV (n=3). (Abbreviation: ATV: atorvastatin, MM: Mixed micelles, QUE: Quercetin)

Histopathology

The histopathology of goat ileum was performed and is shown in Figure 7. According to the histopathology investigation, the formulation altered the tissue microenvironment when it used mixed micelles, but the control tissue experienced no appreciable changes.

The histopathology study revealed that the ATV mixed micelles containing 25 mg of quercetin were more significant than the control in terms of the elongation of epithelial cells. The increased elongation of the epithelium suggested structural alterations, which could be brought on by quercetin.

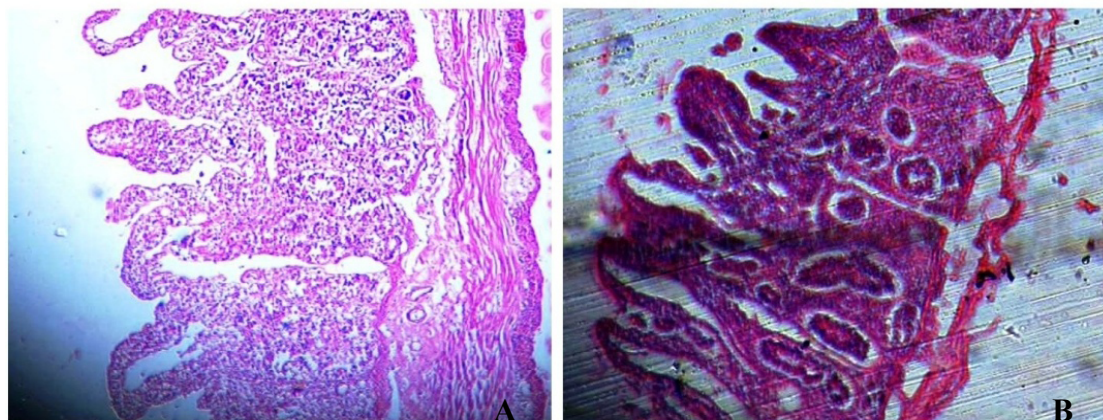


Figure 7. Histopathology study of (A) Control; (B) ATV mixed micelles containing 25mg of quercetin on goat intestine

CONCLUSIONS

ATV-loaded mixed micelles were prepared using the film hydration method. An optimized formulation (F7) was considered to have small vesicles, good entrapment efficiency, and enhanced drug release from mixed micelles. Ex vivo studies of ATV suspension with and without quercetin were conducted using goat intestines. The drug permeation study revealed a noteworthy enhancement in drug penetration when quercetin was present, as compared to the simple suspension. The mixed micelles containing quercetin exhibited a penetration rate that was three times higher than that of the plain ATV suspension and two times higher than that of the ATV-loaded mixed micelles (F7). Based on the results, it can be concluded that quercetin inhibits intestinal drug metabolism of ATV in mixed micellar formulation by preventing the action of Pgp efflux and possibly preventing CYP3A4 drug metabolism. Thus, the prepared ATV mixed micelles could be a promising carrier for improving the oral bioavailability.

CONFLICT OF INTEREST

The authors declare that there is no conflict of interest

AUTHORS OF CONTRIBUTION STATEMENT

Concept (NNP), Manuscript design (NNP, JR), Experiments and data interpretation (NNP, RS), Writing manuscript (NNP, AKD, AB)

REFERENCES

- Abd-Elsalam, W.H., El-Helaly, S.N., Al-mahallawi, A.M., Ahmed, M.A.(2019). The effect of the saturation degree of phospholipid on the formation of a novel self-assembled nano-micellar complex carrier with enhanced intestinal permeability. *International Journal of Pharmaceutics*, 569, 118567. doi: 10.1016/j.ijpharm.2019.118567
- Alqahtani, M.S., Islam, M.S., Podaralla, S. et al. (2017). Food protein-based core-shell nanocarriers for oral drug delivery: effect of shell composition on in vitro and in vivo functional performance of zeinnanocarriers. *Molecular Pharmaceutics* 14: 757–69. doi: 10.1021/acs.molpharmaceut.6b01017
- Bothiraja, C., Kapare, H.S., Pawar, A.P. et al. (2013). Development of plumbagin-loaded phospholipid-Tween® 80 mixed micelles: formulation, optimization, effect on breast cancer cells and human blood/serum compatibility testing. *Therapeutic delivery*, 4(10), 1247-1259. doi: 10.4155/tde.13.92
- Chiappetta, D.A., Hocht, C., Opezzo, J.A. et al.(2013). Intranasal administration of antiretroviral-loaded micelles for anatomical targeting to the brain in HIV. *Nanomedicine*, 8(2), 223-237. doi: 10.2217/nnm.12.104

- Choi, Y.A., Yoon, Y.H., Choi, K. et al.(2015). Enhanced oral bioavailability of morin administered in mixed micelle formulation with PluronicF127 and Tween80 in rats. *Biological and Pharmaceutical Bulletin*, 38(2), 208-217.
- Collnot, E.M., Baldes, C., Wempe, M.F. et al.(2007). Mechanism of inhibition of P-glycoprotein mediated efflux by vitamin E TPGS: influence on ATPase activity and membrane fluidity. *Molecular pharmaceutics*, 4(3): 465-74. doi: 10.1021/mp060121r
- Danaei, M., Dehghankhold, M., Ataei, S. et al.(2018). Impact of particle size and polydispersity index on the clinical applications of lipidic nanocarrier systems. *Pharmaceutics*, 10(2), 57. doi: 10.3390/pharmaceutics10020057
- Dongowski, G., Fritzsich, B., Giessler, J. et al.(2005). The influence of bile salts and mixed micelles on the pharmacokinetics of quinine in rabbits. *European journal of pharmaceutics and biopharmaceutics*, 60 (1), 147-151. doi: 10.1016/j.ejpb.2005.01.003
- Genevieve, G., Satturwar, P., Jones, M.C. et al.(2010). Polymeric Micelles for Oral Drug Delivery. *European journal of pharmaceutics and Biopharmaceutics*, 76, 147-158. doi:10.1016/j.ejpb.2010.06.007
- Helmy, K.Y., Patel, S.A., Nahas, G.R. et al.(2013). Cancer immunotherapy: accomplishments to date and future promise. *Therapeutic delivery*, 4(10), 1307-1320. doi: 10.4155/tde.13.88
- Hsiu, S. L., Hou, Y. C., Wang, Y. H. et al.(2002). Quercetin significantly decreased cyclosporin oral bioavailability in pigs and rats. *Life Sciences*, 72(3), 227-235. doi: 10.1016/s0024-3205(02)02235-x
- Jadhav, P., Bothiraja, C., Pawar, A. (2016). Resveratrol-piperine loaded mixed micelles: formulation, characterization, bioavailability, safety and in vitro anticancer activity. *RSC advances*, 6(114), 112795-112805. doi:10.1039/C6RA24595A
- Jha, S.K., Karki, R., Puttegowda, V.D. et al. (2014). In vitro intestinal permeability studies and pharmacokinetic evaluation of famotidine microemulsion for oral delivery. *International Scholarly Research Notices*, 2014, 1-7. doi: 10.1155/2014/452051
- Kassem, A.A., Abd El-Alim, S.H., Basha, M. et al.(2017). Phospholipid complex enriched micelles: a novel drug delivery approach for promoting the antidiabetic effect of repaglinide. *European journal of pharmaceutical sciences*, 99, 75-84. doi: 10.1016/j.ejps.2016.12.005
- Kesarwani, K., Gupta, R.(2013). Bioavailability enhancers of herbal origin: An overview. *Asian Pacific journal of tropical biomedicine*, 3 (4), 253-266. doi: 10.1016/S2221-1691(13)60060-X
- Kim, M.S., Jin, S.J., Kim, J.S. et al.(2008). Preparation, characterization, and *in vivo* evaluation of amorphous atorvastatin calcium nanoparticles using supercritical antisolvent (SAS) process. *European journal of pharmaceutics and biopharmaceutics*, 69(2), 454-465. doi: 10.1038/s41598-019-52645-0
- Kulthe, S.S., Inamdar, N.N., Choudhari, Y.M. et al.(2011). Mixed micelle formation with hydrophobic and hydrophilic Pluronic block copolymers: implications for controlled and targeted drug delivery. *Colloids and Surfaces B: Biointerfaces*, 88(2), 691-696. doi: 10.1016/j.colsurfb.2011.08.002
- Kushwaha, A.K., Vuddanda, P.R., Karunanidhi, P. et al. (2013). Development and evaluation of solid lipid nanoparticles of raloxifene hydrochloride for enhanced bioavailability. *BioMed Research International*, 2013, 1-9. doi: 10.1155/2013/584549
- Kwon, M., Lim, D.Y., Lee, C.H. et al.(2020). Enhanced intestinal absorption and pharmacokinetic modulation of berberine and its metabolites through the inhibition of P-glycoprotein and intestinal metabolism in rats using berberine mixed micelle formulation. *Pharmaceutics*, 12(9), 882. doi: 10.3390/pharmaceutics12090882

- Li, J., Wang, X., Zhang, T. et al.(2015). A review on phospholipids and their main applications in drug delivery systems. *Asian journal of pharmaceutical sciences*, 10(2), 81-98. doi: 10.1016/j.ajps.2014.09.004.
- Lu, Y., Park, K. (2013). Polymeric micelles and alternative nanonized delivery vehicles for poorly soluble drugs. *International journal of pharmaceuticals*, 453(1), 198-214. doi: 10.1016/j.ijpharm.2012.08.042
- Mu, Y., Fu, Y., Li, J. et al. (2019). Multifunctional quercetin conjugated chitosan nano-micelles with P-gp inhibition and permeation enhancement of anticancer drug. *Carbohydrate Polymers*, 203, 10-18. doi: 10.1016/j.carbpol.2018.09.020
- Nguyen, T.T., Duong, V.A., Maeng, H.J.(2021). Pharmaceutical formulations with P-glycoprotein inhibitory effect as promising approaches for enhancing oral drug absorption and bioavailability. *Pharmaceutics*, 13(7), 1103. doi:10.3390/pharmaceutics13071103
- Palei, N.N., Das, M.K.(2013). Formulation, optimization, and evaluation of solid lipid nanoparticles of lornoxicam. *Latin American journal of pharmacy*, 32(10), 1528-1237. doi:
- Pepic, I., Lovric, J., Filipovic-Grcic, J. (2013). How do polymeric micelles cross epithelial barriers? *European Journal of Pharmaceutical Sciences*, 50(1), 42-55. doi: 10.1016/j.ejps.2013.04.012
- Piazzini, V., D'Ambrosio, M., Luceri, C. et al.(2019). Formulation of nanomicelles to improve the solubility and the oral absorption of silymarin. *Molecules*, 24(9), 1688. doi:10.3390/molecules24091688
- Putri, D.C., Dwiastuti, R., Marchaban, A.K.(2017). Optimization of mixing temperature and sonication duration in liposome preparation. *Journal of Pharmaceutical Sciences and Community*.14(2), 79-85. doi: 10.24071/jpsc.142728
- Qu, X., Zou, Y., He, C., Zhou, Y. et. al. (2018). Improved intestinal absorption of paclitaxel by mixed micelles self-assembled from vitamin E succinate-based amphiphilic polymers and their transcellular transport mechanism and intracellular trafficking routes. *Drug delivery*, 25(1), 210-225. doi:10.1080/10717544.2017.1419513
- Sun, F., Jaspers, T.C.C., van Hasselt, P.M. et al. (2016). A Mixed Micelle Formulation for Oral Delivery of Vitamin K. *Pharmaceutical Research*, 33, 2168–2179. doi:10.1007/s11095-016-1954-9
- Tang, C., Chen, X., Yao, H. et al. (2021). Enhanced oral absorption of Icaritin by using mixed polymeric micelles prepared with a creative acid-base shift method. *Molecules*, 26, 3450. doi: 10.3390/molecules26113450
- Wang, L., Peng, M., Zhu, Y., et al.(2014). Preparation of pluronic/bile salt/phospholipid mixed micelles as drug solubility enhancer and study the effect of the PPO block size on the solubility of pyrene. *Iranian journal of pharmaceutical research*, 13, 1157–1163.
- Weng, W., Wang, Q., Wei, C. et al.(2021). Mixed micelles for enhanced oral bioavailability and hypolipidemic effect of liquiritin: preparation, in vitro and in vivo evaluation. *Drug development and industrial pharmacy*, 47(2), 308-318. doi:10.1080/03639045.2021.1879839
- Xie, Y., Tan, X., Huang, J. et al.(2017). Atorvastatin-loaded micelles with bone-targeted ligand for the treatment of osteoporosis. *Drug Delivery*, 24, 1067–1076. doi: 10.1080/10717544.2017.1347966

Development and Evaluation of Pullulan-Based Mouth Dissolving Film of Furosemide

Aafreen SAHA*, Umesh Kumar ATNERIYA**, Umashankar JOSHI***, Dharmendra SOLANKI****

Development and Evaluation of Pullulan-Based Mouth Dissolving Film of Furosemide

SUMMARY

Mouth-dissolving oral film is an innovative oromucosal route for the systemic delivery of therapeutically/medicinally active drug substances. As we know, furosemide belongs to class IV in BCS classification of drugs, having low solubility and permeability due to strong inter and intramolecular bonds. Due to low aqueous solubility, it exhibits low oral bioavailability. Here, we prepare mouth dissolving film of furosemide to increase its solubility, ultimately enhancing its bioavailability. In this way, we will achieve more rapid drug absorption and the desired pharmacological effect with a quick onset of action by avoiding degradation in gastrointestinal tract (GIT) and first-pass metabolism. This system will provide maximum therapeutic efficacy and stability by reducing the frequency of dosage and improving patient compliance. The present research aimed to prepare pullulan-based mouth dissolving oral films of furosemide used to treat and control hypertension. Pullulan was selected as a film former that exhibits better moisture retention, oxygen barrier, and uniform film-forming properties. Due to the hydrophilic nature of pullulan, it provides quick dissolution. By considering the above points, the film was prepared through the solvent casting method by pullulan as a film-forming polymer, glycerol as a plasticizer, and lepidium sativum mucilage as a natural disintegrating agent known as asaliyo. Disintegration time, drug release, moisture loss, and folding endurance of film were evaluated. Promising batch F6 exhibited better drug dissolution, 98.75±0.09% within 8±0.4 minutes than the other films. The disintegration time for batch F6 was 23±5 sec. It is evident from the above results that it is an innovative dosage form to improve drug delivery, onset of action, and patient compliance.

Key Words: Mouth Dissolving Film, Furosemide, Pullulan, Solvent Casting Method, Bioavailability.

Pullulan Bazlı Ağızda Çözünen Furosemid Filminin Geliştirilmesi ve Değerlendirilmesi

ÖZ

Ağızda çözünen oral film, terapötik/tıbbi açıdan aktif ilaç maddelerinin sistemik olarak verilmesi için yenilikçi bir oromukozal yoldur. Bildiğimiz gibi furosemid, BCS ilaç sınıflandırmasında sınıf IV'e aittir ve güçlü moleküller arası ve molekül içi bağlar nedeniyle düşük çözünürlük ve geçirgenliğe sahiptir. Suda çözünürlüğünün düşük olması nedeniyle oral biyoyararlanımı düşüktür. Bu çalışmada, çözünürlüğünü arttırmak ve sonuçta biyoyararlanımını arttırmak için ağızda çözünen furosemid filmi hazırlıyoruz. Bu sayede gastrointestinal sistemde (GİS) bozulmanın ve ilk geçiş metabolizmasının önüne geçerek daha hızlı ilaç emilimi ve istenen farmakolojik etkiyi elde etmiş olacağız. Bu sistem, dozaj sıklığını azaltarak ve hasta uyumunu artırarak maksimum terapötik etkinlik ve stabilite sağlayacaktır. Mevcut araştırma, hipertansiyonu tedavi etmek ve kontrol etmek için kullanılan furosemidin pullulan bazlı ağızda çözünen oral filmlerini hazırlamayı amaçlamaktadır. Pullulan, daha iyi nem tutma, oksijen bariyeri ve tekdüze film oluşturma özellikleri sergileyen bir film oluşturuç olması nedeniyle seçilmiştir. Pullulan hidrofilitik yapısı nedeniyle hızlı çözünme sağlar. Yukarıdaki hususlar dikkate alınarak, film oluşturuç polimer olarak pullulan, plastikleştirici olarak gliserol ve asaliyo olarak bilinen doğal parçalayıcı madde olarak lepidium sativum müslajı kullanılarak solvent döküm yöntemiyle film hazırlanmıştır. Filmin dağılma süresi, ilaç salımı, nem kaybı ve katlanma dayanıklılığı değerlendirilmiştir. Gelecek vaat eden F6 serisi, diğer filmlere göre 8±0,4 dakika içinde % 98,75±0,09 ile daha iyi ilaç çözünmesi göstermiştir. F6 serisinin parçalanma süresi 23±5 saniye olarak bulunmuştur. Yukarıdaki sonuçlardan, bunun iyileştirilmiş ilaç uygulamasını, etki başlangıcını ve hasta uyumunu iyileştirmeye yönelik yenilikçi bir dozaj formu olduğu açıkça görülmektedir.

Anahtar Kelimeler: Ağızda Çözünen Film, Furosemid, Pullulan, Çözücü Dökme Yöntemi, Biyoyararlanım.

Received: 14.07.2023

Revised: 21.11.2023

Accepted: 22.11.2023

* ORCID: 0009-0004-7250-8492, BM College of Pharmaceutical Education and Research, Indore (Madhya Pradesh) India

** ORCID: 0000-0003-2402-6048, School of Pharmacy, Devi Ahilya Vishwavidyalaya, Indore (Madhya Pradesh) India

*** ORCID: 0009-0006-5426-867X, Shri Bherulal Pharmacy Institute, Indore (Madhya Pradesh) India

**** ORCID: 0000-0001-7093-5985, BM College of Pharmaceutical Education and Research, Indore (Madhya Pradesh) India

° Corresponding Author; Umesh Kumar ATNERIYA

E-mail: atneriya@gmail.com

INTRODUCTION

Mouth dissolving oral film or strip can be defined as “A dosage form that employs aqua dissolving polymer which allows the dosage form to hydrate by saliva, adhere to the mucosa quickly, and disintegrates within few seconds, dissolves and releases medication for oromucosal absorption when placed on the tongue or oral cavity”(Fitzpatrick et. al., 2019). The oral mucosal absorption directly enters the systemic circulation due to being highly vascularized and hence highly permeable by passing gastrointestinal tract (GIT) and first-pass metabolism in the liver. This may be due to a large surface area, facilitating better absorption and patient compliance(Shakya et. al., 2018). The conventional dosage form is substituted by modern developed drug delivery systems as orally fast disintegrating and dissolving films for pediatric, geriatric, dysphagic, schizophrenic, and bed prone patients (Homayun et. al., 2019). These films get hydrated very quickly by soaking saliva when placed on the tongue (Rabe et al., 2019). Generally, hydrophilic polymers with plasticizers are used to prepare films that allow them to quickly release incorporated Active Pharmaceutical Ingredient (API) in just seconds (Orsuwan & Sothornvit, 2018). The Food and Drug Administration (FDA) has approved, furosemide as a loop diuretic that acts on the kidney to ultimately increase the water loss from the body(Khan et. al., 2018). It is most commonly used in edema and various clinical conditions with volume overload, congestive heart failure, high blood pressure, liver and renal failure, including nephrotic syndrome (Gulsun et. al., 2018). Furosemide mouth dissolving film is beneficial as there is ease of administration in patients who have difficulty swallowing, like the elderly, pediatric, bedridden patients, stroke victims, and psychiatric patients (Pawar et. al., 2019). Also, the absorption of drugs is prompt from the pre-gastric area like mouth, pharynx, and esophagus, which show the rapid onset of action. Generally, super disintegrating agents are

added to decrease the disintegration time, which in turn enhances the drug dissolution rate (Dhiman et. al., 2022). Pullulan, a neutral polysaccharide produced using a black yeast-like fungus called *aureobasidium pullulans* from sucrose, and starch as carbon substrates. It is a colorless, odorless, tasteless, white powder that has increased solubility, flexibility, strength, and stability over a wide temperature range (Agrawal et. al., 2022). Due to excellent film formation, mouth feel, edible, water soluble and better mechanical properties, pullulan is extensively used in rapid film making. Despite -these features, pullulan provides better moisture retention and oxygen barrier properties (Liu et al., 2019). Some recent developments show pullulan-based rapid films incorporated APIs like amlodipine besylate (Pezik et. al., 2021), bilastine (Kanugo & Gandhi, 2022), aprepitant (Bala & Sharma, 2018), ropinirole (Meher & Dighe, 2019), for their formulation and evaluation. The type of plasticizer and its concentration play a significant role in producing the film of desired flexibility and reducing the brittleness of the formed film (Edwards et al., 2022). Here, we used glycerol as a plasticizer because it has unique features as an antimicrobial agent, cosolvent, emollient, humectant, plasticizer, sweetening agent, and many more (Singh et. al., 2021). *Lepidium sativum* is used as a natural super disintegrating agent for film (Al-Snafi, 2019). Mucilage of natural origin is advantageous over semi-synthetic and synthetic substances due to its cost-effectiveness, non-toxic and non-irritable properties, easy availability, eco-friendly, biodegradable and biocompatible nature (Soukoulis et. al., 2018). Fenugreek seed mucilage, and *ocimum basilicum* gum are used earlier for the fast disintegrating tablet of amlodipine besylate (Keisandokht et. al., 2022). In the present study, pullulan is mixed with glycerol and *lepidium sativum* in various concentrations to study the film properties like brittleness, folding endurance, disintegration, and dissolution time (Maske et. al., 2022).

MATERIAL AND METHODOLOGY

Material

Furosemide was gifted from IPCA Laboratories, Pithampur, Indore (M.P., India). Pullulan was obtained as a gift sample from Gangwal Chemicals Pvt Ltd, Mumbai. Glycerol was gifted from Glister Pharmaceutical, Rau, Indore (M.P., India). *Lepidium sativum* was procured from SK Traders, Indore (M.P., India). Citric acid and Sucralose were obtained as gift samples from Loba Chemie, Meghnagar (M.P., India)

Method

UV Spectra of Furosemide

10 mg furosemide was accurately weighed (Shimadzu Corporation - EL2204, Japan) and transferred to a 100 mL volumetric flask. It was dissolved and diluted to 100 mL with pH 6.8 phosphate buffer (as per IP, 2014) to obtain a final 100 µg/mL concentration. Dilutions were made to obtain a concentration of 10 µg/mL and scanned by using a UV visible spectrophotometer (Shimadzu-1601, Japan) for λ_{\max} in a range of 200–400 nm in the spectrum for three consecutive times (Kumar & Kumar, 2016). The UV spectra of furosemide were represented in Figure 1.

Solubility Study of Furosemide

For the determination of solubility, an excess amount of furosemide was dissolved in each of 20 mL of different below solvents like water, 0.1 N HCl, dimethyl formamide (DMF), sodium citrate, sodium acetate, phosphate buffer pH 6.8, sodium benzoate, 15% glycerine, dimethyl sulfoxide (DMSO), acetone, methanol separately in the flask. Kept it closed with a rubber cap and placed on a mechanical shaker (REMI Elektrotechnik Motor, Vasai, India) at 37 ± 5 °C for 12 hours, and the solution was allowed to equilibrate for 24 hours undisturbed. Then, the solution is filtered through filter paper. The supernatant was analyzed using a double beam UV spectrophotometer (Shimadzu-1601, Japan) (Zhang et. al., 2022).

Compatibility Study of Furosemide and Excipients by FTIR

The individual pellet of furosemide, pullulan, and the physical mixture was formed to determine the compatibility study. In order to do this, 10 mg of each sample was mixed with dried potassium bromide (KBr) of equal weight. The mixture was properly ground using a pestle and mortar. Pellets were formed by compressing the mixture using a hydraulic press. Transparent pellets formed in this way are scanned by FTIR spectrometer (Nicolet-380, Thermo Scientific, Madison, USA). The spectra are examined over a frequency range of $4000\text{-}200\text{cm}^{-1}$ (Vimalson et al., 2019).

Isolation of Mucilage from *Lepidium sativum* Seeds

Mucilage is present in the outer layer of the seeds. 100 g of seeds were soaked in 1000 mL of distilled water and 5 mL of chloroform for 24 hr. The obtained viscous solution was filtered through a muslin cloth. To the mucilaginous solution, add 1 L of 95% ethanol in the viscous mucilaginous solution to precipitate the mucilage. The precipitated mucilage was collected and dried in a hot air oven (Rasayana scientific-CFC 1001, Surat) at a temperature not exceeding 40 to 45 ± 5 °C until completely dried. The powder was sieved through 80 mesh, weight, and stored in a desiccator for further use (Mahapatra et al., 2021).

Preparation of Mouth dissolving Film of Furosemide

It is an easy and accurate method of formulation of mouth-dissolving film. Water soluble polymer was dissolved in water separately. Furosemide and other excipients were dissolved in methanol. This solution was added to the polymeric solution. Then, the solution was mixed using a mechanical stirrer (REMI Elektrotechnik Motor, Vasai, India) for 45 ± 2 minutes with a rotating speed of 60-80 rpm. The entrapped air was removed by vacuum. The resulting solution

was uniformly spread in a petri plate and dried in a hot air oven (Rasayana scientific-CFC 1001, Surat) at $40\pm 3^{\circ}\text{C}$ for 24 hours. After proper drying, films were cut into the desired dimensions i.e., $2\times 2\text{ cm}^2$, which

40 mg of furosemide was present (Pattewar et. al., 2019). The formula of mouth dissolving film is shown in Table 1.

Table 1. Formulation batches

S. NO.	Ingredients	F 1	F 2	F 3	F 4	F 5	F 6	F 7	F 8
1.	Furosemide	40	40	40	40	40	40	40	40
2.	Pullulan	40	42	45	50	52	55	57	60
3.	Glycerol	05	08	11	14	15	17	23	28
4.	Lepidium Sativum	10	10	10	11	13	14	25	25
5.	Citric acid	15	15	15	15	15	15	15	15
6.	Tween 80	0.06	0.06	0.06	0.06	0.06	0.06	0.06	0.06
7.	Sucralose	3	3	3	3	3	3	3	3
8.	Menthol	2	2	2	2	2	2	2	2
9.	Methanol	q.s.	q.s.	q.s.	q.s.	q.s.	q.s.	q.s.	q.s.
10.	Water	q.s.	q.s.	q.s.	q.s.	q.s.	q.s.	q.s.	q.s.

Sensory evaluation

Appearance is also a key component of sensory evaluation. The vision system is the detector of appearance. We can sense color, intensity, transparency, shininess, and other physical characteristics, including the size and shape of the film. The aroma of mouth dissolving film is perceived through the olfactory system. By somesthesia system, we can evaluate its texture (uniformity, stickiness, rough/smooth). Kinesthesia is also an essential type of sensory evaluation that evaluates the film's mechanical movement like, flexibility, tension, and relaxation (Kemp et. al., 2018).

Film thickness

First of all, make the micrometer screw gauge (Al-Anwar traders, Mumbai, India) reading at zero. Place the film between the spindle and anvil by turning the thimble. Hold the film tightly by turning the ratchet knob until the ratchet slips (a "tick" sound is heard). Now, we will note the reading of film thickness. Each

film was measured at five positions (central and the four corners) and in terms of its length and width. The mean thickness was calculated as measurement results were divided by the number of samples (Wang et al., 2018).

Folding endurance

Folding endurance indicates the brittleness of the film. Schopper type tester (Fibretec Instrument Roorkee-247667, Uttarakhand, India) is another type of apparatus having opposed and moveable jaws (Perdoch et al., 2022). Firstly, we tighten both jaws, insert the film between the place held by both jaws and tighten both sides. Now, release the jaws and apply various tension to the film. As we press the start button, the jaws move and fold numbers are recorded on the screen. During the process, when the film is broken, it is noted as a folding endurance reading. This test was performed on six films of each formulation and mean \pm S.D calculated value (Malviya & Pande, 2021).

Moisture content

It is determined by cutting the film strip of 2×2 cm² dimension and measuring its initial weight by analytical balance (Shimadzu Corporation - EL2204, Japan). Afterward, these strips were placed in a desiccator containing activated silica, and the desiccator was placed inside the incubator to ensure a constant temperature of 37±5 °C for 24 hours. Now, calculate the film's final weight individually until it show a constant weight. Moisture content is estimated by analyzing the weight gain of the film or the difference between the initial and final weight (Fang et. al., 2021).

Surface pH

The test was performed by placing the film of 2x2cm² in a petri dish. The film is moistened with 1 mL of phosphate buffer pH 6.8 and kept for 30 sec. The pH was noted by bringing the electrode of the pH meter (Chemiline-CL110, Aqua mart, Kolkata, India) in contact with the film's surface and allowing equilibration for 1 min. The average of three determinations for each formulation was taken (Kumorek et al., 2020).

Weight variation

It confirms uniformity and supports the quality of the dosage unit. At least six films of each formulation batch are taken of uniform dimension and individually weighed on an analytical balance (Shimadzu Corporation - EL2204, Japan). Note the balance recorded on the screen. Now calculate the average weight of films. Films should have nearly constant weight. As the amount of pullulan increases, the weight of the film also increases. It is helpful to ensure that a film contains the proper amount of excipients and API (Vishvakarma, 2018).

Drug Content Uniformity

Drug content was determined by dissolving the film containing 10 mg of furosemide in 100 mL phosphate buffer pH 6.8 to get 100 µg/mL solutions. An aliquot of 1 mL sample was withdrawn and diluted to 10 mL

with phosphate buffer pH 6.8. Then, the solution was filtered through the whattman filter paper and analyzed by UV-spectrophotometer (Shimadzu-1601, Japan) at 272 nm against a blank prepared using dummy film treated similarly. Content uniformity studies were carried out in triplicate for each batch of the film. The limit of content uniformity is 90-110%.

***In vitro* disintegration studies**

In the petri dish method, the film (2x2 cm²) was placed on a stainless steel wire mesh, which was placed in a petri dish containing 10 mL phosphate buffer pH 6.8 with 37±5 °C temperature. The time required for the film to break and disintegrate was noted as *in vitro* disintegration time. Since the film is expected to disintegrate in the mouth in the presence of saliva, only 10 mL of medium was used. All the measurements are done in triplicate, and the average value is reported (Pawar et. al., 2019).

***In vitro* Dissolution Study**

900 mL phosphate buffer pH 6.8 poured into a stainless steel vessel. Put a single film into the dry basket and immerse the basket into the USP I apparatus (Electrolab- ERD 07, Mumbai). Set the flask at 50 rpm with 37±5 °C temperature. The sink condition is maintained by withdrawing the 5mL sample of the dissolved drug through the pipette at intervals like 1, 2, 4, 6, and 8 minutes and replacing it with fresh dissolution media. The dissolved drug was analyzed by ultraviolet spectrophotometer (Shimadzu-1601, Japan) at λ max 272 (Raza et. al., 2019).

***In vitro* Drug Release Kinetics**

The mechanism of drug release kinetics of furosemide films was analyzed through an *in vitro* study by exploring the following kinetic models (zero order, first order, and Higuchi equations), and release was determined (Sheikh et al., 2020).

Zero order kinetic(constant rate process)

Release of the drug does not depend on reactant concentration(does not vary with increase or decrease

with the concentration of reactant), The zero power of the reactant concentration.

$$C = K_0 t \dots\dots\dots(1)$$

Here, C is the concentration of the drug undergoes reaction at time t.

K_0 is zero order rate constant.

The Concentration vs time plot was plotted with a straight line with a slope equal to K_0 . The graph proves the above theory that drug release from the film does not depend on concentration.

First order kinetic

Release of the drug depends on reactant concentration (vary with increase or decrease with the concentration of reactant).

$$\text{Log } C = \text{Log } C_0 - kt / 2.303 \dots\dots\dots(2)$$

Where C_0 is the initial concentration of the drug, k is the first-order constant, and t is the time.

It proves that the reaction rate is directly proportional to the reactant concentration.

Higuchi's Model

Higuchi's model as cumulative percentage of drug released vs square root of time.

$$Mt/M_\infty = Kht_{1/2} \dots\dots\dots(3)$$

Where Mt/M_∞ is the fraction of drug released at each time t (minutes), Mt is the amount of the drug released in time t (minutes).

M_∞ is the amount of drug released after time ∞ .

K_h represents the Higuchi release kinetic constant.

The system ensures the release of drugs based on Fickian diffusion as a square root of time-dependent process from mouth dissolving film.

Stability Study of Mouth Dissolving Film of Furosemide

The stability study aims to observe the formulation quality, which fluctuates under certain environmental factors like temperature, relative humidity (RH), and light of which storage conditions are to be established. The International Conference of Harmonization (ICH) Guidelines specified the length of study and storage conditions. Stability studies were carried out by placing the film in storage at $25^\circ\text{C} \pm 2^\circ\text{C} / 60 \pm 5\% \text{RH}$ and $40^\circ\text{C} \pm 2^\circ\text{C} / 75 \pm 5\% \text{RH}$ for six months. The effects of temperature and time on the F6 formulation were evaluated. Parameters like folding endurance, surface pH, weight variation, % drug content, disintegration time, and release rate were analyzed (Sahu et al., 2018).

RESULT AND DISCUSSION

UV spectra of Furosemide

10 mg furosemide was accurately weighed (Shimadzu Corporation - EL2204, Japan) and dissolved in 100 mL phosphate buffer pH 6.8 in a volumetric flask and obtained the concentration of 100 $\mu\text{g}/\text{mL}$. Further dilutions were made to obtain a concentration of 10 $\mu\text{g}/\text{mL}$ and scanned using a UV visible spectrophotometer (Shimadzu-1601, Japan), and λ_{max} was found to be 272nm.

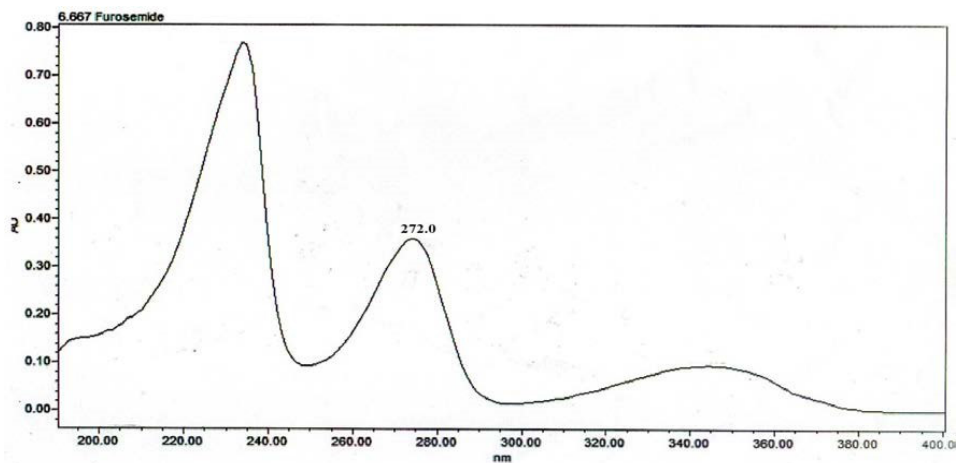


Figure 1. UV Spectra of Furosemide

Solubility Study of Furosemide

Solubility of furosemide in different solvents was done by dissolving it in various below solvents separately. The conclusion shows that furosemide

is practically insoluble in aqua and freely soluble in acetone, and methanol, while 15% glycerine possesses good solubility. The solubility data were expressed in Table 2.

Table 2. Solubility of Furosemide in Different Solvent

S.NO	Solvent	Solubility of Furosemide (mg/ml)
1.	Water	0.01825±0.008
2.	0.1 N HCL	0.0570±0.003
3.	Dimethyl formamide(DMF)	0.0792±0.001
4.	Sodium citrate	0.129±0.009
5.	Sodium acetate	0.239±0.005
6.	Phosphate buffer (pH 6.8)	1.6500 ±0.001
7.	Sodium benzoate	2.157±0.003
8.	15% glycerin	14.6600±0.007
9.	Dimethyl sulfoxide(DMSO)	30±0.002
10.	Acetone	50±0.007
11.	Methanol	50 ±0.009

Solubility result of furosemide in various solvents shown as mean ±S.D.(n=3)

Compatibility study of Furosemide and Excipients by FT-IR

The drug excipient compatibility study was performed by FT-IR spectrometer (Nicolet-380, Thermo Scientific, Madison, USA) to ensure compatibility. No drug-polymer interaction was

observed between the drug and excipients in the entire FT-IR spectrum. The observed peaks indicated the stable nature of furosemide with pullulan and other excipients. The FT-IR spectrums of furosemide, pullulan, and physical mixture of formulation were represented in Figure 2 (a), (b), and (c).

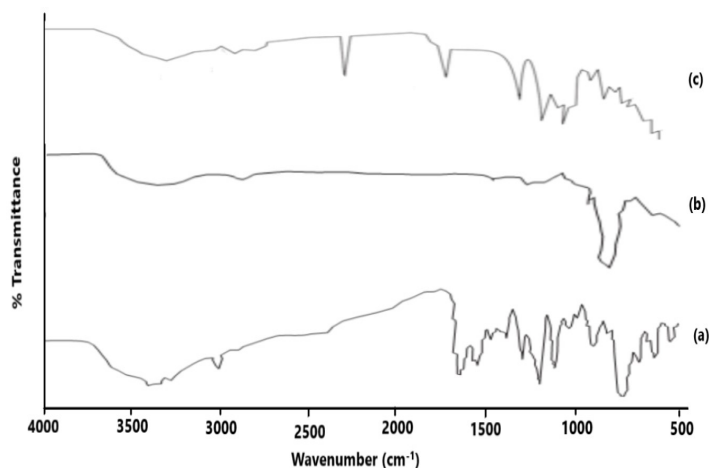


Figure 2. FT-IR Spectrum of Furosemide (a), Pullulan (b) Physical Mixture of Prepared F6 Formulation (c)

FT-IR spectra of pure furosemide are shown in Figure 2 (a). The prominent IR absorption peak of furosemide was attributed to 3647.51 cm^{-1} , indicating O-H hydrogen stretching. 3286.81 cm^{-1} represent N-H stretching, peaks near 3147.05 cm^{-1} showed C-H stretching. It also indicated N-H bending at 1672.34 cm^{-1} . The carbonyl group indicated as stretching at 1568.18 cm^{-1} , and the sulfoxide group showed asymmetric stretching at 1263.44 cm^{-1} . FT-IR spectra of pure pullulan are shown in Figure 2 (b). The prominent IR absorption peaks of pullulan at 3423 cm^{-1} indicated O-H hydrogen stretching. Peaks near 2928 cm^{-1} attributed to C-H asymmetric stretching. Peaks 1636 cm^{-1} , 1460 cm^{-1} indicated as C=O stretching. The glycosidic bond represented as stretching and rocking at 928 cm^{-1} , 849 cm^{-1} , 757 cm^{-1} . The FT-IR spectra of the physical mixture of the prepared formulation were found to be recorded and represented in Figure 2 (c). The band at 3423 cm^{-1} was attributed to O-H stretching vibration. The absorption band 2928 cm^{-1}

was also represented for C-H vibrations of stretching and bending. Wave numbers between $1700\text{--}1200$ were attributed to C-O and C-N stretching vibration due to the presence of protein. Region of glycosidic bond vibration was found at 1058 cm^{-1} while 849 cm^{-1} represents carbohydrate group presence.

Sensory Evaluation

Results from trial studies showed that film is transparent, clear, soft, without air bubbles, uniform in thickness, colorless, and easily removed from a petri dish. It exhibits a shining and glossy appearance with no stickiness, sufficient hardness, and proper plasticity due to the adequate amount of pullulan, glycerol, and lepidium sativum used. Pullulan at 45-55%, glycerol at 14-17%, and 11-14% lepidium sativum form a nontacky, uniform, transparent, and clear film. With less amount of pullulan 5-45%, the film's surface did not form. Less than 14% glycerol and less than 10% lepidium sativum negatively impacted the film's hardness. It possesses no stickiness in film's but has no

clarity. In contrast, the films prepared with more than 55% pullulan, more than 17% glycerol, and more than 14% lepidium sativum form tacky, turbid, and rigid or

brittle film (Choi et. al., 2018). The sensory result was noted in Table 3.

Table 3. Sensory evaluation result

S.NO.	Batch	Surface appearance	Stickiness	Film clarity
1.	F1	Film did not form	Non-sticky	--
2.	F2	Film did not form	Non-sticky	--
3.	F3	Film did not form	Non-sticky	--
4.	F4	Film formed is loose	Non-sticky	Non-clear
5.	F5	Semitransparent film	Non-sticky	Clear
6.	F6	Uniform and transparent film	Non-sticky	Glossy
7.	F7	Brittle	Sticky	Muddy
8.	F8	Brittle	Sticky	Muddy

Film Thickness

Calibrated micrometer screw gauge (Al-Anwar traders, Mumbai, India) was used for the determination of film thickness. With little pullulan concentration from F1 to F3, no film was formed. Hence, no thickness was observed. In F4 and F5, the film developed was loose and semi-transparent, respectively with no sufficient thickness. In comparison, The F6 formulation possessed proper thickness with the appropriate pullulan concentration of 55%. But with more than 55% pullulan in the F7 and F8 batches, the film formed was too thick. That’s why F6 was considered best formulation in the context of thickness. The result of film thickness was expressed in Table 4.

Folding Endurance

Schopper type tester (Fibretec Instrument Roorkee-247667, Uttarakhand, India) was utilized to estimate the film’s brittleness. Folding endurance was analyzed that batch F1 to F3 film had no flexibility due to very low glycerol, *Lepidium sativum* and pullulan concentration. Then, slightly increased the concentration of the above ingredients in the F4, F5, and F6 batches and improved the films as the F6 formulation possessed exact flexibility and no

film breakage was observed. In contrast, more than 17% glycerol and 14% lepidium sativum with higher pullulan concentrations give a brittle film. Hence, the F6 was our best formulation in terms of folding endurance. The Folding endurance result was noted in Table 4.

Moisture Content

Accurate moisture content capacity was observed in formulation F6 because pullulan exhibits suitable moisture retention properties in between 40-55% of the pullulan amount. There is no effect of glycerol and *Lepidium sativum* on the formulations. The result data of moisture content of furosemide film was noted in Table 4.

Surface pH

A digital pH meter with electrode (Chemiline-CL110, Aqua mart, Kolkata, India) was utilized to estimate pH, ultimately to check whether the film exhibits irritation to oral mucosa. All the films had almost near neutral pH but F6 had pH near to saliva pH. There is no effect of the above ingredients on pH observation. The result of the pH of furosemide mouth dissolving film was noted in Table 4.

Weight Variation

Analytical balance (Shimadzu Corporation -

EL2204, Japan) ensured that a film contained the proper amount of excipients and furosemide. The weight variation of the films is directly proportional to the amount of pullulan, glycerol, and *lepidium sativum* used. As we enhanced the concentration of all ingredients, the weight of the film was also enhanced. But batch F6 had the least weight variation due to sufficient amount of pullulan, glycerol, and *Lepidium sativum* used. The weight variation of furosemide film was noted in Table 4.

Drug Content

Drug content was detected by withdrawing the 1 mL sample from 100 µg/mL solutions diluted to 10 mL with phosphate buffer pH 6.8, and analyzed by UV-spectrophotometer (Shimadzu-1601, Japan) at

272 nm wavelength. The drug content uniformity of furosemide film was showed in Table 4.

Disintegration Time

The test was performed by the petri dish method to ensure the onset of action of furosemide film. Pullulan, glycerol, and *Lepidium sativum* are all widely attributed to disintegrating properties of films. With very low concentrations, they had a negative impact on disintegration. But the film of the F6 batch was produced with sufficient disintegration time with an adequate concentration of contents used, such as 55% pullulan, 17% glycerol, and 14% *Leidium sativum*, which exhibit proper film dissolution. The disintegration time of the furosemide film was noted in Table 4.

Table 4. Evaluation result of Film Thickness

S. NO.	Batch	Film Thickness (mm)	Folding endurance	Moisture Content (%)	Surface pH	Weight variation (mg)	Drug contents (%)	Disintegration Time (Sec)
1.	F1	0.005±0.01	97±1	12.30±0.07	6.4±0.4	55.21±0.31	92±0.48	32±5
2.	F2	0.07±0.01	98±5	13.01±0.12	6.2±0.7	57.71±0.22	88±0.36	37±2
3.	F3	0.08±0.02	110±6	14.13±0.40	6.4±0.3	62.31±0.44	86±0.53	43±4
4.	F4	0.09±0.01	94±3	13.24±0.12	6.3±0.22	57.41±0.38	87±0.23	35±4
5.	F5	0.09±0.02	101±4	15.15±0.27	6.7±0.5	63.71±0.17	95±0.51	28±3
6.	F6	0.11±0.02	114±2	10.11±0.33	6.9±0.1	60.21±0.77	97±0.57	23±5
7.	F7	0.12±0.01	99±1	10.44±0.16	6.7±0.15	66.21±0.29	89±0.35	47±4
8.	F8	0.15±0.01	95±2	14.23±0.58	6.5±0.3	57.21±0.56	89±0.46	50±3

The thickness result is shown as mean ±S.D.(n=3), which determines that thickness of the film increases with increasing amount of pullulan. F6 has proper film thickness with appropriate concentration. The folding endurance result is shown as mean ±S.D.(n=3), which expresses the exact brittleness of the film. The folding endurance of the film increases as the amount of plasticizer and polymer increases. F6 shows better mechanical properties like flexibility and strength. Moisture retention result is shown as mean ±S.D.(n=3). F6 has proper moisture retention with a proper concentration of pullulan. Surface pH results are expressed as mean ±S.D.(n=3) and there is no effect of pullulan concentration on film pH, but pH was near to neutral. Hence, no irritation to mucosa occurred. The weight variation result is presented as mean ± S.D.(n=3,) which shows that the amount of pullulan increases, and weight of the film also increases. Drug content results are expressed as mean ± S.D.(n=3), which estimated that F6 possessed the strength of furosemide remains within its specified limit. The disintegration time of each film was measured in triplicate as mean ± S.D. (n=3). The amount of pullulan above 55% showed an increase in disintegration time, but an increase in plasticizer concentration decreased disintegration time.

In vitro Dissolution Study

The test was analyzed through USP apparatus I, Basket apparatus (Electrolab- ERD 07, Mumbai) to explore the rate of drug dissolution (Zayed et. al.,

2020). The dissolution profiles of the furosemide mouth dissolving film were presented in Figure 5, and result was recorded in Table 5.

Table 5. Dissolution Profile of Mouth Dissolving Films

Time (Min)	F1	F2	F3	F4	F5	F6	F7	F8
0	Nil	Nil	Nil	Nil	Nil	Nil	Nil	Nil
1	34.54±0.13	20.35±0.43	25.07±0.46	32.7±0.22	29.24±0.29	27.52±0.37	34.18±0.56	30.94±0.49
2	63.22±0.31	46.47±0.28	46.65±0.47	67.52±0.32	64.49±0.35	48.29±0.54	62.02±0.67	60.32±0.36
4	82.1±0.47	57.98±0.12	78.63±0.36	88.21±0.28	83.74±0.23	83.88±0.76	59.08±0.88	87.63±0.35
6	85.96±0.22	62.98±0.45	85.57±0.34	92.45±0.29	89.41±0.26	92.83±0.39	94.02±0.07	92.15±0.73
8	91.26±0.40	91.44±0.09	92.45±0.29	94.59±0.33	94.79±0.17	98.75±0.09	96.55±0.39	95.47±0.08

The dissolution rate of different sets of furosemide mouth dissolving film was performed by a Basket Dissolution apparatus (USP Type I) at temperature of 37 °C and 50 rpm. The results are shown as Mean±SD (n=3).

With increasing lepidium sativum concentration, disintegration time increases, which ultimately enhances the drug release. The release rate of furosemide was enhanced with pullulan (45 to 55%), which spread the hydrophilic chain around the matrix

system. F6 formulation showed a rapid release of 98.75±0.09 within 8±0.4 min. However, the release profile was decreased at a higher percentage of polymer and disintegrating agent by forming a layer around the drug, which allows the drug release at a slow rate.

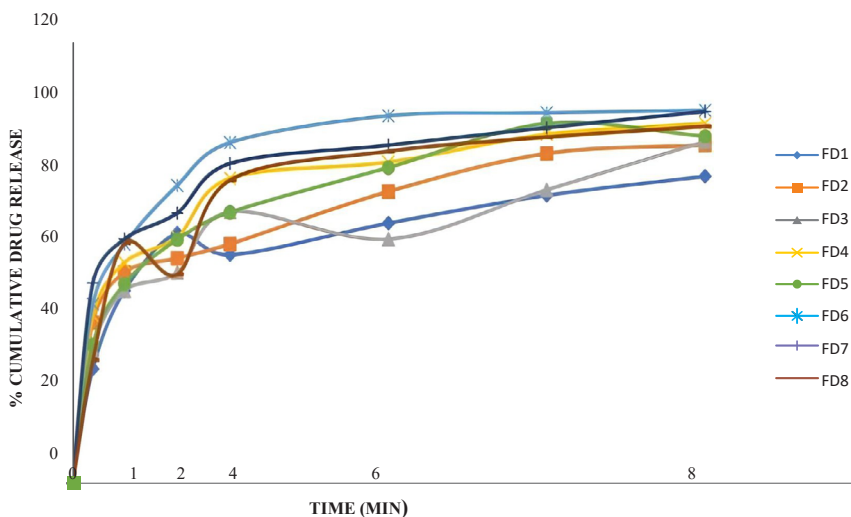


Figure 3. % Cumulative Drug Release v/s Time Plot in Phosphate Buffer pH 6.8

In vitro drug release kinetics

In vitro release data of kinetic models like zero-order, first-order, and Higuchi models were analyzed

to describe the release kinetics. The regression values of all formulations were noted in Table 6.

Table 6. In vitro drug release kinetic data

S. NO.	Batch	Zero order	First order	Higuchi model
1	F1	0.930	0.956	0.964
2	F2	0.884	0.960	0.943
3	F3	0.923	0.955	0.968
4	F4	0.886	0.973	0.960
5	F5	0.833	0.960	0.953
6	F6	0.862	0.976	0.930
7	F7	0.921	0.914	0.905
8	F8	0.928	0.974	0.975

The best model for the furosemide mouth dissolving film release pattern was determined as per the regression data, for the dissolution study, basket dissolution apparatus (USP Type1) was employed. Values are presented as mean±SD (n = 3).

To analyze the release kinetic model, the in vitro release study was performed according to zero order, first order, and diffusion-controlled mechanism through a simplified higuchi model. A certain mechanism was based on the coefficient to determine the parameters studied. If the highest coefficient of the determination is observed, it is favoured for selecting the order of release. Release of all the formulations followed first-order kinetics exhibited a diffusion-controlled mechanism as indicated by the highest coefficient of determination (R²). It was found that the

optimized formulation F6 follows first order-kinetic system as it has the highest value of R².

Stability study of Mouth Dissolving Film of Furosemide

The developed pullulan-based film of furosemide was evaluated for stability studies. The evaluated parameter showed that no notable changes were found in the prepared film. As per the data gathered during six months of storage, it was recapitulated that the fabricated film formulation was stable, and the stability study result was recorded in Table 7.

Table 7. Stability Study of Mouth Dissolving Film of Furosemide.

Evaluation parameters	Observation in months						
	Initial	25°C±2°C/60±5%RH			40°C±2°C/75±5% RH		
	0	2	4	6	2	4	6
Weight variation (mg)*	60.21±0.77	60.09±0.61	59.98±0.22	59.28±0.87	60.18±0.67	59.88±0.56	59.21±0.25
Surface pH **	6.9±0.19	6.9±0.55	6.8±0.89	6.8±1.0	6.9±0.51	6.8±0.24	6.8±0.09
Folding endurance **	114±2	113±1	112± 3	112±2	114±3	113±1	113±2
Drug content (%)**	97.57±0.57	97.62±0.21	97.51±0.11	97.25±0.51	97.68±0.78	97.33±0.29	97.12±0.18
Disintegration time (Sec)**	23±5 sec	23±7sec	24±8 sec	24±9sec	23±6 sec	23±9 sec	24±5 sec
Cumulative drug release (%)***	98.75±0.12	98.54±0.51	98.22±0.18	97.98±0.88	98.78±0.41	98.73±0.57	98.26±0.59

* Each value represent the mean±standard deviation (n=20)

**Each value represent the mean ± standard deviation (n=6)

*** Each value represent the mean ± standard deviation (n=3)

CONCLUSION

The present research aimed to formulate and develop mouth-dissolving oral film and evaluate its different formulations of furosemide to achieve faster drug release to control hypertension. Mouth-dissolving films of diuretic drugs were found to be a better option to control hypertension by way of fast onset of action. Preliminary trials indicated better results for sensory, mechanical properties, and disintegration time. The *in vitro* release of the drug was found to be $98.75 \pm 0.09\%$ within 8 ± 0.4 minutes. The drug content of the optimized formulation was found to be 97 ± 0.57 , no significant difference in drug content was found, and hence, the drug was uniformly distributed in the film. Folding endurance indicates the film brittleness. As concentration of pullulan & glycerol increased, folding endurance also increased, affecting the overall flexibility of the furosemide loaded mouth-dissolving film. The higher value of folding endurance for film proves that the films were strong enough to withstand handling that is 114 ± 2 folds. The *in vitro* disintegration study indicates that the drug's onset of action, 23 ± 5 sec., was found because the increase in plasticizer concentration decreased disintegration time in our formulation F6. More than 14% of *Lepidium sativum* enhances disintegration time, while between 10-14% *lepidium sativum* exhibit proper disintegration profile, and less than 10% possess a negative impact on disintegration time. The mean thickness values for all the batches were 0.07–0.12 mm, indicating uniform cast of respective batches. The surface pH was in the range of 6.5–6.9, close to saliva pH. F6 shows faster release within 8 ± 0.4 minutes. Glycerol also acts as co-solvent hence, it enhances dissolution. Therefore, the F6 formulation is considered as a best and can be used as a fast dissolving oral film as novel drug delivery method. It is a pullulan-based film that exhibits desired moisture retention with faster disintegration time. Due to speedy drug dissolution, it provides quick effects and control hypertension. This film is beneficial for patient convenience and compliance in disease state.

ACKNOWLEDGMENT

The authors would like to express their gratitude to the late Dr. Vimukta Sharma for granting permission to carrying out research work at Department of Pharmaceutics, BM College of Pharmaceutical Education and Research, Indore (MP) India 452020 during the development of this work.

CONFLICT OF INTEREST

The authors declare that there is no conflict of interest.

AUTHOR CONTRIBUTION STATEMENT

Aafreen Shah: Draft manuscript preparation. Umesh Kumar Atneriya: Study conception and design, Analysis and interpretation of results. Umashankar Joshi: Data collection. Dr. Dharmendra Solanki & Umesh K Atneriya: Reviewed the results and approved the final version of the manuscript.

REFERENCES

- Agrawal, S., Budhwani, D., Gurjar, P., Telange, D., & Lambole, V. (2022). Pullulan based derivatives: Synthesis, enhanced physicochemical properties, and applications. *Drug Delivery*, 29(1), 3328-3339.
- Al-Snafi, A. (2019). Chemical constituents and pharmacological effects of *lepidium sativum*. *Int J Curr Pharm Res*, 11(6), 1-10.
- Bala, R., & Sharma, S. (2018). Formulation optimization and evaluation of fast dissolving film of aprepitant by using design of experiment. *Bulletin of Faculty of Pharmacy, Cairo University*, 56(2), 159-168.
- Choi, I., Lee, S. E., Chang, Y., Lacroix, M., & Han, J. (2018). Effect of oxidized phenolic compounds on cross-linking and properties of biodegradable active packaging film composed of turmeric and gelatin. *Lwt*, 93, 427-433.

- Dhiman, J., Dev, D., & Prasad, D. (2022). Superdisintegrants: Brief Review. *Journal of Drug delivery and Therapeutics*, 12(1), 170-175.
- Edwards, L., McCray, N. L., VanNoy, B. N., Yau, A., Geller, R. J., Adamkiewicz, G., & Zota, A. R. (2022). Phthalate and novel plasticizer concentrations in food items from US fast food chains: a preliminary analysis. *Journal of exposure science & environmental epidemiology*, 32(3), 366-373.
- Fang, L., Zeng, J., Zhang, X., & Wang, D. (2021). Effect of veneer initial moisture content on the performance of polyethylene film reinforced decorative veneer. *Forests*, 12(1), 102.
- Fitzpatrick, S. G., Cohen, D. M., & Clark, A. N. (2019). Ulcerated lesions of the oral mucosa: clinical and histologic review. *Head and neck pathology*, 13, 91-102.
- Foo, W. C., Khong, Y. M., Gokhale, R., & Chan, S. Y. (2018). A novel unit-dose approach for the pharmaceutical compounding of an orodispersible film. *International journal of pharmaceutics*, 539(1-2), 165-174.
- Gulsun, T., Borna, S. E., Vural, I., & Sahin, S. (2018). Preparation and characterization of furosemide nanosuspensions. *Journal of Drug Delivery Science and Technology*, 45, 93-100.
- Homayun, B., Lin, X., & Choi, H.-J. (2019). Challenges and recent progress in oral drug delivery systems for biopharmaceuticals. *Pharmaceutics*, 11(3), 129.
- Kanugo, A., & gandhi, Y. (2022). Formulation optimization and evaluation of oral thin film of bilastine for the treatment of allergic conditions. *Journal of Research in Pharmacy*, 26(5).
- Keisandokht, S., Orsat, V., Karboune, S., & Gatamaneni Loganathan, B. (2022). Microwave-assisted extraction of *Ocimum basilicum* L. seed, *Trigonella foenum-graecum* seed, and *Plantago ovata* Forsk seed husk hydrocolloids compared with conventional heating extraction at optimum extraction conditions. *Arabian Journal for Science and Engineering*, 47(5), 5859-5874.
- Kemp, S. E., Hort, J., & Hollowood, T. (2018). Descriptive analysis in sensory evaluation. 1st ed. *Wiley-Blackwell*, 744.
- Khan, T. M., Patel, R., & Siddiqui, A. H. (2018). Furosemide. *StatPearls*, 29763096.
- Kumar, S., & Kumar, M. (2016). Preformulation study of furosemide. *Der Pharmacia Lettre*, 8(13), 214-222.
- Kumorek, M., Minisy, I. M., Krunclová, T., Voršiláková, M., Venclíková, K., Chánová, E. M., Kubies, D. (2020). pH-responsive and antibacterial properties of self-assembled multilayer films based on chitosan and tannic acid. *Materials Science and Engineering: C*, 109, 110493.
- Liu, Y., Liu, Y., Han, K., Cai, Y., Ma, M., Tong, Q., & Sheng, L. (2019). Effect of nano-TiO₂ on the physical, mechanical and optical properties of pullulan film. *Carbohydrate Polymers*, 218, 95-102.
- Mahapatra, A. P. K., Murthy, P., Panda, N., Gupta, A., Paul, B., Malla, S., & Panigrahy, S. (2021). Extraction of lepidium sativum seed mucilage: Optimization of extraction process with maximum yield by using full factorial design. *Journal of Pharmaceutical Research International*, 33(64B), 720-735.

- Malviya, V., & Pande, S. (2021). Development and evaluation of fast dissolving film of fluoxetine hydrochloride. *Research Journal of Pharmacy and Technology*, 14(10), 5345-5350.
- Maske, R. R., Mahajan, V. R., & Bhalerao, S. B. (2022). Polymers used in mouth dissolving film: A review. *World Journal of Advanced Research and Reviews*, 16(3), 378-389.
- Meher, A., & Dighe, N. S. (2019). An overview of fast dissolving oral film. *Journal of Drug delivery and Therapeutics*, 9(4-s), 822-825.
- Orsuwan, A., & Sothornvit, R. (2018). Effect of banana and plasticizer types on mechanical, water barrier, and heat sealability of plasticized banana-based films. *Journal of Food Processing and Preservation*, 42(1), e13380.
- Pattewar, S., Patil, D., & Sharma, S. (2019). Fabrication and characterization of self-microemulsifying mouth dissolving film for effective delivery of piroxicam. *Indian J. Pharm. Sci*, 81, 503-513.
- Pawar, R., Sharma, R., & Darwhekar, G. (2019). Formulation and evaluation of mouth dissolving film of prochlorperazine maleate. *Journal of Drug delivery and Therapeutics*, 9(6), 110-115.
- Pawar, R., Sharma, R., Sharma, P., & Darwhekar, G. (2019). A review on mouth dissolving film. *Journal of Drug delivery and Therapeutics*, 9(6), 206-210.
- Perdoch, W., Cao, Z., Florczak, P., Markiewicz, R., Jarek, M., Olejnik, K., & Mazela, B. (2022). Influence of nanocellulose structure on paper reinforcement. *Molecules*, 27(15), 4696.
- Pezik, E., Gulsun, T., Sahin, S., & Vural, I. (2021). Development and characterization of pullulan-based orally disintegrating films containing amlodipine besylate. *European Journal of Pharmaceutical Sciences*, 156, 105597.
- Rabe, A., Gesell Salazar, M., Michalik, S., Fuchs, S., Welk, A., Kocher, T., & Völker, U. (2019). Metaproteomics analysis of microbial diversity of human saliva and tongue dorsum in young healthy individuals. *Journal of oral microbiology*, 11(1), 1654786.
- Raza, S. N., Kar, A. H., Wani, T. U., & Khan, N. A. (2019). Formulation and evaluation of mouth dissolving films of losartan potassium using 32 factorial design. *Int. J. Pharm. Sci. Res*, 10(3), 1402-1411.
- Sahu, H., Alexander, A., Gupta, S., Yadav, P., Thapa, H., Banjare, T., Diwedi, S. D. (2018). Formulation and evaluation of risperidone loaded mouth-dissolving film. *Research Journal of Pharmacy and Technology*, 11(7), 2922-2925.
- Serrano, D. R., Fernandez-Garcia, R., Mele, M., Healy, A. M., & Lalatsa, A. (2019). Designing fast-dissolving orodispersible films of amphotericin B for oropharyngeal candidiasis. *Pharmaceutics*, 11(8), 369.
- Shakya, A. K., Al-Najjar, B. O., Deb, P. K., Naik, R. R., & Tekade, R. K. (2018). First-pass metabolism considerations in pharmaceutical product development. In *Dosage Form Design Considerations* (pp. 259-286): Elsevier.
- Sheikh, F. A., Aamir, M. N., Shah, M. A., Ali, L., Anwer, K., & Javaid, Z. (2020). Formulation design, characterization and in vitro drug release study of orodispersible film comprising BCS class II drugs. *Pakistan journal of pharmaceutical sciences*, 33.
- Singh, P., Mishra, G., & Dinda, S. C. (2021). Natural excipients in pharmaceutical formulations. *Evidence Based Validation of Traditional Medicines: A comprehensive Approach*, 829-869.

- Soukoulis, C., Gaiani, C., & Hoffmann, L. (2018). Plant seed mucilage as emerging biopolymer in food industry applications. *Current Opinion in Food Science*, 22, 28-42.
- Vimalson, D. C., Anbazhagan, S., Gokul, L., Idhayadharani, S., Ranjith, S., Sabarinathan, J., & Surya, R. (2019). Enhancement of solubility and dissolution characteristics of furosemide by solid dispersion. *World Journal of Pharmaceutical Research*, 11 (8), 696-719.
- Vishvakarma, P. (2018). Design and development of montelukast sodium fast dissolving films for better therapeutic efficacy. *Journal of the Chilean Chemical Society*, 63(2), 3988-3993.
- Wang, B., Fu, X., Song, S., Chu, H. O., Gibson, D., Li, C., Wu, Z. (2018). Simulation and optimization of film thickness uniformity in physical vapor deposition. *Coatings*, 8(9), 325.
- Zayed, G. M., Abd-El Rasoul, S., Ibrahim, M. A., Saddik, M. S., & Alshora, D. H. (2020). In vitro and in vivo characterization of domperidone-loaded fast dissolving buccal films. *Saudi pharmaceutical journal*, 28(3), 266-273.
- Zhang, F., Mao, J., Tian, G., Jiang, H., & Jin, Q. (2022). Preparation and characterization of furosemide solid dispersion with enhanced solubility and bioavailability. *AAPS PharmSciTech*, 23(1), 65.

Investigation of the Effects of Oleuropein on Mouse Detrusor Muscle Contractility

Elif Nur BARUT[°], Ahmet Can OZTURK^{**}, Seckin ENGIN^{***}, Gulin RENDA^{****}

Investigation of the Effects of Oleuropein on Mouse Detrusor Muscle Contractility

SUMMARY

Oleuropein (OLE) is an important bioactive compound isolated from *Olea europaea* L. (olive), the best-known species of the genus *Olea*, which grows in the Mediterranean region and has many biological activities. In this study, we aimed to investigate the effect of OLE on isolated mouse detrusor smooth muscle (DSM) contractility. OLE was isolated from *Olea europaea* L and the effects of OLE on the contractility of DSM strips were investigated using in vitro isolated organ bath systems. The relaxant effect of OLE (10^{-8} - 10^{-3} M) cumulatively on KCl-precontracted strips was evaluated. Moreover, the effect of OLE (10^{-4} and 10^{-3} M) incubation on KCl-, carbachol (CCh)- or electrical field stimulation (EFS)-induced contractile responses of detrusor strips were assessed concentration-dependently. OLE at higher concentration (10^{-3} M) relaxed KCl-precontracted detrusor strips significantly. Moreover, the contractile responses to KCl, CCh, and EFS were significantly decreased in the strips preincubated with OLE (10^{-3} M) ($p < 0.05$). Our results showed that OLE decreased the contractility of isolated mouse detrusor strips in a concentration-dependent manner and thus it would be a promising agent in pathological conditions related to increased bladder contractility such as overactive bladder. Additionally, further studies are needed to elucidate the exact mechanisms of these effects of OLE.

Key Words: Carbachol, detrusor smooth muscle, isolated organ bath, mice, oleuropein

Oleuropeinin Fare Detrusor Kası Kasılması Üzerine Etkilerinin Araştırılması

ÖZ

Oleuropein (OLE), Akdeniz bölgesinde yetişen ve birçok biyolojik aktiviteye sahip olan *Olea* cinsinin en iyi bilinen türü olan *Olea europaea* L. den (zeytin) izole edilen önemli bir biyoaktif bileşiktir. Bu çalışmada *Olea europaea* L. den izole edilen OLE'nin izole fare detrusor düz kas kontraktilesine etkisini incelemeyi amaçladık. OLE, *Olea europaea* L den izole edildi ve in vitro organ banyosu sistemi kullanılarak izole fare detrusor düz kas şeritlerinin kontraktilesi üzerine etkisi incelendi. Kümülatif OLE' (10^{-8} - 10^{-3} M) uygulamasının KCl ile ön-kasılma oluşturulmuş detrusor şeritleri üzerinde gevşetici etkisi araştırıldı. Ayrıca OLE (10^{-4} ve 10^{-3} M) inkübasyonunun KCl, karbakol (CCh) ve elektriksel alan stimülasyonu (EAS) ile indüklenen kasılma yanıtları üzerine konsantrasyona-bağımlı etkisi değerlendirildi. KCl ile ön kasılma oluşturulmuş detrusor şeritlerinde OLE, yüksek konsantrasyonda (10^{-3} M) belirgin gevşeme yanıtına neden oldu. Ayrıca OLE (10^{-3} M) inkübasyonu KCl, CCh ve EAS ile indüklenen kasılma yanıtlarını anlamlı olarak azalttı ($p < 0.05$). Elde ettiğimiz sonuçlar, OLE'nin izole fare detrusor düz kas kontraktilesini konsantrasyona-bağımlı olarak azalttığını ve böylece aşırı aktif mesane gibi mesane kontraktilesinin arttığı patolojik durumlarda umut vaat edici bir ajan olabileceğini göstermektedir. OLE'nin bu etkilerinin mekanizmasının aydınlatılabilmesi için ileri çalışmaların yapılması gerekmektedir.

Anahtar Kelimeler: Karbakol, detrusor düz kası, izole organ banyosu, fare, oleuropein

Received: 12.09.2023

Revised: 24.11.2023

Accepted: 27.11.2023

[°] ORCID: 0000-0003-3284-848X, Department of Pharmacology, Faculty of Pharmacy, Karadeniz Technical University Trabzon, Türkiye.

^{**} ORCID: 0009-0001-6803-4018, Department of Pharmacology, Faculty of Pharmacy, Karadeniz Technical University Trabzon, Türkiye.

^{***} ORCID: 0000-0002-1982-7820, Department of Pharmacology, Faculty of Pharmacy, Karadeniz Technical University Trabzon, Türkiye.

^{****} ORCID: 0000-0001-6323-0338, Department of Pharmacognosy, Faculty of Pharmacy, Karadeniz Technical University Trabzon, Türkiye.

INTRODUCTION

The Oleaceae family includes about 600 species of deciduous trees and shrubs. The genus *Olea*, belonging to the Oleaceae family, consists of 30 species, but *Olea europaea* L. also known as olive tree is the best-known species of the *Olea* genus, used as food and grown in the Mediterranean region. *Olea europaea* is generally grown in tropical and warm temperate regions of the world. It is generally spread in the coastal regions of the Eastern Mediterranean region. Today, 97% of olive trees are located in Mediterranean countries, including Türkiye (Ghanbari et al., 2012; Ozturk et al., 2021). Mediterranean countries have been cultivating olives since ancient times to obtain both oil and medicinal compounds (Topuz & Bayram 2021). The olive leaf extracts have been used for centuries to protect human health against various diseases (Ghanbari et al., 2012). The components responsible for the biological activities of the leaves and fruits of the olive tree are considered phenolic compounds and it is known that their concentrations vary between species. *Olea europaea*, which is widely distributed in Türkiye, contains dominant phenolic oleosides such as oleuropein (OLE), demethyl-oleuropein, ligstroside and oleoside (Omar 2010).

OLE is a phenolic iridoid glycoside, formed by the combination of hydroxytyrosol, elenolic acid, and glucose molecules, predominantly found in the oil and leaves of the plant and it is responsible for the diverse pharmacological effects of *Olea europaea* (Hassen et al., 2015; Rahiman et al., 2019). OLE is a phenolic secoiridoid formed by the combination of hydroxytyrosol, elenolic acid, and glucose molecules (Hassen et al., 2015). The antioxidant, anti-inflammatory, antimicrobial, antifungal, anticancer, hypoglycemic, antihyperlipidemic and cardioprotective effects of OLE have been shown in several *in vivo* and *in vitro* studies (Carrera-González et al., 2013; Sepporta et al., 2014; Hassen et al., 2015). OLE treatment also decreases blood glucose and improves glucose tolerance in animal models of

alloxan or streptozotocin-induced diabetes. It has also been reported that OLE reduces the amount of serum malondialdehyde, increases the amount of reduced glutathione, and has an antioxidant effect by increasing the activity of superoxide dismutase (Qadir et al., 2016; Khalil et al., 2017).

The effects of OLE on vascular smooth muscle contractility have also been investigated. Gilani et al. determined that the leaf extracts of *Olea europaea* had a hypotensive effect due to Ca²⁺ channel blocking action and Scheffler et al. showed that OLE was responsible for this effect (Gilani et al., 2005; Scheffler et al., 2008). In addition, OLE was shown to have a relaxant effect on the contractions induced by phenylephrine in rat thoracic aorta preparations, and endothelial-derived nitric oxide was found to mediate the vasorelaxant effect of OLE (Ilic et al., 2021). In rat gastric fundus, it was shown that OLE caused a marked relaxation in the fundus muscle than other dietary polyphenols, and nitric oxide (NO) formation was responsible for this effect (Rocha et al., 2009). However, the information about the effects of OLE on urinary tract smooth muscle contractility is very limited, and there is no study available reporting its effect on detrusor smooth muscle (DSM) contractility.

Acetylcholine (ACh) is the main neurotransmitter that regulates detrusor contractility. During the micturition phase, ACh stimulates muscarinic receptors that mediate bladder contraction (Merril et al., 2016). DSM relaxation is also mediated by the release of catecholamines from sympathetic nerve terminals and catecholamine-mediated activation of β -adrenoreceptors (Propping et al., 2015). Various ion channels play a major role in the activity of bladder DSM such as voltage dependent calcium and different types of potassium channels. It has been found that voltage-dependent calcium channels allow the calcium influx that results in bladder contraction and it has also been reported that nitric oxide causes relaxation by reducing intracellular calcium levels in DSM (Andersson & Arner 2004; Petkov et al., 2011).

Disturbances in the regulation of detrusor contractility can cause bladder dysfunction, ranging from bladder atony to overactive bladder related to poor quality of life in patients. Currently, medical treatment options for bladder dysfunctions are limited and patient compliance problems may occur due to the side effects of therapeutic agents (Marinkovic, 2019). Therefore, there is an urgent need for potential therapeutics that can regulate bladder contractility with adequate efficacy and appropriate safety profile.

In this study, we aimed to identify the potential effect of OLE on the contractility of the mouse DSM.

MATERIALS AND METHODS

Chemicals

CCh (muscarinic agonist) was purchased from Sigma Aldrich (St. Louis, Missouri, USA). *n*-hexane (104368, Merck), methanol (24229, Riedel-De-Haën), ethyl acetate (100864, Merck), TLC (silica gel aluminum plates, SiO₂ 60 F₂₅₄, 5554, Merck) were used. Silica gel 60 (Kieselgel 60, 70-230 mesh, 107734, Merck) was employed for open column chromatography (CC). Reversed-phase material (LiChroprep C18) (25-40 μm, 09303, Merck) was utilized for vacuum liquid chromatography (VLC). CCh, KCl and OLE were dissolved in distilled water.

Extraction and isolation of OLE

The air-dried and grounded leaves of *O. europaea* (352 g) were extracted with 70% methanol (2 L) at 40 °C by a rotary evaporator under reflux. The procedure was repeated four times, and the extracted materials were filtered. The filtrates had been combined and evaporated to dryness with a rotary evaporator at 40 °C under reduced pressure. The crude extract (69.8 g, yielding 19.8%) was dispersed in a mixture of methanol and water (1:9) and partitioned with *n*-hexane and ethyl acetate, respectively, by using a separatory funnel (Cifa et al, 2018; Otero et al., 2020). The ethyl acetate sub-extract (26.7 g) was subjected to VLC over reversed-phase material (LiChroprep C18), and elution with increasing concentrations of MeOH

in H₂O mixtures (in steps of 10% of MeOH, each 200 mL, fraction volumes 200 mL) as eluent, yielded 5 fractions (fractions A-E). The fractions obtained with the elutions were monitored by the TLC system and combined according to the TLC results. Fraction E (11.3 g) was subjected to chromatographic separation on a silica gel (100 g) column using CHCl₃/MeOH with increasing polarity (100:0 to 90:10 mixtures and combined fractions afforded OLE (6.35 g). The compound's structure was determined by comparing its spectroscopic data to those described in the literature (Zun-Qiu et al., 2015).

Animals

Adult female Balb/C mice (6-8 weeks old) were used in the study. The animals were housed in the humidity and temperature-controlled (22±1 °C) rooms with access to food and water *ad libitum*. The experimental protocol was approved by the Institutional Animal Care and Ethics Committee (Approval number: 2022/04).

DSM strips preparation

The mice were euthanized by cervical dislocation then bladders were identified with abdominal incision and then quickly transferred in Krebs-Henseleit solution (mmol/L: NaCl 118, KCl 4.7, NaH₂PO₄ 1.2, MgSO₄ 1.3, CaCl₂ 2.5, NaHCO₃ 25 ve glucose 11). The sphincter and trigon were removed and DSM strips (3-4 mm long and 2-3 mm wide) were prepared (Engin et al., 2022; Engin et al., 2023).

Contractility studies

The detrusor strips were placed in 30 mL isolated organ baths with Krebs-Henseleit solution at 37 °C and bubbled with carbogen (95% O₂ and 5% CO₂) during the experiments. To determine the tissue contractility, strip was mounted to an isometric force transducer (MAY FDT10A, Commat, Ankara, Türkiye) attached to data acquisition/recording system (BIOPAC MP 35, Goleta, USA). The strips were placed organ bath under 1 g resting tension then stabilized with the equilibrate period for 60 min.

Strips were wash out with fresh bath solution every 20 min. After the equilibration period, DSM strips were contracted with 80 mM KCl to confirm the viability of the strips. All experimental procedures were set up based on previous studies (Engin et al., 2022; Engin et al., 2023).

Effect of OLE on KCl-precontracted DSM strips

To test the effect of OLE on DSM strips precontracted with KCl, KCl (80 mM) was added to the organ bath and the contractile response was waited until it reached a plateau. Then cumulative concentration-dependent responses of OLE (10^{-8} - 10^{-3} M) on DSM strips were recorded. The relaxant response was reported as the percentage of precontraction with KCl.

Effect of OLE on KCl-induced contractions of DSM strips

To investigate the effect of OLE on KCl-induced contractions of DSM strips, the contractile control response was obtained with 80 mM KCl. After a washout period, the strips were incubated with OLE at 10^{-4} M or 10^{-3} M for 20 min and then KCl-induced contractile responses were repeated. The contractile responses were reported as the percentage of maximal control response.

Effect of OLE on CCh-induced contractions of DSM strips

To understand the effect of OLE on CCh-induced contractions of DSM strips, a cumulative response to CCh (10^{-8} - 10^{-4} M) was obtained as a control. Following

an equilibration period, DSM strips were incubated with OLE at 10^{-4} M and 10^{-3} M for 20 min and then concentration-dependent contractile responses to cumulative CCh were repeated. The responses were expressed as the percentage of maximal control contraction induced by CCh.

Effect of OLE on nerve-evoked contractions of DSM strips

To determine the effect of OLE on the nerve-evoked contraction of DSM strips, the contractile responses were assessed by EFS before and after the incubation with OLE (10^{-3} M) for 20 min at the frequencies of 8, 16 and 32 Hz (50 V, 0.2 msec duration) (Engin et al., 2023).

Statistical analysis

Data were expressed as the mean \pm standard error. Statistical analysis was performed using GraphPad Prism (Version 5.01; GraphPad Software, San Diego, CA, USA). The differences between groups were compared with student's *t* test or one-way ANOVA, followed by Bonferroni multiple comparison test and $p < 0.05$ was considered statistically significant.

RESULTS AND DISCUSSION

Effect of OLE on KCl-precontracted DSM strips

OLE at low concentrations (10^{-8} - 10^{-4} M) did not produce a marked relaxation response in KCl-precontracted DSM strips, while the highest concentration of OLE (10^{-3} M) produced a significant relaxation response (Figure 1.).

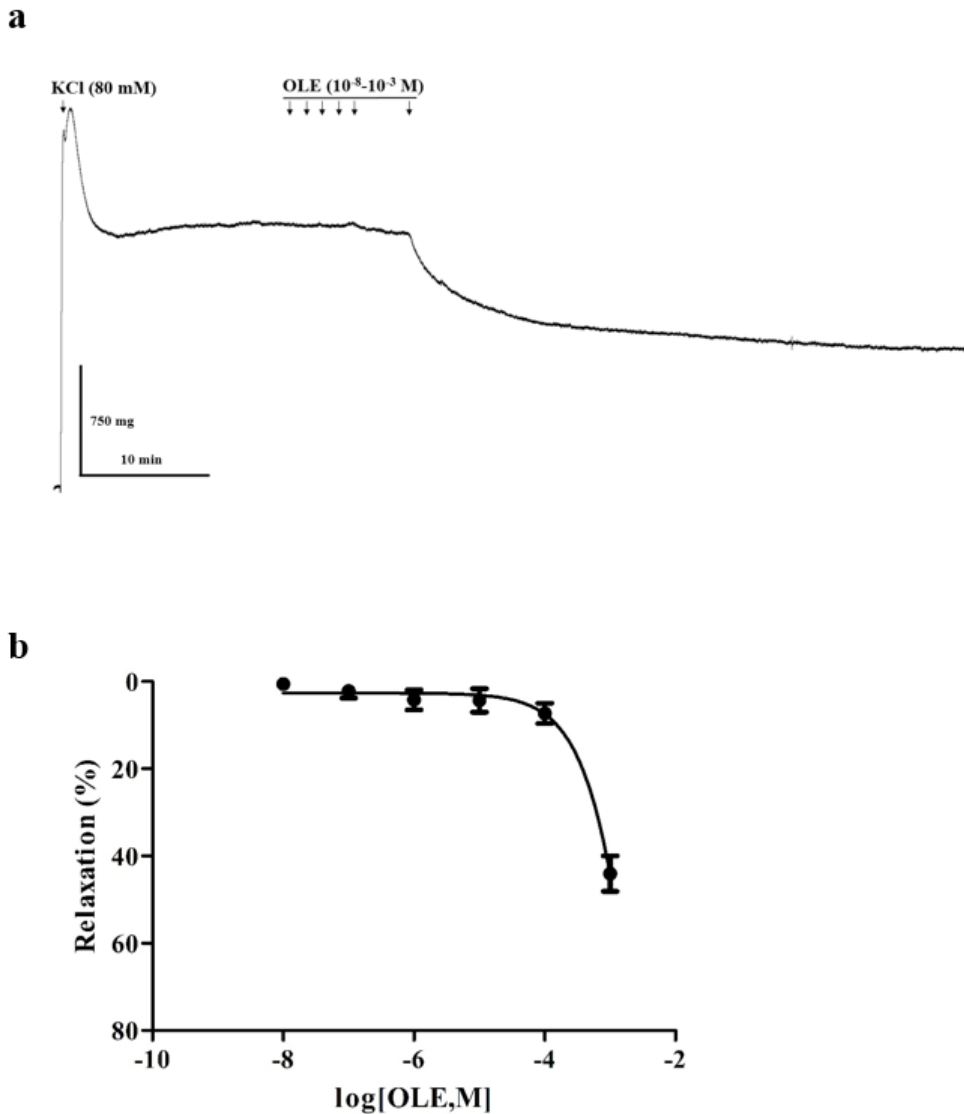


Figure 1. Effect of OLE on the contractility of DSM strips pre-contracted with KCl (80 mM) Data were expressed as mean±standard error (n=4). (a) Representative trace showing the relaxant effect of OLE on DSM strips pre-contracted with KCl. (b) Cumulative concentration-response curve of the inhibitory response induced by OLE (10⁻⁸-10⁻³ M) in KCl pre-contracted DSM strips.

Effect of OLE on KCl-induced contractions of DSM strips

Preincubation with OLE at 10⁻⁴ M did not alter KCl-induced contractions of DSM strips. However,

there was a statistically marked decrease in the KCl-induced contractions after the incubation with OLE at 10⁻³ M (Figure 2., p<0.001).

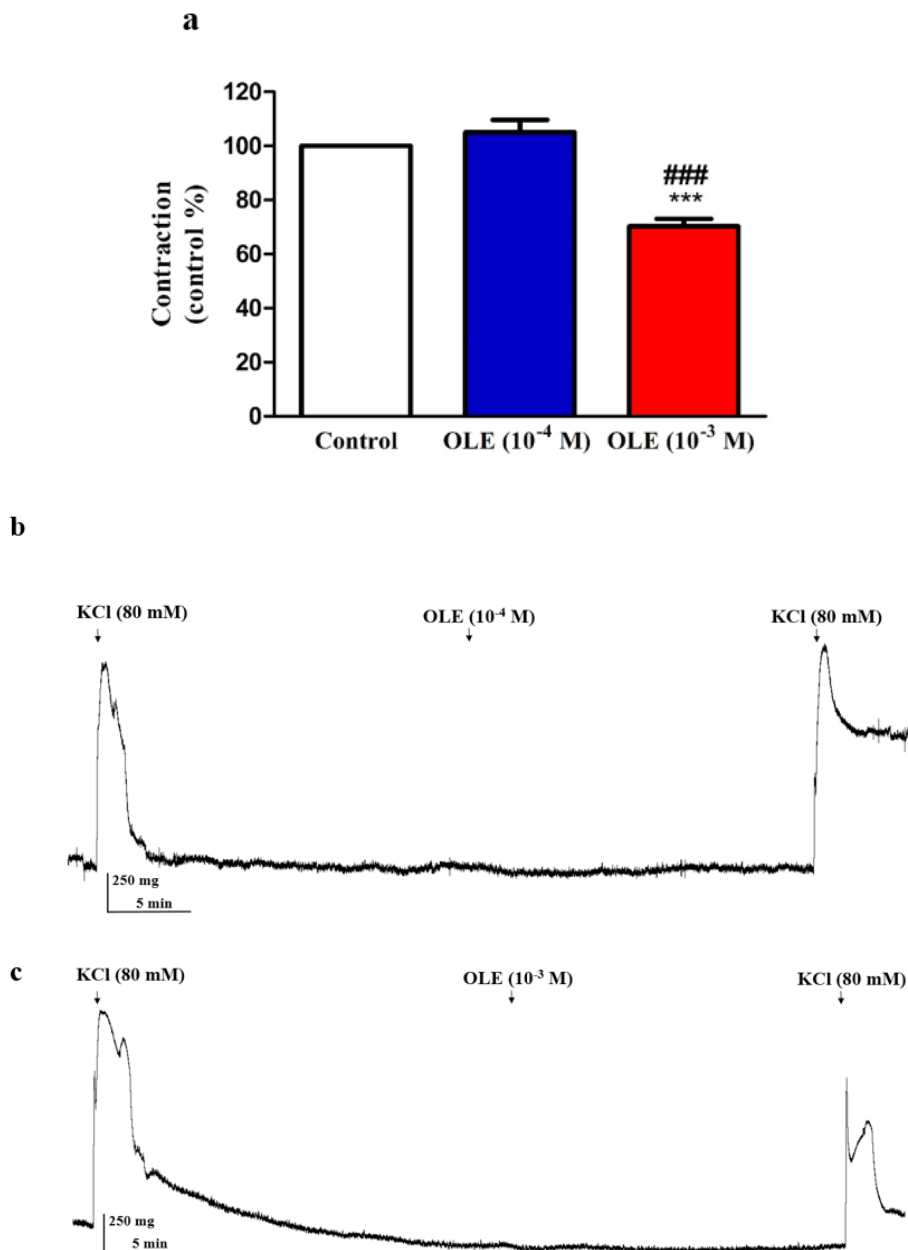


Figure 2. Effect of OLE incubation on KCl-induced contractions of DSM strips. Data were expressed as mean±standard error (n=4). (a) Effect of OLE (10⁻⁴, 10⁻³ M) incubation on the maximum contractile response induced by KCl in DSM strips. Representative trace showing the effect of OLE incubation at (b) 10⁻⁴ M and (c) 10⁻³ M on the maximal contractile response induced by KCl in DSM strips. ***p<0.001 significantly different from the control, ###p<0.001 significantly different from the OLE (10⁻⁴ M).

Effect of OLE on CCh-induced contractions of DSM strips

CCh-induced contractile responses of DSM strips obtained following the incubation with 10⁻⁴ M OLE were similar to the that of control, but a statistically

significant decrease was found in the contractions induced by higher concentrations of CCh (10⁻⁵ and 10⁻⁴ M) after the incubation with 10⁻³ M OLE (Figure 3., p<0.001).

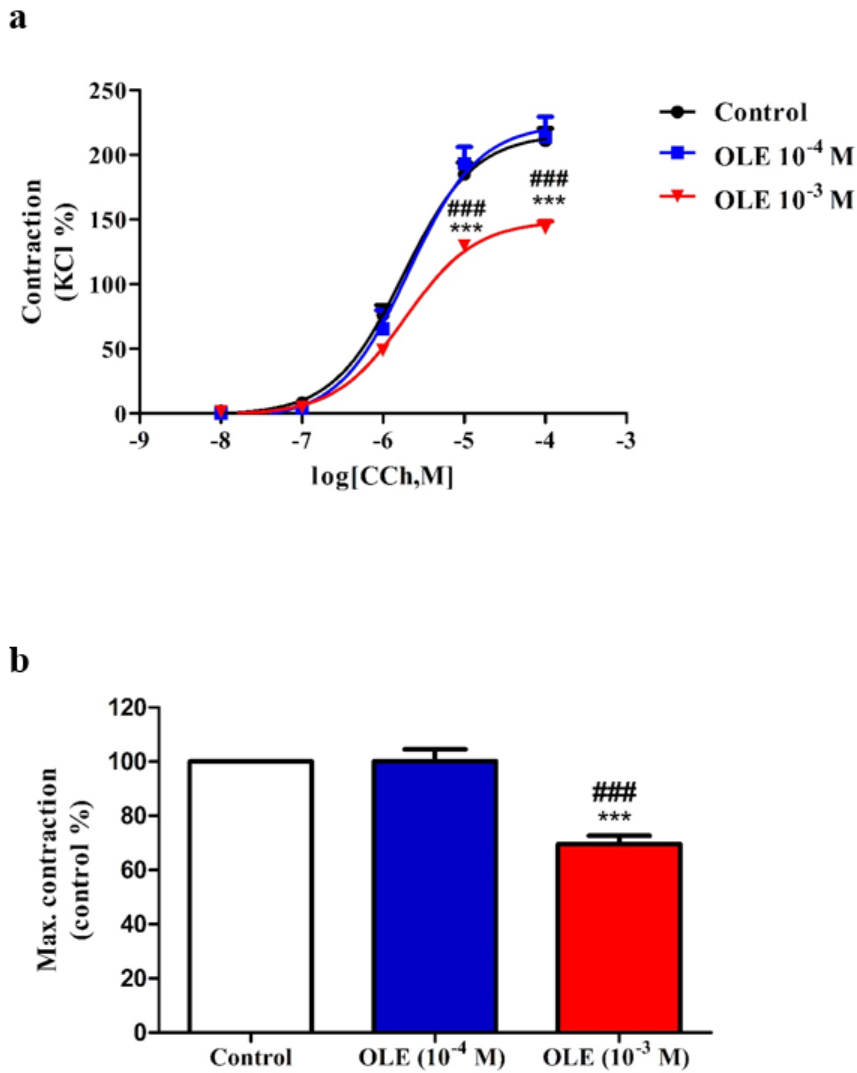


Figure 3. Effect of OLE incubation on CCh-induced contractions of DSM strips. Data were expressed as mean±standard error (n=4). (a) Concentration-response curves showing the inhibitory effect of OLE (10⁻⁴, 10⁻³ M) incubations on CCh-induced contractions in DSM strips. (b) Effect of OLE (10⁻⁴, 10⁻³ M) incubation on the maximum contractile response induced by CCh in DSM strips. ***p<0.001 significantly different from the control, ###p<0.001 significantly different from the control OLE (10⁻⁴ M).

Effect of OLE on nerve-evoked contractions of DSM strips

The contractile responses induced by EFS (8, 16 and 32 Hz) were evaluated in DSM strips after incubation with the highest concentration of OLE

tested, which was observed to reduce contractile responses in previous experiments. After the incubation period with 10⁻³ M OLE, there was a statistically significant decrease in 32 Hz-induced contractions in EFS-induced contractions of DSM strips (Figure 4., p<0.05).

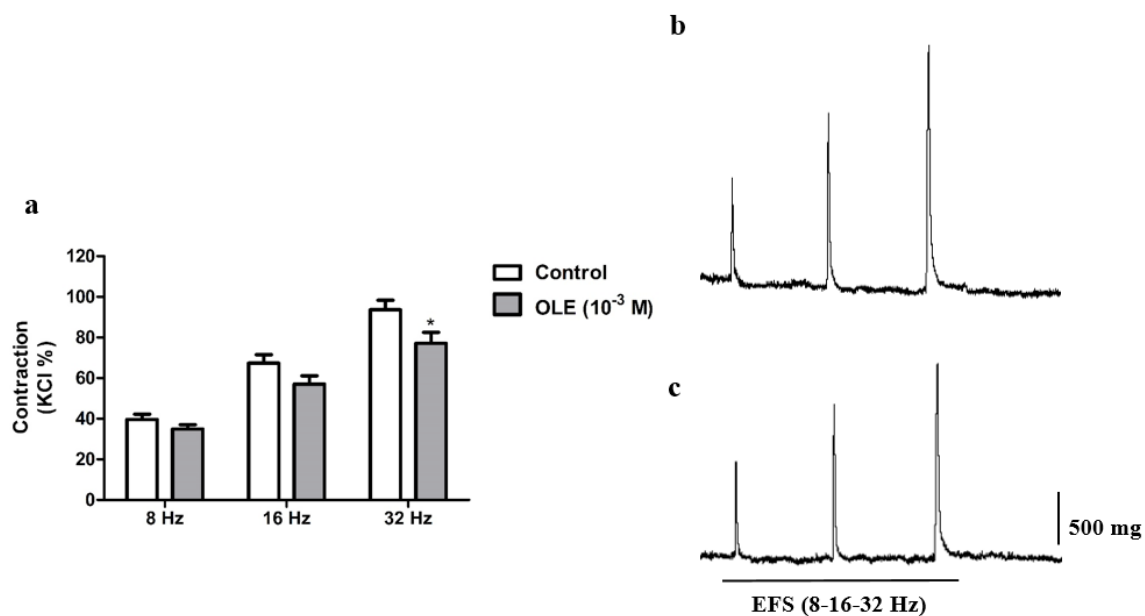


Figure 4. Effect of OLE incubation on EFS-induced neurogenic contractions of DSM strips. Data were expressed as mean±standard error (n=4). (a) Effect of OLE (10⁻³ M) incubation on the maximum contractile response induced by EFS (8-16-32 Hz) in DSM strips. (b) Representative trace showing EFS-induced contractions of DSM strips (b) in the absence (control) and (c) in the presence of OLE (10⁻³ M). *p<0.05 significantly different from the control group.

In our study, we found that the highest concentration of OLE (10⁻³ M) produced a significant relaxation in KCl-precontracted DSM strips. In addition, while there was no significant change in KCl responses following OLE incubation at 10⁻⁴ M compared to the control group, a significant decrease was found in the KCl responses after the OLE incubation at 10⁻³ M. Previous studies have shown that leaf extract of *Olea europaea* mediated vasorelaxation via inhibiting Ca²⁺ channel in aortic smooth muscle, and OLE has been shown the primary bioactive compound responsible for this effect. (Gilani et al., 2005; Scheffler et al., 2008). In line with previous studies, we concluded that high concentrations of OLE may reduce DSM contractility via inhibiting the voltage-sensitive Ca²⁺ channels. We also showed that the CCh-induced contractile responses following the preincubation with OLE at 10⁻⁴ M were not different from the control, but a significant decrease was found in CCh-induced contractile responses of DSM strips after the preincubation with OLE at

10⁻³ M. The reduction of CCh-induced contractions in the presence of OLE may be due to its direct muscarinic receptor antagonist activity or its blocking of intracellular signaling activated by the stimulation of muscarinic receptors.

Detrusor neurogenic contractions are controlled by neurotransmitters such as ACh and ATP via muscarinic and purinergic receptor activation (Fowler et al., 2008). In our study, we observed that incubation with the highest concentration of OLE reduced EFS-induced neurogenic contractions of DSM strips. The mechanisms of the decrement in neurogenic contractions caused by OLE in DSM should be investigated in the presence of various antagonist agents.

CONCLUSION

Disturbances in the regulation of detrusor contractility can cause bladder dysfunction, ranging from bladder atony to overactive bladder. Antimuscarinic drugs and β-agonists are the major therapeutics used

in the pharmacological treatment of overactive bladder, a common bladder dysfunction. However, current pharmacotherapy for overactive bladder has insufficient efficacy and several side effects (Marinkovic, 2019). Therefore, studies are underway to develop potential therapeutics that can regulate bladder contractility with adequate efficacy and appropriate safety profile. In light of our findings, we exhibited that OLE reduces DSM contractility and may be a promising agent in overactive bladder-like bladder dysfunction following the exact mechanism of action clarified.

ACKNOWLEDGEMENTS

This study was supported by the Scientific and Technological Research Council of Turkey, TUBITAK (project number 1919B012206321).

CONFLICT OF INTEREST

The authors declare that there is no conflict of interest.

AUTHOR CONTRIBUTION STATEMENT

Conceptualization: ENB, ACO. Methodology: ENB, SE, GR. Data curation, investigation: ENB, ACO, SE, GR. Funding acquisition: ENB, ACO. Writing original draft: ENB, GR. Review & Editing: ENB, ACO, SE, GR.

REFERENCES

- Andersson, K. E., & Arner, A. (2004). Urinary bladder contraction and relaxation: physiology and pathophysiology. *Physiological Reviews*, 84(3), 935–986. doi:10.1152/physrev.00038.2003
- Carrera-González, M. P., Ramírez-Expósito, M. J., Mayas, M. D., Martínez-Martos, J. M. (2013). Protective role of oleuropein and its metabolite hydroxytyrosol on cancer. *Trends in Food Science & Technology*, 31, 92–99. doi:10.1016/j.tifs.2013.03.003
- Cifá, D., Skrt, M., Pittia, P., Di Mattia, C., & Poklar Ulrih, N. (2018). Enhanced yield of oleuropein from olive leaves using ultrasound-assisted extraction. *Food Science & Nutrition*, 6(4), 1128–1137. doi:10.1002/fsn3.654
- Engin, S., Barut, E. N., Erac, Y., Sari, S., & Kadioglu, M. (2023). The inhibitory effect of escitalopram on mouse detrusor contractility: The role of L-type calcium channels. *Toxicology and Applied Pharmacology*, 461, 116408. doi:10.1016/j.taap.2023.116408
- Engin, S., Kaya Yasar, Y., Barut, E. N., Getboga, D., Erac, Y., & Sezen, S. F. (2022). The inhibitory effect of trimetazidine on detrusor contractility - a potential repositioning of trimetazidine for the treatment of overactive bladder. *The Journal of Pharmacy and Pharmacology*, 74(1), 94–102. doi:10.1093/jpp/rgab072
- Fowler, C. J., Griffiths, D., & de Groat, W. C. (2008). The neural control of micturition. *Nature Reviews Neuroscience*, 9(6), 453–466. doi:10.1038/nrn2401
- Ghanbari, R., Anwar, F., Alkharfy, K. M., Gilani, A. H., & Saari, N. (2012). Valuable nutrients and functional bioactives in different parts of olive (*Olea europaea* L.)-a review. *International Journal of Molecular Sciences*, 13(3), 3291–3340. doi:10.3390/ijms13033291
- Gilani, A. H., Khan, A. U., Shah, A. J., Connor, J., & Jabeen, Q. (2005). Blood pressure lowering effect of olive is mediated through calcium channel blockade. *International Journal of Food Sciences and Nutrition*, 56(8), 613–620. doi:10.1080/09637480500539420
- Hassen, I.E., Casabianca, H., & Hosni, K. (2015). Biological activities of the natural antioxidant oleuropein: exceeding the expectation – A mini-review. *Journal of Functional Foods*, 18, 926–940. doi:10.1016/j.jff.2014.09.001
- Ilic, S., Stojiljkovic, N., Stojanovic, N., Stoilkovic, M., Mitic, K., Salinger-Martinovic, S., & Randjelovic, P. (2021). Effects of oleuropein on rat's atria and thoracic aorta: a study of antihypertensive mechanisms. *Canadian Journal of Physiology and Pharmacology*, 99(1), 110–114. doi:10.1139/cjpp-2020-0363

- Khalili, A., Nekooeian, A. A., & Khosravi, M. B. (2017). Oleuropein improves glucose tolerance and lipid profile in rats with simultaneous renovascular hypertension and type 2 diabetes. *Journal of Asian Natural Products Research*, 19(10), 1011-1021. doi:10.1080/10286020.2017.1307834
- Marinkovic S. P. (2019). New technologies in the management of overactive bladder: current research and future prospects. *Therapeutic Advances in Urology*, 11, 1756287219844669. doi:10.1177/1756287219844669
- Merrill, L., Gonzalez, E. J., Girard, B. M., & Vizzard, M. A. (2016). Receptors, channels, and signalling in the urothelial sensory system in the bladder. *Nature reviews. Urology*, 13(4), 193-204. doi:10.1038/nrurol.2016.13
- Omar, S. H. (2010). Oleuropein in olive and its pharmacological effects. *Scientia Pharmaceutica*, 78(2), 133-154. doi:10.3797/scipharm.0912-18
- Otero, D. M., Oliveira, F. M., Lorini, A., Antunes, B. F., Oliveira, R. M., & Zambiasi, R. C. (2020). Oleuropein: methods for extraction, purifying and applying. *Revista Ceres*, 67(4), 315-329. doi:10.1590/0034-737x202067040009
- Öztürk, M., Altay, V., Gönen, T. M., Unal, B. T., Efe, R., Akçiçek, E., Bukhari, A. (2021). An overview of olive cultivation in Turkey: Botanical Features, Eco-Physiology and Phytochemical Aspects. *Agronomy*, 11(2), 295. doi:10.3390/agronomy11020295
- Petkov G. V. (2011). Role of potassium ion channels in detrusor smooth muscle function and dysfunction. *Nature reviews. Urology*, 9(1), 30-40. doi:10.1038/nrurol.2011.194
- Propping, S., Newe, M., Lorenz, K., Wirth, M. P., & Ravens, U. (2015). β -adrenoceptor-mediated relaxation of carbachol-pre-contracted mouse detrusor. *Urologia Internationalis*, 95(1), 92-98. doi:10.1159/000369075
- Qadir, N. M., Ali, K. A., & Qader, S. W. (2016). Antidiabetic effect of oleuropein from *Olea europaea* leaf against alloxan induced type 1 diabetic in rats, *Brazilian Archives of Biology and Technology*, 59, e16150116. doi:10.1590/1678-4324-2016150116
- Rahiman, S. M., El-Metwally, T. H., Shrivastava, D., Tantry, M. N., & Tantry, B. A. (2019). Oleuropein and oleic acid: A novel emerging dietary target for human chronic diseases, *Indian Journal of Biochemistry and Biophysics*, 56, 263-268. doi:10.56042/ijbb.v56i4.27349
- Rocha, B. S., Gago, B., Barbosa, R. M., & Laranjinha, J. (2009). Dietary polyphenols generate nitric oxide from nitrite in the stomach and induce smooth muscle relaxation. *Toxicology*, 265(1-2), 41-48. doi:10.1016/j.tox.2009.09.008
- Scheffler, A., Rauwald, H. W., Kampa, B., Mann, U., Mohr, F. W., & Dhein, S. (2008). *Olea europaea* leaf extract exerts L-type Ca(2+) channel antagonistic effects. *Journal of Ethnopharmacology*, 120(2), 233-240. doi:10.1016/j.jep.2008.08.018
- Sepporta, M. V., Fucelli, R., Rosignoli, P., Ricci, G., Servili, M., Morozzi, G., Fabiani, R. (2014). Oleuropein inhibits tumour growth and metastases dissemination in ovariectomised nude mice with MCF-7 human breast tumour xenograft, *Journal of Functional Foods*, 8, 269-273. doi:10.1016/j.jff.2014.03.027
- Topuz, S., & Bayram, M. (2022). Oleuropein extraction from leaves of three olive varieties (*Olea europaea* L.): Antioxidant and antimicrobial properties of purified oleuropein and oleuropein extracts, *Journal of Food Processing and Preservation*, 46, e15697. doi:10.1111/jfpp.15697
- Zun-Qiu, W., Gui-Zhou, Y., Qing-Ping, Z., You-Jun, J., Kai-Yu, T., Hua-Ping, C., Ze-Shen, Y. & Qian-Ming, H. (2015). Analysis of the contents and antioxidant activities of oleuropein. *Journal of Food Biochemistry*, 39, 566-574. doi:10.1111/jfbc.12152

Immunosuppressive and Ameliorative Effects of Dietary Combined Herbs Extract of *Curcuma zedoaria* (Christm.) Roscoe and *Phyllanthus niruri* L. in DMBA-induced Breast Cancer Mouse Model

Wira Eka PUTRA*, Anoraga Mona Larasati Sekar MENTARI**,
Devita RATNASARI***, Dhaniar CHAIRUNNIZA****, Arief HIDAYATULLAH*****,
Muhaimin RIFA'I*****

Immunosuppressive and Ameliorative Effects of Dietary Combined Herbs Extract of Curcuma zedoaria (Christm.) Roscoe and Phyllanthus niruri L. in DMBA-induced Breast Cancer Mouse Model

DMBA ile indüklenen Meme Kanseri Fare Modelinde Curcuma zedoaria (Christm.) Roscoe ve Phyllanthus niruri L. Kombine Bitki Ekstrelerinin İmmünsüpresif ve İyileştirici Etkileri

SUMMARY

Cancer continues to be the most prevalent health issue on a worldwide basis. Each year, there is an increased number of new incidence and mortality. Numerous approaches, such as medicinal plant-based treatments, have been put out as therapies. In this study, we aimed to evaluate the immunomodulation effect of dietary combined herbs extract of *Curcuma zedoaria* and *Phyllanthus niruri* (cheral) in 7,12-Dimethylbenz[a]anthracene (DMBA)-induced breast cancer mouse model. The experimental mice were divided into roughly six treatment groups, including administering cheral extract with a series of doses including 1.233 mg/kg BW, 2.466 mg/kg BW, and 4.932 mg/kg BW. Flow cytometry analysis was performed to evaluate immune parameters including NK cells, TNF- α and IFN- γ -expressing NK cells, CD4⁺ TNF- α IFN- γ ⁺ type 1 helper T cells, and CD4⁺ CD25⁺ regulatory T cells population. In this present study, we demonstrated that cheral extract exerts immunosuppressive activity by attenuating the properties of the immune system, such as NK cells, Th1 cells, and regulatory T cells in DMBA-inducing mice to the normal levels. Thus, we suggested that cheral extract has ameliorative potency as alternative or complementary therapy against cancer incidence.

Key Words: Cheral, *Curcuma zedoaria*, DMBA, Immunosuppressive, *Phyllanthus niruri*

ÖZ

Kanser dünya çapında en yaygın sağlık sorunu olmaya devam etmekte, her yıl yeni vaka ve ölüm oranlarında artış yaşanmaktadır. Tıbbi bitki bazlı tedaviler gibi çok sayıda yaklaşım tedavi seçeneği olarak konmuştur. Bu çalışmada, 7,12-Dimetilbenz[a]antrasen (DMBA) ile indüklenen meme kanseri fare modelinde *Curcuma zedoaria* ve *Phyllanthus niruri* (cheral) kombine bitki ekstrelerinin immünomodülatör etkisini değerlendirmeyi amaçladık. Deney hayvanları, 1.233 mg/kg VA, 2.466 mg/kg VA ve 4.932 mg/kg VA dahil olmak üzere bir dizi dozla kombine ekstrelerin (cheral) uygulandığı altı tedavi grubuna ayrıldı. NK hücreleri, TNF- α ve IFN- γ ekspres eden NK hücreleri, CD4⁺ TNF- α IFN- γ ⁺ tip 1 yardımcı T hücreleri ve CD4⁺ CD25⁺ düzenleyici T hücreleri popülasyonu dahil olmak üzere bağışıklık parametrelerini değerlendirmek için akış sitometri analizi yapıldı. Bu çalışmada, kombine ekstrelerin, DMBA'yı indükleyen farelerde NK hücreleri, Th1 hücreleri ve düzenleyici T hücreleri gibi bağışıklık sisteminin özelliklerini normal seviyelere azaltarak immün baskılayıcı aktivite gösterdiği saptandı. Bu nedenle, kombine ekstrelerin kanser vakalarına karşı alternatif veya tamamlayıcı tedavi olarak iyileştirici güce sahip olduğunu düşünmekteyiz.

Anahtar Kelimeler: Cheral, *Curcuma zedoaria*, DMBA, İmmünosüpresif, *Phyllanthus niruri*.

Received: 18.07.2023

Revised: 29.11.2023

Accepted: 30.11.2023

* ORCID:0000-0003-4831-3869, Biotechnology Study Program, Department of Applied Sciences, Faculty of Mathematics and Natural Sciences, Universitas Negeri Malang, East Java, Indonesia.

** ORCID:0000-0002-4187-3671, Department of Biology, Faculty of Mathematics and Natural Sciences, Brawijaya University, East Java, Indonesia.

*** ORCID: 0000-0003-3650-9012, Department of Biology, Faculty of Mathematics and Natural Sciences, Brawijaya University, East Java, Indonesia.

**** ORCID: 0000-0002-6839-3416, Department of Biology, Faculty of Mathematics and Natural Sciences, Brawijaya University, East Java, Indonesia.

***** ORCID: 0000-0003-1929-3635, Health Governance Initiative, United Nations Development Programme Indonesia, Eijkman-RSCM Building, Jakarta, Indonesia

***** ORCID: 0000-0001-5731-2951, Department of Biology, Faculty of Mathematics and Natural Sciences, Brawijaya University, East Java, Indonesia.

INTRODUCTION

Cancer is a broad term for a chronic condition caused by uncontrolled cell proliferation. It is a common disease primarily because of prolonged unhealthy lifestyles like extreme high-calorie diets and high levels of stress, exposure to carcinogens, genetic factors, or a combination of those risk factors (Rock et al. 2020). With more than 19 million newly diagnosed cases and 10 million fatalities annually, it is regarded as one of the leading causes of mortality and one of the most important burdens on healthcare systems and communities globally (Sung et al. 2021). However, the death rate in America has decreased, although this phenomenon may occur only in developed countries with modern and competent healthcare systems and greater ability for earlier diagnosis (Siegel et al. 2021). Nonetheless, some reports indicate that the burden of cancer incidence and mortality, particularly breast cancer, is increasing significantly because breast cancer has surpassed lung cancer as the leading cancer diagnosed regardless of gender, with more than 2.3 million new cases diagnosed in 2020 (Lei et al. 2021, Sung et al. 2021). It accounts for more than 30 percent of the projected new cases in the United States alone during the previous two years among women (Siegel et al. 2022, 2021) the American Cancer Society estimates the numbers of new cancer cases and deaths in the United States and compiles the most recent data on population-based cancer occurrence and outcomes. Incidence data (through 2018, while it accounts for roughly 12% of cases globally, with over 7% of recent fatalities recorded (Sung et al. 2021). One in every eight women in the United States is at risk of developing invasive breast cancer, which can spread to other organs, and one in every 36 women dies from the disease (Britt et al. 2020). Breast cancer patients must be treated as soon as they are diagnosed. Delaying therapy for just three months after the first diagnosis may result in a worse prognosis because breast cancer can progress swiftly into more severe stages. However, in low-to-middle-income nations, most cases are identified later, either locally advanced or metastatic

the chances of survival are very high (Ginsburg et al., 2020). However, women in many settings face complex barriers to early detection, including social, economic, geographic, and other interrelated factors, which can limit their access to timely, affordable, and effective breast health care services. Previously, the Breast Health Global Initiative (BHGI). Because of its complexity, there is currently no universal cure for every type and subtype of cancer.

The immune system plays a vital role in developing and eliminating cancer. It is frequently associated with a persistent inflammatory response. Both innate and adaptive immune components carry out this reaction. It is considered the primary component of the tumor microenvironment, together with the tumor itself, surrounding capillaries, fibroblasts, and extracellular matrix (Henke et al. 2020). Cancer and its surrounding microenvironment are inextricably linked and continually interact. Tumors can impact the microenvironment by releasing extracellular signals, boosting tumor angiogenesis, and establishing peripheral immunological tolerance, whereas immune cells in the microenvironment can influence malignant cell proliferation and development (Korneev et al. 2017, Ghoshdastider et al. 2021). Cancer immunosurveillance is the process by which immune cells continually monitor the tissue to detect and eradicate cancer or pre-cancer cells that exhibit or lose specific surface markers. This method involves several immune cells, including natural killer (NK) cells, macrophages, dendritic cells (DC), helper T cells, and cytotoxic T cells. Furthermore, the immune cells and tumor cells involved produce cytokines, chemicals that carry out intercellular communication in the immune system (Henke et al. 2020, Ghoshdastider et al. 2021).

Because they influence the evolution of chronic inflammatory disorders such as cancer, NK cells are critical components of the inflammatory response. It is an important part of tumor immunosurveillance (Tosello-Tramont et al. 2017, Parisi et al. 2017, Zhang et al. 2021). It is the CD8 T cell equivalent of

innate immunity, which means it may kill tumor cells in the absence of antigen-presenting cells (APCs) by acting directly as cytolytic effector lymphocytes. Resting NK cells are activated to attack cancer by a multi-step signaling mechanism that needs numerous ligations of molecules expressed on their surface. Multiple apoptosis-inducing pathways are triggered by the contacts, including the release of granules containing perforin and granzymes, stimulation of apoptosis via Fas-FasL or TRAIL-TRAIL ligand, and different cytokine and chemokine releases (Zhang et al. 2021, Fang et al. 2018). After activation, NK cells secrete cytokines such as interferon- γ (IFN- γ), tumor necrosis factor- α (TNF- α), granulocyte-macrophage colony-stimulating factor (GM-CSF), and chemokines such as CCL1, CCL2, CCL3, CCL4, CCL5, and CXCL8, which can modulate and activate adaptive immune response effector cells to eliminate cancer cells (Paul & Lal 2017, Marischen et al. 2018). TNF- α and IFN- γ , whose primary role is activating NK cells' lytic capabilities in response to aberrant type I IFNs and other inflammatory cytokines. When NK cells detect cancerous cells, they release cytotoxic granules containing perforin and granzyme, causing cancer cells to undergo apoptosis.

Tumor-infiltrating lymphocytes (TILs) have been identified as a biomarker of anti-tumor response in breast cancer. TIL subsets such as CD4⁺ or CD8⁺ T lymphocytes can identify tumor antigens and kill tumor cells. CD4⁺ helper T cells are primarily involved in tumor immunology and are functionally categorized into Th1, Th2, and Th17 cells based on secretory cytokines and immunologic activities (Zhao et al. 2019, Lee et al. 2019). Th1 helper cells boost macrophage and cytotoxic T-cell responses. The IL-12 generated by antigen-presenting cells in response to antigenic stimulation promotes the polarization of helper T cells into the Th1 subset, which activates the signal transducer and activator of the transcription 4 (STAT4) pathway. They primarily generate pro-inflammatory cytokines, including IL-1, IL-2, IL-12, TNF- α , and IFN- γ , which are linked to a better prognosis in cancer patients because they mediate the

anti-tumor action. Th1 cells' IFN- γ may attract and activate additional NK cells at the tumor site (Wculek et al. 2020, Powell et al. 2019). Another important component in anti-cancer inflammatory responses is regulatory T cells, a subpopulation of T cells identified by the expression of CD4, CD25, and FOXP3, expressing highly immunosuppressive activity against anti-tumor immune responses, explicitly downregulating induction, and proliferation of effector T cells. Because of these qualities, tumor cells secrete CXCL1, CCL2, and CCL20 to attract additional regulatory T cells to the tumor location. They then block the anti-tumor responses from cytotoxic cells by secreting immunomodulatory cytokines such as IL-10, IL-35, and TGF- β (Jean Baptiste et al. 2022, Togashi et al. 2019, Ohue & Nishikawa 2019).

This delicate balance of immune cells in TME has become an attractive area of research, as has the effect of giving bioactive components from diverse herbal and culinary plants. The majority of these studies advocate for a shift in the immune cell balance toward pro-inflammatory cells by promoting helper T cell polarization to the Th1 phenotype, recruiting and promoting the expansion of NK cells as well as their activities, as well as inhibiting T cell polarization to the Th2 phenotype and reducing the activity of regulatory T cells. As a result of the administration of numerous bioactive chemicals, the immune system has been altered by decreasing cancer-promoting factors. Those findings are supported by research on *Withania somnifera*, *Panax genus*, *Rhodiola rosea*, *Coriolus versicolor*, and *Lentinula edodes* (Venturella et al. 2021, Li et al. 2017, Jean Baptiste et al. 2022, Dubey et al. 2021). However, a study focused on Korean red ginseng suggests that it suppresses the Th1 responses by inhibiting Th1 polarization promoted by IL-12 produced by DC (Cho et al. 2019).

Cheral, a combination of *Zedoaria rhizome* (*Curcuma zedoaria* (Christm.) Roscoe) and chamberbitter (*Phyllanthus niruri* L.), is our major focus in this study. Indigenous societies frequently claim that they have anti-cancer effects. However, research on that combination and its impact on

immune cells during cancer is limited. Previous research on *C. zedoaria* and *Phyllanthus* extracts suggests that the extracts' bioactive compounds could remodel the immunosuppressive TME by decreasing Treg infiltration and differentiation and increasing NK cell activity, particularly cytotoxicity, inhibiting IL-2/IL-2R signal-dependent Treg cell differentiation, and preventing metastasis and EMT in the TGF-1-induced signaling pathway. However, the majority of their processes remain unknown (Hou & Fang 2021, Li et al. 2021, Oh et al. 2018, Subramaniam et al. 2019, Tendean & Riwanto 2021, Tjandrawinata et al. 2017). Meanwhile, research reveals that a bioactive ingredient in *Phyllanthus* suppresses B and T cell proliferation and the down-regulation of Th1 (IL-2 and IFN- γ) and Th2 (IL-4) cytokines and CD4⁺ and CD8⁺ cells (Nisar et al. 2018). Therefore, we studied cheral for its potential use as a curative agent for breast cancer using immunity parameters based on the relative quantity of NK cells, CD4TNF- α , CD4IFN- γ , and T-regs in the spleen of the mice model represents the immune response against cancer.

MATERIAL AND METHODS

Experimental design and sample preparation

Combined herbs extract of *C. zedoaria* and *P. niruri* which is called cheral was obtained from Makassar. Pathogen-free female mice were ordered from LPPM, Gadjah Mada University, Yogyakarta. About 24 female mice weighing approximately 20 grams and aged 7-8 weeks were used in this study. The experimental mice underwent an acclimatization procedure for a week. The cages were cleaned daily, and food and water were provided daily, *ad libitum* (Putra & Rifa'i 2020).

A completely randomized design was performed in this study. The treatment was divided into six groups with four replications. Except for the negative control, all of the mice were injected with DMBA (Tokyo Chemical Industry, Japan) for six weeks to induce breast cancer formation. The DMBA group as a positive control was left untreated after the cancer induction (Putra & Rifa'i 2019). The first treatment

group was treated with cisplatin (Dankos Farma-Kalbe Medika, Jakarta) 1 mg/kg BW by subcutaneous injection as a control treatment. The second, third, and fourth treatment group was treated orally with cheral with 1.233 mg/kg BW (CE1); 2.466 mg/kg BW (CE2); and 4.932 mg/kg BW dosage (CE3), respectively for 14 days. The Research Ethics Commission of Brawijaya University issued a declaration of ethical conduct for this study, with reference number 925-KEP-UB.

Immunostaining and flow cytometry analysis

This study's immunostaining and flow cytometry analysis were based on our previous protocols (Putra et al. 2016; Putra et al. 2015). After the mice were sacrificed, the isolated samples from the spleen were mixed with 50 μ l of extracellular antibody, such as anti-NK.1.1, anti-CD4, or anti-CD25 (BioLegend, USA) then incubated in the dark at room temperature for 20 minutes for extracellular antibody labeling. The solution was then incubated at room temperature for 20 minutes with 50 μ l of cytofix (BioLegend, USA). Afterward, 500 μ l of washperm (BioLegend, USA) was applied and incubated at room temperature for 20 minutes before centrifugation. The solution was centrifuged, and the separated pellet was treated with 50 μ l of intracellular antibodies such as anti-TNF- α or anti-IFN- γ (BioLegend, USA) for 20 minutes at room temperature. All solutions were then diluted with 300 μ l of BSA-supplemented PBS before being transferred to a cuvette for flow cytometry analysis (FACS CaliburTM). Further, an *in silico* study related to the evaluation of chemical interaction with specific proteins was performed through the STITCH (<http://stitch.embl.de/>) database (Putra et al. 2023, Putra et al. 2017).

Data and statistical analysis

The data on the relative numbers of NK cells, TH1 cells, and regulatory T cells were obtained via flow cytometry analysis and statistically analyzed using SPSS software version 22.0 for Windows. The gathered data will be evaluated using a normality test to see whether it is regularly distributed and a homogeneity test to see if it is homogenous. The data variance was

then determined using a one-way ANOVA followed by Tukey's Honestly Significant Difference test with a 95% confidence.

RESULTS and DISCUSSION

Immunosuppressive effect of cheral extract toward NK cells expression

According to the flow cytometry analysis, each treatment group's proportion of NK cells produced different outcomes (Figure 1A and 1C). The average relative number of NK cells in negative controls was 3.02%, lower than the DMBA treatment, with a mean relative number of NK cells as high as 3.86%. Furthermore, the cisplatin treatment group had an average relative number of NK cells of 4.07%, higher

than the positive control group. The increase in the relative number of NK cells is suggested due to the response of immunocompetent cells against cancer cells, which need a higher number of NK cells to eliminate the cancer cells. Conversely, cisplatin used in this treatment can suppress cancer-causing mutations by stopping DNA replication, specifically in the DNA adducts segments. Meanwhile, the cheral treatment groups showed continuously lower NK cells' relative number as the treatment dose increased. The CE1 group has an average of 3.16%, the CE2 group has an average of 3.03%, and the CE3 group has 2.48%. Among the cheral treatments, it did not result in a significant difference as the dose progressed. However, this cheral group's result is insignificant compared to negative control groups.

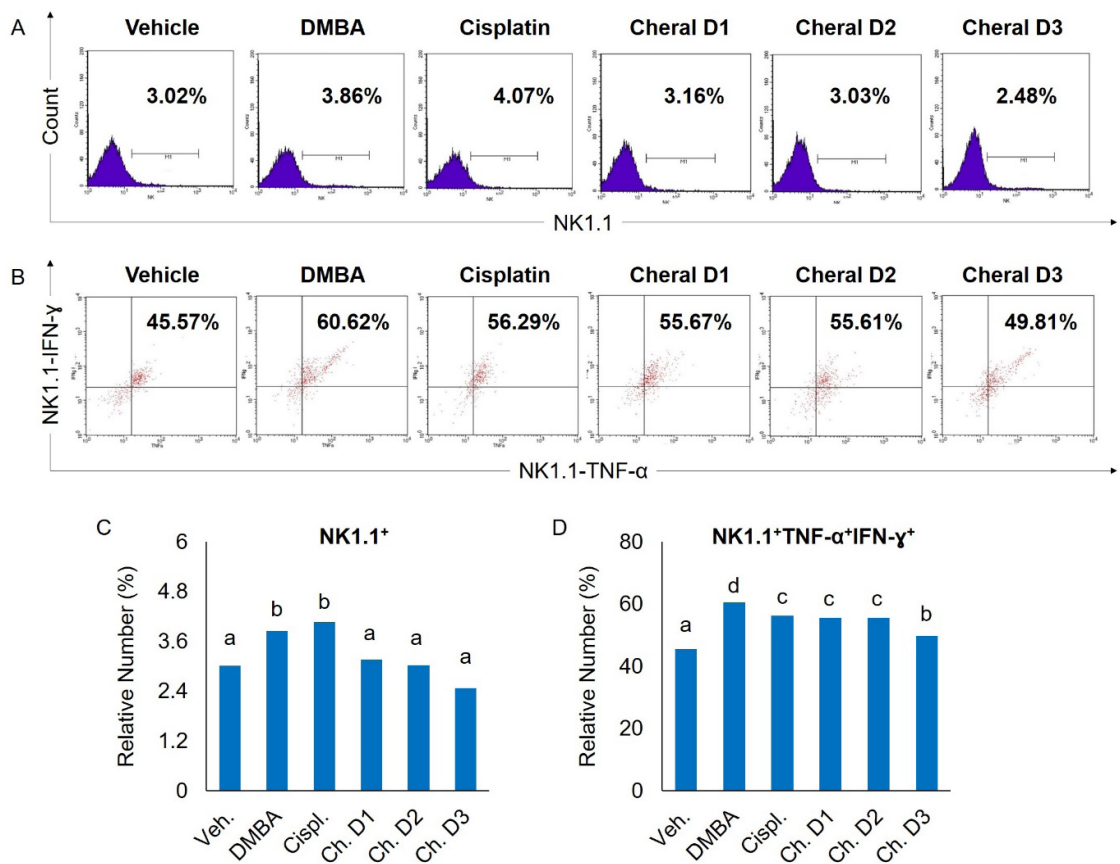


Figure 1. Immunomodulatory effects of cheral extract toward NK1.1⁺ natural killer cells (A and C) and NK1.1⁺TNF-α⁺IFN-γ⁺ natural killer cells (B and D) in DMBA-induced mice. The results were shown as the mean ± SD. Results were considered significant at p < 0.05. Different alphabetic symbols on the graph indicate a significant difference.

Cheral extract attenuates the relative number of NK Cells expressing TNF- α and IFN- γ

TNF- α and IFN- γ are the two major pro-inflammatory cytokines expressed by NK cells. The proportional levels of TNF- α and IFN- γ expressed by NK cells yielded varied results in each treatment group (Figure 1B and 1D). The increasing inflammatory response resulting from DMBA induction in the positive control group resulted in a rising relative number of activated pro-inflammatory cytokines, the TNF- α and IFN- γ , with an average of 60.62%, higher than the negative control, which has an average number of 45.57%. The average relative levels of TNF- α and IFN- γ in the cheral treatment group also decreased compared to the positive control group. Moreover, the CE1 group has an average relative amount of TNF- α and IFN- γ , around 55.67%, whereas the CE2 group has 55.61%. Those two groups had insignificantly different average numbers of TNF- α and IFN- γ compared to each other. Thus, we proposed that those two groups have similar treatment effects. The CE3 group had an average relative level of TNF- α and IFN- γ as low as 49.81%, significantly lower than the two lower dosages. Compared to other treatments, the CE3 group has a lower number of NK cells and their expression of TNF- α and IFN- γ .

Cheral extract constricts the relative number of CD4⁺TNF- α ⁺IFN- γ ⁺ type 1 helper T cells

The cisplatin and cheral treatment groups reduced

the relative number of CD4⁺ T cells expressing the pro-inflammatory cytokine TNF- α ⁺IFN- γ ⁺, also known as Th1, except for the CE1. According to the statistical results, the positive control group had a higher proportion of Th1 cells than the untreated group. There was no significant difference in the number of Th1 cells between the cherals and cisplatin treatment groups ($p>0.05$). The most significant decrease in the relative number of CD4⁺TNF- α ⁺IFN- γ ⁺ cells occurred in the CE2 and CE3 groups, which demonstrated close results to the negative control (Figure 2A and 2C).

Cheral extract reduces the relative number of CD4⁺CD25⁺ regulatory T-cell population

The results showed that the relative number of regulatory T cell populations in breast cancer model mice increased significantly ($p<0.05$) compared to the normal group (Figure 2B and 2D). The increase in the relative number of CD4⁺CD25⁺ T cells in the cancer model may be attributed to the inflammation in cancer patients. Subsequently, a large quantity of tumor antigens presented by MHC II on the surface of the APC cells, causing an increase in population and activation of CD4⁺CD25⁺ T cells, promoting the further proliferation of immunocompetent cells. Compared to the cancer group, cheral treatment group also showed a significantly lower relative number of regulatory T cell populations ($p<0.05$). The highest cheral dose treatment outperformed cisplatin or other cheral doses.

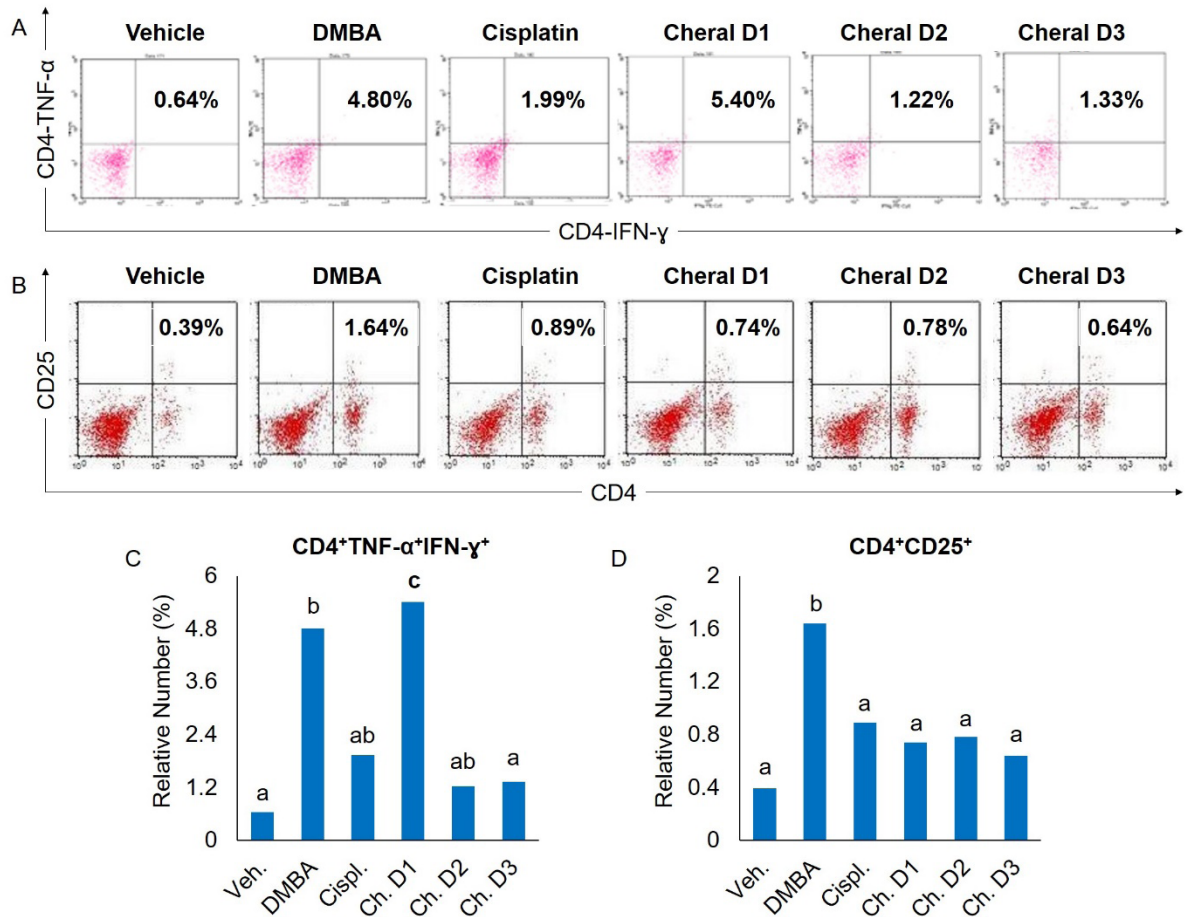


Figure 2. Immunomodulatory effects of cheral extract toward CD4⁺TNF- α ⁺IFN- γ ⁺ T cells (A and C) and CD4⁺CD25⁺ effector T cells (B and D) in DMBA-induced mice. The results were shown as the mean \pm SD. Results were considered significant at $p < 0.05$. Different alphabetic symbols on the graph indicate a significant difference.

The rise in the DMBA-induced group’s NK cell population might be due to the early phases of immunosurveillance mediated by NK cells (Buque et al., 2020). This happens because NK cells constantly monitor the tumor site and recognize growing malignant cells lacking certain self-antigens, such as MHC class I. Tumor cell activation of surface receptors such as CD16, NKG2D, NKp46, DNAM-1, 2B4, NTB-A, and CRACC is also followed by the recognition of missing MHC class I, which triggers the cytotoxic mechanism as well as cytokine production. TNF- α , IFN- γ , and IL-2 generated by CD4⁺ cells, particularly Th1, attract more NK cells

and encourage limited proliferation, increasing their population size as the immune system tries to limit tumor progression (Liu et al. 2021, Meza Guzman et al. 2020). The interaction between the carcinogenic DMBA and cytochrome P-450, on the other hand, promotes DNA adduction and activates a detoxifying process, boosting ROS generation since it transforms DMBA into DMBA-3,4-diol, indicating the existence of free radicals (Mazambani et al. 2019) individual differences in the susceptibility to xenobiotic-induced breast cancer remain unclear. Since epigenetic modifications could control the expression of metabolic enzymes, our goal was to determine whether

epigenome modulated metabolic networks determine susceptibility to xenobiotic-induced breast cancer. The effect of epigenetic background on predisposition to carcinogen 7,12-dimethylbenz(a. Because NK cells are extremely vulnerable to ROS, an increased

concentration of ROS in the TME might result in cell dysfunction as well as triggering apoptosis, favoring an immunological escape mechanism (Kotsafti et al. 2020, Wang et al. 2021).

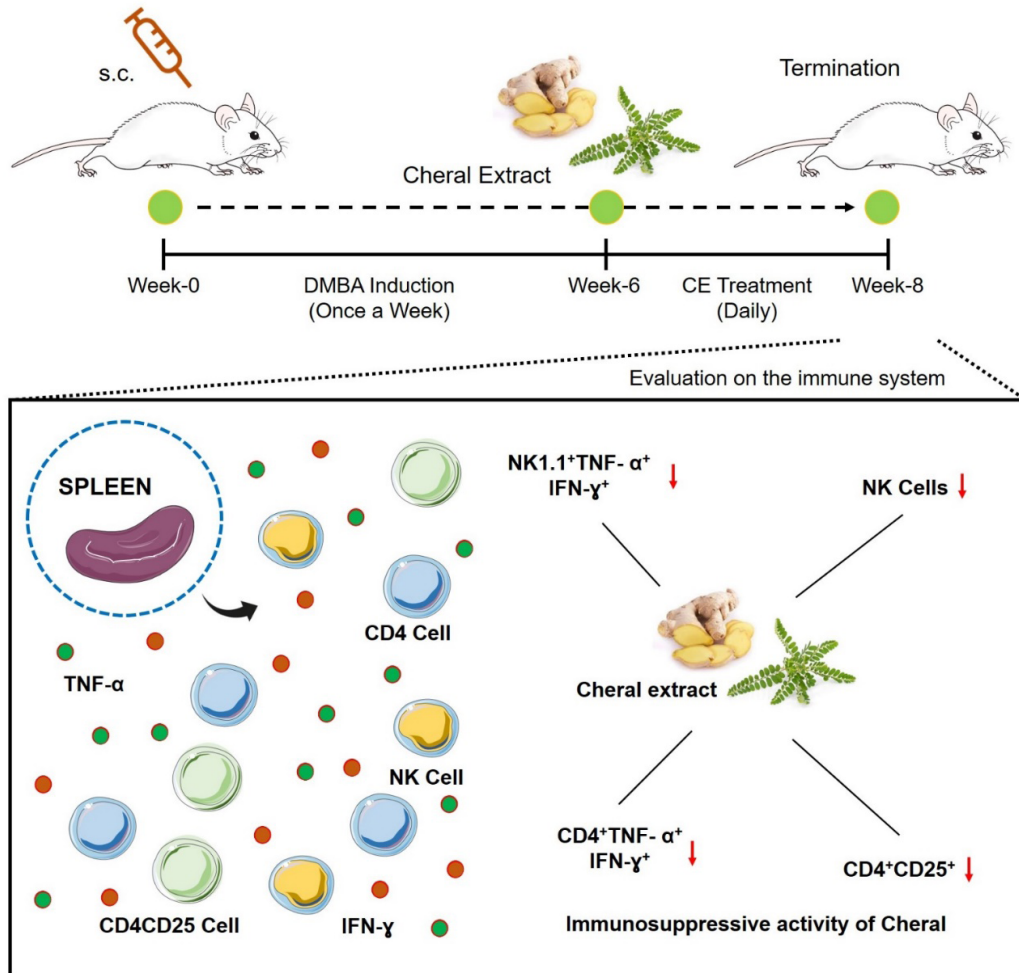


Figure 3. The immunomodulatory role of cheral extract in DMBA-induced breast cancer mouse model

According to certain research, providing bioactive substances may boost the cytotoxic activity of NK cells against tumor cells. Most studies, however, imply that administering bioactive compounds tends to increase the number of NK cells because the bioactive compounds encourage hematopoietic stem cells that develop into NK cells to mature quicker while promoting NK cell proliferation (Huijskens et al. 2015). The findings might imply that administering cheral, which includes many

antioxidants, could reduce oxidative stress generated mainly by ROS, hence improving conditions in the tumor microenvironment (Figure 3). Meanwhile, lower ROS content in the tumor microenvironment may improve NK cells' cytotoxicity and ability to eliminate cancerous cells because the nature of NK cells is susceptible to oxidative stress, particularly in the tumor microenvironment, resulting in a lower number of NK cells required to eliminate cancerous cells effectively (Whiteside 2020, Wang et al. 2021).

The significant rise in both cytokines appears to be unrelated to the number of NK cells. Even though we cannot identify the subset of NK cells from the mice, based on the results obtained, the increase of both cytokines in DMBA-induced mice is likely due to the more dominant subset of NK cells being cytokine-producing NK cells rather than cytotoxic NK cells, which are thought to have lower cytotoxicity but actively express TNF- α and IFN- γ . Furthermore, the NK cell subgroup appears to have not yet reached the fatigued phase. TNF- α continues to cause cancer cell death by activating caspase 8. At the same time, IFN- γ urges DCs to trigger robust CTL responses and further sensitize the cancer cells to NK cytotoxicity by cytotoxic NK cells (Zheng et al. 2019, Wang et al. 2012). In the cisplatin treatment group, the average relative quantity of TNF- α and IFN- γ was lower than the positive control group, at 56.29%. We cannot pinpoint the cause of the decrease. However, it is believed to relate to cisplatin's antineoplastic properties, which interferes with DNA repair mechanisms, primarily in the adducted segment, causing DNA damage and subsequently lowering the number of cancer cells via apoptosis the immune responses by the NK cells (Ghosh 2019).

Typically, the lower number of NK cells and their expression of TNF- α and IFN- γ indicate higher tumor incidence and further tumor progression because it reflects that the NK's function has been impaired. These results contradict other research, favoring a higher number of NK cells and their pro-inflammatory cytokine expression (Tjandrawinata et al. 2017, Hou & Fang 2021, Lee & Cho 2018, Sabry et al. 2019). However, another study stated that curcumin, a dominant bioactive compound in *C. zedoaria*, inhibits the IFN- γ synthesis in NK cells by blocking STAT1 signaling in human pancreatic cancer cells and upregulating the STAT4 and STAT5, which promotes cytotoxicity of the NK cells (Lee & Cho 2018, Fiala 2015, Grudzien & Rapak 2018). The research focuses on an ethanol extract of *Phyllanthus* and found that it significantly reduced the release of IFN- γ , TNF- α ,

IL-1, IL-2, and IL-6. It is claimed that corilagin in the extract significantly inhibited the production of pro-inflammatory cytokines and mediators such as TNF- α , IL-1, IL-6, NO (iNOS), and COX-2 at the protein and gene levels via NF- κ B pathway inhibition. However, this mechanism occurred in cultured cancer cells rather than NK cells (Yuandani et al. 2013, Jantan et al. 2019). It is suggested that the administration of cheral could lower the synthesis of both inflammatory cytokines while enhancing the cytotoxicity of the NK cells, which means shifting the population of NK cells towards the cytotoxic NK cells rather than its cytokines-producing counterparts and directly killing the cancer cells.

The higher number of Th1 in the cancer group is driven by a higher concentration of T-cell stimulating factors, particularly the IL-12 secreted by APCs such as DC. The DCs acquire process and present tumor-associated antigens (TAAs) on MHC molecules in the TME and provide co-stimulation and soluble factors to shape T cell responses. These soluble factors, including IL-12 and IFN- γ , promote T helper polarization towards the Th1 phenotype and increase its relative number (Wculek et al. 2020). The high relative number of Th1 could induce a high degree of anti-tumor responses mediated by the release of pro-inflammatory cytokines and higher recruitment of NK cells to the TME, as mentioned in the previous chapter. Meanwhile, a high concentration of TNF- α in the tumor microenvironment triggers a signaling cascade that activates NF- κ B, initiating the expression of anti-apoptotic genes such as TRAF1 and TRAF2 that could promote tumor survival (Tang et al. 2017). Excessive pro-inflammatory cytokines can promote tumor growth through angiogenesis and cell migration (Esquivel-Velázquez et al. 2015).

The exact reason why the cisplatin treatment group exhibits a significantly lower number of Th1 cells remains unclear. A study suggests that cisplatin downregulates the expression of PD-L2 in DC cells, subsequently enhancing cytokine

synthesis that promotes Th1 polarization, as well as dephosphorylation of STAT6 required for Th2 polarization (Galluzzi et al. 2015, Boustani et al. 2021) accumulating evidence indicates that the efficacy of conventional and targeted anticancer agents does not only involve direct cytostatic/cytotoxic effects, but also relies on the (re, which seems contrary to our results. However, another study suggests that cisplatin induces IL-10 synthesis by activating DC's p38 MAPK and NF- κ B signaling pathways, promoting Th2 cell polarization and inducing DC to adopt a tolerogenic phenotype. Balance shifting towards Th2 promotion hinders the Th1 cell proliferation and polarization (Kim et al. 2016). Because of cisplatin's initial deployment as a cytotoxic drug directly targeting the cancer cell is thought to induce cell death by forming crosslinks in DNA in fast-proliferating cells and initiating apoptosis (Raudenska et al. 2019). It also kills the cancer cell by increasing the expression of the Fas receptor, which recruits a variety of proapoptotic proteins, including caspase-8, to create the death-inducing signaling complex upon stimulation by FasL (Peter et al. 2015, Raudenska et al. 2019). These effects by cisplatin could lower the number of cancer cells, which also reduces the response of DC to promote helper T cell polarization towards the Th1 phenotype trying to eliminate the cancer cells.

The information about the effects of administering *C. zedoaria*, *P. niruri*, or a combination of both towards the population and activity of Th1 cells could possess a similar effect as cisplatin, acting as a cytotoxic agent against cancer cells. A study suggested that α -curcumene contained in *C. zedoaria* extract could activate the caspase-3 and caspase-9 pathways by releasing cytochrome c, inducing apoptosis (Shehna et al. 2022). Similarly, a study showed the alkaloid content of *Phyllanthus* plant called securinine and allosecurinine exerts anti-proliferation activity in several cancer cells. Further, the securinine induces apoptosis through cell cycle arrest activation in HeLa cells (Stefanowicz-Hajduk et al. 2016). Other studies also suggest that *C. zedoaria* and *Phyllanthus* extract

could induce apoptosis in cancer cell through down-regulation of Bcl-2, which act as an inhibitor of Bax and Bak, leading to cytochrome c-induced apoptosis (Lourembam et al. 2019). These mechanisms directly reduced the cancer cell count, simultaneously lowering the immune cell responses involved in TME, such as APCs, CTL, helper T cells, and NK cells. It could be predicted that a lower number of TAA recognized by the DCs could lead to the lower synthesis of the Th1 polarization agent, decreasing the number of Th1 cells in the TME (Wculek et al. 2020, Kim et al. 2016).

TNF- α is also released by macrophage-induced phagocytosis in human malignant mesothelioma. It can increase cell viability, reduce abscess-induced cytotoxicity, and may increase the assemblage of abscess-damaged mesothelium cells prone to malignant transformation. It also contributes to tumor initiation by increasing the production of genotoxic molecules, such as NO and ROS, which can cause DNA damage and mutations. Its expression has also been linked to an increased risk of other types of cancer, including bladder cancer, hepatocellular carcinoma, gastric cancer, and a poor prognosis in many hematological cancers. TNF- α promotes tumor progression rather than tumor initiation by promoting angiogenesis and metastasis and impairing immune surveillance by strongly suppressing many macrophage-activated cytotoxic T-cell activity responses (Cai et al. 2017, Kawanishi et al. 2017). TNF- α expression increases CXCL1/2 production by tumor cells via the NF- κ B activation cascade by releasing an inflammatory modulator protein that can activate the p70S6K protein and the ERK1/2 signaling pathway, providing an advantage for primary tumor cell survival and cell metastasis (Ni et al. 2021). The ILs, TNF- α , and IFN- γ regulate immune function, inflammatory response, and other physiological and pathological activities. These cytokines regulate cell survival, proliferation, and differentiation by signaling through the Jak/STAT and NF- κ B pathways. When ILs and IFN bind to their cognate receptors, Jak Kinase activates and phosphorylates the STAT

protein, allowing STAT dimerization and nuclear translocation. The NF- κ B proteins, including p50, p52, RelA/p65, and RelB, function as dimers and are typically inactively maintained by I κ B proteins. Extracellular stimuli, such as TNF- α secretion, cause I κ B degradation, releasing the NF- κ B complex. The active NF- κ B protein enters the nucleus and interacts with STAT, a transcription factor that regulates a wide range of target genes involved in this process. The TGF- β , with its numerous and critical functions in the immune system, is involved in many ILs, TNF- α , and IFN- γ signaling cascades by regulating the bioavailability and signal transduction of these cytokines. These factors, in turn, influence TGF- β activity in various ways (Esquivel-Velázquez et al. 2015). The TNF- α binds to two receptors, TNFR1

and TNFR2, to initiate a signaling cascade that results in transcriptional regulation of mediators important in tumor cell survival, invasion, angiogenesis, and impaired immune system surveillance. However, the primary receptor mediator of TNF- α in tumor promotion is TNFR1 (Tang et al. 2017). On the other hand, the cheral treatment group reduced the relative number of macrophage cells that secrete both pro-inflammatory cytokines because it contains polyphenol and flavonoid antioxidants, reducing free radical concentration and activity of anti-inflammation and anti-malignancy properties. These bioproperties are not cytotoxic to normal cells, while the anti-cancer effects are limited to tumor cells.

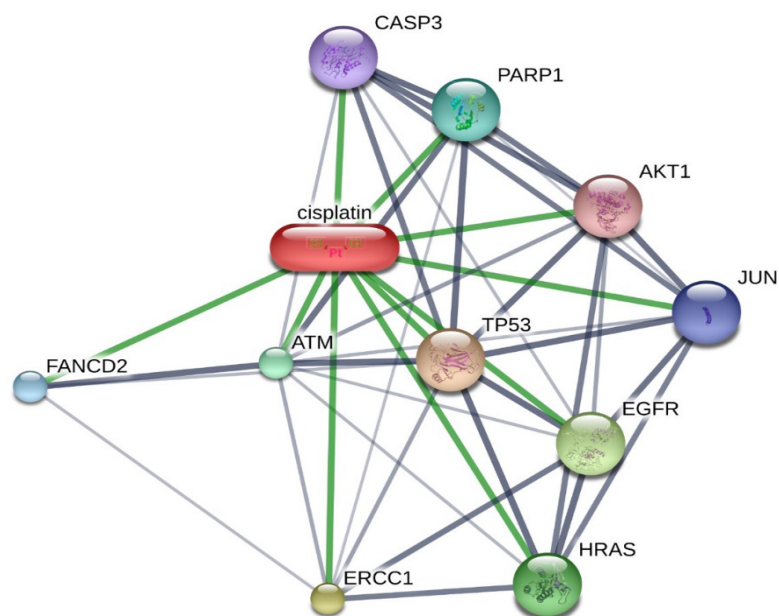


Figure 4. Cisplatin-proteins interaction network analysis. Several proteins showed in the network analysis have responsibility for cancer development and progression.

The CD4⁺CD25⁺ T cell population can modulate the immune system's response to infection, autoimmunity, inflammation, and malignancies. This regulatory T cell typically helps the immune system maintain homeostasis (Okeke & Uzonna 2019). Cancer cells will exploit the Treg population, which

has immunosuppressive properties by inhibiting the activity of dendritic, CTL, and NK cells, resulting in continuous immunological invasion and hastening the development of breast cancer (Jean Baptiste et al. 2022, Togashi et al. 2019, Ohue & Nishikawa 2019). Another study discovered that the cancer mouse

model had more regulatory T lymphocytes in the spleen and lymph nodes than normal mice, which is commonly associated with poor prognosis (Riaz et al. 2017). This phenomenon is expected in the escape phase because tumor cells secrete chemokines such as CXCL1, CCL2, CCL5, CCR6, and CCL20 to recruit more Treg cells into the TME while also promoting Treg cell proliferation (Togashi et al. 2019, Ozga et al. 2021, O'Donnell et al. 2019). Recirculating Treg cells express a high number of IL2R (CD25), which is highly important for its development because it

would actively bind to IL-2, hence inhibiting the immunological response to malignant cells or the environment by lowering the production of cytokines, which also play a role in tumor growth suppression (Chinen et al. 2016). Increased CD25 expression in the CD4⁺ T cell population is primarily due to increased ROS synthesis in the TEM by cancer cells and TAMs during oxidative stress, dampening the immunological response to the cancer cells (Chen, Han, et al. 2015).

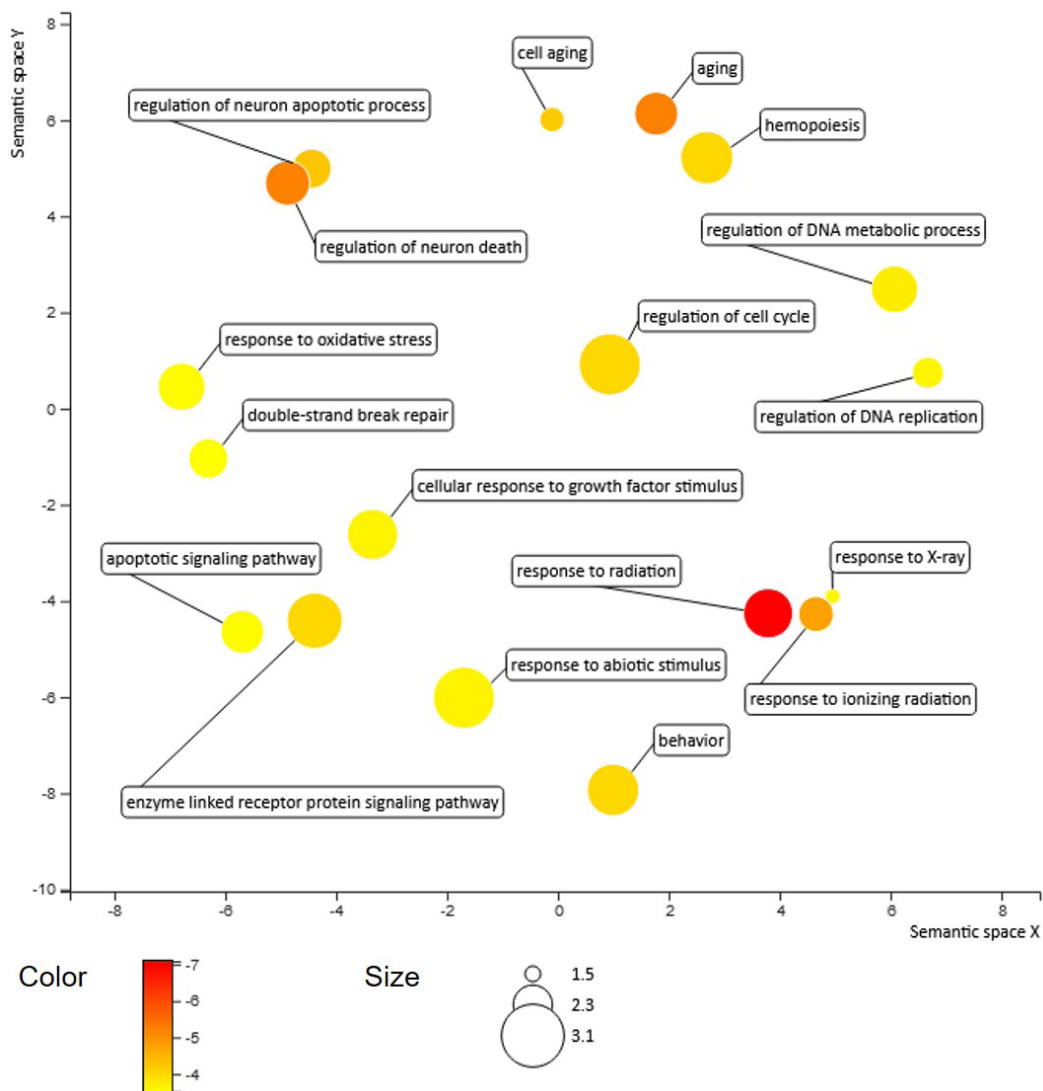


Figure 5. Map visualization of Cisplatin's biological response in the body. The map showed multiple biological processes were affected by Cisplatin.

Cisplatin groups show a lower number of Treg cells in the spleen compared to the DMBA-induced group. Although the exact molecular mechanism is unclear, it is suggested that a lower number of Treg cells in this group is correlated to cisplatin's lymphopenic characteristic which has a direct negative impact on actively proliferating cells, including the Treg cells (Heeren et al. 2019). The fact that the number of Treg cells remains higher than the negative control suggests that the surviving cancer may be feeding the mechanism driving the elevated Treg levels (Chen, et al. 2015).

Cisplatin is an organometallic platinum complex with two chlorine and amine atoms next to one another (Brown et al. 2019). Commonly, patients who have been diagnosed with lymphomas, breast, testicular, ovarian, head and neck, cervical, and sarcomas are still given cisplatin and other platinum-based drugs such as oxaliplatin and carboplatin as first-line medication (Mortensen et al. 2020). Cisplatin has been shown to affect many oncogenes involved in cancer development and remission directly (Figure 4). In addition, various biological processes, including the apoptotic signaling pathway, double-strand break repair, and oxidative stress response, are involved in the impact of cisplatin (Figure 5).

Generally, cisplatin's cytotoxic mechanism is triggered by its interaction with DNA to produce adducts, which induces apoptosis or programmed cell death (Siddik 2003). After entering the cell, cisplatin exerts its lethal effect by losing one chloride ligand, binding to DNA to generate intra-strand DNA adducts, and limiting DNA synthesis and cell growth. DNA lesions resulting from cisplatin-induced DNA damage stimulate DNA repair via NER (nuclear excision repair system) by inhibiting cisplatin-induced cell death via the ATM (ataxia telangiectasia mutated) pathway. Since cisplatin-induced DNA damage activates many signal transduction pathways that can facilitate or inhibit apoptosis, investigations have demonstrated that gene p53 is also related to

DNA damage and repair (De Laurenzi & Melino 2000, Lin & Howell 2006).

These similar outcomes suggested an effect of curcumin that reduced the relative amount of regulatory T cells and its activity by down-regulating CTLA-4, a protein on their cell surface, and interacting with CD80 molecules, causing signal transduction from Treg cells, and FOXP3 which important for T cells differentiation (Paul & Sa 2021, Bose et al. 2015). A study also suggests that curcumin could transform Treg cells into Th1 cells through downregulating FOXP3 and upregulating IFN- γ synthesis (Shafabakhsh et al. 2019). Curcumin could also inhibit the nuclear translocation of p65 and cRel in the regulatory T cells population (Burge et al. 2019). The chamber bitter contains phytochemicals such as Phyllantin and flavonoids, which have the potential to modify and activate the immune system. Previous research has demonstrated that flavonoids can lower the expression of CD25 and IL-2 molecules, scavenging free radicals, lowering ROS levels, and inhibiting NF- κ B activation, resulting in reduced pro-inflammatory cytokines such as IL-1 β , IL-2, IL-6, and TNF- α (Leyva-López et al. 2016).

CONCLUSION

In this present study, we demonstrated that cheral extract exerts immunosuppressive activity by attenuating the properties of the immune system, such as NK cells, Th1 cells, and regulatory T cells in DMBA-inducing mice into normal levels. Further research needs to be carried out, especially to determine the broader effects on the immune system and the specific mechanism of action from cheral extract in treating cancer.

ACKNOWLEDGMENTS

We thank Brawijaya University Malang for providing this study's research instruments and funding (M.R.).

CONFLICT OF INTEREST

The authors declare that there is no conflict of interest.

AUTHOR CONTRIBUTION STATEMENT

Concept and Design (M.R.); Supervision (M.R.); Funding Acquisition (M.R.); Materials (W.E.P., A.M.L.S.M., D.R., D.C., A.H.); Data Collection and Processing (W.E.P., A.M.L.S.M., D.R., D.C.); Analysis and Interpretation (W.E.P., A.H., M.R.); In Silico Study (W.E.P., A.H.); Writing Manuscript (W.E.P., A.H., M.R.); Review and Editing (W.E.P., A.M.L.S.M., D.R., D.C., A.H., M.R.).

REFERENCES

- Bose S, Panda A, Mukherjee S & Sa G. (2015). Curcumin and tumor immune-editing: resurrecting the immune system. *Cell Division* 10: 1–13.
- Boustani J, Joseph Elm, Martin E, Benhmida S, Lecoester B, Tochet F, Mirjolet C, Chevalier C, Thibouw D, Vulquin N, Servagi S, Sun X & Adotévi O. (2021). Cisplatin-based chemoradiation decreases telomerase-specific CD4 TH1 response but increases immune suppressive cells in peripheral blood. *BMC Immunology* 22: 1–9.
- Britt Kl, Cuzick J & Phillips K-A. (2020). Key steps for effective breast cancer prevention. *Nature Reviews Cancer* 20: 417–436.
- Brown A, Kumar S & Tchounwou P. (2019). Cisplatin-based chemotherapy of human cancers. *Journal of Cancer Sciences and Therapy* 11: 1–15.
- Buque A, Bloy N, Petroni G, Kroemer G & Galluzzi L. (2020). NK cells beat T cells at early breast cancer control. *Oncoimmunology* 9: 1–3.
- Burge K, Gunasekaran A, Eckert J & Chaaban H. (2019). Curcumin and intestinal inflammatory diseases: Molecular mechanisms of protection. *International Journal of Molecular Sciences* 20: 1–36.
- Cai X, Cao C, Li J, Chen F, Zhang S, Liu B, Zhang W, Zhang X & Ye L. (2017). Inflammatory factor TNF- α promotes the growth of breast cancer via the positive feedback loop of TNFR1/NF- κ B (and/or p38)/p-STAT3/HBXIP/TNFR1. *Oncotarget* 8: 58338–58352.
- Chen C, Chen Z, Chen D, Zhang B, Wang Z & Le H. (2015). Suppressive effects of gemcitabine plus cisplatin chemotherapy on regulatory T cells in nonsmall-cell lung cancer. *Journal of International Medical Research* 43: 180–187.
- Chen Y, Han F, Cao L-H, Li C, Wang J-W, Li Q, Zheng W, Guo Z-X, Li A-H & Zhou J-H. (2015). Dose-response relationship in cisplatin-treated breast cancer xenografts monitored with dynamic contrast-enhanced ultrasound. *BMC Cancer* 15: 1–9.
- Chinen T, Kannan A, Levine A, Fan X, Klein U, Zheng Y, Gasteiger G, Feng Y, Fontenot J & Rudensky A. (2016). An essential role for IL-2 receptor in regulatory T cell function. *Nature Immunology* 17: 1322–1333.
- Cho M, Choi G, Shim I & Chung Y. (2019). Enhanced Rg3 negatively regulates Th1 cell responses. *Journal of Ginseng Research* 43: 49–57.
- De Laurenzi V & Melino G. (2000). Evolution of Functions within the p53/p63/p73 Family. *Annals of the New York Academy of Sciences* 926: 90–100.

- Dubey S, Singh M, Nelson A & Karan D. (2021). A perspective on *Withania somnifera* modulating antitumor immunity in targeting prostate cancer. *Journal of Immunology Research* 2021: 1–11.
- Esquivel-Velázquez M, Ostoa-Saloma P, Palacios-Arreola Mi, Nava-Castro K, Castro Ji & Morales-Montor J. (2015). The role of cytokines in breast cancer development and progression. *Journal of Interferon & Cytokine Research* 35: 1–16.
- Fang F, Xiao W & Tian Z. (2018). Challenges of NK cell-based immunotherapy in the new era. *Frontiers in Medicine* 12: 440–450.
- Fiala M. (2015). Curcumin and omega-3 fatty acids enhance NK cell-induced apoptosis of pancreatic cancer cells but curcumin inhibits interferon- γ production: Benefits of omega-3 with curcumin against cancer. *Molecules* 20: 3020–3026.
- Galluzzi L, Buqué A, Kepp O, Zitvogel L & Kroemer G. (2015). Immunological effects of conventional chemotherapy and targeted anticancer agents. *Cancer Cell* 28: 690–714.
- Ghosh S. (2019). Cisplatin: The first metal based anticancer drug. *Bioorganic Chemistry* 88: 1–20.
- Ghoshdastider U, Rohatgi N, Mojtavavi Naeini M, Baruah P, Revkov E, Guo YA, Rizzetto S, Wong AML, Solai S, Nguyen TT, Yeong JPS, Iqbal J, Tan Ph, Chowbay B, Dasgupta R & Skanderup AJ. (2021). Pan-cancer analysis of ligand–receptor cross-talk in the tumor microenvironment. *Cancer Research* 81: 1802–1812.
- Ginsburg O. (2020). Breast cancer early detection: A phased approach to implementation. *Cancer* 126: 2379–2393.
- Grudzien M & Rapak A. (2018). Effect of natural compounds on NK cell activation. *Journal of Immunology Research* 2018: 1–12.
- Heeren A, Van Luijk I, Lakeman J, Pocorni N, Kole J, De Menezes Rx, Kenter G, Bosse T, De Kroon C & Jordanova E. (2019). Neoadjuvant cisplatin and paclitaxel modulate tumor-infiltrating T cells in patients with cervical cancer. *Cancer Immunology, Immunotherapy* 68: 1759–1767.
- Henke E, Nandigama R & Ergün S. (2020). Extracellular matrix in the tumor microenvironment and its impact on cancer therapy. *Frontiers in Molecular Biosciences* 6: 1–24.
- Hou Z & Fang G. (2021). Research progress of anti-tumor effects of *Curcuma zedoaria* and its active ingredients through immune regulation mechanism. *Journal of Clinical and Nursing Research* 5: 1–7.
- Huijskens M, Walczak M, Sarkar S, Atrafi F, Senden-Gijsbers B, Tilanus M, Bos G, Wieten L & Germeraad W. (2015). Ascorbic acid promotes proliferation of natural killer cell populations in culture systems applicable for natural killer cell therapy. *Cytotherapy* 17: 613–620.
- Jantan I, Haque M, Ilangkovan M & Arshad L. (2019). An insight into the modulatory effects and mechanisms of action of *Phyllanthus* species and their bioactive metabolites on the immune system. *Frontiers in Pharmacology* 10: 1–19.
- Jean Baptiste S, Le T, Le T, Vu D & Nguyen D. (2022). Anti-cancer immune-modulatory activities of *Panax* genus extracts and bioactive compounds. *Food Reviews International* 38: 1461–1484.

- Kawanishi S, Ohnishi S, Ma N, Hiraku Y & Murata M. (2017). Crosstalk between DNA damage and inflammation in the multiple steps of carcinogenesis. *International Journal of Molecular Sciences* 18: 1–13.
- Kim W, Kim H, Kwon K, Im S-H, Lee B, Ha S-J & Shin S. (2016). Cisplatin induces tolerogenic dendritic cells in response to TLR agonists via the abundant production of IL-10, thereby promoting Th2- and Tr1-biased T-cell immunity. *Oncotarget* 7: 33765–33782.
- Korneev K, Atretkhany K-S, Drutskaya M, Grivennikov S, Kuprash D & Nedospasov S. (2017). TLR-signaling and proinflammatory cytokines as drivers of tumorigenesis. *Cytokine* 89: 127–135.
- Kotsafti A, Scarpa M, Castagliuolo I & Scarpa M. (2020). Reactive oxygen species and antitumor immunity—from surveillance to evasion. *Cancers (Basel)* 12: 1–16.
- Lee H & Cho H. (2018). Improved anti-cancer effect of curcumin on breast cancer cells by increasing the activity of natural killer cells. *Journal of Microbiology and Biotechnology* 28: 874–882.
- Lee H, Jang J, Lee S, Yoo S, Kwon J, Nam S, Bae S, Choi J, Han N & Yoon S. (2019). Inflammatory cytokines and change of Th1/Th2 balance as prognostic indicators for hepatocellular carcinoma in patients treated with transarterial chemoembolization. *Scientific Reports* 9: 1–8.
- Lei S, Zheng R, Zhang S, Wang S, Chen R, Sun K, Zeng H, Zhou J & Wei W. (2021). Global patterns of breast cancer incidence and mortality: A population-based cancer registry data analysis from 2000 to 2020. *Cancer Communications* 41: 1183–1194.
- Leyva-López N, Gutierrez-Grijalva E, Ambriz-Perez D & Heredia J. (2016). Flavonoids as cytokine modulators: A possible therapy for inflammation-related diseases. *International Journal of Molecular Sciences* 17: 1–15.
- Li J, Wang S, Wang N, Zheng Y, Yang B, Wang X, Zhang J, Pan B & Wang Z. (2021). Aiduqing formula inhibits breast cancer metastasis by suppressing TAM/CXCL1-induced Treg differentiation and infiltration. *Cell Communication and Signaling* 19: 1–20.
- Li Y, Pham V, Bui M, Song L, Wu C, Walia A, Uchio E, Smith-Liu F & Zi X. (2017). *Rhodiola rosea* L.: An herb with anti-stress, anti-aging, and immunostimulating properties for cancer chemoprevention. *Current Pharmacology Reports* 3: 384–395.
- Lin X & Howell S. (2006). DNA mismatch repair and p53 function are major determinants of the rate of development of cisplatin resistance. *Molecular Cancer Therapeutics* 5: 1239–1247.
- Liu S, Galat V, Galat4 Y, Lee Y, Wainwright D & Wu J. (2021). NK cell-based cancer immunotherapy: From basic biology to clinical development. *Journal of Hematology & Oncology* 14: 1–17.
- Lourembam R, Yadav A, Kundu G & Mazumder P. (2019). *Curcuma zedoaria* (christm.) roscoe inhibits proliferation of MDA-MB231 cells via caspase-cascade apoptosis. *Oriental Pharmacy and Experimental Medicine* 19: 235–241.
- Magnuson A, Kiner E, Ergun A, Park J, Asinovski N, Ortiz-Lopez A, Kilcoyne A, Paoluzzi-Tomada E, Weissleder R, Mathis D & Benoist C. (2018). Identification and validation of a tumor-infiltrating Treg transcriptional signature conserved across species and tumor types. *Proceedings of the National Academy of Sciences* 115: 10672–10681.

- Marischen L, Englert A, Schmitt A-L, Einsele H & Loeffler J. (2018). Human NK cells adapt their immune response towards increasing multiplicities of infection of *Aspergillus fumigatus*. *BMC Immunology* 19: 39–51.
- Mazambani S, Morris M & Cheriya V. (2019). Epigenome modulated xenobiotic detoxification pathways control DMBA-induced breast cancer in agouti *Avy/a* mice. *Epigenetics* 14: 708–720.
- Meza Guzman L, Keating N & Nicholson S. (2020). Natural killer cells: Tumor surveillance and signaling. *Cancers (Basel)* 12: 1–33.
- Mortensen A, Mohajershojai T, Hariri M, Pettersson M & Spiegelberg D. (2020). Overcoming limitations of Cisplatin therapy by additional treatment with the HSP90 inhibitor Onalespib. *Frontiers in Cell and Developmental Biology* 10: 1–15.
- Ni Y, Zhou X, Yang J, Shi H, Li H, Zhao X & Ma X. (2021). The role of tumor-stroma interactions in drug resistance within tumor microenvironment. *Frontiers in Cell and Developmental Biology* 9: 1–29.
- Nisar M, He J, Ahmed A, Yang Y, Li M & Wan C. (2018). Chemical components and biological activities of the genus *Phyllanthus*: A review of the recent literature. *Molecules* 23: 1–25.
- O'donnell J, Teng M & Smyth M. (2019). Cancer immunoediting and resistance to T cell-based immunotherapy. *Nature Reviews Clinical Oncology* 16: 151–167.
- Oh J-G, Hwang D-J & Heo T-H. (2018). Direct regulation of IL-2 by curcumin. *Biochemical and Biophysical Research Communications* 495: 300–305.
- Ohue Y & Nishikawa H. (2019). Regulatory T (Treg) cells in cancer: Can Treg cells be a new therapeutic target? *Cancer Science* 110: 2080–2089.
- Okeke E & Uzonna J. (2019). The pivotal role of regulatory T cells in the regulation of innate immune cells. *Frontiers in Immunology* 10: 1–12.
- Ozga A, Chow M & Luster A. (2021). Chemokines and the immune response to cancer. *Immunity* 54: 859–874.
- Parisi L, Bassani B, Tremolati M, Gini E, Farronato G & Bruno A. (2017). Natural killer cells in the orchestration of chronic inflammatory diseases. *Journal of Immunology Research* 2017: 1–13.
- Paul S & Lal G. (2017). The molecular mechanism of natural killer cells function and its importance in cancer immunotherapy. *Frontiers in Immunology* 8: 1–8.
- Paul S & Sa G. (2021). Curcumin as an adjuvant to cancer immunotherapy. *Frontiers in Oncology* 11.
- Peter M, Hadji A, Murmann A, Brockway S, Putzbach W, Pattanayak A & Ceppi P. (2015). The role of CD95 and CD95 ligand in cancer. *Cell Death & Differentiation* 22: 549–559.
- Powell M, Read K, Sreekumar B, Jones D & Oestreich K. (2019). IL-12 signaling drives the differentiation and function of a TH1-derived TFH1-like cell population. *Scientific Reports* 9: 13991.
- Putra WE, & Rifa'i M. (2019). Immunomodulatory activities of *Sambucus javanica* extracts in DMBA exposed BALB/c mouse. *Advanced Pharmaceutical Bulletin* 9: 619–623.

- Putra WE, & Rifa'i M. (2020). Assessing the immunomodulatory activity of ethanol extract of *Sambucus javanica* berries and leaves in chloramphenicol-induced aplastic anemia mouse model. *Tropical Life Science Research* 31: 175–185.
- Putra WE, Agusinta AK, Ashar MSAA, Manullang VA, & Rifa'i M. (2023). Immunomodulatory and ameliorative effect of *Citrus limon* extract on DMBA-induced breast cancer in mouse. *Karbala International Journal of Modern Science* 9: 1-14.
- Putra WE, Soewondo A, & Rifa'i M. (2016). Effect of dexamethasone administration toward hematopoietic stem cells and blood progenitor cells expression on BALB/c mice. *Journal of Pure and Applied Chemistry Research* 4: 100-108.
- Putra WE, Soewondo A, & Rifa'i M. (2015). Expression of erythroid progenitor cells and erythrocytes on dexamethasone induced-mice. *Biotropika* 3: 42-45.
- Putra WE, Waffareta E, Ardiana O, Januarisasi ID, Soewondo A, & Rifa'i M. (2017). Dexamethasone-administrated BALB/c mouse promotes proinflammatory cytokine expression and reduces CD4⁺CD25⁺ regulatory T cells population. *Bioscience Research* 14: 201-213.
- Raudenska M, Balvan J, Fojtu M, Gumulec J & Masarik M. (2019). Unexpected therapeutic effects of cisplatin. *Metallomics* 11: 1182–1199.
- Riaz N. (2017). Tumor and microenvironment evolution during immunotherapy with Nivolumab. *Cell* 171: 934–949.
- Rock Cl. (2020). American Cancer Society guideline for diet and physical activity for cancer prevention. *CA: A Cancer Journal for Clinicians* 70: 245–271.
- Sabry M, Zubiak A, Hood S, Simmonds P, Arellano-Ballester H, Cournoyer E, Mashar M, Pockley A & Lowdell M. (2019). Tumor- and cytokine-primed human natural killer cells exhibit distinct phenotypic and transcriptional signatures. *PLoS One* 14: 1–20.
- Shafabakhsh R, Pourhanifeh Mh, Mirzaei H, Sahebkar A, Asemi Z & Mirzaei H. (2019). Targeting regulatory T cells by curcumin: A potential for cancer immunotherapy. *Pharmacological Research* 147: 1–12.
- Shehna S, Sreelekshmi S, Remani P, Padmaja G & Lakshmi S. (2022). Anti-cancer, anti-bacterial and anti-oxidant properties of an active fraction isolated from *Curcuma zedoaria* rhizomes. *Phytomedicine Plus* 2: 1–11.
- Siddik Z. (2003). Cisplatin: mode of cytotoxic action and molecular basis of resistance. *Oncogene* 22: 7265–7279.
- Siegel R, Miller K, Fuchs H & Jemal A. (2021). Cancer statistics, 2021. *CA: A Cancer Journal for Clinicians* 71: 7–33.
- Siegel R, Miller K, Fuchs H & Jemal A. (2022). Cancer statistics, 2022. *CA: A Cancer Journal for Clinicians* 72: 7–33.
- Stefanowicz-Hajduk J, Sparzak-Stefanowska B, Krauze-Baranowska M, & Ochocka JR. (2016). Securinine from *Phyllanthus glaucus* Induces cell cycle arrest and apoptosis in human cervical cancer HeLa cells. *PLoS One* 11: e0165372.
- Subramaniam S, Selvaduray K & Radhakrishnan A. (2019). Bioactive compounds: Natural defense against cancer? *Biomolecules* 9: 1–15.

- Sung H, Ferlay J, Siegel R, Laversanne M, Soerjomataram I, Jemal A & Bray F. (2021). Global cancer statistics 2020: GLOBOCAN estimates of incidence and mortality worldwide for 36 cancers in 185 countries. *CA: A Cancer Journal for Clinicians* 71: 209–249.
- Tang D, Tao D, Fang Y, Deng C, Xu Q & Zhou J. (2017). TNF-alpha promotes invasion and metastasis via NF-kappa B pathway in oral squamous cell carcinoma. *Medical Science Monitor Basic Research* 23: 141–149.
- Tendean M & Riwanto I. (2021). The effects of *Phyllanthus niruri* Linn on infiltrating dendritic cell and ratio of neutrophile/lymphocytes in chemotherapy of Sprague-Dawley rats with colorectal cancer. *Asian Pacific Journal of Cancer Prevention* 22: 3561–3568.
- Tjandrawinata R, Susanto L & Nofiarny D. (2017). The use of *Phyllanthus niruri* L. as an immunomodulator for the treatment of infectious diseases in clinical settings. *Asian Pacific Journal of Tropical Disease* 7: 132–140.
- Togashi Y, Shitara K & Nishikawa H. (2019). Regulatory T cells in cancer immunosuppression — implications for anticancer therapy. *Nature Reviews Clinical Oncology* 16: 356–371.
- Tosello-Tramont A, Surette F, Ewald S & Hahn Y. (2017). Immunoregulatory role of NK cells in tissue inflammation and regeneration. *Frontiers in Immunology* 8: 301–309.
- Venturella G, Ferraro V, Cirlincione F & Gargano M. (2021). Medicinal mushrooms: Bioactive compounds, use, and clinical trials. *International Journal of Molecular Sciences* 22: 1–30.
- Wang L, Kuang Z, Zhang D, Gao Y, Ying M & Wang T. (2021). Reactive oxygen species in immune cells: A new antitumor target. *Biomedicine & Pharmacotherapy* 133: 1–9.
- Wang R, Jaw J, Stutzman N, Zou Z & Sun P. (2012). Natural killer cell-produced IFN- γ and TNF- α induce target cell cytolysis through up-regulation of ICAM-1. *Journal of Leukocyte Biology* 91: 299–309.
- Wculek S, Cueto F, Mujal A, Melero I, Krummel M & Sancho D. (2020). Dendritic cells in cancer immunology and immunotherapy. *Nature Reviews Immunology* 20: 7–24.
- Whiteside T. (2020). NK cells in the tumor microenvironment and thioredoxin activity. *Journal of Clinical Investigation* 130: 5115–5117.
- Yuandani, Ilangkovan M, Jantan I, Mohamad H, Husain K & Abdul Razak A. (2013). Inhibitory effects of standardized extracts of *Phyllanthus amarus* and *Phyllanthus urinaria* and their marker compounds on phagocytic activity of human neutrophils. *Evidence-Based Complementary and Alternative Medicine* 2013: 1–10.
- Zhang C, Hu Y, Xiao W & Tian Z. (2021). Chimeric antigen receptor- and natural killer cell receptor-engineered innate killer cells in cancer immunotherapy. *Cellular & Molecular Immunology* 18: 2083–2100.
- Zhao X, Liu J, Ge S, Chen C, Li S, Wu X, Feng X, Wang Y & Cai D. (2019). Saikosaponin A inhibits breast cancer by regulating Th1/Th2 balance. *Frontiers in Pharmacology* 10: 1–8.

Zheng Y, Li Y, Lian J, Yang H, Li F, Zhao S, Qi Y, Zhang Y & Huang L. (2019). TNF- α -induced Tim-3 expression marks the dysfunction of infiltrating natural killer cells in human esophageal cancer. *Journal of Translational Medicine* 17: 1–12.

Metronidazole Loaded Novel Microemulsion Formulation for Topical Delivery and Characterization With Validated New UPLC Method

Tilbe ÇEVİKELLİ*, Umay Merve GÜVEN**, Ahmet Alper ÖZTÜRK***

Metronidazole Loaded Novel Microemulsion Formulation for Topical Delivery and Characterization With Validated New UPLC Method

SUMMARY

The purpose of the study is to develop metronidazole (MET) containing microemulsion systems for topical application, to overcome limitations of local antibacterial treatments. For preparation of drug loaded microemulsions pseudo-ternary phase diagram technique was applied. IPP as oil phase, Span 80 and Cremophor EL as surfactant, ethanol and propylene glycol as co-surfactant and distilled water was used as aqueous phase. Globule size ranging between 126.8 ± 2.8 to 150.8 ± 1.6 nm and PDI between 0.21 ± 0.02 to 0.35 ± 0.06 were obtained. Zeta potentials of the formulations measured as 0.48 ± 0.08 – 0.68 ± 0.14 mV and conductivity was between 0.5 ± 0.0 and 0.6 ± 0.0 , implicating the formation of w/o emulsions. A UPLC method was developed and validated according to the ICH Q2 (R1) guideline, for quantification of MET, and drug content was calculated as 99.18 ± 0.08 – 99.33 ± 0.12 %. MET release of 80.62 ± 0.86 % for S_{1MET} and 62.06 ± 1.08 % for S_{2MET} formulations at 24h, indicated the control over the MET release by the microemulsions. After 3. and 6. months, no difference observed in physicochemical properties of microemulsions, and MET release showed similar profile; implicating the good stability of formulations.

Key Words: Metronidazole, microemulsion, release kinetics, stability, topical delivery, UPLC.

Topikal Uygulama için Metronidazol Yüklü Yeni Mikroemülsiyon Formülasyonu ve Valide Edilmiş Yeni UPLC Yöntemi ile Karakterizasyonu

ÖZ

Bu çalışmada, lokal etkili topikal antibiyotik uygulamalarında tedavi kısıtlarını aşmak amacıyla metronidazol (MET) içeren mikroemülsiyon formülasyonlarının geliştirilmesi amaçlanmaktadır. Mikroemülsiyon formülasyonları üçgen faz diyagramı tekniğiyle hazırlanmış olup; yağ fazı olarak IPP, yüzey etkin madde olarak Span 80 ve Cremophor EL, yardımcı yüzey etkin madde olarak etanol ve propilen glikol kullanılmış, ve su fazı olarak distile su ilave edilmiştir. Üretilen mikroemülsiyonların damlacık boyutu 126.8 ± 2.8 - 150.8 ± 1.6 nm, PDI değerleri 0.21 ± 0.02 - 0.35 ± 0.06 arasında kaydedilmiş olup; zeta potansiyelleri 0.48 ± 0.08 – 0.68 ± 0.14 mV ve iletkenlikleri 0.5 ± 0.0 and 0.6 ± 0.0 arasında olup yağ içerisinde su tipinde emülsiyon oluşumunu işaret etmektedir. Metronidazol miktar tayinini gerçekleştirmek amacıyla geliştirilen UPLC metodu, ICH Q2 (R1) kriterlerine göre valide edilmiş, ve mikroemülsiyonların MET içeriği 99.18 ± 0.08 – 99.33 ± 0.12 olarak tespit edilmiştir. S_{1MET} formülasyonunun 80.62 ± 0.86 ve S_{2MET} formülasyonunun 62.06 ± 1.08 salım gerçekleştirdiği belirlenerek, mikroemülsiyonların 24 saat boyunca kontrollü MET salımı sağladığı gösterilmiştir. Ayrıca, 3. ve 6. ay sonunda mikroemülsiyonların fizikokimyasal özelliklerini koruduğu ve MET salım profillerinin değişmediği tespit edilerek, formülasyonların iyi stabilite gösterdikleri tespit edilmiştir.

Anahtar Kelimeler: Metronidazol, mikroemülsiyon, salım kinetiği, stabilite, topikal uygulama, UPLC.

Received: 12.09.2023

Revised: 07.12.2023

Accepted: 07.12.2023

* ORCID: 0000-0002-0881-0644, Department of Pharmaceutical Technology, Faculty of Pharmacy, Cukurova University, Adana, Turkey.

** ORCID: 0000-0003-1547-0817, Department of Pharmaceutical Technology, Faculty of Pharmacy, Cukurova University, Adana, Turkey.

*** ORCID: 0000-0001-9596-0538, Department of Pharmaceutical Technology, Faculty of Pharmacy, Anadolu University, Eskişehir, Turkey.

INTRODUCTION

The major barrier for topical delivery is the complicated structure of the skin. Stratum corneum is the topmost layer of the skin, is constituted of dead cells, and this layer is a potential barrier to dermal applied drugs and limits their penetration. The stratum corneum functions as a barrier to hydrophilic drugs and macromolecules. On the contrary, lipophilic molecules can penetrate the intercellular lipids via the transcellular route. The primary obstruction is caused by stratum corneum to penetration of the drug. To overcome this obstruction, many nanosized drug delivery systems have been designed (Benson et al., 2019). Producing a novel therapeutic molecule is not only expensive and time-consuming, but it also frequently fails. However, enhancing these drugs' bioavailability, efficacy, or safety through a various methods may be a more coherent way to use them in the clinic. The researchers have thoroughly investigated several strategies, including stimulant-sensitive targeted pharmaceutical therapy, drug conjugates, therapeutic drug monitoring, and various drug delivery systems (Öztürk & Aygül, 2020; Öztürk et al., 2020). The efficiency of the topically applied antimicrobial drugs depends on the formulation's ability to overcome the stratum corneum barrier, and provide therapeutic activity in the affected area. So, nanosized drug delivery systems aiming to enhance topical penetration are essential to increase its antimicrobial efficacy. Nanosized drug delivery is also preferred to improve solubility of the drugs, to minimize side effects and toxicity, to provide higher drug loading and to increase the bioavailability (Nagula & Wairkar, 2019).

Metronidazole (MET) is a commonly used antibacterial agent in the nitroimidazole class. MET can be used in oral, intravenous and topical dosage forms, and its cutaneous application focuses on the rosacea (Dallo et al., 2023).

Although MET provides antibacterial and antiprotozoal activity, its molecular weight and low lipophilicity limits its activity in topical applications (Dwipayanti et al., 2022). Also, topical antibacterial applications include several disadvantages including drug associated contact dermatitis as a common side effect, minimal depth of penetration resulting in efficacy in only superficial infections, and concerning wound impairment (Bandyopadhyay, 2021).

To overcome these limitations, drug delivery systems for topical application have evolved from simple solutions and creams; to multiphase nanotechnologies, in recent years. They include microemulsions, nanoemulsions, liposomes, niosomes, solid lipid nanoparticles, and dendrimers. Microemulsions are thermodynamically stable liquids; simple and optically isotropic systems constituted by oil, surfactants and water (Tiwari & Sivakumar, 2022). Due to content of surfactants and oil components, these drug delivery systems act as penetration enhancers, and increase the transdermal absorption of the active agent. Use of surfactant, cosurfactant and surfactant mixtures to prepare microemulsions designed for topical administration (Erdal et al., 2020), comprises them in both aqueous and lipid phases; and would be able to penetrate the skin.

Since microemulsions hold significant advantages for topical drug delivery, application of antibacterial agents by the microemulsion systems are well studied in the literature. Pandey et al. (2014) established a microemulsion based hydrogel system that provides 5 hours of MET release for treatment of periodontitis, while Tirnaksız et al. (2012) developed a microemulsion system providing 6 hours of MET release for remission of rosacea. The purpose of the current study was to formulate and evaluate *in vitro* characterization and stability of microemulsion formulations maintaining MET release over 12 hours, as an antibacterial agent.

MATERIALS AND METHODS

Method validation of MET by UPLC

In this study, a new method was developed according to the literature and ICH criteria (Guideline, 2005; Öztürk et al., 2018; Öztürk et al., 2017).

Agilent Technology 1290 Infinity UPLC device was used with reversed-phase Zorbax® Eclipse Plus C18 gravity column (column length: 50 mm, column diameter: 2.1 mm, particle diameter: 1.8 µm). Mobile phase was consisted of 50:50 (v/v/v) acetonitrile:methanol with 0.01 M KHPO₄. Flow rate of the mobile phase was 0.2 mL/min and volume of injection was 0.5 µL. The temperature of the column was set to 40°C while a fluorescent detector was used at 318 nm.

Linearity

Analytes from a standard stock solution of 100 µg/mL of MET were prepared at nine different concentrations between 1-20 µg/mL as six different sets. Absorbance values of analytes were measured to calculate MET concentrations. Calibration curve was acquired by plotting concentration (x) versus peak area (y); regression equation and the correlation coefficient were calculated (n=6).

Limit of detection and limit of quantification (sensitivity)

Detection and quantification limits of an analyte with specified conditions, represent the methods sensitivity. The calibration curve method was applied to calculate the Limit of Detection (LoD) and Limit of Quantitation (LoQ) values of the developed UPLC method for MET quantification. By calculating the standart deviation of y-intercept and slope of curve as recommended by the ICH Q2 (R1) guideline, following equations were used to determine LoD and LoQ (Eq. 1, Eq. 2).

$$LOD = 3.3 \times \sigma/S \quad (\text{Equation 1})$$

$$LOQ = 10 \times \sigma/S \quad (\text{Equation 2})$$

σ = the standard deviation of the response and S = slope of the calibration curve.

Accuracy

Accuracy was determined by calculating the recoveries of known concentrations of MET. Analytes of 10 µg/mL, 30 µg/mL, 50 µg/mL of MET solutions were analyzed and accuracy was determined as the standard deviation of mean from the nominal concentration (n=6).

Precision

Precision is the variance, standard deviation, or coefficient of variation of a set of measurements in the ICH Q2 (R1) guideline. Precision criterion was verified by the repeated absorbance measurements of 10 µg/mL, 25 µg/mL, 50 µg/mL concentrations of MET, and expressed as the RSD% of the results (n=6).

Construction of pseudo-ternary phase diagram

Microemulsion systems must be consisted of specific ratio of three constituents namely: oil, water and mixture of surfactant and cosurfactant (S_{mix}). To establish the exact ratio of these microemulsion components, a pseudo-ternary phase diagram must be constructed. The pseudo-ternary phase diagrams were obtained by using water titration method at the room temperature (Puri et al., 2017).

Isopropyl palmitate (IPP) was selected as an oil component in the microemulsion systems (Alkoholifi et al., 2023). Span® 80 and Cremophor EL were used as surfactants (S), while ethanol and propylene glycol were selected as the cosurfactant (CoS) in S/CoS weight ratios of 1:1, 1:2, 1:3, 1:4, 1:5 and 1:6. As surfactants Span 80 and Cremophor EL were used separately, and as cosurfactants, ethanol and propylene glycol were used in 1:1 ratio as a mixture. For fabrication of pseudo-ternary phase diagram, the weight ratio of oil to mixture of surfactant and cosurfactant at each S_{mix} was varied as 1:9, 2:8, 3:7, 4:6, 5:5, 6:4, 7:3, 8:2, and 9:1, respectively for development of 10 g microemulsion. The mixtures were examined visually and classified as

microemulsions, crude emulsions, or emulgels after being equilibrated (Bharti & Kesavan, 2017; Chen et al., 2007; Nandi et al., 2003).

Based on the microemulsion areas determined from the constructed pseudo-ternary phase diagrams, six formulations containing different proportions of oil, water, and S_{mix} were developed (Çevikelli et al., 2020). Based on these diagrams, suitable concentrations of constituents were selected and utilised in preparation of microemulsions. The phase diagrams have been created utilizing a computer program; the area covered by these points was assumed as microemulsion area and all trials were done in triplicate.

Preparation of MET-loaded microemulsions

Pseudo-ternary phase diagrams were obtained to decide suitable constituents, and their concentration series that arose in a large microemulsion area were chosen. Blank and MET-loaded microemulsions with varied compositions were prepared after identification of microemulsion area from the pseudo-ternary phase diagrams.

The system was stirred using a magnetic stirrer to ensure a thoroughly mix at 25°C. Oil and S_{mix} mixtures were titrated, drop-by-drop, with double distilled water while stirring until the mixture became transparent. The microemulsions were protected from the by storing in dark-brown bottles covered with aluminum foil (Öztürk & Güven, 2019).

Physicochemical characterization of MET-loaded microemulsions

The chosen formulations were taken under the thermodynamic stability tests, in terms of the centrifugation test and heating-cooling cycles. Thermodynamic stability was assessed by the procedure of three cycles between 4°C and 40°C with storage at each temperature for 48 h were studied. Also, the formulations were centrifuged at 3500 rpm for 30 min.

Globule sizes and zeta potential of the formulations were measured using Zetasizer nano ZS (Malvern, UK) at 25°C and polydispersity index (PDI) was reported (Ekinci et al., 2022; Tilki et al., 2023).

The pH value of prepared microemulsion formulations was determined at 25°C with a digital pH meter. All measurements were done in triplicate (Chavhan et al., 2013; Ramasahayam et al., 2015; Zhu et al., 2008).

Drug content

To obtain a clear solution, MET-loaded microemulsions were mixed with methanol and sonicated respectively. Following the sonication, formulations were centrifuged at 1500 rpm for 5 min, to yield a clear supernatant, which were injected to the UPLC for quantification of MET.

In vitro release study

In vitro release studies of MET-containing microemulsion formulations were conducted by the dialysis bag method. The medium used in the release study was phosphate buffer having 7.4 pH. All sets were incubated at 37°C and were shaken at 100 rpm by using a magnetic stirrer. The release medium volume was taken for the study as 50 mL. The formulation (1 mL) was placed in a dialysis bag for the research, and the drug release was evaluated for 24 h. At 0.5, 1, 2, 3, 6, 9 and 12, 24 h, 1 mL of samples were collected. After samples being withdrawn at predetermined time interval, release medium was replaced with an equivalent amount of the fresh medium. The obtained samples were then analyzed for MET quantification by the UPLC. Three replicates were performed for each formulation (Kumbhar et al., 2020; Talaat et al., 2019).

Evaluation of release kinetics

Data were transmitted to the DDSolver program after obtaining the MET release profiles to determine the four most important criteria: coefficient of determination (R^2), adjusted coefficient

of determination ($R^2_{adjusted}$), Akaike information criterion (AIC), and model selection criterion (MSC). To compare various kinetic models, the lowest AIC values, maximum R^2 , $R^2_{adjusted}$, and MSC values were utilized (Öztürk et al., 2021; Öztürk et al., 2020).

Stability of microemulsion formulations

The optimized microemulsion formulations were kept at ambient temperature for six months, and then the clarity, phase separation, globule sizes, PDI, *in vitro* release, and concentration of MET were investigated. Microemulsion samples were analysed at 0, 3 and 6 months, respectively.

Statistical analysis

The collected data (n=3) were presented as

mean±S.D. The Student’s t-test was used to analyze statistical data at the level of $p \leq 0.05$.

RESULTS and DISCUSSION

UPLC method and validations

Linearity

Linearity of MET between 1-20 µg/mL was studied and the regression equation was found to be $y = 1,0232x - 0,3237$ by plotting concentration (x) versus peak area (y). The correlation coefficient (R^2) was determined as 0.9996 and found to be highly significant and suitable (Çağlar et al., 2022). Linearity test results are given in Table 1 and regression curve is shown in Figure 1.

Table 1. Sets and Area/RT values prepared for the linearity study

Conc (µg/mL)	AREA/Rt						Mean	SD	SE
	Set 1	Set 2	Set 3	Set 4	Set 5	Set 6			
1.0	0.798	0.906	0.976	0.908	0.904	0.821	0.885	0.064	0.026
2.5	2.224	2.354	2.405	2.323	2.230	2.194	2.288	0.084	0.034
5.0	4.401	4.433	4.702	4.691	4.504	4.417	4.525	0.137	0.056
7.5	7.286	7.522	7.587	7.131	7.107	7.064	7.283	0.224	0.091
10.0	9.910	9.565	9.979	9.990	9.982	9.613	9.840	0.197	0.080
12.5	12.922	12.735	12.446	12.299	12.754	12.277	12.572	0.268	0.109
15.0	15.233	15.293	15.107	14.886	15.509	14.700	15.121	0.291	0.119
17.5	17.631	17.655	17.265	17.263	17.453	17.581	17.475	0.177	0.072
20.0	20.580	20.362	19.394	20.549	20.720	19.611	20.202	0.558	0.228

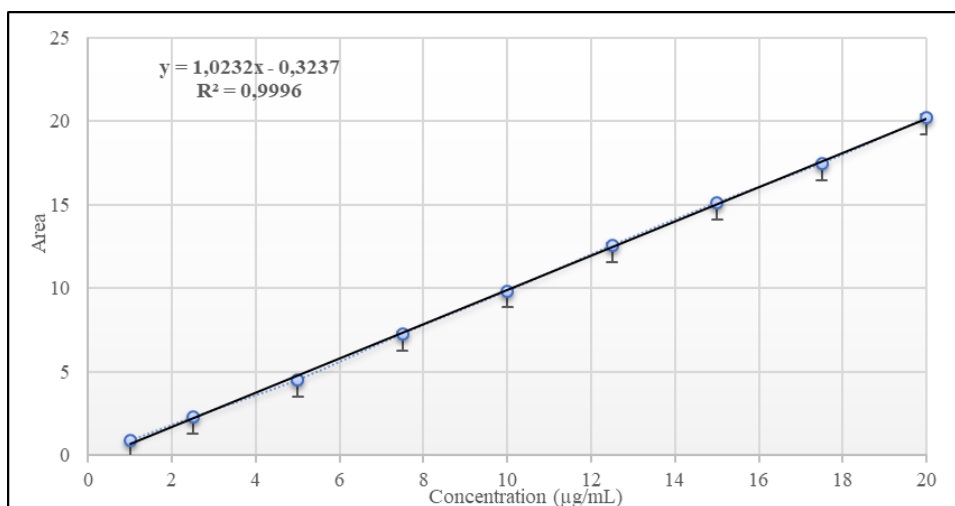


Figure 1. Regression profile of MET.

Limit of detection and limit of quantification (sensitivity)

While LoD and LoQ parameters are interrelated, they cover different properties for the analytic method development and validation. As there are different definitions to describe LoD and LoQ, generally LoD refers to the minimum concentration in a sample under the specified test conditions, but is not found to be quantifiable. The term “LoQ” refers to the minimum concentration of an analyte that can be accurately and precisely measured under the required test conditions. The detection and quantification limits are typically determined using linear regression, signal-to-noise,

limit of blank, and precision-based techniques, as well as blank determination (Guideline, 2005). Linear regression method was applied to calculate LoD and LoQ values for this study and found to be 0.9073 µg/mL and 2.7494 µg/mL, accordingly.

Accuracy

As given in Table 2, recoveries of MET at different concentrations were obtained between 100.4673 – 106.3123%, and relative standard deviation (RSD%) values <2% were calculated for all concentrations studied, which is the acceptance criteria, implicating suitable accuracy for the UPLC method developed for the MET (Çağlar et al., 2022; Guideline, 2005).

Table 2. Accuracy results calculated for the 10 µg/mL, 30 µg/mL and 50 µg/mL of the MET

Area/RT			Concentration		
10 µg/mL	30 µg/mL	50 µg/mL	10 µg/mL	30 µg/mL	50 µg/mL
10.710	30.566	50.747	10.784	30.190	49.914
10.306	30.712	51.079	10.389	30.332	50.238
10.618	30.288	51.863	10.693	29.918	51.005
10.764	30.075	52.125	10.837	29.710	51.261
10.574	30.853	50.785	10.651	30.471	49.951
10.349	30.593	51.290	10.431	30.217	50.444
			Recovery (%)		
			10 µg/mL	30 µg/mL	50 µg/mL
			107.840	100.635	99.828
			103.898	101.109	100.477
			106.938	99.728	102.011
			108.372	99.035	102.522
			106.512	101.570	99.902
			104.312	100.724	100.889
Recovery Mean (%)			106.312	100.467	100.938
Difference (%)			6.312	0.467	0.938
RSD			1.726	0.927	1.101
95% Confidence Interval			1.925	0.975	1.166

Precision

Intermediate precision and repeatability results were calculated for concentrations of 10 µg/mL, 25 µg/mL, 50 µg/mL of the MET to evaluate precision parameter as recommended by the ICH to cover low,

middle and high concentrations of the range, and given in Table 3. RSD% values < 2%, were found to be suitable for ICH Q2(R1) guideline, and method was found to be precise (Guideline, 2005).

Table 3. Precision results of the 10 µg/mL, 25 µg/mL, and the 50 µg/mL of MET

Area/RT			Concentration (10 µg/mL)		
1 st Day	2 nd Day	3 rd Day	1 st Day	2 nd Day	3 rd Day
10.820	10.710	10.053	10.891	10.784	10.142
10.678	10.306	10.585	10.752	10.389	10.661
10.302	10.618	10.417	10.385	10.693	10.497
10.521	10.764	10.716	10.599	10.837	10.789
10.397	10.574	10.643	10.477	10.651	10.718
10.728	10.349	10.792	10.802	10.431	10.864
Mean			10.651	10.631	10.612
Standard Deviation (SD)			0.197	0.183	0.261
Coefficient of Variation (RSD)			1.850	1.726	2.467
95% Confidence Interval			0.206	0.192	0.274
Area/RT			Concentration (25 µg/mL)		
1 st Day	2 nd Day	3 rd Day	1 st Day	2 nd Day	3 rd Day
25.476	26.158	25.801	25.215	25.882	25.533
26.010	25.825	26.231	25.738	25.556	25.953
26.296	26.425	26.638	26.017	26.143	26.351
26.412	26.157	26.321	26.130	25.881	26.041
25.684	25.464	26.124	25.419	25.204	25.848
26.240	26.732	26.978	25.962	26.443	26.684
Mean			24.747	25.851	26.068
Standard Deviation (SD)			0.362	0.434	0.402
Coefficient of Variation (RSD)			1.406	1.680	1.541
95% Confidence Interval			0.380	0.455	0.421
Area/RT			Concentration (50 µg/mL)		
1 st Day	2 nd Day	3 rd Day	1 st Day	2 nd Day	3 rd Day
52.263	50.600	50.747	51.396	49.770	49.914
50.401	52.667	51.079	49.575	51.790	50.238
50.816	51.403	51.863	49.982	50.555	51.005
49.574	50.606	52.125	48.767	49.776	51.261
51.225	52.373	50.785	50.381	51.503	49.951
49.433	53.412	51.290	48.630	52.518	50.444
Mean			49.789	50.985	50.469
Standard Deviation (SD)			1.039	1.130	0.555
Coefficient of Variation (RSD)			2.087	2.217	1.101
95% Confidence Interval			1.090	1.186	0.583

Microemulsions development

A pseudo-ternary phase diagram for the determination of microemulsion region can be constructed by titration method. Constructing a pseudo-ternary phase diagram is important to establish the concentration range of ingredients for the existence range of microemulsion. Microemulsion system is formed when the interfacial tension between water and oil interface is occurred at deficient level. This condition, resulting in a spontaneous dispersion of water phase into oil phase. The pseudo-ternary phase diagram is usually provided by an appropriate selection of surfactants and cosurfactants and their ideal proportions (Lawrence & Rees, 2012). Four different S_{mix} proportions were chosen (1:2, 1:3, 1:4, 1:5) using Span® 80, ethanol and propylene glycol. And then, four different S_{mix} proportions were chosen (1:1, 1:2, 1:3, 1:4) using Cremophor EL, ethanol and propylene glycol. These proportions were created to generate a pseudo-ternary phase diagram, shown in Figure 2. It was observed that the area of the microemulsion region increased as the surfactant/cosurfactant mixture increased. This is probably due to decreased interfacial tension and increased mobility of the system. It was monitored that percentage area of microemulsion area in the most of phase diagrams was most wide-ranging at S/CoS weight ratio of 1:4 compared to others. After determining the Figure 2/c and Figure 2/h shows the larger microemulsion area, formulations used in the next experiments (Table 4) were selected from the weight center of these diagrams

(Öztürk & Güven, 2019). Weight center of these pseudo-ternary phase diagrams were coded as S_1 and S_2 formulations, and MET-loaded microemulsions were produced based on these formulations (S_{1MET} and S_{2MET} , respectively).

Span 80 is a non-ionic surfactant that is biodegradable and nontoxic with low irritant properties. A surfactant for topical administration must decrease the interfacial tension between the oil–water interfaces and have convenient solubilizing capacity for drug (Kogan & Garti, 2006). Cremophor EL is a non-ionic surfactant with a high HLB value; due its less hydrophylic nature, providing a high solubilizing capacity of hydrophobic components with strong emulsifying capacity (Zhang et al., 2020). Due to their advantageous properties and common applications in microemulsion formation, Span 80 and Cremophor EL were chosen as the surfactants in this study.

Cosurfactant is a necessary constituent in the microemulsion development. This component reduces the interfacial tension between oil and water phase and provide a small internal globule size (Laothaweerungsawat et al., 2020). In our study, it has been reported that lipophilic surfactants promote water in oil (w/o) microemulsion formulations. Propylene glycol was used as a vehicle for penetration enhancement. And then, ethanol was chosen as cosurfactant, because of short to medium chain length alcohols are frequently used as co-surfactants to improve the fluidity of interface (Okur et al., 2020).

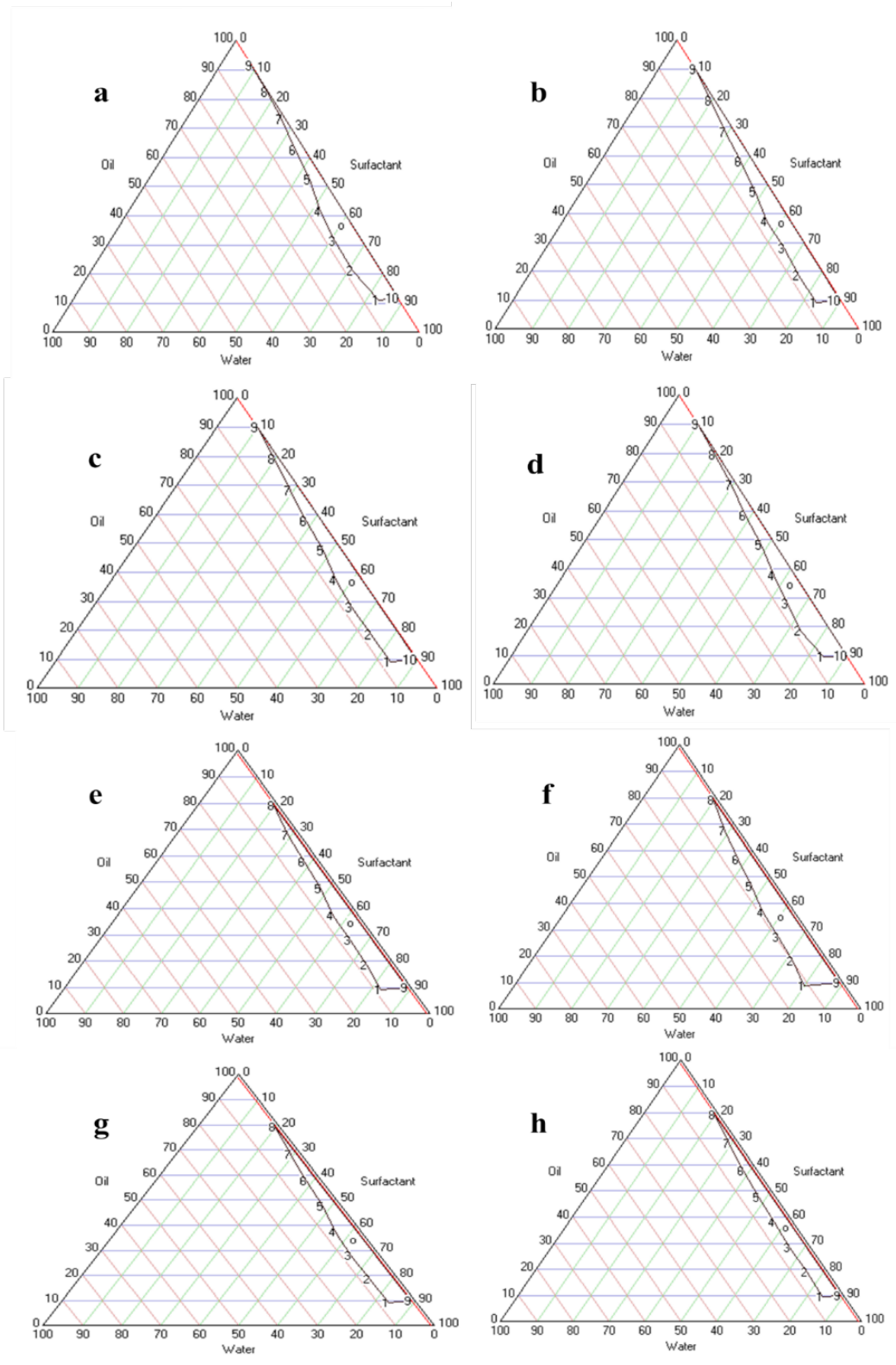


Figure 2. Pseudo-ternary phase diagram of microemulsions composed of oil, surfactant, cosurfactant and water. (a, b, c, d; 1:2, 1:3, 1:4, 1:5 using Span[®] 80, ethanol and propylene glycol) (e, f, g, h; 1:1, 1:2, 1:3, 1:4 using Cremophor EL, ethanol and propylene glycol)

Table 4. Composition of microemulsion formulations (% w/w)

Code / Formulation	IPP	Water	Cremonophor EL	Span 80	Ethanol	Propylene Glycol	MET
S ₁	37.20	3.00	-	11.96	23.92	23.92	-
S _{1MET}	35.34	2.85	-	11.36	22.72	22.72	5
S ₂	35.10	4.60	20.10	-	20.10	20.10	-
S _{2MET}	33.34	4.37	19.09	-	19.09	19.09	5

Physicochemical characterization of metronidazole loaded microemulsions

Physicochemical characterization was required to evaluate the effect of drug loading on microemulsion properties. Visual evaluations of phase separation, undissolved MET, transparency, and clarity of microemulsion formulations were performed (Üstündağ Okur et al., 2019). The prepared blank and MET-loaded microemulsions were clear, transparent, liquid, single phase, no drug precipitation and with homogeneous appearance (Lin et al., 2018; Ryu et al., 2020).

Emulsions usually are thermodynamically unstable systems and may separate when exposed to physical tension. Although microemulsions are visually appear to be homogeneous as a single phase system, in fact they are two phased systems (Hashem et al., 2011). Microemulsions were subjected to centrifugation and heating-cooling cycles to support the absence of no separation. After being subjected to centrifugation, blank and drug-loaded formulations did not show any sign of phase separation, which implicates the physical stability of the microemulsion (Zhu et al., 2008).

It is well known that one crucial factor for drug delivery systems is the vehicle's globule size. Nano globule size provides a larger surface region to interact with the skin, leading to improved permeation of active agents (Sita & Vavia, 2020). The globule sizes and PDI of the prepared microemulsions were determined by using the Dynamic Light Scattering technique. In this technique, laser light hits the globules in the solution and gets dispersed according to the size of the globules

(Altaani et al., 2019). The results of the characterization are summarized in Table 5. Globule size of blank microemulsion formulations was found to be ranged 126.8±2.8 nm to 150.8±1.6 nm. The globule size for S_{1MET} is 142.4±6.4 nm, while S_{2MET} is 162.4±4.6 nm. Globule sizes of MET-loaded formulations were slightly larger than the blank formulations, yet the difference was statistically insignificant ($p > 0.05$).

For monodispersed systems, the PDI index, which measures the distribution of microemulsion globules, is a dimensional number ranging from 0 to 1. Lower value expresses a size distribution of more homogenous for microemulsions (Chavhan et al., 2013; Ramasahayam et al., 2015). All formulations showed a PDI ranging from 0.21±0.02 to 0.35±0.06, suggesting that they are monodispersed.

The pH was found to vary between 4.0 and 7.0 range, optimum for the skin treatment. It is clear from Table 5 that microemulsion systems are within the required physiological pH range accepted. This pH close to skin pH, allows safe and nonirritating use of this formulations as topical application (Hashem et al., 2011).

The zeta potentials of microemulsions were obtained 0.48±0.08 - 0.68±0.14 mV that were being towards neutral. It is established that the stability of lipid based microemulsions containing nonionic surfactants does not depend on the zeta potential (Kumbhar et al., 2020).

Conductivity provides information about the structure of a microemulsion. The literature reported that the w/o type microemulsions stabilized by a

nonionic surfactant has unimportant charge which results in low electrical conductivity. The formulations had conductivity values of $0.5\pm 0.0 - 0.6\pm 0.0 \mu\text{S}/\text{cm}$, near zero, which confirms the formation of w/o type of emulsions (Tirnaksiz et al., 2012). Analysis

for drug content determination was taken by UPLC method and the (%) drug content for microemulsions were found within the suitable limits ($99.18\pm 0.08 - 99.33\pm 0.12 \%$).

Table 5. Characterization of microemulsion formulations (mean \pm SD, n=3)

Storage condition	Duration	Code	pH	Conductivity ($\mu\text{S}/\text{cm}$)	Zeta potential (mV)	Globule size (nm)	PDI	Drug content
Fresh	Initial	S1	5.42 \pm 0.00	0.5 \pm 0.0	0.52 \pm 0.17	126.8 \pm 2.8	0.23 \pm 0.03	-
		S1 _{MET}	5.34 \pm 0.00	0.5 \pm 0.1	0.48 \pm 0.08	142.4 \pm 6.4	0.26 \pm 0.02	99.18 \pm 0.08
		S2	4.98 \pm 0.00	0.6 \pm 0.0	0.64 \pm 0.12	150.8 \pm 1.6	0.21 \pm 0.02	-
		S2 _{MET}	4.86 \pm 0.01	0.6 \pm 0.0	0.68 \pm 0.14	162.4 \pm 4.6	0.24 \pm 0.01	99.33 \pm 0.12
Stored at 4°C	3 month	S1 _{MET}	5.38 \pm 0.00	0.5 \pm 0.0	0.56 \pm 0.14	151.4 \pm 5.0	0.26 \pm 0.02	99.04 \pm 0.16
		S2 _{MET}	4.92 \pm 0.00	0.6 \pm 0.0	0.68 \pm 0.17	174.2 \pm 4.8	0.30 \pm 0.04	99.12 \pm 0.24
	6 month	S1 _{MET}	5.36 \pm 0.01	0.5 \pm 0.1	0.56 \pm 0.18	150.6 \pm 5.6	0.32 \pm 0.02	98.90 \pm 0.16
		S2 _{MET}	4.98 \pm 0.02	0.6 \pm 0.1	0.65 \pm 0.10	170.7 \pm 5.0	0.35 \pm 0.04	98.84 \pm 0.18
Stored at 25°C	3 month	S1 _{MET}	5.44 \pm 0.01	0.5 \pm 0.0	0.44 \pm 0.24	150.4 \pm 3.8	0.26 \pm 0.03	99.13 \pm 0.56
		S2 _{MET}	4.87 \pm 0.03	0.6 \pm 0.0	0.62 \pm 0.17	158.7 \pm 6.2	0.32 \pm 0.02	99.03 \pm 0.32
	6 month	S1 _{MET}	5.38 \pm 0.01	0.5 \pm 0.1	0.48 \pm 0.11	155.7 \pm 8.8	0.33 \pm 0.04	98.92 \pm 0.22
		S2 _{MET}	5.02 \pm 0.00	0.5 \pm 0.1	0.62 \pm 0.15	162.6 \pm 8.6	0.38 \pm 0.08	97.84 \pm 0.48
Stored at 40°C	3 month	S1 _{MET}	5.48 \pm 0.01	0.5 \pm 0.1	0.42 \pm 0.26	156.4 \pm 8.4	0.25 \pm 0.03	98.90 \pm 0.24
		S2 _{MET}	4.88 \pm 0.02	0.4 \pm 0.1	0.58 \pm 0.16	176.4 \pm 10.4	0.30 \pm 0.04	98.24 \pm 0.38
	6 month	S1 _{MET}	5.41 \pm 0.01	0.5 \pm 0.1	0.46 \pm 0.13	164.0 \pm 9.3	0.33 \pm 0.02	98.14 \pm 0.20
		S2 _{MET}	5.06 \pm 0.03	0.4 \pm 0.2	0.52 \pm 0.22	182.4 \pm 3.6	0.35 \pm 0.06	97.76 \pm 0.58

In vitro metronidazole release study

Release profile is a significant parameter in the development of w/o microemulsion for water soluble drugs, because of depending on the solubility of the drug (Kumbhar et al., 2020). The *in vitro* release of MET from microemulsions was studied using the dialysis bag method. The *in vitro* release profile of MET from microemulsion formulation is represented in Figure 3. As expected, two microemulsion formulations showed a decrease in the amount of MET released as well as a delay in the release rate in comparison with the drug release from pure MET solution. The *in vitro* release of pure MET was $98.19 \pm 1.22\%$, within 4 h. Cremophor EL based microemulsion formulation S2_{MET} ($62.66 \pm 1.08\%$) significantly showed the low drug release from

the dialysis membrane within 24 h. The release of the S1_{MET} formulation was found to be $80.62 \pm 0.86\%$ at the end of 24 h. Compared with the formulations, pure MET solution has a rapid release rate, which indicated that the release of metronidazole had been significantly controlled by the microemulsions. Drug release from the S2_{MET} microemulsion was slower than that from the S1_{MET} microemulsion. As the reason for this, incorporation of different surfactants was altered the release profile of the formulation (Ikeuchi-Takahashi et al., 2020). Compared with pure MET solution, there was a significant difference in the release profile of MET from both the formulations ($p \leq 0.05$). Moreover, similar release profiles were obtained for S1_{MET} and S2_{MET} in 3. and 6. months (Figure 3 and 4).

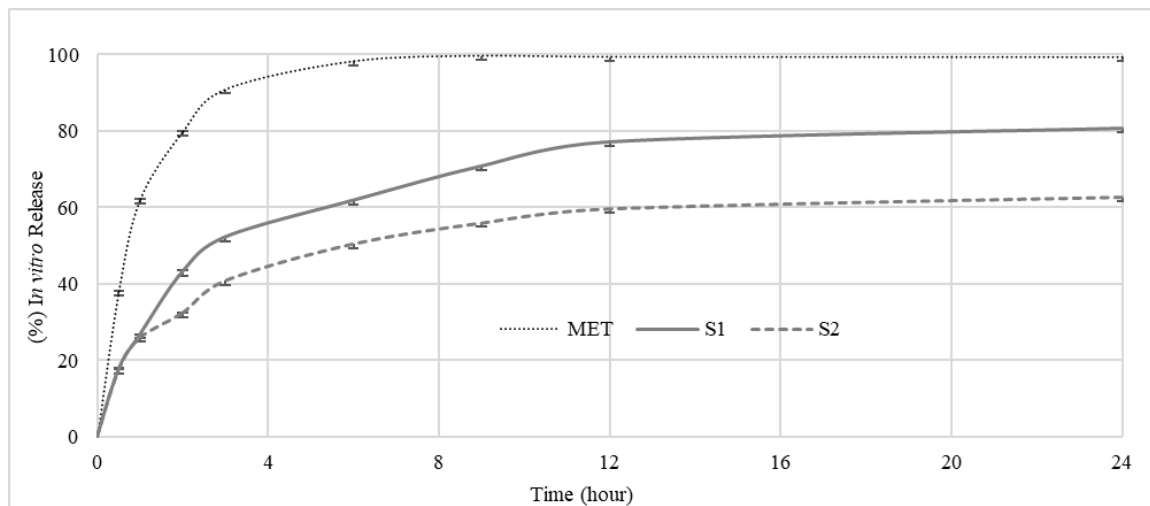


Figure 3. The *in vitro* MET release profiles of the microemulsion formulations and MET solution (n=3).

Evaluation of release kinetics

Kinetic modeling results of MET release from microemulsion formulation are given in Tables 6 and 7 for S1 and S2-coded formulations, respectively. For comparing different kinetic models, the lowest value for AIC; and the highest values of R^2 , $R^2_{adjusted}$ and MSC indicate the best fitting (Kırımloğlu & Öztürk, 2020). Examination of the statistic parameters from Table 6 and Table 7 lead to the conclusion that in formulation, the release kinetics was best defined by the Korsmeyer–

Peppas, Peppas-Sahlin and Weibull models (Scomorosenco et al., 2023). The drug release profile from the formulation may fit more than one model, as previously reported in the literature (Baghirova et al., 2023). The best-fitting release models imply the non-Fickian diffusion mechanism of the drug (Han et al., 2022) and indicate the slow diffusion of MET into the dissolution medium (Miastkowska et al., 2016); decreasing rate of the initial release, followed by the steady release rate of the MET (Jain et al., 2015).

Table 6. Release Kinetics Results for S₁ Coded Formulation

Model	Formulation Code	Evaluation Criteria			
		R ²	R ² _{adjusted}	AIC	MSC
Zero-order	S ₁	-0.056	-0.056	81.283	-0.724
First-order	S ₁	0.791	0.791	66.682	0.899
Higuchi	S ₁	0.818	0.818	65.471	1.033
Korsmeyer-Peppas	S ₁	0.915	0.903	60.611	1.573
Hixson-Crowell	S ₁	0.691	0.691	70.233	0.504
Hopfenberg	S ₁	0.692	0.648	72.201	0.285
Baker-Lonsdale	S ₁	0.953	0.953	53.190	2.398
Peppas-Sahlin 1	S ₁	0.983	0.978	48.021	2.972
Peppas-Sahlin 2	S ₁	0.991	0.989	40.716	3.784
Quadratic	S ₁	0.771	0.738	69.538	0.581
Weibull	S ₁	0.989	0.985	44.187	3.398

Table 7. Release Kinetics Results for S₂ Coded Formulation

Model	Formulation Code	Evaluation Criteria			
		R ²	R ² _{adjusted}	AIC	MSC
Zero-order	S ₂	-0.234	-0.234	77.602	-0.956
First-order	S ₂	0.495	0.495	69.558	-0.063
Higuchi	S ₂	0.771	0.771	62.451	0.727
Korsmeyer-Peppas	S ₂	0.950	0.943	50.770	2.025
Hixson-Crowell	S ₂	0.335	0.335	72.042	-0.339
Hopfenberg	S ₂	0.386	0.299	73.315	-0.480
Baker-Lonsdale	S ₂	0.862	0.862	57.897	1.233
Peppas-Sahlin 1	S ₂	0.996	0.994	30.967	4.225
Peppas-Sahlin 2	S ₂	0.999	0.998	18.842	5.573
Quadratic	S ₂	0.699	0.656	66.895	0.233
Weibull	S ₂	0.986	0.981	41.272	3.080

Stability study

The evaluation of the microemulsions stability is essential for indicating the physicochemical properties were preserved during the storage time, since physicochemical properties of microemulsions as drug delivery systems may affect its drug release profile (Pandey et al., 2014). The characteristic properties of the microemulsions remained unchanged during long-term stability tests. When the microemulsion formulations centrifuged and subjected to heating and cooling cycles, did not result in phase separation or turbidity; confirming that the microemulsions were physically stable. The clarity and stability of the formulations were maintained as indicated by

measurements throughout the storage period. The mean globule size and the PDI of microemulsions are two critical parameters for predicting physical stability (Narala et al., 2019; Sita & Vavia, 2020). No changes of globule size, zeta potential and degradation of MET were observed during six months. There was no statistically significant change between the first and last measurements for any of the characteristics ($p > 0.05$). Furthermore, there was no significant difference ($p > 0.05$) between *in vitro* MET release from formulations and their corresponding stability studies (3 and 6 months, Figure 4). In scope of this study, the microemulsions were found to be suitable carrier systems for the administration of MET through topical application for antibacterial treatment.

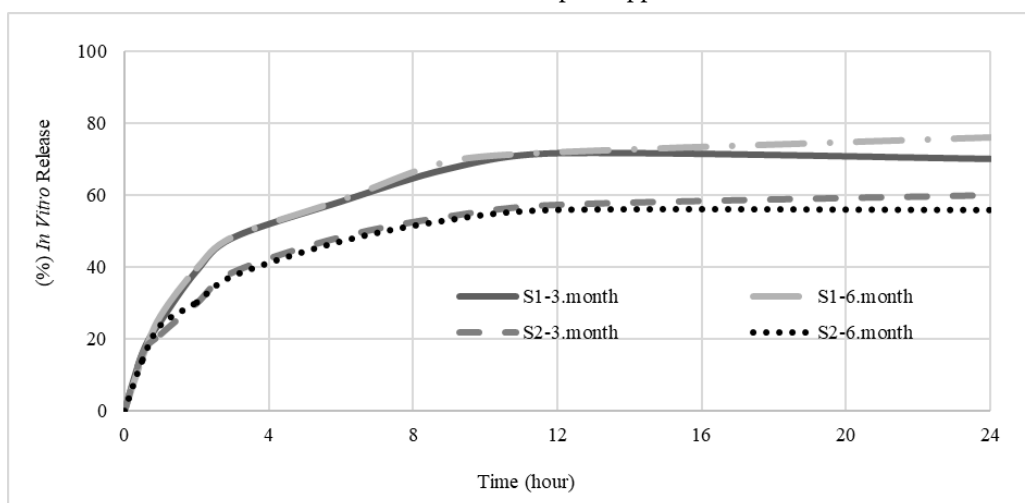


Figure 4. The *in vitro* MET release profile of the microemulsion formulations in 3. and 6. months (n=3).

CONCLUSION

In this work, MET-loaded microemulsions for topical application were developed by the pseudo-ternary phase diagram technique. Globule size, PDI, zeta potential, clarity, viscosity, conductivity, pH values, drug content, and drug release properties of the S_{1MET} and S_{2MET} formulations were satisfactory. Also, long term stability evaluation for six months, indicated good stability in terms of physicochemical properties and the drug release profiles of the formulations. In conclusion of these findings, MET-loaded microemulsions can be considered as a promising alternative for topical treatment.

CONFLICT OF INTEREST

The authors declare that there is no conflict of interest.

AUTHOR CONTRIBUTION STATEMENT

Concept, Experimental Design: (A.A.Ö., U.M.G., T.Ç); Data Collection, Data Processing, Data Analysis: (A.A.Ö., U.M.G., T.Ç); Literature Research, Writing (A.A.Ö., U.M.G., T.Ç); Supervision: (A.A.Ö., U.M.G.)

REFERENCES

- Alkoholifi, F. K., Alam, A., Foudah, A. I., & Yusufoglu, H. S. (2023). Phospholipid-Based Topical Nano-Hydrogel of Mangiferin: Enhanced Topical Delivery and Improved Dermatokinetics. *Gels*, 9(3), 178. <https://doi.org/10.3390/gels9030178>
- Altaani, B. M., Al-Nimry, S. S., Haddad, R. H., & Abu-Dahab, R. (2019). Preparation and characterization of an oral norethindrone sustained release/controlled release nanoparticles formulation based on chitosan. *AAPS PharmSciTech*, 20, 1-14. <https://doi.org/10.1208/s12249-018-1261-3>
- Baghirova, L., Kaya Tilki, E., & Ozturk, A. A. (2023). Evaluation of Cell Proliferation and Wound Healing Effects of Vitamin A Palmitate-Loaded PLGA/Chitosan-Coated PLGA Nanoparticles: Preparation, Characterization, Release, and Release Kinetics. *ACS omega*, 8(2), 2658-2668. <https://doi.org/10.1021/acsomega.2c07232>
- Bandyopadhyay, D. (2021). Topical antibacterials in dermatology. *Indian Journal of Dermatology*, 66(2), 117. https://doi.org/10.4103%2Fijd.IJD_99_18
- Benson, H. A., Grice, J. E., Mohammed, Y., Namjoshi, S., & Roberts, M. S. (2019). Topical and transdermal drug delivery: from simple potions to smart technologies. *Current drug delivery*, 16(5), 444-460. <https://doi.org/10.2174/1567201816666190201143457>
- Bharti, S. K., & Kesavan, K. (2017). Phase-transition W/O microemulsions for ocular delivery: Evaluation of antibacterial activity in the treatment of bacterial keratitis. *Ocular immunology and inflammation*, 25(4), 463-474. <https://doi.org/10.3109/09273948.2016.1139136>
- Chavhan, S. S., Petkar, K. C., & Sawant, K. K. (2013). Simvastatin nanoemulsion for improved oral delivery: design, characterisation, in vitro and in vivo studies. *Journal of microencapsulation*, 30(8), 771-779. <https://doi.org/10.3109/02652048.2013.788085>
- Chen, H., Mou, D., Du, D., Chang, X., Zhu, D., Liu, J., Xu, H., & Yang, X. (2007). Hydrogel-thickened microemulsion for topical administration of drug molecule at an extremely low concentration. *International Journal of Pharmaceutics*, 341(1-2), 78-84. <https://doi.org/10.1016/j.ijpharm.2007.03.052>
- Çağlar, E. Ş., Okur, N. Ü., & Karasulu, H. Y. (2022). Development and validation of an HPLC method for the determination of hyaluronic acid active substance in pharmaceutical formulations. *Journal of Research in Pharmacy*, 26(1). <https://dx.doi.org/10.29228/jrp.108>
- Çevikelli, T., Deniz, O., Güven, U. M., & Demirtürk, E. (2020). Preparation, characterization and in-vitro evaluation of theophylline loaded microemulsion formulations. *Journal of Pharmaceutical Technology*, 1(1), 7-12. <https://doi.org/10.37662/jpt.2020.1>

- Dallo, M., Patel, K., & Hebert, A. A. (2023). Topical Antibiotic Treatment in Dermatology. *Antibiotics*, 12(2), 188. <https://doi.org/10.3390/antibiotics12020188>
- Dwipayanti, K. S., Azhar, M., Rahman, L., Pakki, E., Himawan, A., & Permana, A. D. (2022). Enhanced skin localization of metronidazole using solid lipid microparticles incorporated into polymeric hydrogels for potential improved of rosacea treatment: An ex vivo proof of concept investigation. *International Journal of Pharmaceutics*, 628, 122327. <https://doi.org/10.1016/j.ijpharm.2022.122327>
- Ekinci, M., Öztürk, A. A., Santos-Oliveira, R., & İlem-Özdemir, D. (2022). The use of Lamivudine-loaded PLGA nanoparticles in the diagnosis of lung cancer: Preparation, characterization, radiolabeling with ^{99m}Tc and cell binding. *Journal of Drug Delivery Science and Technology*, 69, 103139. <https://doi.org/10.1016/j.jddst.2022.103139>
- Erdal, M. S., Gürbüz, A., Tan, S. B., Güngör, S., & Özsoy, Y. (2020). In vitro skin permeation and antifungal activity of naftifine microemulsions. *Turkish Journal of Pharmaceutical Sciences*, 17(1), 43. <https://doi.org/10.4274/tjps.galenos.2018.87699>
- Guideline, I. H. T. (2005). Validation of analytical procedures: text and methodology. Q2 (R1), 1(20), 05.
- Han, Y., Liu, S., Du, Y., Li, D., Pan, N., Chai, J., & Li, D. (2022). A new application of surfactant-free microemulsion: Solubilization and transport of drugs and its transdermal release properties. *Journal of the Taiwan Institute of Chemical Engineers*, 138, 104473. <https://doi.org/10.1016/j.jtice.2022.104473>
- Hashem, F. M., Shaker, D. S., Ghorab, M. K., Nasr, M., & Ismail, A. (2011). Formulation, characterization, and clinical evaluation of microemulsion containing clotrimazole for topical delivery. *AAPS PharmSciTech*, 12, 879-886. <https://doi.org/10.1208/s12249-011-9653-7>
- Ikeuchi-Takahashi, Y., Murata, S., Murata, W., Kobayashi, A., Ishihara, C., & Onishi, H. (2020). Development of Morin-Loaded Nanoemulsions Containing Various Polymers; Role of Polymers in Formulation Properties and Bioavailability. *AAPS PharmSciTech*, 21, 1-11. <https://doi.org/10.1208/s12249-020-01670-8>
- Jain, R., Sukla, S. K., Nema, N., & Panday, A. (2015). Drug Nano-particle: a release kinetics. *Journal of Nanomedicine & Nanotechnology*, 6(5), 1.
- Kırmıloğlu, G. Y., & Öztürk, A. A. (2020). Levocetirizine dihydrochloride-loaded chitosan nanoparticles: formulation and in vitro evaluation. *Turkish Journal of Pharmaceutical Sciences*, 17(1), 27. <https://doi.org/10.4274/tjps.galenos.2018.34392>
- Kogan, A., & Garti, N. (2006). Microemulsions as transdermal drug delivery vehicles. *Advances in colloid and interface science*, 123, 369-385. <https://doi.org/10.1016/j.cis.2006.05.014>
- Kumbhar, M. D., Karpe, M. S., & Kadam, V. J. (2020). Development and characterization of water-in-oil microemulsion for transdermal delivery of Eperisone hydrochloride. *Applied Clinical Research, Clinical Trials and Regulatory Affairs*, 7(1), 45-64. <https://doi.org/10.2174/2213476X06666190318120522>
- Laothawerungsawat, N., Neimkhum, W., Anuchapreeda, S., Sirithunyalug, J., & Chaiyana, W. (2020). Transdermal delivery enhancement of carvacrol from *Origanum vulgare* L. essential oil by microemulsion. *International Journal of Pharmaceutics*, 579, 119052. <https://doi.org/10.1016/j.ijpharm.2020.119052>

- Lawrence, M. J., & Rees, G. D. (2012). Microemulsion-based media as novel drug delivery systems. *Advanced drug delivery reviews*, 64, 175-193. <https://doi.org/10.1016/j.addr.2012.09.018>
- Lin, Y.-H., Tsai, M.-J., Fang, Y.-P., Fu, Y.-S., Huang, Y.-B., & Wu, P.-C. (2018). Microemulsion formulation design and evaluation for hydrophobic compound: Catechin topical application. *Colloids and Surfaces B: Biointerfaces*, 161, 121-128. <https://doi.org/10.1016/j.colsurfb.2017.10.015>
- Miastkowska, M., Sikora, E., Ogonowski, J., Zielina, M., & Łudzki, A. (2016). The kinetic study of isotretinoin release from nanoemulsion. *Colloids and Surfaces A: Physicochemical and Engineering Aspects*, 510, 63-68. <https://doi.org/10.1016/j.colsurfa.2016.07.060>
- Nagula, R. L., & Wairkar, S. (2019). Recent advances in topical delivery of flavonoids: A review. *Journal of controlled release*, 296, 190-201. <https://doi.org/10.1016/j.jconrel.2019.01.029>
- Nandi, I., Bari, M., & Joshi, H. (2003). Study of isopropyl myristate microemulsion systems containing cyclodextrins to improve the solubility of 2 model hydrophobic drugs. *AAPS PharmSciTech*, 4(1), 10. <https://doi.org/10.1208/pt040110>
- Narala, A., Guda, S., & Veerabrahma, K. (2019). Lipid nanoemulsions of rebamipide: formulation, characterization, and in vivo evaluation of pharmacokinetic and pharmacodynamic effects. *AAPS PharmSciTech*, 20, 1-9. <https://doi.org/10.1208/s12249-018-1225-7>
- Okur, M. E., Ayla, Ş., Yozgatlı, V., Aksu, N. B., Yoltaş, A., Orak, D., Sipahi, H., & Okur, N. Ü. (2020). Evaluation of burn wound healing activity of novel fusidic acid loaded microemulsion based gel in male Wistar albino rats. *Saudi Pharmaceutical Journal*, 28(3), 338-348. <https://doi.org/10.1016/j.jsps.2020.01.015>
- Öztürk, A., & Güven, U. (2019). Cefaclor monohydrate loaded microemulsion formulation for topical application: Characterization with new developed UPLC method and stability study. *Journal of Research in Pharmacy*, 23(3). <https://doi.org/10.12991/jrp.2019.150>
- Öztürk, A., Yenilmez, E., Arslan, R., ŞENEL, B., & Yazan, Y. (2020). Dexketoprofen trometamol loaded solid lipid nanoparticles (SLNs): Formulation, in vitro and in vivo evaluation. *Journal of Research in Pharmacy*, 24(1). <http://doi.org/10.35333/jrp.2020.114>
- Öztürk, A., & Aygül, A. (2020). Design of cefaclor monohydrate containing nanoparticles with extended antibacterial effect by nano-spray dryer: A nanoenglobing study. *Journal of Research in Pharmacy*, 24(1). <http://doi.org/10.35333/jrp.2020.115>
- Öztürk, A., Güven, U., & Yenilmez, E. (2018). Flurbiprofen loaded gel based topical delivery system: Formulation and in vitro characterization with new developed UPLC method. *ACTA Pharmaceutica Scientia*, 56(4). <http://doi.org/10.23893/1307-2080.aps.05627>
- Öztürk, A. A., Namlı, İ., Güleç, K., & Görgülü, Ş. (2020). Design of lamivudine loaded nanoparticles for oral application by nano spray drying method: a new approach to use an antiretroviral drug for lung cancer treatment. *Combinatorial Chemistry & High Throughput Screening*, 23(10), 1064-1079. <https://doi.org/10.2174/1386207323666200325155020>
- Öztürk, A. A., Yenilmez, E., & Yazan, Y. (2017). Development and validation of high performance liquid chromatography (HPLC) modified method for dexketoprofen trometamol. *Eur Int J Sci Tec*, 6(5), 33-41.

- Öztürk A., Namlı İ., & Aygül, A. (2021). Cefaclor monohydrate-loaded colon-targeted nanoparticles for use in COVID-19 dependent coinfections and intestinal symptoms: Formulation, characterization, release kinetics, and antimicrobial activity. *Assay and drug development technologies*, 19(3), 156-175. <https://doi.org/10.1089/adt.2020.1014>
- Pandey, S., Das, U., & Patil, A. (2014). Formulation and ex-vivo evaluation of metronidazole microemulsion loaded hydrogel for prevention of periodontitis. *Journal of Pharmaceutical Investigation*, 44, 225-236. <https://doi.org/10.1007/s40005-014-0119-2>
- Puri, A., Kaur, A., Raza, K., Goindi, S., & Katare, O. P. (2017). Development and evaluation of topical microemulsion of dibenzoylmethane for treatment of UV induced photoaging. *Journal of Drug Delivery Science and Technology*, 37, 1-12. <https://doi.org/10.1016/j.jddst.2016.09.010>
- Ramasahayam, B., Eedara, B. B., Kandadi, P., Jukanti, R., & Bandari, S. (2015). Development of isradipine loaded self-nano emulsifying powders for improved oral delivery: in vitro and in vivo evaluation. *Drug development and industrial pharmacy*, 41(5), 753-763. <https://doi.org/10.3109/03639045.2014.900081>
- Ryu, K.-A., Park, P. J., Kim, S.-B., Bin, B.-H., Jang, D.-J., & Kim, S. T. (2020). Topical delivery of coenzyme Q10-loaded microemulsion for skin regeneration. *Pharmaceutics*, 12(4), 332. <https://doi.org/10.3390/pharmaceutics12040332>
- Scomorosenco, C., Teodorescu, M., Nistor, C. L., Gifu, I. C., Petcu, C., Banciu, D. D., Banciu, A., & Cinteza, L. O. (2023). Preparation and In Vitro Characterization of Alkyl Polyglucoside-Based Microemulsion for Topical Administration of Curcumin. *Pharmaceutics*, 15(5), 1420. <https://doi.org/10.3390/pharmaceutics15051420>
- Sita, V., & Vavia, P. (2020). Bromocriptine nanoemulsion-loaded transdermal gel: optimization using factorial design, in vitro and in vivo evaluation. *AAPS PharmSciTech*, 21(3), 80. <https://doi.org/10.1208/s12249-020-1620-8>
- Talaat, S. M., Elnaggar, Y. S., & Abdalla, O. Y. (2019). Lecithin microemulsion lipogels versus conventional gels for skin targeting of terconazole: in vitro, ex vivo, and in vivo investigation. *AAPS PharmSciTech*, 20, 1-20. <https://doi.org/10.1208/s12249-019-1374-3>
- Tilki, E., Güven, U., & Kıyan, H. (2023). Ketorolac Tromethamine Loaded Nano-Spray Dried Nanoparticles: Preparation, Characterization, Cell Viability, COL1A1 Gene Simulation and Determination of Anti-inflammatory Activity by In vivo HET-CAM Assay. *Current drug delivery*, 20(6), 830-840. <https://doi.org/10.2174/1567201820666230125144133>
- Tırnaksız, F., Kayış, A., Çelebi, N., Adışen, E., & Erel, A. (2012). Preparation and evaluation of topical microemulsion system containing metronidazole for remission in rosacea. *Chemical and Pharmaceutical Bulletin*, 60(5), 583-592. <https://doi.org/10.1248/cpb.60.583>
- Tiwari, N., & Sivakumar, A. (2022). Biomedical application of microemulsion delivery systems: A review. *Journal of Research in Pharmacy*, 26(5). <http://dx.doi.org/10.29228/jrp.203>
- Zhang, Y., Zhang, K., Wang, Z., Hu, H., Jing, Q., Li, Y., ... & Feng, N. (2020). Transcutol® P/Cremophor® EL/ethyl oleate-formulated microemulsion loaded into hyaluronic acid-based hydrogel for improved transdermal delivery and biosafety of ibuprofen. *AAPS PharmSciTech*, 21, 1-10. <https://doi.org/10.1208/s12249-019-1584-8>

Zhu, W., Yu, A., Wang, W., Dong, R., Wu, J., & Zhai, G. (2008). Formulation design of microemulsion for dermal delivery of penciclovir. *International Journal of Pharmaceutics*, 360(1-2), 184-190. <https://doi.org/10.1016/j.ijpharm.2008.04.008>

In vitro Evaluation of the Effects of *Inula viscosa*'s Different Extracts on Wound Healing and Oxidative Stress in Mouse L929 Fibroblast Cell Line

Ahmet HARMANKAYA^{**}, İrfan ÇINAR^{**}, Muhammed YAYLA^{***},
Sezen HARMANKAYA^{****}, Murat BEYTUR^{*****}, Cem ÖZİÇ^{*****}

In vitro Evaluation of the Effects of *Inula viscosa*'s Different Extracts on Wound Healing and Oxidative Stress in Mouse L929 Fibroblast Cell Line

Inula viscosa'nın Farklı Ekstrelerinin Fare L929 Fibroblast Hücre Hattında Yara İyileşmesi ve Oksidatif Stres Üzerindeki Etkilerinin *In vitro* Değerlendirilmesi

SUMMARY

This study evaluated the effects of extracts prepared using two different methods (decoction extraction and soxhlet ethyl acetate/hexane extraction) from *Inula viscosa* on H₂O₂-induced oxidative stress and wound healing model in mouse L929 fibroblast cells. The cytotoxic effect started to disappear statistically ($p < 0.05$) at concentrations of Soxhlet ethyl acetate/hexane extracts (SoxEHE) in and below 0.1 mg/mL, while the same effect was observed at concentrations of decoction extracts (DE) in and below 0.2 mg/mL. Therefore, 0.2 and 0.02 mg/mL concentrations of DE, and 0.1 and 0.01 mg/mL concentrations of SoxEHEs were used. While cell migration was positively affected in all research concentrations, statistically significant results ($p < 0.05$) were obtained from 0.2 mg/mL of DE and 0.1 mg/mL of SoxEHE extracts. Malondialdehyde (MDA) levels were found to be statistically ($p < 0.05$) decreased, but COL1A1 levels were higher in cell lines treated with oxidative stress + extract than in the cell line treated only with H₂O₂, and reduced glutathione (GSH) levels were higher in cell lines only treated only with extract than in oxidative stress-induced cell lines. Consequently, it has been observed that the extracts have positive effects on migration and oxidative stress. Therefore, *I. viscosa* may serve as a new therapeutic agent for wound healing.

Key Words: Medicinal plants, extraction, scratch assay, cell proliferation, oxidative status

ÖZ

Bu çalışmada *Inula viscosa*'dan iki farklı yöntem (dekoksasyon ekstraksiyonu ve soxhlet etil asetat/hexan ekstraksiyonu) kullanılarak hazırlanan ekstrelerin fare L929 fibroblast hücrelerinde H₂O₂ kaynaklı oksidatif stres ve yara iyileşmesi modeli üzerindeki etkileri değerlendirilmiştir. Soxhlet etil asetat/hexan ekstrelerinin (SoxEHE) 0,1 mg/mL ve altındaki konsantrasyonlarında sitotoksik etki istatistiksel olarak kaybolmaya başlarken ($p < 0,05$), aynı etki dekoksasyon ekstrelerinin (DE) 0,2 mg/mL ve altındaki konsantrasyonlarında da gözlenmiştir. Bu nedenle DE'lerin 0,2 ve 0,02 mg/mL konsantrasyonları ve SoxEHE'lerin 0,1 ve 0,01 mg/mL konsantrasyonları kullanılmıştır. Araştırmanın tüm konsantrasyonlarında hücre migrasyonu olumlu etkilenirken, 0,2 mg/mL DE ve 0,1 mg/mL SoxEHE ekstrelerinden istatistiksel olarak anlamlı sonuçlar ($p < 0,05$) elde edilmiştir. Malondialdehit (MDA) düzeylerinin istatistiksel olarak ($p < 0,05$) azaldığı ancak COL1A1 düzeylerinin oksidatif stres + ekstrakt uygulanan hücre hatlarında, sadece H₂O₂ uygulanan hücre hattına göre daha yüksek olduğu ve indirgenmiş glutatyon (GSH) düzeylerinin oksidatif stresin kaynaklı hücre hatlarına göre yalnızca ekstreyle tedavi edilen hücre hatlarında daha yüksek olduğu görülmüştür. Sonuç olarak ekstrelerin migrasyon ve oksidatif stres üzerinde olumlu etkilerinin olduğu gözlemlenmiştir. Bu nedenle *I. viscosa* yara iyileşmesinde yeni bir terapötik ajan olarak hizmet edebilir.

Anahtar Kelimeler: Tıbbi bitkiler, ekstraksiyon, çizik testi, hücre proliferasyonu, oksidatif stres

Received: 21.09.2023

Revised: 11.12.2023

Accepted: 13.12.2023

* ORCID: 0000-0001-9923-6723, Department of Chemistry, Faculty of Science and Letter, Kafkas University, Kars, Turkey.

** ORCID: 0000-0002-9826-2556, Department of Pharmacology, Faculty of Medicine, Kastamonu University, Kastamonu, Turkey.

*** ORCID: 0000-0002-0659-3084, Department of Pharmacology, Faculty of Medicine, Kafkas University, Kars, Turkey.

**** ORCID: 0000-0003-2498-5003, Department of Food Processing, Kars Vocational College, Kafkas University, Kars, Turkey.

***** ORCID: 0000-0002-7098-5592, Department of Chemistry, Faculty of Science and Letter, Kafkas University, Kars, Turkey.

***** ORCID: 0000-0001-5415-9277, Department of Medical Biology, Faculty of Medicine, Kafkas University, Kars, Turkey

INTRODUCTION

A wound is a deterioration of the cellular, anatomical, and functional continuity of tissue due to a physical, chemical, thermal, microbial, or immunological effect on living tissue. In contrast, wound healing is a biological process involving diverse biochemical and cellular mechanisms designed to restore the structural and functional integrity of injured tissues and enhance physiological conditions (Barku, 2019). Wound healing is a continuous and overlapping process characterized by hemostasis (considered the inflammation stage in the three-stage concept), inflammation, new tissue formation, and the tissue remodeling (Gurtner et al., 2008). Redox signaling and oxidative stress play essential roles in regulating normal wound healing and contribute to specific stages (Sen & Roy, 2008). The formation of reactive oxygen species (ROS) at low concentrations is essential not only for combating invasive microorganisms but also for cellular signaling in the wound healing process (Cano Sanchez et al., 2018). However, even if ROS production is essential for initiating wound repair, excessive ROS formation and uncontrolled oxidative stress in wound healing contribute to persistent and uncontrolled inflammation, which plays a vital role in the pathogenesis of chronic non-healing wounds (Barku, 2019). Problems related to wound healing can occur in the form of swift recovery (such as hypertrophy and keloid scars) (Gurtner et al., 2008), or these problems may be seen as delayed wound healing in especially diabetics or older people (Abe et al., 2000). The healing time of chronic non-healing wounds lasts on average 12 to 13 months and recurs in up to 60 to 70% of patients. If they are not treated, it can lead not only to a loss of function and a decline in quality of life but may also result in mortality (Frykberg & Banks, 2015). While various alternatives, ranging from topical applications (hydrogels, povidone-iodine solution, cadexomer iodine, etc.) to advanced treatment methods such as growth factors, extracellular matrix, and negative pressure wound therapy, exist in wound care (Frykberg & Banks, 2015), these methods sometimes prove insufficient or impractical. Therefore, the scien-

tific world has constantly been searching for effective methods both in practice and cost-wise.

Various herbal products have been used in wound treatment over the years, and these phytochemical compounds have been reported to fight infections, promote blood clotting, and accelerate the healing process. When these wound-healing plants are investigated, it has been claimed that several of them have the potential to increase wound healing owing to their high antioxidant properties (Barku, 2019). The genus *Inula*, belonging to the Asteraceae family, has more than a hundred species, found mainly in Africa, Asia (20 species are also found in China), and Europe, especially in the Mediterranean region (Seca et al., 2014). The *Inula* genus comprises a range of species that have demonstrated medical importance, substantiated by their use in traditional medicine, the biological properties exhibited by their extracts, and the isolation of pure secondary metabolites (Seca et al., 2015). *Inula viscosa* [*Dittrichia viscosa* (L.) Greuter] is used in folk medicine in the Mediterranean region for its anti-inflammatory, antipyretic, antiseptic, antiphlogistic, and balsamic activities, as well as for the treatment of lung and gastroduodenal disorders (Messaoudi et al., 2016). Antioxidant, antibacterial, antifungal, hypoglycemic, hypolipidemic, anticancer, antiparasitic, and phytotoxic effects have also been reported for *I. viscosa* extracts, and it has been argued that these effects originate from sesquiterpenoids, triterpenoids, and flavonoids (Mahmoudi et al., 2016). In the literature review, several reports on extracts and purified metabolites from *I. viscosa* have been identified. However, concerning wound healing, only a morphological study in rats has been encountered. Khalil et al. (Khalil et al., 2007) reported that only 10% aqueous extract of *I. viscosa* healed both the morphological and histological features of wounds. However, no physiopathological studies have shown the effects of different types of extracts obtained from *I. viscosa* on wound healing.

As a result, we examined the *in vitro* effects of different extracts of the *I. viscosa* plant on wound healing

in L929 cells with hydrogen peroxide-induced oxidative stress and levels of oxidative stress parameters such as malondialdehyde (MDA) and reduced glutathione (GSH), and COL1A1 gene expression, which have an effect on healing in this process.

MATERIALS AND METHODS

Preparation and extraction of plant material

The plants collected from Manisa/Akhisar were identified by Asst. Prof. Dr. Mustafa Kemal Altunoğlu (Kafkas University, Faculty of Sciences and Letter, Department of Biology, Kars), the aerial parts were dried in a dry place for two weeks. Dried plants were powdered using an electric blender.

Ethyl acetate/hexane extraction

The plant extract was obtained using a Soxhlet extraction system. The conventional Soxhlet method, which requires minimal training, allows for getting more sample mass and eliminates the need for filtration after the leaching process (Luque de Castro & Priego-Capote, 2010). Briefly, forty (40) grams of the herb were weighed, wrapped in filter paper, and placed in a soxhlet apparatus. Ethyl acetate and n-hexane (3:1 v/v) were used as solvents. The system's temperature reached the optimum level, and the extraction process was terminated after three hours. The remaining solvent in the extract was vaporized at 60 °C in a rotary evaporator until removed entirely. Before testing, dilutions of the ethyl acetate/hexane extract (SoxEHE) (10, 1, 0.1, 0.01, and 0.001 mg/mL) were prepared.

Extraction by method of decoction

In this study, a 2% extract of the plant material was prepared. Twenty grams of the plant were weighed and transferred to a teapot. After adding 1 liter of cold distilled water, the mixture was allowed to come to a boil. After boiling, it was waited for 10 minutes and allowed to cool to room temperature. It was filtered through filter paper to avoid residue (Üstü & Uğurlu, 2018). Dilutions (20, 2, 0.2, 0.02, and 0.002 mg/ml) were prepared from decoction extract (DE) immediately before test.

L929 fibroblast cell proliferation and viability analysis

The L929 (mouse fibroblast cell, ATCC CCL-1) cell line was purchased from the American Type Culture Collection (ATCC, USA) and was used for the experiments. In the liquid nitrogen tank, the cell lines on the cryotube were removed from the tank and kept in a water bath for a short period to dissolve at 37°C. The dissolved cells were cultured in Dulbecco's Modified Eagle's Medium (DMEM) supplemented with 10% fetal bovine serum in 75 cm² plastic flasks. After 48 h, L929 cells were counted in DMEM containing 10% FBS at a density of 2x10⁵ cells/well, and plated in a well plate with 96 wells, and incubated at 37°C in a humid atmosphere containing 5% CO₂. For 24 h, the effects of DE concentrations (20, 2, 0.2, 0.02, and 0.002 mg/mL) and SoxEHE concentrations (10, 1, 0.1, 0.01, and 0.001 mg/mL) in L929 cells were investigated using the MTT method to determine toxic doses of decoction extracts (dissolved in pure water) and ethyl acetate (dissolved in 0.01% DMSO and applied to cells). After the appropriate doses were determined, the cells were planted again in a well plate with 96 wells. For 24 h, the cells were exposed to 2 mg/mL and 0.2 mg/mL decoction and 0.01 mg/mL and 0.001 mg/mL ethyl acetate extracts at different concentrations, and then 3 hours later, H₂O₂ (0.75 mM) was added to the media (Sudsai et al., 2016). After the MTT method was applied to the cells, at the 24th hour, the absorbance was read in each well at 620 nm using a microtiter plate ELISA reader (Epoch Microplate Spectrophotometer, BioTek, USA). The assays were performed a minimum of three times for each repetition. The survival rates of L929 cells were analyzed by comparing them with those of the control wells.

Migration test

The migration of L929 fibroblast cells was examined using the wound healing method. Briefly, L929 cells (2x10⁵ cells/mL) in DMEM containing 10% FBS were seeded into each well of a 24-well plate and in-

cubated at 37°C and 5% CO₂. When the cells formed a complete monolayer in the wells, a scratch was created horizontally in each well with a sterile pipette tip. Cellular debris was removed by washing with PBS and replaced with 2 mL of fresh medium without adding test samples. On day 0, images were taken using the Invitrogen Inverted Microscope, and the wells were photographed at 0, 12, and 24 h by keeping them in the incubator.

Determination of oxidant/antioxidant parameters (MDA, GSH)

L929 cells (2x10⁵ cells/mL) were seeded in each well of 6-well plates (separately for the analysis of MDA and GSH) and incubated in a humid environment containing 5% CO₂ at 37°C. Cells were harvested from 6-well plates using a scraping method and stored at -80°C. Approximately 100 mg of cell lysate

from each group was homogenized with Tissue Lyser on ice in a specific homogenate buffer. The samples were then centrifuged. For biochemical studies, while MDA levels in supernatants were measured colorimetrically using the methods reported by Yoshioka et al. (1979), GSH levels were measured colorimetrically as described by Beutler et al. (1963).

Gene expression analysis by RT-PCR

Total RNA was extracted from actively growing cells using TRIzol Reagent (Sigma). This RNA was then treated with RQ1 DNase I (Promega). Reverse transcription (RT) was carried out following the manufacturer’s instructions (Fermentas) and involved using 1 unit of MMLV reverse transcriptase along with 5 µg of total RNA. Subsequently, the cDNA region corresponding to the COL1A1 protein was amplified using the F and R primers (Table 1).

Table 1. COL1A1 primer list.

Primer Name	Primer List	Tm
COL1A1F	GGCACTCCCGGACCTCAAG	64
COL1A1R	CGGTCACCGTTCTTGCCAG	62

Statistical analysis

Statistical analysis was conducted using Microsoft Excel, and the results were presented as the mean ± standard deviation. For data analysis, one-way variance analysis (ANOVA) was performed using the IBM 25.00 SPSS statistical program, followed by Tukey’s test. p < 0.05 was considered as significant.

RESULTS AND DISCUSSION

Proliferation of L929 and viability analysis

In this study, when the effects of decoction and ethyl acetate extracts on cell proliferation were evaluated separately, DEs demonstrated cytotoxic effects at 20 mg/mL and 2 mg/mL (p<0.05). At doses of 0.2 mg/mL and below, the cytotoxic effect in healthy fibroblast cells began to disappear (Figure 1). The efficacy of 0.2 mg/mL, 0.02 mg/mL, and 0.002 mg/mL were statistically similar (p>0.05). Therefore, we decided to use DE at concentrations of 0.2, and 0.02 mg/

mL in the later stages of our study. The cytotoxic effect of SoxEHEs on healthy fibroblast cells at doses of 10 mg/mL and 1 mg/mL is shown in Figure 1 (p<0.05). This cytotoxic effect was observed to be eliminated at 0.1 mg/mL and lower doses. The effects of SoxEHE at doses of 0.1, 0.01, and 0.001 mg/mL were statistically similar (p>0.05). Therefore, SoxEHE was found to be effective at doses of 0.1 mg/mL, and 0.01 mg/mL.

The effect of H₂O₂ on L929 cells

Analysis of Figure 1 revealed a notable reduction in cell viability in the presence of 0.75 mM H₂O₂, indicating a significant difference compared to the control group (p<0.05). The decoction extract significantly improved cell viability by protecting H₂O₂ damage, especially at a dose of 0.2 mg/mL (p<0.05). Ethyl acetate/hexane extract maintained cell viability significantly against oxidative damage induced by H₂O₂ at a dose of 0.1 mg/mL (p<0.05). Both extracts showed lower effectiveness at decreasing the doses.

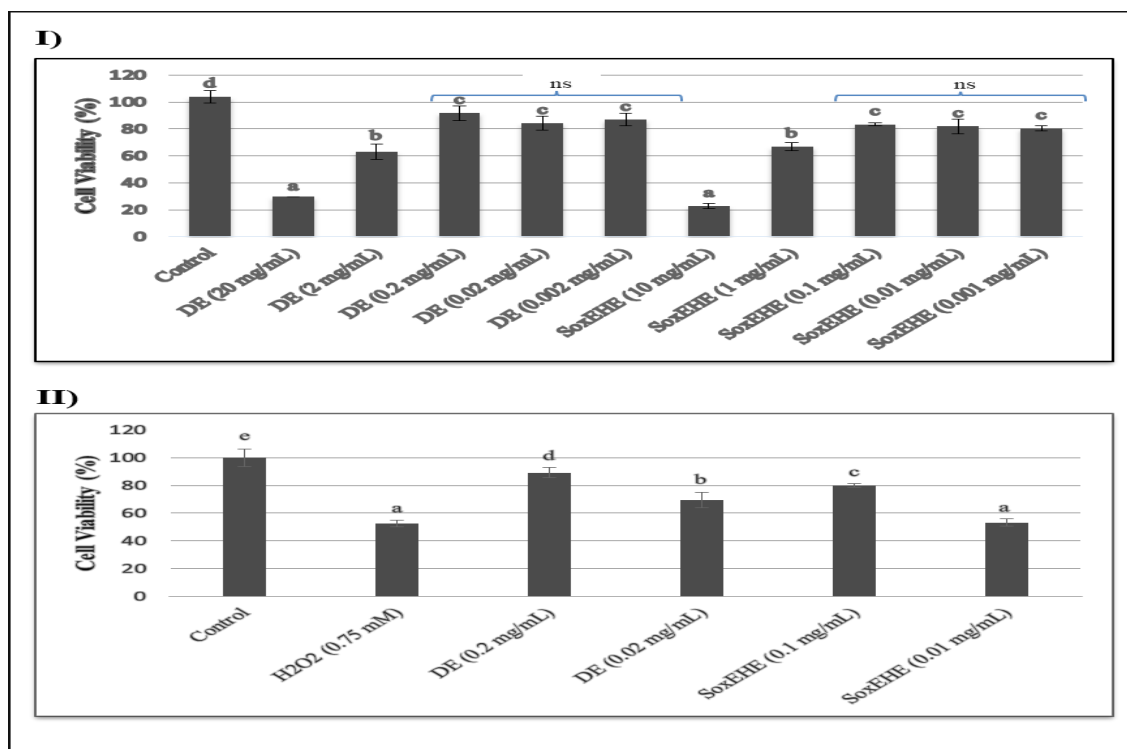


Figure 1. Determination of proliferative and cytotoxic doses of plant extracts (I) and indicating the protective effects of plant extracts against H₂O₂-induced damage (II) on L929 cells (if the letters in the columns are the same, the difference between them is statistically insignificant, p>0.05 ns: the groups included in the line are meaningless with each other, H₂O₂: Hydrogen peroxide, DE: Decoction extract, SoxEHE: Soxhlet ethyl acetate/hexane extract).

Migration test results

An *in vitro* migration test, known as the wound healing test, was conducted to assess how the plant extract influenced the movement of L929 cells toward the scratched area, often referred to as the injury site. According to the results, healthy fibroblast cells exhibited a nearly complete closure tendency by migrating to the wounded area within 24 hours (Figure 2.I; A1-C1). In L929 cells treated with only hydrogen peroxide, it was observed that cell migration was prevented, and this was statistically significant (p<0.05) in the

measurements made at the 12th and 24th hours (Figure 2.I; A2-C2). H₂O₂ showed both a cytotoxic effect by creating oxidative damage and caused the wound to not heal by preventing cell migration. In both doses of DE applied, cell migration to the wounded area significantly increased. Unlike the MTT results, there was more healthy migration, especially at the dose of 0.02 mg/mL (p<0.05) (Figure 2.II; A2-C2). In groups where SoxEHE was applied, cell migration increased in both doses, while it significantly increased cell migration against H₂O₂ at a dose of 0.1 mg/mL (Figure 2.III;A2-C2, 3).

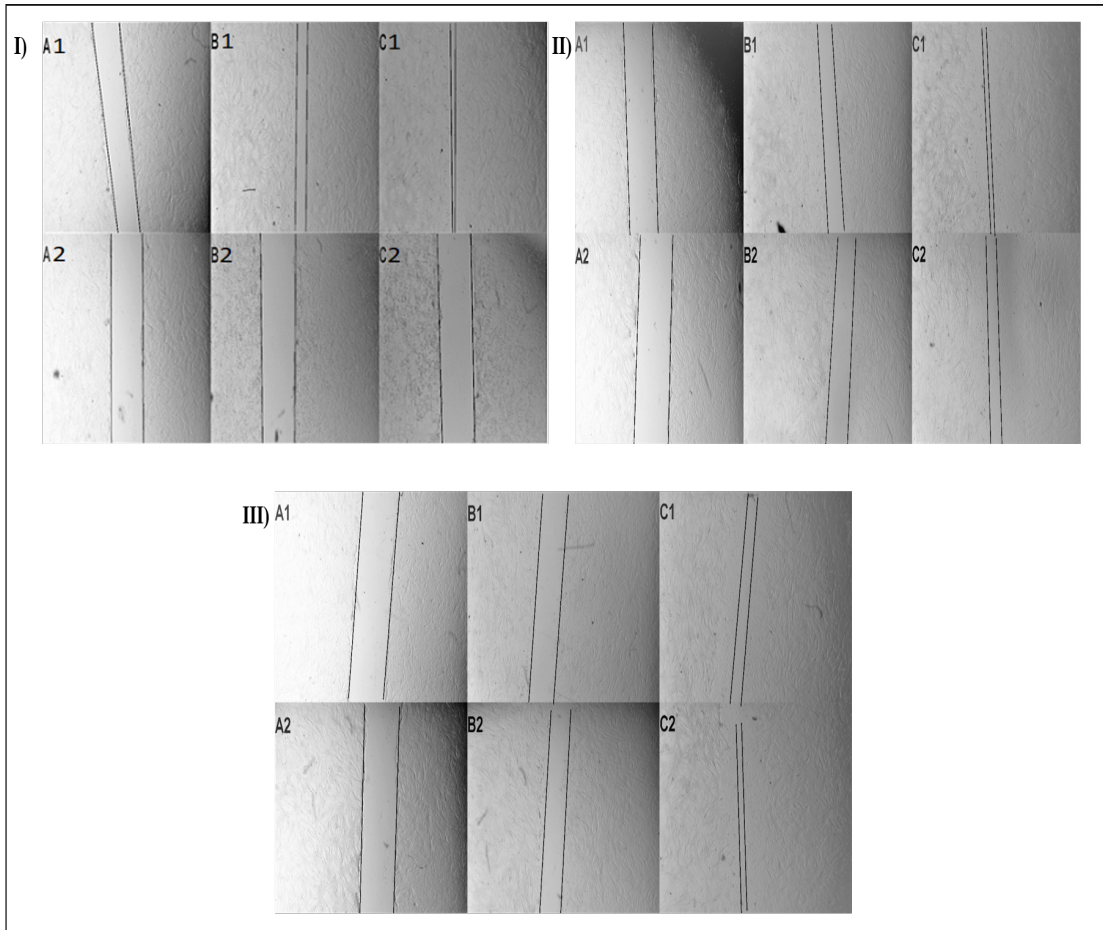


Figure 2. Illustrating of the cell migration under a scratch assay (wound healing method), **I)** the migration of healthy cells (A1: 0th time, B1: 12th hour, C1: 24th hour) and the effect of H₂O₂ application on the cell migration (A2: 0th time, B2: 12th hour, C2: 24th hour), **II)** the effect of DEs (A1: 0.02 mg/mL; 0th time, B1: 0.02 mg/mL; 12th hour, C1: 0.02 mg/mL; 24th hour, A2: 0.2 mg/mL; 0th time, B2: 0.2 mg/mL; 12th hour, C2: 0.2 mg/mL; 24th hour) and **III)** the effect of SoxEHEs (A1: 0.01 mg/mL; 0th time, B1: 0.01 mg/mL; 12th hour, C1: 0.01 mg/mL; 24th hour, A2: 0.1 mg/mL; 0th time, B2: 0.1 mg/mL; 12th hour, C2: 0.1 mg/mL ;24th hour) on cell migration against H₂O₂-induced damage.

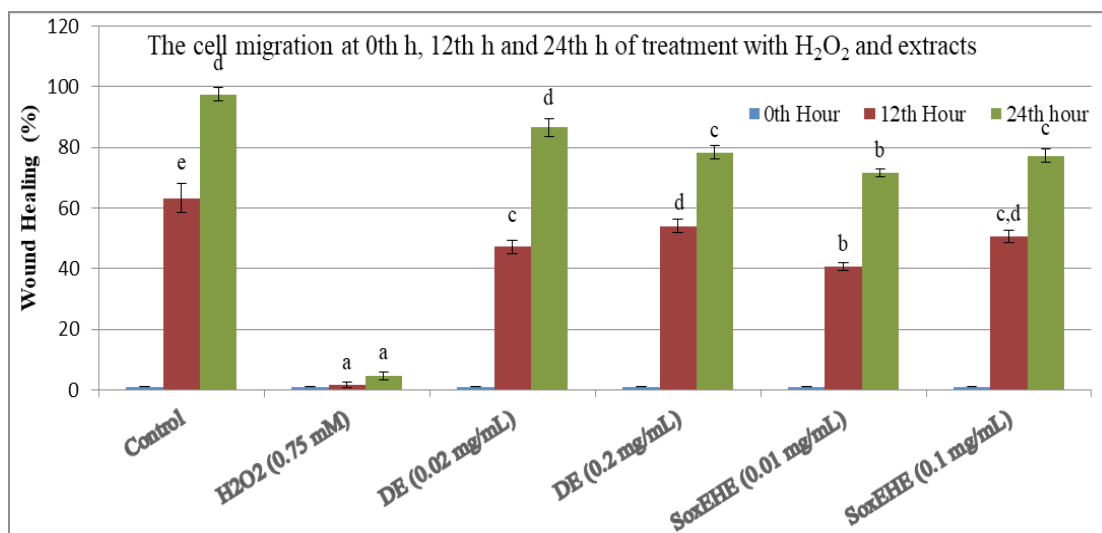


Figure 3. Demonstration of the effect of plant extracts on cell migration in an *in vitro* scratch assay (wound healing method) against damage induced by H₂O₂ in L929 cells as % (If the letters in the columns are the same, the difference between them is statistically meaningless p>0.05, H₂O₂: Hydrogen peroxide, DE: Decoc-tion extract, SoxEHE: Soxhlet ethyl acetate/hexane extract).

Results of MDA and GSH

When the levels of MDA as a signal of lipid per-oxidation were examined in the L929 cell line, it was observed that the highest level (p<0.05) was in the ox-idative stress-induced cell line compared to other cell lines (Fig. 4.). In the cell lines, where the effect of plant extract on oxidative stress was observed, MDA levels were significantly lower (p<0.05) compared to the cell line where only H₂O₂ was applied, but they varied among themselves. The lowest MDA levels in these cell lines (except for the control cell line) were seen in DE (0.02 mg/mL) + H₂O₂ and SoxEHE (0.1 mg/mL) + H₂O₂ cell lines. These results indicated that 0.02 mg/mL concentration of DE and 0.1 mg/mL concentra-

tion of SoxEHE were effective on lipid peroxidation.

When the levels of the tripeptide antioxidant GSH were analyzed in all cell lines, statistically elevated levels (p<0.05) were observed exclusively in the ext-racted cell lines. This finding indicated the effective-ness of plant extracts in enhancing antioxidant capa-city (Fig. 4.). The GSH levels of the plant extract and H₂O₂-treated cell lines decreased statistically (p<0.05) to almost the level of the cell line applied to H₂O₂ alone (except SoxEHE (0.01 mg/mL) + the H₂O₂ cell line) compared to only the plant extract used cell lines. This finding could be explained by GSH depletion during oxidative stress.

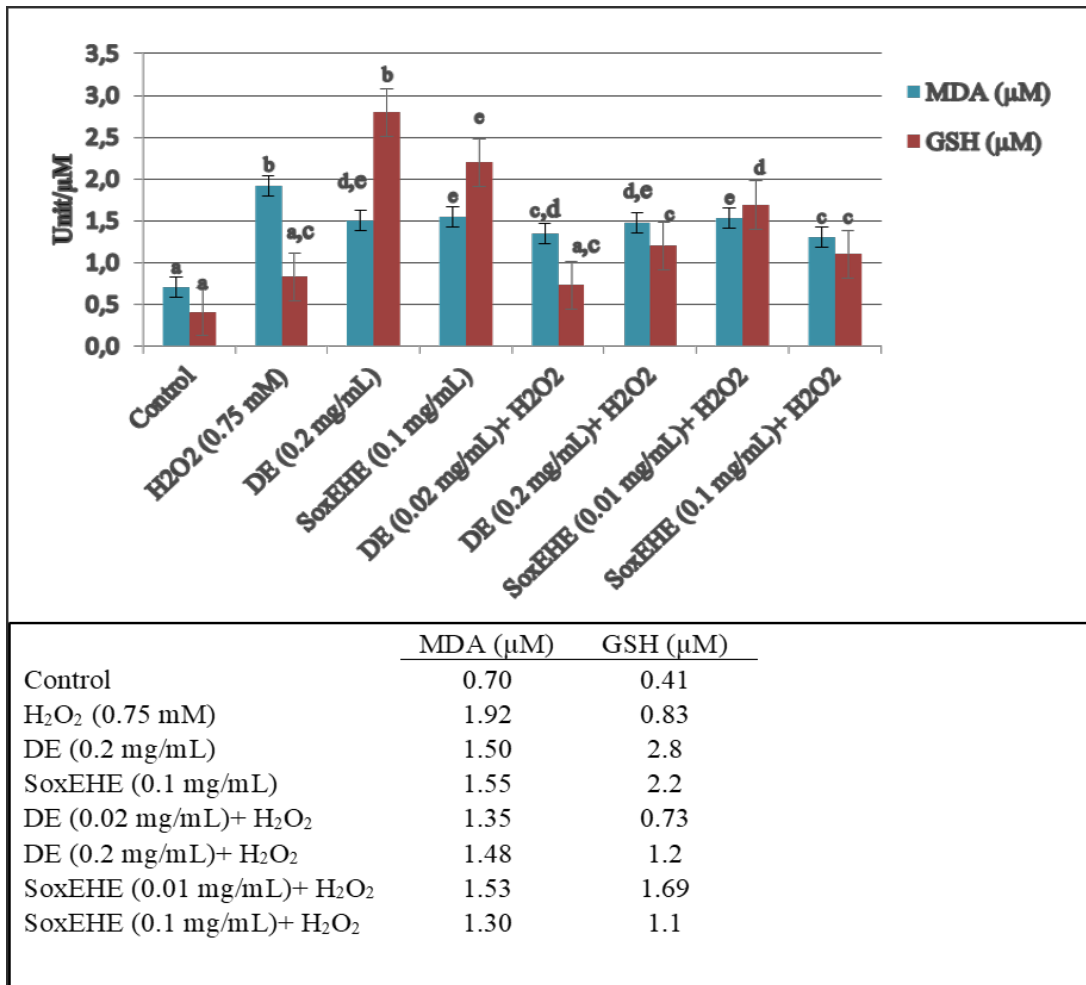


Figure 4. Effect of plant extracts on MDA and GSH levels in an *in vitro* wound healing model against damage caused by H₂O₂ in L929 cells. (If the letters in the columns are the same, the difference between them is statistically insignificant $p > 0.05$, DE: Decoction extract, SoxEHE: Soxhlet ethyl acetate/hexane extract).

mRNA distribution of COL1A1

The mRNA expression levels of COL1A1 were investigated using RT-PCR. The increase in COL1A1 levels in these cell lines (except for the control cell line) were seen in DE (0.2 mg/mL) + H₂O₂ and SoxEHE (0.1 mg/mL). These results indicated that 0.2 mg/mL concentration of DE and 0.1 mg/mL concen-

tration of SoxEHE were effective on wound healing (Figure 5). The level of the GAPDH transcript was the same at all time intervals (Figure 5). When COL1A1 levels as collagen were analyzed in all cell lines, it was found that high levels were only present in the extracted cell lines, therefore, plant extracts were effective in improving collagen capacity (Figure 5).

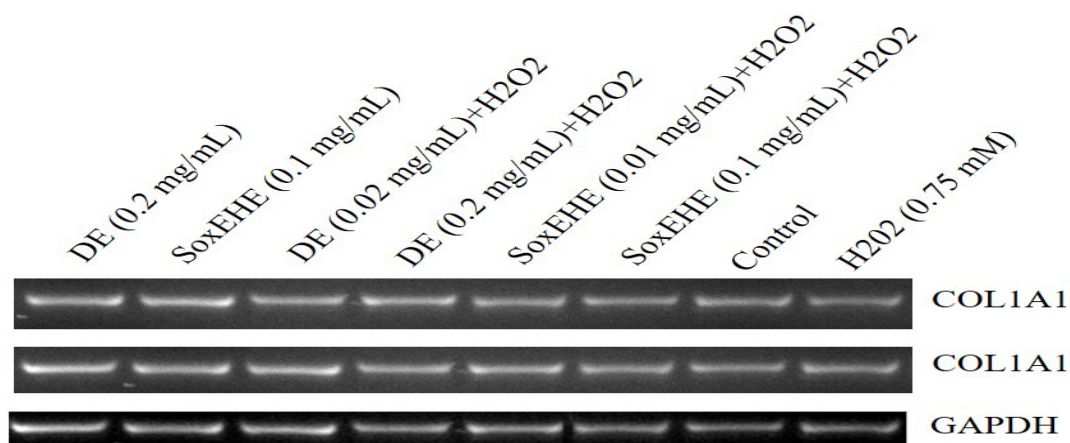


Figure 5. mRNA distribution of COL1A1.

A large percentage of the human population worldwide tends to use herbal medicines because they find them more reliable and easier to access. They also realize synthetic drugs and their side effects. Throughout history, many plant extracts, mixtures, porridge, boiling, and pastes have been used in many countries for the treatment of diseases, cuts, wounds, and burns. Therefore, since ancient times, several herbs and plant-based strategies have been known for their important roles in wound healing and skin regeneration, as well as in their therapeutic application (Barku, 2019).

Scratch testing in fibroblast cell cultures is a method that is widely applied to identify components of wound healing that have been investigated (Liang et al., 2007). Oxidative stress induced by hydrogen peroxide serves as an alternative to assess the antioxidant activity in cells and to delay stress-induced wound healing (Pitz et al., 2016). In this study, *I. viscosa* extracts prepared using different methods were used to test the activity of fibroblast scratch wound healing in H₂O₂-induced L929 cells and the effects of H₂O₂-induced oxidative stress.

As cell proliferation and migration are crucial aspects of tissue formation in the wound healing process, it was essential to establish the non-toxic dosage of the extracts within the specific cell line under investigation for their therapeutic efficacy. Therefore, initi-

ally, the effects of the extracts on the proliferation and cell viability of L929 fibroblast cells were determined. It was determined that dilutions of 0.2 mg/mL and lower for DEs, and 0.1 mg/mL and lower for SoxEHEs were non-toxic, with cell viability exceeding 80%.

In a study in which the cell viability of *I. viscosa* extracts obtained by two different methods was examined using the XTT method, it was reported that 50 µg/mL decoction extract produced a cell viability of over 80% in the L929 fibroblast cell line (Hepokur et al., 2019). The results of this study are consistent with those of our research.

At the concentrations tested in our study, 20 mg/mL of DE and 10 mg/mL of SoxEHE were considered to have cytotoxic effects in the L929 fibroblast cell line (Figure 1). Therefore, it is plausible that extracts or purified phytochemicals obtained from the *Inula* genus may possess antiproliferative properties (Messaoudi et al., 2016; Talib et al., 2012).

Free radicals formed at the basal level during wound healing are necessary for cell signaling and the fight against invasive microorganisms. H₂O₂ facilitates the recruitment of leukocytes to the wound site as a chemoattractant after injury formation, and also participates in the subsequent stages of healing. (Schäfer & Werner, 2008) in particular aged individ-

uals, patients with diabetes, and those treated with immunosuppressive drugs, chemo- or radiotherapy. The mechanisms underlying the impaired healing response are still poorly understood. Recent studies provided strong evidence for a role of oxidative stress in the pathogenesis of non-healing ulcers. Therefore, it is of major importance to identify and functionally characterize the factors involved in the generation and detoxification of ROS. When an excessive amount of free radicals is produced, a condition called oxidative stress occurs, which disrupts the structural integrity of the cell by damaging DNA, carbohydrates, proteins, and especially lipid structures in membranes. Therefore, wound healing is delayed, or the wound cannot heal (Shetty et al., 2008).

Oxidative stress originating from hydrogen peroxide is an alternative method for evaluating the antioxidant activity of extracts in cells (Jose et al., 2019). The determination of MDA, a technique used to measure oxidative stress, is based on the reaction of malondialdehyde formed through peroxidation of polyunsaturated fatty acids with thiobarbituric acid (Yoshioka et al., 1979). In the present study, MDA levels were higher in all groups compared to the control, but the highest level was only in the H₂O₂-treated cell line without statistical difference. This indicates that H₂O₂ induced oxidative stress in this group. Increased ROS levels can inhibit cell migration and proliferation (Steiling et al., 1999). The absence of cell migration and proliferation at the 12th and 24th hours in the group treated with H₂O₂ alone led to the consideration of oxidative stress and the cytotoxic effect of H₂O₂. The levels of MDA in the DE (0.2 mg/mL), SoxEHE (0.1 mg/mL), and extract + H₂O₂ groups were not significantly different. In addition, the fact that cell migration and proliferation were close to the control in groups with oxidative stress and extract shows that the extracts have a positive effect against oxidative stress.

Antioxidants are protein systems designed to counteract the harmful effects of ROS by providing electrons. Therefore, they prevent the capture of elec-

trons from other important molecules such as DNA, proteins, and lipids (Dunnill et al., 2017). Antioxidants include antioxidant enzymes such as GSH reductase, GSH peroxidase, superoxide dismutase (SOD), catalase, and other endogenous free radical scavengers such as α -tocopherol, ascorbic acid, and GSH (Arul et al., 2012). The H₂O₂ effect is an interwoven healing process that is controlled by molecular antioxidants such as SOD, GPx, and phospholipid hydroperoxide glutathione peroxidase (Pitz et al., 2016). Glutathione is an important endogenous antioxidant. It functions as a cellular redox buffer and is crucial in protecting cells from the toxic effects of both endogenous and exogenous electrophilic compounds. (Schäfer & Werner, 2008) in particular aged individuals, patients with diabetes, and those treated with immunosuppressive drugs, chemo- or radiotherapy. The mechanisms underlying the impaired healing response are still poorly understood. Recent studies provided strong evidence for a role of oxidative stress in the pathogenesis of non-healing ulcers. Therefore, it is of major importance to identify and functionally characterize the factors involved in the generation and detoxification of reactive oxygen species (ROS).

In the study, GSH levels were the highest in the DE (0.2 mg/mL) and SoxEHE (0.1 mg/mL) groups compared to other groups. *In vitro* experimental studies have shown that the extract or purified phytochemical compounds obtained from *I. viscosa* have antioxidant activity (Danino et al., 2009; Mohti et al., 2020; Schinella et al., 2002). Although there were no statistical differences between the extract + H₂O₂ groups in terms of GSH levels, there is a statistical decrease ($p < 0.05$) in GSH levels compared to the DE (0.2 mg/mL) and SoxEHE (0.1 mg/mL) groups. The fact that the MDA levels were lower than those of the H₂O₂ group suggests that GSH may have been depleted during migration. The functional importance of antioxidants such as glutathione, ubiquinones, uric acid, lipoic acid, vitamins E and C (ascorbic acid), carotenoids, and phenolic compounds in the wound repair process is suggested by their depletion in healing skin

wounds (Schäfer & Werner, 2008) in particular aged individuals, patients with diabetes, and those treated with immunosuppressive drugs, chemo- or radiotherapy. The mechanisms underlying the impaired healing response are still poorly understood. Recent studies provided strong evidence for a role of oxidative stress in the pathogenesis of non-healing ulcers. Therefore, it is of major importance to identify and functionally characterize the factors involved in the generation and detoxification of ROS. In a study in which the L929 fibroblast cell line was treated with the GSH blocker, buthionine sulfoximine, cell death occurred following GSH depletion, and GSH protected the cells from death (Zucker et al., 1997). In another study, wounds were reported to heal faster when GSH was applied topically to wounds in diabetic rats. These studies have shown that glutathione benefits wound repair (Mudge et al., 2002).

Fibroblasts, the primary cell type in the dermis, are responsible for the production and remodeling of the extracellular matrix during wound healing. Collagen, type III, alpha 1 (COL3A1) and Collagen, type I, alpha 1 (COL1A1) are well-established as major constituents of the extracellular matrix (ECM) found in the dermal tissues of the skin (McFarland et al., 2011). Beare et al. (2003) observed that the wounds of mice with a mutant collagen type-I gene (COL1A1^{tr}) healed more slowly than those of wild-type mice. Hashimoto et al. (2020) reported that the COL3A1 gene was down-regulated on all surfaces throughout the cell culture. Their research did not reveal any significant variances in the expression of the COL1A1 gene among the three different surfaces in the cell culture. In the present study, we investigated the effect of this collagen (COL1A1) in wound healing. The increase in COL1A1 levels in these cell lines (except for the control cell line) were seen in DE (0.2 mg/mL) + SoxEHE (0.1 mg/mL). These results indicated that the concentration of 0.2 mg/mL for DE and 0.1 mg/mL for SoxEHE were effective in wound healing (Figure 5.). The level of the GAPDH transcript was the same at all time intervals (Figure 5.). When COL1A1 levels as collagen were analyzed in all

cell lines, it was found that high levels were only present in the extracted cell lines. Therefore, plant extracts were effectively improved collagen capacity (Figure 5). In another study, it was reported that COL1A1 and COL3A1 levels increased in parallel with the formation of the fibroblast cell layer (Wiegand et al., 2021).

According to the literature, the antioxidant, antibacterial, and other biological activities of *I. viscosa* are known to originate from sesquiterpenes, triterpenoids, and flavonoids. Mohti et al. (2020) reported that extracts obtained from *I. viscosa* exhibited strong antioxidant properties through various techniques, attributing this effect to the phenolic acid and flavonoid derivatives present in the extracts. Similarly, Mahmoudi et al. (2016) found that the methanolic extract of *I. viscosa* leaves possessed a phenolic profile, particularly rich in mono- and dicaffeoylquinic acids, indicating a high antioxidant capacity of the extract. In another study, Khalil et al. (2007) suggested that *I. viscosa* extract promoted the healing of excision wounds in mice, proposing that this effect could be attributed to the anti-inflammatory properties of inuviscolide, a sesquiterpene found in the extract. In our study, we think that the proliferative and antioxidative effects of *I. viscosa* extracts originate from these flavonoids and sesquiterpenes.

CONCLUSION

Different extraction methods can unearth various phytochemicals in plants. Decoction extraction is less costly than Soxhlet extraction (in terms of chemicals and equipment). In our study, it was observed that extracts obtained from *I. viscosa* plant exhibited a positive effect on both migration and oxidative stress parameters in the L929 cell line, where oxidative stress occurs. In this context, *I. viscosa* may be a potential agent for the treatment of wounds. However, further investigation through preclinical and clinical studies is necessary to explore this in more detail.

ACKNOWLEDGEMENTS

We thank Asst. Prof. Mustafa Kemal Altunoğlu.

CONFLICT OF INTEREST

The authors declare that there is no conflict of interest.

AUTHOR CONTRIBUTION STATEMENT

AH: Conceptualization; Formal analysis; Investigation; Methodology; Writing-original draft; Writing-review & editing. Data curation; Resources. **İÇ:** Conceptualization; Formal analysis; Investigation; Methodology; Resources. **MY:** Conceptualization; Formal analysis; Investigation; Methodology; Resources. **SH:** Investigation; Resources **MB:** Investigation; Resources. **CÖ:** Investigation; Methodology; Resources; Writing-review & editing.

REFERENCES

- Abe, Y., Inagaki, K., Fujiwara, A., & Kuriyama, K. (2000). Wound healing acceleration of a novel transforming growth factor- β inducer, SEK-1005. *European Journal of Pharmacology*, 408(2), 213–218. [https://doi.org/10.1016/S0014-2999\(00\)00766-4](https://doi.org/10.1016/S0014-2999(00)00766-4)
- Arul, V., Masilamoni, J. G., Jesudason, E. P., Jaji, P. J., Inayathullah, M., Dicky John, D. G., Vignesh, S., & Jayakumar, R. (2012). Glucose oxidase incorporated collagen matrices for dermal wound repair in diabetic rat models: A biochemical study. *Journal of Biomaterials Applications*, 26(8), 917–938. <https://doi.org/10.1177/0885328210390402>
- Barku, V. (2019). Wound Healing: Contributions from Plant Secondary Metabolite Antioxidants. In *Wound Healing - Current Perspectives*. IntechOpen. <https://doi.org/10.5772/intechopen.81208>
- Beare, A. H. M., O’Kane, S., Krane, S. M., & Ferguson, M. W. J. (2003). Severely impaired wound healing in the collagenase-resistant mouse. *The Journal of Investigative Dermatology*, 120(1), 153–163. <https://doi.org/10.1046/j.1523-1747.2003.12019.x>
- Beutler, E., Duron, O., & Kelly, B. M. (1963). Improved Methods for Determination of Blood Glutathione. *Journal of Laboratory Clinics Medicine*, 61, 882–888.
- Cano Sanchez, M., Lancel, S., Boulanger, E., & Nevieri, R. (2018). Targeting Oxidative Stress and Mitochondrial Dysfunction in the Treatment of Impaired Wound Healing: A Systematic Review. *Antioxidants (Basel, Switzerland)*, 7(8), 98. <https://doi.org/10.3390/antiox7080098>
- Danino, O., Gottlieb, H. E., Grossman, S., & Bergman, M. (2009). Antioxidant activity of 1,3-dicaffeoylquinic acid isolated from *Inula viscosa*. *Food Research International*, 42(9), 1273–1280. <https://doi.org/10.1016/j.foodres.2009.03.023>
- Dunnill, C., Patton, T., Brennan, J., Barrett, J., Dryden, M., Cooke, J., Leaper, D., & Georgopoulos, N. T. (2017). Reactive oxygen species (ROS) and wound healing: the functional role of ROS and emerging ROS-modulating technologies for augmentation of the healing process. *International Wound Journal*, 14(1), 89–96. <https://doi.org/10.1111/iwj.12557>
- Frykberg, R. G., & Banks, J. (2015). Challenges in the Treatment of Chronic Wounds. *Advances in Wound Care*, 4(9), 560–582. <https://doi.org/10.1089/wound.2015.0635>
- Gurtner, G. C., Werner, S., Barrandon, Y., & Longaker, M. T. (2008). Wound repair and regeneration. *In Nature* (Vol. 453, Issue 7193). <https://doi.org/10.1038/nature07039>
- Hashimoto, T., Kojima, K., & Tamada, Y. (2020). Higher Gene Expression Related to Wound Healing by Fibroblasts on Silk Fibroin Biomaterial than on Collagen. *Molecules (Basel, Switzerland)*, 25(8). <https://doi.org/10.3390/molecules25081939>

- Hepokur, C., Budak, Y., Karayel, H. basri, Selvi, B., & Yaylim, İ. (2019). Investigation of Cytotoxic Effects of *Inula viscosa* Extract. *Cumhuriyet Science Journal*, 40(3), 578–582. <https://doi.org/10.17776/csj.437993>
- Jose, G. M., Raghavankutty, M., & Kurup, G. M. (2019). Attenuation of hydrogenperoxide-induced oxidative damages in L929 fibroblast cells by sulfated polysaccharides isolated from the edible marine algae *Padina tetrastromatica*. *Journal of Bioactive and Compatible Polymers*, 34(2), 150–162. <https://doi.org/10.1177/0883911519835144>
- Khalil, E. A., Afifi, F. U., & Al-Hussaini, M. (2007). Evaluation of the wound healing effect of some Jordanian traditional medicinal plants formulated in Pluronic F127 using mice (*Mus musculus*). *Journal of Ethnopharmacology*, 109(1), 104–112. <https://doi.org/10.1016/j.jep.2006.07.010>
- Liang, C. C., Park, A. Y., & Guan, J. L. (2007). *In vitro* scratch assay: A convenient and inexpensive method for analysis of cell migration *in vitro*. *Nature Protocols*, 2(2), 329–333. <https://doi.org/10.1038/nprot.2007.30>
- Luque de Castro, M. D., & Priego-Capote, F. (2010). Soxhlet extraction: Past and present panacea. *Journal of chromatography A*. 1217(16), 2383-2389. <https://doi.org/10.1016/j.chroma.2009.11.027>
- Mahmoudi, H., Hosni, K., Zaouali, W., Amri, I., Zargouni, H., Hamida, N. Ben, Kaddour, R., Hamrouni, L., Nasri, M. Ben, & Ouerghi, Z. (2016). Comprehensive Phytochemical Analysis, Antioxidant and Antifungal Activities of *Inula viscosa* Aiton Leaves. *Journal of Food Safety*, 36(1), 77–88. <https://doi.org/10.1111/jfs.12215>
- McFarland, K. L., Glaser, K., Hahn, J. M., Boyce, S. T., & Supp, D. M. (2011). Culture medium and cell density impact gene expression in normal skin and abnormal scar-derived fibroblasts. *Journal of Burn Care and Research*, 32(4), 498–508. <https://doi.org/10.1097/BCR.0b013e3182223cb1>
- Messaoudi, M., Chahmi, N., El-Mzibri, M., Gmouh, S., Amzazi, S., Benbacer, L., & El-Hassouni, M. (2016). Cytotoxic Effect and Chemical Composition of *Inula viscosa* from Three Different Regions of Morocco. *European Journal of Medicinal Plants*, 16(4), 1–9. <https://doi.org/10.9734/EJMP/2016/28340>
- Mohti, H., Taviano, M. F., Cacciola, F., Dugo, P., Mondello, L., Marino, A., Crisafi, G., Benameur, Q., Zaid, A., & Miceli, N. (2020). *Inula viscosa* (L.) Aiton leaves and flower buds: Effect of extraction solvent/technique on their antioxidant ability, antimicrobial properties and phenolic profile. *Natural Product Research*, 34(1), 46–52. <https://doi.org/10.1080/14786419.2019.1569659>
- Mudge, B. P., Harris, C., Gilmont, R. R., Adamson, B. S., & Rees, R. S. (2002). Role of glutathione redox dysfunction in diabetic wounds. *Wound Repair and Regeneration: Official Publication of the Wound Healing Society [and] the European Tissue Repair Society*, 10(1), 52–58. <https://doi.org/10.1046/j.1524-475x.2002.10803.x>
- Pitz, H. D. S., Pereira, A., Blasius, M. B., Voytena, A. P. L., Affonso, R. C. L., Fanan, S., Trevisan, A. C. D., Ribeiro-Do-Valle, R. M., & Maraschin, M. (2016). *In vitro* Evaluation of the Antioxidant Activity and Wound Healing Properties of Jaboticaba (*Plinia peruviana*) Fruit Peel Hydroalcoholic Extract. *Oxidative Medicine and Cellular Longevity*, 2016. <https://doi.org/10.1155/2016/3403586>
- Schäfer, M., & Werner, S. (2008). Oxidative stress in normal and impaired wound repair. *Pharmacological Research*, 58(2), 165–171. <https://doi.org/10.1016/j.phrs.2008.06.004>
- Schinella, G. R., Tournier, H. A., Prieto, J. M., Mordujovich De Buschiazzi, P., & Ríos, J. L. (2002). Antioxidant activity of anti-inflammatory plant extracts. *Life Sciences*, 70(9), 1023–1033. [https://doi.org/10.1016/S0024-3205\(01\)01482-5](https://doi.org/10.1016/S0024-3205(01)01482-5)

- Seca, A. M. L., Grigore, A., Pinto, D. C. G. A., & Silva, A. M. S. (2014). The genus *Inula* and their metabolites: From ethnopharmacological to medicinal uses. *Journal of Ethnopharmacology*, *154*(2), 286–310. <https://doi.org/10.1016/j.jep.2014.04.010>
- Seca, A. M. L., Pinto, D. C. G. A., & Silva, A. M. S. (2015). Metabolomic Profile of the Genus *Inula*. *Chemistry & Biodiversity*, *12*(6), 859–906. <https://doi.org/10.1002/cbdv.201400080>
- Sen, C. K., & Roy, S. (2008). Redox signals in wound healing. *Biochimica et Biophysica Acta*, *1780*(11), 1348–1361. <https://doi.org/10.1016/j.bbagen.2008.01.006>
- Shetty, S., Udupa, S., & Udupa, L. (2008). Evaluation of antioxidant and wound healing effects of alcoholic and aqueous extract of *Ocimum sanctum* Linn in rats. *Evidence-Based Complementary and Alternative Medicine*, *5*(1), 95–101. <https://doi.org/10.1093/ecam/nem004>
- Steiling, H., Munz, B., Werner, S., & Brauchle, M. (1999). Different types of ROS-scavenging enzymes are expressed during cutaneous wound repair. *Experimental Cell Research*, *247*(2), 484–494. <https://doi.org/10.1006/excr.1998.4366>
- Sudsai, T., Wattanapiromsakul, C., & Tewtrakul, S. (2016). Wound healing property of isolated compounds from *Boesenbergia kingii* rhizomes. *Journal of Ethnopharmacology*, *184*, 42–48. <https://doi.org/10.1016/j.jep.2016.03.001>
- Talib, W. H., Abu Zarga, M. H., & Mahasneh, A. M. (2012). Antiproliferative, antimicrobial and apoptosis inducing effects of compounds isolated from *Inula viscosa*. *Molecules*, *17*(3), 3291–3303. <https://doi.org/10.3390/molecules17033291>
- Üstü, Y., & Uğurlu, M. (2018). Herbal Teas in Phytotherapy. *Ankara Medical Journal*, *18*(1), 18–21. <https://doi.org/10.17098/amj.409053>
- Wiegand, C., Hipler, U.-C., Elsner, P., & Tittelbach, J. (2021). Keratinocyte and Fibroblast Wound Healing *In vitro* Is Repressed by Non-Optimal Conditions but the Reparative Potential Can Be Improved by Water-Filtered Infrared A. *Biomedicines*, *9*(12), 1802. <https://doi.org/10.3390/biomedicines9121802>
- Yoshioka, T., Kawada, K., Shimada, T., & Mori, M. (1979). Lipid peroxidation in maternal and cord blood and protective mechanism against activated-oxygen toxicity in the blood. *American Journal of Obstetrics and Gynecology*, *135*(3), 372–376. [https://doi.org/10.1016/0002-9378\(79\)90708-7](https://doi.org/10.1016/0002-9378(79)90708-7)
- Zucker, B., Hanusch, J., & Bauer, G. (1997). Glutathione depletion in fibroblasts is the basis for apoptosis-induction by endogenous reactive oxygen species. *Cell Death and Differentiation*, *4*(5), 388–395. <https://doi.org/10.1038/sj.cdd.4400258>

Design, Development, and Characterization of Lyophilized Posaconazole-Loaded Mixed Micelles for Improved Fungal Treatment and Stability

Adesh KURANE*, Rutuja CHOUGALE**, Vibhuti THAKUR***, Kiran PATIL****, Shalaka PATKI*****, John DISOUZA*****, Ashok HAJARE*****

Design, Development, and Characterization of Lyophilized Posaconazole-Loaded Mixed Micelles for Improved Fungal Treatment and Stability

SUMMARY

Posaconazole (POS), a BCS class II drug with the low solubility of the drug prevents its absorption in the body leading to suboptimal drug levels and reduced treatment effectiveness. To address this issue, this research aimed to develop a lyophilized powder of Posaconazole-loaded mixed micelles (POS-MMs) using Pluronic F68® (PF68) and Soluplus® to enhance fungal treatment and stability. A 32-factorial design optimized the POS-MMs formulation by varying PF68 and Soluplus® concentrations. Various characterization techniques were employed, including particle size analysis, zeta potential (ZP) measurement, FTIR, DSC, and XRPD. In vitro drug release studies indicated sustained release with 79.4% released within 24 hrs, while in vitro hemolysis studies confirmed safety and biocompatibility. Lyophilization with lactose as a cryoprotectant was successful, yielding a stable formulation over three months. The optimized POS-MMs exhibited a particle size (PS) of 66.30 ± 2.10 nm, a high % entrapment efficiency (%EE) of $94.88 \pm 2.4\%$, and a desirable ZP of -51.1 ± 2.4 mV. These findings highlight the potential of POS-MMs to enhance the therapeutic outcomes of POS in the treatment of fungal infections. In addition, lyophilized powder is a promising technique for improving the stability of POS-MMs.

Key Words: Fungal infection, lyophilization, mixed micelles, posaconazole, stability.

Geliştirilmiş Mantar Tedavisi ve Stabilité için Liyofilize Posaconazol Yüklü Karışık Misellerin Tasarımı, Geliştirilmesi ve Karakterizasyonu

ÖZ

Posaconazol (POS), düşük çözünürlüğü nedeniyle ilacın vücutta absorpsiyonunun önleyerek optimal düzeyin altında ilaç seviyelerine neden olan ve tedavinin etkinliğini azaltan bir BCS Sınıf II ilaçtır. Bu sorunu çözmek için, bu araştırmada, Pluronic F68® (PF68) ve Soluplas® kullanarak hazırlanan posakonazol yüklü karışık misellerin (POS-MMs) liyofilize tozunun geliştirilmesi ile mantar tedavisinin iyileştirilmesi ve stabilitenin artırılması amaçlanmıştır. POS-MMs formülasyonları, PF68 ve soluplas® konsantrasyonları değiştirilerek 32 faktöriyel tasarım ile optimize edilmiştir. Partikül boyutu analizi, zeta potansiyel (ZP) ölçümü, FTIR, DSC ve XRPD dahil olmak üzere çeşitli karakterizasyon teknikleri uygulanmıştır. İn vitro hemoliz çalışmaları biyoyumluluğu doğrularken in vitro ilaç salım çalışmaları 24 saatte %79,4 salım ile sürekli salımı göstermiştir. Kriyoprotektan olarak laktoz ile liyofilizasyon başarılı olmuştur ve üç ay boyunca stabil bir formülasyon elde edilmiştir. Optimize POS-MM'ler, $66,30 \pm 2,10$ nm partikül boyutu (PS), $94,88 \pm 2,4$ ile yüksek yükleme kapasitesi (%EE) ve istendiği gibi $-51,1 \pm 2,4$ mV ZP sergilemiştir. Bu bulgular, POS-MM'lerin mantar enfeksiyonlarının tedavisinde POS'un terapötik sonuçlarını geliştirme potansiyelini vurgulamaktadır. Ayrıca liyofilize toz, POS-MM'lerin stabilitesini artırmak için umut verici bir tekniktir.

Anahtar Kelimeler: Mantar enfeksiyonu, liyofilizasyon, karışık miseller, posakonazol, stabilite.

Received: 23.07.2023

Revised: 27.12.2023

Accepted: 27.12.2023

* ORCID: 0009-0004-9408-9399, Department of Quality Assurance, Tatyasaheb Kore College of Pharmacy, Warananagar - 416113, Shivaji University, Kolhapur-416004, Maharashtra, India.

** ORCID: 0000-0002-6312-8066, Department of Quality Assurance, Bharati Vidyapeeth College of Pharmacy, Kolhapur- 416013, Shivaji University, Kolhapur-416004, Maharashtra, India.

*** ORCID: 0009-0009-9963-4743, Department of Quality Assurance, Tatyasaheb Kore College of Pharmacy, Warananagar - 416113, Shivaji University, Kolhapur-416004, Maharashtra, India.

**** ORCID: 0000-0002-3248-6063, Department of Quality Assurance, Tatyasaheb Kore College of Pharmacy, Warananagar - 416113, Shivaji University, Kolhapur-416004, Maharashtra, India.

***** ORCID: 0009-0009-2862-9015, Department of Pharmaceutics, Tatyasaheb Kore College of Pharmacy, Warananagar - 416113, Shivaji University, Kolhapur-416004, Maharashtra, India.

***** ORCID: 0000-0002-9807-7932, Department of Pharmaceutics, Tatyasaheb Kore College of Pharmacy, Warananagar - 416113, Shivaji University, Kolhapur-416004, Maharashtra, India.

***** ORCID: 0000-0002-2728-6155, Department of Pharmaceutics, Bharati Vidyapeeth College of Pharmacy, Palus, Sangli- 416310, Dr. Babasaheb Ambedkar Technological University, Lonere, Maharashtra, India.

° Corresponding Author; Kiran S. PATIL
E-mail: kspatil.tkcp@gmail.com

INTRODUCTION

Posaconazole (POS), a broad-spectrum antifungal agent, has shown great potential in treating various fungal infections. However, its inherent physico-chemical instability, particularly in aqueous formulations, poses significant challenges to its storage and administration. To overcome this limitation, incorporating POS into mixed micelles (MMs) has emerged as a promising approach to enhance its stability and solubility (Ribeiro, 2022).

MMs are self-assembled structures composed of amphiphilic molecules, which form colloidal nanoparticles in aqueous media. These nanoparticles can encapsulate hydrophobic drugs within their hydrophobic core, providing an ideal environment for their protection. However, the long-term stability of such formulations remains a concern, especially during storage and transportation.

There are various ways by which stability can be achieved, such as lyophilization, spray drying, fluidized bed drying, coating, etc. Lyophilization, also known as freeze-drying, is widely used in pharmaceutical formulation and preservation (Kuperkar, 2022). It involves the removal of water from a sample by sublimation under reduced pressure and low temperatures, resulting in the formation of a dry, stable product (Trenkenschuh, 2021)

The previous literature revealed that POS micelles have been developed using Tween 80 as a surfactant. However, concerns arise due to the cytotoxic effects of Tween 80 at high concentrations or prolonged exposure, potentially affecting cell viability and function. Moreover, Tween 80 can lead to micelle aggregation, precipitation, and phase separation, impacting long-term stability (Thakral, 2021). Allergic reactions, including skin irritation and itching, can occur with Tween 80-containing micelles. Alternatively, researchers have utilized TPGS, but its limited solubility may hinder its effectiveness as a solubilizing agent, especially for poorly soluble drugs. Additionally, the thin-film hydration technique employed for micelle

preparation can be time-consuming, labor-intensive, and prone to batch-to-batch variability, potentially affecting micelle properties and drug stability (Vinchurkar, 2021). These considerations highlight the need for exploring alternative surfactants and simplified micelle preparation methods to overcome these limitations. MMs exhibit multifunctionality by offering solubilization of hydrophobic drugs, improving drug bioavailability, and providing controlled drug release, making them versatile drug delivery systems (Jin, 2022).

Hence, this research aims to utilize the scalable solvent evaporation method to prepare Posaconazole loaded mixed micelles (POS-MMs) using novel Pluronic F68 (PF68) and Soluplus®. This will be achieved by employing a 3² full factorial design, followed by thorough characterization of the resulting MMs, to enhance the treatment of various fungal infections. The full factorial design is a prevalent and efficient approach used to understand the influence of multiple factors, and their interactions, and to prevent batch failure. It enables systematic analysis and process optimization. Further, research work is extended to lyophilize the liquid formulation to convert the stable solid POS-MMs form to improve its long-term storage.

MATERIAL AND METHODS

Materials

POS was kindly supplied by Lupin, Mumbai. PF68 and Soluplus® were procured from Sigma Aldrich and BASF, respectively. Analytical grade Methanol and distilled water were purchased from Fine Chemical, Mumbai. Lactose was purchased from Sigma-Aldrich.

Critical micelle concentration determination

The Critical Micelle Concentration (CMC) of PF68, Soluplus®, and their combination was determined using the iodine UV-visible spectrophotometric technique. KI/I₂ solution was added to different copolymer solutions, and absorbance was measured at 366 nm using a UV-visible spectrophotometer (Agilent 1800) (Suzuki, 2023).

Preparation of POS-MMs

The solvent evaporation technique was used for the preparation of POS-MMs. To prepare POS-MMs, 10 mg of POS, 10 mg of Soluplus®, and 95 mg of PF68 were combined with 2 mL of methanol and subjected to sonication for 5 min. The resulting mix was then gradually added to 10 mL of deionized distilled water and stirred for 6 hrs at room temperature, enabling methanol to evaporate. Afterward, the mixture was centrifuged at 2000 rpm for 5 min, and the supernatant was collected to analyze the % entrapment efficiency (%EE), particle size (PS), and Zeta potential (ZP) (Patil, 2022; Ugwu, 2022).

Optimization of the formulation

Optimization of formulation has a great influence on the composition and development method of

MMs. A 3² factorial design was employed, using Design Expert® VR software, to examine how different formulations impact micelle properties. Nine unique combinations were investigated, with each formulation parameter set at three levels (-1, 0, +1) for PF68 concentration and Soluplus® concentration. The evaluation focused on two dependent variables: PS (Y₁) and %EE (Y₂). Preliminary studies were conducted before the implementation of the experimental design to select three levels of independent variables. During optimization using experimental design, the formulation components and other processing variables were kept constant. The coded levels translated to the experimental units, experimental runs, and their factor combinations considered in the present study are summarized in Table 1 (Hajare, 2021).

Table 1. Levels of independent variables in 3² factorial design

Coded Values Level	Independent Variables values	
	Factor 1 (X ₁) PF68 Concentration (mg)	Factor 2 (X ₂) Soluplus® Concentration (mg)
-1	0.8	0.06
0	1.1	0.08
+1	1.4	0.10

Characterization of POS-MMs

%Entrapment efficiency and %drug loading capacity

The micellar dispersion underwent a process to assess the drug %entrapment capability of the micelles.

$$\%EE = \frac{(Weight\ of\ encapsulated\ POS)}{Weight\ of\ POS\ used\ for\ micelle\ preparation} \times 100 \quad \text{Eq. (1)}$$

$$\%DLC = \frac{Weight\ of\ encapsulated\ POS}{Weight\ of\ POS\ used\ for\ micelle\ preparation + combined\ weight\ of\ both\ PF68\ and\ Soluplus^{\circledR}} \times 100 \quad \text{Eq. (2)}$$

Where,

Weight of feeding POS = Quantity of POS that is added to the formulation

Weight of total polymers = Combined weight of both PF68 and Soluplus®

The amount of encapsulated POS was measured spectrophotometrically at 262 nm after dilution with methanol. The %EE and percent drug loading capacity (%DLC) were determined using the following formulas. (Patil, 2021):

Particle size and zeta potential measurements

The Horiba particle size analyzer was employed to assess the PS and ZP of the MMs. The PS was determined using dynamic light scattering (DLS). To perform PS analysis, 1 mL of the supernatant obtained from the POS-MMs was diluted with deionized dis-

tilled water to a final volume of 10 mL and then subjected to analysis using the particle size analyzer (Jain, 2019).

Drug-excipient compatibility study

Fourier transform infrared spectroscopy (FTIR)

The compatibility of POS, Soluplus®, and PF68 was investigated using FTIR spectroscopy. The FTIR spectra of both plain POS and final POS-MMs were recorded using an FTIR spectroscopy (Agilent, Alpha 100508) (Baviskar, 2022).

Differential scanning calorimetric study

The thermal behavior of plain POS and POS-MMs was analyzed using a differential scanning calorimeter (DSC; SDT Q600 V20.9 Build 20) with an intracooler under a dry inert nitrogen atmosphere, where powder samples were heated at 10 °C per min from 10 °C to 500 °C in hermetically sealed punctured aluminum pans (Patil, 2022).

Powder X-ray diffraction

An X-ray powder diffraction (XRPD) (Bruker D8 Advance) with Cu-K radiation ($\lambda = 1.54$) was employed for the crystallographic analysis of plain POS and POS-MMs. The diffractometer operated at a voltage of 40 kV and 50 mA, with scans conducted at 0.02° increments ranging from 5° to 100° diffraction angle (2 θ) at a rate of 1 s/step. For accurate measurements, both plain POS and POS-MMs were scanned against a zero backdrop (Hajare, 2020).

In vitro drug release study

Drug release study

The purpose of this study was to explore the drug release characteristics employing UV-visible spectrophotometry as the analytical technique. First, the calibration of the POS was carried out in pH 7.4 medium. Then calibration curve was meticulously con-

structed to derive an equation enabling the precise calculation of drug release percentages. To maintain the robustness and reproducibility of the findings, each experiment was replicated three times. Then, the release behavior of plain POS and POS-MMs was determined using the dialysis bag technique. A drug solution containing 10 mg of POS was prepared and placed in dialysis tubes with a molecular weight cut-off of 12000 Da, securely sealed to prevent leakage. The release study was conducted in a pH 7.4 medium with samples withdrawn at various time intervals (1, 2, 4, 8, and 24 hrs), and the collected samples were analyzed by measuring absorbance at 262 nm to estimate the percentage of drug release (Patil, 2023).

Drug release kinetics study:

The drug release profile of the optimized MMs batch was analyzed to calculate the coefficient of determination (R^2) and determine the appropriate model that describes its release pattern. Various models, including zero-order, first-order, Higuchi, and Korsmeyer-Peppas, were tested to assess the fitting of the release data and identify the most suitable model for the MMs formulation (Patil, 2023).

In vitro hemolysis study

Hemolysis was evaluated by measuring the hemolysis percentage using human blood samples. The process included extracting fibrinogen from a 5 mL blood sample, combining it with the 0.9% NaCl solution, centrifuging, and collecting the supernatant. Red blood cell pellets were washed, dispersed, and diluted to prepare a 2% erythrocyte pellet solution. Samples containing POS, blank PF68 and Soluplus® MMs, and POS-MMs (A1), along with positive and negative controls, were incubated, and centrifuged, and their absorbance was measured at 420 nm to quantify hemolysis. The percentage of hemolysis was calculated using the following formula (Manjusha, 2023).

$$\%Hemolysis = \frac{Absorbance\ of\ samp - Absorbance\ of\ negative\ control}{Absorbance\ of\ positive\ control - Absorbance\ of\ negative\ control} \times 100 \quad Eq. (3)$$

Lyophilization of POS-MMs

Preparation of lyophilized POS-MMs

A precisely measured volume of 1 mL of the optimized batch composition of POS-MMs (A1) was combined with 15% w/v lactose and filled into glass vials with a capacity of 3 mL and these vials were subjected to pre-freezing at a temperature of -20 °C for 12 hrs. After pre-freezing, the vials were subjected to lyophilization using a Martin Christ lyophilizer. The lyophilization process involved setting the shelf temperature at -42 °C and maintaining the condenser temperature at -50 °C. A vacuum of 0.1 mBar was applied for 48 hrs, following the protocol from previous literature. Subsequently, the dried formulation underwent secondary drying. The vials were placed in a vacuum chamber with a pressure of 0.06 mBar for 12 hrs and then sealed under vacuum (Patil, 2022).

Characterization of lyophilized POS-MMs

After the process, the final product was obtained in the form of loose cakes. These cakes were further characterized to assess particle size, %EE, % drug loading capacity (%DLC), moisture content, SEM, and reconstitution time. The stability of the POS-MMs formulation was aimed to be proved by these characterization studies (Szente, 2021).

Scanning electron microscopy (SEM)

Morphological analysis was conducted using Scanning Electron Microscopy (JEOL JSM-6360, Japan). The samples underwent fixation on a brass stub with double-sided adhesive tape, and electrical conductivity was achieved by applying a platinum coating (6 nm/min) in a vacuum (6 Pa) using a Hitachi Ion Sputter (E-1030) for 120 s at 15 mA. The SEM images were analyzed using an image analysis system (Image-Inside Ver 2.32) (Singh, 2020).

Determination of moisture content

Moisture analysis of dried products was performed using a Karl Fischer Titrator (Vigo – Matric M.D.). Accurately, 20 mL of anhydrous methanol

was transferred to the titration vessel and titrated to the endpoint. A sample of 10 µl of water, accurately measured, was used to standardize the Karl Fischer reagent. Accurately weighed samples were suspended in anhydrous methanol, and titration was carried out to the electromagnetic endpoint (Joseph, 2019).

Determination of reconstitution time

The Thiermann method was utilized to quantify the reconstitution times of lyophilized products. Each sample was reconstituted with 1 mL of sterile water for injection, and the process involved adding the solution onto the inner wall of the vial to ensure a smooth flow. Quantitative measurement determined the time required for the solution to achieve homogeneity without visible aggregates, thereby establishing the reconstitution time (Thiermann, 1998; Patil, 2023).

Stability study

Following the ICH Q1A R2 guideline for stability studies, the stability of the POS-MMs was assessed by storing them at a temperature range of 2–8 °C for 3 months (ICH Q1A(R2) guidelines, Hajare, 2021).

Statistical Analysis

Formulation and optimization data are averages of triplicates and expressed as means with \pm SDs. The influence of formulation development variables on the response variables was statistically evaluated using ANOVA at a significance level of 0.05 with the Design-Expert® version (Stat-Ease Inc.) (Hajare, 2021). The polynomial equation, 3D response surface graphs, and contour plots to study the interaction of independent variables on dependent variables were established by applying ANOVA using Design-Expert® software. The data are presented as the mean \pm standard deviation of three independent experiments. The obtained results were analyzed using one-way ANOVA and two-way ANOVA, and $p < 0.05$ indicated a statistically significant difference (Patil, 2022).

RESULTS AND DISCUSSION

In this research, POS-MMs were prepared by employing the solvent evaporation method and subsequently lyophilized to address the challenges related to stability and drug release.

Selection of formulation components

Soluplus® is a copolymer known for its exceptional solubilizing properties, which make it highly suitable for enhancing the solubility of poorly water-soluble drugs. By effectively solubilizing hydrophobic drugs, Soluplus® improves their dissolution rate and enhances their bioavailability, leading to better absorption and therapeutic efficacy. Moreover, Soluplus® demonstrates remarkable stability, safeguarding the encapsulated drug against degradation and physical changes. Acting as a protective barrier, it prevents drug precipitation and maintains the chemical integrity of the drug during formulation and storage (Attia, 2023). This ensures consistent and reliable drug delivery, minimizing the potential for variability in drug performance. On the other hand, PF68 is known for providing enhanced stability and protection, particularly for sensitive drugs, proteins, and nanoparticles. It acts as a shielding barrier, safeguarding the encapsulated

payload from enzymatic degradation, pH changes, and physical stress. By preserving the stability and integrity of the encapsulated substances, PF68 ensures the efficacy and reliability of the drug delivery system (Fatima, 2022). Hence, by combining Soluplus® and PF68 the MMs of POS were prepared.

Critical micelle concentration

In a study by Patil et al., CMC of PF68, Soluplus®, and POS-MMs was determined using the iodine spectrophotometric method. The obtained CMC values were 0.037 mM, 0.0029 mM, and 0.033 mM, respectively. The POS-MMs exhibited a lower CMC than the other copolymers, suggesting enhanced stability when diluted in biological fluids. This indicates that MMs are less likely to disintegrate or experience drug leakage when exposed to biological environments (Patil, 2021).

Formulation optimization using a 3² factorial design

Initial experiments were conducted, and formulation optimization was performed by considering two factors: the concentration of PF68 (X_1) and the concentration of Soluplus® (X_2). The impact of these variables on the %EE and PS was investigated.

Table 2. 3² factorial design batches and the results of their characterization

Formulation code	Drug (mg)	Factor 1 (X_1) PF68 Concentration (mg)	Factor 2 (X_2) Soluplus® Concentration (mg)	Response 1 (Y_1) %EE (%)	Response 2 (Y_2) Particle size (nm)
A1	10	0.8	0.06	94.88±2.4	66.30±2.10
A2	10	0.8	0.08	91.60±2.1	77.31±1.18
A3	10	0.8	0.10	88.30±2.1	85.92±1.14
A4	10	1.1	0.06	92.46±1.6	75.56±2.10
A5	10	1.1	0.08	92.15±2.1	84.27±2.20
A6	10	1.1	0.10	90.67±1.9	92.69±2.24
A7	10	1.4	0.06	90.47±1.2	82.77±1.13
A8	10	1.4	0.08	91.82±2.2	85.70±2.41
A9	10	1.4	0.10	93.57±2.1	99.64±2.60

Values are mean ± SD (n = 3).

Among the nine batches of POS-MMs, the A1 batch was selected as the optimized formulation due to its high %EE (94.88±2.4%) and small particle size (66.3±2.1 nm) (Gaikwad, 2023).

%Entrapment efficiency and %drug loading capacity

The %EE of the optimized batch A1 was found to be 94.88±2.4%, and the %DLC was found to be 98.20±1.2%.

Effect of formulation variables on %EE

The %EE of the POS-MMs formulations ranged from 88.3 ± 2.1% to 94.88 ± 2.4%. It was observed that an increase in the concentration of PF68 and Soluplus® led to a decrease in %EE. Based on this observation,

the optimum concentrations were determined to be 0.8 mg for PF68 and 0.06 mg for Soluplus® (Table 2). The factors and their interactions influencing %EE were represented using coded variables in the following equation:

$$%EE = + 91.75 - 0.1650A - 0.9017B + 2.40AB \quad \text{Eq. (4)}$$

The regression model equation (Eq. 1) suggests that the concentration of PF68 (X_1) and Soluplus® (X_2) exert a negative influence on the entrapment of the drug within the MM. The significant model term is indicated by the model F-value of 191.49 and $p < 0.05$, implying the model's significance with X_1 and X_2 . Moreover, the contour plot (Figure 1A.) and the 3D response plot (Figure 1B.) both illustrate the negative effects of X_1 and X_2 on the %EE (Li, 2023).

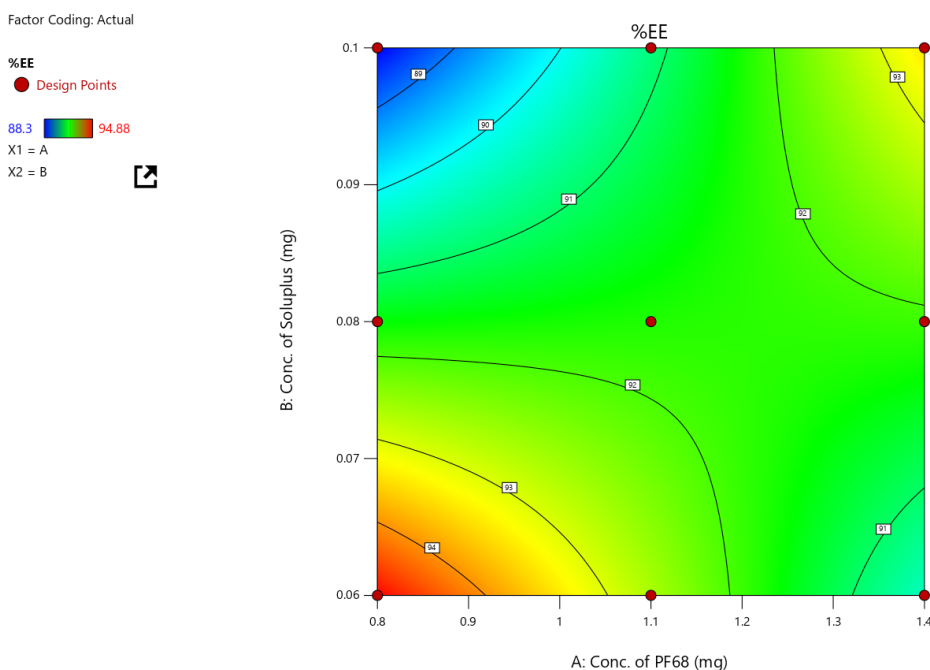


Figure 1A. Contour plot of %EE

Factor Coding: Actual

%EE

Design Points:

● Above Surface

○ Below Surface

88.3  94.88

X1 = A

X2 = B

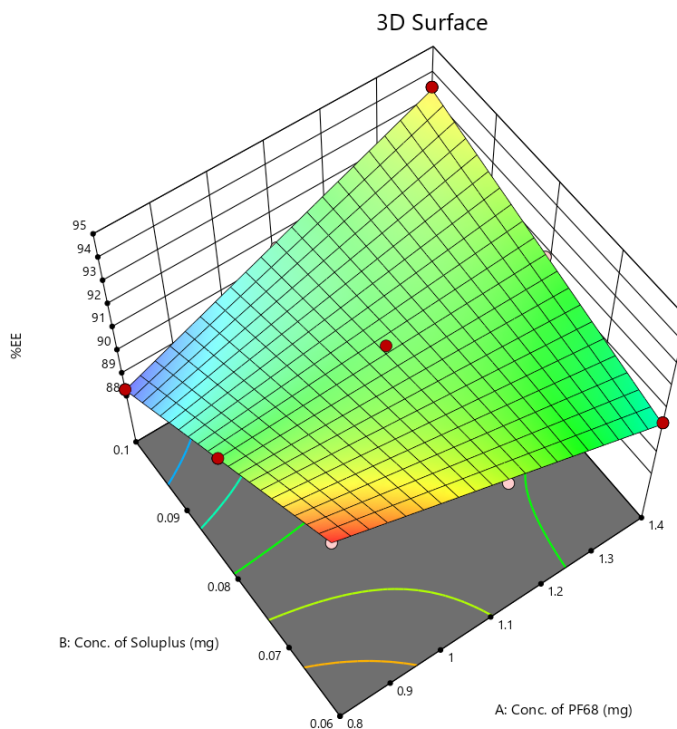


Figure 1B. 3D surface response plot of %EE

Effect of formulation variables on particle size

The particle size of the POS-MMs formulations varied between 66.3 ± 2.1 nm and 99.6 ± 2.6 nm. It was observed that the particle size increased with an increase in the concentration of PF68 and Soluplus[®]. Consequently, the optimal concentrations were determined to be 0.8 mg for PF68 and 0.06 mg for Soluplus[®]. The factors and their interactions influencing the particle size were represented in the following equation:

$$\text{Particle size} = + 83.34 + 6.43A + 8.93B \quad \text{Eq. (5)}$$

The regression model equation (Eq. 2) suggests that the concentration of PF68 (X_1) and Soluplus[®] (X_2) have a positive impact on the particle size of the MMs. The significance of the model term is indicated by the model F-value of 82.77 and $p < 0.05$, indicating that the model is significant with X_1 and X_2 . Furthermore, the contour plot (Figure 2A.) and the 3D response plot (Figure 2B.) both illustrate the positive effects of X_1 and X_2 on the particle size (Liu, 2022).

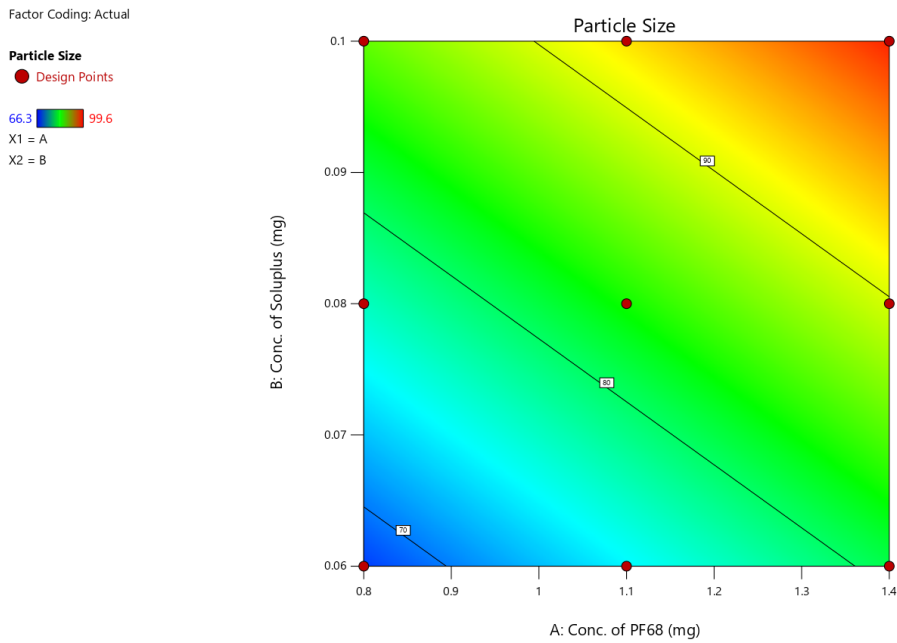


Figure 2A. Contour plot of particle size

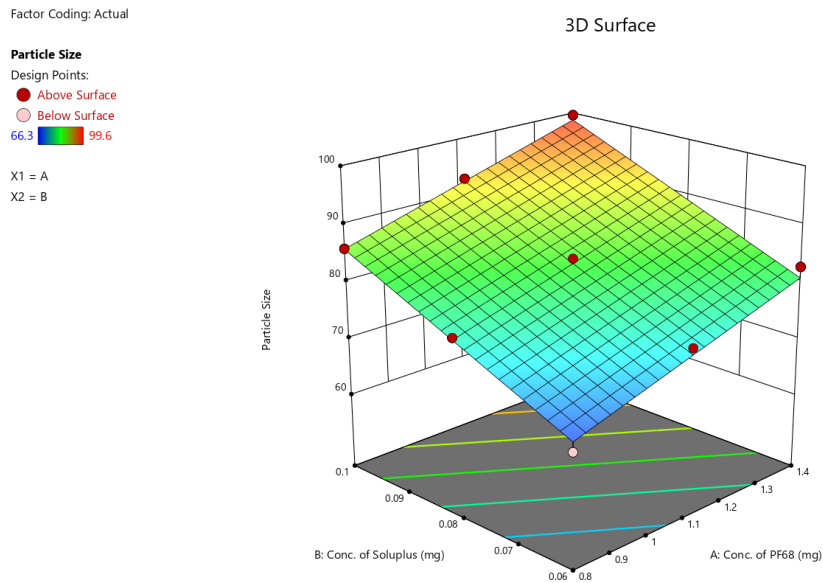


Figure 2B. 3D surface response plot of particle size

Particle size and zeta potential analysis

The optimized batch A1 displayed a PS of 66.30 ± 2.10 nm (with a PDI of 0.062) and a ZP of -51.1 ± 2.4 mV, as depicted in (Figures 3A and 3B). The PS was determined using dynamic light scattering (DLS). The nanoscale dimensions of the MMs are advanta-

geous in fungal treatment, as they enable better penetration and more effective targeting of the infection site. The smaller PS offers an increased surface area for interaction, improved bioavailability, and enhanced cellular uptake, as fungal cells have specific mechanisms to internalize smaller particles more efficiently

(Zhang, 2023). Further, the high observed ZP of the MMs indicates excellent stability and the presence of strong electrostatic repulsion between micelles. This phenomenon plays a crucial role in preventing micelle aggregation or coalescence, which is particularly significant in applications such as drug delivery,

where the stable dispersion of micelles is essential for the efficient transportation of active compounds. As reported by Feng et al. (2016), higher zeta potentials (usually > 30 mV) indicate stronger electrostatic repulsive forces, which are beneficial for maintaining a stable water dispersion formulation (Feng, 2016).

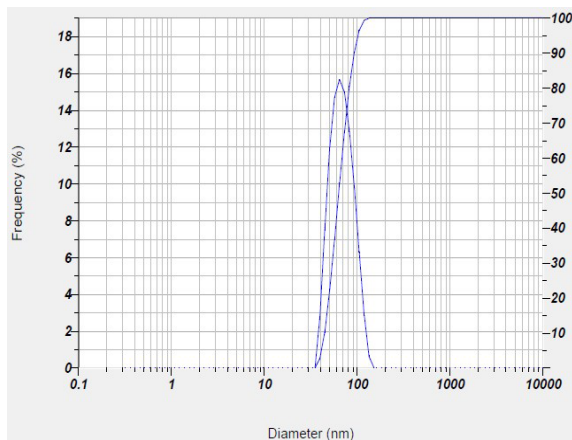


Figure 3A. PS of optimized batch

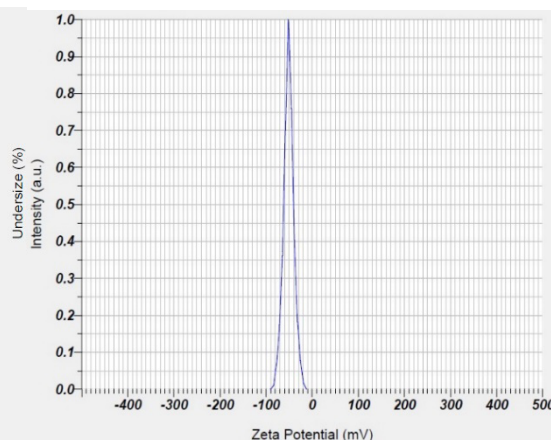


Figure 3B. ZP of optimized batch

Drug-excipient compatibility study

FTIR spectroscopy

Figure 4 shows the overlain FTIR spectrum of plain POS and the optimized formulation POS-MMs (A1). In the FTIR spectrum of POS, characteristic peaks were observed at 2966.73 cm^{-1} , corresponding to the stretching vibrations of C-H in the aromatic rings; 1685.72 cm^{-1} , representing the stretching vi-

bration of the C=O bond; and 1509.46 cm^{-1} , indicating the stretching vibration of C=C in the aromatic rings of POS. IR spectroscopic studies were conducted on POS, PF68, and Soluplus® to evaluate potential drug-excipient interactions. The results indicate that the characteristic drug peaks remain unaltered, suggesting no significant chemical interactions between POS and the excipients. This confirms the stability of POS in its formulation (Hajare, 2021).

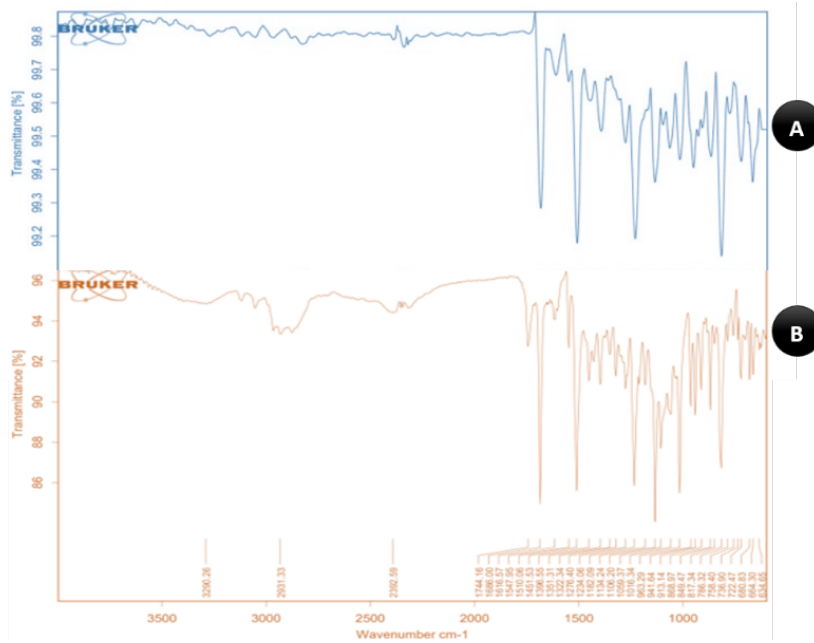


Figure 4. Overlain FTIR spectra of (A) plain POS and (B) POS-MMs A1 formulation

DSC analysis

Figure 5 displays the DSC thermograms obtained under a dry inert nitrogen atmosphere for plain POS and the POS-MMs (A1) formulation. The DSC thermogram of plain POS exhibited a broad peak at 169.98 °C, corresponding to its melting point. The DSC thermograms of the excipients in the formulation showed

endothermic peaks at different temperatures, namely 138.58 °C, 155.17 °C, 215.00 °C, and 229.81 °C, representing their respective thermal events. In the POS-MMs (A1) formulation, the melting point peak of POS was no longer observed, suggesting amorphization within the MMs. This observation indicates that POS has been successfully entrapped and dispersed within the MMs (Hajare, 2020).

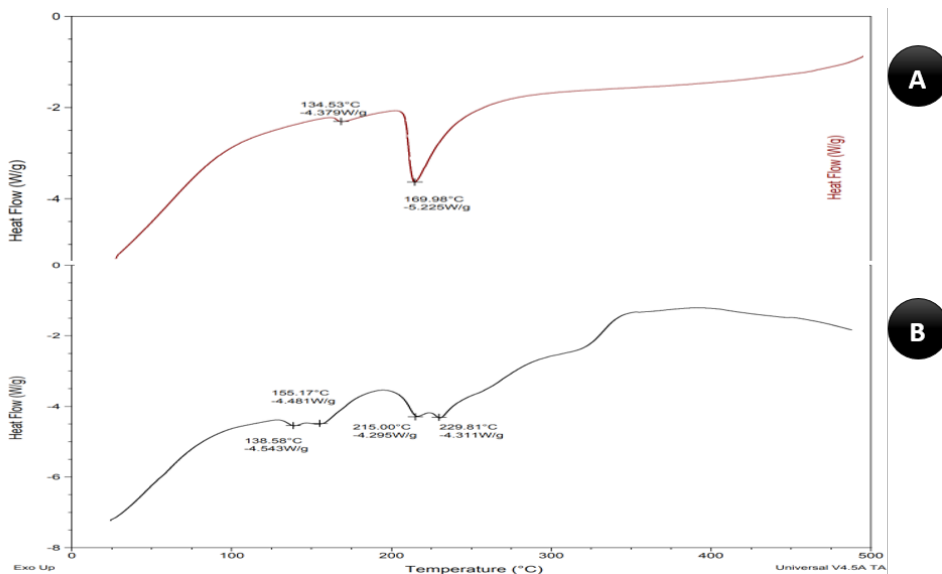


Figure 5. DSC thermograms of (A) plain POS and (B) POS-MMs A1 formulation

XRPD analysis

Figure 6 presents the XRPD patterns of plain POS and POS-MMs. The XRPD pattern of plain POS displayed distinct diffraction peaks, suggesting its crys-

talline nature. In contrast, the XRPD pattern of POS-MMs exhibited broadened peaks with decreased intensities, indicating partial amorphization of the drug within the micellar formulation (Patil, 2022).

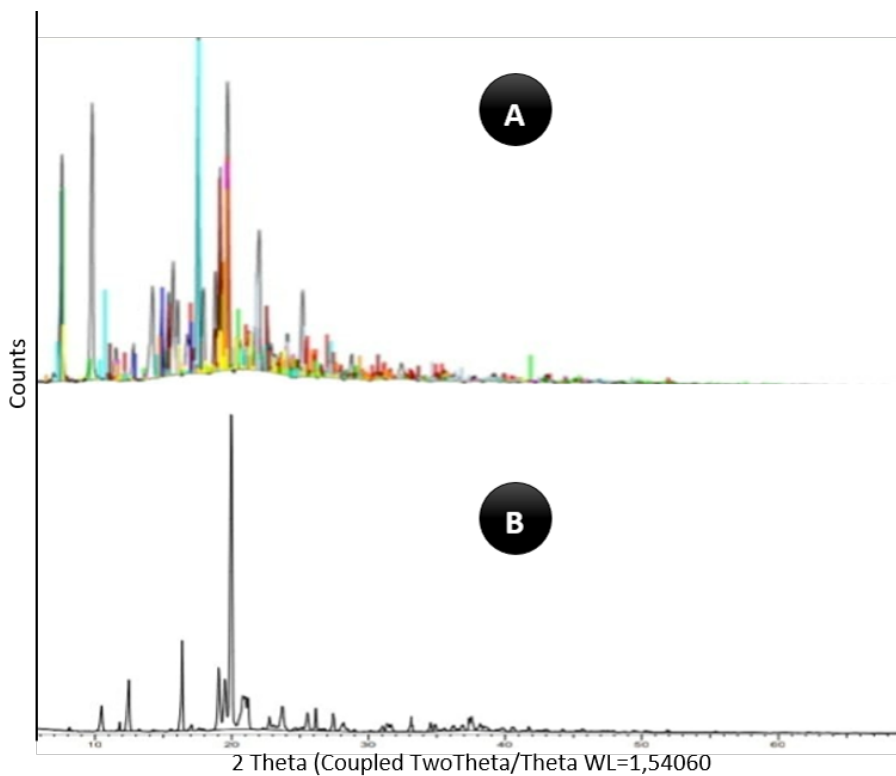


Figure 6. XRPD of (A) plain POS and (B) POS-MMs A1 formulation

In vitro drug release study

Drug release study

Figure 7 illustrates the release profiles of POS from both plain POS dispersion and POS-MMs (A1). In the PBS (pH 7.4) medium containing 0.5% w/v Tween 80, plain POS dispersion exhibited over 90% drug release within 12 hrs, indicating a rapid release profile. On

the other hand, POS-MMs demonstrated sustained release behavior, with a release of 79.4% within 24 hrs ($p < 0.01$). The sustained release of POS from POS-MMs helps provide a continuous and controlled release of POS over an extended period, reducing the frequency of administration, enhancing its efficacy against fungal pathogens, and potentially improving patient compliance (Gupta, 2020).

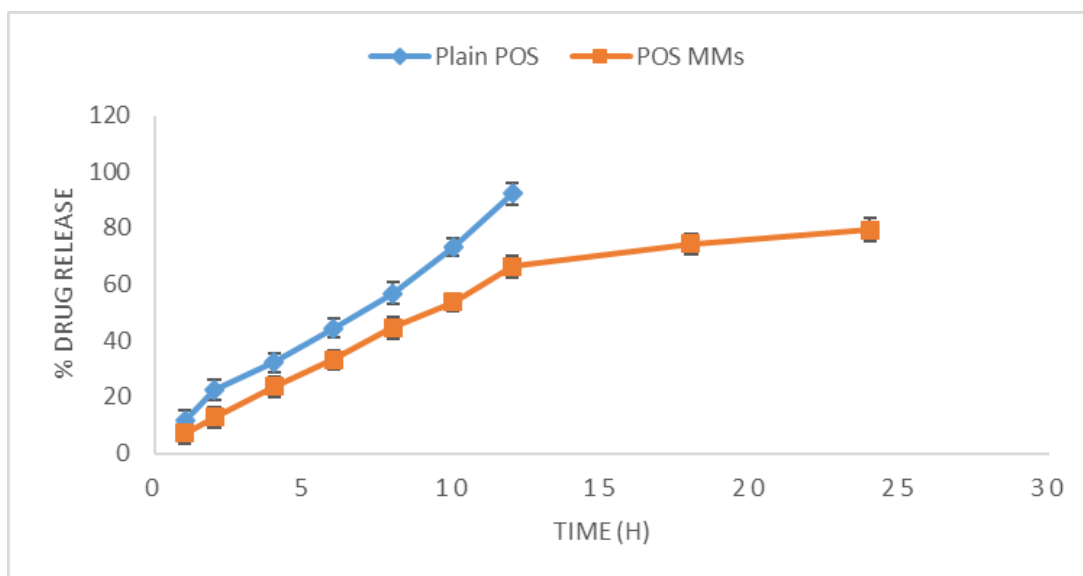


Figure 7. In vitro drug release study from (A) plain POS and (B) POS-MMs A1 formulation

Drug release kinetics study

To determine the mechanism of POS release from MMs, *in vitro* release data was fitted to various drug release kinetics models. The results indicated that the Korsmeyer-Peppas model (Figure 8) provided the

best fit, suggesting that the release of POS from the MMs occurs through matrix diffusion. This implies that the drug molecules diffuse from the micellar core into the surrounding aqueous medium (Zlotnikov, 2023).

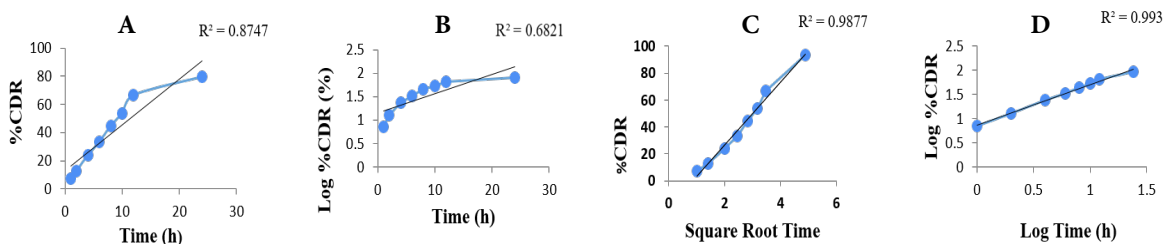


Figure 8. Comparative plots of (A) zero-order release kinetics, (B) first-order release kinetics, (C) Higuchi (SQRT) release kinetics, and (D) Korsmeyer-Peppas model for *in vitro* release profile of the optimized POS-MMs formulation

***In vitro* hemolysis study**

Devices and drug carriers derived from nanotechnology are becoming viable substitutes for traditional small-molecule drugs, and assessing their compatibility with blood components *in vitro* is an essential aspect of early preclinical development (Dobrovolskaia, 2008). In micelle-based drug delivery systems, *in vitro* hemolysis studies are of paramount importance, serving as an early assessment of biocompatibility and safety evaluation. These studies enable the detection and mitigation of hemolytic activity, contributing to safer drug delivery systems. They also provide predictive value for *in vivo* behavior, help meet regulatory requirements, and contribute to a deeper understanding of micelle interactions with biological compo-

nents.

Figure 9 illustrates the results of the *in vitro* hemolysis study, which compared plain POS, blank PF68 and Soluplus® MMs, and POS-MMs. The positive control exhibited complete hemolysis, while the negative control showed minimal hemolysis. At various concentrations, regular POS caused more hemolysis at 50 µg/ml compared to both blank MMs and POS-MMs at the same concentration. Significantly, POS-MMs showed much lower hemolysis ($p < 0.01$) than plain POS at the same concentration. This finding highlights the favorable biocompatibility and safety of POS-MMs for intravenous administration (Khumaini, 2023).

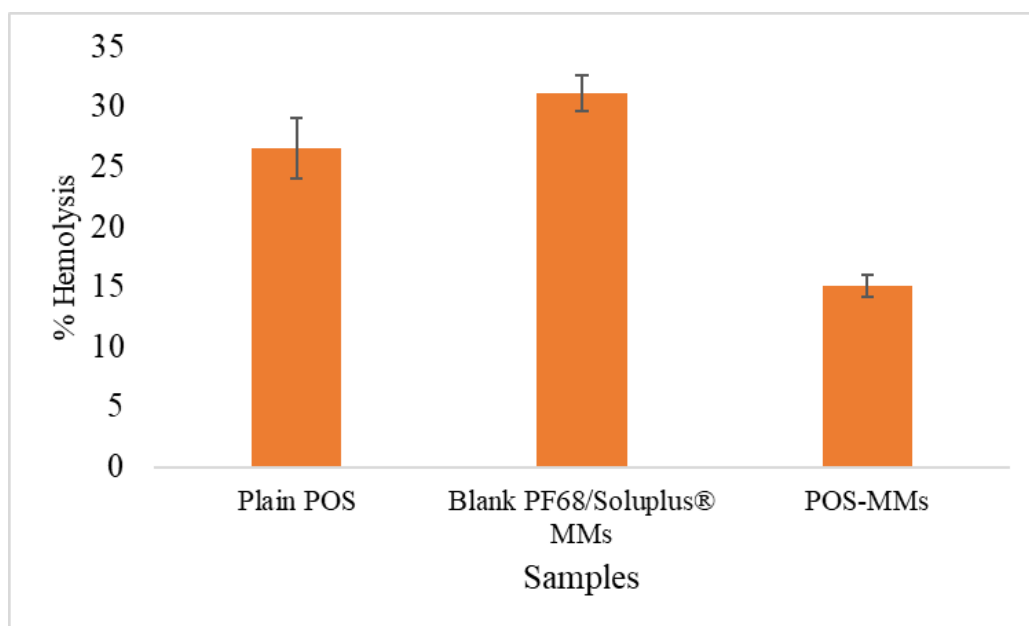


Figure 9. Results of hemolysis studies of plain POS, blank MMs, and optimized formulation (A1)

Characterization of lyophilized POS-MMs

The lyophilization of POS-MMs with 15% lactose as a cryoprotectant, as reported by Cheng (2020), has significantly enhanced the stability of the formulation. The increase in PS to 70.1 ± 2.5 nm after lyophilization is due to the coating of the micelles by the cryoprotectant. When administered, these larger micelles can exhibit prolonged circulation times in the blood-

stream and enhanced drug release at the target site, contributing to more effective and sustained treatment against fungal infections. The decrease in ZP of lyophilized POS-MMs to -25.3 ± 2.8 mV demonstrates that lyophilization effectively prevented particle aggregation and maintained uniform particle dispersion. Furthermore, the high %EE of $96.46 \pm 4.1\%$ and %DLC of $99.21 \pm 0.9\%$ indicate that the active pharmaceutical ingredient (API) remains well-preserved within the

microspheres. The low moisture content of $2.49 \pm 0.5\%$ confirms the absence of moisture-induced degradation. Additionally, the rapid RT of 46 ± 4 sec highlights the ease with which the lyophilized POS-MMs can be redispersed, emphasizing preserving the microsphere integrity and drug release characteristics. Figure 11 represents the powdered formulation and the recon-

stitution product of the lyophilized POS-MMs. These collective findings underscore the critical role of lyophilization in maintaining the stability of POS-MMs, making them an attractive option for pharmaceutical applications where long-term stability and controlled drug release are essential (Bergonzi, 2020).

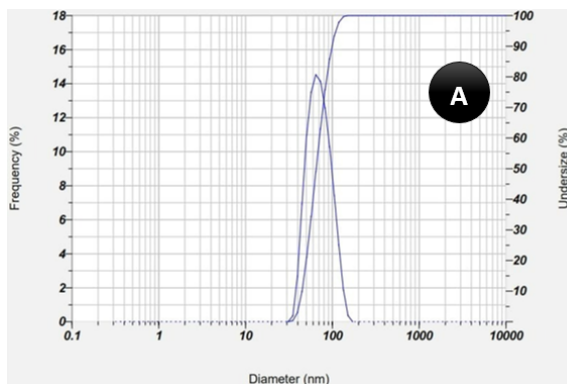


Figure 10A. PS lyophilized POS-MMs and



Figure 11A. Lyophilized POS-MMs and

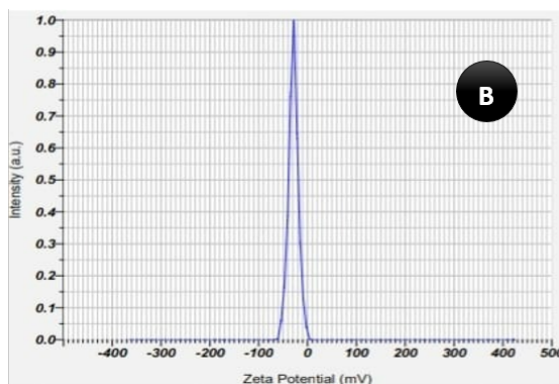


Figure 10B. ZP of lyophilized POS-MMs



Figure 11B. Solution of POS-MMs after reconstitution

SEM was utilized to investigate the surface morphology of the POS-MMs, as depicted in Figure 12. The SEM images revealed that the POS-MMs exhib-

ited irregularly folded, porous, and flocculated amorphous morphology, characterized by a smooth surface (Baviskar, 2022).

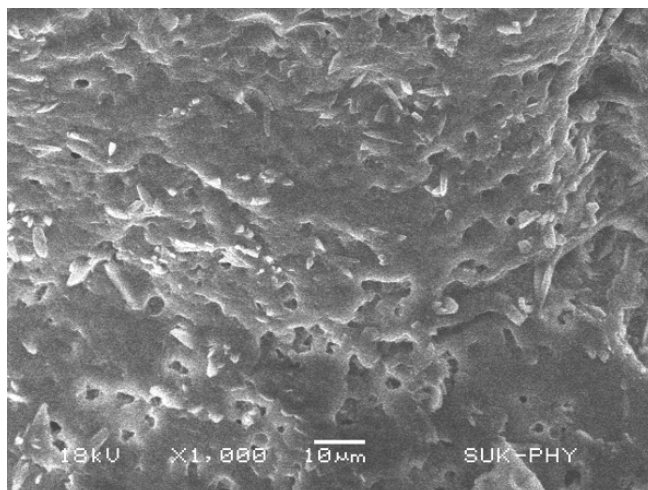


Figure 12. SEM images of POS-MMs

Stability study

Following the ICH Q1A R2 guideline for stability studies, the stability of the POS-MMs was assessed by storing them at a controlled temperature of 2–8 °C for three months. After this period, the %EE of the POS-MMs was determined to be 80.34%, as reported in Table 3 (Bhendale, 2023). A comparison between

the stability of POS-MMs and lyophilized POS-MMs revealed that the PS of the liquid MMs increased rapidly, accompanied by a significant change in the %EE. In contrast, the lyophilized POS-MMs remained stable with minimal changes in %EE and particle size, demonstrating their superior stability compared to the liquid formulation (ICH Q1A(R2) guidelines).

Table 3. Stability study

Sampling Time	POS-MMs			Lyophilized POS-MMs		
	%EE (%)	Particle Size (nm)	%DLC	%EE (%)	Particle Size (nm)	%DLC
0 day	94.88±2.4	66.3±1.2	98.20±1.2	96.46±4.1	70.1±2.5	99.21±0.9
1 month	90.20±0.8	68.4±0.5	97.12±2.1	96.10±3.2	71.2±3.1	98.45±1.4
2 month	88.50±1.3	69.1±1.1	95.34±0.7	95.84±3.7	71.8±2.4	96.79±2.9
3 month	80.34±1.4	75.4±0.7	91.24±1.4	95.30±2.8	72.4±2.3	95.28±1.7

CONCLUSION

In conclusion, using PF68 and Soluplus® as excipients in the formulation of POS-MMs offers several advantages. The POS-MMs containing 0.08 mg PF68 and 0.06 mg Soluplus® exhibit a high %DLC, allowing for efficient encapsulation of POS. These excipients improve the stability of POS by protecting it from degradation and interactions with external factors. The micelles formed using PF68 and Soluplus® demonstrate controlled drug release, enabling sustained therapeutic effects.

The solvent evaporation method is simpler, less time-consuming, and more reproducible. It allows for the precise control of micelle composition and drug loading. This method ensures uniform drug distribution within the mixed micelles, resulting in consistent drug release profiles. Furthermore, the stability of the POS-MMs was further enhanced through the lyophilization process. Lyophilization effectively preserved the MMs structure, prevented drug degradation, and maintained drug loading efficiency. The resulting lyophilized powder exhibited improved sta-

bility during storage and handling, making it a more practical and reliable formulation. These findings contribute to the development of stable and efficient drug delivery systems, paving the way for improved therapeutic outcomes in treating fungal infections.

CONFLICT OF INTEREST

The authors declare that there is no conflict of interest

AUTHOR CONTRIBUTION STATEMENT

Concept (AK, KP), Design (AK, KP), Data Collection or Processing (AK, RC, VT, SP), Analysis and Interpretation (RC, KP, SP, JD, AH), Literature Search (AK, RC, VT), Writing (AK, RC, VT, KP, SP, JD, AH)

List of abbreviations

PF68: Pluronic F68[®]

POS-MMs: Posaconazole-loaded mixed micelles

FTIR: Fourier Transform Infrared spectroscopy

DSC: Differential scanning calorimetry

XRPD: X-ray powder diffraction

Hrs: hours

%EE: % entrapment efficiency

PS: Particle size

MMs: Mixed micelles

KI: Potassium iodide

I₂: Iodine

ZP: Zeta potential

%DLC: % drug loading capacity

POS: posaconazole

S: second

Da: Dalton

nm: Nanometer

DLS: Dynamic light scattering

CMC: Critical micelle concentration

SD: Standard deviation

REFERENCES

- Abdul Hussein HA, Maraie NK. (2022). Tenoxicam-loaded polymeric micelles material: Formulation, optimization, and evaluation. *Mater Today*. 61:672–80.
- Attia MS, Elshahat A, Hamdy A, Fathi AM, Emad-El-din M, Ghazy FE, Chopra H, Ibrahim TM. (2023). Soluplus[®] as a solubilizing excipient for poorly water-soluble drugs: Recent advances in formulation strategies and pharmaceutical product features. *J Drug Deliv Sci Technol*. 104519.
- Baviskar PS, Mahajan HS, Chandankar SM, Agrawal YO. (2022). Development and evaluation of N-acetyl glucosamine-decorated vitamin-E-based micelles incorporating resveratrol for cancer therapy. *J Drug Deliv Sci Technol*. 78:103965.
- Bergonzi MC, Vasarri M, Marroncini G, Barletta E, Degl'Innocenti D. (2020). Thymoquinone-loaded soluplus[®]-solutol[®] HS15 mixed micelles: preparation, *in vitro* characterization, and effect on the SH-SY5Y cell migration. *Molecules*. 25(20):4707.
- Bhendale M, Singh JK. (2023). Molecular insights on morphology, composition, and stability of mixed micelles formed by ionic surfactant and nonionic block copolymer in water using coarse-grained molecular dynamics simulations. *Langmuir*. 39:5031–40.
- Cheng Q, Qin W, Yu Y, Li G, Wu J, Zhuo L. (2020). Preparation and characterization of PEG-PLA genistein micelles using a modified emulsion-evaporation method. *J Nanomater*. 2020:1-5.
- Dobrovolskaia MA, Clogston JD, Neun BW, Hall JB, Patri AK, McNeil SE. (2008). Method for analysis of nanoparticle hemolytic properties *in vitro*. *Nano letters*. 8(8):2180-7.
- Fatima M, Karwasra R, Almalki WH, Sahebkar A, Kesharwani P. (2022). Galactose engineered nano-

- carriers: Hopes and hypes in cancer therapy. *Eur Polym J.* 111759.
- Feng B, Ashraf MA, Peng L. (2016). Characterization of particle shape, zeta potential, loading efficiency, and outdoor stability for chitosan-ricinoleic acid loaded with rotenone. *Open Life Sci.* 11(1):380-6.
- Gaikwad DS, Chougale RD, Patil KS, Disouza JI, Hajare AA. (2023). Design, development, and evaluation of docetaxel-loaded niosomes for the treatment of breast cancer. *Futur J Pharm Sci.* 9:1-13
- Gupta A, Costa AP, Xu X, Lee SL, Cruz CN, Bao Q, Burgess DJ. (2020). Formulation and characterization of curcumin-loaded polymeric micelles produced via continuous processing. *Int J Pharm.* 583:119340.
- Hajare A, Dol H, Patil K. (2021). Design and development of terbinafine hydrochloride ethosomal gel for enhancement of transdermal delivery: *In vitro*, *in vivo*, molecular docking, and stability study. *J Drug Deliv Sci Technol.* 61:102280.
- Hajare AA, Velapure PD, Rathod PN, Patil KS, Chopade SS. (2020). Formulation and evaluation of solid lipid nanoparticle gel for topical delivery of clobetasol propionate to enhance its permeation using silk sericin as permeation enhancer. *Int J Pharm Sci Res.* 11:2356-65.
- International Council for Harmonisation of Technical Requirements for Pharmaceuticals for Human Use (ICH). ICH Harmonised Tripartite Guideline: Stability Testing of New Drug Substances and Products Q1A(R2). ICH; 2003. Available from: ICH Guideline
- Jain AK, Thareja S. (2019). *In vitro* and *in vivo* characterization of pharmaceutical nanocarriers used for drug delivery. *Artif Cells Nanomed Biotechnol.* 47(1):524-39.
- Jin GW, Rejinold NS, Choy JH. (2022). Multifunctional polymeric micelles for cancer therapy. *Polymers.* 14(22):4839.
- Joseph E. (2019). Residual moisture determination in lyophilized drug products. *Pharmaceutical Technology.* 43(11):30-9.
- Khumaini Mudhar Bintang MA, Tipmanee V, Srichana T. (2023). Colistin sulfate-sodium deoxycholate sulfate micelle formulations; molecular interactions, cell nephrotoxicity, and bioactivity. *J Drug Deliv Sci Technol.* 79:104091.
- Kuperkar K, Patel D, Atanase LI, Bahadur P. (2022). Amphiphilic block copolymers: their structures, and self-assembly to polymeric micelles and polymersomes as drug delivery vehicles. *Polymers.* 14(21):4702.
- Li X-Y, Shi L-X, Shi N-N, Chen W-W, Qu X-W, Li Q-Q, et al. (2023). Multiple stimulus-response berberine plus baicalin micelles with particle size-charge-release triple variable properties for breast cancer therapy. *Drug Dev Ind Pharm.* 49:189-206.
- Liu J, Liu D, Bi J, Liu X, Lyu Y, Verkerk R, et al. (2022). Micelle separation conditions based on particle size strongly affect carotenoid bioaccessibility assessment from juices after *in vitro* digestion. *Food Res Int.* 151:110891.
- Manjusha V, Reshma LR, Anirudhan TS. (2023). Mesoporous silica gated mixed micelle for the targeted co-delivery of doxorubicin and paclitaxel. *J Drug Deliv Sci Technol.* 79:104032.
- Osouli M, Abdollahizad E, Alavi S, Mahboubi A, Abbasian Z, Haeri A, Dadashzadeh S. (2023). Biocompatible phospholipid-based mixed micelles for posaconazole ocular delivery: Development, characterization, and *in vitro* antifungal activity. *J. Biomater. Appl.* 37(6):969-78.
- Patil KS, Hajare AA, Manjappa AS, Dol HS. (2023).

- Vacuum foam drying of docetaxel mixed micelles for improved stability and ovarian cancer treatment. *J Drug Deliv Sci Technol.* 86:104747.
- Patil K, Patil J, Bharade S, Disouza J, Hajare A. (2023). Design and development of sodium alginate/carboxymethyl cellulose *in situ* gelling system for gastroretentive delivery of lisinopril. *J Pharm Res.* 27(2).
- Patil KS, Hajare AA, Manjappa AS, More HN, Disouza JI. (2021). Design, development, *in silico*, and *in vitro* characterization of Docetaxel-loaded TPGS/Pluronic F 108 mixed micelles for improved cancer treatment. *J Drug Deliv Sci Technol.* 65:102685.
- Patil KS, Hajare AA, Manjappa AS, More HN, Disouza JI. (2022). Design, Development, *In Silico*, and *In Vitro* Characterization of Camptothecin-Loaded Mixed Micelles: *In Vitro* Testing of Verapamil and Ranolazine for Repurposing as Adjuvant Therapy in Cancer. *J Pharm Innov.* 1-9.
- Patil SS, Chougale RD, Manjappa AS, Disouza JI, Hajare AA, Patil KS. (2022). Statistically developed docetaxel-laden mixed micelles for improved therapy of breast cancer. *OpenNano.* 8:100079
- Ribeiro AI, Dias AM, Zille A. (2022). Synergistic effects between metal nanoparticles and commercial antimicrobial agents: A review. *ACS Appl. Nano Mater.* 5(3):3030-64.
- Singh S, Kuca K, Kalia A. (2020). Alterations in Growth and Morphology of *Ganoderma lucidum* and *Volvariella volvaceae* in Response to Nanoparticle Supplementation. *Mycobiology.* 48(5):383-91.
- Suzuki N, Taura D, Komichi Y. (2023). Critical micelle concentration and partition coefficient of mixed micelles: Analysis of ternary systems based on Markov chain model and simple mixture model. *J Mol Liq.* 376:121383
- Szente L, Puskás I, Sohajda T, Varga E, Vass P, Nagy ZK, Farkas A, Várnai B, Béni S, Hazai E. (2021). Sulfobutylether-beta-cyclodextrin-enabled antiviral remdesivir: Characterization of electrospun-and lyophilized formulations. *Carbohydr Polym.* 264:118011.
- Thakral S, Sonje J, Munjal B, Suryanarayanan R. (2021). Stabilizers and their interaction with formulation components in frozen and freeze-dried protein formulations. *Adv Drug Deliv Rev.* 173:1-9.
- Thiermann H, Schreiner R, Eyer P. (1998). Dissolution kinetics of unstable drugs in two-compartment autoinjectors: Analysis of the individual shaking behaviour and influence of various shaking parameters on the dissolution rate of HI 6 in an automated system, *Int J Pharm.* 170;23-32.
- Trenkenschuh E, Friess W. (2021). Freeze-drying of nanoparticles: How to overcome colloidal instability by formulation and process optimization. *Eur J Pharm Biopharm.* 165:345-60.
- Ugwu CE, Oraeluno JN, Eze KC, Ezenma CO, Nwankwo AO. (2022). PEGylated aceclofenac solid lipid microparticles homolipid-based solidified reverse micellar solutions for drug delivery. *Heliyon [Internet].* 8:e09247.
- Vinchurkar RH, Kuchekar AB. (2021). Polymeric micelles: a novel approach towards nano-drug delivery system. *Biosci Biotechnol Res Asia.* 18(4):629-49.
- Zhang W, Taheri-Ledari R, Ganjali F, Mirmohammadi SS, Qazi FS, Saeidirad M, Kashti Aray A, Zarei-Shokat S, Tian Y, Maleki A. (2023). Effects of morphology and size of nanoscale drug carriers on cellular uptake and internalization process: a review. *RSC advances.* 13(1):80-114.
- Zlotnikov ID, Streltsov DA, Belogurova NG, Ku-

dryashova EV. (2023). Chitosan or cyclodextrin grafted with oleic acid self-assemble into stabilized polymeric micelles with potential of drug carriers. *Life (Basel)*. 13:2.

Bilayer Nanofiber Scaffold Incorporated with Mupirocin and Thyme Essential Oil for Synergistic Activity Against Bacterial Wound Infections

Kisan JADHAV[°], Shivani GHARAT^{**}, Shradha B. ADHALRAO^{***}

Bilayer Nanofiber Scaffold Incorporated with Mupirocin and Thyme Essential Oil for Synergistic Activity Against Bacterial Wound Infections

SUMMARY

This study aimed to fabricate a bilayer nanofiber scaffold using an electrospinning process, incorporating a drug and oil-containing polymeric emulsion to enhance its effectiveness against bacterial wound infections. The research focused on characterizing the scaffold's morphology, chemical composition, thermal behavior, porosity, swelling ratio, drug release kinetics, in-vitro permeation, ex vivo skin permeation, and antimicrobial activity. Results from in-vitro drug permeation studies demonstrated an initial rapid release of Mupirocin (53% in 6 h) followed by sustained release (92.17% in 72 h). In comparison, Thyme Essential Oil exhibited a release profile with an initial burst followed by sustained release (85.45% release in 10 h). The ex vivo skin permeation data revealed greater permeability compared to conventional films; notably, the bilayer nanofiber scaffold exhibited superior antibacterial activity compared to single-layer Mupirocin and Thyme Essential Oil scaffolds, indicating a synergistic effect between Mupirocin and Thyme Essential Oil. This research offers an innovative approach to wound management with potential clinical implications.

Key Words: Bilayer nanofiber scaffold, Wound infections, Mupirocin, synergistic activity, Thyme essential oil, Antibacterial activity.

Bakteriyel Yara Enfeksiyonlarına Karşı Sinerjistik Aktivite için Mupirosin ve Kekik Uçucu Yağı ile Birleştirilmiş Çift Tabakalı Nanofiber İskele

ÖZ

Bu çalışma, bakteriyel yara enfeksiyonlarına karşı etkinliği arttırmak için bir ilaç ve yağ içeren polimerik emülsiyon içeren bir elektroöğirme işlemi kullanarak çift tabakalı bir nanofiber iskele üretmeyi amaçlamaktadır. Araştırma, iskelenin morfolojisini, kimyasal bileşimini, termal davranışını, porozitesini, şişme oranını, ilaç salım kinetiğini, in vitro permeasyonunu, ex vivo deri permeasyonunu ve antimikrobiyal aktivitesini karakterize etmeye odaklanmıştır. In vitro ilaç permeasyon çalışmalarından elde edilen sonuçlara göre, Mupirosin başlangıçta hızlı bir salım (6 saatte %53) ve ardından sürekli salım (72 saatte %92,17) göstermiştir. Buna karşılık Kekik Esansiyel Yağı, sürekli salım (10 saatte %85,45 salım) ile devam eden bir ilk patlama etkisi ile salım profili sergilemiştir. Ex vivo cilt permeasyonu verileri, geleneksel filmlere kıyasla daha fazla geçirgenlik ortaya çıkarmıştır; özellikle, çift tabakalı nanofiber iskele, tek tabakalı Mupirosin ve Kekik Uçucu Yağı iskelelerine kıyasla üstün antibakteriyel aktivite sergilemiş ve bu, Mupirosin ve Kekik Uçucu Yağı arasında sinerjistik bir etki olduğunu göstermiştir. Bu araştırma, potansiyel klinik etkiler ile yara tedavisine yenilikçi bir yaklaşım sunmaktadır.

Anahtar Kelimeler: Çift tabakalı nanofiber iskele, Yara enfeksiyonu, Mupirosin, sinerjistik aktivite, Kekik uçucu yağı, Antibakteriyel aktivite.

Received: 19.08.2023

Revised: 17.01.2024

Accepted: 19.01.2024

[°] ORCID: 0000-0001-7563-3935, Department of Pharmaceutics, Bharati Vidyapeeth's College of Pharmacy, Sector 3A, CBD Belapur, Navi Mumbai-400614, Maharashtra, India.

^{**} ORCID: 0000-0003-4972-8863, Department of Pharmaceutics, Bharati Vidyapeeth's College of Pharmacy, Sector 3A, CBD Belapur, Navi Mumbai-400614, Maharashtra, India.

^{***} ORCID: 0000-0002-6065-1839, Department of Pharmaceutics, Bharati Vidyapeeth's College of Pharmacy, Sector 3A, CBD Belapur, Navi Mumbai-400614, Maharashtra, India.

INTRODUCTION

The presence of wounds is an inevitable part of patient care, and the risk of infection is a common concern in wound management. Currently, commercially available formulations of mupirocin, an antimicrobial agent commonly used in wound care, have shown effectiveness in preventing and treating infections. However, there is growing concern about the emergence of bacterial resistance to mupirocin, necessitating the exploration of alternative strategies to improve its efficacy (Alkilani et al., 2015).

In recent literature, nanofiber-based wound dressings have gained attention as a promising approach for delivering antimicrobial drugs. Nanofibers offer advantages such as a high surface area-to-volume ratio, increased porosity, and the ability to precisely control drug release. These attributes make them ideal for targeted drug delivery to wound sites while minimizing microbial penetration (Kamble et al., 2016).

Electrospinning, a widely employed technology for nanofiber production, offers ease of handling, precise control over fiber diameter, and cost-effectiveness. This method provides a platform to develop innovative wound dressings that can optimize drug release profiles and enhance therapeutic outcomes (Thenmozhi et al., 2017).

Mupirocin (MUP), a potent antimicrobial agent produced by the Gram-negative bacterium *Pseudomonas fluorescens*, has demonstrated effectiveness against various bacterial strains. However, it is essential to optimize its delivery to wounded tissues, as oral administration leads to the gradual breakdown of mupirocin into an inactive metabolite (Abbas et al., 2019).

Addressing the concern of mupirocin resistance, this study aims to formulate an electrospun bilayer nanofiber scaffold incorporating both Mupirocin and Thyme Essential Oil (TEO). The combination of these agents is expected to synergistically enhance their antibacterial effects, providing a potential solution to

combat bacterial resistance and improve the therapeutic efficacy of wound care. Propolis and its combination with MUP against methicillin-resistant *Staphylococcus aureus* (MRSA) in nasal carriage of rabbits were found to result in a more profound reduction in bacterial cell count and inflammatory response (Onlen et al., 2007). Thyme Essential Oil (*Thymus vulgaris* L.), known for its natural antimicrobial properties and ability to reduce inflammation, holds promise as an adjunct to mupirocin in wound management (Rather et al., 2021).

In recent developments, MUP-loaded nanoemulsions have emerged as a promising solution for the treatment of superficial skin infections. These nanoemulsions, formulated with the inclusion of eucalyptus oil (EO), offer a novel approach to combat such infections effectively (Alhasso et al., 2023).

Moreover, for the management of invasive *Staphylococcus aureus* infections, a parenteral delivery system known as Nano-MUP has been devised. This innovative approach, involving liposome protection and enhanced drug delivery mechanisms, has shown remarkable improvements in antimicrobial efficacy, particularly within infected organs and *Staphylococcus aureus*-harboring phagocytic cells (Goldmann et al., 2019).

Furthermore, an important endeavor in this field has been the development of MUP nanoparticle-loaded hydrogel (MLH), with a primary focus on ensuring its biocompatibility for rat model wound healing and its safety for cell lines. Notably, the results have been promising, as evidenced by wound contraction, reduced secretion, increased development of new blood vessels, stimulation of hair follicle cells, and other wound healing indicators in burn wounds. In comparison to alternative treatment groups, MLH, and hydrogel have demonstrated superior performance in facilitating the healing process, marking a significant advancement in wound care strategies. These developments underscore the potential of Mupirocin formulations to revolutionize the treatment of skin

infections and wound management (Kamlungmak et al., 2021).

It's worth noting that commercially available Mupirocin formulations come in the form of creams and ointments, providing additional options for patients and healthcare providers in addressing skin infections (Bakkiyaraj et al., 2017).

In summary, this research focuses on developing an innovative electrospun bilayer nanofiber scaffold with MUP and TEO to address the challenge of bacterial resistance and improve the treatment of bacterial wound infections.

Preparation of MUP-PCL-TEO-PVA bilayer nanofiber scaffold



Figure 1. Electrospinning setup (E-SPIN NANO) for fabrication of MUP-PCL-TEO-PVA bilayer nanofiber scaffold.

Preparation of Electrospinning solutions

MUP-PCL polymeric solution

MUP-loaded PCL polymer solution was prepared based on a modified version of an existing technique (Chen et al., 2018). Using magnetic stirring, a precisely weighed amount of PCL was solubilized in DCM over 24 hours at room temperature, yielding a homogeneous solution with a 10% (w/v) concentration. The PCL solution was then gradually added MUP (2 % w/v) while being vigorously stirred for 24 hours.

MATERIALS AND METHODS

Materials

Kawman Pharma Ltd. Mumbai, India. generously provided MUP. Polycaprolactone (Mn, 80,000) was purchased from Otto Chemie Pvt Ltd. Mumbai, India. The source of the Thymus vulgaris essential oil was Naturalis essential oil, India. Polyvinyl alcohol and Tween 80 were obtained from Research Lab Fine Chem Industries and Loba Chemie Pvt. Ltd. Respectively. Dichloromethane AR grade and Methanol AR grade were gained from S.D. Fine Chemicals, Mumbai, India. The additional ingredients together with solvents belonging to analytical grade were utilized.

TEO- PVA loaded polymeric emulsion

To incorporate the oil in the polymeric solution, an o/w emulsion formulation was selected. The TEO-loaded emulsion was prepared by accurately weighing PVA (7% w/v) and dissolving in distilled water at 60-80°C along with 2 hours of constant magnetic stirring, to get a homogeneous solution. Then TEO (1% w/v) was dissolved in Tween 80 (3% w/v) and this oil-surfactant mixture was slowly added to the PVA solution (polymeric aqueous phase) and kept

nearly to 24 hours on magnetic stirring at room temperature to get a homogenous emulsion (KesiciGüler et al., 2019).

Preparation of bilayer nanofiber scaffold

The electrospinning technique for this investigation was carried out using the electrospinning device Espin Nano (as shown in Figure 1.). It consists of an adjustable DC power supply, a syringe, a stainless-steel needle, as well a syringe pump. The experimental criteria containing flow rate, supply voltage, tip-to-collector distance, as well as drum speed, were set based on previous literature as well as experimental conditions (Li et al., 2018). Processing for electrospinning was done at ambient temperature and 55% relative humidity. A syringe pump's flow rate was controlled using a 10 mL syringe having a 24-gauge metallic needle. The metal needle was charged using a high-voltage power source including an applied voltage of 18 kV, and on an aluminium foil-coated drum collector moving at 400–500 rpm, the fibers were collected. The flow rate was kept constant at 1 mL/h, and the tip-to-collector distance was set to 13 cm. For the preparation of bilayer nanofiber scaffolds, a first layer containing, TEO loaded PVA emulsion was deposited on aluminum foil followed by the second layer of MUP-loaded PCL solution. After that, a vacuum was applied to the fibers that had gathered from the aluminium foil upon the collector.

Gas Chromatography

The investigation employed an HP 6890 gas chromatography with a flame ionization detector (FID) and a 30 m x 0.25 mm HP-5 (cross-linked Phenyl-Methyl Siloxane) column with 0.25 µm film thickness from Agilent. The essential oil samples (0.1 µL) were injected straight into the column. With a flow rate of 1, 4 mL min⁻¹ and a split-less operation, helium was employed as the carrier gas. The column was kept at 40°C for five minutes, then elevated to 230°C at a rate of 10°C min⁻¹, and lastly from 230 to 280°C at a rate of 30°C min⁻¹.

Mass spectrometry analysis

A Hewlett Packard 6890 mass selective detector and a Hewlett Packard 6890 gas chromatograph were used to examine the oil using gas chromatography-mass spectrometry (GC-MS). The MS operating conditions were as follows: Ionisation potential is 70 Ev; ionization current, 2 A; ion source temperature is 200°C, and resolution is 1000. From 30 to 450 m/z, mass units were tracked. With retention indices related to n-alkanes. The chromatographic conditions were the same as those employed for GC analysis.

Characterization of electrospun MUP-PCL-TEO-PVA bilayer nanofiber scaffold

Scanning Electron Microscopy (SEM)

SEM was utilized for analyzing the surface morphological properties as well as the fiber diameter of electrospun nanofiber scaffolds. Using the FEI Quanta 200 SEM, nanofiber samples were imaged at varying magnifications after being gold-sputter-coated. At least 50 randomly chosen fibers were measured to estimate the fabrication's nanofiber membrane's average diameter.

Thickness

A Yuzuki digital micrometer was used to measure the nanofiber scaffold's thickness. Three samples() were measured at different areas of the nanofiber scaffold.

Porosity

The porous nature produced by the patches was measured using a procedure that has already been discussed. Absolute ethanol was used to immerse the scaffolds until they were saturated scaffolds were weighed before and after they had been soaked in alcohol. Porosity was measured using the equation given below:

$$\text{Eq. (A.1): } P = P = \frac{W_2 - W_1}{\rho V_1} \times 100$$

where W_1 and W_2 are the scaffolds' relative weights before and after being immersed in alcohol; V_1 represents the volume previously immersed in

alcohol which was determined using the formula for the dressing's length, breadth, and height (Thakur et al., 2008).

Swelling ratio:

The nanofibrous scaffold was cut into equal portions and submerged in PBS (pH 7.4) for nearly 24 hours which represents medium conditions to gauge the level of swelling. After using filter paper to gently wipe away any water that had stuck to the surface, the scaffolds were promptly weighed.

$$\text{Eq. (A.2): } DS = \frac{W_w - W_d}{W_d} \times 100$$

In the above equation, DS stands for the amount of swelling, while W_w and W_d are the scaffolds' respective wet and dry weights (Tanriverdi et al., 2018).

Fourier-transform infrared spectroscopy (FTIR)

A Fourier transform infrared spectrometer (SHIMADZU IR spirit) was utilized to get the infrared spectra of the electrospun scaffolds. After drying in a vacuum oven, nanofibrous mats were applied to the diamond crystal for investigation. The investigation included the spectral region from 4000 cm^{-1} to 400 cm^{-1} . For every spectrum, scans were recorded. To determine whether the formulation was causing any chemical interactions, the absorption peaks were examined.

Differential scanning calorimetry (DSC)

DSC (Hitachi 7020) was used to investigate thermal characteristics. As a reference, an empty aluminium pan was used. Using an aluminium sealed pan, DSC measurements were conducted from 10 to $300 \text{ }^\circ\text{C}$ at a heating rate of $10 \text{ }^\circ\text{C/minute}$. Oil or Liquid holding sample pans were used to characterize TEO. For each measurement, a sample size of 5–10 mg was used. During the measurement, nitrogen gas was used to purge the sample cell. In the context of DSC, melting refers to the process of a substance transitioning from a solid to a liquid state under the influence of increasing temperature. DSC measures the heat flow associated with the phase transition, allowing for the

characterization of melting temperatures and enthalpies of materials.

% Entrapment efficiency (% EE)

To ascertain the % EE, the quantity of medication that was not trapped in the nanofibers was assessed. The nanofiber mat formed was diluted appropriately with methanol and then subjected to centrifugation for 30 minutes at 10,000 rpm. Utilizing a UV/VIS spectrophotometer with a wavelength of 230 nm, the quantity of free medicine in the supernatant was calculated. A similar process was followed to determine the TEO content at 274 nm. The quantity of drug that was absorbed was determined by comparing the initial drug content with the free drug in the supernatant. The experiment was conducted in triplicate using three different samples.

In vitro drug release

In vitro drug release of nanofiber scaffold was carried out as per described in the earlier method. By inserting a known mass and approximate size ($4 \times 4 \text{ cm}^2$) of material in 60 mL of PBS (pH=7.4) at 37°C , drug release from the MUP-loaded nanofiber scaffolds was assessed. 1.0 mL of solution was moved to a sample vial from the test solution at predefined sample collection intervals. The amount of drug released was determined by a UV spectrometer (Shimadzu UV-1800) at a wavelength of 230 nm and the cumulative release percentage of MUP at various times was determined based on the calibration curve. TEO release was also detected using a UV spectrometer at 274 nm wavelength.

The amount of MUP and TEO released were calculated from:

$$\text{Eq. (B.1): } y = 0.0243c + 0.0397 \quad (R^2 = 0.995)$$

where c is the concentration of MUP (mg/L) and y is absorbance.

$$\text{Eq. (B.2): } y = 0.0606x - 0.0044 \quad (R^2 = 0.996)$$

where c is the concentration of TEO (mg/L) and y is absorbance.

***In vitro* drug permeation**

In vertical Franz diffusion cells, 22 ml of pH 7.4 phosphate-buffered saline (PBS) were added to the produced bilayer electrospun scaffolds (JN CIENCE-TECH). The complete scaffold was present in the diffusion cell's receptor chamber, which was below the sampling port. The scaffold showed promising wettability throughout the tests and maintained the entire immersion without any additional support. The interior compartments of the Franz cells were covered with cellulose membrane, while the outside jacket of the cells was kept at 37° C and agitated at 200 rpm. 1 ml of sample was taken out of the sampling port and replaced at the proper intervals between 1 and 72 hours with an equal volume of the new buffer. Shimadzu UV-1800 spectrometer was used to measure overall drug concentrations for MUP and TEO at wavelengths of 230 nm and 274 nm, respectively.

***Ex vivo* studies**

For the *ex vivo* study, a male white Wistar rat weighing 180–200 g was sacrificed by chloroform inhalation method. Abdominal hair was shaved off after scarification. The sample of injured tissue had the adherent fat and dirt thoroughly removed. Before beginning the diffusion studies, the skin sample was immersed in phosphate buffer saline solution for 30 min. [Approval statement: The above-mentioned project, "Bilayer Nanofiber Scaffold Incorporated with Mupirocin and Thyme Essential Oil for Synergistic Activity Against Bacterial Wound Infections." (Protocol No.-BVCP/IAEC/07/2020) consisting of male white Wistar rat has been reviewed and approved by the IAEC. Humane care of the obtained animal used in animal studies was done as per the IAEC guidelines]. Vertical Franz diffusion cells with a diffusional surface area of 1 cm² and 32 ml of receptor cell volume were used for *ex vivo* permeation tests. First, the scaffold was fully submerged in the diffusion cell's receptor compartment underneath the sampling port. Second, a pH 7.4 phosphate buffered solution was added to the receptor compartments. The receptor phase was sustained

at 37°C by employing a circulated water bath with stirring at 200 rpm. Diffusion barriers were made out of rat skin. Then, over 72 hours, 1 ml aliquots were regularly taken out and refilled with a similar amount of receptor fluid. This adequate further diluting of receiver contents was assessed with a UV spectrophotometer. The cumulative amount of drug permeated across the skin (ug/cm²) was plotted against time (hr). The slope of the linear section of the graph was used to calculate the steady-state flux "J." Eq. 1 was used to calculate the Permeability Coefficient "Kp."

$$\text{Eq. (C): } K_p = J/C_0$$

Where C_0 is the drug concentration in the donor phase and J is the flux (Tas et al., 2007)

Antimicrobial studies

For antimicrobial assessment of electrospun nanofibers, the individual scaffolds of MUP-PCL, TEO-PVA, and combined bilayer scaffold of MUP-PCL-TEO-PVA was verified contrary to three microorganisms, *S. aureus*, *E. coli*, and *P. aeruginosa* using zone inhibition techniques to evaluate their antimicrobial action. Cultures of *S. aureus*, *E. coli*, and *P. aeruginosa* with a concentration of 10⁸ CFU/ml were prepared on nutrient agar plates. A scaffold specimen with a diameter of 0.9 cm was positioned on top of a 100, l of 10⁸ CFU/mL bacteria solution that had been spread out on an agar plate. Each sample's inhibitory region was quantified (Chen et al., 2017).

RESULTS AND DISCUSSION

Chemical composition of the essential oil

The output of essential oils was 1.0%. Freshly separated essential oil was a golden liquid with a strong, narcotic aroma. Sesquiterpene hydrocarbons, oxygenated sesquiterpenes, monoterpene hydrocarbons, and others were the five groups into which the constituents of essential oils were divided (Table 1). Thyme essential oil's GC and GC-MS analysis revealed 41 components, accounting for 97.85% of all detectable compounds. The main components of the oil were camphor (39.39%), camphene (17.57%),

α -pinene (9.55%), 1,8-cineole (5.57), borneol (5.03%), and β -pinene (4.32%). Less than 2% of other components were found overall (Table 1). The most significant monoterpene hydrocarbons, camphene, α -pinene,

β -pinene, and myrcene, were present in thyme essential oil. The oil's most prevalent component class (54.82%) was oxygenated monoterpenes.

Table 1. Chemical composition of the essential oil.

Compound	Content %	Compound	Content %
Tricyclene	0.64	Terpinene-4-ol	2.21
Alpha-thyjene	0.46	Para-cymen-8-ol	0.28
Alpha pinene	9.35	Alpha terpineol	0.57
Camphene	17.19	Verbenone	0.13
Beta pinene	4.23	Carveol 1	0.22
Myrcene	3.21	Carvacrol methyl ethyl	0.11
Alpha terpinen	0.27	Bornyl acetate	0.40
Para cymene	1.19	Thymol	0.24
1,8-cineole	5.45	Alpha-copaene	0.30
Trans Beta ocimene	0.09	Beta-bourbonene	0.12
Gama terpinene	0.55	Alpha-Gurjunene	0.66
Cis-sabinene hydrate	0.46	Beta-caryophyllene	0.09
Camphenilone	0.31	Aromadendrene	0.11
Alpha-terpinolene	0.11	Alpha-clemene	0.22
Linalol	0.14	Germacrene-d	0.23
Alpha-thyhone	0.29	Bicyclogermacrene	0.13
Nealloocimene	0.53	Spathulenol	0.73
Camphor	38.54	Caryophellene oxide	0.56
Borneol	4.92	Beta-oplepenone	0.07

Scanning Electron Microscopy (SEM)

SEM was used to validate the creation of nanofibers. SEM images revealed the development of casually oriented uniform and homogeneous fibers having a diameter range of 325–419 nm. It is assumed that the

drug was encapsulated and molecularly disseminated within the electrospun fibers because the photos did not indicate the existence of the drug crystals and/or aggregates on the surface (Figure 2.)(Kamble et al., 2016).

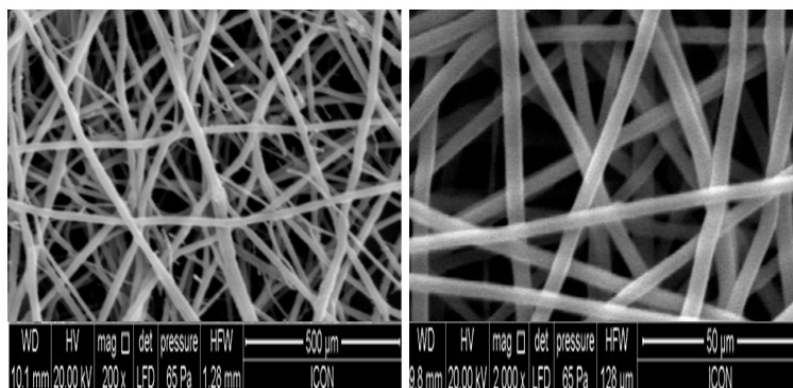


Figure 2. SEM images of electrospun MUP-PCL-TEO-PVA bilayer nanofiber scaffold.

Thickness

The thickness of nanofiber scaffold was confirmed by utilizing Yuzuki digital micrometer. Three samples were measured which give thickness 107 μm , 109 μm , and 113 μm respectively which shows the optimum thickness of nanofiber scaffold attributed to the ideal wound dressing material. The number of nanofibrous layers that cover each other increases as the thickness of nanofibrous scaffolds does, which causes a reduction in air permeability and an enhancement in the compaction and tightness of the nanocomposite scaffold (Ghasemi-Mobarakeh et al., 2009).

Porosity

The porosity of the MUP-PCL-TEO-PVA bilayer nanofiber scaffold by the alcohol immersion method was found to be 82% which indicates good porosity. Electrospinning creates scaffolds with a greater porosity compared to previous techniques (Li et al., 2019). A bacterial wound dressing benefits from the scaffolds' high porosity, which helps to promote hydration and prevent infection (Li et al., 2018). The highly porous nature of the patches may assist in removing discharge from the injury site as well as avoid wound infection. Additionally, the great amount of porous nature present acts as an advantage in delivering nutrients and O_2 to the cells connected to the dressings (Liang et al., 2016).

Swelling ratio

A gravimetric approach was used to determine the swelling index of electrospun nanofiber materials. The loading and release behavior of medication is significantly influenced by the nanofibers' swelling index. The degree of swelling of MUP-PCL-TEO-PVA scaffolds in PBS pH 7.4 after 24 h was 257.43%. However, after maximum swelling (351.57%) was noted at 12 h. In all cases, additional extensions of time revealed a reduction in the intensity of edema. This decline in

inflammation is mostly because of the breakdown of polymers, which causes the leakage of polymer from the nanofiber patch and reduces edema. The nanofibers' strong hydrophilicity and excellent swelling capabilities allow them to collect exudates at the wound site and keep it moist.

FTIR

The physical and chemical interactions of the polymers were studied using FTIR spectroscopy. The spectra of the MUP-PCL-TEO-PVA bilayer nanofiber scaffold exhibited preservation of all the characteristic bands (Figure 3a). Due to the lack of any chemical interaction, there was also no significant shifting of the existing bands or the emergence of new bands, indicating the compatibility of all nanofiber scaffold components. From the above overlay plot (Figure 3b.) of a pure drug (MUP), PCL, PVA, TEO, TWEEN 80, and nanofibers scaffold it has been observed that the medicine and the excipients utilized do not physically interact.

In the comprehensive FTIR analysis, the spectra of a film formulation containing the drug MUP alongside excipients such as PCL, PVA, TWEEN80 along TEO, were meticulously examined. By comparing these spectra with the isolated peaks of the drug MUP, a noteworthy revelation was observed. The distinct peaks corresponding to C-H Bending (806.14 cm^{-1}), CO-O-CO Stretching (1044.04 cm^{-1}), C-O Stretching (1143.17 cm^{-1}), C-N Stretching (1221.62 cm^{-1}), N-H Bending (1469.79 cm^{-1}), and C=C Stretching (1653.78 cm^{-1}) in drug MUP were found to be harmoniously echoed in the formulation's spectra. Furthermore, the presence of specific peaks associated with TEO and PCL within the formulation was also noted. This compelling evidence collectively suggests that there is no discernible interaction between the drug MUP and the selected excipients, thus affirming the compatibility of the drug with the formulation components.

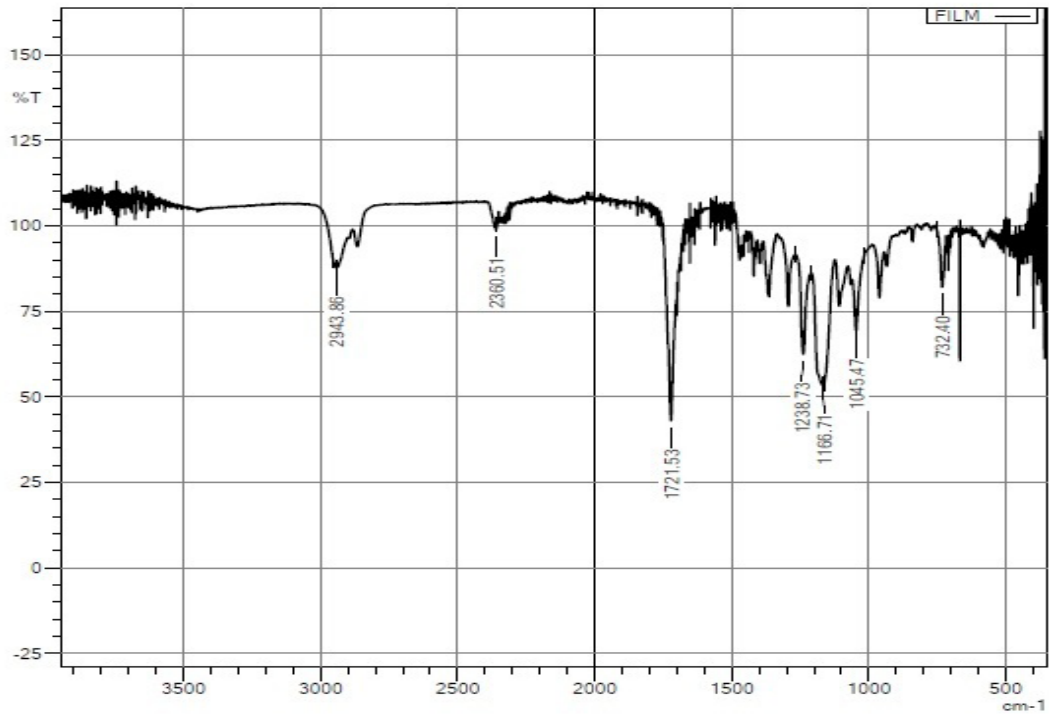


Figure 3a. FTIR spectra of MUP-PCL-TEO-PVA bilayer nanofiber scaffold.

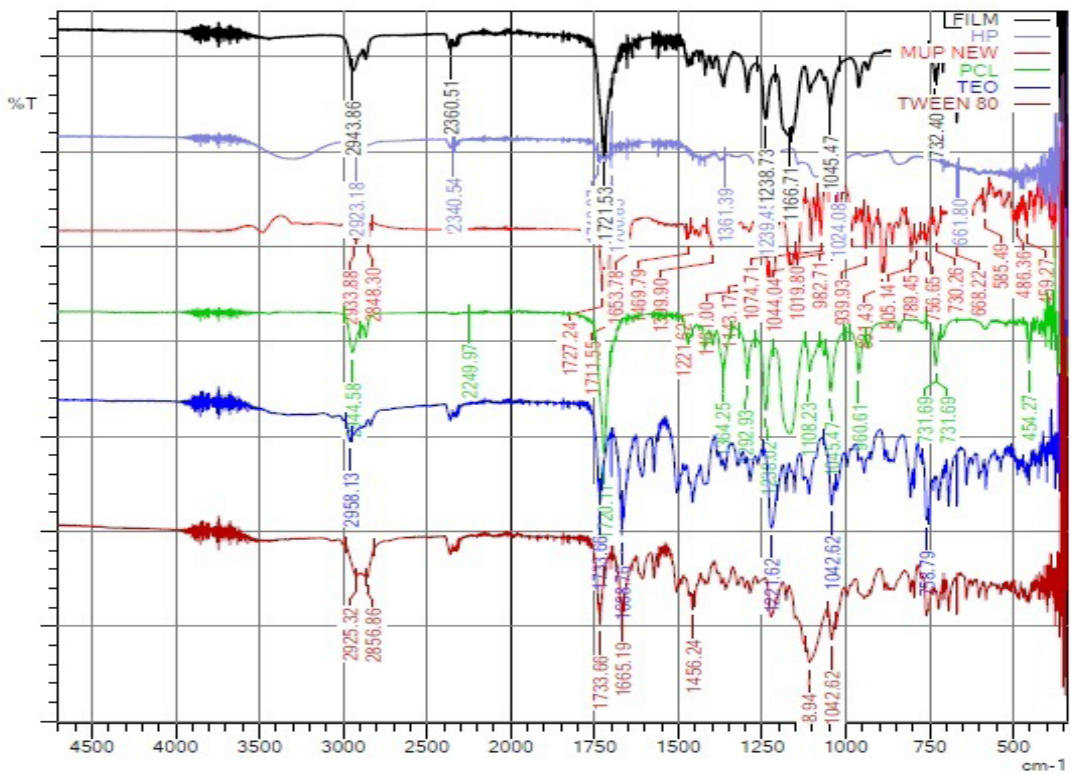


Figure 3b. Overlay plot of the pure drug (MUP), PCL, PVA, TEO, and TWEEN 80.

DSC

DSC is a technique for determining the temperature and energy variations associated with a compound's phase transitions, which aids in determining the degree of crystallinity. The crystalline character of MUP was confirmed by its abrupt endothermic peak at 71.5°C, which corresponds to its melting point Figure 4a. Also, TEO oil exhibited an endothermic peak at 215°C (Figure 4b). The DSC thermogram of both

the polymer used in formulation i.e., PCL shows endothermic peaks at 57.7°C and PVA shows endothermic peaks at 192.7°C respectively. However, the MUP-PCL-TEO-PVA bilayer nanofiber scaffold showed an endothermic peak only at 53.3°C and 193.0°C for two polymers PCL and PVA respectively as shown in (Figure 4c) whereas, peaks associated with MUP and TEO melting points were not present which indicates the whole amorphization and solubilization respectively when nanofibers formulations were prepared.

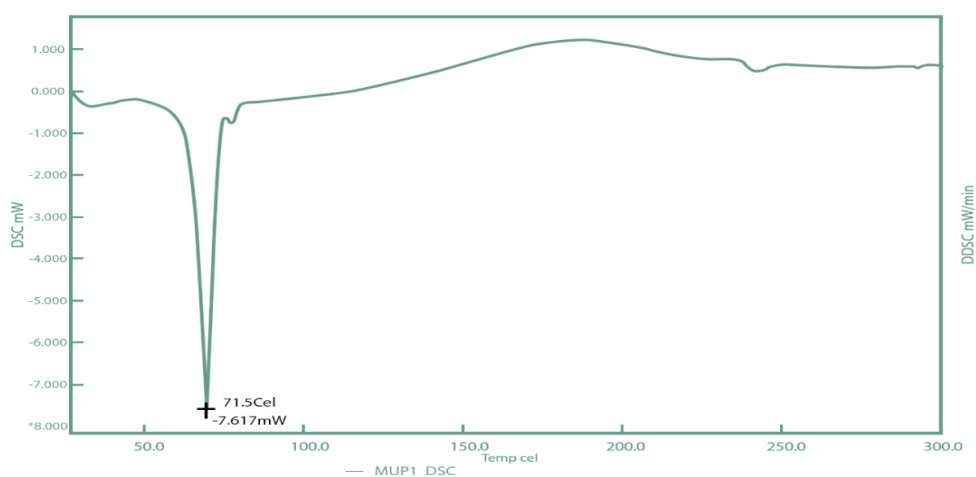


Figure 4a. DSC thermogram of pure MUP.

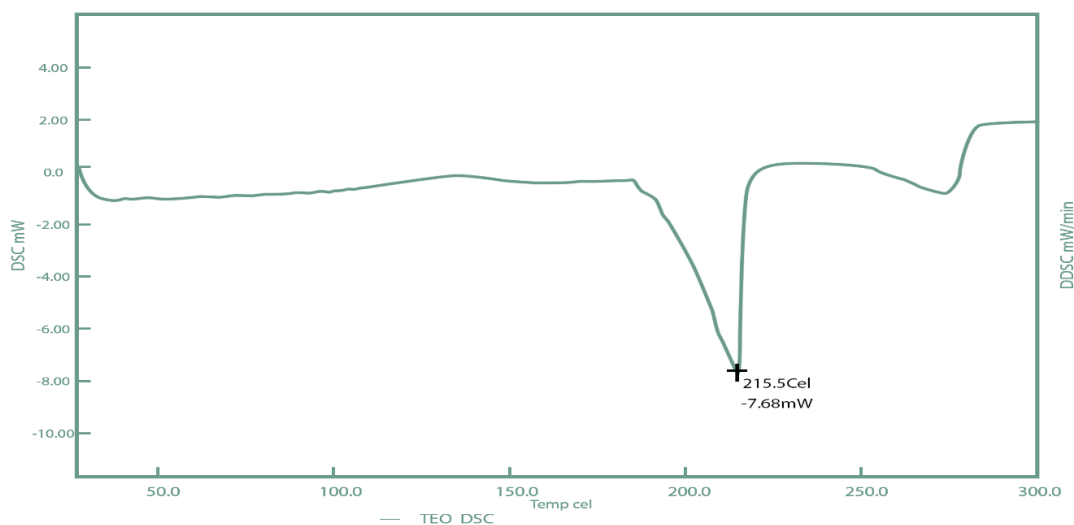


Figure 4b. DSC thermogram of TEO.

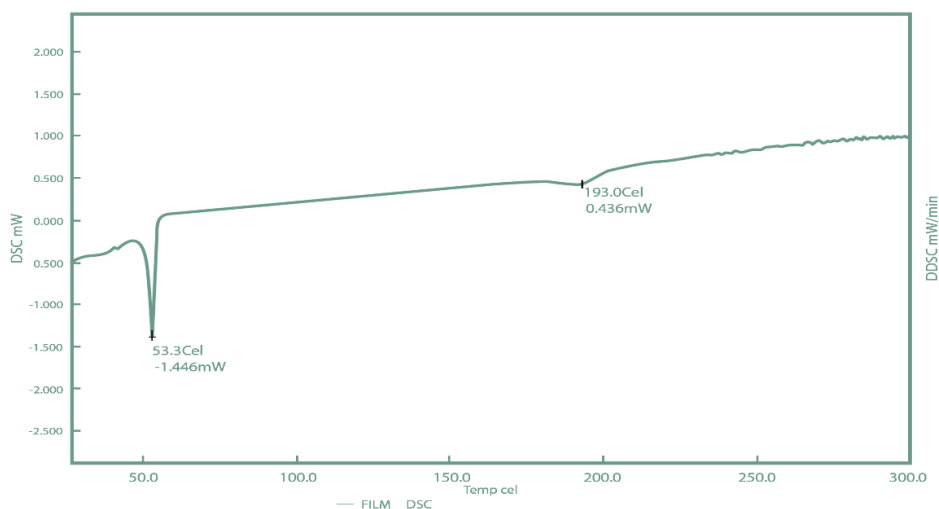


Figure 4c. Thermogram of MUP-PCL-TEO-PVA bilayer nanofiber scaffold

% Entrapment efficiency (% EE)

The % EE of the final optimized batch of bilayer nanofiber scaffold of MUP-PCL-TEO-PVA was studied using the UV spectroscopic method. The %EE of bilayer nanofiber scaffold was found to be 97.39 % and 93.06 % respectively for MUP and TEO.

In vitro drug release

The drug release profiles of an optimized batch from the MUP-PCL-TEO-PVA bilayer nanofiber scaffold are illustrated in Figure 5. The calibration curves of MUP at 230 nm were $R^2 = 0.995$ and TEO at 274 nm was $R^2 = 0.9961$. MUP displayed a prolonged release from the bilayer nanofiber scaffold for 3 days. A two-stage release profile initially showed rapid release and thereafter showed a slower sustained release. Figure 5 displays the results of a sustained release profile of MUP from the Bilayer nanofiber scaffold for 3 days. The initial rapid release of MUP from the bilayer nanofiber scaffold resulted in the release of 40.55% of the total MUP content in the first 6 hours. With the sustained release, another approximately 53% was released from the bilayer scaffold in the following 72 hours. TEO exhibited a two-stage release, initially showed rapid release, and thereafter slower sustained release was observed. About 48% of TEO was released from the bilayer nanofiber scaffold in the first hours. The cumulative drug release increased steadily to 87% in the following 10 hours.

Though identical drug release profiles could be seen for MUP as well as TEO, 49% of the TEO exhibited burst release during the first hour, whereas 27% of the MUP dispersed out of the nanofiber scaffold simultaneously. This was explained by the fact that intense chemical linkage bonds of PCL and MUP conjugated to the fiber, resulted in a lower release ability of MUP in comparison to TEO. Thyme essential oil with a burst release profile can quickly reduce the microbial load in the wound, promoting faster wound healing by creating a more favorable environment for tissue repair. MUP, while slower to release, can provide a sustained antimicrobial effect, ensuring continuous inhibition of microbes even after the initial rapid action of thyme essential oil. The combined action of both agents can be effective in addressing both the immediate need for rapid microbial reduction and the longer-term need for sustained antimicrobial activity, ultimately contributing to improved wound healing outcomes. Drug release from the bilayer nanofiber scaffolds is dependent on the concentration of polymers used and the flow rate of polymeric solutions for electrospinning. This means polymers with a smaller size range with a larger interfacial area, thus promoting the controlled release of the drug from the formulation. Multiple options for controlling release time profiles are available with electrospun medicated fibers having a multilayer structure.

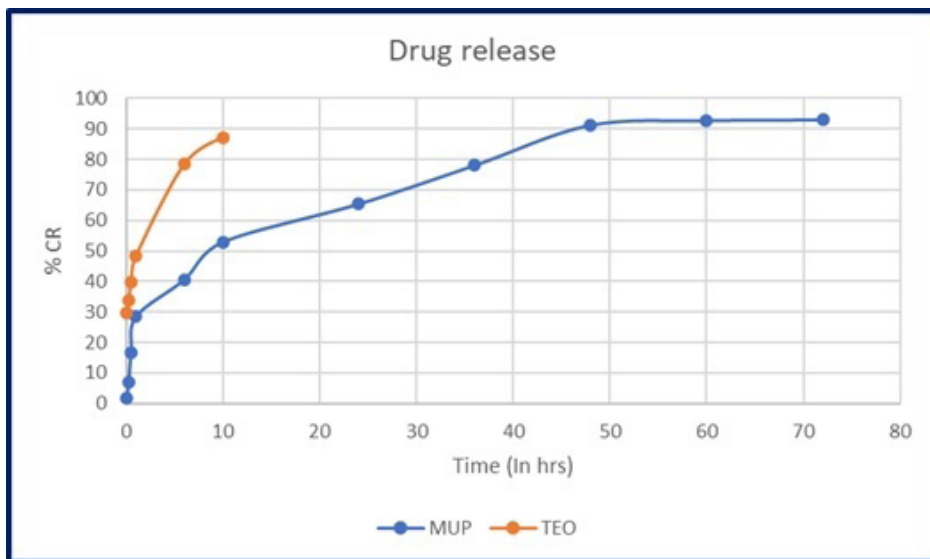


Figure 5. *In vitro* drug release of MUP and TEO from the MUP-PCL-TEO-PVA bilayer nanofiber scaffold.

***In vitro* drug permeation**

The *in vitro* drug permeation study of the MUP-PCL-TEO-PVA bilayer nanofiber scaffold was conducted using a Franz diffusion cell for 72 h. The drug permeation study was conducted for 72 hours. From acquired results (Figure 6), it was found that MUP showed initial rapid release and thereafter a slower

sustained release achieving 92.17% drug release after 72 h whereas TEO showed 85.45% release in 10 h with initial burst release and thereafter a sustained release profile. *In vitro*, drug permeation studies interpret the diffusion-derived drug delivery from nanofiber scaffold by following the KorsmeyerPeppas plot.

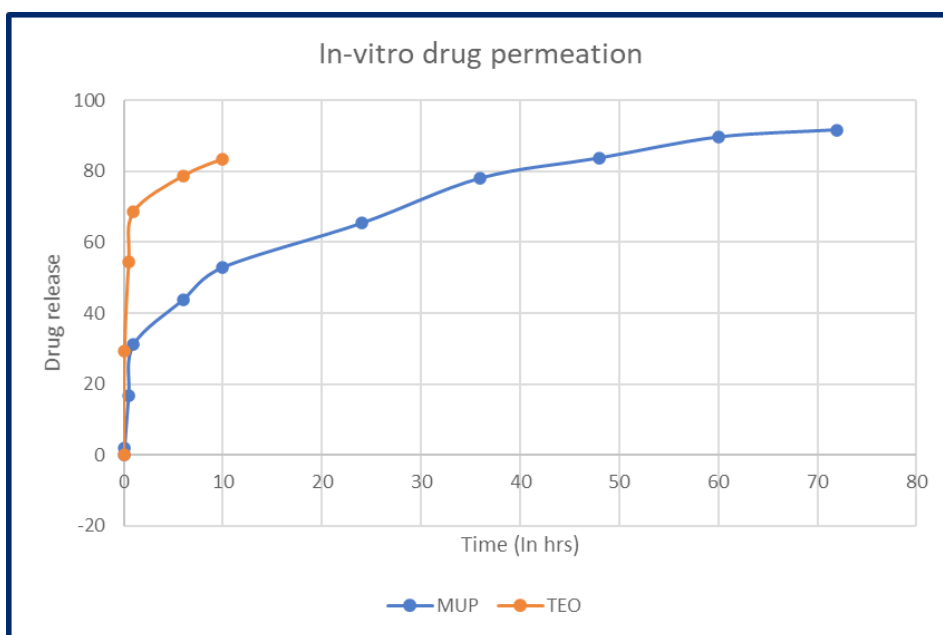


Figure 6. *In vitro* drug permeation of MUP and TEO from the MUP-PCL-TEO-PVA bilayer nanofiber scaffold.

Ex vivo studies

The *ex vivo* skin permeation study was performed by utilizing Franz diffusion cell for the MUP-PCL-TEO-PVA bilayer nanofiber scaffold. Here the skin is not whole in injured tissue. The study was carried out for 72 hours. From the results, it was found that MUP showed initial rapid release followed by a slower sustained release achieving 91.67% of drug release

whereas TEO showed 83.45% release in 10 h with initial burst release followed by sustained release profile (Figure 7). The *ex vivo* skin permeation data displayed that for the MUP-PCL-TEO-PVA bilayer nanofiber scaffold the flux of nanofiber mats was found to be 5.12 and permeability was found to be 0.00425 which is greater than that of conventional cast film. BVCP/IAEC/07/2020 is the proposal no. for *ex vivo* studies.

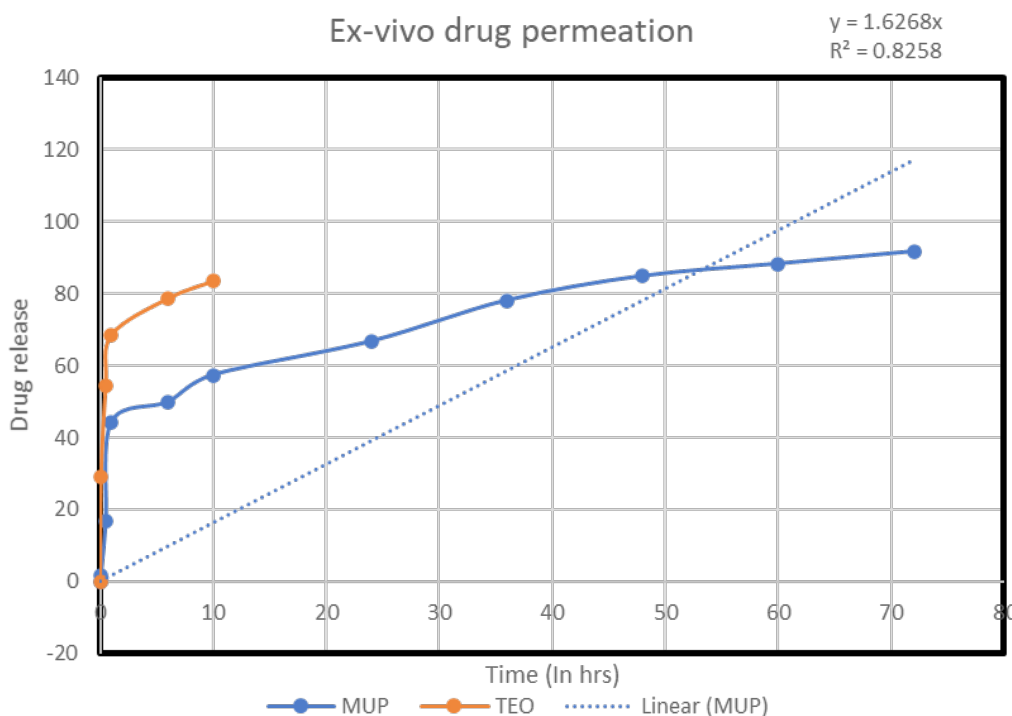


Figure 7. *Ex vivo* skin permeation from MUP-PCL-TEO-PVA bilayer nanofiber scaffold.

Antimicrobial studies

Antibacterial activity of individual scaffolds of MUP-PCL, TEO-PVA, and combined bilayer scaffold of MUP-PCL-TEO-PVA was verified in contrast to 3 microorganisms, *S. aureus*, *E. coli*, and *P. aeruginosa* to evaluate their antimicrobial action. The inhibitory region formed by the respective sample was evaluated. Figure 8 shows the activity of MUP-PCL, TEO-PVA, and combined bilayer scaffold. Zone of in-

hibition for *S. aureus* was shown as 17 mm, 11 mm, and 21 mm by MUP alone, TEO alone, and bilayer MUP-PCL-TEO-PVA respectively. The activity of MUP-PCL, TEO-PVA, and combined bilayer scaffold for *P. aeruginosa*, shows the inhibitory region as 14 mm, 8 mm, and 17 mm respectively. The activity of MUP-PCL, TEO-PVA and combined bilayer scaffold for *E. coli* shows the inhibitory region as 11 mm, 6 mm, and 12 mm respectively.

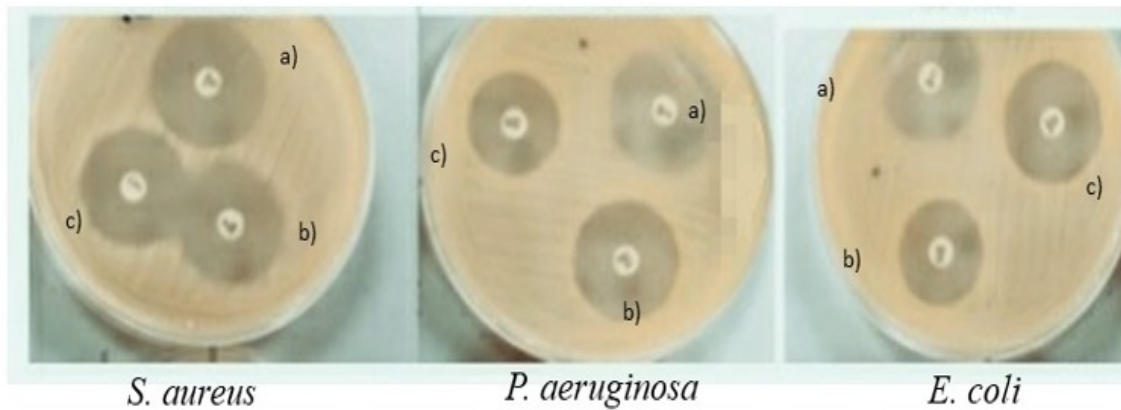


Figure 8. Antibacterial activity of MUP-PCL-TEO-PVA bilayer nanofiber scaffold against *S. aureus*, *P. aeruginosa*, and *E. coli*. [(a) MUP-PCL-TEO-PVA bilayer nanofiber scaffold, (b) MUP+PCL scaffold, (c) TEO+ PVA scaffold]

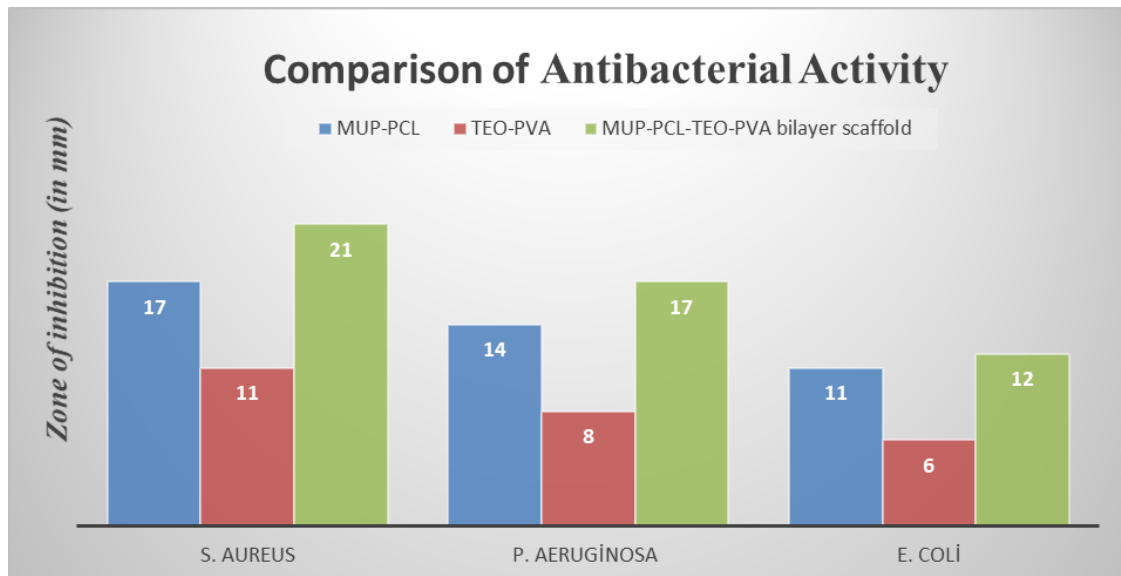


Figure 9. Statistical representation comparing the antibacterial activity of MUP-PCL-TEO-PVA bilayer nanofiber scaffold against *S. aureus*, *P. aeruginosa*, and *E. coli*. [(a) MUP-PCL-TEO-PVA bilayer nanofiber scaffold, (b) MUP+PCL scaffold, (c) TEO+ PVA scaffold]

The bilayer MUP-PCL-TEO-PVA scaffold exhibited outstanding action in contrast to all tested microorganisms, through the toughest action counter to *S. aureus* (21 mm), following this with *P. aeruginosa* (17 mm), and lastly *E. coli* (12 mm). Generally, this bilayer nanofiber scaffold displayed noteworthy action contrary to *S. aureus*, *E. coli*, as well as *P. aeruginosa*. The comparison is showcased in the Figure 9. To determine whether the observed differences in anti-

bacterial activity are statistically significant, a one-way ANOVA was conducted followed by Tukey's Honestly Significant Difference test (post hoc Analysis). Based on the post hoc analysis, the comparison between MUP-PCL and TEO-PVA has a p-value of 0.08, which is not statistically significant ($p > 0.05$). However, the comparisons between MUP-PCL-TEO-PVA and both MUP-PCL ($p = 0.02$) and TEO-PVA ($p = 0.04$) are statistically significant ($p < 0.05$). In this scenario, it

concludes that MUP-PCL-TEO-PVA has the highest antibacterial efficacy among the tested scaffolds. Thus, the scaffold produced here possibly will increase efficacy in treating bacterial-infected injuries due to the combined antibacterial effect of MUP and TEO. Mupirocin is a potent antibacterial agent and is extensively utilized by medical practitioners as a topical ointment to cure various topical wounds. MUP acts in contrast to a wide range of bacteria by resisting bacterial protein and RNA production by reversibly blocking isoleucyl-transfer RNA (Perumal et al., 2014).

CONCLUSION

In conclusion, this study successfully fabricated a novel MUP-PCL-TEO-PVA bilayer nanofiber scaffold using the electrospinning technique. The choice of polymer concentrations and electrospinning parameters played a critical role in determining drug release, % EE, and nanofiber structure. Notably, nanofibers composed of 10% PCL and 7% PVA exhibited favourable % EE and controlled drug release properties.

Characterization studies, including FTIR and DSC analyses, provided compelling evidence of the successful incorporation of both MUP and TEO within the nanofiber matrix. Furthermore, SEM images confirmed the formation of uniform and homogeneous nanofibers, essential for their efficacy as wound dressings.

In vitro drug permeation studies revealed distinct release profiles for MUP and TEO, with MUP initially displaying a rapid release followed by sustained drug release over 72 hours. Conversely, TEO exhibited an initial burst release followed by a sustained release pattern, reaching a significant level of release within 10 hours. This differential release kinetics could offer a tailored approach to wound treatment, allowing for rapid antimicrobial action (MUP) alongside lon-

ger-lasting benefits (TEO).

The *ex vivo* skin permeation data demonstrated that the MUP-PCL-TEO-PVA bilayer nanofiber scaffold exhibited superior permeability compared to conventional cast films, indicating its potential for improved transdermal drug delivery.

Most importantly, the antibacterial activity assessment highlighted the synergistic effect of MUP and TEO within the bilayer nanofiber scaffold. The increased zone of inhibition observed in the MUP-PCL-TEO-PVA bilayer scaffold, as compared to single-layer MUP and TEO scaffolds, underscores the potential of this innovative approach in combating bacterial infections more effectively.

Overall, our study offers a promising avenue for advanced wound care through the development of a bilayer nanofiber scaffold that combines the strengths of MUP and Thyme Essential Oil, potentially reducing bacterial resistance and improving treatment outcomes for bacterial wound infections.

ACKNOWLEDGEMENTS

This work was supported by AICTE by providing financial support under the Research Promotion Scheme (File No. 8-4/RIFD/RPS/policy-1/2017-2018) for the purchase of ESPIN NANO equipment and chemicals to carry out the research work. We are immensely grateful to Kawman Pharma Ltd. Mumbai, India, for providing the sample of MUP.

CONFLICT OF INTEREST

Authors declare that there is no conflict of interest.

AUTHOR CONTRIBUTION STATEMENT

In the collaborative endeavour of developing the mupirocin and thyme essential oil bilayer nanofiber scaffold for synergistic activity against bacterial wound infections, each author played a distinctive

role, contributing to various aspects of the research. Author Dr. Kisan JADHAV was instrumental in formulating the initial hypothesis, laying the foundation for our investigation. Shivani GHARAT actively engaged in the experimental design and execution, overseeing the intricate process of scaffold development. Simultaneously, Shradha ADHALRAO took charge of preparing the study text, ensuring clarity and coherence in presenting our findings. All authors collaborated in reviewing the text, collectively refining the manuscript to meet rigorous scientific standards. Statistical analysis and interpretation of the data were meticulously conducted by Shivani GHARAT, utilizing advanced methodologies to derive meaningful conclusions. Shradha ADHALRAO spearheaded the extensive literature research, grounding our work in existing knowledge and identifying gaps in understanding. The collaborative effort extended to critical discussions and consensus-building throughout the research journey, ultimately culminating in a comprehensive and impactful contribution from each author to the successful completion of this study.

REFERENCES

- Alkilani A.Z., McCrudden M.T.C., Donnelly R.F. (2015). Transdermal drug delivery: Innovative pharmaceutical developments based on disruption of the barrier properties of the stratum corneum. *Pharmaceutics*, 7, 438–470. <https://doi.org/10.3390/pharmaceutics7040438>.
- Abbas M., Hussain T., Arshad M., Ansari A.R., Irshad A., Nisar J. (2019). Wound healing potential of curcumin cross-linked chitosan/polyvinyl alcohol. *International Journal of Biological Macromolecules*, 140, 871–876. <https://doi.org/10.1016/j.ijbiomac.2019.08.153>
- Alhasso B., Ghori M.U., Conway B.R. (2023). Development of Nanoemulsions for Topical Application of Mupirocin, *Pharmaceutics*, 15(2), 378–380. <https://doi.org/10.3390/pharmaceutics15020378>
- Bakkiyaraj D., Sritharadol R., Padmavathi A.R., Nakpheng T., Srichana T. (2017). Anti-biofilm properties of a mupirocin spray formulation against *Escherichia coli* wound infections, *Biofouling*, 33, 591–600. <https://doi.org/10.1080/08927014.2017.1337100>.
- Chen X., Zhao R., Wang X., Li X., Peng F., Jin Z. (2017). Electrospun mupirocin loaded polyurethane fiber mats for anti-infection burn wound dressing application. *Journal of Biomaterials Science, Polymer Edition*, 28, 162–176. <https://doi.org/10.1080/09205063.2016.1262158>.
- Ghasemi-Mobarakeh L., Morshed M., Karbalaie K., Fesharaki M.A., Nematollahi M., Nasr-Esfahani M.H. (2009). The thickness of electrospun poly (ϵ -caprolactone) nanofibrous scaffolds influences cell proliferation, 32, 679–689. <https://doi.org/10.1177/03913988090320030>
- Goldmann O., Cern A., Müssen M., Rohde M., Weiss W., Barenholz Y. (2019). Liposomal mupirocin holds promise for systemic treatment of invasive *Staphylococcus aureus* infections. *Journal of Controlled Release*, 316, 292–301. <https://doi.org/10.1016/j.jconrel.2019.11.007>
- Kamble R.N., Gaikwad S., Maske A., Patil S.S. (2016). Fabrication of electrospun nanofibers of BCS II drug for enhanced dissolution and permeation across skin. *Journal of Advanced Research*, 7, 483–489. <https://doi.org/10.1016/j.jare.2016.03.009>.

- Kamlungmak S., Nakpheng T., Kaewpaiboon S., Bintang MAKM., Prom-in S., Chunhachaichana C. (2021). Safety and Biocompatibility of Mupirocin Nanoparticle-Loaded Hydrogel on Burn Wound in Rat Model. *Biological and Pharmaceutical Bulletin*, 44(11), 1707–1716. <https://doi.org/10.1248/bpb.b21-00397>
- KesiciGüler H., Cengiz C.F., SesliÇetin E. (2019). Antibacterial PVP/cinnamon essential oil nanofibers by emulsion electrospinning. *Journal of the Textile Institute*, 110, 302–310. <https://doi.org/10.1080/00405000.2018.1477237>.
- Liang D., Lu Z., Yang H., Gao J., Chen R. (2016). Novel Asymmetric Wetttable AgNPs/Chitosan Wound Dressing: In Vitro and in Vivo Evaluation. *ACS Applied Materials and Interfaces*, 8, 3958–3968. <https://doi.org/10.1021/acsami.5b11160>.
- Li J., Zhou Y., Yang J., Ye R., Gao J., Ren L. (2019). Fabrication of gradient porous microneedle array by modified hot embossing for transdermal drug delivery. *Materials Science and Engineering C*, 96, 576–582. <https://doi.org/10.1016/j.msec.2018.11.074>.
- Li X., Wang C., Yang S., Liu P., Zhang B. (2018). Electrospun PCL/mupirocin and chitosan/ lidocaine hydrochloride multifunctional double layer nanofibrous scaffolds for wound dressing applications. *International Journal of Nanomedicine*, 13, 5287–5299. <https://doi.org/10.2147/IJN.S177256>.
- Onlen Y., Duran N., Atik E., Savas L., Altug E., Yakan S. (2007). Antibacterial activity of propolis against MRSA and synergism with topical mupirocin. *Journal of Alternative and Complementary Medicine*, 13, 713–718. <https://doi.org/10.1089/acm.2007.7021>.
- Perumal S., Ramadass S.K., Madhan B. (2014) Sol-gel processed mupirocin silica microspheres loaded collagen scaffold: A synergistic bio-composite for wound healing. *European Journal of Pharmaceutical Sciences*, 52, 26–33. <https://doi.org/10.1016/j.ejps.2013.10.006>.
- Rather A.H., Wani T.U., Khan R.S., Pant B., Park M., Sheikh F.A. (2021). Prospects of polymeric nanofibers loaded with essential oils for biomedical and food packaging applications. *International Journal of Molecular Sciences*, 22, 12-28. <https://doi.org/10.3390/ijms22084017>.
- Thenmozhi S., Dharmaraj N., Kadirvelu K., Kim H.Y.(2017). Electrospun nanofibers: New generation materials for advanced applications. *Materials Science and Engineering B: Solid-State Materials for Advanced Technology*, 217, 36–48. <https://doi.org/10.1016/j.mseb.2017.01.001>.
- Thakur R.A., Florek C. A., Kohn J., Michniak B.B. (2008) Electrospun nanofibrous polymeric scaffold with targeted drug release profiles for potential application as wound dressing. *International Journal of Pharmaceutics*, 364, 87–93. <https://doi.org/10.1016/j.ijpharm.2008.07.033.3>,

- Tanriverdi S.T., Suat B., Azizoğlu E., Köse FA., Özer Ö.(2018). In-vitro evaluation of dexpanthenol-loaded nanofiber mats for wound healing. *Tropical Journal of Pharmaceutical Research*, 17, 387–394. <https://doi.org/10.4314/tjpr.v17i3.1>.
- Tas C., Ozkan Y., Okyar A., Savaser A. (2007). In vitro and ex vivo permeation studies of etodolac from hydrophilic gels and effect of terpenes as enhancers. *Drug Delivery*, 14, 453–459. <https://doi.org/10.1080/10717540701603746>.

Protective Role of *Pistacia palaestina* Boiss. Fruit and Leaf Extracts in Isoproterenol-Induced Cardiac Ischemia

Mehmet Sina İÇEN*, Hande YÜCE**, Neşe BAŞAK TÜRKMEN***, Aslı TAŞLIDERE****, Dilan AŞKIN ÖZEK*****, Songül ÜNÜVAR*****

Protective Role of Pistacia palaestina Boiss. Fruit and Leaf Extracts in Isoproterenol-Induced Cardiac Ischemia

Pistacia palaestina Boiss. Meyve ve Yaprak Ekstrelerinin İzoproterenol Kaynaklı Kardiyak İskemide Koruyucu Rolü

SUMMARY

Myocardial infarction (MI) is one of the leading causes of death worldwide. This study aimed to investigate the protective effects of *Pistacia palaestina* Boiss (PP) leaf and fruit extracts, which are thought to have antioxidant and anti-inflammatory activity, in isoproterenol (ISO)-induced MI. 80 Sprague-Dawley rats were divided into ten groups. The control group was given 0.9% isotonic sodium chloride saline. PP leaf and fruit extracts at doses of 250 mg/kg and 500 mg/kg were administered by oral gavage for 21 days. ISO 100 mg/kg subcutaneously was administered to the MI and MI-treatment groups on the 17th and 18th days of the experiment. Thiobarbituric acid reactive substances (TBARS) and glutathione (GSH) levels, catalase (CAT), superoxide dismutase (SOD), and glutathione peroxidase (GPx) activities were measured in heart tissue. In serum, troponin T, CK-MB; pro-inflammatory cytokine necrosis factor- α (TNF- α), interleukin-1 β (IL-1 β), and IL-6; anti-inflammatory IL-10 levels were determined by the ELISA method. Heart tissue was examined by hematoxylin-eosin staining. While lipid peroxidation indicator TBARS activity increased in the MI group, antioxidant enzyme activities and GSH levels decreased. While troponin T, CK-MB, TNF- α , IL-1 β , and IL-6 levels increased, anti-inflammatory IL-10 levels decreased. Low and high dose PP leaf and fruit extracts significantly decreased TBARS, troponin T, CK-MB, TNF- α , IL-1 β , and IL-6 levels improved antioxidant enzyme activity, and GSH and IL-10 levels. PP ameliorated cardiac biomarkers and histopathological changes in ISO-induced MI by suppressing oxidative stress and inflammation. PP extracts may play an important cardioprotective role in the treatment of MI through their antioxidant and anti-inflammatory effects.

Key Words: *Pistacia palaestina* boiss, myocardial infarction, isoproterenol, antioxidant, anti-inflammatory activity, cardiac markers.

ÖZ

Miyokard enfarktüsü (MI) dünya çapında önde gelen ölüm nedenlerinden biridir. Bu çalışmada antioksidan ve antiinflamatuvar aktiviteye sahip olduğu düşünülen *Pistacia palaestina* Boiss (PP) yaprak ve meyve ekstrelerinin izoproterenol (ISO)-indüklü MI'da koruyucu etkilerinin araştırılması amaçlanmıştır. 80 adet Sprague-Dawley sıçan 10 gruba ayrıldı. Kontrol grubuna %0,9 izotonik sodyum klorür verildi. 250 mg/kg ve 500 mg/kg dozlarında PP yaprak ve meyve ekstreleri 21 gün süreyle gavaj yoluyla uygulandı. MI ve MI-tedavi gruplarına deneyin 17. ve 18. günlerinde ISO 100 mg/kg subkutan olarak uygulandı. Kalp dokusunda tiyobarbitürik asit reaktif maddeleri (TBARS) ve glutatyon (GSH) düzeyleri, katalaz (CAT), süperoksit dismutaz (SOD) ve glutatyon peroksidaz (GPx) aktiviteleri ölçüldü. Serumda troponin T, CK-MB; proinflamatuvar sitokin nekroz faktörü-alfa (TNF- α), interlökin-1 β (IL-1 β) ve IL-6; antiinflamatuvar IL-10 düzeyleri ELISA yöntemiyle belirlendi. Kalp dokusu hematoksilen-eozin boyama ile incelendi. MI grubunda lipid peroksidasyon göstergesi TBARS aktivitesi artarken, antioksidan enzim aktiviteleri ve GSH seviyeleri azaldı. Troponin T, CK-MB, TNF- α , IL-1 β ve IL-6 düzeyleri artarken antiinflamatuvar IL-10 düzeyleri azaldı. Düşük ve yüksek doz PP yaprak ve meyve ekstreleri TBARS, troponin T, CK-MB, TNF- α , IL-1 β , IL-6 düzeylerini önemli ölçüde azaltmış, antioksidan enzim aktivitelerini, GSH ve IL-10 düzeylerini iyileştirmiştir. PP, oksidatif stres ve inflamasyonu baskılayarak ISO-indüklü MI'daki kardiyak biyobelirteçleri ve histopatolojik değişiklikleri düzeltmiştir. PP ekstreleri antioksidan ve antiinflamatuvar etkileriyle MI tedavisinde önemli bir kardiyoprotektif rol oynayabilir.

Anahtar Kelimeler: *Pistacia palaestina* Boiss, miyokard enfarktüsü, izoproterenol, antioksidan, antiinflamatuvar aktivite, kardiyak belirteçler.

Received: 17.09.2023

Revised: 26.01.2024

Accepted: 29.01.2024

* ORCID: 0000-0002-1411-7184, Department of Pharmacognosy Faculty of Pharmacy, Inonu University, Malatya, Türkiye.

** ORCID: 0000-0003-2907-2019, Department of Pharmaceutical Toxicology, Faculty of Pharmacy, Inonu University, Malatya, Türkiye.

*** ORCID: 0000-0001-5566-8321, Department of Pharmaceutical Toxicology, Faculty of Pharmacy, Inonu University, Malatya, Türkiye.

**** ORCID: 0000-0003-3902-3210, Department of Histology and Embryology, Faculty of Medicine, Inonu University, Malatya, Türkiye.

***** ORCID: 0000-0001-9075-4807, Department of Pharmaceutical Toxicology, Faculty of Pharmacy, Inonu University, Malatya, Türkiye.

***** ORCID: 0000-0001-8454-490X, Department of Pharmaceutical Toxicology, Faculty of Pharmacy, Inonu University, Malatya, Türkiye.

° Corresponding Author: Dilan AŞKIN ÖZEK
E-mail: daskin@firat.edu.tr

INTRODUCTION

In 2020, 928.741 people in the United States and approximately 19.05 million people worldwide died from cardiovascular disease (Tsao et al. 2023). Myocardial infarction (MI), one of the most common cardiovascular diseases, is characterized by insufficient blood circulation feeding the heart and causes irreversible acute necrosis (Mechanic et al. 2022). Although there are many surgical and pharmacological treatment methods for MI and ischemic heart diseases, these methods are insufficient in reversing the damage to the heart and improving the changing biochemical parameters. Developing new molecules that reduce damage to the heart and have fewer side effects is of vital importance for reducing MI complications and mortality.

Subcutaneous administration of isoproterenol (ISO), a synthetic catecholamine, and β -adrenergic receptor agonist, has been reported to induce infarction-like myocardial lesions (El-Gohary & Allam, 2017). The ISO-induced cardiac ischemia model is often used to investigate new treatment modalities against MI, myocardial ischemia, and cardiac fibrosis in experimental animals. ISO causes progressive cardiotoxicity at low doses, whereas it causes acute cardiac damage at high doses (Allawadhi et al. 2018). ISO causes mitochondrial damage and increased oxidative stress, resulting in changes in cardiac biochemical parameters that lead to cardiac damage (Nwokocha et al. 2017, Allawadhi et al. 2018). Therefore, products of natural origin with antioxidant properties can reduce the damage by protecting against cardiac damage caused by MI (Feng et al. 2019).

Recent studies have suggested that phytotherapeutics are effective in the prevention and treatment of cardiovascular diseases (Deng et al. 2015; Allawadhi et al. 2018; Feng et al. 2019). The genus *Pistacia* has recently attracted attention in the field of phytotherapy as an important source of phenolic compounds, terpenoids, monoterpenes, flavonoids, alkaloids, saponins, fatty acids, and sterols. It has been reported

that different parts of these plants, such as the leaves, trunk, bark, arborvitae, and fruit, have different uses. Its medicinal uses are mentioned in ancient pharmacopoeias, Ayurveda, traditional Chinese medicine, Iranian folk medicine, and other similar sources. As a result of the increased interest in the use of *Pistacia* species, studies have been conducted to evaluate various properties, such as antioxidant, antimicrobial, antiviral, anticholinesterase, anti-inflammatory, antinociceptive, antidiabetic, antitumor, antihyperlipidemic, antiatherosclerotic, and hepatoprotective properties (Tomaino et al. 2010; Hosseinzadeh et al. 2012; Rauf et al. 2017). It has been reported that the seeds of the *Pistacia vera* L. plant are used as cardioprotective and exhilarating (Sobhani et al. 2017). In the literature review about *Pistacia palaestina* Boiss (PP), another species of this genus, research has suggested that the amounts of essential oils vary depending on the region where the plant grows. The essential oil obtained from the leaves of the plant collected from Osmaniye was analyzed by gas chromatography-mass spectrometry (GC-MS), and it was determined that it contained α -pinene (19.9%) as the major compound. In addition, the antibacterial and insecticidal activities of essential oils have been reported (Ulukanli et al. 2014). The contents of the essential oils obtained separately from the leaves, thuja, raw and ripe fruits of the plant collected in Jordan, and the major compounds were α -pinene in the leaf (61.3%), α -pinene in the thuja (49.4%), and (E)-ocimene (41.3%) in the raw fruit and (E)-ocimene (33.8%) were detected in ripe fruit (Flamini et al. 2004). In another study conducted in Lebanon, 29 components were found in the essential oil obtained from the fruits of the plant, and the main components with the highest ratios were sabinene (17.08%) and limonene (8.56%). The antiviral activity of the plant evaluated in vitro was found to be low (Loizzo et al. 2008). It has been reported that the essential oil obtained from the seeds of the plant collected in Lebanon inhibits the proliferation of K562 human leukemia cells (Lampronti et al. 2005). In the human hepatocyte cell line (HepG2), PP extracts

showed cytotoxic activity by reducing cell viability (Saad et al. 2006). Although content analysis has been performed for PP leaves and fruits, their biological activities are not yet fully known. Studies on its biological activity are limited. However, it is known that in traditional medicine, ripe fruits of PP are consumed as food by adding them to the medicinal herb mixture called zahter (Flamini et al. 2004). PP likely has a powerful antioxidant and anti-inflammatory activity due to the high amounts of α -pinene, (E)-ocimene, sabinene, and limonene components found in its fruits and leaves.

This study aimed to determine the cardioprotective role of low and high doses of leaf and fruit extracts of the PP in ISO-induced MI in rats. To determine the antioxidant capacity of the extracts, thiobarbituric acid reactive substances (TBARS) and glutathione (GSH) levels, catalase (CAT), superoxide dismutase (SOD), and glutathione peroxidase (GPx) activities were measured in heart tissue. Levels of the pro-inflammatory cytokines interleukin-1 β (IL-1 β), IL-6, tumor necrosis factor-alpha (TNF- α), and anti-inflammatory cytokine IL-10 were evaluated in the blood serum. Additionally, the creatine kinase-myocardial band (CK-MB) and troponin T levels, which are biomarkers of cardiac ischemia, were determined. Histopathological examination of heart tissues was

performed using hematoxylin-eosin staining.

MATERIALS AND METHOD

Preparation of Plant Extract

The leaves and fruits of the PP plant, which were collected in the Pütürge district of Malatya province in the Eastern Anatolia Region, from the end of August to early September 2020, were dried in the shade. Diagnosis of PP plant İnönü University Faculty of Pharmacy, Department of Pharmaceutical Botany, the lecturer was made by Prof. Dr. Turan Arabacı. PP samples were kept in the herbarium of İnönü University Faculty of Pharmacy with the number S11032. Dried leaves and fruits were carefully separated and weighed. 530 g of leaves and 420 g of fruit were weighed and ground in a grinder and macerated with a sufficient amount of 80% ethanol (Sigma-Aldrich, Cas no: 64-7-5, Germany) at room temperature for 24 hours. The extract was filtered using filter paper. The filtrate was collected, and 80% ethanol was added to the plant again, and macerated again for 24 h. The filtrates collected in this way, 7 repetitions in total, were concentrated under low pressure in the rotavapor (Laborota 4011-digital, Heidolph, Germany) at temperatures not exceeding 45°C and dried with a lyophilizer. The extract amounts and yields are presented in Table 1.

Table 1. Amount of PP leaves and fruits used for extraction, amount of extraction obtained, and yield.

PP	Amount (g)	Obtained extract (g)	Yield (%)
Leaf	530	86.13	16.25%
Fruit	420	78.36	18.65%

Establishment of the Cardiac Ischemia Model

Eighty Sprague-Dawley rats with an average weight of 250-300 g were used in this study. Rats were obtained from the İnönü University Experimental Animals Production and Research Center. This study was carried out with the approval of the İnönü University Animal Experiments Local Ethics Committee dated 25.02.2020 and numbered 2020/3-4. Rats were divided into ten groups; control, MI, MI+PP leaf (250 mg/kg), MI+PP leaf (500 mg/kg), MI+PP fruit (250

mg/kg), MI+PP fruit (500 mg/kg), PP leaf (250 mg/kg), PP leaf (500 mg/kg), PP fruit (250 mg/kg), PP fruit (500 mg/kg). The control group was given 0.9% isotonic sodium chloride (NaCl) saline by gavage for 21 days. The control group was injected subcutaneously (sc) with saline on the 17th and 18th days of the experiment. ISO (100 mg/kg, Sigma-Aldrich, Cas no: 51-30-9, China) was dissolved in 0.9% NaCl and injected sc into the right thigh of the rat for two consecutive days, 24 hours apart, to induce MI (Boarescu

et al. 2019). 250 mg/kg and 500 mg/kg doses of PP leaf and fruit extracts were dissolved in 0.1% CMC (carboxy methyl cellulose) and administered by gastric gavage for 21 days. The rats were sacrificed at the end of the 21st day. The heart tissue was carefully removed, and divided vertically into two pieces, and the left atrium and ventricle were stored at -80°C for biochemical examination. The right atrium and ventricle were fixed with 10% formalin.

Biochemical Examination of Heart Tissue

Heart tissue samples were stored at -80°C until biochemical enzyme analysis. Before the analysis, the heart tissues were washed with physiological saline, weighed, diluted 1:10, and homogenized using a Teflon glass homogenizer in 20 mM Tris-HCl (pH 7.4) buffer. Some homogenates were separated and used for TBARS and CAT activity measurements. The remaining homogenates were centrifuged at 3.500 rpm for 30 min for GSH, SOD, and GPx analyses in a refrigerated centrifuge (NF 800R, Nüve, Türkiye), and supernatants were collected.

Determination of TBARS Levels

The levels of thiobarbituric acid reactive substance (TBARS), a lipid peroxidation marker, were determined using the Yagi method in homogenized heart tissue (Yagi, 1998). Tissue homogenate was precipitated with 10% trichloroacetic acid (TCA, Sigma-Aldrich, Cas no: 76-03-9, Germany) (pH: 3.5) and kept in a hot water bath (Memmert, Germany) for 15 minutes. The mixture was then cooled and centrifuged at 3000 rpm for 10 min. The remaining supernatant was carefully removed. The supernatant was incubated with thiobarbituric acid (TBA, Merck, L55063680 731, Germany) in a 95°C water bath for 50 min and cooled. The absorbance of the pink complex formed as a result of the reaction of malondialdehyde with TBA was measured at 532 nm using a spectrophotometer (T60 UV/VIS, Enotek, UK).

Determination of GSH Levels

10% TCA (0.2 M, pH: 8.9) was added to the heart

tissue homogenate and tissue was precipitated for 10 min at 3500 rpm. The resulting supernatants were added with tris-ethylenediamine tetraacetic acid (EDTA, Sigma-Aldrich, Cas no: 6381-92-6, USA) and 0.01 M 5,5'-dithiobis (2-nitrobenzoic acid) (1:9) buffer solution was added. By adding 0.01 mol/L DTNB (5-5'-dithiobis – nitro benzoic acid) to the mixture, it is reduced by sulfhydryl compounds and forms a yellow complex, which is a disulfide compound. The absorbance of this yellow compound was measured at 412 nm in a spectrophotometer (Sedlak & Lindsay, 1968).

Determination of SOD Activity

The superoxide radical formed during the conversion of xanthine to uric acid by xanthine oxidase reacts with nitroblue tetrazolium (NBT) in the environment to form purple-colored formazan. In the presence of superoxide dismutase in the environment, because the superoxide radical formed is converted to hydrogen peroxide, NBT reduction and, therefore, formazan formation will decrease. The reduction of formazan formation was determined spectrophotometrically by measuring at 560 nm. Enzyme activity that inhibited NBT reduction by 50% was considered SOD activity (Sun et al. 1968).

Determination of CAT Activity

Homogenates of heart tissue were subjected to sanitation for 3×10 seconds in a cold environment. Hydrogen peroxide was gradually added to the pH=7 buffer solution prepared with $\text{NaH}_2\text{PO}_4 \cdot 2\text{H}_2\text{O}$ and $\text{NaH}_2\text{PO}_4 \cdot 12\text{H}_2\text{O}$. Buffer solution was added to the samples at a ratio of 300:1, and the decrease in absorbance as a result of the breakdown of hydrogen peroxide by catalase was measured at a wavelength of 240 nm. This decrease in absorbance is directly proportional to enzyme activity (Aebi, 1974).

Determination of GPx Activity

To determine the GPx activity, a buffer solution consisting of NaH_2PO_4 , NaH_2PO_4 , and EDTA was prepared. Reduced glutathione, NADPH, and sodium

azide were dissolved separately in a buffer solution. GSH reductase dissolves ammonium sulfate solution. These separately prepared solutions were added to the sample and incubated for 30 min. Hydrogen peroxide was added to the mixture, and the decrease in absorbance was immediately measured in a spectrophotometer at 340 nm for 2 min. The decrease in absorbance was directly proportional to glutathione peroxidase activity (Paglia & Valentine 1967).

Determination of Total Protein Amount

The amount of total protein in the heart tissue was measured according to the method determined by Lowry et al. (Lowry et al. 1951) Reagent A, consisting of CuSO_4 and anhydrous sodium citrate, and reagent B, consisting of Na_2CO_3 and NaOH , was mixed at a ratio of 1:50 and added to the sample. Thus, alkaline copper (Cu^{2+}) forms a complex with peptide bonds, and every 7 or 8 amino acid residues are bonded to 1 atom of Cu. When Folin-Cieolteu reagent was added to the reaction, a purple-blue color was formed, and the color change of these samples was measured with a spectrophotometer at 700 nm. Parameters measured in heart tissue homogenates were normalized according to the amount of protein.

ELISA Analysis

Four mL of blood taken from all experimental groups was centrifuged at 2500 g for 10 minutes at room temperature, separated into serum, and stored at -80°C until analysis. Troponin T (E0311Ra), CK-MB (E0311Ra), $\text{TNF-}\alpha$ (E0764Ra), $\text{IL-1}\beta$ (E0107Ra), IL-6 (E0135Ra), and IL-10 (E0108Ra) levels were determined at 450 nm by using commercially available ELISA kits (Bioassay Technology Laboratory, China) and ELISA plate reader (Biotek Instruments Inc., USA).

Histopathological Analysis

Heart tissues were fixed in 10% formalin. Tissues undergoing follow-up procedures were enclosed in paraffin blocks. Sections of 5 μm thickness were taken from the prepared blocks with a microtome knife

system (Leica RM 2245), and the hematoxylin-eosin staining method was applied to the sections. Tissues were examined for necrosis, mononuclear cell infiltration, hemorrhage, and vascular occlusion using a Leica DFC 280 light microscope and Leica Q Win Image Analysis System (Leica Microsystems Imaging Solutions, Cambridge, UK). The histopathological damage score was calculated according to the findings obtained.

Statistical Analysis

SPSS 12.0 (SPSS Inc.; Chicago, IL, USA) was used for the analyses. The Kruskal-Wallis test was used for intergroup comparisons for histopathological examinations. The difference between the groups was evaluated with the Bonferroni Mann-Whitney U test. One-way ANOVA followed by Tukey's post-hoc test was used to statistically evaluate the biochemical parameters and ELISA results. $p < 0.05$ was considered significant. Data are shown as mean \pm SEM.

RESULTS and DISCUSSION

Biochemical Results

CAT, SOD, and GPx activities and TBARS, GSH levels of PP plant leaf and fruit extracts in rat heart tissue are given in Table 2. TBARS levels, which indicate the amount of lipid peroxidation, were statistically significantly higher in the MI group compared to all other groups. However, it was determined that PP treatment significantly reduced the increase in TBARS caused by ISO. GSH levels, which are antioxidant defense system elements, and CAT, SOD, and GPx activities were significantly decreased in the MI group. Leaf and fruit extracts of PP ameliorated the decrease in antioxidant enzyme activity. It was observed that fruit extract treatment at a dose of 500 mg/kg decreased TBARS levels and increased antioxidant enzyme levels more than other treatment groups, but this was not statistically significant.

Table 2. TBARS, GSH levels, and CAT SOD, GPx activities in rats (Mean±SEM, n=8).

Groups	TBARS (nmol/g tissue)	GSH (nmol/mL)	CAT (U/mg protein)	SOD (U/mg protein)	GPx (U/mg protein)
Control	11.97±0.73	94.75±1.96	0.032±0.0017	40.66±1.70	269.1±4.8
MI	20.48±1.12 [*]	58.84±2.98 [*]	0.018±0.0005 [*]	22.52±1.75 [*]	153.6±2.7 [*]
MI+PP leaf 250 mg/kg	15.99±0.61 ^{*,#}	78.94±3.00 ^{*,#}	0.024±0.0012 ^{*,#}	31.28±0.82 ^{*,#}	193.9±8.2 ^{*,#}
MI+PP leaf 500 mg/kg	15.76±0.67 ^{*,#}	71.44±4.20 [*]	0.025±0.0010 ^{*,#}	31.04±0.85 ^{*,#}	198.3±6.0 ^{*,#}
PP leaf 250 mg/kg	10.66±0.90 [#]	95.25±2.27 [#]	0.034±0.0019 [#]	39.33±1.52 [#]	270.7±7.3 [#]
PP leaf 500 mg/kg	11.24±0.99 [#]	94.44±4.08 [#]	0.032±0.0010 [#]	40.01±1.18 [#]	272.1±2.8 [#]
MI+PP fruit 250 mg/kg	15.54±0.65 ^{*,#}	78.08±2.18 ^{*,#}	0.025±0.0005 [*]	31.20±1.05 ^{*,#}	198.3±5.9 ^{*,#}
MI+PP fruit 500 mg/kg	14.17±0.64 ^{*,#}	78.20±4.40 ^{*,#}	0.026±0.0010 [*]	32.40±0.070 ^{*,#}	200.8±3.7 ^{*,#}
PP fruit 250 mg/kg	10.88±0.33 [#]	94.67±2.75 [#]	0.030±0.0005 [#]	40.73±0.75 [#]	274.7±4.0 [#]
PP fruit 500 mg/kg	11.05±0.17 [#]	98.92±2.44 [#]	0.034±0.0015 [#]	42.77±1.26 [#]	270.1±2.9 [#]

: Significant compared to the control group (: $p < 0.05$), #: Significant compared to the MI group (#: $p < 0.05$). (CAT: catalase, GPx: glutathione peroxidase, GSH: glutathione, SOD: superoxide dismutase, TBARS: thiobarbituric acid reagents, PP: *Pistacia palaestina* Boiss)

The effect of PP leaf and fruit extracts on serum troponin T, CK-MB, TNF- α , IL-1 β , IL-6, and IL-10 levels is given in Figure 1. According to the results, the levels of cardiac serum markers troponin T, CK-MB, and pro-inflammatory cytokine TNF- α , IL-1 β , and IL-6 increased in the MI group with the administration of ISO. On the other hand, anti-inflammatory IL-10 levels decreased. This increase in pro-inflammatory cytokine levels caused by ISO in MI groups

was statistically decreased in both doses (250 mg/kg and 500 mg/kg) in the treatment groups (MI+PP leaf and MI+PP fruit). It was observed that the decrease in troponin T, CK-MB, and proinflammatory cytokine levels was more pronounced in the treatment with 500mg/kg fruit extracts. The cytokine levels of the groups given PP alone (Groups 7, 8, 9, and 10) were similar to the control group in the fruit and leaf groups for both doses.

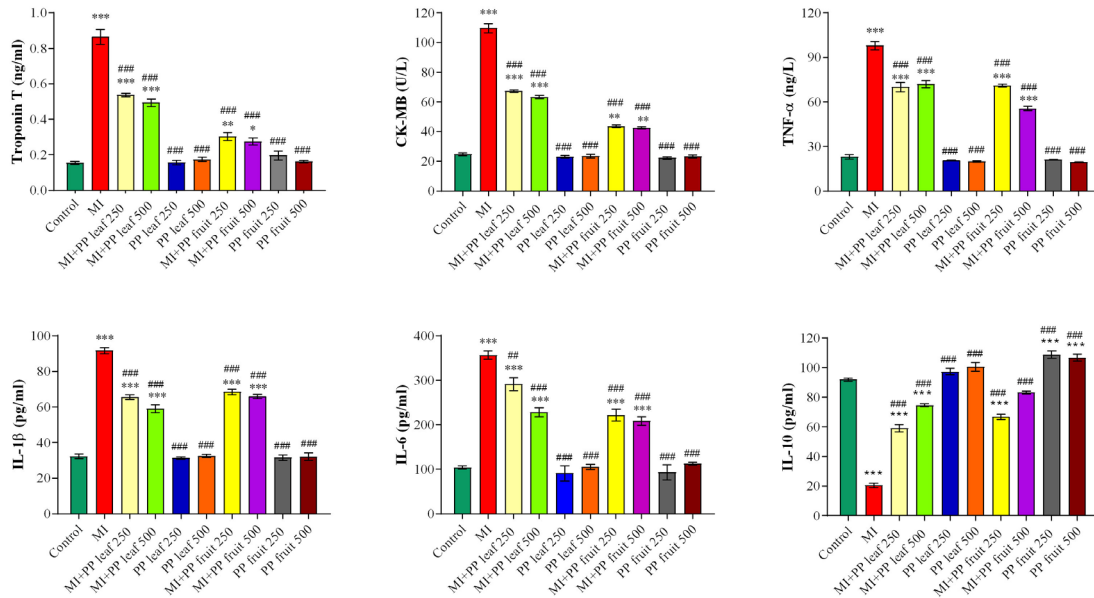


Figure 1. All values are presented as mean±SEM (n=8). *Pistacia palaestina* Boiss (PP) leaves and fruits (250 mg/kg and 500 mg/kg) in isoproterenol-induced myocardial infarction (MI); Effect on troponin T, creatine kinase-myocardial band (CK-MB), tumor necrosis factor-alpha (TNF-α), interleukin-1 beta (IL-1β), interleukin-6 (IL-6) and interleukin-10 (IL-10) levels. Values with different superscripts in the same column are statistically significantly different ($p < 0.05$).

: Significant compared to the control group (: $p < 0.05$, **: $p < 0.01$, ***: $p < 0.001$)

#: Significant compared to the MI group (**: $p < 0.01$, ***: $p < 0.001$)

Histopathological Results

In the control group (Figure 2A, 2B), heart tissue was observed in normal histological appearance. Myofibril loss (Figure 3A, 3C, 3D), vascular congestion (white arrows) (Figure 3B, 3D), cell infiltration (Figure 3D), hemorrhage (black stars) (Figure 3C, 3E), necrosis thick black arrows) (Figure 3E), cells with eosinophilic cytoplasm, pycnotic nuclei (Figure 3C, 3F), and vacuolization (thin black arrows) (Figure 3F) were observed in the MI group. A small amount of hemorrhage and cell infiltration was observed in the heart muscle fibers in the MI+PP fruit 250 mg/kg group (Figure 4A, 4B) and the MI+PP fruit 500 mg/kg group (Figure 4C, 4D). A small amount of cell in-

filtration was observed in the cardiac muscle fibers in the PP fruit 250 mg/kg group (Figure 5A, 5B), and a small amount of hemorrhage in the heart muscle fibers in the PP fruit 500 mg/kg group (Figure 5C, 5D). In the MI+PP leaf, 250 mg/kg group (Figure 6A, 6B) and in the MI+PP leaf 500 mg/kg group (Figure 6C, 6D), hemorrhage in the heart muscle fibers and moderate cell infiltration compared to the MI group were observed. A small amount of hemorrhage and cell infiltration was observed in the cardiac muscle fibers in the PP leaf 250 mg/kg group (Figure 7A, 7B), whereas a small amount of vascular congestion was observed in the cardiac muscle fibers in the PP leaf 500 mg/kg group (Figure 7C, 7D).

CONTROL

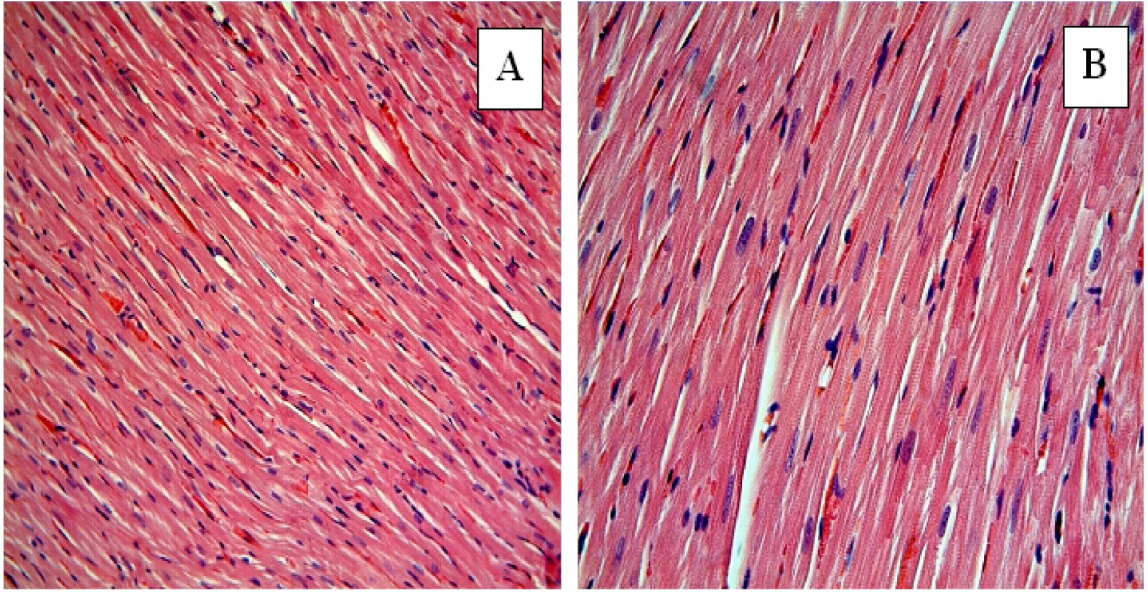


Figure 2. Heart tissue in the control (A, B) group showed a normal histological appearance. A: H-E; X20, B: H-E; X40.

MI

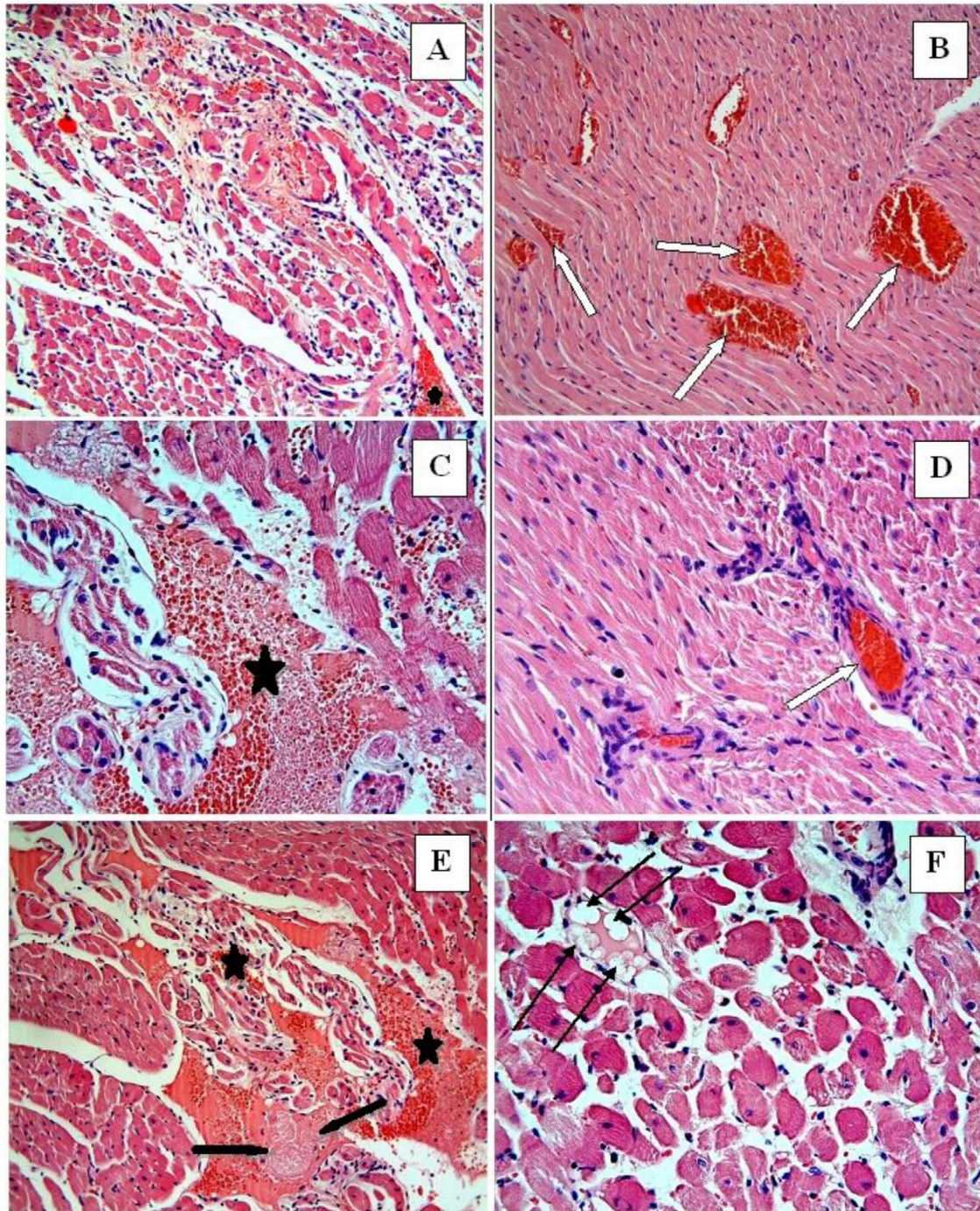


Figure 3. Myofibril loss (A, C, D), vascular congestion (white arrows) (B, D), mononuclear cell infiltration (D), hemorrhage (black stars) (C, E), necrosis (thick black arrows) (E), cells with eosinophilic cytoplasm and pycnotic nuclei (C, F), vacuolization (thin black arrows) (F) were observed in MI group. A, B, E: H-E; X20, C, D, F: H-E; X40. (MI: Myocardial infarction)

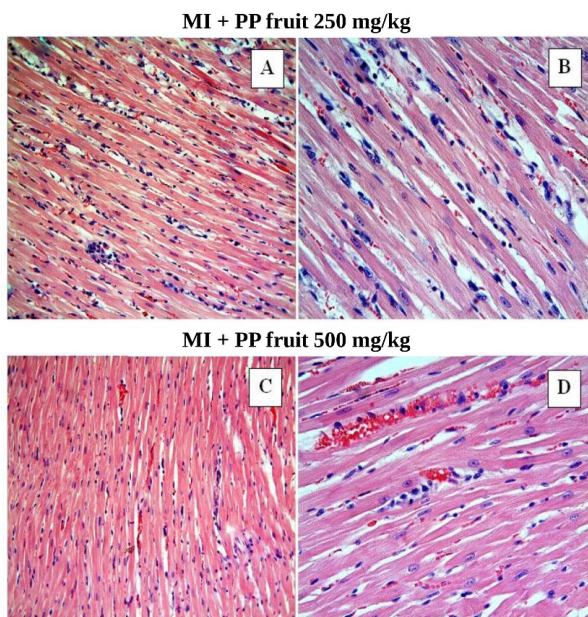


Figure 4. A small amount of hemorrhage and cell infiltration was observed in the heart muscle fibers in the MI+PP fruit 250 mg/kg group (A, B) and the MI+PP fruit 500 mg/kg group (C, D). A, C: H-E; X20, B, D: H-E; X40. (PP: *Pistacia palaestina* Boiss)

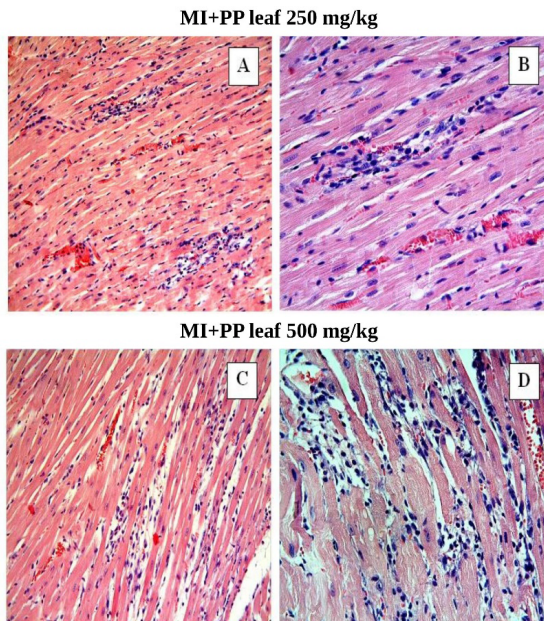


Figure 6. In the MI+PP leaf 250 mg/kg group (A, B) and the MI+PP leaf 500 mg/kg group (C, D), hemorrhage in the heart muscle fibers and moderate cell infiltration were observed compared to the MI group. A, C: H-E; X20, B, D: H-E; X40.

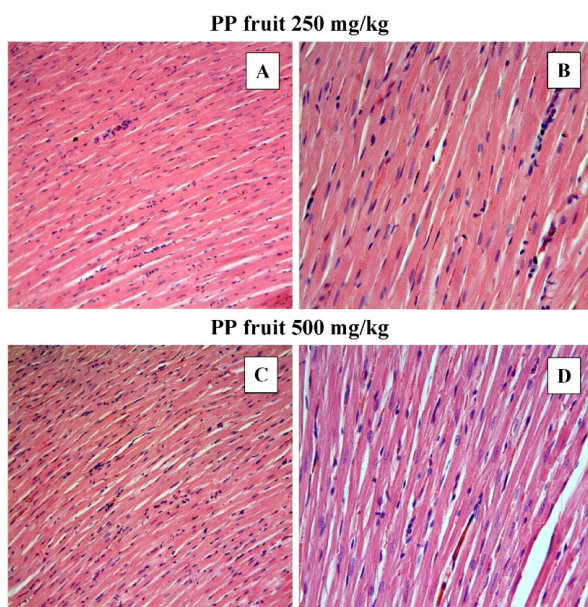


Figure 5. A small amount of cell infiltration was observed in the cardiac muscle fibers in the PP fruit 250 mg/kg group (A, B), and a small amount of hemorrhage in the cardiac muscle fibers in the PP fruit 500 mg/kg group (C, D). A, C: H-E; X20, B, D: H-E; X40.

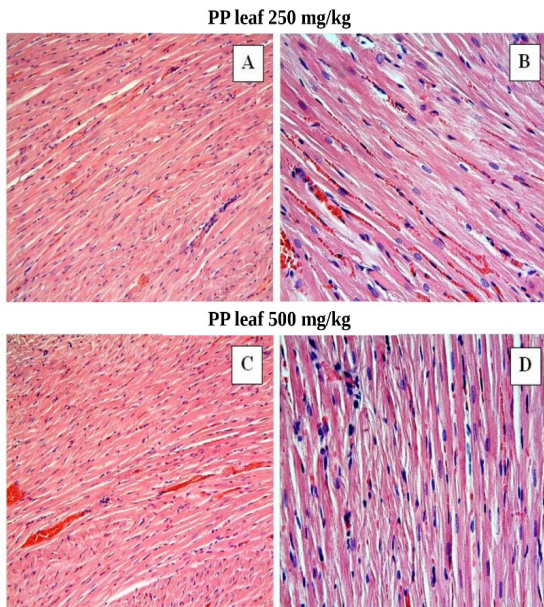


Figure 7. A small amount of hemorrhage and cell infiltration in the cardiac muscle fibers was observed in the PP leaf 250 mg/kg group (A, B), and a small amount of vascular congestion in the cardiac muscle fibers in the PP leaf 500 mg/kg group (C, D). A, C: H-E; X20, B, D: H-E; X40.

Myocardial infarction causes permanent and progressive cardiac damage. After MI, oxidative stress, inflammatory responses, and mitochondrial dysfunction increase, and apoptotic pathways are disrupted, resulting in necrosis and cell death (Schirone et al. 2022). Previous studies have reported that oxidative stress, inflammatory pathways, and mitochondrial dysfunction increase, and histopathological changes occur in cardiomyocytes during ISO-induced MI (Allawadhi et al. 2018; Feng et al. 2019; Xing et al. 2022). Oxidative stress, which increases with the production of free radicals and disruption of the scavenging balance through antioxidant mechanisms, further promotes myocardial hypoxia reactions with the secretion of proinflammatory mediators. This causes increased cardiac damage (Giordano, 2005). Therefore, we investigated the protective role of the fruit and leaf extracts of PP, which have antioxidant and anti-inflammatory activities, in ISO-induced MI.

In this study, we determined that the application of ISO caused an increase in TBARS levels in heart tissue. ISO increases lipid peroxidation, free radicals, and ROS production in heart tissue. In addition, it inhibits antioxidant defense mechanisms, and as a result of this imbalance, oxidative stress increases in cardiomyocytes and tissue damage occurs (Long et al. 2012; Zaafan et al. 2013). As suggested by previous studies, it is thought that ISO may cause cardiovascular damage by inducing oxidative stress in the heart (Goyal et al. 2015; Ganapathy et al. 2020; Zhang et al. 2021; Althunibat et al. 2022). Our study results are consistent with and support previous studies. Zhang et al. reported that ISO reduces GSH levels and CAT, SOD, and GPx activities (Zhang et al. 2021). Ganapathy et al. showed in their study that the *Thraatchathi chooranam* plant, which has antioxidant properties, reduces the increased TBARS levels and increases the levels of antioxidant defense system elements (GSH, CAT, SOD, GPx) in ISO-induced MI (Ganapathy et al. 2020). In the literature, many studies show that natural products with antioxidant properties increase antioxidant enzyme activities in ISO-induced

MI (El-Gohary & Allam, 2017; Allawadhi et al. 2018; Huang et al. 2018; Ardjmand et al. 2019; Feng et al. 2019; Althunibat et al. 2022). Similarly, in our study, PP fruit and leaf extracts reduced ISO-induced oxidative stress by decreasing TBARS levels and increasing GSH levels, CAT, SOD, and GPx activity. In this study, the antioxidant properties of fruit and leaf extracts were similar. This effect is attributed to the high antioxidant capacity of *P. palaestina*. Therefore, PP may be an effective protective agent against cardiac damage caused by MI.

Troponin, a protein specific to skeletal and cardiac muscle fibers, is a highly sensitive and specific indicator of myocardial injury. In the event of a cardiac attack, it passes from the muscle tissue to the systemic circulation due to cardiac degeneration. With cardiovascular damage, the level of troponin in the blood rises (Tiwari et al. 2012). The CK-MB isoenzyme, which is especially located in cardiac muscle cells, is a highly sensitive marker with increased blood levels in major heart diseases and in patients diagnosed with acute MI (Karimkhani et al. 2021). In this study, troponin T and CK-MB levels increased in the ISO-induced MI group, consistent with previous findings. Troponin T and CK-MB levels were significantly decreased in all treatments with PP extracts. In another study, antioxidant treatment after ISO-induced MI improved oxidative stress parameters but slightly reduced serum troponin T levels and did not sufficiently reduce CK-MB levels (Ardjmand et al. 2019). As observed in our study, the use of PP, a natural antioxidant, before and after MI improved cardiac parameters more effectively. In addition, we suggest that high-dose fruit extracts may be more effective in treatment, since high-dose fruit extract treatment reduces troponin T and CK-MB levels more significantly.

Cytokines are produced by various cells, have a polypeptide structure, and are intercellular communication tools. It regulates the immune and inflammatory events of cells, including growth, healing, inflammation, and systemic response to injury. TNF- α ,

IL-1 β , and IL-6 are the main proinflammatory cytokines. IL-10, which is one of the anti-inflammatory cytokines, is a factor that inhibits cytokine synthesis (Huang et al. 2018; Ahmed & Ivashkiv, 2000). TNF- α is a cell signaling protein involved in systemic inflammation and is one of the cytokines that make up the acute phase reaction. TNF- α levels were also increased in regions without infarction area after chronic MI. However, it has been suggested that inflammatory cytokine levels decrease and survival rate increases after MI in TNF- α knockout mice in cardiac tissue (Sun et al. 2004). These results may suggest that TNF- α inhibition may reduce cardiac damage caused by MI. It has been reported that IL-1 β and IL-6 have both harmful and protective effects during MI (Fuchs et al. 2003; Jong et al. 2016; Schirone et al. 2022). In a stress period, the inflammatory response is necessary for the cell survival. However, highly increased inflammation may exacerbate MI injury. Therefore, it is recommended not to suppress the inflammation excessively, especially in the acute phase of MI. However, reducing the levels of these cytokines, whose role has been proven in cardiac damage, is seen as an effective strategy (Schirone et al. 2022).

Previous studies have suggested that the levels of inflammatory factors, including IL-1 β , IL-6, and TNF- α , are increased in the ISO-induced MI model (Huang et al. 2018; Ganapathy et al. 2020; Mohamed et al. 2021; Schirone et al. 2022; Xing et al. 2022; Cinar et al. 2022). In this study, while TNF- α , IL-1, and IL-6 levels in pro-inflammatory cytokines increased in the ISO-induced MI group, they decreased significantly with PP treatment. While the anti-inflammatory IL-10 level decreased in the MI group, it increased in the treatment groups. Significant reduction in proinflammatory cytokines and upregulation of anti-inflammatory IL-10 in the treatment groups were remarkable.

In this study, it was shown that ISO causes severe myofibril loss, vascular occlusion, hemorrhage, necrosis, and infiltration of heart muscle cells. The pathological findings decreased, and partial improve-

ment was observed in the groups treated with both doses of PP fruit and leaves. Although no histopathological changes were observed in the control group, a small amount of cell infiltration and bleeding was observed in the groups in which only PP extract was applied. Huang et al. showed that ISO induces inflammatory cell infiltration and bleeding in hematoxylin-eosin staining of heart tissue (Huang et al. 2018). When another study group examined the histological structures of myocardial cells under a light microscope, they found that the myocytes of rats in the ISO-induced MI group were severely damaged. In addition, they detected necrotic myofibril structures, mononuclear cell infiltration, edema, and vascular occlusion (Karimkhani et al. 2021). Several recent studies have suggested that antioxidant and anti-inflammatory compounds may reduce cardiac damage caused by ISO (Abbas, 2016; Kalkan et al. 2018; Ganapathy et al. 2020). Based on our study results, we can suggest that PP administration may reduce immunologically induced cardiovascular damage by reducing inflammatory cytokines and increasing antioxidant enzyme activity.

In this study, the cardioprotective roles of PP leaf and fruit extracts, a member of the *Pistacia* genus with antioxidant and anti-inflammatory properties grown in Malatya, were evaluated in an ISO-induced MI rat model. In all treatment groups, the lipid peroxidation indicator TBARS levels; the pro-inflammatory cytokines TNF- α , IL-1 β , and IL-6; the cardiac damage indicator troponin T; and CK-MB levels decreased. Low- and high-dose extracts of PP increased anti-inflammatory IL-10 levels and antioxidant enzyme activities. Improved antioxidant mechanisms and decreased inflammation also reduce histopathological changes, indicating tissue damage. PP leaf and fruit extracts may play an important cardioprotective role in treating MI with their antioxidant and anti-inflammatory effects on heart tissue. With this study, it was suggested for the first time that PP extracts have antioxidant, anti-inflammatory, and cardioprotective effects against cardiac damage. Our study results showed that PP extracts can be considered as a natu-

ral and new treatment alternative for cardiovascular diseases. However, its effectiveness is insufficient for treatment. In addition to its effectiveness, comprehensive research on its safety, optimum dose, and cellular mechanism of action is required.

CONCLUSION

For the first time, this study found that PP leaf and fruit extracts reduced oxidative stress and inflammatory response in cardiac tissue, improved histopathological changes, and ameliorated ISO-induced MI. However, more comprehensive and advanced mechanistic studies are needed regarding the protective role of this plant in heart diseases.

ACKNOWLEDGMENT

This study was supported by IUBAP (İnönü University Scientific Research Project Unit) numbered TSA-2020-2146. All authors would like to thank Prof. Dr. Turan Arabacı, who identified *Pistacia palaestina* Boiss. plant material.

CONFLICT OF INTEREST

The authors declare that there is no conflict of interest.

AUTHOR CONTRIBUTION STATEMENT

M.S.İ., literature search, research concepts, design, experimental studies; H.Y., literature search, experimental studies, data acquisition, design; N.B.T., experimental studies, manuscript writing, research concepts, design; A.T., experimental studies, data analysis; D.A.Ö., data analysis, manuscript writing, literature search, experimental studies; S.Ü., data analysis, conducting the research, interpreting the data, compiling and revising the article

REFERENCES

Abbas A. M. (2016). Cardioprotective effect of resveratrol analogue isorhapontigenin versus omega-3 fatty acids in isoproterenol-induced myocardial infarction in rats. *Journal of physiology and biochemistry*, 72(3), 469–484. <https://doi.org/10.1007/s13105-016-0494-4>

Aebi, H. (1974). Catalase. In *Methods of enzymatic analysis* (pp. 673-684). Academic press.

Ahmed, S. T., & Ivashkiv, L. B. (2000). Inhibition of IL-6 and IL-10 signaling and Stat activation by inflammatory and stress pathways. *Journal of immunology* (Baltimore, Md.: 1950), 165(9), 5227–5237. <https://doi.org/10.4049/jimmunol.165.9.5227>

Allawadhi, P., Khurana, A., Sayed, N., Kumari, P., & Godugu, C. (2018). Isoproterenol-induced cardiac ischemia and fibrosis: Plant-based approaches for intervention. *Phytotherapy research: PTR*, 32(10), 1908–1932. <https://doi.org/10.1002/ptr.6152>

Althunibat, O. Y., Abduh, M. S., Abukhalil, M. H., Aladaileh, S. H., Hanieh, H., & Mahmoud, A. M. (2022). Umbelliferone prevents isoproterenol-induced myocardial injury by upregulating Nrf2/HO-1 signaling, and attenuating oxidative stress, inflammation, and cell death in rats. *Biomedicine & pharmacotherapy = Biomedecine & pharmacotherapie*, 149, 112900. <https://doi.org/10.1016/j.biopha.2022.112900>

Ardjmand, A., Shahaboddin, M. E., Mazoochi, T., & Ghavipankeh, G. (2019). Ameliorative effects of cerebrolysin against isoproterenol-induced myocardial injury in male rats. *Life sciences*, 227, 187–192. <https://doi.org/10.1016/j.lfs.2019.04.056>

Boarescu, P. M., Chirilă, I., Bulboacă, A. E., Boçşan, I. C., Pop, R. M., Gheban, D., & Bolboacă, S. D. (2019). Effects of Curcumin Nanoparticles in Isoproterenol-Induced Myocardial Infarction. *Oxidative medicine and cellular longevity*, 7847142. <https://doi.org/10.1155/2019/7847142>

Cinar, I., Yayla, M., Tavaci, T., Toktay, E., Ugan, R. A., Bayram, P., & Halici, H. (2022). In Vivo and In Vitro Cardioprotective Effect of Gossypin Against Isoproterenol-Induced Myocardial Infarction Injury. *Cardiovascular toxicology*, 22(1), 52–62. <https://doi.org/10.1007/s12012-021-09698-3>

- Deng, X. Y., Chen, J. J., Li, H. Y., Ma, Z. Q., Ma, S. P., & Fu, Q. (2015). Cardioprotective effects of timosaponin B II from *Anemarrhena asphodeloides* Bge on isoproterenol-induced myocardial infarction in rats. *Chemico-biological interactions*, 240, 22–28. <https://doi.org/10.1016/j.cbi.2015.08.001>
- El-Gohary, O. A., & Allam, M. M. (2017). Effect of vitamin D on isoprenaline-induced myocardial infarction in rats: possible role of peroxisome proliferator-activated receptor- γ . *Canadian journal of physiology and pharmacology*, 95(6), 641–646. <https://doi.org/10.1139/cjpp-2016-0150>
- Feng, L., Ren, J., Li, Y., Yang, G., Kang, L., Zhang, S., Ma, C., Li, J., Liu, J., Yang, L., & Qi, Z. (2019). Resveratrol protects against isoproterenol induced myocardial infarction in rats through VEGF-B/AMPK/eNOS/NO signalling pathway. *Free radical research*, 53(1), 82–93. <https://doi.org/10.1080/10715762.2018.1554901>
- Flamini, G., Bader, A., Cioni, P. L., Katbeh-Bader, A., & Morelli, I. (2004). Composition of the essential oil of leaves, galls, and ripe and unripe fruits of Jordanian *Pistacia palaestina* Boiss. *Journal of agricultural and food chemistry*, 52(3), 572–576. <https://doi.org/10.1021/jf034773t>
- Fuchs, M., Hilfiker, A., Kaminski, K., Hilfiker-Kleiner, D., Guener, Z., Klein, G., Podewski, E., Schieffer, B., Rose-John, S., & Drexler, H. (2003). Role of interleukin-6 for LV remodeling and survival after experimental myocardial infarction. *FASEB journal: official publication of the Federation of American Societies for Experimental Biology*, 17(14), 2118–2120. <https://doi.org/10.1096/fj.03-0331fj>
- Ganapathy, R., Ramachandran, A., Shivalingaiah, S. B., Bishir, M., Bhojaraj, S., Sridhar, S., Mohan, S. K., Veeraraghavan, V. P., Chidambaram, S. B., Essa, M. M., & Qoronfleh, M. W. (2020). Cardioprotective potential of polyphenols rich Thraathathi Chooranam against isoproterenol induced myocardial necrosis in experimental rats. *BMC complementary medicine and therapies*, 20(1), 356. <https://doi.org/10.1186/s12906-020-03124-x>
- Giordano F. J. (2005). Oxygen, oxidative stress, hypoxia, and heart failure. *The Journal of clinical investigation*, 115(3), 500–508. <https://doi.org/10.1172/JCI24408>
- Goyal, S. N., Sharma, C., Mahajan, U. B., Patil, C. R., Agrawal, Y. O., Kumari, S., Arya, D. S., & Ojha, S. (2015). Protective Effects of Cardamom in Isoproterenol-Induced Myocardial Infarction in Rats. *International journal of molecular sciences*, 16(11), 27457–27469. <https://doi.org/10.3390/ijms161126040>
- Hosseinzadeh, H., Sajadi Tabassi, S. A., Milani Moghadam, N., Rashedinia, M., & Mehri, S. (2012). Antioxidant Activity of *Pistacia vera* Fruits, Leaves and Gum Extracts. *Iranian journal of pharmaceutical research: IJPR*, 11(3), 879–887.
- Huang, H., Geng, Q., Yao, H., Shen, Z., Wu, Z., Miao, X., & Shi, P. (2018). Protective effect of scutellarin on myocardial infarction induced by isoprenaline in rats. *Iranian journal of basic medical sciences*, 21(3), 267–276. <https://doi.org/10.22038/ijbms.2018.26110.6415>
- Jong, W. M., Ten Cate, H., Linnenbank, A. C., de Boer, O. J., Reitsma, P. H., de Winter, R. J., & Zuurbi-er, C. J. (2016). Reduced acute myocardial ischemia-reperfusion injury in IL-6-deficient mice employing a closed-chest model. *Inflammation research: official journal of the European Histamine Research Society*, 65(6), 489–499. <https://doi.org/10.1007/s00011-016-0931-4>
- Kalkan, F., Parlakpınar, H., Disli, O. M., Tanrıverdi, L. H., Özhan, O., Polat, A., Cetin, A., Vardi, N., Otlu, Y. O., & Acet, A. (2018). Protective and therapeutic effects of dexpanthenol on isoproterenol-induced cardiac damage in rats. *Journal of cellular biochemistry*, 119(9), 7479–7489. <https://doi.org/10.1002/jcb.27058>

- Karimkhani, H., Özkoç, M., Shojaolsadati, P., Uzuner, K., Donmez, D. B., & Kanbak, G. (2021). Protective Effect of Boric Acid and Omega-3 on Myocardial Infarction in an Experimental Rat Model. *Biological trace element research*, 199(7), 2612–2620. <https://doi.org/10.1007/s12011-020-02360-z>
- Lampronti, I., Saab, A., & Gambari, R. (2005). Medicinal plants from Lebanon: effects of essential oils from Pistacia palaestina on proliferation and erythroid differentiation of human leukemic K562 cells. *Minerva Biotechnologica*, 17(3), 153.
- Loizzo, M. R., Saab, A. M., Tundis, R., Statti, G. A., Menichini, F., Lampronti, I., Gambari, R., Cinatl, J., & Doerr, H. W. (2008). Phytochemical analysis and in vitro antiviral activities of the essential oils of seven Lebanon species. *Chemistry & biodiversity*, 5(3), 461–470. <https://doi.org/10.1002/cbdv.200890045>
- Long, J., Gao, M., Kong, Y., Shen, X., Du, X., Son, Y. O., Shi, X., Liu, J., & Mo, X. (2012). Cardioprotective effect of total paeony glycosides against isoprenaline-induced myocardial ischemia in rats. *Phytomedicine: international journal of phytotherapy and phytomedicine*, 19(8-9), 672–676. <https://doi.org/10.1016/j.phymed.2012.03.004>
- Lowry, O. H., Rosebrough, N. J., Farr, A. L., & Randall, R. J. (1951). Protein measurement with the Folin phenol reagent. *The Journal of biological chemistry*, 193(1), 265–275.
- Mechanic, O. J., Gavin, M., & Grossman, S. A. (2022). Acute Myocardial Infarction. In *StatPearls*. StatPearls Publishing.
- Mohamed, M. E., Abduldaium, M. S., & Younis, N. S. (2021). Cardioprotective Effect of Linalool against Isoproterenol-Induced Myocardial Infarction. *Life (Basel, Switzerland)*, 11(2), 120. <https://doi.org/10.3390/life11020120>
- Nwokocho, C., Palacios, J., Simirgiotis, M. J., Thomas, J., Nwokocho, M., Young, L., Thompson, R., Cifuentes, F., Paredes, A., & Delgoda, R. (2017). Aqueous extract from leaf of Artocarpus altilis provides cardio-protection from isoproterenol induced myocardial damage in rats: Negative chronotropic and inotropic effects. *Journal of ethnopharmacology*, 203, 163–170. <https://doi.org/10.1016/j.jep.2017.03.037>
- Paglia, D. E., & Valentine, W. N. (1967). Studies on the quantitative and qualitative characterization of erythrocyte glutathione peroxidase. *The Journal of laboratory and clinical medicine*, 70(1), 158–169.
- Rauf, A., Patel, S., Uddin, G., Siddiqui, B. S., Ahmad, B., Muhammad, N., Mabkhot, Y. N., & Hadda, T. B. (2017). Phytochemical, ethnomedicinal uses and pharmacological profile of genus Pistacia. *Biomedicine & pharmacotherapy = Biomedecine & pharmacotherapie*, 86, 393–404. <https://doi.org/10.1016/j.biopha.2016.12.017>
- Saad, B., Dakwar, S., Said, O., Abu-Hijleh, G., Al Battah, F., Kmeel, A., & Azizeh, H. (2006). Evaluation of medicinal plant hepatotoxicity in co-cultures of hepatocytes and monocytes. *Evidence-based complementary and alternative medicine: eCAM*, 3(1), 93–98. <https://doi.org/10.1093/ecam/nel002>
- Schirone, L., Forte, M., D'Ambrosio, L., Valenti, V., Vecchio, D., Schiavon, S., Spinosa, G., Sarto, G., Petrozza, V., Frati, G., & Sciarretta, S. (2022). An Overview of the Molecular Mechanisms Associated with Myocardial Ischemic Injury: State of the Art and Translational Perspectives. *Cells*, 11(7), 1165. <https://doi.org/10.3390/cells11071165>
- Sedlak, J., & Lindsay, R. H. (1968). Estimation of total, protein-bound, and nonprotein sulfhydryl groups in tissue with Ellman's reagent. *Analytical biochemistry*, 25(1), 192–205. [https://doi.org/10.1016/0003-2697\(68\)90092-4](https://doi.org/10.1016/0003-2697(68)90092-4)

- Sobhani, Z., Nami, S. R., Emami, S. A., Sahebkar, A., & Javadi, B. (2017). Medicinal Plants Targeting Cardiovascular Diseases in View of *Avicenna*. *Current pharmaceutical design*, 23(17), 2428–2443. <https://doi.org/10.2174/1381612823666170215104101>
- Sun, M., Dawood, F., Wen, W. H., Chen, M., Dixon, I., Kirshenbaum, L. A., & Liu, P. P. (2004). Excessive tumor necrosis factor activation after infarction contributes to susceptibility of myocardial rupture and left ventricular dysfunction. *Circulation*, 110(20), 3221–3228. <https://doi.org/10.1161/01.CIR.0000147233.10318.23>
- Tiwari, R. P., Jain, A., Khan, Z., Kohli, V., Bharmal, R. N., Kartikeyan, S., & Bisen, P. S. (2012). Cardiac troponins I and T: molecular markers for early diagnosis, prognosis, and accurate triaging of patients with acute myocardial infarction. *Molecular diagnosis & therapy*, 16(6), 371–381. <https://doi.org/10.1007/s40291-012-0011-6>
- Tomaino, A., Martorana, M., Arcoraci, T., Monteleone, D., Giovinazzo, C., & Saija, A. (2010). Antioxidant activity and phenolic profile of pistachio (*Pistacia vera* L., variety Bronte) seeds and skins. *Biochimie*, 92(9), 1115–1122. <https://doi.org/10.1016/j.biochi.2010.03.027>
- Tsao, C. W., Aday, A. W., Almarzooq, Z. I., Anderson, C. A. M., Arora, P., Avery, C. L., Baker-Smith, C. M., Beaton, A. Z., Boehme, A. K., American Heart Association Council on Epidemiology and Prevention Statistics Committee and Stroke Statistics Subcommittee (2023). Heart Disease and Stroke Statistics-2023 Update: A Report From the American Heart Association. *Circulation*, 147(8), e93–e621. <https://doi.org/10.1161/CIR.0000000000001123>
- Ulukanli, Z., Karabörklü, S., Öztürk, B., Çenet, M., & Balcilar, M. (2014). Chemical Composition, Antibacterial and Insecticidal Activities of the Essential Oil from the *Pistacia terebinthus* L. Spp. Palaestina (B oiss.) (A nacardiaceae). *Journal of Food Processing and Preservation*, 38(3), 815-822. <https://doi.org/10.1111/jfpp.12035>
- Xing, Z., Yang, C., He, J., Feng, Y., Li, X., Peng, C., & Li, D. (2022). Cardioprotective Effects of Aconite in Isoproterenol-Induced Myocardial Infarction in Rats. *Oxidative medicine and cellular longevity*, 2022, 1090893. <https://doi.org/10.1155/2022/1090893>
- Yagi K. (1998). Simple assay for the level of total lipid peroxides in serum or plasma. *Methods in molecular biology* (Clifton, N.J.), 108, 101–106. <https://doi.org/10.1385/0-89603-472-0:101>
- Zaafan, M. A., Zaki, H. F., El-Brairy, A. I., & Kenawy, S. A. (2013). Protective effects of atorvastatin and quercetin on isoprenaline-induced myocardial infarction in rats. *Bulletin of Faculty of Pharmacy, Cairo University*, 51(1), 35–41.
- Zhang, X., Li, X., Wang, C., Li, H., Wang, L., Chen, Y., Feng, J., Ali Alharbi, S., & Deng, Y. (2021). Ameliorative effect of ferruginol on isoprenaline hydrochloride-induced myocardial infarction in rats. *Environmental toxicology*, 36(2), 249–256. <https://doi.org/10.1002/tox.23030>

Comparative Study of The Anti-Inflammatory Pathway Enzyme Activities of Selected Plant Extracts from Lamiaceae Family

Kubra SENER*, Murat EKİCİ**, Ekrem Murat GONULALAN***, Ebru BODUR****

Comparative Study of The Anti-Inflammatory Pathway Enzyme Activities of Selected Plant Extracts from Lamiaceae Family

SUMMARY

In this study, the effects of selected plants from the Lamiaceae family (*Mentha piperita* L., *Salvia officinalis* L., *Lavandula officinalis* Chaix., *Scutellaria orientalis* L. and *Melissa officinalis* L.) on the activities of lipoxygenase-12/15 (LOX-12/15), cyclooxygenase-2 (COX-2) and acetylcholinesterase (AChE) enzymes, which have an essential place in the inflammation pathway, were determined. They have been studied as an alternative to inhibitor drugs that have many side effects. The metabolomic profiles of the extracts were defined by GC-MS and LC-qTOF-MS methods. The antioxidant parameters of the extracts were investigated by DPPH+ radical scavenging activity and TAC methods. The time-dependent scavenging capacity of extracts for DPPH+ radicals varies depending on the extracts, time, and concentration. The potential inhibitory effects of the extracts on 12-15-LOX, COX-2, and AChE enzymes were compared with metabolomics analysis. Our combined results suggest that the extracts have potential use as anti-inflammatory agents.

Key Words: Anti-inflammatory, Lamiaceae, lipoxygenase, cyclooxygenase, acetylcholinesterase, metabolomic.

Lamiaceae Familyasından Seçilen Bitki Ekstrelerinin Anti-İnflamatuvar Yolak Enzim Aktivitelerinin Karşılaştırmalı Çalışması

ÖZ

Bu çalışmada Lamiaceae familyasından seçilmiş bitkilerin (*Mentha piperita* L., *Salvia officinalis* L., *Lavandula officinalis* Chaix., *Scutellaria orientalis* L. ve *Melissa officinalis* L.) inflamasyon yolağında önemli bir yeri olduğu bilinen lipoksijenaz-12/15 (LOX-12/15), siklooksijenaz-2 (COX-2) ve asetilkolinesteraz (AChE) aktiviteleri üzerine etkileri araştırılmıştır. İnflamasyon sürecinde yan etkileri fazla bulunan inhibitör ilaçlara alternatif olmaları açısından bu bitki ekstrelerinin etkinlikleri incelenmiştir. Ekstrelerin metabolomik profilleri GC-MS ve LC-qTOF-MS yöntemleriyle tanımlanmıştır. Ekstrelerin antioksidan potansiyelleri, DPPH+ radikal süpürücü etki ve TAC yöntemleriyle araştırılmıştır. DPPH+ radikalinin zamana bağlı süpürücü etkileri incelendiğinde, ekstrelerin zamana ve konsantrasyona bağlı olarak etkilerinin değiştiği bulunmuştur. Ekstrelerin 12-15-LOX, COX-2 ve AChE enzimleri üzerindeki potansiyel inhibitör etkileri incelenmiş ve elde edilen sonuçların metabolomik profilleri korelasyon analizi ile karşılaştırılmıştır. Elde edilen sonuçlar, ekstrelerin potansiyel anti-inflamatuvar ajanlar olarak kullanıma sahip olduğunu düşündürmektedir.

Anahtar Kelimeler: Anti-inflamatuvar, Lamiaceae, lipoksijenaz, siklooksijenaz, asetilkolinesteraz, metabolomik.

Received: 15.11.2023

Revised: 01.02.2024

Accepted: 01.02.2024

* ORCID:0000-0002-8759-9444, Gazi University, Faculty of Science, Department of Biology, Ankara, Türkiye

** ORCID: 0000-0002-3402-177X, Gazi University, Faculty of Science, Department of Biology, Ankara, Türkiye

*** ORCID: 0000-0002-8171-3824, Afyonkarahisar Health Sciences University, Faculty of Pharmacy, Department of Pharmacognosy, Afyonkarahisar, Türkiye

**** ORCID:0000-0001-5829-5487, Hacettepe University, Faculty of Medicine Department of Medical Biochemistry, Ankara, Türkiye

° Corresponding Author: Ebru BODUR

E-mail: bodurebru@yahoo.com

INTRODUCTION

Tissue damage, destruction, and prolonged persistent infection are associated with chronic inflammation. In this process, tissue damage occurs through imbalances in blood flow, increased permeability in vascular tissues, synthesis of reactive oxygen derivatives (ROS), and activation and migration of leukocytes (Shah, 2008).

Inflammation is a very complex process, and various mediators such as prostaglandins (PGs), leukotrienes (LTs), phospholipase A₂ (PLA₂), cyclooxygenases (COXs), and lipoxygenases (LOXs) are involved (Busse, 1998). COX and LOX enzymes are convert arachidonic acid (AA) to biologically active leukotrienes and prostaglandins (Gilroy,

Tomlinson, & Willoughby, 1998). The formation of the inflammatory response also has various effects on the nervous system, where acetylcholine (ACh) is the neurotransmitter that plays a critical role (Massoulié, Pezzementi, Bon, Krejci, & Vallette, 1993). Borovikova et al. (2000) reported that ACh effectively inhibited peripheral macrophages and mediated the inflammatory response by inhibiting the release of proinflammatory mediators, including tumor necrosis factor (TNF- α) (Borovikova et al., 2000). These results show that acetylcholinesterase (AChE) may induce ACh-dependent macrophage deactivation, hence forming an important of the cholinergic anti-inflammatory (CAI) pathway (Figure 1).

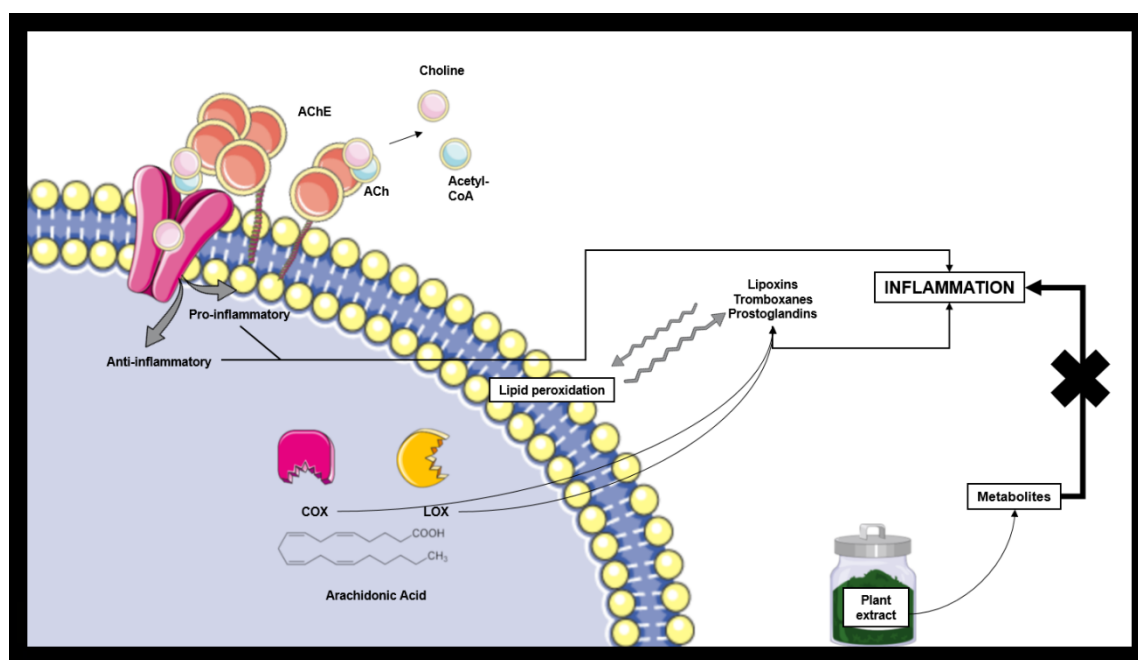


Figure 1. Potential inflammation pathways associated with AChE, LOX, and COX

Steroidal glucocorticoids can reduce cytokine-induced gene expression, and non-steroidal anti-inflammatory (NSAID) drugs, which target cyclooxygenase (COX) enzyme isoforms, can regulate the uncontrolled inflammatory response (Barnes, 1998; Vane, 1971). However, long-term use of these drugs causes undesirable side effects, including ulcers and cardiovascular disorders (Baron et al., 2008; Rostom et al., 2002). The discovery of less toxic

dual LOX/COX and AChE inhibitors is essential to overcome these disadvantages.

Since the beginning of human history, medicinal and aromatic plants have been used for many purposes, such as food, medicine, cosmetics, and spices. The first records of the use of plants for medicinal purposes date back to B.C. (Demirezer, 2010). Turkey has a very diverse ecosystem waiting to be discovered. Advances in the biological sciences have enabled

them to evaluate the therapeutic potential of various plant species (Mesquita et al., 2019).

The Lamiaceae (Labiatae) family is a cosmopolitan family that includes plants in herbaceous, shrub, or tree forms and is of great economic importance in many parts of the world. It is mainly distributed in the Mediterranean and Central Asia (Suddee, Paton, & Parnell, 2004). The Lamiaceae family also has a vital role in the flora of Turkey and is the third most affluent family, with a 44.2% endemism rate (Baser & Kırimer, 2014). Plants of the Lamiaceae family have a rich content of secondary metabolites and are used in phytotherapy (Fecka & Turek, 2008). These secondary metabolites display many biological activities such as antioxidant, antimicrobial, antiviral (Sökmen et al., 2004), anti-inflammatory effects –especially as inhibitors of LOX-COX enzymes (Juergens, Stöber, & Vetter, 1998) and AChE (Orhan, Senol, Ozturk, Akaydin, & Sener, 2012).

The development of technology leads to the increased use of omics technologies. Metabolomics, an omics technology that investigates all metabolic components of the organism rather than scanning a single metabolite, is beginning to be used in the content analysis of plant extracts, especially in pharmacology (Ulrich-Merzenich et al., 2007). Metabolomics research leads to pharmacologically active substances obtained by scanning the content analysis of materials such as plant extracts. These have formed new ways to treat various diseases (Kamatou, Makunga, Ramogola, & Viljoen, 2008). Investigating the correlation of biologically active components determined by metabolomics studies with bio-activity studies is a new approach and necessary for further studies.

In this study, plant species of *Mentha piperita* L., *Salvia officinalis* L., *Lavandula officinalis* Chaix., *Scutellaria orientalis* L., and *Melissa officinalis* L. from the Lamiaceae family, known to have biologically active secondary metabolites, were selected. Given these selected plant extracts' antioxidant and anti-

inflammatory potential, we aimed to determine their inhibitory effects on COX-2, 12/15-LOX, and AChE enzymes, if any. Determination of the possible double/triple enzyme inhibitor potential of these plant extracts would enable a new approach to develop ligands in the inflammation pathway.

Our combined results display that *S. officinalis* L. and *M. officinalis* methanol extracts have LOX/COX dual inhibitor potentials. *M. officinalis* L. extract may be a potential natural triple LOX/COX/AChE enzyme inhibitor.

MATERIALS AND METHOD

Chemicals

Trizma hydrochloride, sodium hydroxide, 2,2-diphenyl-1-picrylhydrazyl (DPPH), lipoxidase (*Glycine max* Type I), dimethyl sulfoxide (DMSO), Quercetin and Tween-20 were obtained from Sigma-Aldrich (St. Louis, MO, USA). Linoleic acid was purchased from Calbiochem, Germany. Total Antioxidant Capacity (TAC) Assay Kit and COX-2 Inhibitor Screening Assay Kit (Fluorometric) were obtained from Biovision (USA). All other chemicals used were of the best analytical grade.

Plant Materials and Extraction Procedures

Plants (*Lavandula officinalis* Chaix., *Melissa officinalis* L., *Mentha piperita* L., and *Salvia officinalis* L.) were collected from the culture area of Selçuk University Faculty of Agriculture, Department of Field Crops. *Scutellaria orientalis* L. was collected from the Ankara-Beytepe region during flowering periods. The herbarium specimen numbers of the plants are as follows, respectively (TBÇ-L-001, TBÇ-M-001, TBÇ-M-002, TBÇ-S-001 and HUEF 20016).

The parts to be used were separated after the plant samples were dried at room temperature, free from moisture, in a sun-free environment. The aerial parts of the plants were used in this study. These parts were powdered with the help of a grinder. 5 g of dried and powdered plant samples were weighed, extracted at 40°C under reflux for 30 minutes with

50 ml of methanol, and then filtered. After the filtrate was separated, the remaining solid phase was extracted a second time at the same temperature, with 30 ml of methanol under reflux for 15 minutes. The filtrates were combined, a rotary evaporator removed the solvent, and a dry extract was obtained by lyophilization. For DPPH radical scavenging assays, powdered plant extracts were weighed and dissolved in methanol. For Trolox equivalent determination, the solvent used was absolute ethanol. The extracts were dissolved in 1% dimethylsulfoxide (DMSO) for enzymatic assays.

DPPH⁺ radical scavenging activity

The radical scavenging capacity of extracts was determined by DPPH⁺ (1,1-diphenyl-2-picrylhydrazyl) assay according to Brand-Williams Cuvelier and Berset method (Brand-Williams, Cuvelier, & Berset, 1995). Briefly, 50 µl of the extracts dissolved in MeOH (200-1.56 µg/ml, in the final) was transferred to 96-well plates. 1 mM 150 µl DPPH⁺ radical was added to samples and standard. After 30 min of incubation, the absorbance was read at 517 nm with the microplate reader SpectraMax i3. In addition, the radical scavenging effects of the samples were investigated over time (0-90 minutes). Quercetin was used as the standard for all radical scavenging activity assays. All assays were carried out in triplicate. The antioxidant activity values of all materials were calculated according to the following formula:

$$\%Inhibition: \frac{A_0 - A_{sample}}{A_0} \times 100 \quad (1)$$

where A_0 is the absorbance value consisting of MeOH and DPPH⁺ for extracts and Quercetin, A_{sample} is the absorbance with extracts or standard. The EC_{50} value was determined by a linear regression curve.

Total antioxidant capacity: Trolox equivalent

The 2,2'-azinobis-(3-ethylbenzothiazoline-6-sulfonic acid) (ABTS•⁺) radical is used to measure the total radical scavenging capacity. This method is based on the discoloration of ABTS•⁺ by antioxidant compounds. The stable free radical scavenging ability

of the molecules is compared with Trolox (6-hydroxy-2,5,7,8-tetramethylchroman-2-carboxylic acid), a water-soluble analog of vitamin E (Huang, Ou, Hampsch-Woodill, Flanagan, & Deemer, 2002). Determination of the total antioxidant capacity of the extracts was performed using the TAC Assay Kit (Biovision, Catalog No: #K274-100, USA) according to the manufacturer's instructions. Trolox was used as a standard in the concentration range of 0-20 nmol/µl. The total antioxidant capacities of the extracts are given as nmol/µl Trolox equivalent value. All assays were carried out in triplicate. All samples (Trolox and extracts) were prepared in absolute methanol.

COX-2 activity assay

A commercial COX-2 Inhibitor Screening Kit (Biovision, Catalog #K547-100, U.S.A) was used to determine the effects of extracts on COX-2 (EC: 1.14.99.1) enzyme activity. Generally, this assay is based on the fluorometric detection of prostaglandin G_2 produced by the COX enzyme in AA metabolism. The extracts were dissolved in 1% DMSO and were transferred to the microplate with 80 µl of substrate-free activity medium. The reaction was initiated by adding 10 µl of AA as the substrate. The change in fluorescence intensity was measured at Ex/Em = 535/587 nm wavelengths, kinetically at 25°C for 10 minutes in a microplate reader (SpectraMax i3). All assays were carried out in triplicate. % Inhibition values were given according to Formula (1): where A_0 is the initial, -uninhibited- enzyme activity consisting of enzyme, substrate and solvent; A_{sample} is an enzyme activity with extracts. A linear regression curve determined the IC_{50} value.

12-15/LOX activity assay

The protocol used to determine the effects of extracts on 12/15-LOX enzyme activity was carried out with some modifications (Tappel, 1962; Ulusu, Ercil, Sakar, & Tezcan, 2002). The activity mixture was prepared as 1 ml. It contained 1.5 µg/ml of the enzyme (Lipoxidase from Glycine max, Type-1, EC: 1.13.11.12) and various concentrations of extracts in

50 mM sodium borate buffer (pH 9.0) in the final. The reaction was started by adding substrate (Linoleic acid, LA) after extracts were incubated with enzyme for 5 minutes at 25°C. The change in absorbance was monitored with quartz cuvettes in Shimadzu UV1700 UV-Vis spectrophotometer at 234 nm, kinetically at 25°C for 1 minute. While all extracts were dissolved in 5% DMSO, LA was suspended in 50 mM sodium borate buffer pH 9.0 containing % 0.2 Tween-20 in the final. % Inhibition values were given according to Formula (1): where A_0 is the initial, -uninhibited-enzyme activity consisting of enzyme, substrate, and solvent; A_{sample} is an enzyme activity with extracts. A linear regression curve determined the IC_{50} value.

AChE activity assay

The Ellman assay in 96-well plates determined Acetylcholinesterase (AChE, EC 3.1.1.7) activity with a final volume of 200 μ l (Ellman, Courtney, Andres Jr, & Featherstone, 1961; Gok, Zeybek, & Bodur, 2016). AChE activity was measured using acetylthiocholine (ATCh) as substrate at a final concentration of 1 mM in 50 mM 3-(N-morpholino) propanesulfonic acid buffer (MOPS) pH 7.4, 0.25 mM 5,5'-Dithiobis (2-Nitro Benzoic Acid (Ellman's Reagent, DTNB) and varying concentration of extracts (containing %0.05 DMSO in the final) at 412 nm for 1 minute, kinetically. % Inhibition values were given according to Formula (1): where A_0 is the initial, -uninhibited-enzyme activity consisting of enzyme, substrate and, solvent; A_{sample} is an enzyme activity with extracts. A linear regression curve determined the IC_{50} value.

Metabolomics analysis

GC-MS

Gas chromatography-mass spectrometry (GC-MS) analysis was carried out as described previously (Nemutlu et al., 2015). 100 μ g/ml plant sample was prepared with methanol. GC-MS (Shimadzu GCMS-QP2010 Ultra) was used for metabolomic profiles, and

DB-5MS was chosen as the stationary phase column. After the procedure, the data were analyzed with AMDIS and SpectConnect software. Myristic acid was used as an internal standard in this metabolomics analysis.

LC-qTOF-MS

LC-qTOF-MS metabolomic analysis was performed as described previously with minor modifications (Gonulalan et al., 2020). Metabolites were separated by C18 column in LC-qTOF-MS system (Agilent 6530). Natural product databases [Universal Natural Products Database (UNPD), KNApSAcK, and PlantCyc] were scanned for metabolite identification. The mass tolerance is fitted at ten ppm. Only structures with a score greater than six were correctly identified. Phenylalanine was used as an internal standard in this metabolomics analysis.

Statistical analysis

Statistical analyses of enzymatic and scavenging activity assays were performed with GraphPad Prism 8.4.2 software. Values are given as means \pm SEM (Standard error mean) of at least triplicate experiments. Statistical analyses for all experiments were calculated using one-way ANOVA analysis, followed by Post-Hoc tests. Values of $p \leq 0.05$ were considered statistically significant. Microsoft Excel was used for the correlation analysis between metabolomic and activity data.

RESULTS and DISCUSSION

DPPH⁺ radical scavenging activity

In comparing the results of the DPPH⁺ radical scavenging activity of the plant extracts, Quercetin was used as a control. The EC_{50} of quercetin was found as 2.92 ± 8.54 μ g/ml. *M. officinalis* L. displayed the highest DPPH⁺ radical scavenging activity; EC_{50} : 25.75 ± 13.41 μ g/ml (Figure 2). EC_{50} values of all extracts were statistically significant as compared to Quercetin ($P \leq 0.05$, Figure 2).

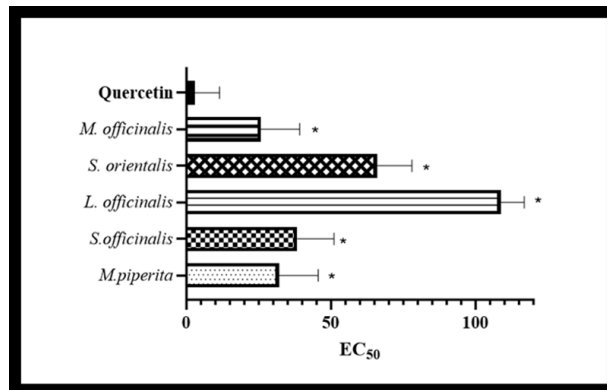


Figure 2. DPPH⁺ radical scavenging effect of the Lamiaceae extracts n=3, EC₅₀ values are given ±SEM * Compared to quercetin p<0.05.

The results confirm that all extracts have antioxidant properties comparable to Quercetin. Next, we evaluated the time-dependent radical scavenging effects of extracts. When the time-dependent scavenging capacities of DPPH⁺ radicals were examined, reliant on the extracts, time, and concentration, the effects were varied (Figure 3).

Generally, all extracts displayed a steady inhibition over the observed period. *M. piperita* L., *S. officinalis* L. and *S. orientalis* L. extracts displayed a concentration-dependent increase in DPPH⁺ scavenging activity. *M. officinalis* L. and *S. officinalis* L. displayed the highest DPPH⁺ scavenging activity (Figure 3).

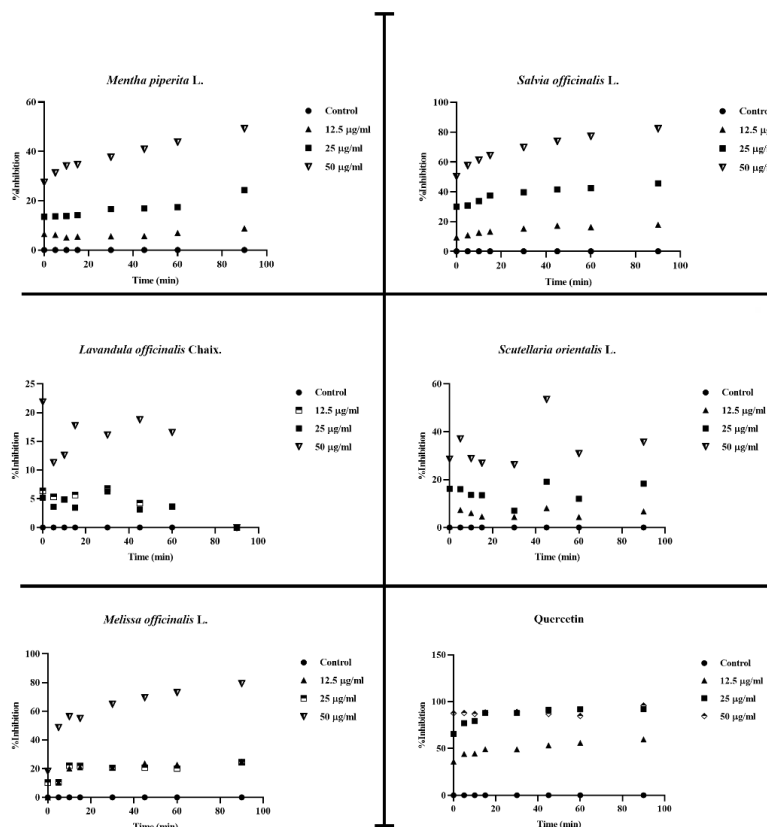


Figure 3. Time-dependent DPPH⁺ radical scavenging effect of the Lamiaceae extracts

Total antioxidant capacity: Trolox equivalent

The total antioxidant capacities of the extracts are given as Trolox Equivalent values (nmol/μL). The

highest antioxidant activity belonged to *M. piperita* L. (Table 1; 50 μg/ml: 726.62±0.02 nmol/ μl Trolox Equivalent).

Table 1. Total antioxidant capacity of Lamiaceae extracts as Trolox equivalent

Concentration (μg/ml)	<i>M.piperita</i> L.	<i>S.officinalis</i> L.	<i>L.officinalis</i> Chaix.	<i>S. orientalis</i> L.	<i>M. officinalis</i> L.
	nmol/ μl Trolox Equivalent				
6.25	128.15±0.01	103.87±0.01	53.06±0.02	132.64±0.01	222.57±0.02
12.5	298.08±0.01	171.31±0.01	59.80±0.02	137.14±0.01	312.50±0.01
25	578.24±0.02	336.33±0.01	60.25±0.01	192.00±0.01	553.51±0.01
50	726.62±0.02	400.63±0.02	73.29±0.02	260.34±0.01	676.26±0.01

n=3, Trolox equivalent values are given ±SEM

COX-2 enzyme activity assay

Inhibitory potentials of the extracts were screened against COX-2 enzyme activity at 0-400 μg/ml. The results are given in Table 2 as IC₅₀ values. According to our results, all of the extracts displayed COX-2 enzyme inhibition in varying degrees. The highest inhibitory activity belonged to *L. officinalis* Chaix. (IC₅₀: 6.24±13.70 μg/ml), which was followed by *M. officinalis* L., with the IC₅₀ value of 16.65±9.09 μg/ml. The plant extract with the highest IC₅₀ value and the lowest inhibitor potential was determined as *M. piperita* L. for the COX-2 enzyme (Table 2).

12-15/LOX enzyme activity assay

The IC₅₀ values indicating the effects of Lamiaceae extracts at different concentrations on 12/15 Lipoxygenase enzyme activity are in Table 2. The highest inhibitory activity belonged to *M. piperita* L. which was 14.98±9.23 μg/ml (Table 2). *M. officinalis* L. and *S. officinalis* L. extracts displaying similar IC₅₀ values also have high 12/15 LOX inhibitory potential (Table 2).

AChE enzyme activity assay

In addition to COX-2 and 12-15/LOX enzymes, the effects of Lamiaceae extracts on AChE enzyme were investigated. According to our results, all extracts except *S. orientalis* L. displayed AChE inhibition. The highest AChE inhibitory potential was displayed by *M.*

officinalis L., which had an IC₅₀ value of 157.97±1.62 μg/ml. The other three plant extracts displayed IC₅₀ values in 345-455 μg/ml (Table 2).

Table 2. Inhibitory effects (IC₅₀ values) of Lamiaceae extracts on COX-2, 12-15/LOX, and AChE enzyme activities

Extracts	Enzymes, IC ₅₀ (μg/ml)		
	COX-2	12-15/LOX	AChE
<i>M. piperita</i> L.	69.98±13.70	14.98±9.23	455.55±6.77
<i>S.officinalis</i> L.	26.44±17.68	42.54±37.70	432.31±5.22
<i>L. officinalis</i> Chaix.	6.23±13.25	329.48±44.77	345.52±1.86
<i>S. orientalis</i> L.	30.43±12.32	96.63±55.70	ND*
<i>M. officinalis</i> L.	16.65±9.09	35.73±16.75	157.97±1.62

*Not detected.

GC-MS

After analysis of GC-MS chromatograms, 1745 mass spectral properties were found, of which 295 were analyzed using retention index libraries. We determined 81 organic acids and derivatives, 69 organic compounds, 48 lipids and lipid-like molecules, 37 benzenoids, and 28 organoheterocyclic-type compounds (Supplementary data 1a).

LC-qTOF-MS

Secondary metabolites were determined with LC-qTOF-MS analysis, and 362 metabolites were identified using MS/MS databases. Among the

metabolites identified, 60 flavonoid glycosides and aglycones with flavone, isoflavone, flavonol, methylated flavonoids, and flavonol skeletons were the most common group. Fourteen anthocyanidin glycosides were determined as the other major secondary metabolite group. In addition, coumarin, catechin, terpenoids, and hydroxycinnamic acid-type

compounds were detected (Supplementary data 2a).

Also, we have found that metabolites belong to fatty acyls (fatty acid esters, fatty acids and conjugates, fatty acyl glycosides, fatty amides, fatty alcohols, and linoleic acids and derivatives) as a result of GC-MS and LC-QTOF-MS analyses (Table 3).

Table 3. Fatty acyls determined in extracts

Class	Sub Class	Compound Name	Presence in membrane
Fatty Acyls	Fatty acid esters	Methyl Stearate	+
	Fatty acyl glycosides	Lactobionic acid	-
		Lactitol	-
		Maltitol	-
		Turanose	-
		Palatinitol	+
	Fatty amides	Adipamide	-
	Fatty alcohols	1-hexadecanol	-
	Lineolic acids and derivatives	Linoleic acid	+
		Methyl linolenate	-
	Fatty acids and conjugates	Oleic acid	+
		Capric acid	+
		Pimelic acid	+
		Maleamic acid	-
		Methyl oleate	-
		2-isopropylmalic acid	-
		3-hydroxy-3-methylglutaric acid (dicrotalic acid)	-
		Citramalic acid	+
		Methyl palmitate	+
		Methyl palmitoleate	-
		Palmitic acid	+
		Stearic acid	+
		Arachidic acid	+
		Heptadecanoic acid	+
		Myristic acid	+
		Palmitoleic acid	+
		4-acetylbutyric acid	-
		Lauric acid	-
		Trans,trans-muconic acid	+
		2,3-dimethylsuccinic acid	-
		Behenic acid	+
		Methyl hexacosanoate	-
		Itaconic acid	+
	Tetracosanoic acid	+	
16-Hydroxyhexadecanoic acid	+		
cis,cis-Muconic acid	+		
Sebacate	+		
Suberic acid	+		
Methyl octadecanoate	-		
3-Hydroxyisovaleric acid	+		

Correlation analysis

The findings obtained by correlation analyses of LC-QTOF-MS and GC-MS analysis are shown in Table 4. LC-qTOF-MS correlation analyses show that 13, 24, and 77 positively correlated metabolites with

12-15/LOX, COX-2, and AChE enzymes, respectively. On the other hand, GC-MS correlation analyses show that 22, 13, and 66 positively correlated metabolites with 12-15/LOX, COX-2, and AChE enzymes, respectively ($r \geq 0.70$; Table 4).

Table 4. Correlation analyses between metabolites and enzyme activities

	Number of positively correlated metabolites ($r \geq 0.70$)			Number of negatively correlated metabolites ($r \leq -0.70$)		
	12-15/LOX	COX-2	AChE	12-15/LOX	COX-2	AChE
LC-QTOF-MS	13	24	77	63	47	33
GC-MS	22	13	66	44	24	29

*r: Correlation coefficient

Antioxidant activity is widely used to characterize biological materials (López-Alarcón & Denicola, 2013). Plants contain various phytochemicals or bioactive molecules that can neutralize free radicals and delay the progression of many chronic diseases associated with oxidative stress and ROS (Ani, Varadaraj, & Naidu, 2006). Lamiaceae family plants have rich secondary metabolite content (Fecka & Turek, 2008). It is known that these secondary metabolites have many antioxidant properties and are effective in many anti-inflammatory pathways (Paun et al., 2018).

This study determined the radical scavenging effects and the total antioxidant capacity of the selected Lamiaceae extracts. When the radical scavenging effects of *M. piperita* L., *S. officinalis* L., and *M. officinalis* L. extracts were compared with the literature our extracts were found to have higher antioxidant activity than previous studies (Albano et al., 2012; Derwich, Chabir, Taouil, & Senhaji, 2011; Koksál, Bursal, Dikici, Tozoglu, & Gulcin, 2011). Moreover, *L. officinalis* Chaix. results are very close to those reported in literature (Spiridon et al., 2011).

In addition, time-dependent (0-90 minutes) radical scavenging capacities of the extracts' at determined concentrations (12.5, 25, and 50 µg/ml) were investigated. Generally, all extracts displayed a steady scavenging effect over the observed period.

While the radical scavenging capacities of the extracts did not change over time, they were nevertheless concentration-dependent. All plant extracts displayed a higher scavenging effect with higher (50 µg/ml) extract concentrations. *M. officinalis* L. and *Salvia officinalis* L. plant extracts displayed the highest DPPH⁺ scavenging activity. These two plants displayed an 80 % inhibition on the DPPH⁺ radical formation over a period of 90 minutes (Figure 3). It is thought that the high efficiency of our extracts in antioxidant and radical scavenging activities may be related to the secondary metabolite components in their content. A comparison of the radical scavenging effects with Quercetin and the total antioxidant capacity with Trolox suggests that our extracts have strong antioxidant properties (Table 1).

Given the extracts' potential to inhibit cyclooxygenase (COX) and lipoxygenase (LOX) enzymes, the results of *S. officinalis* L. and *M. officinalis* L. extracts are promising. The IC₅₀ values of *S. officinalis* L. and *M. officinalis* L. for COX-2 enzyme were 26.44±17.68 and 16.65±9.09 µg/ml, respectively. Moreover, 12/15-LOX enzyme IC₅₀ values of the *S. officinalis* L. and *M. officinalis* L. were 42.54±37.70 and 35.73±16.75 µg/ml, respectively (Table 2). It is seen that the inhibition values of both extracts for both enzymes are very close. These findings may be related to the similarity of secondary compounds

and, or the synergistic and antagonistic effects of the secondary metabolites in the extract. Metabolomics analyses show that our extracts are rich in flavonoids and anthocyanidins. Coumarin, catechin, terpenoids, and hydroxycinnamic acid-type compounds are commonly found in these extracts.

Plants from the Lamiaceae family display inhibitory effects on the inflammation pathway enzymes. Alonazi et al. (2021) showed that *Salvia lanigera* ethanol and water extracts inhibited COX-2 and 5-LOX enzymes in human colorectal cancer cell lines (HCT-116 and Lovo) without causing any cytotoxicity (Alonazi et al., 2021). Another study on COX enzyme showed that hydroalcoholic extracts of *L. officinalis* inhibited inflammation through and COX-1 COX-2 activity (Husseini et al., 2016). Also, the anti-inflammatory activity of menthol and peppermint oil was investigated on human monocytes *in vitro*. Juergens et al. found that menthol and peppermint oil are potential inhibitors for LOX and COX pathways (Juergens et al., 1998). In another study with rats, 800 mg/kg of *M. officinalis* L. was found to cause 50% inhibition of COX-2 levels in tissues (Hamza, Ahmed, Elwey, & Amin, 2016). *In vitro* study with *S. baicalensis* L., the IC₅₀ value for the COX-2 and 5-LOX enzyme of the extract was found to be 15 µg/ml and 25 µg/ml, respectively (Burnett, Jia, Zhao, & Levy, 2007).

Acetylcholinesterase (AChE) enzyme is the neurotransmitter in cholinergic synapses (Massoulié et al., 1993). Several plants and their metabolites are used in folk medicine to alter cognitive function, alleviate other neurodegenerative disorder symptoms, and prevent memory loss (Howes, Perry, & Houghton, 2003). Literature findings show that *Salvia* and *Melissa* genus have promising key metabolites that inhibit AChE and butyrylcholinesterase enzymes (Castro et al., 2021; Gülçin et al., 2016). In addition, the large-scale study by Miyazawa et al. showed that *Mentha* essential oils and their metabolites also have a strong AChE inhibitory potential (Miyazawa, Watanabe, Umemoto, & Kameoka, 1998).

This is the first study that incorporates both the metabolomic profiles and correlation of the inhibition potentials of these metabolites on LOX COX and AChE enzymes, especially fatty acyl metabolites. Through correlation analyses of LC-qTOF-MS and GC-MS, it was seen that a group of metabolites were positively correlated with the inhibitions of AChE>12-15/LOX>COX-2 enzymes, respectively (Table 4). We found 77 and 66 metabolites positively correlated with the AChE enzyme with LC-qTOF-MS and GC-MS analyses, respectively. Surprisingly, correlation analyses revealed that through LC-qTOF-MS and GC-MS analyses, 63 and 44 negatively correlated metabolites were found for 12-15/LOX enzyme. The number of metabolites correlated with COX-2 enzyme by LC-qTOF-MS and GC-MS analyses were 47 and 24, respectively. The correlation type was negative, as it was with the 12/15/ LOX enzyme (Table 4).

The inhibition studies of our extracts show promising results. The extracts contain many primary and secondary metabolites that display antioxidant and anti-inflammatory activity. We believe that these activities of plant extracts may be due to the synergistic/antagonistic effects of different metabolites instead of single active metabolites.

It is known that the fatty acyls linoleic and arachidonic acid are involved in anti-inflammatory effects. Considering AChE is a member of the cholinergic anti-inflammatory pathway, we have previously investigated their potential as acetylcholinesterase inhibitors. We found that linoleic acid, linolenic acid, and arachidonic acid have inhibitory effects on human erythrocyte AChE and characterized the interaction of these fatty acyls with the AChE enzyme through docking studies (Akay, Şener, Sari, & Bodur, 2023). In this study, we determined that the Lamiaceae feature fatty acyl metabolites (fatty acid esters, fatty acids, and conjugates, fatty acyl glycosides, fatty amides, fatty alcohols, and linoleic acids and derivatives) as a result of GC-MS and LC-QTOF-MS analyses. Through

these analyses, we find that the dual LOX/COX inhibitory potential of *S. officinalis* L. and the triple LOX/COX/AChE inhibitory potential of *M. officinalis* positively correlate with fatty acyl type compounds. *M. officinalis* contains relatively more of these compounds than others, which may be the source of the triple effect. Therefore, further studies are needed to clarify the metabolite or metabolites responsible for the activity.

ACKNOWLEDGEMENTS

This study was funded by Gazi University Scientific Research Projects (BAP) (Project number: 05/2020-23).

The figure was partly generated using Servier Medical Art, provided by Servier, licensed under a Creative Commons Attribution 3.0 unported license (Access on 10 August, 2022).

CONFLICT OF INTEREST

Authors declare that there is no conflict of interest.

AUTHOR CONTRIBUTION STATEMENT

EB and ME conceived the study; KS performed the experiments, collected and analyzed the data, EMG provided the plant extracts and performed the metabolic analysis, EB and KS wrote the manuscript; EMG and ME made manuscript revisions.

REFERENCES

- Akay, M. B., Şener, K., Sari, S., & Bodur, E. (2023). Inhibitory Action of Omega-3 and Omega-6 Fatty Acids Alpha-Linolenic, Arachidonic and Linoleic acid on Human Erythrocyte Acetylcholinesterase. *The Protein Journal*, 42(2), 96-103.
- Albano, S., Lima, A. S., Miguel, M. G., Pedro, L. G., Barroso, J. G., & Figueiredo, A. C. (2012). Antioxidant, anti-5-lipoxygenase and antiacetylcholinesterase activities of essential oils and decoction waters of some aromatic plants. *Records of natural products*, 6(1), 35-48.
- Alonazi, M. A., Jemel, I., Moubayed, N., Alwhibi, M., El-Sayed, N. N. E., & Bacha, A. B. (2021). Evaluation of the in vitro anti-inflammatory and cytotoxic potential of ethanolic and aqueous extracts of *Origanum syriacum* and *Salvia lanigera* leaves. *Environmental Science and Pollution Research*, 28(16), 19890-19900.
- Ani, V., Varadaraj, M., & Naidu, K. A. (2006). Antioxidant and antibacterial activities of polyphenolic compounds from bitter cumin (*Cuminum nigrum* L.). *European Food Research and Technology*, 224(1), 109-115.
- Barnes, P. J. (1998). Anti-inflammatory actions of glucocorticoids: molecular mechanisms. *Clinical science*, 94(6), 557-572.
- Baron, J. A., Sandler, R. S., Bresalier, R. S., Lanas, A., Morton, D. G., Riddell, R., . . . Demets, D. L. (2008). Cardiovascular events associated with rofecoxib: final analysis of the APPROVe trial. *the Lancet*, 372(9651), 1756-1764.
- Baser, K. H. C., & Kırımer, N. (2014). Essential oils of Anatolian Apiaceae-A profile. *Natural Volatiles and Essential Oils*, 1(1), 1-50.
- Borovikova, L. V., Ivanova, S., Zhang, M., Yang, H., Botchkina, G. I., Watkins, L. R., . . . Tracey, K. J. (2000). Vagus nerve stimulation attenuates the systemic inflammatory response to endotoxin. *Nature*, 405(6785), 458-462.
- Brand-Williams, W., Cuvelier, M.-E., & Berset, C. (1995). Use of a free radical method to evaluate antioxidant activity. *LWT-Food science and Technology*, 28(1), 25-30.
- Burnett, B., Jia, Q., Zhao, Y., & Levy, R. (2007). A medicinal extract of *Scutellaria baicalensis* and *Acacia catechu* acts as a dual inhibitor of cyclooxygenase and 5-lipoxygenase to reduce inflammation. *Journal of medicinal food*, 10(3), 442-451.

- Busse, W. W. (1998). Leukotrienes and Inflammation. *American Journal of Respiratory and Critical Care Medicine*, 157(6), S210-S213. doi:10.1164/ajrccm.157.6.mar-1
- Castro, M. F. V., Stefanello, N., Assmann, C. E., Baldissarelli, J., Bagatini, M. D., da Silva, A. D., . . . Morsch, V. M. (2021). Modulatory effects of caffeic acid on purinergic and cholinergic systems and oxi-inflammatory parameters of streptozotocin-induced diabetic rats. *Life Sciences*, 277, 119421.
- Demirezer, L. (2010). *Bitkilerin tıpta kullanılması konusundaki sorumluluklarımız*. Paper presented at the Bitkilerle Tedavi Sempozyumu, Zeytinburnu.
- Derwich, E., Chabir, R., Taouil, R., & Senhaji, O. (2011). In-vitro antioxidant activity and GC/MS studies on the leaves of *Mentha piperita* (Lamiaceae) from Morocco. *International Journal of Pharmaceutical Sciences and Drug Research*, 3(2), 130-136.
- Ellman, G. L., Courtney, K. D., Andres Jr, V., & Featherstone, R. M. (1961). A new and rapid colorimetric determination of acetylcholinesterase activity. *Biochemical pharmacology*, 7(2), 88-95.
- Fecka, I., & Turek, S. (2008). Determination of polyphenolic compounds in commercial herbal drugs and spices from Lamiaceae: thyme, wild thyme and sweet marjoram by chromatographic techniques. *Food Chemistry*, 108(3), 1039-1053.
- Gilroy, D. W., Tomlinson, A., & Willoughby, D. A. (1998). Differential effects of inhibitors of cyclooxygenase (cyclooxygenase 1 and cyclooxygenase 2) in acute inflammation. *European journal of pharmacology*, 355(2-3), 211-217.
- Gok, M., Zeybek, N. D., & Bodur, E. (2016). Butyrylcholinesterase expression is regulated by fatty acids in HepG2 cells. *Chemico-Biological Interactions*, 259, 276-281.
- Gonulalan, E. M., Nemitlu, E., Bayazeid, O., Koçak, E., Yalçın, F. N., & Demirezer, L. O. (2020). Metabolomics and proteomics profiles of some medicinal plants and correlation with BDNF activity. *Phytomedicine*, 74, 152920. doi:https://doi.org/10.1016/j.phymed.2019.152920
- Gülçin, İ., Scozzafava, A., Supuran, C. T., Koksal, Z., Turkan, F., Çetinkaya, S., . . . Alwasel, S. H. (2016). Rosmarinic acid inhibits some metabolic enzymes including glutathione S-transferase, lactoperoxidase, acetylcholinesterase, butyrylcholinesterase and carbonic anhydrase isoenzymes. *Journal of enzyme inhibition and medicinal chemistry*, 31(6), 1698-1702.
- Hamza, A. A., Ahmed, M. M., Elwey, H. M., & Amin, A. (2016). *Melissa officinalis* protects against doxorubicin-induced cardiotoxicity in rats and potentiates its anticancer activity on MCF-7 cells. *PLoS one*, 11(11), e0167049.
- Howes, M. J. R., Perry, N. S., & Houghton, P. J. (2003). Plants with traditional uses and activities, relevant to the management of Alzheimer's disease and other cognitive disorders. *Phytotherapy research: An international journal devoted to pharmacological and toxicological evaluation of natural product derivatives*, 17(1), 1-18.
- Huang, D., Ou, B., Hampsch-Woodill, M., Flanagan, J. A., & Deemer, E. K. (2002). Development and validation of oxygen radical absorbance capacity assay for lipophilic antioxidants using randomly methylated β -cyclodextrin as the solubility enhancer. *Journal of Agricultural and Food chemistry*, 50(7), 1815-1821.
- Husseini, Y., Sahraei, H., Meftahi, G. H., Dargahian, M., Mohammadi, A., Hatef, B., . . . Alibeig, H. (2016). Analgesic and anti-inflammatory activities of hydro-alcoholic extract of *Lavandula officinalis* in mice: possible involvement of the cyclooxygenase type 1 and 2 enzymes. *Revista Brasileira de Farmacognosia*, 26, 102-108.

- Juergens, U., Stöber, M., & Vetter, H. (1998). The anti-inflammatory activity of L-menthol compared to mint oil in human monocytes in vitro: a novel perspective for its therapeutic use in inflammatory diseases. *European journal of medical research*, 3(12), 539-545.
- Kamatou, G. P. P., Makunga, N. P., Ramogola, W. P. N., & Viljoen, A. M. (2008). South African Salvia species: A review of biological activities and phytochemistry. *Journal of ethnopharmacology*, 119(3), 664-672. doi:https://doi.org/10.1016/j.jep.2008.06.030
- Koksal, E., Bursal, E., Dikici, E., Tozoglu, F., & Gulcin, I. (2011). Antioxidant activity of Melissa officinalis leaves. *Journal of Medicinal Plants Research*, 5(2), 217-222.
- López-Alarcón, C., & Denicola, A. (2013). Evaluating the antioxidant capacity of natural products: A review on chemical and cellular-based assays. *Analytica chimica acta*, 763, 1-10.
- Massoulié, J., Pezzementi, L., Bon, S., Krejci, E., & Vallette, F.-M. (1993). Molecular and cellular biology of cholinesterases. *Progress in neurobiology*, 41(1), 31-91.
- Mesquita, L. S. S. d., Luz, T. R. S. A., Mesquita, J. W. C. d., Coutinho, D. F., Amaral, F. M. M. d., Ribeiro, M. N. d. S., & Malik, S. (2019). Exploring the anticancer properties of essential oils from family Lamiaceae. *Food Reviews International*, 35(2), 105-131.
- Miyazawa, M., Watanabe, H., Umemoto, K., & Kameoka, H. (1998). Inhibition of acetylcholinesterase activity by essential oils of Mentha species. *Journal of agricultural and food chemistry*, 46(9), 3431-3434.
- Nemutlu, E., Zhang, S., Xu, Y.-Z., Terzic, A., Zhong, L., Dzeja, P. D., & Cha, Y.-M. (2015). Cardiac resynchronization therapy induces adaptive metabolic transitions in the metabolomic profile of heart failure. *Journal of cardiac failure*, 21(6), 460-469.
- Orhan, I. E., Senol, F. S., Ozturk, N., Akaydin, G., & Sener, B. (2012). Profiling of in vitro neurobiological effects and phenolic acids of selected endemic Salvia species. *Food Chemistry*, 132(3), 1360-1367.
- Paun, G., Neagu, E., Moroeanu, V., Albu, C., Ursu, T.-M., Zandirescu, A., . . . Radu, G. L. (2018). Anti-inflammatory and antioxidant activities of the Impatiens noli-tangere and Stachys officinalis polyphenolic-rich extracts. *Revista Brasileira de Farmacognosia*, 28, 57-64.
- Rostom, A., Dube, C., Wells, G. A., Tugwell, P., Welch, V., Jolicoeur, E., . . . Lanas, A. (2002). Prevention of NSAID-induced gastroduodenal ulcers. *Cochrane database of systematic reviews*, 2002(4).
- Shah, B. (2008). Role of Leukotriene in Inflammation and Antileukotriene Therapy. *Journal of Pharmacy Research*.
- Sökmen, M., Serkedjieva, J., Daferera, D., Gulluce, M., Polissiou, M., Tepe, B., . . . Sokmen, A. (2004). In vitro antioxidant, antimicrobial, and antiviral activities of the essential oil and various extracts from herbal parts and callus cultures of Origanum acutidens. *Journal of Agricultural and Food chemistry*, 52(11), 3309-3312.
- Spiridon, I., Colceru, S., Anghel, N., Teaca, C. A., Bodirlau, R., & Armatu, A. (2011). Antioxidant capacity and total phenolic contents of oregano (Origanum vulgare), lavender (Lavandula angustifolia) and lemon balm (Melissa officinalis) from Romania. *Natural product research*, 25(17), 1657-1661.
- Suddee, S., Paton, A., & Parnell, J. (2004). A taxonomic revision of tribe Ocimeae Dumort. (Lamiaceae) in continental South East Asia II. Plectranthinae. *Kew Bulletin*, 379-414.
- Tappel, A. (1962). [71] Lipoxidase. In *Methods in enzymology* (Vol. 5, pp. 539-542): Elsevier.

- Ulrich-Merzenich, G., Zeitler, H., Jobst, D., Panek, D., Vetter, H., & Wagner, H. (2007). Application of the “-Omic-” technologies in phytomedicine. *Phytomedicine*, 14(1), 70-82. doi:10.1016/j.phymed.2006.11.011
- Ulusu, N. N., Ercil, D., Sakar, M. K., & Tezcan, E. F. (2002). Abietic acid inhibits lipoxygenase activity. *Phytotherapy research*, 16(1), 88-90.
- Vane, J. R. (1971). Inhibition of prostaglandin synthesis as a mechanism of action for aspirin-like drugs. *Nature new biology*, 231(25), 232-235.

Financial Development of the Turkish Pharmaceutical Sector During and After the Pandemic: Sector Panel Data Analysis for the Period 2018-2022

Mustafa ÖZYEŞİL*, Havane TEMBELO**

Financial Development of the Turkish Pharmaceutical Sector During and After the Pandemic: Sector Panel Data Analysis for the Period 2018-2022

Pandemi Dönemi ve Sonrasında Türkiye İlaç Sektörünün Finansal Gelişimi: 2018-2022 Dönemi Sektör Panel Veri Analizi

SUMMARY

This study examines the effects of the COVID-19 pandemic on the financial performance of the Turkish pharmaceutical industry between 2018 and 2022. Financial indicators in the sector were examined and analyzed through the data set covering the periods before, during and, after the pandemic. The hypotheses on which the research focuses predict the impact of the pandemic process on the pharmaceutical industry. The ADF unit root tests concentrate on four different financial indicators in the sector and, it was determined that these indicators were stationary at normal levels. Hausman test results showed that a fixed-effect model is the most suitable for the panel data model. However, upon detecting autocorrelation and heteroscedasticity problems in the model, the Panel GLS model was applied. Structural break analysis revealed unexpected changes in the periods determined as the second quarter of 2020 and the first quarter of 2022. These periods mark when the effects of the COVID-19 pandemic are particularly evident. Additionally, new recorded case data of COVID-19 shows how the pandemic's impact on the industry has changed. It was observed that pandemic conditions became evident in April and May 2020, and February 2022 marked the highest number of cases. This study aims to evaluate the sector's future potential by examining in detail the changes in the financial performance of the Turkish pharmaceutical industry before, during and, after the pandemic.

Key Words: COVID-19 Pandemic, Turkish Pharmaceutical Industry, Financial Performance, Panel Data Analysis, Sectoral Changes

ÖZ

Bu çalışma, COVID-19 salgınının Türk ilaç sektörünün 2018-2022 yılları arasındaki finansal performansı üzerindeki etkilerini incelemektedir. Araştırmanın odaklandığı hipotezler, pandemi sürecinin ilaç endüstrisi üzerindeki etkisini öngörüyor. ADF birim kök testleri sektörde dört farklı finansal göstereye odaklanmıştır ve bu göstergelerin normal seviyelerde durduğu tespit edilmiştir. Hausman testi sonuçları sabit etkili modelin panel veri modeli için en uygun seçenek olduğunu göstermiştir. Ancak modelde otokorelasyon ve değişen varyans sorunlarının tespit edilmesi üzerine robust tahminci Panel GLS modeli uygulanmıştır. Yapısal kırılma analizi, 2020 yılının ikinci çeyreği ve 2022 yılının ilk çeyreği olarak belirlenen dönemlerde beklenmedik değişikliklerin yaşandığını ortaya koymuştur. Bu dönemler, özellikle Covid-19 salgınının etkilerinin belirgin olduğu dönemlere işaret etmektedir. Ek olarak, kaydedilen yeni COVID-19 vaka verileri, salgının sektör üzerindeki etkisinin zaman içinde nasıl değiştiğini göstermektedir. Pandemi koşullarının 2020 Nisan ve Mayıs aylarında belirginleştiği, en fazla vaka sayısının ise Şubat 2022'de görüldüğü tespit edilmiştir. Bu çalışma, Türk ilaç sektörünün pandemi öncesinde, pandemi sırasında ve sonrasında finansal performansında meydana gelen değişiklikleri detaylı bir şekilde inceleyerek sektörün gelecek potansiyelini değerlendirmeyi amaçlamaktadır.

Anahtar Kelimeler: COVID-19 Pandemisi, Türkiye İlaç Sektörü, Finansal Performans, Panel Veri Analizi, Sektörel Değişimler

Received: 23.11.2023

Revised: 06.02.2024

Accepted: 08.02.2024

* ORCID: 0000-0002-4442-7087, İstanbul Aydın Üniversitesi, Anadolu Bil Meslek Yüksekokulu, İşletme Yönetimi (İngilizce), mozyesil@aydin.edu.tr

** ORCID: 0000-0003-3394-4166, İstanbul Aydın Üniversitesi, Lisansüstü Eğitim Enstitüsü, İşletme, havanetembelo@stu.aydin.edu.tr

INTRODUCTION

The COVID-19 pandemic has significantly and extensively affected global health systems, economies, and industries (IMF, 2020, October 13). The analysis of these impacts is crucial for comprehending the performance of specific sectors and evaluating the long-term effects of the pandemic (Company, 2020). The pharmaceutical industry is essential in contributing to treatment and prevention processes during this pandemic period and providing a remarkable case study in terms of industry and financial performance (World Bank, 2020). The COVID-19 pandemic has spread rapidly worldwide since its first days and has affected many sectors. This impact has revealed how critical investments and health policies in public health are on a global scale. However, the effect of the pandemic was not only limited to the health field, it also radically shook the economic balances.

This study examines the financial performance of the Turkish pharmaceutical industry between 2018 and 2022. It evaluates the effects of the COVID-19 pandemic on the sector over a broad time, including before, during and, after the pandemic. This analysis is carried out to understand the short and long-term effects of the pandemic on the financial performance of the industry, to evaluate the resilience of the industry and, to predict possible future scenarios. Turkey has seriously felt the effects of this global crisis in terms of both public health and, the economy. One of the sectors where economic waves are felt is the pharmaceutical sector, which is directly at the center of the pandemic. The pandemic has been a period in which research on vaccines and treatment methods has accelerated and, the pharmaceutical industry has entered an important race on a global scale. In this process, Turkey has closely experienced the dynamics, national and international competition and, financial performance of the pharmaceutical industry.

The flow of the study consists of an analysis section that will start with a literature review to

understand the effects of the COVID-19 pandemic on the pharmaceutical industry, then provide a detailed explanation of the methodology and data set used, and then present the findings. The findings will conclude by a summary of the sector's performance during pandemic periods and a discussion of possible future directions in the conclusion.

Purpose of the Study and Contribution to the Literature

This study analyzes the financial performance of the Turkish pharmaceutical industry between 2018 and 2022 with the impact of the COVID-19 pandemic. Existing studies in the literature generally focus on a specific time or avoid covering broader periods. This study examines financial changes in the sector in detail by covering a broad period, including the periods before, during and, after the pandemic. It offers a solid methodology with panel data analysis. This study contributes significantly to the literature by providing a more comprehensive perspective to understand the effects of the pandemic on the pharmaceutical industry.

Turkish Pharmaceutical Sector Analysis Before and After Covid-19

Turkey has a crucial pharmaceutical market due to its geographical location, population density and, investments in health services. In previous years, the Turkish pharmaceutical industry has shown stable growth, generally recording an increase of 5-7% on an annual basis. Both local pharmaceutical manufacturers and branches of global companies in Turkey play an active role in the market. While Turkey is very active in pharmaceutical imports, it also exports medicines to many regions, especially the Middle Eastern countries, North Africa, and the Turkish Republic. Primarily domestic pharmaceutical companies have allocated more budget to Research and Development (R&D) investments every year and thus tried to encourage domestic drug production (TISD, 2022).

The COVID-19 pandemic has significantly affected the pharmaceutical industry in Turkey, as well as all over the world. There has been a tremendous increase in demand, especially for drugs used to combat the virus. The pandemic has caused disruptions in supply chains, leading to temporary issues in drug availability. The pandemic has again shown how critical domestic pharmaceutical production and R&D studies are. In this direction, state-supported R&D projects and domestic pharmaceutical production incentives have increased (TUIK, 2023).

Turkey experienced difficulties importing some critical medicines, especially during the pandemic. However, in this process, it tried to eliminate this deficiency by increasing its domestic production capacity. At the same time, Turkey's export capacity in some pharmaceuticals has also increased (TITCK, 2023).

The demand for pharmaceuticals, which showed a stable growth in the pre-COVID-19 period, has increased significantly during the pandemic, especially in antiviral drugs and drugs used in supportive treatment. The pandemic has revealed how vital supply chains are. In this process, the Turkish pharmaceutical industry has taken essential steps in diversifying the supply chain and supporting domestic production (TISD, 2022). It is predicted that R&D investments and innovation will increase further in Turkey after COVID-19. Domestic drug production and domestic vaccine studies sector's potential in this field. While Turkey's pharmaceutical industry continues to be a part of global supply chains, it is expected to have a more active role, especially in the regional market (TUIK, 2023).

The COVID-19 pandemic has brought challenges and opportunities to the Turkish pharmaceutical industry. In this process, the sector has taken crucial steps to strengthen the supply chain, increase R&D investments and, support domestic production. In the coming years, it is expected that the sector will continue to grow by maintaining its resilient structure

and, playing a more active role in the international market.

The statistics of the pharmaceutical industry for the period 2018-2022 are shown in (Table 1) below:

Table 1. World Pharmaceutical Market Size and Growth Rate for the Period 2018-2022 (www.statista.com)

Year	World pharmaceutical market size (billion USD)	World pharmaceutical market growth rate (%)
2018	1.200	5.2%
2019	1.320	6.4%
2020	1.450	10.3%
2021	1.600	11.7%
2022	1.750	10.0%

As seen in the table, the world pharmaceutical market grew by approximately 50% from 2018 to 2022. This growth is due to increasing population, aging population and, increase in chronic diseases. The pharmaceutical industry has a sector with high growth potential and, is expected to grow further in the coming years.

Expenditures and R&D investments in the pharmaceutical sector in Turkey in the 2018-2022 period are shown in Table 2 below:

Table 2. Pharmaceutical Expenditures and R&D Investments in Turkey for the Period 2018-2022 (www.tuik.gov.tr)

Year	Pharmaceutical Expenditures (billion TL)	Pharmaceutical Sector R&D Investments (billion TL)
2018	24.7	1.9
2019	27.2	2.2
2020	30.6	2.6
2021	34.7	3.1
2022	38.9	3.6

The table shows pharmaceutical expenditures and pharmaceutical sector R&D investments in Turkey between 2018-2022. As seen in the table, pharmaceutical expenditures are increasing every year. Pharmaceutical spending, which were 24.7

billion TL in 2018, increased to 38.9 billion TL in 2022. Pharmaceutical industry R&D investments are also growing every year. R&D investments in the pharmaceutical industry, 1.9 billion TL in 2018, increased to 3.6 billion TL in 2022. The reason for the increase in pharmaceutical expenditures is the growing and aging population of Turkey. While Turkey's population was 84 million 339 thousand 385 in 2018, it increased to 84 million 681 thousand 757 in 2022. Turkey's population is aging and, the proportion of the population aged 65 and over is increasing. The population rate of 65 years and over, 12 million 419 thousand 529 in 2018, increased to 13 million 244 thousand 979 in 2022.

Increase in R&D investments in the pharmaceutical industry is due to the development of new drugs and the improvement of existing drugs. New drugs with enhanced effectiveness in treating diseases and fewer side effects are currently under development. By improving existing drugs, more effective and affordable medicines are being developed to treat diseases.

As a result, pharmaceutical expenditures and pharmaceutical sector R&D investments in Turkey are increasing yearly. The reason for this increase is the increase and aging of Turkey's population, the development of new drugs and, the improvement of existing drugs.

Statistics of the Turkish pharmaceutical market for the period 2018-2022 are shown in Table 3 below:

Table 3. Türkiye Pharmaceutical Market Size and Growth Rate for the Period 2018-2022 (www.statista.com)

Year	Turkish pharmaceutical market size (billion TL)	Turkish pharmaceutical market growth rate (%)
2018	40 billion	9.7%
2019	44 billion	9.2%
2020	48 billion	8.9%
2021	52 billion	8.6%
2022	56 billion	8.3%

According to the table above, Turkey's pharmaceutical market grew by approximately 20% from 2018 to 2022. This growth is due to increasing population, aging population and, increase in chronic diseases. The Turkish pharmaceutical industry has a high growth potential and is expected to grow further in the coming years. Many foreign pharmaceutical companies operate in the Turkish pharmaceutical market, along with domestic pharmaceutical manufacturers. Turkey's largest pharmaceutical companies include Abdi İbrahim, Bayer, Bristol-Myers Squibb, GlaxoSmithKline, Janssen, Novartis, Roche, Sanofi and Pfizer.

Turkish Pharmaceutical Industry Crisis Management and Future Expectations During The Covid-19 Pandemic

The Covid-19 epidemic rapidly affected Turkey, as it did worldwide. The epidemic deeply affected the Turkish pharmaceutical industry. During the epidemic, the demand for medicines increased, and, the supply chain was disrupted. This situation led to an increase in drug prices and a decrease in drug availability (TITCK, 2023). While the health systems of countries attempted to respond quickly to this situation, the pharmaceutical industry also played a critical role in the process. Representatives of the pharmaceutical industry in Turkey swiftly implemented crisis management strategies. The Turkish pharmaceutical industry took various measures against the COVID-19 epidemic. These measures include the development of new drugs and vaccines, increasing drug production and, improving drug distribution (Health, 2023).

In the meetings held under the leadership of TITCK, strategies regarding potential drug shortages, raw material supply and, how to maintain the drug distribution network were determined. The measures taken, especially to maintain chronic patients' medication access, became one of the cornerstones of crisis management (TITCK, 2023). According to data from the World Health Organization, the impact

of Covid-19 on the global pharmaceutical industry was significant (WHO, 2023). Turkey managed this process by increasing domestic production and strengthening the supply chain. Domestic pharmaceutical manufacturers have developed alternative solutions to the problems experienced in global pharmaceutical supply by making additional investments in R&D studies.

The pandemic process has revealed the adaptive and innovative capacity of the Turkish pharmaceutical industry. The pharmaceutical industry's successful management of this crisis can serve as an example for similar situations in the future (OECD, 2020). In this process, the importance of digitalization for the pharmaceutical industry was once again seen. Digital health platforms, telemedicine, and, e-health solutions will have a vital place in the future of the pharmaceutical industry (Company, 2020). In particular, pharmaceutical tracking and tracing systems will rapidly be included in the digitalization process.

Additionally, Turkey is expected to take a more active role in global competition in biotechnological drugs and vaccine development. Increasing in R&D investments will further strengthen Turkey's position in the pharmaceutical industry. A continuous observation and analysis process is required to understand how the epidemic shapes the global pharmaceutical market and Turkey's position. These analyses will play a critical role in shaping the future of the pharmaceutical industry.

The Turkish pharmaceutical industry is expected to grow after the epidemic. This growth will result from factors such as the developing of new drugs and vaccines, increasing drug production and, improving drug distribution (TUBİTAK, 2023).

Literature Review

Acar and Ozturk (2020) examined the impact of the COVID-19 epidemic on the Turkish pharmaceutical industry. The study consists of data collected from all pharmaceutical companies

in Turkey. The data set includes variables such as companies' financial performance, research and development expenditures, workforce and, exports. In the study, time series analysis and comparative analysis were used. According to the findings, the COVID-19 epidemic had a significant negative impact on the Turkish pharmaceutical industry. As a result, according to the study, the epidemic negatively affected companies' financial performance, research and development expenditures, workforce and, exports (Acar & Öztürk, 2020).

Bayraktar and Demirtas (2021) their study aims to examine the effects of the COVID-19 epidemic on the Turkish pharmaceutical industry using time series analysis. For this purpose, they worked on a data set consisting of data collected from all pharmaceutical companies in Turkey. This data set includes variables such as companies' financial performance, research and development expenditures, workforce and, exports. The findings of the study indicate that the COVID-19 epidemic has a significant negative impact on the Turkish pharmaceutical industry. As a result, it has been determined that the COVID-19 epidemic negatively affects the financial performance, research and development expenditures, workforce, and, exports of companies (Bayraktar & Demirtaş, 2021).

Çakar and Gunes (2022) examined the effects of the COVID-19 epidemic on the Turkish pharmaceutical industry using comparative analysis. Companies' financial performance, research and development expenditures, workforce and, exports are included in the analysis. According to the analysis results, it has been determined that the global perception has a significantly negative impact on the Turkish pharmaceutical industry (Çakar & Güneş, 2022).

Gurcan and Sonmez (2021) examined the impact of the global epidemic on the production of the Turkish pharmaceutical industry in their study. The data set includes variables such as companies' production quantity, production value, and production cost. In the study, time series analysis and comparative

analysis were used. The findings of the study show that the COVID-19 pandemic has had a significant negative impact on Turkish pharmaceutical industry production. The epidemic has negatively affected the industry's production amount, production value and, production cost (Gürcan & Sönmez, 2021).

Sen and Ozturk (2021) aim to examine the impact of the COVID-19 epidemic on the financial performance of the Turkish pharmaceutical industry in their study. The data included in the analysis in the study comprise variables such as companies' sales revenue, net profit, and equity capital. In the study, time series analysis and, comparative analysis were used. According to the analysis results of the survey, COVID-19 negatively affected the sales revenue, net profit, and, equity capital of the sector (Şen & Öztürk, 2021).

Gokcek and Oztekin (2022) examined the impact of the COVID -19 epidemic on the Turkish pharmaceutical industry using econometric analysis. The study includes variables such as sales revenue, net profit and, equity capital collected from all

pharmaceutical companies in Turkey. In the study, regression analysis was used. The analysis results show that the COVID-19 epidemic negatively affected the sales revenue, net profit, and, equity capital of the sector, indicating a significant negative impact on the Turkish pharmaceutical industry (Gökçek & Öztekin, 2022).

Covid-19 and Financial Performance Of The Turkish Pharmaceutical Industry

Sample Structure

Quarterly or annual financial reports of nine pharmaceutical companies whose shares are traded on Borsa Istanbul in Turkey between 2018 and 2023 will be used to compare performance before, during and, after the pandemic. In addition, the amount of pharmaceutical sales in Turkey during COVID-19 and, the revenues obtained from these sales and, the periodic data of the investments made by pharmaceutical companies for R&D will also be used in the analysis.

Summary information of the companies included in the sample is shown in Table 4 below:

Table 4. Summary information of the companies included in the sample (www.isyatirim.com)

Equity Code	Title	Closing Price (TRL)	Market Value (mn)	Market Value (mn \$)	Free Float Rate (%)	Capital (mn TRL)
ANGEN	Anatolia Biotechnology	14.57	3205.4	118.5	29.5	220
DEVA	Deva Holding	72.6	14521.4	536.7	17.8	200
ECILC	Eczacıbaşı İlaç	44.58	30548.9	1129.2	18.7	685.3
GENIL	Gene Pharmaceuticals	67	20100	742.9	22.6	300
LKMNH	Lokman Hekim Engurusag	35.8	1288.8	47.6	71.6	36
MEDTR	Meditera Medical Equipment	37.02	4405.4	162.8	20.5	119
SELEC	Selcuk Pharmaceutical Warehouse	51.3	31857.3	1177.5	14.9	621
TNZTP	Tapdi Oxygen	37.34	4779.5	176.7	21.9	128
TRILC	Turk Pharmaceuticals and Serum Industry	11.4	1844.6	68.2	59.9	161.8

The table shows the share values of 10 publicly traded pharmaceutical companies in Turkey. As seen in the table, Anatolia Biotechnology has the highest market value, with 3205.4 million TL. Deva Holding has the second highest market value, with 14521.4 million TL. Eczacıbaşı İlaç has the third highest market value, with 30548.9 million TL.

The data in the table points to the growth potential of the pharmaceutical industry in Turkey. The high market values of the companies operating in the sector show that the industry attracts attention from investors. It is expected that the sector's growth will continue as companies operating in the industry open up to foreign markets and develop new products.

MATERIAL and METHOD

The research aims to answer the hypotheses set below:

H₁: The financial performance of the pharmaceutical industry in Turkey was positively affected during the COVID-19 pandemic.

H₂: Financial growth expectations in the pharmaceutical industry are high after the Covid-19 pandemic.

Research data was conducted between 2018 and 2022 with a quarterly frequency. E-VIEWS 13 and STATA 17 statistical programs were used to analyze study's hypotheses.

A- Hypothesis-1

The study will consider the five most influential companies in the pharmaceutical industry in this

research. The data of these companies were collected from the Public Disclosure Platform (www.kap.org.tr). The five companies researched are shown in Table 5.

Table 5. Pharmaceutical Industry Companies of the Study

Firm No	Title
1	Deva Holding (DEVA)
2	EIS Eczacıbaşı İlaç Industrial and Financial Investment Inc. (ECILC)
3	Lokman Hekim Engurusag Health Tourism Education Services and Construction Contracting Inc. (LKMNH)
4	Selçuk Pharmaceutical Inc. (SELEC)
5	Turkish Pharmaceuticals and Serum Industry Inc. (TRILC)

To analyze the first hypothesis, data will be utilized in quarterly and, cross-sectional forms for five companies. Since the data of the study are cross-sectional, the Panel Data model was used to investigate the effect of independent variables on the dependent variable (Baltagi, 2005). Before estimating the panel data model, a unit root test will be performed to determine whether the data is stationary. Hausman and LM tests will be used to select the method of the panel data model from common effect, fixed effect and, random effect methods. Panel data assumptions will be tested and, the final model will be estimated. The variables used in the first hypothesis are shown in Table 6 (Hausman, 1978).

Table 6. Variables

	Variables		Abbreviation
Independent Variable	Inventory Turnover Ratio	Inventory Turnover Ratio	SD
	Net Profit and Loss Margin %	Net Profit and Loss Margin %	NKZM
	ROA	Return on Asset	ROA
Dependent Variable	ROE	Return on Equity	ROE

For the first hypothesis, the financial performance measure ROE ratio was determined. Other variables were determined as independent variables. Structural

break tests were conducted to answer the final panel model estimated hypothesis. Before the analysis, the series will be tested to be stationary.

RESULTS and DISCUSSION

Unit Root Test

First of all, since the data are quarterly, seasonal effects were investigated and, the seasonality effects of the series were eliminated in the residual and average values of the series (Levin, 2002). Dickey and Fuller (1979) ADF method was used for standard unit root tests (Dickey & Fuller, 1979). The results of the ADF test are shown in Figures 1 to 4.

```
. xtunitroot fisher SD, dfuller lags(1)

Fisher-type unit-root test for SD
Based on augmented Dickey-Fuller tests

H0: All panels contain unit roots      Number of panels =    5
Ha: At least one panel is stationary    Number of periods =   20

AR parameter: Panel-specific          Asymptotics: T -> Infinity
Panel means:   Included
Time trend:    Not included
Drift term:    Not included           ADF regressions: 1 lag
```

		Statistic	p-value
Inverse chi-squared(10)	P	40.4624	0.0000
Inverse normal	Z	-3.2793	0.0005
Inverse logit t(29)	L*	-4.1940	0.0001
Modified inv. chi-squared	Pm	6.8116	0.0000

Figure 1. SD ADF Unit Root Test

PM statistic values of the ADF test show the final ADF result. If the probability value of this statistic is less than 0.05, the test rejects the null hypothesis. The SD variable rejects the null hypothesis in the ADF test. Therefore, the SD series is stationary.

```
. xtunitroot fisher NKZM, dfuller lags(1)

Fisher-type unit-root test for NKZM
Based on augmented Dickey-Fuller tests

H0: All panels contain unit roots      Number of panels =    5
Ha: At least one panel is stationary    Number of periods =   20

AR parameter: Panel-specific          Asymptotics: T -> Infinity
Panel means:   Included
Time trend:    Not included
Drift term:    Not included           ADF regressions: 1 lag
```

		Statistic	p-value
Inverse chi-squared(10)	P	28.6305	0.0014
Inverse normal	Z	-2.1335	0.0164
Inverse logit t(29)	L*	-2.7323	0.0053
Modified inv. chi-squared	Pm	4.1659	0.0000

Figure 2. NKZM % ADF Unit Root Test

Figure 2 shows the ADF test results of the NKZM. The NKZM variable rejects the null hypothesis in the ADF test. Therefore, the NKZM series is stationary.

```
. xtunitroot fisher ROE, dfuller lags(1)

Fisher-type unit-root test for ROE
Based on augmented Dickey-Fuller tests

H0: All panels contain unit roots      Number of panels =    5
Ha: At least one panel is stationary    Number of periods =   20

AR parameter: Panel-specific          Asymptotics: T -> Infinity
Panel means:   Included
Time trend:    Not included
Drift term:    Not included           ADF regressions: 1 lag
```

		Statistic	p-value
Inverse chi-squared(10)	P	26.5194	0.0031
Inverse normal	Z	-2.3066	0.0105
Inverse logit t(29)	L*	-2.4297	0.0108
Modified inv. chi-squared	Pm	3.6939	0.0001

Figure 3. ROE ADF unit root test

Figure 3 shows the ADF test results of the ROE variable. The series of the ROE variable rejects the null hypothesis in the ADF test. Therefore, the ROE series is stationary.

```
. xtunitroot fisher ROA, dfuller lags(1)

Fisher-type unit-root test for ROA
Based on augmented Dickey-Fuller tests

H0: All panels contain unit roots      Number of panels =    5
Ha: At least one panel is stationary    Number of periods =   20

AR parameter: Panel-specific          Asymptotics: T -> Infinity
Panel means:   Included
Time trend:    Not included
Drift term:    Not included           ADF regressions: 1 lag
```

		Statistic	p-value
Inverse chi-squared(10)	P	69.7479	0.0000
Inverse normal	Z	-4.9131	0.0000
Inverse logit t(29)	L*	-7.9865	0.0000
Modified inv. chi-squared	Pm	13.3600	0.0000

Figure 4. ROA ADF Unit Root Test

Figure 4 shows the ADF test results of the ROA variable. The series of the ROA variable rejects the null hypothesis in the ADF test. Therefore, the ROA series is stationary.

Hausman Test

After estimating the panel data model with random and fixed effect models, the Hausman test was used to select the most appropriate and safe model between these two models. The null hypothesis of the Hausman test is that the coefficient difference is not systematic, and this shows that the appropriate model is a random effect model. Figure 5 shows the Hausman test results.

```
. hausman fixed random, sigmamore
```

	Coefficients		(b-B) Difference	sqrt(diag(V_b-V_B)) Std. err.
	(b) fixed	(B) random		
NKZM	-.1268414	-.1342088	.0073674	.0079524
ROA	-1.000361	-.0044389	-.9959225	.2093532
SD	.0032511	-.0011773	.0044284	.001984

```

b = Consistent under H0 and Ha; obtained from xtreg.
B = Inconsistent under Ha, efficient under H0; obtained from xtreg.

Test of H0: Difference in coefficients not systematic

chi2(3) = (b-B)'[(V_b-V_B)^(-1)](b-B)
        = 29.61
Prob > chi2 = 0.0000

```

Figure 5. Hausman Test

According to the continuation of the Hausman test, the null hypothesis is rejected. Therefore, the most suitable model is the fixed-effects panel data model. Tests for autocorrelation, heteroskedasticity, and multicollinearity were conducted to examine the identified panel data model.

Heteroskedasticity, Autocorrelation and, Multiple Linear Dependency Test

Heteroskedasticity refers to a situation where the variance of the residual term or error term in a regression model varies significantly. Wald test was used to detect heteroscedasticity. The null hypothesis of this test is that the model has no heteroskedasticity. Figure 6 shows Wald Heteroskedastic Test results.

```
. xttest3
```

```

Modified Wald test for groupwise heteroskedasticity
in fixed effect regression model

H0: sigma(i)^2 = sigma^2 for all i

chi2 (5) = 39.49
Prob>chi2 = 0.0000

```

Figure 6. Wald Heteroskedasticity Test

The probability values of the Wald Heteroskedastic test reject the null hypotheses. This result shows that the model has heteroscedasticity.

The Breusch-Godfrey test was used to determine the absence of autocorrelation in the model variables. The null hypothesis of this test is that there is no

autocorrelation between the variables. Figure 7 shows the results of the Breusch Godfrey autocorrelation test (Breusch & Pagan, 1979).

```
. estat bgodfrey, lags(1)
```

```

Breusch-Godfrey LM test for autocorrelation

```

lags(p)	chi2	df	Prob > chi2
1	34.658	1	0.0000

```

H0: no serial correlation

```

Figure 7. Breusch-Godfrey Autocorrelation Test

The results of Breusch-Godfrey (1979) test reject the null hypothesis. Therefore, it was determined that there was autocorrelation between the series. The specified fixed-effect panel data model has autocorrelation and heteroskedasticity problems, and the fixed-effect Panel GLS model will be used to eliminate these problems.

Belsley (1973), variance inflation factor (VIF) measures the amount of multicollinearity in regression analysis. Multicollinearity exists when there is a correlation between more than one independent variable in a multiple regression model. Figure 8 shows the results of the VIF test (Belsley, 1973).

```
. estat vif
```

Variable	VIF	1/VIF
SD	1.00	0.999024
ROA	1.00	0.999048
NKZM	1.00	0.999976
Mean VIF	1.00	

Figure 8. VIF test

If the VIF test values are more than 3, it is determined that there is a variance inflation factor, but since the VIF test results of the study are less than 3, it is determined that there is no VIF problem in the model.

Panel GLS Model and Panel Structural Break

Tests

```
. xtglm ROE NKZM ROA SD, panels(correlated) corr(ar1)
Cross-sectional time-series FGLS regression
Coefficients: generalized least squares
Panels: heteroskedastic with cross-sectional correlation
Correlation: common AR(1) coefficient for all panels (0.5605)
Estimated covariances = 15 Number of obs = 100
Estimated autocorrelations = 1 Number of groups = 5
Estimated coefficients = 4 Time periods = 20
Wald chi2(3) = 91.52
Prob > chi2 = 0.0000
```

ROE	Coefficient	Std. err.	z	P> z	[95% conf. interval]	
NKZM	-.110125	.0135335	-8.14	0.000	-.1366501	-.0835998
ROA	-.6485697	.2194349	-2.96	0.003	-1.078654	-.2184852
SD	.0066564	.0026107	2.55	0.011	.0015395	.0117733
_cons	.1962587	.0199419	9.84	0.000	.1571734	.2353441

Figure 9. Panel GLS model

Figure 9 shows Greene’s (1986) panel GLS results. Panel GLS results determined that the effects of the determined independent variables were significant, and, this result indicates that the variables in the future Structural Break tests were selected correctly (Greene, 1986).

In econometrics and statistics, a structural break is an unexpected change in the parameters of regression models over time that can lead to significant forecast errors and overall unreliability. This issue has been popularized that instability of coefficients often leads to prediction failure and, therefore we should routinely test for structural stability. Structural stability is a central issue in all applications of linear regression models.

Dvoretzky, Kiefer and Wolfowitz (1956) investigate the possibility of a structural break in the regression using the DKW test (Dvoretzky, Kiefer, & Wolfowitz, 1956). The null hypothesis of the DKW test is that there is no structural break. Additionally, this test will predict the date of the structural break. Figure 10 shows the results of the DKW test.

```
. xtbreak test ROE NKZM ROA SD, breaks(2) hypothesis(1)
Test for multiple breaks at unknown breakdates
(Ditzen, Karavias & Westerlund, 2021)
H0: no break(s) vs. H1: 2 break(s)
----- Bai & Perron Critical Values -----
Test Statistic 1% Critical Value 5% Critical Value 10% Critical Value
-----
supW(tau) 4.43 4.82 4.00 3.58
Estimated break points: 2020q2 2022q1
Trimming: 0.15
```

Figure 10. DKW Structural Fracture Test

In the regression determined according to the results of the DKW test, structural breaks occurred in 2 data. These dates are determined as the second quarter data of 2020 and the first quarter data of 2022. This estimate was estimated at the 5% significance level.

KT test tests whether each series has a structural break at specified dates. This test is performed once on each series and makes predictions by observing only the data of the series. According to the KT test results, a structural break exists in the series on the dates determined in the DKW test results.

Figure 11 shows the data on recorded new cases of COVID-19.

Daily New Cases in Turkey

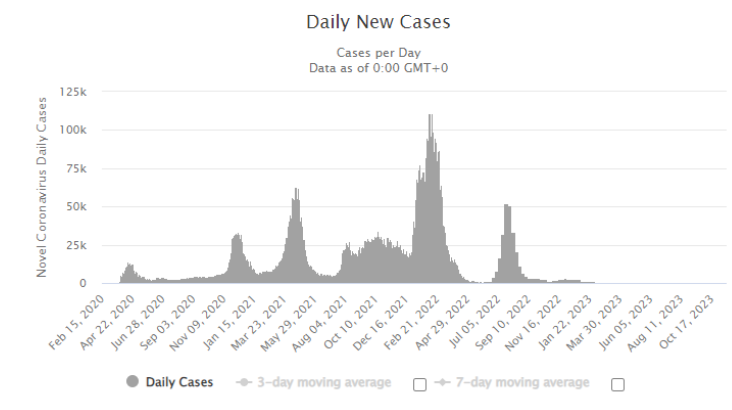


Figure 11. COVID-19 daily cases

According to the figure, COVID-19 reached pandemic conditions in April and May 2020. In addition, the COVID-19 pandemic was the cause of the highest number of cases in February 2022. These data confirm the result of the study.

B- Hypothesis 2

To analyze the second hypothesis of the study, data were collected in time series. Since time series models are used in this hypothesis, the financial growth variables will be the three variables determined in Table 7. The other variable was determined as the independent variable.

Table 7. Second hypotheses variables

Abbreviation	Variable	Frequency	
Snkzm	Net profit and loss margin	Quarter	Dependent
CCV	Covid-19 quarter cases	Quarter	Independent
sROE	Return on Equity	Quarter	Independent
sHSG	Stock returns of five companies in the pharmaceutical industry	Quarter	Independent

In the second hypothesis, the NKZM variable was determined as the financial growth rate in the pharmaceutical industry. After creating a VAR model in this hypothesis, the effects of the independent variables on the dependent variable will be investigated in the following eight quarters with the impact-response test. Since the series of this hypothesis are quarterly data, seasonal effects have been eliminated.

VAR takes into account the lags of the variables of the model, so the optimal lag of the model must be determined (Akaike, 1974). VAR lag criteria were used to determine the optimal lag, and, the statistical values of these criteria are shown in Figure 12. Among the requirements in Figure 12, AIC, SC and, HQ, the most appropriate with the smallest value at zero lag. The values of the results show that the AIC information criterion is the most appropriate. The AIC shows that the most appropriate lag of the VAR model is only the first lag.

VAR Lag Order Selection Criteria
 Endogenous variables: SNKZM CCV SROE SHSG
 Exogenous variables: C
 Date: 11/19/23 Time: 21:08
 Sample: 2018Q1 2022Q4
 Included observations: 18

Lag	LogL	LR	FPE	AIC	SC	HQ
0	-222.8999	NA	1045547.	25.21110	25.40896	25.23838
1	-190.4253	46.90781*	177910.4	23.38059	24.36989*	23.51700
2	-168.4359	21.98938	127776.8*	22.71510*	24.49584	22.96064*

* indicates lag order selected by the criterion
 LR: sequential modified LR test statistic (each test at 5% level)
 FPE: Final prediction error
 AIC: Akaike information criterion
 SC: Schwarz information criterion
 HQ: Hannan-Quinn information criterion

Figure 12. VAR Optimal Lag

The optimal lag of the VAR is the second lag determined in the AIC criterion, so that the VAR model will be estimated with lags of 1 and 2 for Hypothesis tests.

Roots of Characteristic Polynomial
 Endogenous variables: SNKZM CCV SROE SHSG
 Exogenous variables: C
 Lag specification: 1 2
 Date: 11/19/23 Time: 21:11

Root	Modulus
0.960772	0.960772
-0.871329	0.871329
-0.023143 - 0.811058i	0.811389
-0.023143 + 0.811058i	0.811389
0.387822 - 0.495514i	0.629238
0.387822 + 0.495514i	0.629238
-0.444113	0.444113
0.374113	0.374113

No root lies outside the unit circle.
 VAR satisfies the stability condition.

Figure 13. VAR Stability Test

If the values of the VAR Stability test are less than 1, it will be determined that the VAR model is stable. Since the values of the results were less than 1, it was determined that the estimated VAR model was stable.

VAR serial correlation LM test checks whether the model passes with the LM test. The null hypothesis of this test is that the model has a serial correlation at the specified lag. The results of the LM test are shown in Figure 14.

VAR Residual Serial Correlation LM Tests
 Date: 11/19/23 Time: 21:15
 Sample: 2018Q1 2022Q4
 Included observations: 18

Null hypothesis: No serial correlation at lag h

Lag	LRE* stat	df	Prob.	Rao F-stat	df	Prob.
1	16.62332	16	0.4104	0.991367	(16, 6.7)	0.5407
2	15.94837	16	0.4566	0.923666	(16, 6.7)	0.5829
3	61.68518	16	0.0000	37.04876	(16, 6.7)	0.0000

Figure 14. VAR Serial Correlation Test

According to the results of the LM test, the model accepts the null hypothesis at the first and second lags, but it was determined that the third lag had a serial correlation. Therefore, it was determined that there was no serial correlation with the estimated VAR model 1 and 2 lags.

The Johansen Co-integration approach uses maximum likelihood estimation to estimate the number of cointegration relationships and the parameters of these relationships (Johansen, 1991). It consists of VAR estimates that include the differences and levels of non-stationary series. Figure 15 shows the Johansen Co-integration test results. According to the Trace test statistics in Figure 15, it is seen that there is a long-term relationship between the variables examined. The null hypothesis of this test is the absence of a long-term relationship. As shown in the figure, rejecting at most one probability value, there are two cointegration equations in the model.

Unrestricted Cointegration Rank Test (Trace)

Hypothesized No. of CE(s)	Eigenvalue	Trace Statistic	0.05 Critical Value	Prob.** Critical Value
None *	0.997660	140.2578	47.85613	0.0000
At most 1 *	0.822667	37.28095	29.79707	0.0057
At most 2	0.369454	7.875564	15.49471	0.4788
At most 3	0.002097	0.035681	3.841465	0.8501

Figure 15. Cointegrating Test

Figure 16 shows the estimated cointegration equation. To determine the significance of the estimate, which is the model of the study, in the cointegration equation, the coefficients of the equation will be divided by the standard error of the series. If the positive result is greater than two, it will be determined that the variable significantly affects the dependent variable in the long term.

1 Cointegrating Equation
 Log-Likelihood: -108.9619

Normalized cointegrating coefficients (standard error in parenth...

	SNKZM	CCV	SROE	SHSG
1	-8.04237104...	6.731303407...	0.276394823...	1.328705940...
		0.121655790...	0.009158676...	

Figure 16. Cointegration Equation

According to the results of dividing the coefficients by the standard error, CCV, SROE and, SHSG variables significantly affect the dependent variable in the long term.

After determining that the VAR model and cointegration equation are significant, we can be sure of the results of the impulse response model. Figure 17 shows the results of the impulse test.

Accumulated Response to Cholesky One S.D. (d.f. adjusted) Innovations

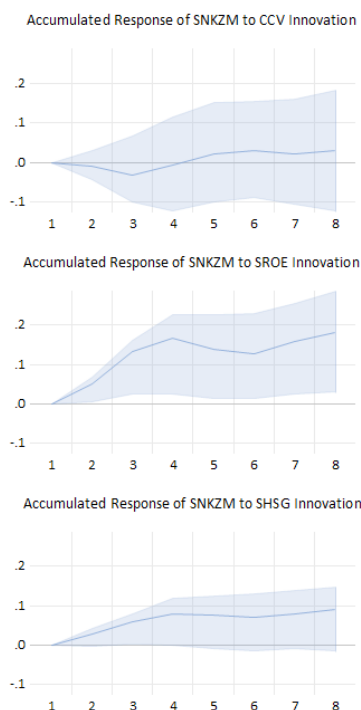


Figure 17. Impulse Test Results

According to the results of the impulse response test, a positive shock effect of the CCV variable negatively affects the NKZM value for up to three periods. After the third period, the shock will have a positive impact, and, this effect will continue until the eighth period.

The positive shock of the SROE variable affects the NKZM variable positively. This effect has a positive growth rate and will only have a negative growth rate in the fourth and sixth periods.

The positive shock of the SHSG variable affects the NKZM variable positively. This effect will continue at a constant growth rate.

This study has examined the financial performance of the Turkish pharmaceutical sector from 2018 to 2022 in the context of the impacts of the COVID-19 pandemic. Other studies have similarly investigated how the Turkish pharmaceutical sector was affected by the pandemic. These studies have emphasized the

adverse effects of the pandemic on significant variables within the industry, such as financial performance, R&D expenditures, workforce, and exports.

Acar and Ozturk's study indicated a significant negative impact of the pandemic on the Turkish pharmaceutical industry, supporting the notion that it affected a broad spectrum of elements, including financial performance, R&D expenditures, workforce, and exports. Likewise, the studies conducted by Bayraktar and Demirtas, and Cakar and Gunes also supported these findings, highlighting the adverse effects of the pandemic on various facets of the sector.

Moreover, the studies by Gurcan and Sonmez, as well as Sen and Ozturk, yielded similar outcomes, demonstrating the adverse effects of the pandemic on the Turkish pharmaceutical industry. Gurcan and Sonmez delved into production-oriented elements like production quantity, value, and cost, indicating the sector's exposure to this unfavorable impact on production activities.

Additionally, the panel data analysis in this study revealed distinct fluctuations in the effects of the pandemic during specific periods. The structural break analysis emphasized the pronounced impact of the pandemic starting from the second quarter of 2020, showing significant alterations in sector performance during these periods. Furthermore, it observed how the relationship between COVID-19 case data and financial performance evolved.

These comparative analyses underscore the extensive and diverse adverse effects of the pandemic on the Turkish pharmaceutical industry. However, this study, in particular, provided a more detailed perspective by focusing on the evolution of pandemic effects over time.

CONCLUSION

In conclusion, these comparative analyses highlight the value of employing different analytical methods to understand the sector's response to the pandemic and the changes in its financial performance. Future studies could expand on these findings and deeply

evaluate the sector's potential by utilizing larger datasets or employing different methodologies.

The COVID-19 pandemic has had profound social, economic and, health impacts in Turkey, as well as all over the world. As stated at the beginning of this study, we aim to analyze in depth how the pharmaceutical industry in Turkey responded to this unexpected and far-reaching crisis, and what the industry's future expectations are.

Throughout the pandemic, the Turkish pharmaceutical industry has faced a sudden increase in drug demand, disruptions in supply chains, and, fluctuations in drug prices. However, the sector has taken a series of strategic measures to overcome these difficulties, thus managing to keep supply continuity at the highest level and meet the pharmaceutical needs of the public.

With the active contributions of the Turkish Ministry of Health and TÜBİTAK, studies on new drugs and vaccines continue rapidly. At the same time, improvements in pharmaceutical production and distribution processes have increased the overall resilience of the sector and enabled it to respond to quickly changing needs.

This study examined in detail the financial performance of the Turkish pharmaceutical industry between 2018 and 2022 under the impact of the COVID-19 pandemic. Analyses conducted to understand the short and long-term effects of the pandemic on the sector have highlighted unexpected changes in financial indicators during specific periods. In particular, the financial resilience and volatility of the industry were observed in the periods ranging from before the pandemic to during and after the pandemic. The panel data analysis and structural break analysis showed that the pandemic had a substantial impact, especially from the second quarter of 2020, and that there were substantial changes in sector's performance during these periods. It was also observed how changes in the financial performance of the industry evolved in correlation with COVID-19

case data. The results of this study provide a significant perspective to understand the pharmaceutical industry's ability to adapt to pandemic conditions and the resilience of the sector. Future studies may expand on the findings of this study through analysis with larger data sets or the use of different methodologies and evaluate the future potential of the sector in more detail.

Limitations of the Study

This study has some limitations. For example, the data set used in the analysis covers a specific period, which may not allow long-term trends to be fully captured. Additionally, since the panel data analysis method is based on certain assumptions, the results may be affected if these assumptions are not met. However, since the study was limited to specific financial indicators, the impact of other variables in the sector may not have been thoroughly evaluated.

Future Directions

The findings of this study provide an essential basis for future research. In particular, more in-depth studies can be conducted on companies' strategies, international competition and, sectoral innovations in the post-pandemic period in the pharmaceutical industry. In addition, analyzing other variables such as labor force dynamics and R&D investments, in addition to the financial indicators on which this study focuses, may provide a vital breakthrough for future research.

Implications

The findings of this study may influence the decision-making processes of companies and regulators in the pharmaceutical industry. In particular, considering the uncertainties and changing trends in the sector during the pandemic is, crucial for companies to make their strategies flexible and adaptable. Additionally, the impact of these findings on regulations in the industry may shape future policy-making processes and contribute to the sustainable growth of the industry.

CONFLICT of INTEREST

The authors declare that there is no conflict of interest

AUTHOR CONTRIBUTION STATEMENT

Developing hypothesis (MÖ, HT), experimenting (MÖ, HT), preparing the study text (MÖ, HT), reviewing the text (MÖ, HT), statistics (MÖ, HT), analysis and interpretation of the data (MÖ, HT), literature research (MÖ, HT).

REFERENCES

- Acar, T., & Öztürk, G. (2020). The Impact of the Covid-19 Epidemic on the Turkish Pharmaceutical Industry. *Journal of Business Research*, 119.
- Akaike, H. (1974). A new look at the statistical model identification. . *IEEE Transactions on Automatic Control*, 19((6)), 716-723.
- Baltagi, B. H. (2005). *Econometric analysis of panel data (3rd ed.)*. . John Wiley & Sons.
- Bayraktar, D., & Demirtaş, M. (2021). Effects of the Covid-19 Epidemic on the Turkish Pharmaceutical Industry: A Time Series Analysis. *Journal of Economic Studies*, 48(2), 249-266.
- Belsley, D. A. (1973). The Variance inflation factor. *Journal of the American Statistical Association*, 68(341), 92-101.
- Breusch, T. S., & Pagan, A. R. (1979). A Simple Test for Heteroscedasticity and Random Coefficient Variation. *Econometrica*, 47(5), 1287-1294.
- Company, M. &. (2020, November 10). *The Pharmaceutical Industry in 2020: A Year of Transformation*. Retrieved from McKinsey & Company. (2020). The Pharmaceutical Industry in 2020: A Year of Transformation: <https://www.mckinsey.com/capabilities/risk-and-resilience/our-insights/covid-19-implications-for-business-2020>
- Çakar, M., & Güneş, G. (2022). Effects of the Covid-19 Epidemic on the Turkish Pharmaceutical Industry: A Comparative Analysis. *Journal of Applied Economics*, 25(1), 113-132.
- Dickey, D. A., & Fuller, W. A. (1979). Distribution of the Estimators for Autoregressive Time Series with a Unit Root. *Journal of the American Statistical Association*, 74(366), 427-431.
- Dvoretzky, A., Kiefer, J., & Wolfowitz, J. (1956). On the Sample Distribution of the Maximum of Empirical Distribution Functions. *Annals of Mathematical Statistics*, 27(1), 642-650.
- Gökçek, S., & Öztekin, S. (2022). The Impact of the Covid-19 Pandemic on the Turkish Pharmaceutical Industry: An Econometric Analysis. *Journal of Business Research*, 136,, 102745.
- Greene, W. H. (1986). Asymptotic Properties of the Generalized Least Squares Estimator in Panel Data Models with Cross-sectional Heteroskedasticity and Autocorrelation. *Econometrica*, 54(3), 717-739.
- Gürçan, E., & Sönmez, A. (2021). The Effect of Turkish Pharmaceutical Industry Production on the Covid-19 Pandemic. *Journal of Economics and Administrative Sciences*, 27(1), 131-146.
- Hausman, J. A. (1978). Specification Tests in Econometrics. *Econometrica*, 46(6), 1251-1271.
- Health, T. M. (2023, November 10). *Precautions for the Turkish Pharmaceutical Industry during the COVID-19 Pandemic*. Retrieved from Turkish Ministry of Health: https://www.saglik.gov.tr/?_Dil=2
- IMF. (2020, October 13). *A Long and Uneven Road to Recovery*. Washington, DC: International Monetary Fund.
- Johansen, S. (1991). Estimation and Hypothesis Testing of Cointegration Vectors in Gaussian Vector Autoregressive Models. *Econometrica*, 59(6), 1551-1580.

- Levin, A. L. (2002). Unit root tests in panel data: Asymptotic and finite-sample properties. *Journal of Econometrics*, , 108(1), 1-24.
- OECD. (2020, November 10). *Health Sector Responses to COVID-19 in OECD Countries*. Retrieved from OECD: <https://www.oecd.org/coronavirus/en/policy-responses>
- Pharmaceutical Expenditures and R&D Investments in Turkey for the Period 2018-2022, www.tuik.gov.tr.
- Public Disclosure Platform (www.kap.org.tr).
- Şen, G., & Öztürk, G. (2021). The Impact of the Covid-19 Pandemic on the Financial Performance of the Turkish Pharmaceutical Industry. *Journal of Business Research*, 123, , 102689.
- TISD. (2022, January 10). *TISD*. Retrieved from Turkish Pharmaceutical Industry Association: https://www.ieis.org.tr/static/shared/publications/pdf/5822m1wt_turkish-pharmaceut
- TITCK. (2023, October 25). *TITCK*. Retrieved from Türkiye Pharmaceutical Industry Analysis: https://www.ieis.org.tr/static/shared/publications/pdf/111023mFyM_turkish_pharmaceutical_market_2022.pdf
- TUBİTAK. (2023, October 25). *Scientific and Technological Research Council of Türkiye*. Retrieved from TUBİTAK: https://www.tubitak.gov.tr/tubitak_content_files/english/TUBITAKcatalogue.pdf
- TUIK. (2023, November 10). *Türkiye Pharmaceutical Industry Statistics*. Retrieved from Turkish Statistical Institute: https://www.tuik.gov.tr/media/announcements/istatistiklerle_turkiye.pdf
- Türkiye Pharmaceutical Market Size and Growth Rate for the Period 2018-2022; www.statista.com
- WHO. (2023, October 25). *The Impact of COVID-19 on the Global Pharmaceutical Industry*. Retrieved from World Health Organization: <https://www.atlantis-press.com/article/125978330.pdf>
- World Bank. (2020, October 25). *World Bank*. Retrieved from World Bank. (2020). *The Global Economic Outlook During the COVID-19 Pandemic: A Changed World*. Washington, DC: World Bank: <https://www.worldbank.org/en/news/feature/2020/06/08/the-global-economic-outlook-during-the-covid-19-pandemic-a-changed-world>
- World Pharmaceutical Market Size and Growth Rate for the Period 2018-2022, www.statista.com.

The Inhibitory Effect of Trimethylamine (TMA), an Intestinal Bacterial Metabolite, on Endothelial Vasorelaxation in Rat Mesenteric Artery

Melike Hacer ÖZKAN*

The Inhibitory Effect of Trimethylamine (TMA), an Intestinal Bacterial Metabolite, on Endothelial Vasorelaxation in Rat Mesenteric Artery

SUMMARY

The effect of the gut microbiota metabolite trimethylamine-(TMA) in isolated vessels is unknown. Previously TMAO, the hepatic oxidation product of TMA, at 3 mM has been shown to inhibit endothelium-dependent vasorelaxations of isolated arteries only after 24-hour interaction. In this study, the effects of TMA (at 1 mM) on endothelium-dependent relaxations with acute (1 or 4 hours) and longer (24 hours) incubation periods were evaluated in superior mesenteric arteries of rats. Acute exposure to TMA of 1 hour significantly inhibited acetylcholine-stimulated endothelium-derived hyperpolarizing (EDH) type relaxations, and this inhibition gradually intensified as the incubation period was prolonged to 4 and 24 hours. The area under the curves (AUCs) of the relaxation-response curves after 1 and 24 hours after TMA incubation were found to be significantly different from each other. In contrast, similar AUC values were obtained after 4 and 24 hours of incubation. Contractile responses to phenylephrine, and nitric oxide (NO)-mediated relaxations of acetylcholine were similar in arteries before and after pretreatment with TMA for 24 hours. These data indicate that TMA selectively inhibits EDH-type relaxations in rat isolated mesenteric arteries. Although the inhibitory effect of TMA intensifies over time, it appears to be more pronounced during acute incubation periods. The findings strengthen the evidence that TMA is a more toxic metabolite on vascular tone than TMAO.

Key Words: Endothelial dysfunction, TMA, vascular, metabolite, mesenteric artery, rat.

Bağırsak Bakteriyel Metaboliti Trimetilaminin (TMA) Sıçan Mezenter Arterinde Endotel-aracılı Geşeme Üzerindeki İnhibitör Etkisi

ÖZ

Bağırsak mikrobiyota metaboliti trimetilamin'in (TMA) izole damarlardaki etkisi henüz bilinmemektedir. Daha önce, TMA'nın hepatic oksidasyon ürünü olan TMAO'nun izole arterlerde 3 mM konsantrasyonda 24 saatlik inkübasyon sonrası endotel-bağımlı geşemeleri seçici olarak inhibe ettiği gösterilmiştir. Buradaki çalışmada sıçan izole superior mezenter arterlerinde TMA'nın (1 mM) akut (1 ve 4 saat) ve daha uzun (24 saat) süreli inkübasyonu sonrası endotel- bağımlı geşemeler üzerindeki direkt etkileri incelendi. TMA'ya 1 saatlik akut maruz kalma, asetilkolin ile stimüle edilen endotel-kaynaklı hiperpolarizan (EDH)-tipi geşemeleri anlamlı olarak inhibe etti ve bu inhibisyon inkübasyon süresi 4 ve 24 saate uzatıldıkça şiddetlendi. Ne var ki, 1 ve 24 saatlik TMA inkübasyonu sonrasında geşeme-yanıt eğrilerinin eğri altında kalan alanları (AUC) birbirine göre anlamlı derecede farklı iken, 4 ve 24 saatlik inkübasyon sonrasında benzerdi. Fenilefrin ile elde edilen kasılmalar ve asetilkolin ile stimüle edilen nitrik oksit (NO)-aracılı geşemeler, 24 saatlik TMA inkübasyonu sonrası değişmedi. Bu veriler TMA'nın EDH-tipi geşemeleri selektif olarak inhibe ettiğini göstermektedir. Her ne kadar TMA'nın inhibitör etkisi zamana bağlı şiddetlense de, bunun akut inkübasyon dönemlerinde daha belirgin olduğu görülmektedir. Bulgular, TMA'nın vasküler tonus üzerinde TMAO'dan daha toksik bir metabolit olduğuna dair kanıtları güçlendirmektedir.

Anahtar Kelimeler: Endotel disfonksiyonu, TMA, vasküler, metabolit, mezenter arter, sıçan.

Received: 31.01.2024

Revised: 25.02.2024

Accepted: 26.02.2024

* ORCID: 0000-0003-1339-2616, Hacettepe Üniversitesi, Eczacılık Fakültesi, Eczacılık Meslek Bilimleri Bölümü, Farmakoloji A.B.D.

* Corresponding Author; Melike Hacer ÖZKAN
E-mail: melikeo@hacettepe.edu.tr

INTRODUCTION

Trimethylamine (TMA) is produced as an intermediate digestion product of animal foods through the metabolism of the intestinal microbiota. After passing the systemic circulation, TMA is immediately metabolized to trimethylamine N-oxide (TMAO) via flavin-monooxygenase-3 (FMO-3)-mediated oxidation in hepatic tissue (al-Waiz, Mikov, Mitchell, & Smith, 1992). Clinical studies show that TMAO is independently associated with cardiovascular disease (CVD) and that the risk of myocardial damage can be predicted by the plasma level of TMAO (Roncal, Martinez-Aquilar, Orbe, Ravassa, Fernandez-Montero,... Paramo, 2019). Essentially level of both metabolites in the circulatory system increases in patients having renal dysfunction or trimethylaminuria (Treacy, Akerman, Chow, Youil, Bibeau, Lin,... Forrest, 1998; Bain, Faull, Fornasini, Milne, & Evans, 2006). However, the direct vascular effects of these metabolites remain to be solved. Although TMA is known to be a more toxic metabolite on cells than TMAO, a limited number of *in vitro* studies have comparatively examined the vascular effects of TMA together with TMAO in the same experimental design. Both TMA and TMAO might change vascular tone. In human umbilical arteries, the potency and efficacy of TMA-induced contractile responses have been reported to be significantly higher than TMAO (Ongun, Orgul, Celik, & Bariskaner, 2023). We have also reported at pharmacological concentrations that TMAO impairs endothelium-derived and hyperpolarizing vasodilation in the rat isolated mesenteric artery, which implies the contribution of TMAO to endothelial disruption (Hamad, Ozkan, & Uma, 2021; Ongun, Orgul, Celik, & Bariskaner, 2023). However, no studies have investigated whether TMA could influence the function of endothelium in rat isolated mesenteric arteries. In the current study, the experimental protocol was applied with TMA at 1 mM concentration in both acute (1 hour and 4 hours) and long-term exposure times (24 hours) in rat small-sized arteries by measuring *ex vivo* isolated vessel function.

MATERIAL AND METHODS

Twenty-eight male Sprague Dawley rats 200-250 g in weight were purchased from Kobay Company (Ankara, Türkiye). The ethical approval was obtained by the local ethics committee of Hacettepe University (No: 2018-45). The animals were anesthetized by CO₂ and euthanized by decapitation. The feeding branch of superior mesenteric artery was carefully dissected and cleaned from adipose and connective tissues. The four mesenteric arterial rings were obtained from one rat mesenteric artery, and the rings were mounted into the organ baths of 5 ml. Isometric tensions were measured using a transducer and recorded on a computer. The rings were precontracted with phenylephrine submaximally, and then endothelium-dependent relaxations were obtained by cumulative acetylcholine concentrations (0.1 nM - 10 µM). After the first relaxation responses to acetylcholine, N(gamma)-nitro-L-arginine methyl ester (L-NAME) (100 µM)+indomethacin (INDO; 10 µM) were applied into the baths for 45 min to obtain endothelium-derived hyperpolarizing (EDH)-type vasorelaxations. Thereafter, the rings were incubated with TMA (1 mM) at increasing exposure times. For 1- and 4-hour incubations, the rings were exposed to TMA in Krebs-Henseleit Solution (KHS) of organ baths. Then acetylcholine responses were repeated in the presence of the inhibitors, as mentioned above. 24-hour-incubations (unpaired data) were carried out with tissue culture studies, in which arterial rings were pretreated with TMA in a cell culture medium containing DMEM (0.5 mL) and penicillin/streptomycin (1%) in an incubator at 37 °C for 24 hours. PBS was applied to the rings as a solvent control. At the end of the incubation period, TMA- and PBS-treated rings were mounted to organ baths, and the remaining experimental protocol were conducted, as mentioned over. In addition to EDH-type relaxations, NO-mediated relaxations of acetylcholine were also obtained in TMA-treated rings in the presence of apamin (APA; 50 nM)+INDO (10 µM) and TRAM-34

(1 μ M) for 45 min. To examine vascular contractility, cumulative contractions to phenylephrine (10 μ M - 100 μ M) were obtained in TMA-treated rings for 4 hours and 24 hours.

Phenylephrine (Sigma, P6126), acetylcholine (Sigma-Aldrich, A6625), L-NAME (Sigma, N-5751) and apamin (Sigma-Aldrich, A-1289) were prepared in distilled water. Indomethacin (Sigma, I-7378) was prepared with sodium bicarbonate-water mixture. KHS (mM): NaCl 118.0, KCl 4.7, MgSO₄ 1.2, CaCl₂ 2.5, KH₂PO₄ 1.2, NaHCO₃ 25.0 and glucose 11.1. NaCl was replaced with equimolar KCl to create an 80 mM KCl solution.

DMEM (D-5796) and penicillin-streptomycin (P-4333) were from Sigma. TMA (Sigma-Aldrich, 243205) was dissolved in PBS at pH 7.4.

Results are shown as the Mean \pm Standard Error of the Mean (SEM). Contractions are expressed % of contraction obtained with high KCl (80 mM), and relaxations % of precontraction. The area under the curves (AUCs) are expressed as arbitrary units (a.u). pD₂ values are represented as the -logEC₅₀, the half maximal effect occurred by sigmoid curve fitting (GraphPad, Prism 8). Two response curves were analysed with two-way ANOVA. Multiple comparisons were done using one-way ANOVA and Tukey's or Dunnett's post-hoc tests. P<0.05 was considered significant.

RESULTS AND DISCUSSION

In this *ex vivo* study, it was examined whether TMA showed similar disruptive effects as its hepatic

metabolite TMAO on endothelium-dependent relaxation in the rat isolated mesenteric artery. The TMA concentration was chosen as 1 mM to avoid a possible cytotoxic effect that may occur above this concentration (Jaworska, Bielinska, Gawryskopczynska, & Ufnal, 2019). In rat mesenteric arteries, endothelium-dependent relaxations are mainly mediated by EDH and NO. To examine EDH-type vasorelaxations, cumulative and endothelium-dependent relaxations of acetylcholine were first obtained in the presence of L-NAME (100 μ M)+INDO (10 μ M). The same preparations were then pretreated with 1 mM TMA in bath media for 1 and 4 hours of acute exposure. Acetylcholine-induced EDH-type relaxations were significantly reduced by 1- and 4-hour TMA incubation (Figure 1A and 1B). The acute effects of TMA on the EDH-type relaxations were detected as early as 1 hour and intensified within 4 hours. We have previously shown that acute treatment with 3 mM TMAO does not cause any changes in EDH-type in the same preparations, and the responses to acetylcholine are significantly reduced by increasing the incubation time to 24 hours (Hamad, Ozkan, & Uma, 2021). Similar to this data, extending the incubation period with 1 mM TMA up to 24 hours caused a more significant decrease in EDH-mediated relaxations compared to 1-hour incubation (Figure 1C). However, similar inhibitions were obtained with 4 and 24 hours of incubations. The AUC values of the relaxation-response curves obtained with acetylcholine after 1 and 24 hours of TMA incubation were found to be significantly different compared to each other (p< 0.05) (Figure 1D).

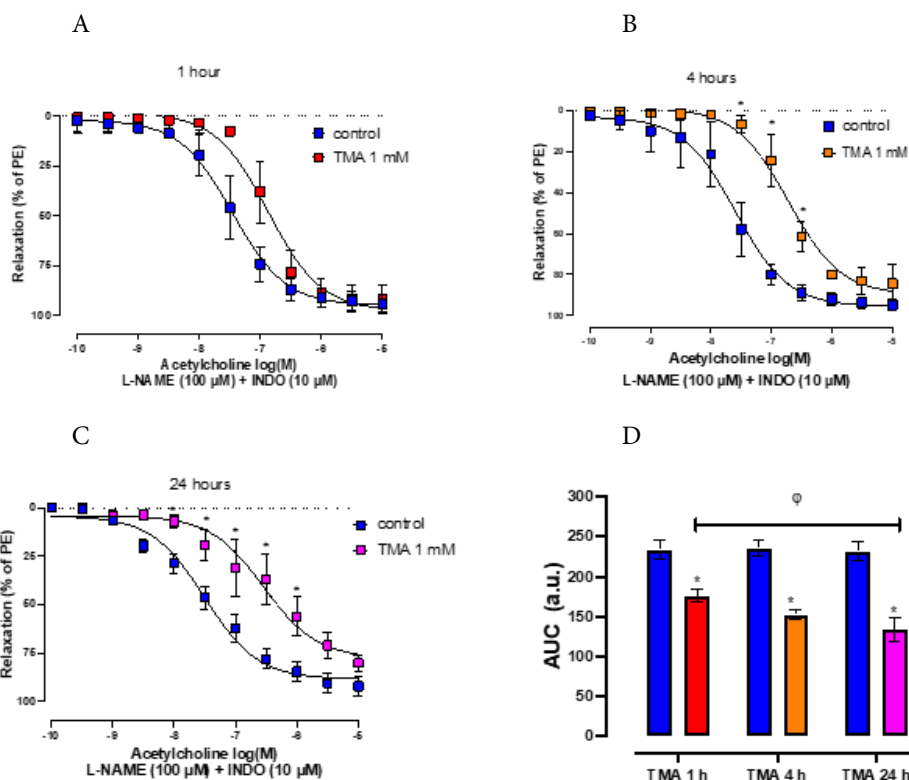


Figure 1. Acetylcholine-induced EDH-type vasorelaxations after 1-, 4- or 24-hour TMA exposure in mesenteric arteries after precontraction with phenylephrine (PE; 0.3 μ M). Concentration-dependent relaxations obtained with acetylcholine in the presence of L-NAME (100 μ M) and indomethacin (INDO: 10 μ M) significantly decreased after 1 hour (A), 4 hours (B), and 24 hours (C) of incubation with TMA (1 mM). The AUC values (D) of the relaxation-response curves obtained with acetylcholine after 1 and 24 hours of TMA incubation were significantly different compared to each other (n=7) (*significantly different from its control; ϕ significantly different from 1-hour incubation with TMA) (p<0.05).

In another series of experiments, long-term TMA incubations were done in organ culture media to evaluate its effect on NO relaxations. After 24 hours of exposure to TMA in cell-culture medium, the arterial rings were placed in organ baths, and then acetylcholine-stimulated endothelium-dependent and NO-mediated relaxations were obtained in the presence of TRAM-34+INDO+APA. Interestingly, these responses were unchanged in mesenteric arteries treated with 1 mM TMA or its solvent PBS for 24 hours (Figure 2).

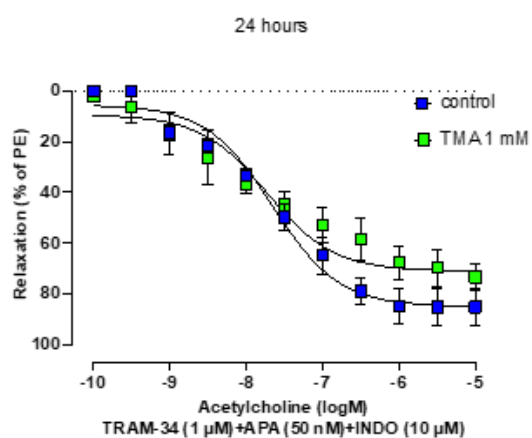


Figure 2. Acetylcholine-induced NO-mediated vasorelaxations after 24 hours of TMA (1 mM) or PBS (control) exposure in rat mesenteric arteries incubated with TRAM-34+INDO+APA. The long-term tissue presence of TMA did not lead to a change in the amplitude or sensitivity of the relaxations to acetylcholine (n=7).

Phenylephrine-induced cumulative contractions were also found to be TMA-resistant after 24-hour incubation (Figure 3).

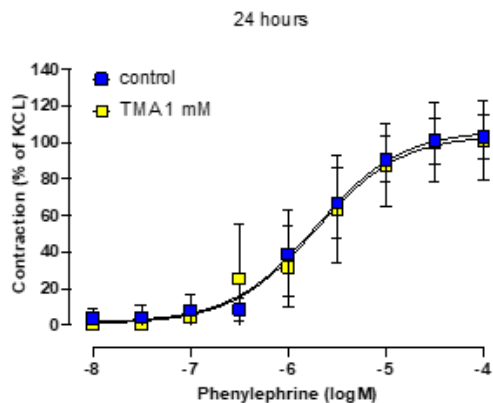


Figure 3. Phenylephrine-induced contractions after 24 hours of TMA (1 mM) exposure in rat isolated mesenteric arterial rings. The long-term presence of TMA in bath media did not affect the contractile responses in the mesenteric arterial rings (n=7).

In this study, we conducted *ex vivo* experiments to examine the possible effects of TMA, the precursor of TMAO, on endothelium-dependent vasorelaxations obtained with acetylcholine. TMA and TMAO levels in plasma increase in cardiovascular patients with decreased glomerular filtration rates, and in aged rats (Jaworska, Bielinska, Gawrys-Kopczynska, & Ufnal, 2019). Previously, we have shown no deterioration in endothelium-dependent relaxations obtained with acetylcholine after 1 or 4 hours of acute exposure to TMAO (1 or 3 mM) in rat isolated mesenteric arteries. However, TMAO at 3 mM concentration selectively inhibited EDH-type relaxations in response to acetylcholine when the incubation period was prolonged up to 24 hours (Hamad, Ozkan, & Uma, 2021). In the current study, a similar experimental protocol was applied to investigate whether TMA would worsen endothelium-dependent relaxations similarly to TMAO. Interestingly, TMA at 1 mM concentration inhibited EDH-type vasorelaxations to acetylcholine as early as acute incubations of 1 and 4 hours. However, extending the duration of treatment with TMA to 24 hours maintained a decrease in EDH-type responses, but those were similar to that obtained at 4-hour incubation group. Although previously we have shown that TMAO has a time-dependent progression in its

destructive effects, leading to a decrease in EDH-type vasorelaxations (Hamad, Ozkan, & Uma, 2021), the inhibitory potency of TMA on the same type of relaxations might appear more pronounced and severe in the acute exposure periods. These data propose that TMA can worsen endothelial function in a much shorter time and more severely than TMAO when its level increases in acute cardiovascular events (Jaworska, Konop, Hutsch, Perlejewski, Radkowska, Grochowska, ... Ufnal, 2020; Hamad, Ozkan, & Uma, 2021). The signaling pathways and subsequent events triggered by TMA in vascular endothelium are precisely unknown. The inhibition of EDH-type relaxations with TMA may be due to TMA somehow inhibiting membrane hyperpolarization through post-receptor events, thus preventing calcium-activated potassium channels from opening and vasorelaxation. However, to support this, some specific experiments such as membrane potential or calcium measurements in the vascular endothelium need to be done. Previously some G-protein coupled receptors like Olf78 and Gpr41 expressed on endothelium, the target of short-chain fatty acids, which are gut microbiota metabolites, which implies such a target may also apply to TMA or TMAO (Natarajan, Hori, Flavanhan, Steppan, Flavanhan, Berkowitz, & Pluznick, 2016). Recently, TMA has been suggested to be an agonist for trace amine-associated receptor 5 (TAAR5) in human olfactory epithelial cells (Wallrabenstein, Kuklan, Weber, Zborala, Werner, Altmuller, ... Gisselmann, 2013). However, it remains unclear what the target molecules are that mediate the effect of TMA on vascular endothelium or smooth muscle layer. Interestingly, the FMO-3 enzyme subtype, which is responsible for the oxidation of TMA to TMAO, has also been detected in rat aortic perivascular adipose tissue (Restini, Fink, & Watts, 2021). Since perivascular adipose tissue functions with anticontractile effects in regulating vascular tone (Chang, Garcia-Barrío, & Chen, 2020), it may also play a modulatory role in TMA metabolism and trigger the conversion to TMAO, a less toxic molecule, against increasing plasma TMA levels. All these studies provide that TMA might play a potential role in vascular diseases and contribute to endothelial dysfunction through direct and, or indirect effects on the endothelium.

In conclusion, the findings of the current study confirm that TMA inhibits EDH-type vasorelaxations without causing disruption with NO-mediated relaxations like TMAO. Moreover, short exposure periods to TMA are sufficient to reduce EDH-type relaxations in rat isolated mesenteric arteries.

ACKNOWLEDGEMENT

This study was granted by the Scientific Research Projects Coordination Unit of Hacettepe University (No: 7655).

CONFLICT OF INTEREST

The authors declare that there is no conflict of interest.

REFERENCES

- al-Waiz, M., Mikov, M., Mitchell, S. C., & Smith, R. L. (1992). The exogenous origin of trimethylamine in the mouse. *Metabolism*, *41*(2), 135-136. doi:10.1016/0026-0495(92)90140-6
- Bain, M. A., Faull, R., Fornasini, G., Milne, R. W., & Evans, A. M. (2006). Accumulation of trimethylamine and trimethylamine-N-oxide in end-stage renal disease patients undergoing haemodialysis. *Nephrol Dial Transplant*, *21*(5), 1300-1304. doi:10.1093/ndt/gfk056
- Chang, L., Garcia-Barrio, M. T., & Chen, Y.E. (2020). Perivascular Adipose Tissue Regulates Vascular Function by Targeting Vascular Smooth Muscle Cells. *ATVB* *6*, 1094-1109. doi: 10.1161/ATVBAHA.120.312464
- Hamad, A., Ozkan, M. H., & Uma, S. (2021). Trimethylamine-N-oxide (TMAO) Selectively Disrupts Endothelium-Dependent Hyperpolarization-Type Relaxations in a Time-Dependent Manner in Rat Superior Mesenteric Artery. *Biol Pharm Bull*, *44*(9), 1220-1229. doi:10.1248/bpb.b20-00767
- Jaworska, K., Bielinska, K., Gawrys-Kopczynska, M., & Ufnal, M. (2019). TMA (trimethylamine), but not its oxide TMAO (trimethylamine-oxide), exerts haemodynamic effects: implications for interpretation of cardiovascular actions of gut microbiome. *Cardiovasc Res*, *115*(14), 1948-1949. doi:10.1093/cvr/cvz231
- Jaworska, K., Konop, M., Hutsch, T., Perlejewski, K., Radkowski, M., Grochowska, M., ... Ufnal, M. (2020). Trimethylamine But Not Trimethylamine Oxide Increases With Age in Rat Plasma and Affects Smooth Muscle Cells Viability. *J Gerontol A Biol Sci Med Sci*, *75*(7), 1276-1283. doi:10.1093/gerona/glz181
- Natarajan, N., Hori, D., Flavahan, S., Steppan, J., Flavahan, N. A., Berkowitz, D. E., & Pluznick, J. L. (2016). Microbial short chain fatty acid metabolites lower blood pressure via endothelial G protein-coupled receptor 41. *Physiol Genomics*, *48*(11), 826-834. doi:10.1152/physiolgenomics.00089.2016
- Ongun, M. C., Orgul, G., Celik, C., & Bariskaner, H. (2023). Contractile effect of trimethylamine and trimethylamine-n-oxide on isolated human umbilical arteries. *J Obstet Gynaecol Res*, *49*(7), 1736-1742. doi:10.1111/jog.15656
- Restini, C. B. A., Fink, G. D., & Watts, S. W. (2021). Vascular reactivity stimulated by TMA and TMAO: Are perivascular adipose tissue and endothelium involved? *Pharmacol Res*, *163*, 105273. doi:10.1016/j.phrs.2020.105273
- Roncal, C., Martinez-Aquilar, E., Orbe, J., Ravassa, S., Fernandez-Montero, A., ... Paramo, J.A. (2019). Trimethylamine-N-Oxide (TMAO) Predicts Cardiovascular Mortality in Peripheral Artery Disease. *Scientific Reports*, *9*, 15580. doi: 10.1038/s41598-019-52082-z
- Treacy, E. P., Akerman, B. R., Chow, L. M., Youil, R., Bibeau, C., Lin, J., ... Forrest, S. M. (1998). Mutations of the flavin-containing monooxygenase gene (FMO3) cause trimethylaminuria, a defect in detoxication. *Hum Mol Genet*, *7*(5), 839-845. doi:10.1093/hmg/7.5.839
- Wallrabenstein, I., Kuklan, J., Weber, L., Zborala, S., Werner, M., Altmüller, J., ... Gisselmann, G. (2013). Human trace amine-associated receptor TAAR5 can be activated by trimethylamine. *PLoS One*, *8*(2), e54950. doi:10.1371/journal.pone.0054950

Effect of n-Hexane Extract from *Tanacetum argenteum* (Lam.) Willd. subsp. *argenteum* on the Secretion of Proinflammatory Cytokines in THP-1 Cell Line

Ege ARZUK^{*}, Fuat KARAKUŞ^{**}, Gökay ALBAYRAK^{***}, Ali ERGÜÇ^{****}, İclal TAN^{*****}, Ecrin ATIŞ^{*****}

Effect of n-Hexane Extract from Tanacetum argenteum (Lam.) Willd. subsp. argenteum on the Secretion of Proinflammatory Cytokines in THP-1 Cell Line

Tanacetum argenteum (Lam.) Willd subsp. argenteum n-Hekzan Ekstresinin THP-1 Hücre Hattında Proinflamatuvar Sitokinlerin Salgılanması Üzerine Etkisi

SUMMARY

Inflammation is an initial biological process that involves the activation of the immune system in response to injury, infection or exposure to toxic agents. During this process, cytokines, small proteins produced by immune cells, play a vital role in regulating the immune response. Inflammatory cytokines, including interleukins, tumor necrosis factor- α , nitric oxide, and interferon-gamma, initiate the immune response and promote inflammation. Natural products are frequently a source of potential anti-inflammatory compounds, and screening natural products can lead to the discovery of novel bioactive compounds. The present study aimed to investigate the effects of n-hexane extract from *Tanacetum argenteum* subsp. *argenteum* on the lipopolysaccharide-induced inflammatory response in human macrophages THP-1 cell. Cells were incubated with different concentrations of n-hexane extract, and the inhibitor effects of the extract exposure on various cytokine secretions were determined. The findings demonstrated that n-hexane extract dramatically decreased the levels of interleukin-6, interleukin-1 β , and tumor necrosis factor- α in differentiated THP-1 cells, indicating the remarkable anti-inflammatory potential of the extract. The n-hexane extract inhibited the secretion of interleukin-6 and interleukin-1 β even at the lowest dose of 1 μ g/ml. However, a significant reduction in tumor necrosis factor- α secretion was observed at 5 μ g/ml and above concentrations. Importantly, the results of the study indicated that both the n-hexane extract and its active component, parthenolide, exhibit comparable effects. Furthermore, in silico analysis of toxicogenomic data revealed the interactions between the active component of the n-hexane extract and interleukin-6, interleukin-1 β , and tumor necrosis factor.

Key Words: *Tanacetum argenteum* subsp. *argenteum*, inflammatory response, human macrophage cells, toxicogenomic data analysis

ÖZ

İnflamasyon, infeksiyon, hasar ya da toksik ajanlara maruz kalmaya yanıt olarak immün sistemin aktivasyonunu içeren biyolojik süreçtir. Bu süreç sırasında, immün hücreleri tarafından üretilen küçük proteinler olan sitokinler, inflamatuvar cevabın düzenlenmesinde hayati bir rol oynar. İnterlökinler, tümör nekroz faktörü- α , nitrik oksit ve interferon-gama gibi inflamatuvar sitokinler immün yanıtı başlatır ve inflamasyonun indüklenmesine yol açar. Doğal ürünler sıklıkla anti-inflamatuvar aktivite potansiyeli olan bileşiklerin kaynağı olup ve çalışmalar yeni biyoaktif bileşiklerin keşfine yol açabilir. Bu çalışma, *Tanacetum argenteum* subsp. *argenteum*'dan hazırlanan n-hekzan ekstresinin THP-1; insan makrofaj hücresinde lipopolisakkarit ile indüklenen inflamatuvar yanıt üzerindeki etkilerini araştırmayı amaçlamıştır. Hücreler farklı konsantrasyonlarda n-hekzan ekstresi ile inkübe edilmiş ve hücrelerin ekstre maruziyetinin çeşitli sitokinlerin sekresyonları üzerindeki inhibitör etkisi belirlenmiştir. Sonuçlar, n-hekzan ekstresinin farklılaştırılmış THP-1 hücrelerinde interlökin-6, interlökin-1 β ve tümör nekroz faktörü- α düzeyini önemli ölçüde azalttığını ve ekstrenin anti-inflamatuvar potansiyelini ortaya koymuştur. N-hekzan ekstresi, en düşük doz olan 1 μ g/ml'da bile interlökin-6 ve interleukin-1 β ekspresyonunu inhibe etmiştir. Ancak, interlökin-6 sekresyonunda 5 μ g/ml ve üzeri konsantrasyonlarda anlamlı azalma gözlenmiştir. Daha da önemlisi, çalışmanın sonuçları n-hekzan ekstresi ile aktif bileşeni olan parthenolidin karşılaştırılabilir etkiler sergilediğini göstermiştir. Ayrıca, toksikogenomik verilerin in silico analizi n-hekzan ekstresinin aktif bileşeni ile interlökin-6, interlökin-1 β ve tümör nekroz faktörü arasındaki etkileşimleri ortaya koymuştur.

Anahtar Kelimeler: *Tanacetum argenteum* subsp. *argenteum*, inflamatuvar cevap, insan makrofaj hücreleri, toksikogenomik veri analizi

Received: 28.12.2023

Revised: 26.02.2024

Accepted: 27.02.2024

^{*} ORCID: 0000-0002-3239-4855, Department of Pharmaceutical Toxicology, Faculty of Pharmacy, Ege University, İzmir, Türkiye

^{**} ORCID: 0000-0002-5260-3650, Department of Pharmaceutical Toxicology, Faculty of Pharmacy, Van Yüzüncü Yıl University, Van, Türkiye

^{***} ORCID: 0000-0002-5729-0796, Department of Pharmaceutical Botany, Faculty of Pharmacy, İzmir Kâtip Çelebi University, İzmir, Türkiye

^{****} ORCID: 0000-0002-9791-4399, Department of Pharmaceutical Toxicology, Faculty of Pharmacy, İzmir Kâtip Çelebi University, İzmir, Türkiye

^{*****} ORCID: 0009-0001-2006-5480, Faculty of Pharmacy, Ege University, İzmir, Türkiye

^{*****} ORCID: 0009-0001-8475-8067, Faculty of Pharmacy, Ege University, İzmir, Türkiye

INTRODUCTION

The inflammation process is a coordinated response involving the activation of signaling pathways and aims to initiate tissue repair and protect the body from further damage (Chen et al., 2017). Inflammatory stimuli, including pathogens, toxins, or endogenous factors, can trigger signaling pathways in cells, stimulating the production of inflammatory mediators. Inflammatory cytokines bind to specific receptors on the surface of immune cells, including interleukin-1 receptor (IL-1R), toll-like receptors, tumor necrosis factor (TNF) receptor and IL-6 receptor (Dinarello et al., 2018; Parameswaran & Patial, 2010; Tanaka et al., 2014). Once activated, these receptors can initiate intracellular signaling pathways that stimulate the excessive production of pro-inflammatory cytokines and chemokines. These molecules recruit immune cells to the area of inflammation, enhance their activation and survival, and induce tissue damage or repair (Kany et al., 2019). The precise balance of these inflammatory responses is critical for protecting cells from infection or tissue injury and maintaining tissue homeostasis. However, dysregulated, excessive and chronic inflammation contributes to the development of various diseases, such as diabetes, rheumatoid arthritis, cancer and cardiovascular diseases (Chen et al., 2017). Therefore, the underlying mechanisms of inflammatory processes in multiple diseases and developing or identifying novel and effective inflammatory compounds are essential for the therapeutic strategies of numerous diseases (Furman et al., 2019).

Multiple investigations have been conducted to identify natural products, including herbal extracts and phytochemicals, that can act as anti-inflammatory agents and improve the therapeutic effect of synthetic drugs (Nisar et al., 2023). *Tanacetum argenteum* (Lam.) Willd. subsp. *argenteum* (Asteraceae) is an essential annual plant found exclusively in Inner

and South Anatolia (Albayrak et al., 2017). Previous studies have shown that the subspecies of *T. argenteum* differ in their total flavonoid components and levels of parthenolide. *T. argenteum* subsp. *argenteum* has been found to have the highest levels of both parthenolide and total flavonoid among all the subspecies (Orhan et al., 2015). Therefore, it is essential to investigate the biological activities of *T. argenteum* subsp. *argenteum* and determine the potential therapeutic effects of all extracts and pure compounds. In our previous study, we demonstrated that the *n*-hexane extract of this plant exhibited significant activity in the iNOS assay, and we also conducted an MTT assay to determine the cytotoxicity potential of related plant extracts. *N*-hexane extract was found to exhibit potent cytotoxicity to PC-3 cells (Albayrak et al., 2017). However, the anti-inflammatory activity of this extract had not been examined in terms of possible suppression of the secretion of various cytokines.

In the present study, we aimed to investigate the potential anti-inflammatory effects of the *n*-hexane extract from *T. argenteum* subsp. *argenteum* on lipopolysaccharide (LPS)-treated THP-1 cells. LPS was utilized to induce inflammation and promote the secretion of inflammatory cytokines in cells. We incubated differentiated THP-1 cells with increasing concentrations of *n*-hexane extract following LPS stimulation to determine the effects of the extract on the levels of interleukin (IL)-6, IL-1 β and tumor necrosis factor- α (TNF- α). Furthermore, we performed an *in silico* toxicogenomic data analysis to predict the compound responsible for suppressing cytokine secretion. In our previous publication, we confirmed the presence of the parthenolide compound in the *n*-hexane extract using thin layer chromatography (TLC) (Albayrak et al., 2017), and in the current study, we employed high performance liquid chromatography (HPLC) for the same purpose. Moreover, we conducted a toxicogenomic evaluation of its interaction with genes and proteins based on the parameters we measured experimentally.

MATERIAL AND METHODS

Cell Culture and Materials

THP-1 (ATTC, TIB-202, USA) human monocyte cells were grown in RPMI-1640 medium supplemented with 10% fetal bovine serum. The cells were kept at 37°C under 5% CO₂ to maintain an appropriate environment for their survival. All experiments were conducted after the treatment of the monocytes with 25 µM of phorbol 12-myristate 13-acetate (PMA) for 24 hours. This treatment was applied to differentiate the monocytes into adherent macrophages used in the subsequent experiments. IL-6 (cat. no. ab46027), IL-1β (cat. no. ab214025) and TNF-α (cat. no. ab181421) assay kits were provided by Abcam (MA, U.S.A.). PMA, parthenolide, and all other chemicals were obtained from Sigma-Aldrich (Darmstadt, Germany).

Preparation and HPLC-UV Analysis of *N*-hexane Extract

The aerial parts of the plant were collected from Mount Nemrut, Adiyaman, in 2022, and the plant material was identified by Prof. Şura Baykan Ozturk. A voucher specimen was stored in the herbarium of the Faculty of Pharmacy of Ege University (IZEF 6029). The aerial parts of the plant were dried with a constant airflow in shadow. Then the dried material was powdered in a grinder to be ready for extraction. The plant parts (100 g) were extracted with *n*-hexane (200 mL) using an ultrasonic water bath 2 times, each for 6 hours. After filtration with filter paper, the obtained extract was evaporated to dryness with a rotary evaporator under low pressure at 40°C. The extract was kept at 4°C until the bioactivity experiments.

HPLC analysis was performed to determine whether the activity of *n*-hexane extract is due to the presence of parthenolide, a significant bioactive molecule of *T. argenteum*. The HPLC analyses were carried out in accordance with the previously described method (Avula et al., 2006). In brief, the solutions of parthenolide and extract were prepared

in DMSO and diluted with mobile phase B. 500 ppm standard parthenolide solution and 200 ppm *n*-hexane extract were analyzed by employing the ACE5-C18 column (100 Å, 5 µm, 4.6 x 250 mm) with gradient elution of mobile phase A (water) and mobile phase B (acetonitrile: methanol (90:10, %v/v)). The flow rate was 1 ml/min, and the wavelength range detection was 210 nm.

Treatment of Cells with *N*-hexane Extract and Inflammation Induction by LPS

Differentiated THP-1 cells (pretreated with 25 µM PMA for 24 hours) were categorized into four groups: one group served as the control (medium without LPS and extract), another group was exposed to LPS, the third group was treated with parthenolide before LPS treatment, and the last group was treated with *n*-hexane extract before LPS treatment.

Stock solutions of parthenolide and *n*-hexane extract were prepared in DMSO. Following, appropriate amounts of cell medium were used to dilute stock solutions to desired final concentrations. The final concentration of DMSO did not exceed 1%. The cells were incubated with increasing concentrations of parthenolide (0-5 µg/ml) or *n*-hexane extract (0-100 µg/ml) for 2 hours. After the incubation period, the cells were then stimulated with the LPS (final concentration: 2µM) for 24 hours. The working final concentration of LPS was selected in accordance with the literature (Liu et al., 2018). 2 µM is the dose level of LPS that induces inflammation and the secretion of inflammatory cytokines without leading to cytotoxicity in the differentiated THP-1 cells. Moreover, the cytotoxicity of 2 µM LPS was also controlled in our laboratory via MTT assay, and no significant cytotoxic effect was seen (data not shown), similar to a previous study (Liu et al., 2018). Subsequently, the measurement of IL-6, IL-1β and TNF-α were conducted by commercial kits.

Measurement of IL-1β, IL-6 and TNF-α Levels

The levels of IL-1β (ab214025), IL-6 (ab46027) and TNF-α (ab181421) in the cell supernatant were mea-

sured using ELISA kits according to the manufacturer's instructions. After the incubation period, as detailed above, 40 µl of supernatants were collected and transferred to novel wells. Subsequently, the specific antibody cocktails of each ELISA kit were added to wells, and the mixture was incubated for 1 hour again at room temperature. Then, TMB solution was added, and following 10 minutes, absorbance was measured by operating a microplate reader at a wavelength of 450 nm (Zhang et al., 2020). Experiments were repeated three times and conducted in triplicate.

Identification of Shared Genes Associated with Both Parthenolide and Inflammatory Processes

We examined the Comparative Toxicogenomics Database data to investigate the potential correlation between parthenolide and inflammation (Davis et al., 2023). The MyVenn tool was utilized to identify shared genes associated with parthenolide and inflammation from a dataset retrieved on December 25, 2023 (Davis et al., 2023).

Investigating Interactions Among Genes and Proteins

GeneMANIA was employed to examine the network of interactions among genes, with a specific focus on *Homo sapiens* as the target organism (Franz et al., 2018). In the investigation of protein-protein interactions (PPI) linked to parthenolide and inflammation, the String v.12 database was utilized, setting a minimum required interaction score threshold of 0.9, and the organism chosen was *Homo sapiens* (Szklarczyk et al., 2023). The analysis included the utilization of Cytoscape version 3.10.1 (Shannon et al., 2003). Furthermore, to pinpoint the essential proteins contributing to inflammation, the Network Analyzer Cytoscape plugin was employed to evaluate betweenness (BC), closeness (CC), degree centralities (DC), and number of undirected edges.

Statistical Analysis

All data were expressed as mean ± standard error.

Results were compared by one-way ANOVA analysis employing the GraphPad Prism. A statistically significant difference was considered when the p-value was less than 0.05%.

RESULTS AND DISCUSSION

Previous studies of *Tanacetum* species primarily focused on their chemical composition and potential therapeutic effects, including anti-inflammatory, anti-oxidant and anti-cancer properties (Jain et al., 1999; Rosselli et al., 2012; Vilhelmova et al., 2020). Nasri et al. reported that the anti-inflammatory effects were detected only in the alcoholic extract of *T. balsamita*, and quercetin is responsible for the observed effects (Nasri et al., 2014). Bukhari et al. studied several extracts of *T. artemisioides* and demonstrated that *n*-hexane extract had the highest anti-inflammatory potential. *T. argenteum* subsp. *argenteum* is an endemic and essential plant (Bukhari et al., 2007). However, there is limited research on its biological and therapeutic potential. In our previous study, we evaluated the anti-inflammatory activity of *T. argenteum* subsp. *argenteum* employing NF-κB and iNOS assays, and we found that the *n*-hexane extract had higher anti-inflammatory potential than the others similar to *T. artemisioides* (Albayrak et al., 2017). Therefore, in this follow-up study, we investigated the possible inhibition of the *n*-hexane extract on the secretion of inflammatory cytokines in THP-1 cells.

First, we determined the presence of parthenolide in *n*-hexane extract by the HPLC-UV system. As shown in Figure 1, the blue chromatogram displays the retention time of the standard parthenolide molecule. The retention time of parthenolide (500 ppm) was 17.85 min. The red chromatogram indicates the primary molecular peak in the 200 ppm *n*-hexane extract. The retention time of the main peak was 17.9 min. Upon analyzing the two chromatograms, it was observed that the *n*-hexane extract predominantly comprised parthenolide (Figure 1).

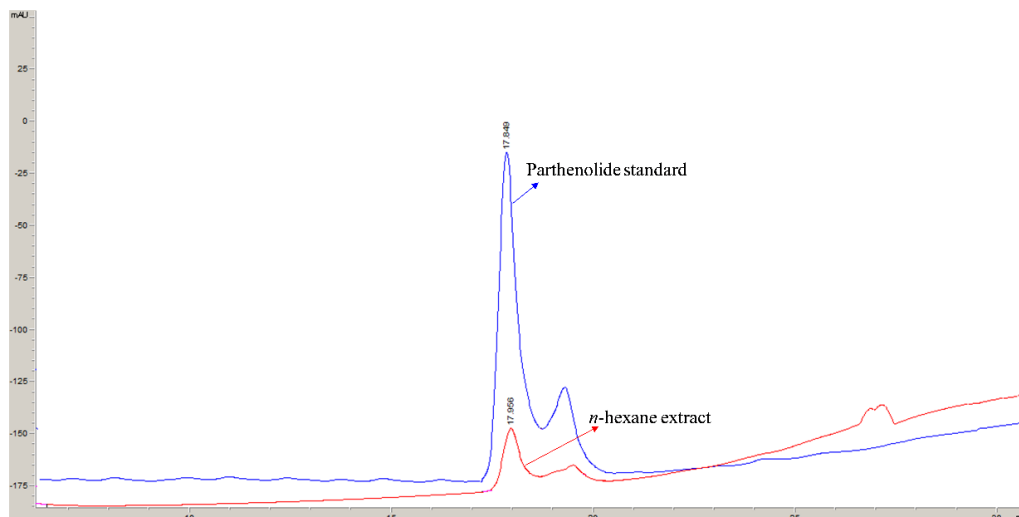


Figure 1. The HPLC-UV (210 nm) analysis. Blue chromatogram, parthenolide standard; red chromatogram, *n*-hexane extract.

Then, we exposed differentiated THP-1 cells to 2 μ M LPS for 24 hours and detected IL-6, IL-1 β , and TNF- α expression levels using ELISA. The final concentration level of LPS was determined as the dose value that triggers inflammation without causing cytotoxicity in the cell based on a previous study (Liu et al., 2018) and our laboratory experience. The incubation of differentiated THP-1 cells with 2 μ g/

mL LPS resulted in a significant increase in the levels of inflammatory cytokines, including IL-6, IL-1 β , and TNF- α , compared to the control. Following LPS exposure, IL-6, IL-1 β levels and TNF- α levels increased from 8.6 \pm 0.44 pg/ml to 31.2 \pm 0.57 pg/ml, 325.12 \pm 1.56 pg/ml to 570.3 \pm 1.75 pg/ml, and 180.33 \pm 1.18 pg/ml to 420.63 \pm 1.77 pg/ml, respectively, indicating the efficient induction of inflammation (Figure 2-4).

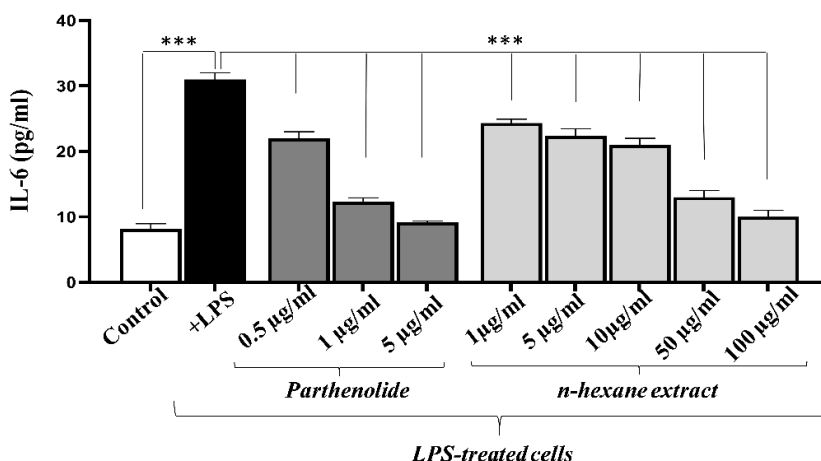


Figure 2. The effects of *n*-hexane extract on the levels of IL-6 in LPS-treated THP-1 cells. Cells were incubated with various concentrations of parthenolide (0.5-5 μ g/ml) or *n*-hexane extract (1-100 μ g/ml) for 24h. The control group comprised cells incubated solely in the medium, without LPS, parthenolide or *n*-hexane extract. *** $p < 0.0001$.

Then, the anti-inflammatory effects of increasing concentrations of *n*-hexane extract were investigated in the presence of excessive inflammation in THP-1 cells stimulated with LPS. In order to evaluate the anti-inflammatory potential of the extract, cells were also treated with parthenolide standard. As shown in Figure 2, IL-6 secretion was measured as 31.2±0.57 pg/ml in LPS-treated cells. Unsurprisingly, parthenolide exposure decreased IL-6 levels compared to cells

incubated with LPS alone. Cells treated with 0.5, 1, and 5 µg/ml of parthenolide exhibited 22.4±0.57, 12.33±0.31, and 9.27±0.12 pg/ml IL-6 secretion, respectively. Furthermore, *n*-hexane extract markedly reduced the secretion of IL-6 compared to only LPS-treated cells; the inhibitory effect started at 1µg/ml and increased in a dose-dependent manner. Treatment with 1-100 µg/ml *n*-hexane extract resulted in 24.3±0.31-10.2±0.57 pg/ml IL-6 secretion in cells.

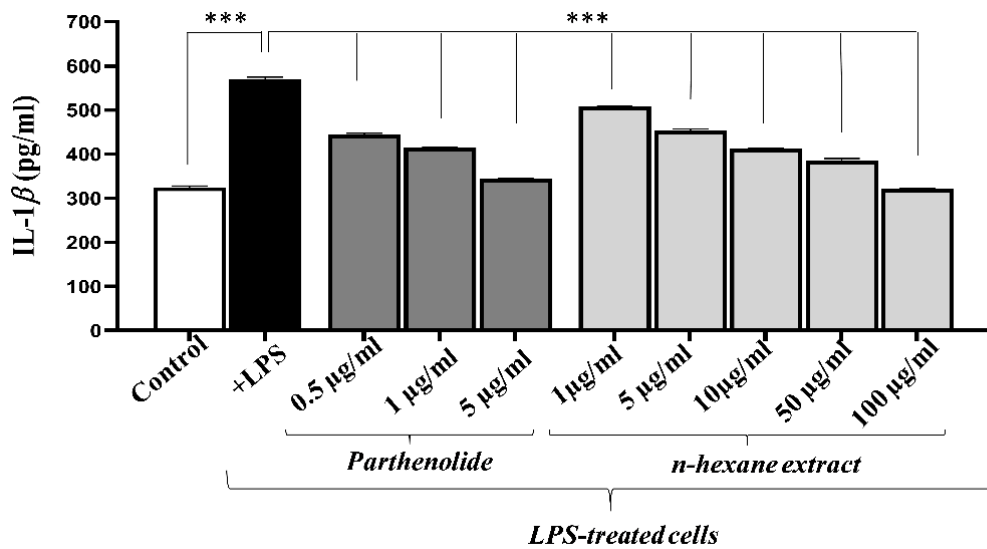


Figure 3. IL-1β levels of LPS-treated THP-1 cells after the incubation with the *n*-hexane extract or parthenolide. The cells representing the control group were incubated only in the medium, without the presence of LPS or extract. *** p < 0.0001.

Moreover, parthenolide or *n*-hexane extract treatment dramatically diminished the secretion of IL-1β and TNF-α in differentiated THP-1 cells, as illustrated in Figures 3-4. IL-1β levels were measured as 445.3±1.12 pg/ml, 414.02±0.94 pg/ml, and 344.5±0.84 pg/ml with the treatment of 0.5 µg/ml, 1 µg/ml, and 5 µg/ml of parthenolide, while the level was 570.3±1.75 pg/ml in cells treated only with LPS (Figure 3). In a similar trend, 0.5, 1, and 5 mg/ml parthenolide also decreased TNF-α levels from 420.63±1.77 pg/ml to 382.67±1.18pg/ml, 342.23±0.27 pg/ml, and 215.08±0.61 pg/ml in LPS-treated cells, respectively (Figure 4). At a concentration of 1 µg/

ml, the *n*-hexane extract did not significantly alter the level of TNF-α, while a significant decrease in IL-1β levels was detected. 1 µg/ml *n*-hexane extract decreased IL-1β levels from 570.3±1.75 pg/ml to 507.9±0.41 pg/ml (Figure 3). Furthermore, the levels of IL-1β and TNF-α secretion were significantly reduced with higher doses of the extract; treatment with 5 µg/ml extract resulted in 353.16±0.82 pg/ml TNF-α and 453.64±1.15 pg/ml IL-1β secretion. At the highest dose studied (100 µg/ml), IL-1β and TNF-α levels were measured as 321.36±0.81 and 201.7±1.26 pg/ml, respectively (Figures 3-4).

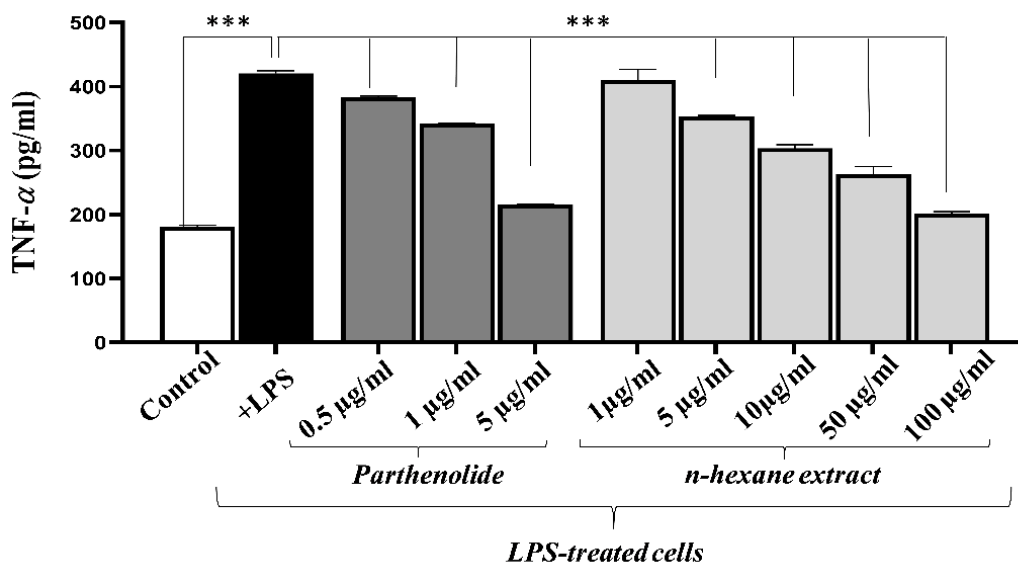


Figure 4. The effects of *n*-hexane extract and parthenolide on the levels of TNF- α in LPS-treated THP-1 cells. The control group comprised cells incubated solely in the medium, without LPS or extract. *** $p < 0.0001$.

The observed effect of *n*-hexane extract might be caused by apolar sesquiterpene lactones that contain γ -lactone (Gören et al., 2002). These lactones have multiple biological activities, including cytotoxic, anti-inflammatory and anti-oxidant properties (Pican et al., 1986; Gören et al., 2002). Our previous study determined the presence of parthenolide in *n*-hexane extract by TLC (Albayrak et al., 2017), and in the current study, we demonstrated that *n*-hexane extract contains parthenolide by HPLC (Figure 1). Parthenolide is a natural compound belonging to the sesquiterpene lactone family known as germacranolides (Mathema et al., 2012). It is well-known for its potent anti-inflammatory (Kwok et al., 2001) and anti-oxidant properties (Al-Fatlawi et al., 2015). These activities make it a promising candidate

for developing new drugs to treat various diseases. Therefore, we suggest that parthenolide contributes to the anti-inflammatory effects of the *n*-hexane extract. Indeed, *n*-hexane extract exhibited similar effects on anti-inflammatory markers as parthenolide. As part of our research, we carried out a toxicogenomic analysis to anticipate how parthenolide interacts with the parameters that we measured by *in vitro* studies. First, genes related to parthenolide and inflammation were identified from the CTD database. Then, common genes were extracted using the MyVenn tool. The initial exploration of CTD data revealed that 197 genes are associated with inflammation, while 66 genes are linked to parthenolide. Nineteen genes were identified as shared between inflammation and parthenolide (Figure 5A).

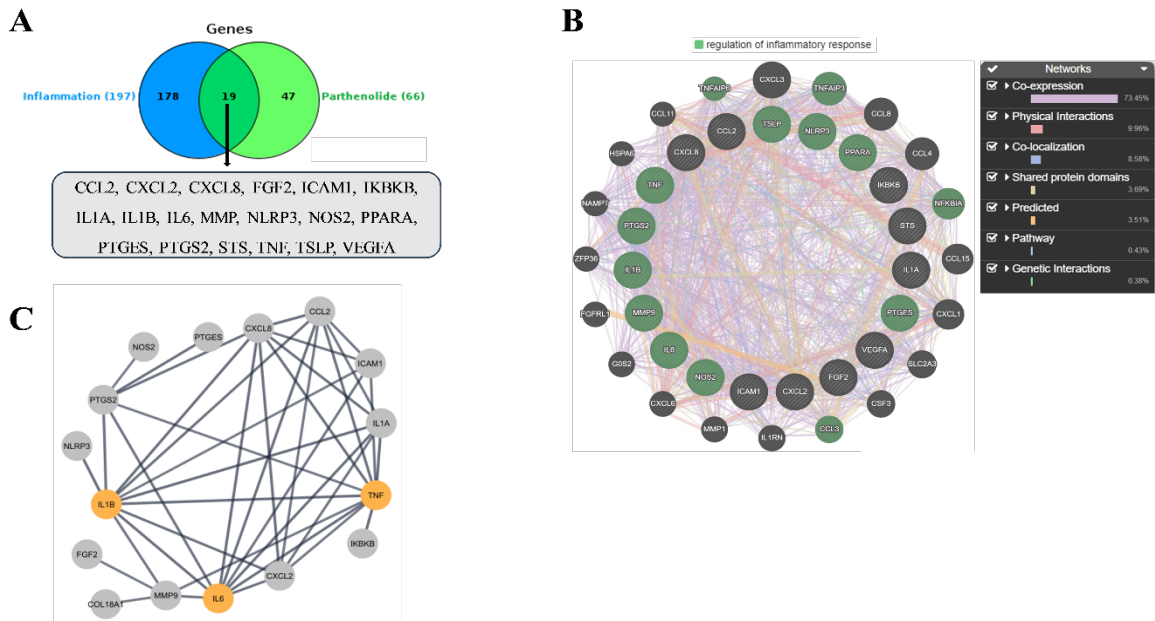


Figure 5. Toxicogenomic analysis. A, Venn diagram shows overlapped genes for inflammation and parthenolide; B, Gene-gene interactions were predicted by GeneMANIA; C, Protein-protein interactions were predicted using the String database and visualized with the Cytoscape software.

The common genes were input into the GeneMANIA online plug-in, generating hypotheses and analyzing the function and interaction of genes, resulting in a connected network. The analysis revealed that co-expressions accounted for 73.45% and were the predominant factors among the overlapping genes. This result suggests that these genes exhibit similar expression levels across conditions in a gene expression study. Nodes in the inner ring represent common genes, while nodes in the outer ring depict genes associated with these common genes, according

to GeneMANIA. Additionally, fourteen green nodes indicate genes related to the regulation of the inflammatory response, with a false discovery rate of 5.52×10^{-15} (Figure 5B). Furthermore, the PPIs of the nineteen common genes displayed 19 nodes and 39 edges (Figure 5C), with a PPI enrichment p-value of $< 1.0 \times 10^{-16}$. In the centrality analysis, the most critical genes among these common genes, related to both parthenolide and inflammation, were identified as IL6, IL-1 β , and TNF, ranking in the top three (Table 1).

Table 1. Centrality analysis of common genes between parthenolide and inflammation

Common Genes	Degree	Closeness Centrality	Betweenness Centrality	Number Of Undirected Edges
TNF	10	0.750	0.242	10
IL-1 β	10	0.750	0.242	10
IL-6	9	0.714	0.109	9
CXCL8	8	0.625	0.032	8
CCL2	7	0.556	0.004	7
IL1A	6	0.536	0	6
PTGS2	6	0.577	0.257	6
CXCL2	6	0.536	0	6
ICAM1	5	0.517	0	5
MMP9	5	0.556	0.257	5
COL18A1	1	0.366	0	1
FGF2	1	0.366	0	1
NLRP3	1	0.441	0	1
IKBKB	1	0.441	0	1
PTGES	1	0.375	0	1
NOS2	1	0.375	0	1
PPARA	0	0	0	0
STS	0	0	0	0
TSLP	0	0	0	0

We have concluded that the anti-inflammatory properties of *n*-hexane extract may be due to parthenolide, based on both *in silico* and *in vitro* analyses.

CONCLUSION

The findings indicated that exposure to the *n*-hexane extract of *T. argenteum* subsp. *argenteum* reduced the secretion of IL-6, IL-1 β , and TNF- α in differentiated THP-1 cells as similar to parthenolide standard. Moreover, toxicogenomic data also demonstrate that parthenolide interacts with these three cytokines, considering the shared genes between parthenolide and inflammation. This study suggests that parthenolide, the significant component of the

extract, may be responsible for the anti-inflammatory effects of *n*-hexane extract. Further experiments are being conducted to examine the phytochemical properties and other biological activities of parthenolide and *n*-hexane extract from *T. argenteum* subsp. *argenteum*.

ACKNOWLEDGEMENTS

We thank Ege University Faculty of Pharmacy, Pharmaceutical Sciences Research Center (FABAL) for supplying the microplate reader. Our special thanks to Prof. Ayşe Nalbantsoy (Ege University, Bioengineering Department). The authors thank Prof. Dr Ayşe Nalbantsoy for providing the parthenolide standard and Dr Aysegül Kaymak Özdemir for THP-1 cells.

CONFLICT OF INTEREST

The authors declare that there is no conflict of interest.

AUTHOR CONTRIBUTION STATEMENT

Concept and Design (EA), resources and materials (EA, FK, GA), data collection and processing (EA, FK, GA, AE), analysis and/or interpretation (EA, FK, AE, GA, IT, EA), literature search (EA, FK, AE, GA, IT, EA), writing (E.A), critical reviews (EA, FK, AE, GA, IT, EA)

REFERENCES

- Albayrak G., Nalbantsoy A., Baykan Ş. (2017). In vitro cytotoxic and anti-inflammatory activities of *Tanacetum argenteum* (lam.) Willd. subsp. *argenteum* extract. *Turkish journal of pharmaceutical sciences*, 14, 231-236. <https://doi.org/10.4274/tjps.42714>
- Al-Fatlawi, A. A., Al-Fatlawi, A. A., Irshad, M., Rahisuddin, & Ahmad, A. (2015). Effect of parthenolide on growth and apoptosis regulatory genes of human cancer cell lines. *Pharmaceutical biology*, 53(1), 104-109. <https://doi.org/10.3109/13880209.2014.911919>
- Avula, B., Navarrete, A., Joshi, V. C., & Khan, I. A. (2006). Quantification of parthenolide in *Tanacetum* species by LC-UV/LC-MS and microscopic comparison of Mexican/US feverfew samples. *Die Pharmazie*, 61(7), 590-594.
- Bhadoriya, S. S., Mishra, V., Raut, S., Ganeshpurkar, A., & Jain, S. K. (2012). Anti-Inflammatory and Antinociceptive Activities of a Hydroethanolic Extract of *Tamarindus indica* Leaves. *Scientia pharmaceutica*, 80(3), 685-700. <https://doi.org/10.3797/scipharm.1110-09>
- Bukhari, I. A., Khan, R. A., Gilani, A. U., Shah, A. J., Hussain, J., & Ahmad, V. U. (2007). The analgesic, anti-inflammatory and calcium antagonist potential of *Tanacetum artemisioides*. *Archives of pharmaceutical research*, 30(3), 303-312. <https://doi.org/10.1007/BF02977610>
- Chen, L., Deng, H., Cui, H., Fang, J., Zuo, Z., Deng, J., Li, Y., Wang, X., & Zhao, L. (2017). Inflammatory responses and inflammation-associated diseases in organs. *Oncotarget*, 9(6), 7204-7218. <https://doi.org/10.18632/oncotarget.23208>
- Davis, A. P., Wieggers, T. C., Johnson, R. J., Sciaky, D., Wieggers, J., & Mattingly, C. J. (2023). Comparative Toxicogenomics Database (CTD): update 2023. *Nucleic acids research*, 51(D1), D1257-D1262. <https://doi.org/10.1093/nar/gkac833>
- Dinarello, C. A. (2018). Overview of the IL-1 family in innate inflammation and acquired immunity. *Immunological reviews*, 281(1), 8-27. <https://doi.org/10.1111/imr.12621>
- Franz, M., Rodriguez, H., Lopes, C., Zuberi, K., Montojo, J., Bader, G. D., & Morris, Q. (2018). GeneMANIA update 2018. *Nucleic acids research*, 46(W1), W60-W64. <https://doi.org/10.1093/nar/gky311>
- Furman, D., Campisi, J., Verdin, E., Carrera-Bastos, P., Targ, S., Franceschi, C., Ferrucci, L., Gilroy, D. W., Fasano, A., Miller, G. W., Miller, A. H., Mantovani, A., Weyand, C. M., Barzilai, N., Goronzy, J. J., Rando, T. A., Effros, R. B., Lucia, A., Kleinstreuer, N., & Slavich, G. M. (2019). Chronic inflammation in the etiology of disease across the life span. *Nature medicine*, 25(12), 1822-1832. <https://doi.org/10.1038/s41591-019-0675-0>

- Gören, N., Arda, N., & Çaliskan, Z. (2002). Chemical characterization and biological activities of the genus *Tanacetum* (Compositae). *Studies in natural products chemistry*, 27, 547-658 [https://doi.org/10.1016/S1572-5995\(02\)80044-8](https://doi.org/10.1016/S1572-5995(02)80044-8)
- Jain, N. K., & Kulkarni, S. K. (1999). Antinociceptive and anti-inflammatory effects of *Tanacetum parthenium* L. extract in mice and rats. *Journal of Ethnopharmacology*, 68(1-3), 251-259. [https://doi.org/10.1016/s0378-8741\(99\)00115-4](https://doi.org/10.1016/s0378-8741(99)00115-4)
- Kany, S., Vollrath, J. T., & Relja, B. (2019). Cytokines in Inflammatory Disease. *International journal of molecular sciences*, 20(23), 6008. <https://doi.org/10.3390/ijms20236008>
- Kwok, B. H., Koh, B., Ndubuisi, M. I., Elofsson, M., & Crews, C. M. (2001). The anti-inflammatory natural product parthenolide from the medicinal herb Feverfew directly binds to and inhibits IkappaB kinase. *Chemistry & biology*, 8(8), 759-766. [https://doi.org/10.1016/s1074-5521\(01\)00049-7](https://doi.org/10.1016/s1074-5521(01)00049-7)
- Liu, X., Yin, S., Chen, Y., Wu, Y., Zheng, W., Dong, H., Bai, Y., Qin, Y., Li, J., Feng, S., & Zhao, P. (2018). LPS-induced proinflammatory cytokine expression in human airway epithelial cells and macrophages via NF- κ B, STAT3 or AP-1 activation. *Molecular medicine reports*, 17(4), 5484-5491. <https://doi.org/10.3892/mmr.2018.8542>
- Mathema, V. B., Koh, Y. S., Thakuri, B. C., & Sillanpää, M. (2012). Parthenolide, a sesquiterpene lactone, expresses multiple anti-cancer and anti-inflammatory activities. *Inflammation*, 35(2), 560-565. <https://doi.org/10.1007/s10753-011-9346-0>
- Nisar, A., Jagtap, S., Vyavahare, S., Deshpande, M., Harsulkar, A., Ranjekar, P., & Prakash, O. (2023). Phytochemicals in the treatment of inflammation-associated diseases: the journey from preclinical trials to clinical practice. *Frontiers in pharmacology*, 14, 1177050. <https://doi.org/10.3389/fphar.2023.1177050>
- Orhan, I. E., Tosun, F., Gülpınar, A. R., Kartal, M., Duran, A., Mihoglugil, F., Akalgan, D. (2015). LC-MS quantification of parthenolide and cholinesterase inhibitory potential of selected *Tanacetum* L. (Emend. Briq.) taxa. *Phytochemistry letters*, 11, 347-352. <https://doi.org/10.1016/j.phytol.2014.10.003>
- Parameswaran, N., & Patial, S. (2010). Tumor necrosis factor- α signaling in macrophages. *Critical reviews in eukaryotic gene expression*, 20(2), 87-103. <https://doi.org/10.1615/critrevueukargeneexpr.v20.i2.10>
- Picman A. (1986). Biological activities of sesquiterpene lactones. *Biochemical systematics and ecology*, 3(14), 255-281.
- Rosselli, S., Bruno, M., Raimondo, F. M., Spadaro, V., Varol, M., Koparal, A. T., & Maggio, A. (2012). Cytotoxic effect of eudesmanolides isolated from flowers of *Tanacetum vulgare* ssp. *siculum*. *Molecules* (Basel, Switzerland), 17(7), 8186-8195. <https://doi.org/10.3390/molecules17078186>
- Shannon, P., Markiel, A., Ozier, O., Baliga, N. S., Wang, J. T., Ramage, D., Amin, N., Schwikowski, B., & Ideker, T. (2003). Cytoscape: a software environment for integrated models of biomolecular interaction networks. *Genome research*, 13(11), 2498-2504. <https://doi.org/10.1101/gr.1239303>

- Szklarczyk, D., Kirsch, R., Koutrouli, M., Nastou, K., Mehryary, F., Hachilif, R., Gable, A. L., Fang, T., Doncheva, N. T., Pyysalo, S., Bork, P., Jensen, L. J., & von Mering, C. (2023). The STRING database in 2023: protein-protein association networks and functional enrichment analyses for any sequenced genome of interest. *Nucleic acids research*, 51(D1), D638–D646. <https://doi.org/10.1093/nar/gkac1000>
- Tanaka, T., Narazaki, M., & Kishimoto, T. (2014). IL-6 in inflammation, immunity, and disease. *Cold Spring Harbor perspectives in biology*, 6(10), a016295. <https://doi.org/10.1101/cshperspect.a016295>
- Vilhelmova, N., Simeonova, L., Nikolova, N., Pavlova, E., Gospodinova, Z., Antov, G., Galabov, A., & Nikolova, I. (2020). Antiviral, Cytotoxic and Antioxidant Effects of *Tanacetum Vulgare* L. Crude Extract In Vitro. *Folia medica*, 62(1), 172–179. <https://doi.org/10.3897/folmed.62.e49370>
- Zhang, Z., Sun, Y., & Chen, X. (2020). NLRC5 alleviated OGD/R-induced PC12-cell injury by inhibiting activation of the TLR4/MyD88/NF- κ B pathway. *The Journal of international medical research*, 48(8), 300060520940455. <https://doi.org/10.1177/0300060520940455>

Endocrine Disrupting Effects of Flame Retardants on Thyroid System

İrem İYİĞÜNDOĞDU*, İsmet ÇOK***

Endocrine Disrupting Effects of Flame Retardants on Thyroid System

SUMMARY

Accumulating scientific evidence shows that thyroid hormone synthesis and signaling are now recognized as one of the critical targets of environmental chemicals, especially of endocrine disruptors. Endocrine disrupting chemicals (EDCs) are artificial chemicals and consist of different types of molecules, for instance some pesticides, plasticizers, flame retardants (FRs), surfactants, many of which can interfere with thyroid hormone synthesis or their actions. FRs, essential members of endocrine disruptors, share similarities in their chemical structures when compared with thyroid hormones, and there are accumulating scientific findings pointing out that they may take part in dysfunction of thyroid hormone homeostasis. The primary aim of using FRs is to minimize the risk of fire and prevent its spreading. The potential effects of exposure to FRs on the thyroid and thyroid hormones have gained importance since they may easily migrate into the surrounding environment and are mainly found in house dust. Within the framework of the results of some experimental animal and in vitro studies, as well as limited human studies researching the consequences of FRs on the thyroid system, this paper aims to make a general assessment of whether these chemicals have a role in some thyroid diseases. Although the information that FRs with endocrine disrupting properties may have an effect on thyroid hormone levels and cause disruption in the thyroid system is still in its infancy, there is emerging evidence that some members of FRs may have thyroid disrupting properties.

Key Words: Flame retardants, thyroid hormones, endocrine disruptors, thyroid toxicity.

Alev Geciktiricilerin Tiroid Sistem Üzerindeki Endokrin Bozucu Etkileri

ÖZ

Sayı giderek artan bilimsel bulgular çevreden maruz kalınan kimyasallar için, özellikle de endokrin bozucular olarak adlandırılan kimyasal grubu açısından, tiroid hormon sentezi ve sinyalizasyonunun önemli bir hedef haline geldiğini göstermektedir. Endokrin bozucu kimyasallar (EBK) insan yapımı kimyasallardır ve çok çeşitli moleküllerden oluşur. Bunlara bazı pestisitler, plastizerler, alev geciktiriciler (AG), surfaktanlar örnek verilebilir, bu kimyasalların çoğu tiroid hormon sentezine veya bu hormonların aktivitelerine müdahale etmektedir. AGLer endokrin bozucuların önemli bir üyesidir, kimyasal yapıları tiroid hormonlarıyla benzerlik göstermektedir ve tiroid hormon homeostazının disfonksiyonunda rol oynayabileceğini gösteren bulguların sayısı artmaktadır. AGLerin kullanımının birincil amacı yangın riskini olabildiğince azaltmak ve yayılmasını önlemektir. Kolayca çevreye sızabilmeleri ve özellikle ev tozunda bulunabilmeleri nedeniyle AGLere maruziyetin tiroid ve tiroid hormonları üzerine potansiyel etkileri önem kazanmıştır. Tiroid sistem üzerine AGLerin etkilerini inceleyen bazı deneysel hayvan çalışmaları ve in vitro çalışmalar, bunun yanı sıra sınırlı sayıda insan çalışmasının sonuçları çerçevesinde, bu çalışmamızın amacı bu kimyasalların bazı tiroid hastalıklarında bir role sahip olup olmayacağı hakkında genel bir değerlendirme yapmaktır. Her ne kadar endokrin bozucu etkileri olan AGLerin tiroid hormon seviyelerini etkileyebileceği ve tiroid sistemde bozukluklara yol açabileceği bilgisi çok yeni olsa da, AGLerin bazı üyelerinin tiroid bozucu özelliklere sahip olduğuna dair bulgular ortaya çıkmaktadır.

Anahtar Kelimeler: Alev geciktiriciler, tiroid hormonları, endokrin bozucular, tiroid toksisitesi.

Received: 14.09.2023

Revised: 24.01.2024

Accepted: 29.01.2024

* ORCID: 0000-0001-9780-2488, Dept. of Toxicology, Faculty of Pharmacy, Gazi University, Ankara, Turkey.

** ORCID: 0000-0003-3128-677X, Dept. of Toxicology, Faculty of Pharmacy, Gazi University, Ankara, Turkey.

INTRODUCTION

A significant number of synthetic chemical compounds have emerged; they have been produced and transferred into our surrounding environment since the mid-1930s till today (Yeung et al., 2011). Between 1950-2000, the production of chemical substances increased 60 times in mass, and global chemical sales increased over two times between 2004-2014 (Bolinus et al., 2018). The precise amount of chemicals on the global market is unknown; however, recently it is reported that the number of industrial chemicals and mixtures which have been registered for production are more than 350,000 (Brack et al., 2022). In 2018, total chemical consumption was 303 million tons in 27 member countries of the EU, and 221 million tons of this amount consisted of chemicals that are accepted to be hazardous to health. In addition, the use and production of chemical substances increased 16 times over the last 70 years in the USA (Sutton et al., 2012). It is calculated that this number refers to 13.000 kg for every individual living in the USA (Wang et al., 2016). In a research conducted by FDA, over 1800 chemicals were determined to interfere with one or more of three different pathways of endocrine system (androgen, eustrogen, and thyroid) (De Falco & Laforgia, 2021). Evidence is increasing day by day that exogenous chemicals, which have an effect on hormone production and hormone effects and are classified under the name of Endocrine Disrupting Chemicals (EDCs), can disrupt the established biological balance and cause significant changes in the protection of both our body and public health (Kahn et al., 2020). World Health Organisation (WHO) characterizes an endocrine disruptor as “an exogenous substance or mixture that alters function(s) of the endocrine system and consequently causes adverse health effects in an intact organism, or its progeny, or (sub) populations” (WHO, 2013). In light of this definition, ten critical characteristics of EDCs have now been identified. These characteristics include interaction or activation of hormone receptors, antagonizing these receptors,

altering hormone receptor expression, changing signal transduction among cells that respond to hormones, causing differences in synthesis, transport, distribution, or circulating levels, and finally, metabolism or clearance of hormones; and lastly altering the fate cells that function in the production of hormones or responding to hormones (La Merrill et al., 2020).

EDCs are a group of compounds with different chemical structures (Cok, 2021). There is a consensus today that acknowledged or potential EDCs might be present in industrial and consumer products. EDCs, which we might be exposed to intentionally or unintentionally in our daily life through different consumer products, are seen in a wide range of possible exposure sources from our food to the air we inhale. In addition to regulatory health authorities such as WHO, the US Environmental Protection Agency (EPA), United Nations Environment Programme (UNEP) and European Union (EU); many scientific establishments, mainly Endocrine Society, accept EDCs as a global problem and work on developing programmes in order to decrease the number of EDCs and exposure to these compounds. Due to the accumulating scientific evidence regarding the role of EDCs, particularly in hormone-related diseases such as diabetes, reproductive diseases, neurodevelopmental diseases, breast cancer, prostate cancer, both the public and health authorities are concerned about exposure and potential adverse effects of these substances (Encarnação et al., 2019).

Thyroid hormones, which are among the most important hormones vital for a healthy life, are involved in various physiological processes. These include bone remodelling, mental status, cardiac function and regulation of metabolism. Therefore, normal functioning of the thyroid is substantial for maintaining psychological and physiological health. Furthermore, thyroid hormones have a crucial role in fetal development because levels of thyroid hormones need to be normal for the development

of the brain. In case of deficit in the levels of these hormones; neuronal growth and differentiation in the hippocampus, cerebral cortex, and cerebellum is reduced. Moreover, maternal thyroid homeostasis has a vital role in fetal development (Boas et al., 2012).

The synthesis and storage of thyroid hormones take place in the thyroid gland. Their transportation to target cells occurs through binding to thyroid hormone-distributing proteins facilitating the process; however, free hormones are the ones that can be transferred into the cell. The levels of thyroid hormones in our bloodstream are strictly controlled by the hypothalamus-pituitary-thyroid (HPT) axis which consists of the hypothalamus, the pituitary and thyroid gland; and it depends on a negative feedback mechanism. If the levels of T4 and T3 in the blood are perceived to be low, pituitary gland secretes thyroid stimulating hormone (TSH) and forms a stimuli promoting the thyroid gland. Consequently, additional thyroid hormones are synthesized and increasingly released to preserve the levels of hormones in a narrow range. The liver and kidney take part in the deactivation and clearance of these hormones. Deiodinating enzymes regulate the levels of thyroid hormones at the cellular level. In order to evaluate thyroid function clinically, levels of TSH/T4/T3 in serum or plasma are used. If a decrease in serum T4 without the combination of increased TSH is observed, it gives an idea of hypothyroxinemia; however, differing from this case, if both a reduction in T4 and increased TSH are observed, then overt hypothyroidism can be considered. Total T4 seems to be the main parameter in developmental toxicology guideline studies. The main purpose of thyroid hormones is to control gene transcription. The control of the thyroid signaling mechanism is essential for mammalian brain development because different degrees of thyroid hormones are needed for some specific brain subregions. Maternal T4 seems to be the only source of hormones for the developing fetus during the early stages of pregnancy; therefore, it is precisely controlled by transporters and deiodinases

in the placenta T3 concentrations in the brain only depend on deiodinase activity in the brain since only T4 is able to be transferred to the fetal brain. Functioning of the thyroid gland of human fetuses begins in mid pregnancy. In the later stages of the pregnancy, during the third trimester, majority of neural circuits are seen to appear and they continue developing beyond adolescence (Gilbert et al., 2020).

Major causes of thyroid-related dysfunctions include thyroid cancer, autoimmune thyroid diseases and deficiencies in iodine and some other micronutrients (Brent, 2010). It has been suggested that environmental iodine deficiency, some medical treatments including radiation therapy, autoimmune diseases and some genetic disorders may affect the development of these disorders. Moreover, recent researches have indicated that exposure to some EDCs originating from consumer products that are used in our daily lives, may have a role in the increase of thyroid-related diseases (Alsen et al., 2021). Since thyroid diseases are prevalent endocrine diseases and affect approximately more than 200 million people worldwide, there is an increasing awareness of thyroid-related diseases in societies (Keestra et al., 2021). Thyroid hormone system is very vulnerable since EDCs can affect thyroxine and its active metabolites throughout the whole process including precise feedback regulation, synthesis and distribution of this prohormone and metabolism, and action of these compounds. Most of the effects attributed to EDCs occur at the pre-receptor control of T3 ligand availability to T3 receptors, which results in thyroid hormone action due to mediation by ligands. All of the different components of this system; including thyroid hormone transporters, deiodinases, enzymes functioning in metabolism and T3-receptor forms, might play a role in mediation of adverse effects. Epidemiological results concerning EDC exposure and thyroid hormone related conditions point out that human development, specifically the maturing of the brain throughout the fetal and neonatal period, growth, differentiation, can be affected by EDCs.

When EDCs interfere with iodide or thyroid hormone transport, they may cause substantial and irreversible alterations on brain development and functions which can be seen from the parameters including cognition, behavior, or Intelligence quotient (IQ) deficits in later life. Also, metabolic processes in adult and aging humans may be open to adverse effects of

EDCs (Köhrle & Frädrieh, 2021). It is observed that bisphenol A, phthalates, perfluorinated chemicals, and brominated flame retardants (BFRs) may be among the substances with thyroid-disrupting properties (Boas et al., 2012). Some examples of possible thyroid disruptors are listed in Table 1 (Kabir et al., 2015).

Table 1. Examples of potential thyroid disruptors, the way they act, and the consequences on the thyroid system (Kabir et al., 2015)

Thyroid Disruptors	Mechanism of Action	Biological effect
Phthalates	-Preventing the entry of iodide into thyroid cell -Binding with thyroid transport protein competitively	-Reduced synthesis of T3 and T4 -Potential impact on fetal brain T4 production
Polychlorinated biphenyls (PCBs)	-Binding with thyroid transport protein competitively -Elevated metabolism in the liver -Inhibition of sulfation reaction -Inhibition of TSH receptor -Inhibiting the activity of the deiodinase enzyme -Changes in binding to thyroid receptor	-Potential impact on fetal brain T4 production -Enhanced biliary metabolism of T3 and T4 -Potential reduction of peripheral T3 synthesis due to reduced sulfation of thyroid hormones -Lower level of production of T3 and T4 -Reduced peripheral T3 synthesis -Changes in the gene transcription mediated by thyroid hormones
Triclosan	-Inhibition of sulfation reaction	-Potential reduction of peripheral T3 synthesis due to reduced sulfation of thyroid hormones
Chlordane	-Causing changes in the transport across the cell membrane	-A higher level of biliary elimination of T3 and T4
Flame Retardants	-Binding with thyroid transport protein competitively -Changes in binding to thyroid receptor	-Potential impact on fetal brain T4 production -Changes in the gene transcription mediated by thyroid hormones

FLAME RETARDANTS

Flame retardants (FRs) are compounds that are applied in order to lower flammability and prevent fires from starting and spreading (Yao et al., 2021). The idea of protection from fire appeared for the first time in Egypt thousands of years ago, later on alum solutions were applied to wooden battleships. However, the first FRs patent was registered in 1735. In 1820, J.L. Lussac played a major role in the history of FRs with his work on the resistance of curtains to flames in Parisian theaters. Afterwards progress of working on flame retardancy continued; emerge of halogenated, phosphorus and nitrogen based FRs in 1980 and organophosphate flame retardants (OPFRs) in 2003 can be named as critical events throughout this process (Vahabi et al., 2021). FRs are mainly applied to furniture such as upholstery, mattresses, carpets and curtains; electrical devices such as laptops, computers,

phones and televisions; materials that are used in the construction process, for example, wires and cables that electricity runs through; materials that take part in insulation, such as polyurethane and polystyrene insulation foams; products like seats of the vehicle or the covers of these seats and overhead compartments and other materials in transportation such as cars, planes, and trains (Shaw et al., 2014).

FRs are categorized into two main groups which are additive FRs and reactive FRs. Additive FRs are added to combustibles, in contrast reactive FRs take part in chemical reactions to make that material more resistant to flame (Yao et al., 2021). The difference between additive and reactive FRs is that additives are applied after polimerization and no covalent bonds are formed between FRs and the material whereas reactive ones are applied during polimerization and have chemical bonds with the material (Dishaw et al.,

2014). General characteristics of FRs (Kozłowski et al., 2014) are described in Figure 1.

There are several advantages of FRs such as prevention of fires or keeping the fire growth slow, reduced loss of property, reduced injuries and death due to fires, reduced environmental contamination due to fires. At the same time, the critical disadvantage of FRs is that they may migrate out of the products and are released to the surroundings (Purser, 2014). FRs are found in the indoor air, dust and outdoor environment due to volatilization and leaching from the treated materials (Dishaw et al., 2014). In addition, the increasing amount of toxicity information due to exposure from the use of these substances has become a general concern.

Exposure of human beings to FRs take place in three ways which are diet, inhalation, and ingesting or dermally absorbing dust particles. Children's exposure is higher than adults because of ingesting more dust particles via hand-to-mouth and object-to-mouth activities (Dishaw et al., 2014). Most FRs share similarity with thyroid hormones in terms of chemical structure and are thought to take part in the disorder of thyroid hormone homeostasis (Mughal & Demeneix, 2017). The disrupting effects of FRs, that have been used from past to present or are used today, on thyroid functions and hormones of laboratory animals and humans are tried to be evaluated below in groups.



Figure 1. General characteristics of FRs (Kozłowski et al., 2014)

Polybrominated diphenyl ethers

Back in the 1970s after the application of polybrominated biphenyls were withdrawn, polybrominated diphenyl ethers (PBDEs) were preferred to be used due to flammability standards. PBDEs have no chemical bonds with the material that they are in; thus, they can be released from those products, contaminate the air, and become a component of dust. They may be released to the surrounding environment during the manufacturing process or due to wearing down of materials (Shaw et al., 2014). Due to such concerns, PBDEs were phased out and organophosphate esters (OPEs) appeared as alternatives (Doherty et al., 2019). Penta-PBDE was limited in Europe in 2002 and in the US in 2005 (Castorina et al., 2017).

When possible effects of PBDEs are considered, the thyroid system seems to be the primary target of PBDEs and their hydroxylated metabolites (Dishaw et al., 2014). Biotransformation of PBDEs results in hydroxylated-BDEs (OH-BDEs) and bromophenols. The structure of OH-BDEs has similarities with endogenous thyroid hormones; therefore, it might be the causing factor of part of PBDE toxicity. According to these toxicity results, effects on neurodevelopment can be seen as the prominent example of this toxicity. Thus, thyroid hormones are substantial components of cell migration and synaptogenesis in the brain and generally appropriate neurodevelopment. It is thought that behavioral/neurodevelopmental effects of PBDEs might happen due to impaired regulation of thyroid hormone throughout critical developmental windows (Dingemans et al., 2011; Dishaw et al., 2014).

In various studies, PBDEs have been chosen as the subject because of their risk of resulting in endocrine disruption and other adverse effects (Kim & Oh, 2014). In a study conducted on human serum, the disrupting mechanism of polychlorinated biphenyls (PCBs), PBDEs, and new flame retardants (NFRs) were evaluated by investigating TH-regulated proteins and gene expression. In this study, some of

the compounds in these groups were observed to have a strong binding affinity towards thyroglobulin, TSH, gene expression of thyroid hormone receptor α - (TR α) and β - (TR β), thyroxine-binding globulin (TBG), and iodothyronine deiodinase I (ID1). Levels of TSH, TBG and expression of TR α were lower among highly exposed group; however, higher expression of ID1 was observed (Guo et al., 2019). In a different study, serums from blood samples of 140 pregnant women were analyzed for PBDEs, phenolic metabolites, and thyroid hormones. A significant positive association was found between BDE47, 99 and 100 and free and total T4 levels, and also between these compounds and total T3 levels higher than normal range (Stapleton et al., 2011). In a different study concerning PBDEs, the association of 10 PBDE congeners and free and total T4 and TSH were investigated among 270 pregnant women. It was found that as the concentration of individual congeners increased 10-folds each time, it resulted in a decrease of TSH between 10.9% and 18.7%. There was a significant enhancement in the odds of subclinical hyperthyroidism among participants who were exposed the most to Σ PBDEs and BDEs 100 and 153. No significant relation was observed between PBDEs and free and total T4. Study's findings suggested that PBDEs are related to decreased TSH during pregnancy (Chevrier et al., 2010). As a different exposed group, office workers were seen as the subject of a study in which serum samples were used and whether an association exist between PBDE concentrations in serum and thyroid hormones was investigated. It was found that an inverse relationship existed between total T4 and each PBDE congener. On the other hand, total T3, free T4 or TSH and PBDEs in the serum did not present a strong relationship. The findings of the research pointed out that being exposed to PBDE may cause a decrease in the binding of T4 to serum T4 binding proteins (Makey et al., 2016). As another possible exposure group, adult male sport fish consumers were studied in order to observe whether an association exists between PBDE body burdens and several aspects concerning the thyroid

system. Serums were collected from 405 participants and analysed for different chemicals and hormones including PBDE congeners, thyroglobulin antibodies, T4, T3, TSH, and T4-binding protein. Measures of T4 and PBDEs were observed to be positively associated. In contrast PBDEs were negatively related with total T3 and TSH in 308 men who did not have conditions of diabetes or thyroid dysfunction. In addition, PBDEs had a positive association with percentage of T4 bound to albumin, on the contrary had an inverse association with the percentage of T4 bound to TBG. Study's findings suggested that PBDE exposure had a link with increased thyroglobulin antibodies and T4 (Turyk et al., 2008). In a research, in which the exposed population consisted of children, researchers investigated the relation of PBDEs and NFRs with thyroid hormone. The study was conducted on 174 school students who reside around a petrochemical complex with questionnaires and blood samples. It was found that there was a significant association between the sum of thirteen PBDE congeners and eight types of NFRs and T3 levels (Guo et al., 2018). In another study, researchers examined serum hormone levels in men recruited from an infertility clinic and determined 31 PBDE congeners and 6 alternate FRs in their house dust. Beside other findings of the study, when hormones related to the thyroid system was evaluated, considerable positive associations between serum levels of free T4 and total T3 and pentaBDEs were seen. In addition, octaBDEs were found to be positively related with serum free T4 and TSH (Johnson et al., 2013). In a study, which was conducted on female participants, whether PBDE concentrations in serum had a link with thyroid disease among women was investigated. The possibility of thyroid disease increased among those with the highest concentrations of BDE47, 99 and 100 in serum. Authors concluded that these compounds were related to thyroid disease and that the effects were observed to be greater in post-menopause (Allen et al., 2016). In a different study considering exposure of children, researchers collected serum

samples of children who attended to a school in town with an e-waste recycling area and of children from a school in a control area. Levels of PCBs and halogen FRs were determined to be much higher in the exposed group when compared with the control group. It was shown that internal exposure levels were closely related with responses of thyroid hormone related proteins and gene expression. An increase in the expression of ID1, a decrease in levels of TSH and expression of TR α - were observed due to more extensive exposure concentrations (Guo et al., 2020). On the contrary to studies mentioned above, Eggesbo and coworkers (2011) investigated the association of BFRs including six PBDEs with neonatal TSH via milk samples of 239 mothers. As a result, there was no significant association between important toxic PBDE congeners (BDE-47, 99, 153, 154, 209) and hexabromocyclododecane (HBCD) and TSH (Eggesbø et al., 2011).

When the effects of metabolites of PBDEs were considered, Li and coworkers (2010) found in their study that OH-PBDEs showed elevated thyroid hormone activities compared to PBDEs. Hydrogen bonding was seen between OH-PBDEs and TR β (Li et al., 2010). 172 adults, who were not exposed because of occupation but lived in a FRs production region, provided serum samples for a study. When levels of PBDEs in serum and thyroid function parameters were evaluated, it was seen that a significant and positive association was seen between serum levels of some BDE congeners (BDE-47, 100, 99) and FT3, TT3, TT4 and thyroid peroxidase antibody (Zhao et al., 2021).

In a study conducted on adult male Sprague Dawley rats, the effects of a BFRs mixture on the reproductive system and thyroid function were examined. Beside other findings of the study, when the impact on thyroid system was examined, it was seen that the highest dose led to thyroid toxicity which was seen as hypertrophy of the thyroid gland epithelium and decreased levels of serum T4. Epithelium of thyroid

gland seemed thinner at lower doses; however, there were no alterations in the hormone levels (Ernest et al., 2012). In utero exposure of CD-1 mice in an in vivo study demonstrated that PBDE-209 resulted in reduced serum T3 in offspring; however, it did not reduce T4 (Tseng et al., 2008).

Tetrabromobisphenol A, Tetrachlorobisphenol A and Hexabromocyclododecane

Tetrabromobisphenol A (TBBPA) and tetrachlorobisphenol A (TCBPA) are applied as FRs in different products including plastic products, building materials, synthetic textiles and paints, their molecular formulas are shown in Figure 2. Approximately one third of total FRs use consists of TBBPA though TBBPA has the potential of being persistent in the environment and bioaccumulate (Kitamura et al., 2002). Due to phasing out of penta- and octa- BDE-based FRs, different BFRs including TBBPA and HBCDs have been seen as alternatives to be used instead of PBDEs. Besides human tissues, marine sediments and biota are among the environmental matrices in which these compounds

are detected (Kim & Oh, 2014).

Kim and Oh (2014) examined the relationship between TBBPA and HBCDs and thyroid hormones and environmental factors using serum samples of infant-mother pairs (26 infants had congenital hypothyroidism and 12 infants were healthy). It is indicated that maternal transfer of these compounds are important and a weak correlation was seen between TBBPA and thyroid hormones, positively related to fT4 while negatively related to T3 (Kim & Oh, 2014). In another study focusing on TBBPA and TCBPA, TBBPA and TCBPA were evaluated according to their thyroid hormonal-disrupting activity, and a comparison was made between these compounds and bisphenol A. It was observed that TBBPA and TCBPA caused an inhibition in the binding of T3 to the thyroid hormone receptor. In rat pituitary cell line GH3 cells, these compounds caused an increase in proliferation and stimulated growth hormone production. According to the results of this study it is concluded that TBBPA and TCBPA may function as thyroid hormone agonists (Kitamura et al, 2002).

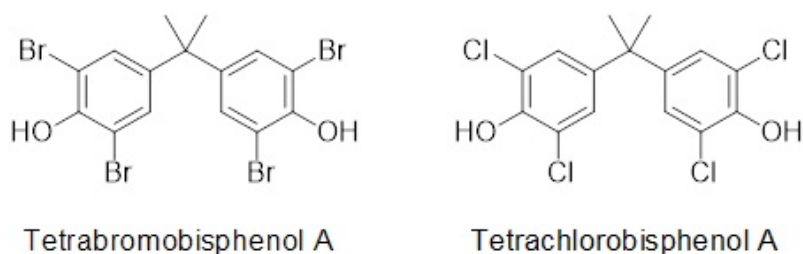


Figure 2. Structural formulas of TBBPA and TCBPA (Kitamura et al., 2002)

Phosphorus Flame Retardants

PBDEs are gradually being phased out because of their toxic effects, some of which are developmental toxicity, endocrine-disrupting effects, immunotoxicity, and neurotoxicity. Phosphorus flame retardants (PFRs) are seen as alternatives that are relatively efficient and safe (Zhang et al., 2016). PFRs consist of three main categories including organic, inorganic, and halogen-containing PFRs.

PFRs are mostly active in the solid phase of burning materials however some of them might show their action in the gas phase. Some PFRs are mixed into the polymer, while some have chemical bonds with the polymer. If the concentrations are compared, it is observed that the concentrations of PFRs in the environment seem to be higher than those of PBDEs. When exposure through indoor air is considered, exposure to concentrations of PFRs appears to be

higher than concentrations of PBDEs (Van der Veen & de Boer, 2012). Automobiles, offices, and homes are among the places in which PFRs have been found. In the US, Canadian, Asian, European, and Australian populations, detectable levels of PFR metabolites have been determined in urine. It is suggested that metabolite levels differ according to age, and higher exposures are seen in younger ages (Hoffman et al., 2017).

Organophosphate Flame Retardants

This group of FRs have taken place in the production for more than thirty years, and the application of these compounds have been increased as a result of the restriction of PBDEs, and some of the most well-known examples of OPFRs are listed in Table 2 (Castorina et al., 2017). OPFRs show their effect through increasing char formation, which results in a physical barrier between the material and the ignition source (Dishaw et al., 2014). OPFRs are classified as additive FRs (Doherty et al., 2019; Yao et al., 2021) and categorized as halogenated and non-halogenated aryl phosphates esters. They have primarily been used instead of PBDEs in the past twenty years (Wang et al., 2020). Textiles, glues, building materials, plastic products, chemicals, paints, furniture, baby products, electronic devices, and printed circuit boards are among the usage areas of OPFRs (Du et al., 2019; Ren et al., 2016; Yao et al., 2021). Therefore, they can easily leach into the environment (Ren et al., 2016; Yao et al., 2021) and have been detected in water, air, sediment, and dust (Yao et al., 2021). Preliminary data is suggesting direct human exposure to OPFRs through the measurement of dust samples and foam of baby products (Castorina et al., 2017).

Organophosphate esters (OPEs) are detected in office spaces, residential housing, and childcare environments. OPEs are particularly determined in indoor air and dust of indoor environments (Doherty et al., 2019). Routes of exposure to these compounds include inhaling dust in the indoor environment, ingesting dust or contaminated food, respiration

of contaminated air, consumption of contaminated water, dermal absorption (Ding et al., 2019; Doherty et al., 2019). Metabolites of OPEs were detected in human biological matrices; placenta, urine, and breast milk can be given as examples. This may suggest that OPEs have the potential to accumulate in the human body (Ding et al., 2019). Urinary metabolites of some OPFRs are shown in Table 3.

An increasing number of studies have demonstrated that OPFRs may lead to carcinogenesis, neurotoxicity, and endocrine-disrupting activity (Yao et al., 2021). Also, it is demonstrated in experimental animal models that OPEs may lead to neurotoxicity, the disruption of the endocrine system, developmental toxicity, adverse reproductive issues, and other systemic effects (Ren et al., 2016).

As an example of OPFRs, when TDCPP is examined, it is seen that this compound is found in different environmental compartments such as indoor air, dust, and drinking water. It is mainly applied to polyurethane foams for the furniture. TDCPP is found to be relatively toxic when compared to other OPFRs according to acute toxicity results (Wang et al., 2013). TDCPP can induce different types of toxicities including developmental toxicity, nerve toxicity, hepatic toxicity, endocrine disrupting toxicity, nephron toxicity, acute toxicity and reproductive toxicity in animals (Wang et al., 2020). Also, it is suggested in an animal study that mRNA expression of thyroid hormone receptors and associated genes could be significantly upregulated due to TDCPP exposure (Wang et al., 2013).

Another example of OPFRs is TPHP, which is suggested in the literature to have the potential to interfere with thyroid function (Preston et al., 2017). According to present studies, several different toxicities are related to TPHP, including genotoxicity, reproductive toxicity, developmental toxicity, neurotoxicity, metabolic disruption, and endocrine effects (Castorina et al., 2017).

Table 2. Examples of OPFRs, their structural formula, chemical nomenclature, and abbreviated name (Doherty et al., 2019)

Structural Formula	Chemical Nomenclature	Abbreviation
	Tris (1,3-dichloro isopropyl) phosphate	TDCPP
	Tris (1-chloro-2-isopropyl) phosphate	TCIPP
	Tris (2-chloroethyl) phosphate	TCEP
	Triphenyl phosphate	TPHP

In the study by Ren and coworkers (2016) the activities of four OPEs including trimethylphosphate (TMP), TCEP, triethylphosphate (TEP), and TDCPP against thyroid hormone nuclear receptor were examined via *in vitro* methods. Results demonstrated that these compounds had agonistic activity towards TR β , and TDCPP was found to be the most potent compound. In addition, it was found that these studied OPEs could fit into the ligand binding pocket of TR β , and again TDCPP was bound more functionally. Overall, the authors suggested that disruption of the thyroid system by OPEs may occur through a mechanism involving the activation of TR (Ren et al., 2016). On the contrary to this study, in a study which took place in China, researchers used *in silico*, *in vitro* and *in vivo* methods in order to examine the thyroid hormone disrupting activity of nine phosphorus containing FRs. Their results suggested that some of

these compounds showed antagonistic activity on TR β , including tributyl phosphate (TNBP), tricresyl phosphate (TMPP), TCIPP, and TDCPP. It is reported that this effect may be observed due to the direct binding of PFRs to TR. Due to the T3 antagonistic activity of TNBP and TMPP, the viability of GH3 cell lines significantly decreased in the presence of T3. The authors concluded that some PFRs have the possibility to disrupt thyroid hormones (Zhang et al., 2016).

In an *in vivo* study, domestic chicken eggs were exposed to TCEP and TDCPP and several aspects including thyroid hormone pathway and thyroid hormone levels were examined. Beside its other effects, TDCPP caused a reduction in plasma free T4 levels. The authors suggested that findings on phenotypic responses may be observed due to disruption of the thyroid hormone axis since it has a substantial role for normal growth and development of birds (Farhat

et al., 2013). In a different animal study, researchers exposed chicken embryos to OPFRs which are tris(2-butoxyethyl) phosphate (TBOEP), and TEP. Several aspects were evaluated, including thyroid hormone levels. Plasma T4 concentrations were observed to be decreased due to TEP doses (Egloff et al., 2014). An animal study conducted on fish demonstrated the possible effect of parental exposure to TDCPP on the thyroid endocrine system and the growth of zebrafish. The results showed that this compound was transferred to the offspring from adult zebrafish. In F1 larvae, a critical decrease was observed in T4 while there was a considerable increase in T3, also the transcription of some genes and expression of proteins that take part in the HPT axis were disrupted. These observations demonstrated that parental exposure to TDCPP could lead to the induction of thyroid disruption in the offspring (Ren et al., 2019). In a study using zebrafish embryos some aspects, such as whole-body concentrations of thyroid hormones and transcriptional profiles of genes that take part in the HPT axis, were evaluated. Due to TDCPP exposure, whole body T4 levels decreased and whole body T3 levels increased, which suggested the disruption of the thyroid endocrine system. Furthermore, being exposed to TDCPP led to an important increase in the transcription of genes that take part in thyroid development and thyroid hormone synthesis. According to the results of this study, it is reported that TDCPP caused endocrine disruption of the thyroid system (Wang et al., 2013). In another study, TDCPP exposure on adult zebrafish was examined, and when thyroid hormone homeostasis was evaluated, it was seen that plasma T4 and 3,5,3'-triiodothyronine levels considerably reduced in F0 females and F1 larvae/eggs. According to the results of the study, the authors concluded that TDCPP is capable of being passed on to the offspring due to the exposure of the parent and may result in the disruption of thyroid function and developmental neurotoxicity (Wang et al., 2015). In a study examining the transgenerational profile of TDCPP and polystyrene nanoplastics (PS-NPs) and

their impact on thyroid disruption in zebrafish, it was seen that when parent zebrafish were exposed to TDCPP either alone or combined with PS-NPs, it resulted in the induction of thyroid disruption in both adult zebrafish and offsprings. T4 and T3 levels decreased, and this seemed to affect the thyroid dysfunction of offspring due to transgenerational factors (Zhao et al., 2021).

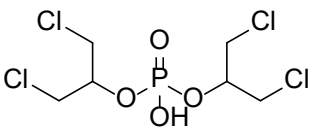
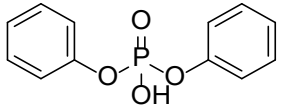
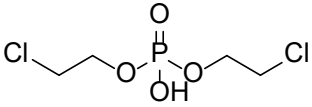
In a study which examined the effects of a different member of OPFRs, researchers used embryonic/larval zebrafish to examine the toxic effects of TPHP on thyroid endocrine system. In order to define the underlying mechanisms of such effects, rat pituitary (GH3) and thyroid follicular (FRTL-5) cell lines were used. According to the findings on the cell lines, it was suggested that TPHP stimulated thyroid hormone synthesis in the thyroid gland. Results with zebrafish larvae showed that TPHP caused important increases in T3 and T4 levels. Also, the expression of genes in thyroid hormone synthesis increased. In addition, the expression of genes that are linked with metabolism, elimination, and transport of thyroid hormones were significantly upregulated due to TPHP exposure. The authors indicated that in the early stages of zebrafish life, due to the disruption of central regulation and hormone synthesis pathways, TPHP could cause an increase in thyroid hormone levels (Kim et al., 2015).

Meeker and Stapleton (2010) investigated the association between TDCPP and TPHP and hormone levels and reproductive system parameters, and house dust was used in order to analyze the exposure. In addition to the findings about the reproductive system, the results showed that an increase in the TDCPP was related to a decrease in free T4 (Meeker & Stapleton, 2010). Prenatal urinary levels of OPE metabolites (mOPEs), concentrations of FT3, FT4, TSH, and some oxidative stress parameters in pregnant women and neonatal TSH heel blood were measured in newborns in a different study. A positive relation was seen between the concentrations of DBP and DPHP and either maternal or neonatal TSH levels; however,

no such relation was seen with maternal FT3 and FT4 levels. In addition, 8-OHdG was observed to mediate the association between neonatal TSH and DPHP, which led to the idea that DNA damage may take part in the disorder of fetal thyroid function (Y. Yao et al., 2021). Previous research has led to the assumption that disruption of thyroid hormones caused by FRs may elevate cancer risk because increased TSH levels and chronic iodine deficiency are well-known factors on the risk of various types of cancer (Mughal & Demeneix, 2017). However, a study in which 100 females who were diagnosed with papillary thyroid cancer and 100 controls were recruited in order to determine the levels of six PFRs metabolites in urine, demonstrated a different perspective. The findings suggested that there are no associations between PFRs and papillary thyroid cancer risk (Deziel et al., 2018). Also, Hoffman and coworkers (2017) investigated whether higher exposure to FRs has an association

with an elevated risk of papillary thyroid cancer. It is reported that higher concentrations of FRs in household dust had a relationship with an increase in the risk of papillary thyroid cancer. This was observed especially for BDE-209 and TCEP. TCEP was linked with larger and more aggressive tumors, while BDE-209 was related to less aggressive tumors with smaller sizes. Overall, it was indicated that there may be an association between FRs in the home, BDE-209 and TCEP in particular, and papillary thyroid cancer (Hoffman et al., 2017b). In another study concerning the metabolites of OPFRs, the association between urinary DPHP concentrations and thyroid hormones was investigated in 51 adults. No significant link was seen between total T3, TSH, free T4 and DPHP, but it was found that particularly among women, being exposed to TPHP might be related to increased total T4 levels (Preston et al., 2017).

Table 3. Examples of urinary metabolites of several OPFRs (Doherty et al., 2019)

Structural Formula of Metabolite	Urinary Metabolite	Parent Compound
	Bis (1,3-dichloro isopropyl) phosphate (BDCIPP)	TDCPP
	Diphenyl phosphate (DPHP)	TPHP
	Bis (2-chloroethyl) phosphate (BCEP)	TCEP

CONCLUSION

Although legal regulations are made by health authorities and regulatory agencies try to prevent people from being exposed to FRs from various sources, the widespread use of these chemicals makes exposure inevitable. In this review, we focused on the effects of FRs on the thyroid system, but the potential health effects of FRs are not limited to

thyroid disruption. Exposure to FRs has been linked to various health risks, including neurological and developmental disorders, reproductive problems, and cancer. It should not be forgotten that the role of the dysfunction of hormones and hormone homeostasis, especially thyroid hormones, in the development of these diseases cannot be denied. As the use of FRs is in high amounts in all societies and new data are provided about their toxicity profiles over time, the use of some

members of these chemicals such as PBDEs has been restricted or prohibited. Moreover, although some of them were banned many years ago due to their toxic effects, they can still be found in the environment in high concentrations today. The best example of this can be given as BDE 209, which was added to Annex A of the Stockholm Convention on POPs (Persistent Organic Pollutants) in 2017. Results of experimental animal studies have shown that BDE 209 causes reductions in thyroid hormone levels and thyroid gland enlargement, and is an endocrine disruptor by causing a decrease in serum triiodothyronine.

As can be understood from this review, although there are enough scientific signals to draw our attention to the effects of FRs on the thyroid system, more human-sourced signals are needed to reach a complete conclusion. In fact, this review is intended to encourage further studies of human data on disorders of the thyroid system resulting from FRs exposure.

This review has been prepared to serve as a stimulus for further study of complex/controversial experimental animal results as well as human data. It is important to continue researching the potential hazards of FRs, and take measures to minimize exposure to these chemicals, especially for vulnerable populations such as infants, young children and pregnant women.

ACKNOWLEDGEMENTS

The authors would like to thank the Gazi University Academic Writing Application and Research Center for proofreading the article.

CONFLICT OF INTEREST

The authors declare that there is no conflict of interest.

AUTHOR CONTRIBUTION STATEMENT

Determination of the Subject (İÇ), Literature Research (İİ, İÇ), Preparing the Study Text (İİ, İÇ), Reviewing the Text (İÇ,İİ)

REFERENCES

- Allen, J. G., Gale, S., Zoeller, R. T., Spengler, J. D., Birnbaum, L., & McNeely, E. (2016). PBDE flame retardants, thyroid disease, and menopausal status in US women. *Environmental Health*, 15(1), 1-9. doi: 10.1186/s12940-016-0141-0
- Alsen, M., Sinclair, C., Cooke, P., Ziadkhanpour, K., Genden, E., & van Gerwen, M. (2021). Endocrine disrupting chemicals and thyroid cancer: an overview. *Toxics*, 9(1), 14. doi: 10.3390/toxics9010014
- Boas, M., Feldt-Rasmussen, U., & Main, K. M. (2012). Thyroid effects of endocrine disrupting chemicals. *Molecular and Cellular Endocrinology*, 355(2), 240-248. doi: 10.1016/j.mce.2011.09.005
- Bolinus, D. J., Sobek, A., Löf, M. F., & Undeman, E. (2018). Evaluating the consumption of chemical products and articles as proxies for diffuse emissions to the environment. *Environmental Science: Processes & Impacts*, 20(10), 1427-1440. doi: 10.1039/c8em00270c
- Brack, W., Barcelo Culleres, D., Boxall, A., Budzinski, H., Castiglioni, S., Covaci, A., . . . Kandie, F. (2022). One planet: one health. A call to support the initiative on a global science-policy body on chemicals and waste. *Environmental Sciences Europe*, 34(1), 1-10. doi: 10.1186/s12302-022-00602-6
- Brent, G. A. (2010). Environmental exposures and autoimmune thyroid disease. *Thyroid*, 20(7), 755-761. doi: 10.1089/thy.2010.1636
- Castorina, R., Butt, C., Stapleton, H. M., Avery, D., Harley, K. G., Holland, N., . . . Bradman, A. (2017). Flame retardants and their metabolites in the homes and urine of pregnant women residing in California (the CHAMACOS cohort). *Chemosphere*, 179, 159-166. doi: 10.1016/j.chemosphere

- Chevrier, J., Harley, K. G., Bradman, A., Gharbi, M., Sjödin, A., & Eskenazi, B. (2010). Polybrominated diphenyl ether (PBDE) flame retardants and thyroid hormone during pregnancy. *Environmental Health Perspectives*, 118(10), 1444-1449. doi: 10.1289/ehp.1001905
- Cok, İ. (2021). Chemistry of endocrine disruptors. Tarım O, editor. Endokrin Bozucular. Ankara. *Türkiye Klinikleri*, 1st ed, Ankara, Turkey 11-18.
- De Falco, M., & Laforgia, V. (2021). Combined effects of different endocrine-disrupting chemicals (EDCs) on prostate gland. *International Journal of Environmental Research and Public Health*, 18(18), 9772. doi: 10.3390/ijerph18189772
- Deziel, N. C., Yi, H., Stapleton, H. M., Huang, H., Zhao, N., & Zhang, Y. (2018). A case-control study of exposure to organophosphate flame retardants and risk of thyroid cancer in women. *BMC Cancer*, 18(1), 1-10. doi: 10.1186/s12885-018-4553-9
- Ding, J., Deng, T., Ye, X., Covaci, A., Liu, J., & Yang, F. (2019). Urinary metabolites of organophosphate esters and implications for exposure pathways in adolescents from Eastern China. *Science of the Total Environment*, 695, 133894. doi: 10.1016/j.scitotenv.2019.133894
- Dingemans, M. M., van den Berg, M., & Westerink, R. H. (2011). Neurotoxicity of brominated flame retardants:(in) direct effects of parent and hydroxylated polybrominated diphenyl ethers on the (developing) nervous system. *Environmental Health Perspectives*, 119(7), 900-907. doi: 10.1289/ehp.1003035
- Dishaw, L. V., Macaulay, L. J., Roberts, S. C., & Stapleton, H. M. (2014). Exposures, mechanisms, and impacts of endocrine-active flame retardants. *Current Opinion in Pharmacology*, 19, 125-133. doi: 10.1016/j.coph.2014.09.018
- Doherty, B. T., Hammel, S. C., Daniels, J. L., Stapleton, H. M., & Hoffman, K. (2019). Organophosphate esters: are these flame retardants and plasticizers affecting children's health? *Current Environmental Health Reports*, 6, 201-213. doi: 10.1007/s40572-019-00258-0
- Du, J., Li, H., Xu, S., Zhou, Q., Jin, M., & Tang, J. (2019). A review of organophosphorus flame retardants (OPFRs): occurrence, bioaccumulation, toxicity, and organism exposure. *Environmental Science and Pollution Research*, 26, 22126-22136. doi: 10.1007/s11356-019-05669-y
- Eggesbø, M., Thomsen, C., Jørgensen, J. V., Becher, G., Odland, J. Ø., & Longnecker, M. P. (2011). Associations between brominated flame retardants in human milk and thyroid-stimulating hormone (TSH) in neonates. *Environmental Research*, 111(6), 737-743. doi: 10.1016/j.envres.2011.05.004
- Egloff, C., Crump, D., Porter, E., Williams, K. L., Letcher, R. J., Gauthier, L. T., & Kennedy, S. W. (2014). Tris (2-butoxyethyl) phosphate and triethyl phosphate alter embryonic development, hepatic mRNA expression, thyroid hormone levels, and circulating bile acid concentrations in chicken embryos. *Toxicology and Applied Pharmacology*, 279(3), 303-310. doi: 10.1016/j.taap.2014.06.024
- Encarnação, T., Pais, A. A., Campos, M. G., & Burrows, H. D. (2019). Endocrine disrupting chemicals: Impact on human health, wildlife and the environment. *Science Progress*, 102(1), 3-42. doi: 10.1177/0036850419826802
- Ernest, S. R., Wade, M. G., Lalancette, C., Ma, Y.-Q., Berger, R. G., Robaire, B., & Hales, B. F. (2012). Effects of chronic exposure to an environmentally relevant mixture of brominated flame retardants on the reproductive and thyroid system in adult male rats. *Toxicological Sciences*, 127(2), 496-507. doi: 10.1093/toxsci/kfs098

- Farhat, A., Crump, D., Chiu, S., Williams, K. L., Letcher, R. J., Gauthier, L. T., & Kennedy, S. W. (2013). In ovo effects of two organophosphate flame retardants—TCPP and TDCPP—on pipping success, development, mRNA expression, and thyroid hormone levels in chicken embryos. *Toxicological Sciences*, 134(1), 92-102. doi: 10.1093/toxsci/kft100
- Gilbert, M. E., O'Shaughnessy, K. L., & Axelstad, M. (2020). Regulation of thyroid-disrupting chemicals to protect the developing brain. *Endocrinology*, 161(10), bqaa106. doi: 10.1210/endo/bqaa106
- Guo, L.-C., Liu, T., Yang, Y., Yu, S., Gao, Y., Huang, W., . . . Zhang, Y. (2020). Changes in thyroid hormone related proteins and gene expression induced by polychlorinated biphenyls and halogen flame retardants exposure of children in a Chinese e-waste recycling area. *Science of the Total Environment*, 742, 140597. doi: 10.1016/j.scitotenv.2020.140597
- Guo, L.-C., Xiao, J., Zhang, Y., Yu, S., Lin, H., Su, G., . . . Rutherford, S. (2018). Association between serum polybrominated diphenyl ethers, new flame retardants and thyroid hormone levels for school students near a petrochemical complex, South China. *Chemosphere*, 202, 476-482. doi: 10.1016/j.chemosphere.2018.03.120
- Guo, L.-C., Yu, S., Wu, D., Huang, J., Liu, T., Xiao, J., . . . Zeng, W. (2019). Disruption of thyroid hormone regulated proteins and gene expression by polychlorinated biphenyls, polybrominated diphenyl ethers and new flame retardants in residents of an e-waste region. *Environmental Pollution*, 254, 112925. doi: 10.1016/j.envpol.2019.07.093
- Hoffman, K., Lorenzo, A., Butt, C. M., Adair, L., Herring, A. H., Stapleton, H. M., & Daniels, J. L. (2017). Predictors of urinary flame retardant concentration among pregnant women. *Environment International*, 98, 96-101. doi: 10.1016/j.envint.2016.10.007
- Hoffman, K., Lorenzo, A., Butt, C. M., Hammel, S. C., Henderson, B. B., Roman, S. A., . . . Sosa, J. A. (2017b). Exposure to flame retardant chemicals and occurrence and severity of papillary thyroid cancer: a case-control study. *Environment International*, 107, 235-242. doi: 10.1016/j.envint.2017.06.021
- Johnson, P. I., Stapleton, H. M., Mukherjee, B., Hauser, R., & Meeker, J. D. (2013). Associations between brominated flame retardants in house dust and hormone levels in men. *Science of the Total Environment*, 445, 177-184. doi: 10.1016/j.scitotenv.2012.12.017
- Kabir, E. R., Rahman, M. S., & Rahman, I. (2015). A review on endocrine disruptors and their possible impacts on human health. *Environmental Toxicology and Pharmacology*, 40(1), 241-258. doi: 10.1016/j.etap.2015.06.009
- Kahn, L. G., Philippat, C., Nakayama, S. F., Slama, R., & Trasande, L. (2020). Endocrine-disrupting chemicals: implications for human health. *The Lancet Diabetes & Endocrinology*, 8(8), 703-718. doi: 10.1016/S2213-8587(20)30129-7
- Keestra, S., Höggqvist Tabor, V., & Alvergne, A. (2021). Reinterpreting patterns of variation in human thyroid function: An evolutionary ecology perspective. *Evolution, Medicine, and Public Health*, 9(1), 93-112. doi: 10.1093/emph/eoaa043

- Kim, S., Jung, J., Lee, I., Jung, D., Youn, H., & Choi, K. (2015). Thyroid disruption by triphenyl phosphate, an organophosphate flame retardant, in zebrafish (*Danio rerio*) embryos/larvae, and in GH3 and FRTL-5 cell lines. *Aquatic Toxicology*, *160*, 188-196. doi: 10.1016/j.aquatox.2015.01.016
- Kim, U.-J., & Oh, J.-E. (2014). Tetrabromobisphenol A and hexabromocyclododecane flame retardants in infant-mother paired serum samples, and their relationships with thyroid hormones and environmental factors. *Environmental Pollution*, *184*, 193-200. doi: 10.1016/j.envpol.2013.08.034
- Kitamura, S., Jinno, N., Ohta, S., Kuroki, H., & Fujimoto, N. (2002). Thyroid hormonal activity of the flame retardants tetrabromobisphenol A and tetrachlorobisphenol A. *Biochemical and Biophysical Research Communications*, *293*(1), 554-559. doi: 10.1016/S0006-291X(02)00262-0
- Kozłowski, R., Muzyczek, M., & Walentowska, J. (2014). Flame retardancy and protection against biodeterioration of natural fibers: State-of-Art and Future Prospects. In *Polymer green flame retardants* (pp. 801-836): Elsevier.
- Köhrle, J., & Frädlich, C. (2021). Thyroid hormone system disrupting chemicals. *Best Practice & Research Clinical Endocrinology & Metabolism*, *35*(5), 101562. doi: 10.1016/j.beem.2021.101562
- La Merrill, M. A., Vandenberg, L. N., Smith, M. T., Goodson, W., Browne, P., Patisaul, H. B., . . . Woodruff, T. J. (2020). Consensus on the key characteristics of endocrine-disrupting chemicals as a basis for hazard identification. *Nature Reviews Endocrinology*, *16*(1), 45-57. doi: 10.1038/s41574-019-0273-8
- Li, F., Xie, Q., Li, X., Li, N., Chi, P., Chen, J., . . . Hao, C. (2010). Hormone activity of hydroxylated polybrominated diphenyl ethers on human thyroid receptor- β : in vitro and in silico investigations. *Environmental Health Perspectives*, *118*(5), 602-606. doi: 10.1289/ehp.0901457
- Makey, C. M., McClean, M. D., Braverman, L. E., Pearce, E. N., He, X.-M., Sjödin, A., . . . Webster, T. F. (2016). Polybrominated diphenyl ether exposure and thyroid function tests in North American adults. *Environmental Health Perspectives*, *124*(4), 420-425. doi: 10.1289/ehp.1509755
- Meeker, J. D., & Stapleton, H. M. (2010). House dust concentrations of organophosphate flame retardants in relation to hormone levels and semen quality parameters. *Environmental Health Perspectives*, *118*(3), 318-323. doi: 10.1289/ehp.0901332
- Mughal, B. B., & Demeneix, B. A. (2017). Flame retardants and increased risk of thyroid cancer. *Nature Reviews Endocrinology*, *13*(11), 627-628. doi: 10.1038/nrendo.2017.123
- Preston, E. V., McClean, M. D., Henn, B. C., Stapleton, H. M., Braverman, L. E., Pearce, E. N., . . . Webster, T. F. (2017). Associations between urinary diphenyl phosphate and thyroid function. *Environment International*, *101*, 158-164. doi: 10.1016/j.envint.2017.01.020
- Purser, D. (2014). Fire safety performance of flame retardants compared with toxic and environmental hazards. In *Polymer Green Flame Retardants* (pp. 45-86): Elsevier.
- Ren, X., Cao, L., Yang, Y., Wan, B., Wang, S., & Guo, L. (2016). In vitro assessment of thyroid hormone receptor activity of four organophosphate esters. *Journal of Environmental Sciences*, *45*, 185-190. doi: 10.1016/j.jes.2015.12.021
- Ren, X., Wang, W., Zhao, X., Ren, B., & Chang, L. (2019). Parental exposure to tris (1, 3-dichloro-2-propyl) phosphate results in thyroid endocrine disruption and inhibition of growth in zebrafish offspring. *Aquatic Toxicology*, *209*, 132-141. doi: 10.1016/j.aquatox.2019.02.004

- Shaw, S. D., Harris, J. H., Berger, M. L., Subedi, B., & Kannan, K. (2014). Brominated flame retardants and their replacements in food packaging and household products: Uses, human exposure, and health effects. *Toxicants in Food Packaging and Household Plastics: Exposure and Health Risks to Consumers*, 61-93. doi:10.1007/978-1-4471-6500-2_3
- Stapleton, H. M., Eagle, S., Anthopolos, R., Wolkin, A., & Miranda, M. L. (2011). Associations between polybrominated diphenyl ether (PBDE) flame retardants, phenolic metabolites, and thyroid hormones during pregnancy. *Environmental Health Perspectives*, 119(10), 1454-1459. doi: 10.1289/ehp.1003235
- Sutton, P., Woodruff, T. J., Perron, J., Stotland, N., Conry, J. A., Miller, M. D., & Giudice, L. C. (2012). Toxic environmental chemicals: the role of reproductive health professionals in preventing harmful exposures. *American Journal of Obstetrics and Gynecology*, 207(3), 164-173. doi: 10.1016/j.ajog.2012.01.034
- Tseng, L.-H., Li, M.-H., Tsai, S.-S., Lee, C.-W., Pan, M.-H., Yao, W.-J., & Hsu, P.-C. (2008). Developmental exposure to decabromodiphenyl ether (PBDE 209): effects on thyroid hormone and hepatic enzyme activity in male mouse offspring. *Chemosphere*, 70(4), 640-647. doi: 10.1016/j.chemosphere.2007.06.078
- Turyk, M. E., Persky, V. W., Imm, P., Knobeloch, L., Chatterton Jr, R., & Anderson, H. A. (2008). Hormone disruption by PBDEs in adult male sport fish consumers. *Environmental Health Perspectives*, 116(12), 1635-1641. doi: 10.1289/ehp.11707
- Vahabi, H., Laoutid, F., Mehrpouya, M., Saeb, M. R., & Dubois, P. (2021). Flame retardant polymer materials: An update and the future for 3D printing developments. *Materials Science and Engineering: R: Reports*, 144, 100604. doi:10.1016/j.mser.2020.100604
- Van der Veen, I., & de Boer, J. (2012). Phosphorus flame retardants: properties, production, environmental occurrence, toxicity and analysis. *Chemosphere*, 88(10), 1119-1153. doi: 10.1016/j.chemosphere.2012.03.067
- Wang, A., Padula, A., Sirota, M., & Woodruff, T. J. (2016). Environmental influences on reproductive health: the importance of chemical exposures. *Fertility and Sterility*, 106(4), 905-929. doi: 10.1016/j.fertnstert.2016.07.1076
- Wang, C., Chen, H., Li, H., Yu, J., Wang, X., & Liu, Y. (2020). Review of emerging contaminant tris (1, 3-dichloro-2-propyl) phosphate: Environmental occurrence, exposure, and risks to organisms and human health. *Environment International*, 143, 105946. doi: 10.1016/j.envint.2020.105946
- Wang, Q., Lai, N. L.-S., Wang, X., Guo, Y., Lam, P. K.-S., Lam, J. C.-W., & Zhou, B. (2015). Bioconcentration and transfer of the organophorous flame retardant 1, 3-dichloro-2-propyl phosphate causes thyroid endocrine disruption and developmental neurotoxicity in zebrafish larvae. *Environmental Science & Technology*, 49(8), 5123-5132. doi: 10.1021/acs.est.5b00558
- Wang, Q., Liang, K., Liu, J., Yang, L., Guo, Y., Liu, C., & Zhou, B. (2013). Exposure of zebrafish embryos/larvae to TDCPP alters concentrations of thyroid hormones and transcriptions of genes involved in the hypothalamic-pituitary-thyroid axis. *Aquatic Toxicology*, 126, 207-213. doi: 10.1016/j.aquatox.2012.11.009
- World Health Organization. (2013), State of the science of endocrine disrupting chemicals 2012: World Health Organization, https://apps.who.int/iris/bitstream/handle/10665/78102/WHO_HSE_PHE_IHE_2013.1_eng.pdf, Accessed 28.07.2023
- Yao, C., Yang, H., & Li, Y. (2021). A review on organophosphate flame retardants in the environment: Occurrence, accumulation, metabolism and toxicity. *Science of the Total Environment*, 795, 148837. doi: 10.1016/j.scitotenv.2021

- Yao, Y., Li, M., Pan, L., Duan, Y., Duan, X., Li, Y., & Sun, H. (2021). Exposure to organophosphate ester flame retardants and plasticizers during pregnancy: thyroid endocrine disruption and mediation role of oxidative stress. *Environment International*, 146, 106215. doi: 10.1016/j.envint.2020.106215
- Yeung, B. H., Wan, H. T., Law, A. Y., & Wong, C. K. (2011). Endocrine disrupting chemicals: Multiple effects on testicular signaling and spermatogenesis. *Spermatogenesis*, 1(3), 231-239. doi: 10.4161/spmg.1.3.18019
- Zhang, Q., Ji, C., Yin, X., Yan, L., Lu, M., & Zhao, M. (2016). Thyroid hormone-disrupting activity and ecological risk assessment of phosphorus-containing flame retardants by in vitro, in vivo and in silico approaches. *Environmental Pollution*, 210, 27-33. doi: 10.1016/j.envpol.2015.11.051.
- Zhao, X., Yang, X., Du, Y., Li, R., Zhou, T., Wang, Y., . . . Shi, Z. (2021). Polybrominated diphenyl ethers in serum from residents living in a brominated flame retardant production area: Occurrence, influencing factors, and relationships with thyroid and liver function. *Environmental Pollution*, 270, 116046. doi: 10.1016/j.envpol.2020.116046